Physics of Atomic Nuclei, Vol. 63, No. 4, 2000, pp. 523–524. Translated from Yadernaya Fizika, Vol. 63, No. 4, 2000, pp. 581–582.

IN MEMORIAM OF F. L. SHAPIRO

Fedor L'vovich Shapiro (April 6, 1915–January 30, 1973)

The articles that are presented under this rubric are dedicated to the 85th anniversary of the birth of Professor Fedor L'vovich Shapiro, a prominent physicist and a corresponding member of the USSR Academy of Sciences. A *rara avis* among nuclear physicists, Shapiro was a broad-minded person, known for his wide erudition and passionate enthusiasm for science. A man of principles, he was simultaneously kind and considerate to people, who loved and held him in high esteem for these generous qualities.

Shapiro was born in Gomel on April 6, 1915. He graduated from school at 15 years of age and entered an electrotechnical school. Being only 19 years old, he proposed an original method for converting thermal energy into electric energy by changing the magnetic flux generated by controlled variations in the temperature of a ferromagnetic core near the Curie point. In 1936, Shapiro entered the Faculty of Physics at Moscow State University. In 1941, he graduated from it with honors. In the same year, he joined the army as a volunteer and was seriously wounded. After the war, Shapiro became a postgraduate student of I. M. Frank at the Institute of Physics (USSR Academy of Sciences, Moscow) and, from then on, remained a close associate of this teacher. In those years, he also became an assistant professor at the Department of Nuclear Physics of the Faculty of Physics, Moscow State University. After finishing his postgraduate studies, Shapiro—together with E.L. Feinberg, L.E. Lazarev, L.V. Groshev, and I.V. Shtranikh—embarked on investigations into subcritical uranium–graphite systems. The results of these investigations, which were performed at the Institute of Physics within the program for developing nuclear weapons in the USSR, formed the basis of his candidate's dissertation, which he successfully defended in 1949.

In the early 1950s, Shapiro's group developed a spectrometer for recording neutrons by the time of their moderation in lead. This spectrometer was used in an extensive series of experiments that studied neutron–nucleus interactions and which showed, among other things, that the cross section for neutron capture by nuclei can deviate from the $1/v$ law (an explanation of this phenomenon was also given in Shapiro's studies). Along with research work, Shapiro delivered lectures on neutron physics at the Faculty of Physics at Moscow State University (his students dubbed these lectures Shapiro's special course). His lectures were characterized by extreme clarity and precision of presentation; as a teacher, he was able to explain involved physics problems in very simple and comprehensive terms.

In 1958, Shapiro became a deputy director of the Laboratory of Neutron Physics (headed by I. M. Frank) at the Joint Institute for Nuclear Research. In 1960, a pulsed fast-neutron reactor was commissioned at this laboratory, and Shapiro was among those who evolved the program of scientific investigations for this reactor. The program included investigations of the total and partial cross sections for neutron–nucleus interactions and the development of a method for polarizing resonance neutrons with energies between 1 eV and a few tens of keV that was previously unavailable to researchers.

The aforementioned reactor was used in a series of experiments that were able to measure the spins and magnetic moments of neutron resonances in nuclei and to determine the amplitudes for low-energy neutron scattering on a deuteron.

While continuing his studies in neutron physics, Shapiro took part in investigations of the Mössbauer effect. As a matter of fact, Shapiro became the pioneer of this new method of gamma spectroscopy in the Soviet Union. He developed the classical theory of the Mössbauer effect. Together with I.Ya. Barit and M.I. Podgoretsky, he indicated for the first time that, with the aid of the Mössbauer effect, an experiment aimed at testing the implications of the general theory of relativity could be implemented on the Earth. In the course of this experiment, it proved possible to observe the shift of the photon frequency in gravitational and inertial fields. For this, Shapiro proposed using narrow gamma lines as a source of photons. As a result, a velocity sweep of the 92-keV gamma-line resonance in the ^{67}Zn nucleus was obtained for the first time with a relative energy resolution of about 10^{-15}, which still remains a record value.

In 1961, Shapiro indicated that slow neutrons from pulsed fast-neutron reactors could be employed in investigations into condensed-matter physics. He developed a highly sensitive method of inverse geometry. This method made it possible to study thermal vibrations of atoms in solid bodies and liquids and to measure self-diffusion coefficients in the critical state of liquid–vapor systems. Together with the Polish physicist B. Buras, Shapiro substantiated the application of the neutron-time-of-flight method to diffraction investigations. In addition, the method of neutron dif-

1063-7788/00/6304-0523$20.00

fraction at magnetic structures in strong pulsed fields was implemented under his supervision.

In 1964, he became a member of the Editorial Board of the journal *Uspekhi Fizicheskikh Nauk* (known in the English-speaking world as *Soviet Physics—Uspekhi*).

In April 1968, Shapiro proposed using ultracold neutrons in a device for seeking the electric dipole moment of the neutron (such searches are of paramount importance for testing the conservation of T invariance). In the summer of the same year, a group of experimentalists headed by Shapiro observed for the first time ultracold neutrons (gas of elementary particles, neutrons) that were created with the aid of the low-energy pulsed fast-neutron reactor installed at the Laboratory of Neutron Physics and which were confined within a vessel made from ordinary matter.

After that, Shapiro initiated experiments with ultracold neutrons at more powerful stationary reactors at the Kurchatov Institute of Atomic Energy (Moscow), Research Institute for Atomic Reactors (Dmitrovgrad), and Institute of Nuclear Physics (Kazakh SSR Academy of Sciences, Alma-Ata).

Shapiro fell seriously ill in 1971 and passed away on January 30, 1973 three months before his 58th birthday.

For his scientific and pedagogical achievements, Fedor L'vovich Shapiro was rewarded with various state decorations and prizes. The degree of professor was conferred upon him in 1967. In 1968, he was elected to corresponding membership in the USSR Academy of Sciences.

The name of Fedor L'vovich Shapiro belongs to the history of physics and will ever be remembered by those who had a privilege to know him.

L. B. Pikelner
A. V. Strelkov

Physics of Atomic Nuclei, Vol. 63, No. 4, 2000, pp. 525–529. Translated from Yadernaya Fizika, Vol. 63, No. 4, 2000, pp. 583–588.

IN MEMORIAM OF F. L. SHAPIRO

Measurements of a Partial Cross Section for the Reaction ^{58}Ni(n, γ_0)^{59}Ni

Yu. P. Popov*, A. V. Voinov, S. S. Parzitski, N. A. Gundorin, D. G. Serov, A. P. Kobzev, and P. V. Sedyshev

Joint Institute for Nuclear Research, Dubna, Moscow oblast, 141980 Russia

Received August 9, 1999

Abstract—The partial cross section for radiative neutron capture accompanied by gamma transitions to the ground state of the ^{59}Ni nucleus was measured as a function of energy by a new neutron-spectrometry method that employed the shift of a primary gamma transition in response to a change in the energy of the captured neutron. The reaction ^{7}Li(p, n)^{7}Be was used as source of neutrons for the present measurements. The protons that induced this reaction were accelerated by a Van de Graaff electrostatic generator to energies exceeding the reaction threshold by 60 keV, in which case an appropriate geometry of the experiment permitted irradiation of the sample under study with neutrons whose energy ranged between 10 and 120 keV. The partial widths of some resonances and radiative strength function for hard primary $M1$ gamma transitions were determined in addition to the above cross sections. © *2000 MAIK "Nauka/Interperiodica".*

1. INTRODUCTION

At present, there exists a vast body of experimental data on the parameters of neutron resonances in nuclei, as well as experimental and estimated data on cross sections for radiative neutron capture. The most comprehensive compilations of such data can be found in well-known libraries like ENDF/B and JENDL. At the same time, experimental information about partial gamma transitions accompanying neutron capture is less comprehensive, covering a limited range of neutron energies and a very limited range of nuclei (no such information is available for the majority of nuclei). In all probability, this is because partial cross sections for the reactions being discussed are small, requiring highly efficient experimental methods involving the spectrometry of the recorded gamma radiation. For those cases, the application of the time-of-flight method for neutron spectrometry is limited because of its low efficiency.

In the present study, the partial cross sections for radiative neutron capture were measured by a new method employing the shift of the energy of the primary gamma transition triggered by resonance-neutron capture in relation to the energy of the analogous transition following thermal-neutron capture [1, 2]. For the first time, the capabilities of this method were demonstrated by Thomson *et al.* [3], who were able to record two resonances in silicon by using a reactor-neutron beam filtered by a boron layer. However, those authors failed to extract any information from their results other than the experimental resonance widths. At the same time, this new method, which is being refined in our laboratory, makes it possible to measure not only the partial cross sections for gamma transitions to the ground and the first excited state of a daughter nucleus but also partial radiative widths. The latter enables a determination of $E1$ and $M1$ radiative strength functions [2]. In this connection, we believe that the analysis of averaged radiative-capture cross sections that was performed in the experiments of F.L. Shapiro's group with the first spectrometer using the time of neutron moderation in lead [4] may prove promising in extracting neutron strength functions.

At the first stage of refining the method, we employed Fe and Ni samples, for which the partial gamma widths for some of the strongest resonances (for the most part, s-wave resonances) had been measured by the time-of-flight method [5, 6]. This provided reference values for our relative measurements of cross sections and made it possible to test the new procedure.

2. DESCRIPTION OF THE EXPERIMENTAL PROCEDURE

In measuring partial cross sections for the reaction ^{58}Ni(n, γ_0)^{59}Ni, we recorded primary gamma transitions to the ground state of the daughter nucleus ^{59}Ni. The spin–parity of this state is $I^\pi = 3/2^-$; therefore, the multipolarity of these transitions is $E1$ for s-wave resonances and $M1$ for p-wave resonances.

The arrangement of the equipment in the neutron beam is schematically illustrated in Fig. 1. A sample that was made from natural nickel and which had a thickness of 4 mm and a shape similar to that of a ring was exposed to a flux of neutrons from the reaction ^{7}Li(p, n)^{7}Be. The protons that induced this reaction were accelerated by a Van de Graaff electrostatic generator to energies exceeding the reaction threshold by

* e-mail: ypopov@nf.jinr.ru

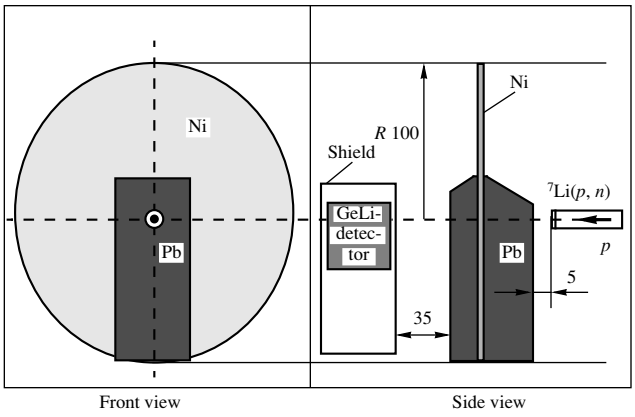

Fig. 1. Layout of the experimental setup.

60 keV, whereby irradiation of the sample with neutrons of energies between 10 and 120 keV was ensured. A lead block shielded the germanium detector used from hard gamma radiation originating from the reaction ^{7}Li(p, γ). A compact geometry of the experiment made it possible to achieve optimal efficiency both for photon detection and for the irradiation of the sample with neutrons.

The measurements were performed in short series of one-hour runs (the total time of measurements was about 70 h). After that, the resulting spectra, preliminarily corrected for the drift of the electronics amplification factor, were summed. For a drift indicator, we used background peaks that were invariably present in the measured spectra and which represented the well-known doublet of gamma transitions to the ground and the first excited state of ^{57}Fe nuclei generated in the reaction ^{56}Fe(n, γ)^{57}Fe induced by thermal (background) neutrons incident on iron nuclei that were in abundance both in structure materials and in the equipment of the experimental hall.

The background was measured without any sample in the time intervals between the experimental series. The bulk of the background was due to Compton scattering that photons originating from the radiative capture of neutrons scattered and moderated in surrounding materials, including the material of the massive magnet used to rotate the proton beam, suffered in the germanium detector.

The energy resolution of this spectrometric method was determined almost completely by the resolution of the germanium detector at the energies of the photons under investigation, amounting to about 8 keV in our case.

A section of the experimental gamma spectrum for gamma transitions to the ground state of the daughter nucleus is displayed in Fig. 2. The corresponding background, also presented in this figure, shows no peaks that could distort the sought effect.

3. RESULTS OF MEASUREMENTS AND THEIR ANALYSIS

The area of the primary gamma transition under the peak corresponding to the ith neutron resonance can be represented as

$$A_i \sim k_i \phi_i \varepsilon_i \lambda_i^2 g_i \frac{\Gamma_{ni}\Gamma_{\gamma i}^{p}}{\Gamma_i}, \qquad (1)$$

where Γ_{ni} is the neutron width of the ith resonance, $\Gamma_{\gamma i}^{p}$ is the partial radiative width, Γ_i is the total resonance width, ϕ_i is the neutron flux, and g_i is the spin factor. Since the sample used proved to be thick for some strong neutron resonances, a correction factor k_i that takes into account multiple neutron scattering in the sample and changes in the neutron flux over the thickness because of self-absorption was introduced in (1). For each resonance, this factor was computed by the Monte Carlo method. We used the neutron-resonance parameters from the compilation presented in [7]. The angular and energy dependences of the neutron flux were calculated by using the known cross sections for the reaction ^{7}Li(p, n)^{7}Be [8] and its kinematical features and by taking into account the overall geometry of the experiment (see Fig. 1). We have also introduced a correction for inefficiency of photon detection, considering that points occurring at different distances from the sample center are hit by neutrons of different energies.

The background conditions in the presence of the sample are different from those in the absence of it, because, in the former case, there arise neutrons scattered by the sample and Compton tails from nuclei of the ^{61}Ni isotope (its binding energy is B_n = 10598 keV) that are present in the sample. In processing the spectra, the background under the peaks was therefore approximated separately by background functions in the regions to the right and to the left of the effect being detected. The boundaries of the effect were determined by the interval of energies of the neutrons hitting the sample. For an approximating function, we used a polynomial of the second degree. Upon background subtraction, the area under the peak for each resonance was evaluated with the aid of computer fits that were obtained with the peak positions fixed strictly at $E_\gamma = B_n + E_0[A/(A+1)]$, where A is the atomic weight of the target, E_0 is the neutron-resonance energy, and B_n = 8999.43 keV is the neutron binding energy. In addition to strong resonances, which are responsible for the formation of peaks, the experimental spectrum features a large number of weak resonances [7]. It was assumed that these weak resonances form the continuous distribution of gamma-transition intensities in the region of well-resolved strong peaks. This is the reason why the adjustable function was taken in the form of the sum of Gaussian functions (which represented the peaks) and a smooth function. For a first approximation, we used a polynomial for the latter.

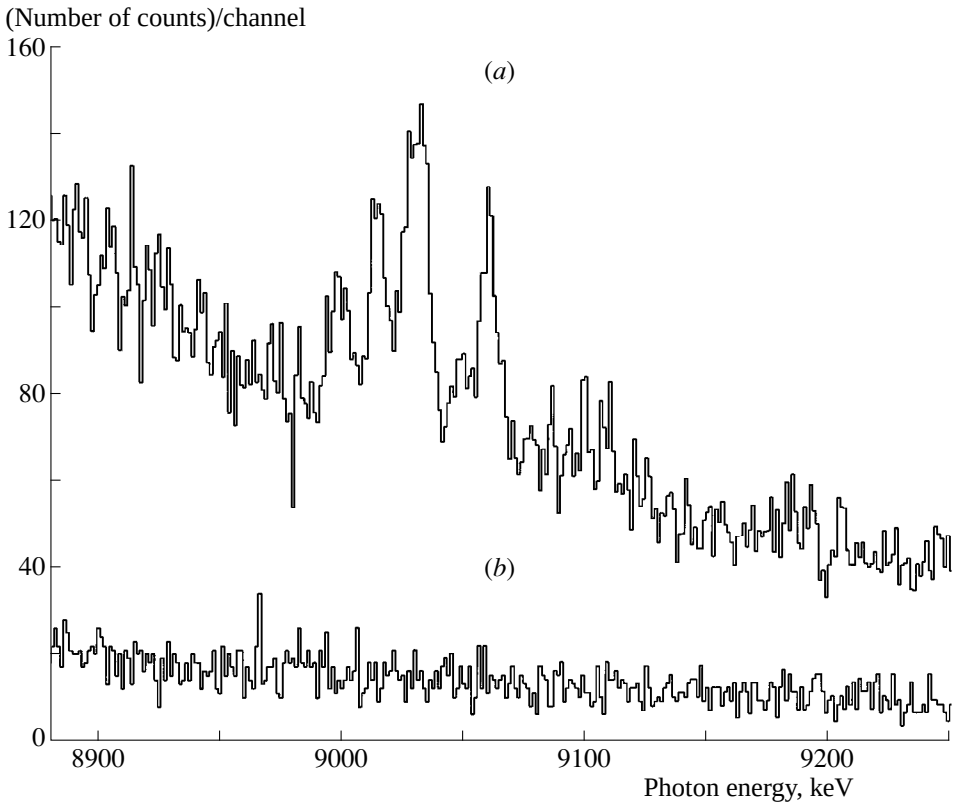

Fig. 2. (*a*) Experimental spectrum taken with a Ni sample: section that corresponds to gamma transitions populating the ground state of the ^{59}Ni nucleus (the data-accumulation time is 70 h); (*b*) background spectrum measured without a Ni sample (the data-accumulation time is 16 h).

Because the mean spacing between the resonances under study and the resolution of the method were 2 and 8 keV, respectively, the experimental curve was analyzed by the method of successive approximations. First, only those resonances were taken into account whose positions coincided with experimental peaks. After that, other resonances (the strongest ones, according to [7]) were added in order to improve the shape of the fitted curve and to minimize the χ^2 value. The procedure of adding resonances was terminated when this no longer resulted in the reduction of χ^2, leading simultaneously to the growth of the error in A_i. The total area of the resonances was used in the cases where they were closely spaced ($E_i - E_{i+1} \le 0.5$ keV).

3.1. Partial Parameters of Neutron Resonances

The relative area values for the E_0 = 15.28 keV resonance and for the E_0 = 26.07 + 26.64 keV and E_0 = 32.26 + 32.38 keV summed resonance pairs proved to be proportional to the corresponding partial widths from [5]. The proportionality factor was used for an absolute normalization of our relative values of the resonance areas. The results of this normalization are shown graphically in Fig. 3 and in the table, where the quoted errors are purely statistical. As a result, we additionally obtained the partial-width values for the E_0 = 36.12 keV resonance and for the E_0 = 51.91 + 52.22 keV unresolved resonances. The reason behind the discrepancy for the E_0 = 20.00 + 21.12 keV summed resonance pair (see table) has yet to be clarified.

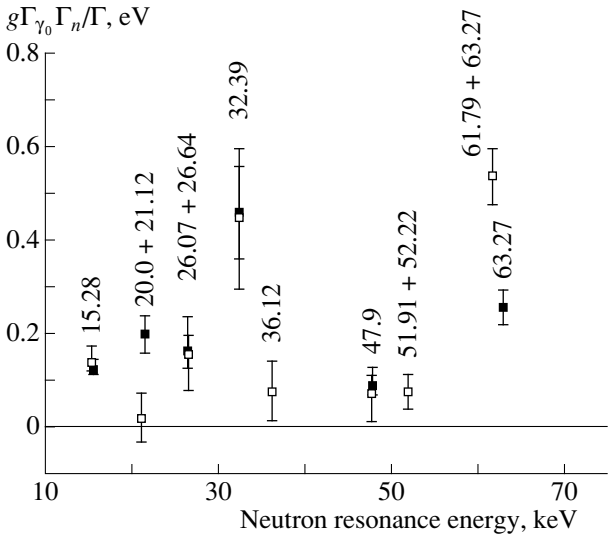

Fig. 3. Partial parameters $g\Gamma_{\gamma_0}\Gamma_n/\Gamma$ of neutron resonances: (closed boxes) our data and (open boxes) data from [5].

Parameters of neutron resonances in ^{58}Ni (the underlined values are used for the absolute normalization of our results)

E_0, keV	J^π [7]	$g\Gamma_\gamma\Gamma_n/\Gamma$, eV [7]	$g\Gamma_{\gamma_0}\Gamma_n/\Gamma$, eV	$g\Gamma_{\gamma_0}\Gamma_n/\Gamma$, eV [5]
15.28	$1/2^+$	1.21	0.140(27)	<u>0.124(17)</u>
20.002 + 21.12	$1/2^-$	0.25 + 0.69	0.017(53)	0.196(41)
26.07 + 26.64	$1/2^-$	0.28 + 0.89	0.155(79)	<u>0.159(35)</u>
32.26 + 32.38	$1/2^+ + 3/2^-$	0.46 + 1.35	0.443(152)	<u>0.456(98)</u>
36.12	$1/2^+$	1.19	0.074(63)	–
47.89	$3/2^-$	1.3	0.068(57)	0.088(19)
51.91 + 52.22	$3/2^-$	0.82 + 1.0	0.074(34)	–
61.79 + 63.27	$1/2^+ + 1/2^-$	1.43 + 2.3	0.538(60)	–
63.27	$1/2^+$	2.3		0.258(33)

The absolute normalization of the partial widths made it possible to rescale our experimental spectrum into the dependence of the absolute partial cross section for the reaction ^{58}Ni(n, γ_0)^{59}Ni as displayed in Fig. 4, which also shows the cross section calculated by using the partial parameters obtained here for neutron resonances (see table) with allowance for neutron absorption and rescattering in the sample.

3.2. Radiative Strength Function

A transition to the absolute values of the neutron-resonance parameters makes it possible to estimate not only the partial reaction cross section but also the radiative strength function. According to [7], about 45 p-wave resonances occur in the energy region studied in our experiment. This enables us to deduce the mean partial parameters of neutron resonances and, in particular, to calculate the radiative strength function for primary $M1$ gamma transitions to the ground state of the ^{59}Ni.

The radiative strength function was computed by the conventional formula

$$k_{M1} = \Gamma_{ij}^{M1}/D_i E_\gamma^3. \quad (2)$$

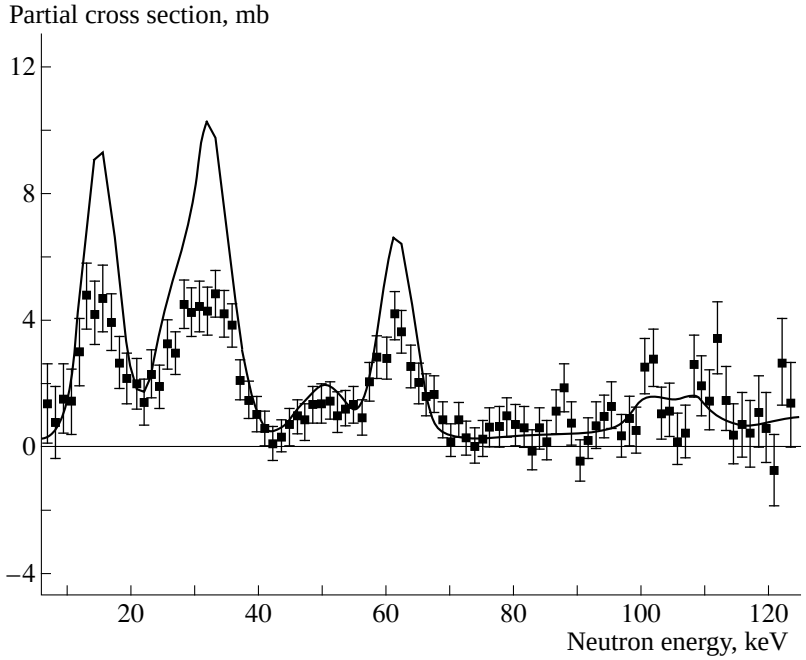

Fig. 4. Partial cross section for the reaction ^{58}Ni(n, γ_0)^{59}Ni: (points) experimental data that were corrected for the neutron flux, but which do not involve corrections for rescatterings and absorption in the sample; (curve) partial cross section that was calculated on the basis of the values obtained in this study for the partial parameters of neutron resonances (see table) and which take into account rescatterings and absorption in the sample.

For p-wave resonances, the mean value of the partial width Γ_{ij} was evaluated by taking into account all p-wave resonances having a specific spin value and occurring in the energy region being studied. In doing this, we included both strong resonances that manifested themselves as individual peaks in the experimental spectrum and weak resonances that contributed to the continuous pedestal (the contribution of weak resonances amounted to some 40% of the contribution of all resonances populating this energy region). In the calculation, we assumed, in accordance with the statistical model, that the radiative strength function takes the same value for resonances with different spins. The mean spacing between the spin-1/2 and spin-3/2 p-wave resonances was computed by using data from [7].

For the mean value of the $M1$ radiative strength function, the above procedure yields $k_{M1} = (12 \pm 6) \times 10^{-9}$ MeV^{-3}. The quoted error includes statistical uncertainties in approximating the experimental spectrum, errors in averaging over resonances in computing the mean values of Γ_n/Γ and the mean level spacing, and the error associated with Porter–Thomas fluctuations of the partial widths with respect to gamma transitions.

Obviously, the radiative-strength-function value obtained on the basis of the procedure outlined above depends on the way of background subtraction (that is, on the form of the function used to approximate the background, on the boundaries of the regions where the background was studied, and on some other similar factors). Bearing this in mind, we performed a test calculation of the radiative strength function within an exponential approximation of the background instead of the above approximation in terms of a second-degree polynomial. The result of this test calculation is $k_{M1} = (10 \pm 5) \times 10^{-9}$ MeV^{-3}. Variations in the boundaries of the background intervals change the k_{M1} value within the quoted statistical errors.

The value obtained here for k_{M1} complies well with data from [5] and with the compilation presented in [9].

4. CONCLUSION

We have demonstrated the capabilities of a new method of neutron spectroscopy. The efficiency of this method is higher than that of the time-of-flight method. The energy resolution of the method is determined by the resolution of a germanium detector in recording gamma transitions of energies in the range 6–9 MeV. This is, however, sufficient for studying light and medium-mass nuclei for which the spacing between the resonances is greater than or commensurate with the resolution of the germanium detector.

The high resolution of the method has enabled us to analyze not only strong resonances manifesting themselves as individual peaks but also weak resonances contributing to the continuous spectrum. Owing to this, we have been able to estimate the resonance parameters averaged over a large number of resonances. This has been demonstrated in calculating the mean value of the $M1$ radiative strength function.

Further plans are associated with studying gamma transitions that populate not only the ground state of the daughter nucleus but also its excited states, as well as with refining procedures for analysis of continuous spectra. This will make it possible to estimate the mean values of the partial parameters of neutron resonances, of the partial cross sections, and of radiative strength functions for heavier nuclei.

ACKNOWLEDGMENTS

We are grateful to I. A. Chepurenko and to the entire personnel of the EG-5 Van de Graaff electrostatic generator for ensuring stable operation of this device.

REFERENCES

1. Yu. P. Popov, P. V. Sedyshev, and M. V. Sedysheva, JINR Rapid Commun. (Dubna), No. 6[80]-96, 79 (1996).
2. Yu. V. Popov *et al.*, in *Proceedings of ISINN-6* (JINR, Dubna, 1998), no. E3-98-202, p. 319; Yad. Fiz. **62**, 886 (1999) [Phys. At. Nucl. **62**, 827 (1999)].
3. V. J. Thomson, A. V. López, W. V. Prestvich, *et al*., Nucl. Instrum. Methods **126**, 263 (1975).
4. Yu. P. Popov and F. L. Shapiro, Zh. Éksp. Teor. Fiz. **42**, 988 (1962) [Sov. Phys. JETP **15**, 683 (1962)]; Yu. P. Popov and Yu. I. Fenin, Zh. Éksp. Teor. Fiz. **43**, 2000 (1963) [Sov. Phys. JETP **16**, 1409 (1963)].
5. H. Beer, R. R. Spenser, and F. Kaeppeler, Z. Phys. A **284**, 173 (1978).
6. H. Komano, M. Igashira, M. Shimizu, *et al.*, Phys. Rev. C **29**, 345 (1984).
7. S. I. Suchoruchkin, Z. N. Soroko, and V. V. Deriglazov, in *Landolt–Bornstein/New Series*, Vol. 16/B: *Table of Neutron Resonance Parameters*, Ed. by H. Schopper (Springer-Verlag, 1998).
8. J. H. Gibbons and H. W. Newson, in *Fast Neutron Physics*, Ed. by J. B. Marion and J. L. Fowler (Interscience, 1960), Vol. 1, p. 133.
9. J. Kopecky and M. Uhl, in *Proceedings of a Specialists Meeting on Measurement, Calculation and Evaluation of Photon Production Data, Bologna, Italy, 1964*, p. 119.

Translated by A. Isaakyan

Physics of Atomic Nuclei, Vol. 63, No. 4, 2000, pp. 530–538. From Yadernaya Fizika, Vol. 63, No. 4, 2000, pp. 589–597.

IN MEMORIAM OF F. L. SHAPIRO

Measurements of Delayed-Neutron Yields from Thermal-Neutron-Induced Fission of ^{235}U, ^{233}U, ^{239}Pu, and ^{237}Np*

S. B. Borzakov, A. N. Andreev, E. Dermendjiev[1)], A. Filip[2)], W. I. Furman, Ts. Panteleev, I. Ruskov, Yu. S. Zamyatnin, and Sh. Zeinalov

Joint Institute for Nuclear Research, Dubna, Moscow oblast, 141980 Russia

Received August 9, 1999

Abstract—The experimental results on delayed-neutron yields from thermal-neutron-induced fission of some actinides in the IBR-2 pulsed reactor are presented. A method of periodic irradiation without displacement of the sample was used. The measurements of delayed-neutron total yields in thermal-neutron-induced fission of ^{239}Pu, ^{233}U, and ^{237}Np and in cold-neutron-induced fission of ^{235}U, ^{233}U, and ^{239}Pu were carried out. All values were obtained with the use of the value of β_0 for (n_{th} + ^{235}U) as a reference. Precise measurements of decay curves in the time interval 5–350 ms for ^{235}U and ^{239}Pu were performed. © *2000 MAIK "Nauka/Interperiodica".*

1. INTRODUCTION

It is well known that the emission of delayed neutrons (DN) after neutron-induced fission of heavy nuclei has a fundamental significance for the realization of a controllable fission chain reaction. The yields and time characteristics of delayed neutrons from the thermal-neutron-induced fission of the main reactor isotopes (^{235}U, ^{239}Pu, and ^{233}U) are some of the most important nuclear reactor constants used in reactor-kinetics calculations [1–5]. An accuracy of 3% for ^{235}U, 4% for ^{239}Pu, and 6% for ^{233}U has now been achieved for DN yields. The requirements for the accuracy of the parameters have continued to increase, especially in connection with the problems of reactor safety [4, 5].

However, despite a considerable number of measurements, the discrepancy in the obtained data is significant. This discrepancy is especially seen when comparing the DN data obtained by using two radically different methods for determining the DN parameters: (1) DN decay curve measurements with a subsequent approximation with six exponentials and determination of DN parameters: decay constants λ_i and weights a_i; (2) calculation of the group parameters by summation of all precursor yields included in this group. In the second case, the DN yield for a given precursor ν_{di} is equal to the product of the cumulative yield of the precursor Y_i and the neutron-emission probability P_{ni}. For example, the experimentally achieved accuracy in the DN yield for one of the well-studied cases (thermal-neutron-induced fission of ^{239}Pu) is 4%, but the calculated value of the DN yield ν_d is 10% above the experimental one [6]. Moreover, the boundaries of the six groups have an arbitrary character and vary in different works [7, 8]. One should mention that the values of the parameters for the fifth and the sixth group are determined with the poorest accuracy (20–40%) because of their short decay periods (less than 1 s). This is comparable with the time needed, in some works, to move a sample from the irradiation position to the position of DN recording.

As a consequence, the values of ν_d and $\beta_0 = \nu_d/\nu$ (where $\nu = \nu_d + \nu_p$ is the total number of fission neutrons and ν_p is the number of prompt neutrons per fission event) are the subject of continuing efforts to improve their accuracy.

The total-yield determination for DN from the thermal-neutron-induced fission of ^{233}U, ^{239}Pu, and ^{237}Np and from the cold-neutron-induced fission of ^{233}U, ^{235}U, and ^{239}Pu (by using the data on ν_d from the thermal-neutron-induced fission of ^{235}U as a reference) is the subject of this work. Our specific interest in the investigation of fission characteristics for ^{237}Np was stimulated by the recent work by Lisowski *et al.* [9], who demonstrated that ^{237}Np is a promising isotope for accelerator-driven energy production and waste transmutation. Also, one of the purposes of this work was to check experimentally the existence of DN groups with very short periods (less than 0.1 s) in thermal-neutron-induced fission of ^{235}U and ^{239}Pu, which is due to the existence of such isotopes as ^{94}Br, ^{99}Rb, ^{100}Rb, and ^{102}Sr.

2. METHOD

To study the short-lived DN groups in the millisecond time range, a method of periodic irradiation of the

* This article was submitted by the authors in English.

[1)] Institute for Nuclear Research and Nuclear Energy, BAS, Sofia, Bulgaria.

[2)] CEA, Cadarache, France.

1063-7788/00/6304-0530$20.00 © 2000 MAIK "Nauka/Interperiodica"

samples without displacement was developed at the Frank Laboratory of Neutron Physics (JINR, Dubna). Since the method has been discussed in detail elsewhere [10–12], we present here a short summary with relevant formulas.

The IBR-2 pulsed reactor [13] was used as a neutron source. The reactor pulses with a half-width of 230 μs at a repetition frequency of 5 Hz and a high intensity of the pulse neutron flux (the peak power is about 1350 MW) give a unique possibility to study DN with short decay periods. The pulse reactor allows us to carry out the periodic irradiation of samples and to measure the DN in the time intervals between the pulses. The detection of prompt neutrons and DN under the same conditions allows one to determine the β_0 value with good accuracy.

In the case of a periodic sample exposure, the counting rate for DN decreases with time t according to the expression

$$n_d(t) = N_f \nu_d \varepsilon_d \sum_{i=1}^{6} \frac{a_i}{\Delta t} \frac{1-\exp(-\lambda_i \Delta t)}{1-\exp(-\lambda_i T)} \exp(-\lambda_i t), \quad 0 < t < T - \Delta t, \tag{1}$$

where N_f is the number of fission events; ε_d is the detector efficiency for DN; λ_i and a_i are the decay constant corresponding to the half-life $T_{1/2,i}$ ($\lambda_i = \ln 2/T_{1/2,i}$) and the relative yield for the ith group of the DN $\left(\sum a_i = 1\right)$, respectively; Δt is the irradiation time; and T is the time interval between neutron bursts. The value of t is measured from the end of the irradiation time. This formula uses the well-known six-group approximation of Keepin [1] and takes into account the periodic irradiation of the target.

If the count numbers of prompt (measured in some time interval $[t_0, t_1]$) and delayed neutrons (in a time interval $[t_1, t_2]$), N_p and N_d, respectively, are known from the experiment, one can calculate the value of β_0 using the formulas given below.

In particular, the total number of DN is

$$S_d = \frac{N_d}{\varepsilon_d} F(T, \Delta t, t_1, t_2), \tag{2}$$

where $F(T, \Delta t, t_1, t_2)$ is a function that can be obtained from (1) and which takes into account the finite time interval of the DN measurement,

$$F(\Delta t, T, t_1, t_2) = \left[\sum_{i=1}^{6} \frac{a_i}{\lambda_i \Delta t} \frac{1-\exp(-\lambda_i \Delta t)}{1-\exp(-\lambda_i T)} \times (\exp(-\lambda_i t_1) - \exp(-\lambda_i t_2)) \right]^{-1}. \tag{3}$$

The number of prompt fission neutrons is

$$S_p = N_p/\varepsilon_p, \tag{4}$$

where ε_p is the detector efficiency for prompt neutrons. Obviously, we have

$$\nu_d/\nu_p = S_d/S_p \tag{5}$$

and

$$\beta_0 = \frac{\nu_d/\nu_p}{1+\nu_d/\nu_p}. \tag{6}$$

Therefore, the determination of the β_0 value is reduced to measurements of the detector counts for prompt and delayed neutrons and the ratio of their detection efficiencies.

The main advantage of this method lies in the fact that it is not necessary to know the absolute detector efficiency, the neutron flux, and the sample mass for these measurements. On the other hand, the measurements of DN from the short-life groups are carried out with a background from other groups with longer periods, which reaches saturation a few minutes after the start of irradiation.

3. THE EXPERIMENTAL SETUP

The measurements were performed at the Isomer setup (see Fig. 1), which was described in detail in [11, 12]. The Isomer facility was placed 27 m from the reactor core, and the time-of-flight method allowed the energy of the incident neutrons to be determined. The neutrons from the reactor core passed through a bent mirror guide (cross section 150×15 mm^2), which considerably suppressed the background from fast neutrons and photons. The thermal-neutron-flux density at the exit of the mirror guide was 6×10^5 n cm^{-2} s^{-1}.

The Isomer facility consists of a slow neutron chopper and a 4π neutron detector. The chopper is a Cd disk with two slits. The rotation of the chopper was synchronized with the reactor neutron bursts. The chopper served the following purposes: (1) to cut off the tail of cold neutrons quickly (during a time of about 1 ms) and to produce neutron pulses with a width of 10–40 ms, depending on the size of the slits and the rotation phase; (2) to suppress the reactor neutrons between these pulses. By shifting the chopper phase relative to the neutron bursts, one can choose different energy intervals of incident neutrons.

The neutron detector consists of 12 ^{3}He counters in a polyethylene moderator. The counters can be placed either in an internal ring ($\varnothing$ = 22.5 cm) or in an external ring ($\varnothing$ = 33 cm). The sample was placed in the central hole ($\varnothing$ = 15 cm) of the detector. To avoid recording thermal neutrons scattered by the sample, the detector was shielded inside by a Cd tube. The outside of the detector was covered with a 5-cm borated-polyethylene shield against the environment scattered neutrons.

The high-intensity neutron burst from the reactor causes a pileup of prompt-fission-neutron pulses during the exposure. Also, the dead time of the electronics used in these measurements leads to additional count

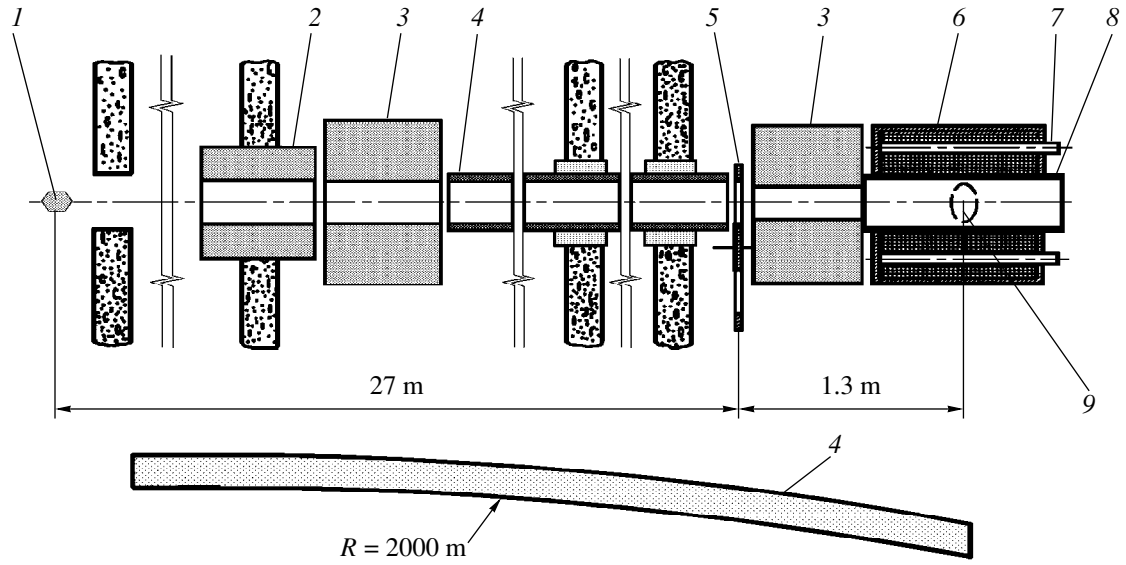

Fig. 1. The scheme of the Isomer setup: (*1*) IBR-2 reactor core and moderator, (*2*, *3*) collimators, (*4*) bent mirror guide, (*5*) chopper, (*6*) neutron detector, (*7*) ^{3}He counters, (*8*) Cd tube, and (*9*) sample.

losses. Therefore, special attention was paid to the correct estimation of the loss of prompt neutrons. The total dead time of the acquisition system, τ, was measured by the usual method of two neutron sources. The main part of the measurements were carried out with $\tau = 5.5$ μs; other measurements were performed with improved electronics ($\tau = 2.5$ μs). The conditions of the experiments were chosen such that the total correction of the number of detected prompt fission neutrons obtained in such measurements was not more than a few percent.

CAMAC-based electronics, connected to a PC, were used in the experiments to collect the data.

4. MEASUREMENTS

In this section, we present the results of the DN yield measurements for the $^{233, 235}$U, ^{239}Pu, and ^{237}Np isotopes and the decay-curve measurements for the ^{235}U and ^{239}Pu isotopes performed in our work.

Table 1. Characteristics of the samples used in the measurements

Isotope	Weight, g	Enrichment, %	Chemical compound	Backing
^{235}U	0.025	90	Oxide	Al
^{235}U	7.0	90	Metal	–
^{233}U	0.067	98.1	Oxide	Ni
^{239}Pu	0.057	95.2	Metal	–
^{239}Pu	20.0	99.9	Metal	–
^{237}Np	40.4	99.999	Oxide	Ni

Due to the large thermal-neutron-fission cross section, the samples used to measure the DN yield values for the main reactor isotopes had masses of about 25–70 mg. Since the thermal-neutron cross section for ^{237}Np is rather small, we used a sample of ^{237}Np with a mass of 40 g. For the decay-curve measurements, much larger samples of ^{235}U and ^{239}Pu (with masses of 7 and 20 g, respectively) were used. Some characteristics of the samples used are shown in Table 1.

4.1. Delayed-Neutron Yields

A typical spectrum measured with the ^{235}U sample over 18 h is shown in Fig. 2. The background was measured with a 1.5-mm Cd filter in the beam just behind the chopper. The background was due to (a) the (α, *n*) reaction on the backings and on the oxygen in the oxides of the isotopes and (b) the scattering of fast reactor neutrons in the sample. To reduce the first part of the background, Ni foils for the backings or metallic samples were used. The background value in the time interval $[t_1, t_2]$ for the DN counting was approximately 15% for ^{235}U, 30% for ^{233}U, and 45% for ^{239}Pu.

Our preliminary results were obtained from a number of runs that measured the effect for several hours and the consequent measurement of the background for approximately the same time [14]. To ensure the long-term stability of the results, we repeated the measurements with improved detector electronics, software, and automatic system, which allowed us to alternate the measurements of the effect and the background with a period of 20 min. The ratio of the efficiencies for delayed and prompt neutrons was obtained from the measurements with the ^{235}U sample at a mean energy of 0.023 eV and a value of $\beta_0 = (0.680 \pm 0.020)\%$. The lat-

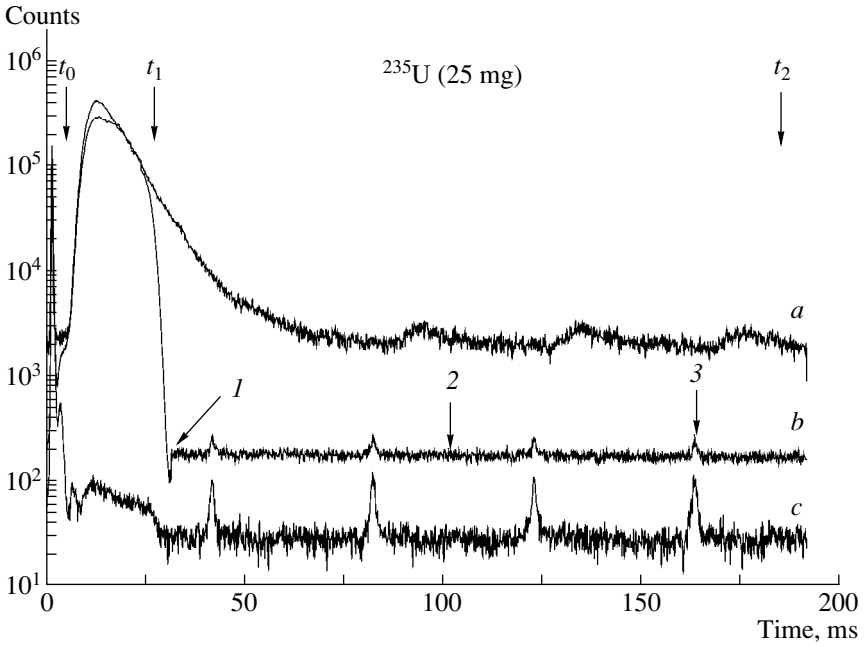

Fig. 2. The experimental time distributions of the detector counts measured with a ^{235}U sample: (*a*) without chopper, (*b*) with chopper, and (*c*) with a Cd filter in the beam. (*1*) Cutoff point of the reactor thermal-neutron-flux, (*2*) delayed neutrons measured for interval $[t_1, t_2]$, and (*3*) "satellites" of the main burst due to the specific design of the IBR-2 reactor.

ter was derived by using the recommended values of $\nu_d = 0.01653$ [5] and $\nu = 2.4320 \pm 0.0036$ [15]. The resulting ratios of the efficiencies were $\varepsilon_d/\varepsilon_p = 1.32 \pm 0.04$ and $\varepsilon_d/\varepsilon_p = 1.08 \pm 0.035$ for internal and external rings, respectively. These values were in good agreement with the calculations made by the Monte Carlo method, which were performed with the help of the MCNP code [16].

A typical spectrum measured with the ^{239}Pu sample (57 mg) is shown in Fig. 3.

The β_0 values were measured for the neutron-energy intervals having mean energies of 0.003 and 0.023 eV. These energy intervals were chosen by changing the phase of the neutron chopper. A Be filter was used to perform measurements with cold neutrons with a mean energy of about 0.003 eV (see Fig. 4). Several runs of about 10–15 h each were carried out for each isotope. The statistical errors were less than 0.5% for ^{235}U and ^{233}U and less than 1.0% for ^{239}Pu. The total error was calculated as a standard deviation from the weighted mean value obtained from all runs and the error in the reference.

The data for the main reactor isotopes are shown in Table 2.

We should stress that the final experimental error in β_0 includes both the experimental error itself and the error of the reference used. The main contribution to the final experimental error arises from the error of the reference used (~3%). The experimental error itself is much lower (~1.5%) and determined by the statistics of prompt neutrons and by their losses.

One can see from Table 2 that there is no energy dependence for the β_0 values in the studied energy region. Therefore, we calculated the mean values of β_0, and, using the known values of ν from [15], we obtained the values of ν_d, shown in Table 3.

In conclusion, the values of β_0 and ν_d for the isotopes presented are in agreement with previously measured data obtained with thermal neutrons and have an accuracy comparable with that of the recommended evaluated data [5, 17].

Measuring the β_0 value for thermal-neutron-induced fission of ^{237}Np is an extremely difficult task because

Table 2. The β_0 values (in %) for different energies of the initial neutrons and their ratios (in parentheses) to the reference β_0 [^{235}U(n_{th}, *f*)] for ^{235}U, ^{233}U, and ^{239}Pu

Isotope	$E_n = 0.003$ eV	$E_n = 0.023$ eV
^{235}U	0.683 ± 0.021 (1.004 ± 0.009)	0.680 ± 0.021 (1.000)
^{233}U	0.274 ± 0.009 (0.403 ± 0.006)	0.267 ± 0.009 (0.393 ± 0.006)
^{239}Pu	0.227 ± 0.011 (0.334 ± 0.013)	0.234 ± 0.008 (0.344 ± 0.004)

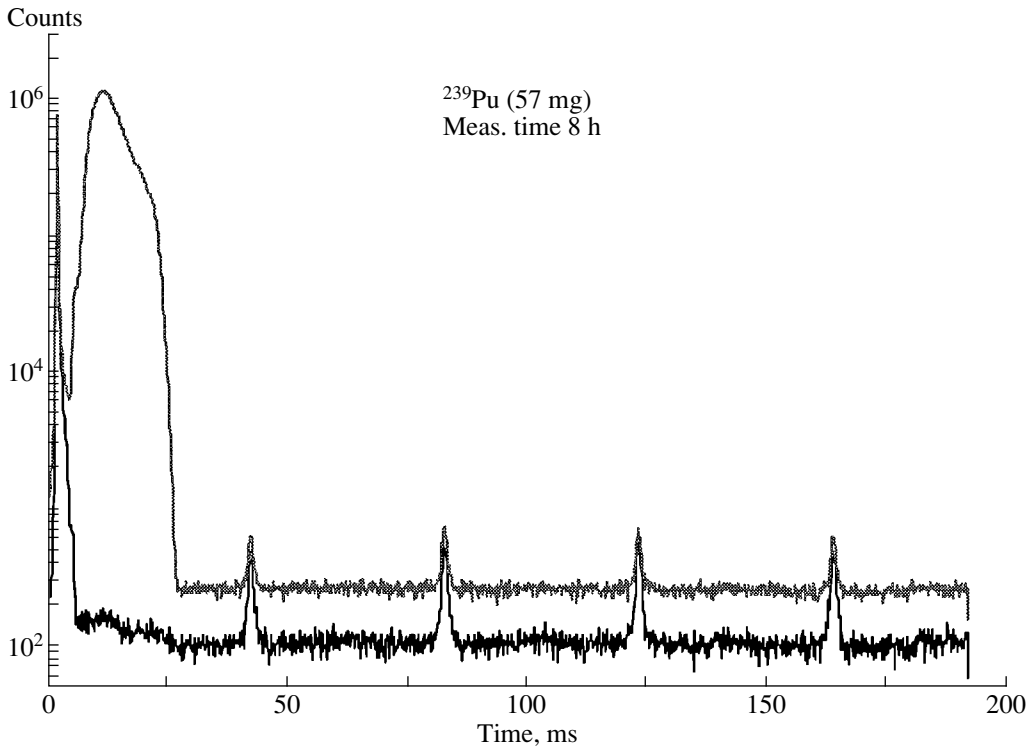

Fig. 3. The experimental time distributions measured for the ^{239}Pu sample with and without Cd filter.

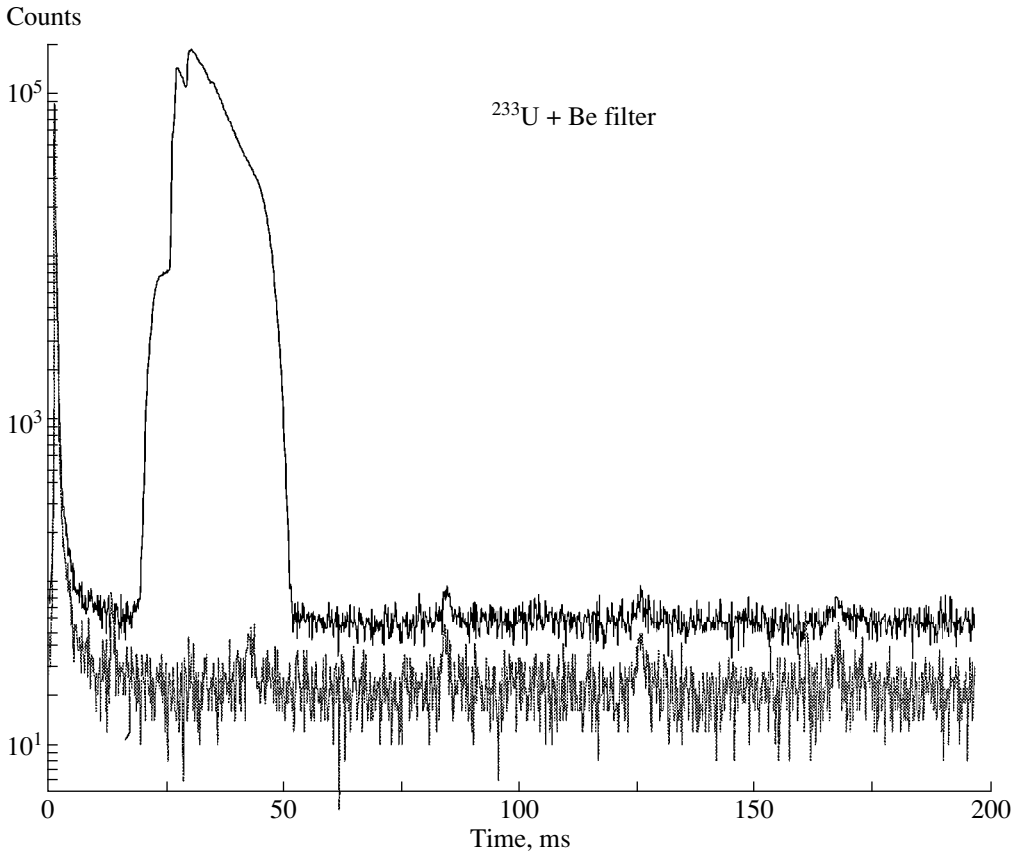

Fig. 4. The experimental time distributions measured for the ^{233}U sample and Be filter with and without Cd filter.

Table 3. Values obtained for β_0 and ν_d, along with the data from the literature

Isotope	β_0, %	ν	ν_d	
			our data	other data
^{233}U	0.270 ± 0.009	2.4946 ± 0.0040	0.006735 ± 0.00022	0.00667 ± 0.00029 [29]
^{239}Pu	0.232 ± 0.008	2.8799 ± 0.0090	0.00668 ± 0.00023	0.00653 ± 0.00026 [5]

Table 4. The values of ν_d for ^{237}Np

$\nu_d \times 10^2$	Reference	Comment	$\nu_d \times 10^2$	Reference	Comment
1.25 ± 0.11	This work	Thermal neutrons	1.26 ± 0.07	[25]	Fast neutrons (1.3 MeV)
1.14 ± 0.11	[19]	Thermal neutrons	1.14 ± 0.12	[6]	Calculation
1.29 ± 0.04	[22]	Fast neutrons (144 keV)	1.07 ± 0.10	[27]	Fast neutrons
1.18 ± 0.13	[23]	Fast neutrons	1.00–1.14	[26]	0.4–1.2 MeV
1.22 ± 0.03	[24]	Fast neutrons			

^{237}Np has a very small fission cross section (21.5 mb [18]) and a relatively large neutron background due to the (α, n) reaction. Up to now, only two attempts to measure the value of ν_d for the thermal-neutron-induced fission of ^{237}Np are known: our preliminary result [14] and a measurement made by a similar method, but with another acquisition system [19].

Because the thermal-neutron-fission cross section for ^{237}Np is 3×10^4 times smaller than that for ^{235}U and that for ^{239}Pu, determination of the possible admixture is a very important task. Therefore, the ^{237}Np sample was chemically purified from ^{235}U and ^{239}Pu contamination to reduce their concentrations to a value less than 10^{-6} g/g. The concentration of ^{239}Pu was measured by the method of α spectroscopy, which gave the limit of 10^{-6} g/g. Unfortunately, the methods of α and γ spectroscopy do not allow the concentration of ^{235}U to be determined with good sensitivity. To solve this prob-

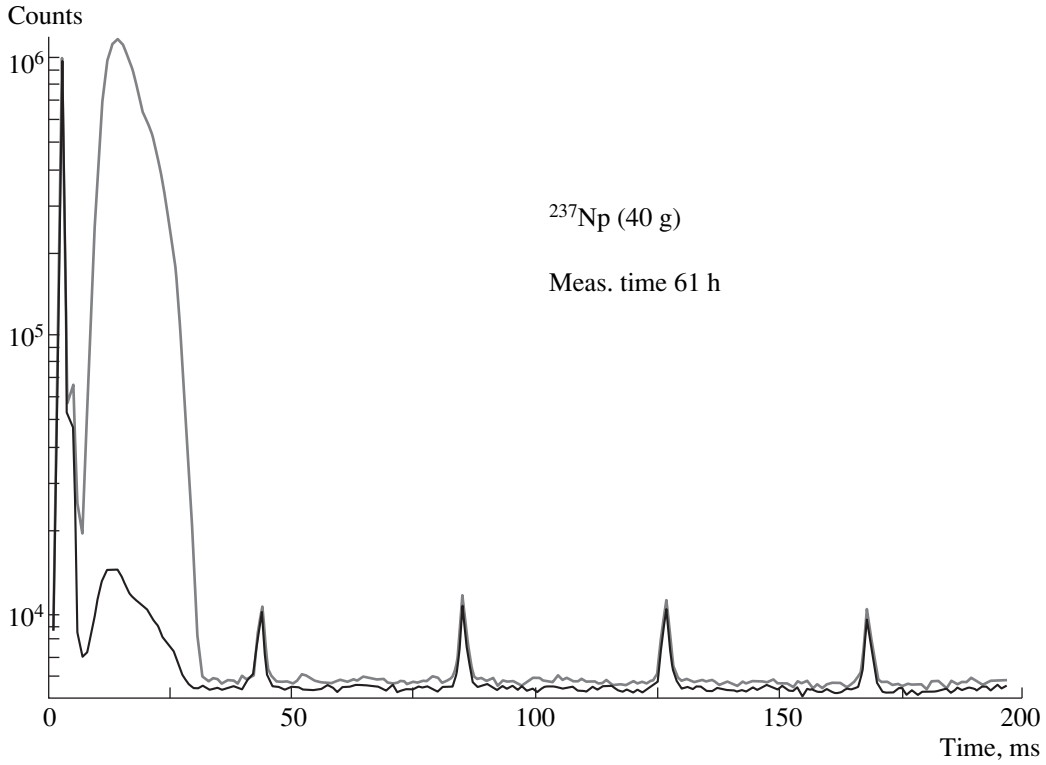

Fig. 5. The experimental spectrum for ^{237}Np. The channel width is equal to 1.024 ms (see the caption under Fig. 3).

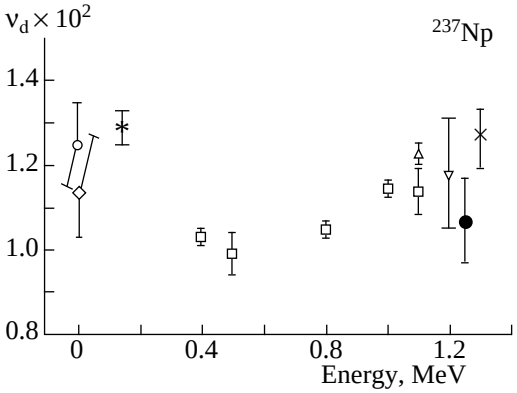

Fig. 6. ν_d for ^{237}Np as a function of neutron energy: (◇) [19], (∗) [22], (▽) [23], (△) [24], (×) [25], (□) [26], (●) [27], and (○) this work.

lem, the method of neutron resonance spectroscopy was used. For this purpose, an ionization chamber with the same purity ^{237}Np (weight 88 mg) was made. The measurements were carried out at the 16-m flight base of the IBR-30 booster, with a pulse width of 4 μs [20]. The results showed no indications of the strongest resonances of ^{235}U in the measured spectra. The conclusion that the concentration of ^{235}U was less than 10^{-5} g/g was made from these data.

The measured time spectrum of the DN for ^{237}Np is shown in Fig. 5. One should note that, despite the large mass of the sample, the number of DN counts was only about 5–6% relative to the background. Any further increase in the sample mass was useless and was limited by the flux attenuation due to the large radiative-capture cross section for thermal neutrons in the sample. As the result of ten runs of measurements (5–12 h each), we obtained

$$\beta_0 = (0.506 \pm 0.030)\%.$$

Taking into account the known value of $\nu = 2.47 \pm 0.14$ [21], one can obtain the value of ν_d, which is shown in Table 4 and in Fig. 6, along with the measured [19, 22–27] data for thermal- and fast-neutron-induced fission.

In conclusion, it is worth noting that the values of ν_d for the thermal-neutron-induced fission of ^{237}Np are in reasonable agreement with published data obtained for fast neutrons [22–27]. Some evidence for an energy dependence of ν_d as shown in Fig. 6 have to be confirmed by following more precise measurements.

4.2. Decay-Curve Measurements

The time dependence of the DN counting rate after irradiation with thermal neutrons (decay curve) was measured for ^{235}U (7 g) and ^{239}Pu (20 g) in time intervals up to 350 ms. The results are shown in Figs. 7 and 8 for ^{235}U and ^{239}Pu, respectively. In this case, the background was less than 0.2%. Each experimental point in Figs. 7 and 8 represents a time interval of 1.024 ms and has statistical errors less than 0.3% for ^{235}U and 0.2% for ^{239}Pu.

It is interesting to check the consistency between the time dependence of the DN yield measured by our Iso-

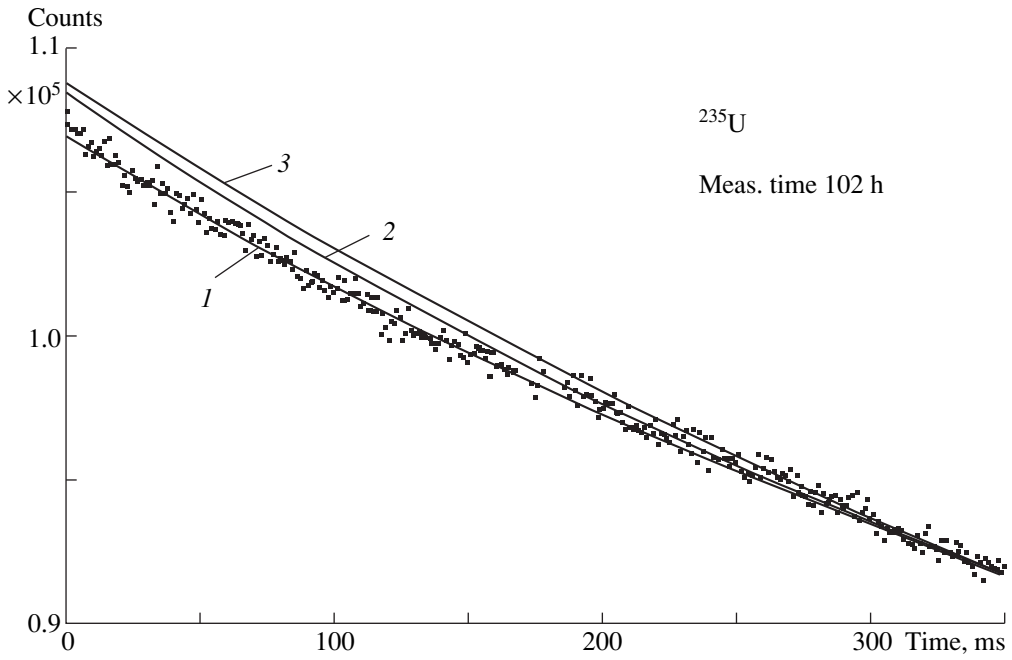

Fig. 7. The experimental time dependence of DN for ^{235}U and the decay curves calculated on the basis of different six-group approximations: (*1*) Keepin–Tuttle [1, 2], (*2*) Waldo *et al.* [27], and (*3*) Mills *et al.* [28].

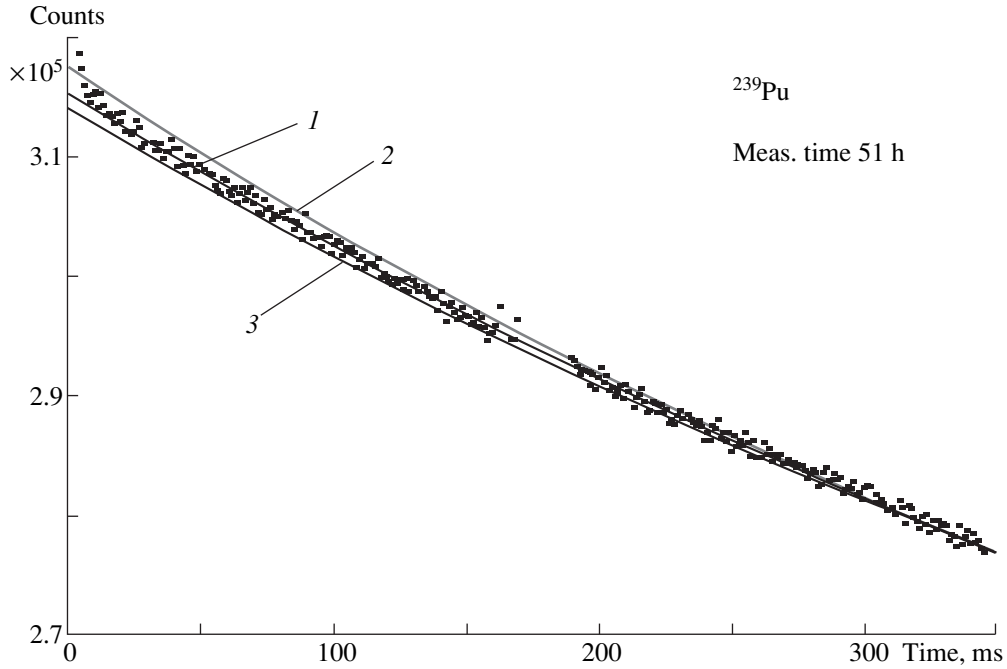

Fig. 8. A DN decay curve for ^{239}Pu and the calculated ones using the six-group set of DN constants: (*1*) Keepin–Tuttle [1, 29], (*2*) Wahl [7], and (*3*) Waldo *et al*. [27].

mer facility and the decay curves calculated by equation (1) within different six-group approximations [1, 2, 7, 27–29]. The calculated curves were normalized to the experimental data at the 350-ms time point.

One can see from these figures that the best agreement between the measured data and the calculated curves is achieved with the Keepin–Tuttle parameter set.

To check the existence of the DN groups with shorter periods, a fit of the ^{235}U data was made with the Keepin–Tuttle parameter set by adding a seventh group with $T_{1/2,7}$ = 50 ms. The conclusion should be drawn that the seventh group is absent at a level of $a_7 < 5.2 \times 10^{-3}$ (with a probability of 95%). A more detailed analysis of the decay curves will be made in a separate paper.

ACKNOWLEDGMENTS

We wish to thank Drs. Yu.V. Grigoriev, V.B. Pavlovich, G.V. Buklanov, S.M. Soloviev, and V.N. Konev for providing fissile samples for these measurements and S.S. Pavlov and V.Yu. Konovalov for their help with the measurements.

This work was supported by the ISTC (project no. 471), the Russian Foundation for Basic Research (project no. 95-02-03740), and the CEA-JINR Agreement.

REFERENCES

1. G. R. Keepin, *Physics of Nuclear Kinetics* (Addison-Wesley, Reading, 1965).
2. R. J. Tuttle, Nucl. Sci. Eng. **56**, 37 (1975).
3. V. M. Sluchevskaya and I. P. Matveenko, in *Probl. At. Sci. and Tech. Nucl. Data* (Moscow, 1980), Part 3 (38), p. 29.
4. A. Filip and A. D'Angelo, in *Nuclear Data for Science and Technology, Jülich, 1991* (Springer-Verlag, Berlin, 1992), p. 946.
5. J. Blachot *et al.*, OECD-NEA, NEASRP-L-323 (1990).
6. M. C. Brady and T. R. England, Nucl. Sci. Eng. **103**, 129 (1989).
7. A. C. Wahl, At. Data Nucl. Data Tables **39**, 1 (1988).
8. G. Rudstam, Nucl. Sci. Eng. **80**, 238 (1982).
9. P. W. Lisowski *et al.*, in *Nuclear Data for Science and Technology, Jülich, 1991* (Springer-Verlag, Berlin, 1992), p. 92.
10. E. Dermendjiev, V. M. Nazarov, S. S. Pavlov, *et al.*, Preprint No. E3-93-6, JINR (Dubna, 1993).
11. S. B. Borzakov, E. Dermendjiev, Yu. S. Zamyatnin, *et al.*, At. Energ. **79**, 231 (1995).
12. S. B. Borzakov, E. Dermendjiev, Yu. S. Zamyatnin, *et al.*, Preprint No. R3-94-447, JINR (Dubna, 1994).
13. V. D. Ananiev *et al.*, At. Energ. **57**, 227 (1984).
14. S. B. Borzakov *et al.*, in *Nuclear Data for Science and Technology, Trieste, 1997* (Bologna, 1997), Vol. 1, p. 497.
15. H. Tellier, in *Nuclear Data Standards for Nuclear Measurements* (NEA OECD, 1992), p. 90.
16. *MCNP—A General Monte Carlo N Particle Transport Code*, Version 4A, Ed. by J. F. Briesmeister, Los Alamos Lab. Report LA-12625 (1993).
17. J. F. Conant and P. F. Palmedo, Nucl. Sci. Eng. **44**, 173 (1971).

18. S. F. Mughabghab *et al.*, *Neutron Cross Sections* (Academic, New York, 1984), Vol. 1, Part B.
19. Sh. S. Zeinalov *et al.*, Preprint No. R3-98-17, JINR (Dubna, 1998).
20. I. M. Frank, Sov. J. Part. Nucl. **2**, 807 (1972).
21. A. Thierens *et al.*, Nucl. Phys. A **342**, 229 (1980).
22. H. H. Saleh, T. A. Parish, and N. Shinohara, Nucl. Sci. Eng. **125**, 51 (1997).
23. A. N. Gudkov *et al.*, At. Energ. **66**, 100 (1989).
24. G. Benedetti *et al.*, Nucl. Sci. Eng. **80**, 379 (1982).
25. A. A. Malinkin *et al.*, *Probl. At. Sci. and Tech. Phys. Nucl. Reactors* (1992), Part 3, p. 37.
26. V. M. Piksaĭkin *et al.*, *XIV Workshop on Nuclear Fission, Obninsk, 1998.*
27. R. W. Waldo *et al.*, Phys. Rev. C **23**, 1113 (1981).
28. R. W. Mills *et al.*, in *Nuclear Data for Science and Technology, Jülich, 1991* (Springer-Verlag, Berlin, 1992), p. 86.
29. R. J. Tuttle, *IAEA Report*, INDC(NDS)-107/G + Special, 1979, p. 29.

Physics of Atomic Nuclei, Vol. 63, No. 4, 2000, pp. 539–544. Translated from Yadernaya Fizika, Vol. 63, No. 4, 2000, pp. 598–604.

IN MEMORIAM OF F. L. SHAPIRO

Investigation of Parity Violation and Interference Effects in the Angular Distributions of Fragments Originating from ^{233}U Fission Induced by Resonance Neutrons

V. P. Alfimenkov, A. N. Chernikov, A. M. Gagarski[1)], S. P. Golosovskaya[1)], I. S. Guseva[1)], I. S. Krasnoshchekova[1)], L. Lason[2)], Yu. D. Mareev, V. V. Novitsky, G. A. Petrov[1)], V. I. Petrova[1)], A. K. Petukhov[1)], L. B. Pikelner, Yu. S. Pleva[1)], V. E. Sokolov[1)], M. I. Tsulaia[3)], and V. M. Tsulaia[3)]

Joint Institute for Nuclear Research, Dubna, Moscow oblast, 141980 Russia

Received August 9, 1999

Abstract—Three interference asymmetry effects in the angular distributions of fragments originating from ^{233}U fission induced by resonance neutrons were measured. The energy dependences of the asymmetry factors being studied show sizable irregularities that are associated, according to modern theory, with the interference of *s* and *p* resonances at the stage of a compound nucleus. The basic features of weak *p*-wave resonances in the low-energy region were obtained from a global theoretical analysis of the asymmetry factors as functions of energy. The first estimates of nuclear matrix elements of weak interaction were derived for a few *p*-wave resonances. © *2000 MAIK "Nauka/Interperiodica".*

1. INTRODUCTION

The present study reports on experiments that have been performed to continue implementing a vast program of investigations into the asymmetry of the emission of fragments originating from the interactions of neutrons with fissile nuclei [1–7]. In experiments with ^{233}U nuclei, we have studied parity-nonconserving (PNC) and parity-conserving (PC) left–right (LR) and forward–backward (FB) effects. The objective of this investigation was to compare experimental data with the existing theoretical results and to estimate some parameters of low-lying *p*-wave resonances, including the matrix elements of weak interaction mixing states of opposite parities.

In slow-neutron-induced fission, angular correlations can be represented as

$$W(\mathbf{p}_f) = 1 + \alpha_{nf}(\boldsymbol{\sigma}_n \cdot \mathbf{p}_f) + \alpha_{nf}^{\mathrm{LR}}(\mathbf{p}_f \cdot [\boldsymbol{\sigma}_n \times \mathbf{p}_n]) + \alpha_{nf}^{\mathrm{FB}}(\mathbf{p}_f \cdot \mathbf{p}_n), \quad (1)$$

where $\mathbf{p}_f$ and $\mathbf{p}_n$ are unit vectors in the directions of, respectively, the light-fragment momentum and the momentum of neutrons that induced fission; $\boldsymbol{\sigma}_n$ is a unit pseudovector aligned with the neutron polarization; and α_{nf}, $\alpha_{nf}^{\mathrm{LR}}$, and $\alpha_{nf}^{\mathrm{FB}}$ are the asymmetry factors for the PNC, LR, and FB effects, respectively.

According to the existing theories [8, 9], the effects being considered are associated with the resonance structure of the neutron cross section; they are due to the mixing of compound states of opposite parities. As is shown below, all the coefficients α are similar and depend on the same resonance parameters. There are, however, two exceptions. First, this is not so for the dependence of α_{nf} on the matrix element of weak interaction. Second, the mixing of levels for this effect occurs only at equal spins of *s*- and *p*-wave resonances. For even effects, there is no this restriction.

For the general case of mixing of several *s*- and *p*-wave resonances, Sushkov and Flambaum [8] showed that the angular distribution of fission fragments is given by

$$W_{\mathrm{PC}}(\mathbf{p}_f) \sim \sum_{ss'}(2J_s + 1)U_s U_{s'}^* \delta_{J_s J_{s'}} + \sum_{spj} Q(J_s J_p j K I) \times \mathrm{Re}\left\{U_s U_{pj}^*((\mathbf{p}_f \cdot \mathbf{p}_n) - i\beta_j(\mathbf{p}_f \cdot [\boldsymbol{\sigma}_n \times \mathbf{p}_n]))\right\}, \quad (2)$$

[1)] Petersburg Nuclear Physics Institute, Russian Academy of Sciences, Gatchina, 188350 Russia.
[2)] University of Lodz, Lodz, Poland.
[3)] Institute of Physics, Georgian Academy of Sciences, ul. Tamarashvili 6, GE-380077 Tbilisi, Republic of Georgia.

where

$$U_s = \frac{\pm\sqrt{\Gamma_s^n(J_s)}F_s}{E - E_s + i\Gamma_s/2}, \quad U_{pj} = \frac{\pm i\sqrt{\Gamma_p^n(J_p, j)}F_p}{E - E_p + i\Gamma_p/2}; \quad (3)$$

$$W_{\mathrm{PNC}}(\mathbf{p}_f) \sim \sum_{ss'}(2J_s + 1)U_s U_{s'}^* \delta_{J_s J_{s'}} + \sum_{ss'p} Q\left(J_p J_{s'} \frac{1}{2} KI\right)\mathrm{Re}\, U_{sp} U_{s'}^* (\boldsymbol{\sigma}_n \cdot \mathbf{p}_f) \quad (4)$$

with

$$U_{sp} = \frac{\sqrt{\Gamma_s^n(J_s)}\langle p|H_W|s\rangle F_p}{(E - E_s + i\Gamma_s/2)(E - E_p + i\Gamma_p/2)}. \quad (5)$$

In the above expressions, E is the neutron energy, E_s (E_p) is the energy of the s-wave (p-wave) resonance; Γ_s^n and Γ_s^f (Γ_p^n and Γ_p^f) are, respectively, the neutron and the fission width of the s-wave (p-wave) resonance; j is the total angular momentum of the neutron; J_s, $J_{s'}$ and J_p are the spins of the s- and p-wave compound states; K is the projection of the spin J onto the symmetry axis of a fissile nucleus; $F_s = \sqrt{\Gamma_s^f}\, e^{i\phi_s^f}$ and $F_p = \sqrt{\Gamma_p^f} e^{i\phi_p^f}$ are the fission amplitudes featuring phase factors; $\langle p|H_W|s\rangle$ is the matrix element featuring weak interaction; and

$$\beta = \begin{cases} 1, & \text{at } j = 1/2 \\ -1/2, & \text{at } j = 3/2. \end{cases}$$

The factors $Q(J_s J_p jKI)$ in (2) and (4) depend only on the angular momenta. For PC interference effects, we have

$$Q(J_s J_p jKI) = 2\sqrt{3}(2J_s + 1)(2J_p + 1)\sqrt{2j + 1} \times (-1)^{1 + j - I - K} \begin{Bmatrix} 1/2 & 1 & j \\ J_p & I & J_s \end{Bmatrix} \begin{pmatrix} J_s & J_p & 1 \\ K & -K & 0 \end{pmatrix}. \quad (6)$$

Expression (6) holds for the PNC effect as well, but we must bear in mind the constraint $j = 1/2$.

Considering that the main contribution to the fission cross section $\sigma_f(E)$ comes from s-wave resonances and using equations (2) and (4), we can show that, over a segment of width ΔE, the asymmetry factors can be represented as

$$\alpha_{nf}^{\mathrm{FB}}(E) = \frac{1}{\Delta E \sigma_f(E)} \times \int_{E - \Delta E/2}^{E + \Delta E/2} \left[\sum_{spj} Q(J_s J_p jKI)\mathrm{Re}(U_s U_{pj}^*)\right] dE', \quad (7)$$

$$\alpha_{nf}^{\mathrm{LR}}(E) = \frac{1}{\Delta E \sigma_f(E)} \times \int_{E - \Delta E/2}^{E + \Delta E/2} \left[\sum_{spj} Q(J_s J_p jKI)\mathrm{Im}(\beta U_s U_{pj}^*)\right] dE', \quad (8)$$

$$\alpha_{nf}(E) = \frac{1}{\Delta E \sigma_f(E)} \times \int_{E - \Delta E/2}^{E + \Delta E/2} \left[\sum_{ss'p} Q\left(J_p J_{s'} \frac{1}{2} KI\right)\mathrm{Re}(U_{sp} U_{s'}^*)\right] dE'. \quad (9)$$

The asymmetry factors are much greater in the region of p-wave resonances than in the region of s-wave resonances. This is because the values of the fission cross section $\sigma_f(E)$ are different at these resonances.

A global analysis of all three effects considered above, which was performed over a wide integral of neutron energies, yielded new information about the parameters of p-wave resonances and about the matrix element of weak interaction. It should be noted that, by measuring various cross sections, it is hardly possible to detect directly p-wave resonances in nuclei like ^{233}U and ^{235}U. This is because, in relation to the neutron width of an s-wave resonance, the neutron width of a p-wave resonance involves the suppression factor $(kR)^2$, where k is the neutron wave number, while R is the radius of the nucleus being considered. In the region around a few keV, this factor is about 10^{-5}. It is clear that, in the $^{233, 235}$U nuclei, which are characterized by a very high level density, it is hardly possible to detect such weak resonances.

2. EXPERIMENTAL EQUIPMENT AND MEASUREMENTS

The present study is devoted to a measurement and a global theoretical analysis of the energy dependences of PNC and PC asymmetry effects in ^{233}U fission induced by resonance neutrons. Similar investigations of our group for ^{235}U were reported previously in [5–7].

By using unpolarized-neutron beams from the IBR-30 reactor (Dubna) [10], the effect of forward–backward asymmetry for ^{233}U was measured in [2–4] in the neutron-energy range from thermal energies to 70 eV. In order to detect fission fragments and to separate them into light and heavy ones, we evolved a 16-section fast ionization chamber [5, 11].

The first measurements of PNC and PC (LR) effects were performed in a polarized-neutron beam from the WWR-M reactor at Gatchina. A crystal monochromator was used there as a medium where the beam neutrons were polarized, on one hand, and where they deposited energy, on the other hand; it enabled an investigation of only a narrow neutron-energy region below 2 eV [1, 3, 4]. In the present study, we performed

measurements in a beam of polarized resonance neutrons from the IBR-30 reactor (POLYANA facility) [12]. A new fast fission chamber that was divided into 40 sections and which made it possible to detect both LR and PNC effects was developed for these measurements [5]. The total weight of the ^{233}U isotope in the chamber was about 2 g.

A beam of polarized neutrons, with the degree of polarization being 60%, was obtained by passing the neutrons through a polarized proton target. A collimator of area 70×70 cm^2 was positioned in front of the inlet of the chamber. Targets containing ^{233}U layers were arranged in such a way that their planes were parallel to the neutron-beam direction, coinciding with the plane spanned by the neutron momentum and the direction of vertical neutron polarization. The emission of a fixed-mass fragment to the left or to the right of this plane made it possible to measure the corresponding LR effect. In the order to measure the PNC effect, we rotated the chamber through a right angle about the beam direction in such a way that the target planes were orthogonal to the direction of neutron polarization; after that, we measured the fragment yields in this direction and in the direction opposite to it.

By spectroscopically measuring the kinetic energies of fragments, we were able to break down the set of fragments into two groups comprising light and heavy fragments. The direction of neutron polarization could be reversed by means of an adiabatic flipper.

The main objective of our experiment was to determine the asymmetry factor. For light fragments, it was defined as

$$\alpha = \frac{N_L^+ - N_L^-}{N_L^+ + N_L^-}, \qquad (10)$$

where N_L^+ and N_L^- are the normalized numbers of light-fragment counts for two directions of the polarization. The asymmetry factor for heavy fragments was defined in a similar way.

In our experimental results, we introduced corrections for the chamber length (of about 80 cm), for a background accompanying the measurements, for overlaps of light and heavy fragments in the spectrum because of a poor resolution, for a large solid angle (about 2π) of fragment emission, and for the degree of neutron polarization. The absence of spurious instrumental effects was checked by performing additional measurements in a beam of unpolarized neutrons.

3. BASIC EXPERIMENTAL RESULTS

The results obtained in our experiment by measuring asymmetry effects are displayed in Fig. 1. The factors $\alpha_{nf}^{\mathrm{FB}}$, $\alpha_{nf}^{\mathrm{LR}}$, and α_{nf} are presented over a wide range of neutron energies from 20 meV to 70 eV. We can see that the energy dependence of these factors is quite

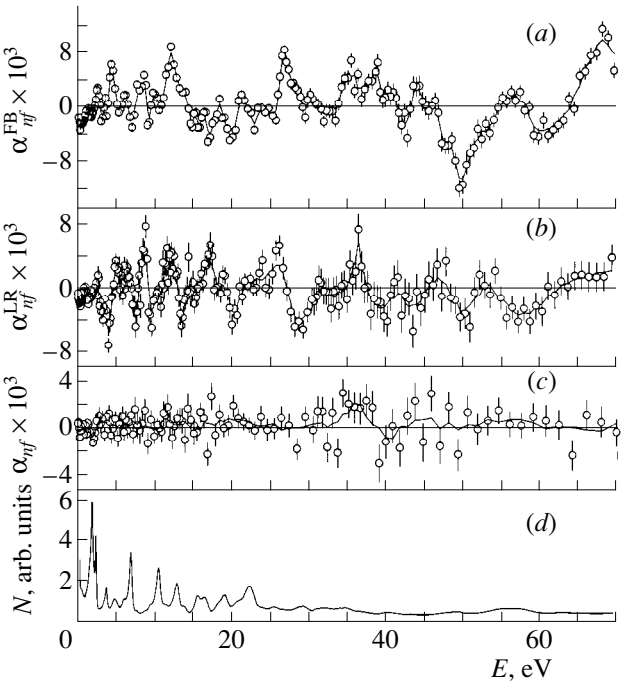

Fig. 1. Asymmetries of fragment emission from neutron-induced fission of ^{233}U versus the neutron energy in the range 0.02–70 eV: (*a*) PC FB interference effect, (*b*) PC LR interference effect, (*c*) PNC interference effect, and (*d*) experimental spectrum of ^{233}U fission. The curves in Figs. 1*a*–1*c* represent theoretical fits.

complicated, as might have been expected on the basis of the theoretical predictions from [8, 9]. The maximal magnitude of PC effects amounts to 1%, while that for PNC effects is a few times less. Therefore, the statistical accuracy is insufficient, in the latter case, for determining weak-interaction matrix elements for many resonances.

Figure 1*d* shows the experimental spectrum of ^{233}U fission versus the energy of the neutrons that caused fission. All resonances visible in the figure are *s*-wave ones—the *p*-wave resonances do not show up in the spectrum, as was indicated above. As the energy of the neutrons is increased, the energy resolution becomes poorer; in view of this, it is not reasonable to analyze asymmetries at energies above 15–20 eV. It should be noted that, sometimes, the energy widths of the observed irregularities exceed considerably the total resonance widths [13]. In all probability, this is due to the overlap of the neighboring sections of the spectrum in the case of a poor resolution.

4. THEORETICAL ANALYSIS OF THE DATA AND DISCUSSION OF THE RESULTS

A theoretical analysis of our data was performed for all three interference effects in ^{233}U fission at neutron energies from 20 meV to 15 eV (see Figs. 2, 3), where the energy resolution was still satisfactory.

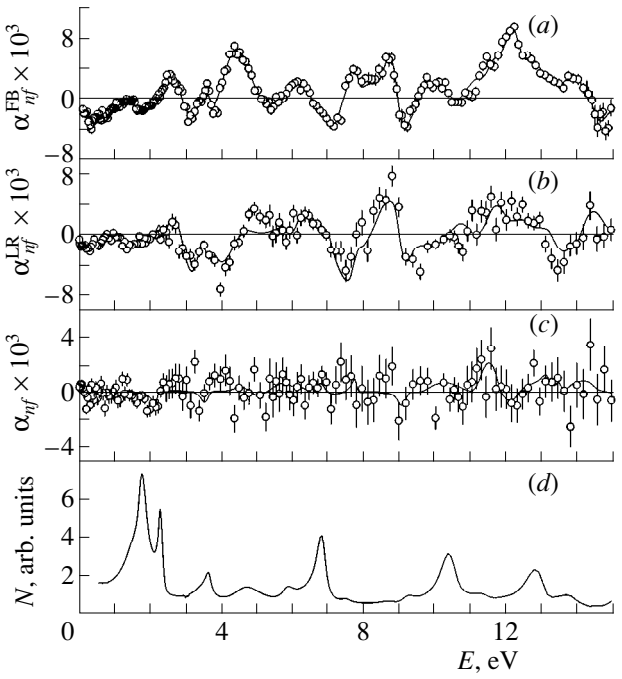

Fig. 2. As in Fig. 1, but for neutron-energy range 0.02–15 eV.

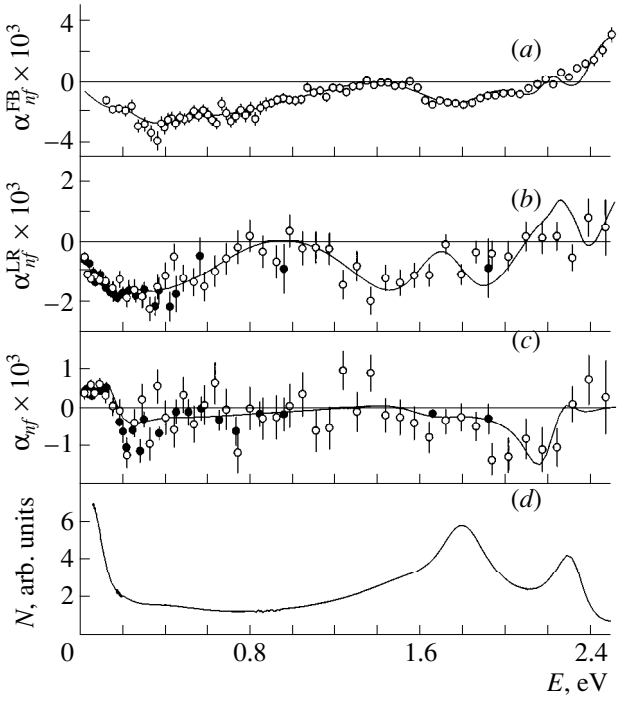

Fig. 3. As in Fig. 1, but for low neutron energies between 0.02 and 2.5 eV: (open circles) results of the present study (IBR-30) and (closed circles) results borrowed from [1, 3, 4] (WWR-M).

The main objective of this analysis was to verify whether it is possible describe experimental data in terms of expressions (7) and (8), which represent PC effects and which involve many levels, and to estimate the *p*-wave-resonance parameters, which were then used to extract the matrix elements of weak interaction from the relevant data.

As a first step in determining the parameters of the *p*-wave resonances from the energy dependences of the LR and FB effects, the theoretical values of the asymmetry factors were fitted to the corresponding experimental values by varying the parameters of the *p*-wave resonances, the known parameters of the *s*-wave resonances [13] and the above expressions being taken into account in doing this. In the range 0.02–15 eV, we included 30 *s*-wave resonances in our calculation. The parameters of the *p*-wave resonances were fitted within specific energy intervals of width ΔE. In doing this, we varied the following parameters of the *p*-wave resonances: the resonance energy E_p, the partial neutron widths $\Gamma^n_{p,1/2}$ and $\Gamma^n_{p,3/2}$ ($\Gamma^n_{p,1/2} + \Gamma^n_{p,3/2} = \Gamma^n_p$), the fission width Γ^f_p, and the phase factor $\Delta\phi^f_{sp} = \phi^f_p - \phi^f_s$. The radiative width was fixed at $\Gamma^\gamma_p = 40$ meV, while the total width was taken to be $\Gamma_p = \Gamma^\gamma_p + \Gamma^f_p$. It was also assumed that a given section of the spectrum features only one or two *p*-wave resonances, whose spins are 2 or 3. In the case of an unsatisfactory fit, we tried the spins of 1 and 4.

The parameters were obtained by using the least squares method as implemented on the basis of the FUMILI code. The results for 18 *p*-wave resonances are listed in the table.

As a next step in data processing, we fitted the PNC effect. In order to do this, the experimental dependence of the asymmetry factor α_{nf} was described in terms of the known parameters of the *s*-wave resonances and the parameters found for the *p*-wave resonances. Here, we considered that only those *s*-wave and *p*-wave resonances that have identical spins contribute to the effect being considered [8]. Apart from the fixed parameters of the *s*- and *p*-wave resonances, the expression for α_{nf} features only one free parameter, the weak-interaction matrix element, which is determined by the least squares method. Figure 2 displays the fitted curves that were obtained as the result of a global analysis of the FB and LR effects (Figs. 2*a*, 2*b*) and of the PNC effect (Fig. 2*c*) over the neutron-energy interval from 20 meV to 15 eV. It can be seen that the resulting curves describe the experimental points fairly well.

Figure 3 singles out the low-energy section between 20 meV and 2.5 eV, where the experimental data are much more precise and much more comprehensive than in the region of high energies. Figure 3 also displays the results obtained previously by measuring the LR and PNC asymmetries in the experiment that employed thermal neutrons from the WWR-M reactor at Gatchina and a polarizing crystal-diffraction monochromator. We can see that the experimental data obtained by the different methods are consistent and

Parameters of the *p*-wave resonances as obtained in describing the LR and FB effects (Γ_p^{nl} is the reduced width; the rest of the notation is explained in the main body of the text)

	E_p, eV	J_p	Γ_p^{nl}, meV	Γ_p^f, meV	$\Gamma_{p,1/2}^n/\Gamma_p^n$	$\Delta\phi_{sp}^f$, rad
1	0.19 ± 0.02	3	≤0.1	90 ± 20	0.50 ± 0.05	1.6 ± 0.1
2	0.34 ± 0.07	3	5.1 ± 0.3	1700 ± 100	0.99 ± 0.01	2.75 ± 0.05
3	0.41 ± 0.04	4	6.5 ± 1.5	330 ± 80	0.00	1.05 ± 0.30
4	1.52 ± 0.03	2	1.35 ± 0.15	500 ± 30	0.99 ± 0.01	−0.25 ± 0.15
5	1.95 ± 0.04	2	≤0.1	350 ± 50	0.90 ± 0.05	3.1 ± 0.2
6	3.01 ± 0.03	3	3.2 ± 0.3	870 ± 40	0.68 ± 0.03	1.3 ± 0.1
7	3.53 ± 0.02	3	0.6 ± 0.10	250 ± 30	0.85 ± 0.02	0.15 ± 0.15
8	4.58 ± 0.04	(3)	0.55 ± 0.05	860 ± 60	0.01 ± 0.01	–1.30 ± 0.15
9	4.85 ± 0.05	2	≤0.1	760 ± 90	0.99 ± 0.01	1.5 ± 0.2
10	6.62 ± 0.04	(3)	7.8 ± 1.3	1700 ± 100	0.05 ± 0.03	–2.3 ± 0.15
11	6.71 ± 0.04	3	6.8 ± 1.3	1050 ± 50	0.15 ± 0.03	1.0 ± 0.2
12	7.77 ± 0.05	(3)	0.3 ± 0.1	1150 ± 100	0.02 ± 0.02	0.25 ± 0.4
13	9.08 ± 0.03	3	0.75 ± 0.10	370 ± 40	0.47 ± 0.04	1.25 ± 0.10
14	9.79 ± 0.14	3	0.7 ± 0.1	2500 ± 100	0.96 ± 0.03	0.00 ± 0.05
15	11.73 ± 0.04	(3)	0.3 ± 0.07	430 ± 130	0.02 ± 0.02	0.0 ± 0.03
16	12.30 ± 0.03	2	1.2 ± 0.1	500 ± 50	0.13 ± 0.05	0.45 ± 0.10
17	13.14 ± 0.01	3	0.8 ± 0.3	280 ± 150	0.98 ± 0.02	1.9 ± 0.3
18	14.34 ± 0.07	(3)	0.15 ± 0.05	400 ± 150	0.11 ± 0.11	0.65 ± 0.25

that they are reproduced satisfactorily by the results of our theoretical analysis. A significant PNC effect is observed only at energies of about 0.2 and 2.0 eV. Unfortunately, the statistical accuracy achieved in the present experiment is insufficient for describing this small effect in greater detail.

The *p*-wave-resonance parameters that are listed in the table were deduced as the result of applying our fitting procedure, which involved some assumptions. Therefore, the quoted errors reflect the quality of the fit under the condition that the number of the *p*-wave resonances within a given segment and some other hypotheses were chosen correctly. These errors do not include uncertainties that are associated with changes in the hypotheses and which appear to be systematic errors.

Systematic errors stem, in particular, from the absence of some data on the *s*-wave resonances. Information about the spins of these resonances in ^{233}U is scanty, and there are no data on the projections of their angular momenta on the fission axis (*K* values). In view of this, we always set $K = 1$ in implementing our fitting procedure, because this is the most probable value at $J = 2$ or 3. Among the *s*-wave-resonance parameters that are determined from fitting, the energies of the *s*-wave resonances and their total widths are the most stable ones, because these are directly related to the positions and widths of the structures observed in the energy dependences of the asymmetry factors.

The parameter $\Delta\phi_{sp}^f$, whose values are quoted in the table, represents the phase difference between the fission amplitudes for the case where the *s*- and the *p*-wave resonances are mixed. However, we cannot assign rigorous meaning to it in the representation being considered. It is retained in the expressions for fission amplitudes, but the opinions as to whether the phase in question is a real physical parameter that can change differ. In our calculations, it is rather a normalization factor that can be used as an adjustable parameter.

In fitting the reduced neutron widths of *p*-wave resonances, we considered that they involve two components corresponding to two values of the neutron angular momentum, $\Gamma_{p,1/2}^n$ and $\Gamma_{p,3/2}^n$. Their sum is equal to the total neutron width Γ_p^n. The table quotes the values of the reduced neutron widths Γ_p^{nl} and of the ratio $\Gamma_{p,1/2}^n/\Gamma_p^n$. For three resonances, we present only an upper bound on Γ_p^{nl}, while the corresponding ratios lie in a broad interval between zero and unity. For the resonance-spin value of $J_p = 1$ or 4 ($J_p = I \pm 3/2$), we have only one component, $\Gamma_p^n = \Gamma_{p,3/2}^n$. In view of this, the fitting was initially performed with the J_p values of 2 or 3; in those cases where the above ratio proved to be close to zero, the spin value of 1 or 4 was probable. Despite this, the parenthetical value of (3) was left in

the table, because a better value of χ^2 was obtained in fitting with a spin of 3 than in fitting with a spin of 1 or 4.

The matrix elements $\langle p|H_W|s\rangle$ from a fit to the PNC-asymmetry factor could be estimated only for energies below 2 eV, where the statistical accuracy of the measured PNC-asymmetry factors was sufficiently high. Presented immediately below are the results for the above matrix element:

E_p, eV	0.19	0.34	1.95
$\langle p\|H_W\|s\rangle$, meV	0.15	0.05	–1.0

The errors in determining the matrix elements amount to some 30%. For other *p*-wave resonances, we were able to estimate only an upper limit. The result is $|\langle p|H_W|s\rangle| \le 10^{-3}$ eV. This is because the statistical accuracy becomes much poorer as we go over to *p*-wave resonances at higher energies.

5. CONCLUSION

A global analysis of PC asymmetry effects in fission (that is, FB and LR effects) and of the PNC effect furnishes information about *p*-wave resonances and about the character of the angular distributions of diverging light and heavy fragments and makes it possible to compare experimental data with theoretical predictions. In this context, it is important to perform relevant measurements over a sufficiently broad energy interval containing at least 15–20 resonances, in which case it is possible to reveal the character of fluctuations and to estimate relevant mean values. In the present study, we have performed such a comprehensive experiment with the ^{233}U isotope. Previously, we conducted similar measurements with ^{235}U [7].

A measurement of the angular distributions of fragments emitted from aligned nuclei [14] would be an interesting extension of the investigations described here. The results of such experiments would provide missing information about the projections K of the spins for *s*-wave resonances. Unfortunately, experiments with aligned nuclei are very complicated technically; therefore, their results can hardly be expected in the near future.

An investigation into interference effects is very promising for the ^{239}Pu nucleus. That the level density in this nucleus is less than those in the uranium isotopes is expected to simplify a theoretical description of experimental data and to render this description less ambiguous. In addition, only two values of $K = 0$ and 1 are possible for *s*-wave resonances in plutonium at the spin value of $I = 1/2$. This circumstance also reduces the number of unknown parameters included in the description. All this is expected to increase the reliability of the results to appear. Experiments of this type are complicated by the alpha-particle activity of ^{239}Pu nuclei, which prevents the use of sufficiently large targets.

It should be noted that, in experiments like those that are described above, a considerable refinement of results can be expected from the use of sources characterized by a higher intensity and a better resolution, such as LANSCE in Los Alamos or IREN projected in Dubna. This is especially important for measurements of small PNC effects.

ACKNOWLEDGMENTS

This work was supported in part by the Russian Foundation for Basic Research (project nos. 93-02-3979 and 97-02-19-6846).

REFERENCES

1. G. A. Petrov, G. V. Val'ski, A. K. Petukhov, *et al.*, Nucl. Phys. A **502**, 297 (1989).
2. V. P. Alfimenkov, I. S. Guseva, G. A. Petrov, *et al.*, in *Proceedings of ISINN-3* (JINR, Dubna, 1995), p. 276.
3. A. M. Gagarski, S. P. Golovskaya, I. S. Guseva, *et al.*, Preprint No. NP-29-1995, PNPI RAS (Petersburg Nuclear Physics Inst., Russian Academy of Sciences, 1995), 2056.
4. V. P. Alfimenkov, G. V. Val'skiĭ, A. M. Gagarski, *et al.*, Yad. Fiz. **58**, 799 (1995) [Phys. At. Nucl. **58**, 737 (1995)].
5. V. P. Alfimenkov, A. N. Chernikov, L. Lason, *et al.*, Preprint No. E3-97-106, JINR (Dubna, 1997).
6. A. M. Gagarski, I. S. Guseva, G. A. Petrov, *et al.*, in *Proceedings of ISINN-5* (JINR, Dubna, 1997), p. 182.
7. V. P. Alfimenkov, A. N. Chernikov, L. Lason, *et al.*, Nucl. Phys. A **645**, 31 (1999).
8. O. P. Sushkov and V. V. Flambaum, Usp. Fiz. Nauk **136**, 3 (1982) [Sov. Fiz. Usp. **25**, 1 (1982)].
9. V. E. Bunakov and V. P. Gudkov, Nucl. Phys. A **401**, 93 (1983).
10. V. L. Aksenov, N. A. Dikansky, V. L. Lomidze, *et al.*, JINR Commun. (Dubna), No. E3-92-110 (1992).
11. A. M. Gagarski, G. A. Petrov, A. K. Petukhov, *et al.*, Preprint No. 1634, LNPI (Leningrad Nuclear Physics Inst., USSR Academy of Sciences, 1990).
12. V. P. Alfimenkov, Yu. D. Mareev, L. B. Pikel'ner, *et al.*, Yad. Fiz. **54**, 1489 (1991) [Sov. J. Nucl. Phys. **54**, 907 (1991)].
13. S. F. Mughabghab, *Neutron Cross Sections* (Academic, New York, 1984), Vol. 1, Part B.
14. D. I. Tambovtsev, L. K. Kozlovsky, N. N. Gonin, *et al.*, Yad. Fiz. **60**, 981 (1997) [Phys. At. Nucl. **60**, 877 (1997)].

Translated by A. Isaakyan

Physics of Atomic Nuclei, Vol. 63, No. 4, 2000, pp. 545–547. Translated from Yadernaya Fizika, Vol. 63, No. 4, 2000, pp. 605–608.

IN MEMORIAM OF F. L. SHAPIRO

Time Focusing of Neutrons

A. I. Frank* and R. Gähler[1)]

Joint Institute for Nuclear Research, Dubna, Moscow oblast, 141980 Russia

Received October 14, 1999

Abstract—The possibility of time focusing for very slow neutrons is considered. This focusing may prove very useful in solving the problem of accumulating ultracold neutrons in a trap that are generated by a pulsed source. Diffraction at a phase grating moving across a beam or resonance neutron-spin flip is proposed to implement time-controlled changes in the neutron energy. © *2000 MAIK "Nauka/Interperiodica".*

In this article, we would like to attract the attention of researchers to the possibility of time focusing of very slow neutrons generated by a pulsed source. This focusing may prove useful in developing new-generation sources of ultracold neutrons (UCN). Figure 1 illustrates the physics behind our proposal.

Suppose that, at the instant $t = 0$, neutrons are emitted from the point $x = 0$ in the positive direction of the x axis and that the velocities of these neutrons are distributed over a certain interval. The time of neutron arrival at the observation point $x = L$, t_L, is distributed over the interval $t_{\min} < t_L < t_{\max}$. We assume that some device, a time lens, capable of changing the neutron energy by $\Delta E(t)$ according to a preset time law in the interval $t_1 < t < t_2$ is positioned at the point $x = a$. The principle underlying the operation of the time lens will be considered below. For now, we only require that, upon traversing the lens, the velocities of the neutrons be such that the neutrons arrive at the observation point simultaneously at the instant $t_L = t_0$; that is,

$$\frac{a}{v_a} + \frac{b}{v_b} = t_0, \quad a + b = L, \tag{1}$$

where v_a and v_b are the neutron velocities before and after traversing the lens, respectively.

We then have

$$\Delta E(t) = \frac{m}{2}\left|\left(\frac{b}{t_0 - t}\right)^2 - \left(\frac{a}{t}\right)^2\right|, \quad t = \frac{a}{v_a}, \quad t_1 < t < t_2. \tag{2}$$

In optics, image formation is associated with a transformation of the angular distribution of rays; likewise, time focusing is accompanied by changes in the velocity distribution, as can clearly be seen from Fig. 1. Concurrently, the duration of the neutron pulse is transformed, which makes it possible to introduce the concept of time magnification, M. For a relatively small energy transfer, $|\Delta E| \ll E$, the thin-lens formula

$$M = \frac{T}{\tau}, \quad M = -\frac{b}{a}, \tag{3}$$

where τ and T are the durations of the primary pulse and of its "image," respectively, holds.

The possibility of neutron time focusing seems appealing in connection with the long-standing problem of the accumulation of UCNs from a pulsed source. It was first indicated by F.L. Shapiro in 1964 that, if we inject UCNs into a neutron trap at the instant of pulsed-reactor burst and isolate the trap after the completion of the burst and if there are no losses, the UCN density in the trap will correspond to the peak neutron density, which can exceed the time-averaged density by a few orders of magnitude [1].

The majority of fundamental experiments with UCNs employ the so-called accumulation regime, in which case the removal of UCNs from the trap is either absent or very small (see, for example, [2]). Under such conditions, the Shapiro expression for the neutron-density gain takes the form

$$G = 1 + \left(1 - \frac{\tau_1}{\theta}\right)\left(\frac{\tau_1}{\theta} + \frac{\Sigma\mu}{S}\right)^{-1}, \tag{4}$$

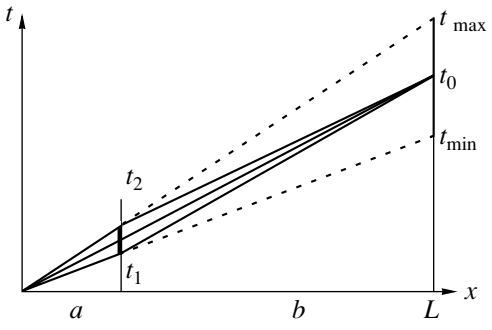

Fig. 1. Time focusing.

* e-mail: frank@nf.jinr.ru

1) Technische Universität München, James Frank Strasse, 85747 Garching, Germany.

where τ_1 is the time over which the gate is open (this time exceeds the duration of the neutron burst), θ is the time interval between the successive reactor bursts, S is the area of the converter surface emitting UCNs,[2] Σ is the area of the inner surface of the UCN vessel, and μ is the probability of UCN loss in one event of reflection from the vessel wall.

In current experiments, we have $\mu \approx 10^{-5}$ [3]. At reasonable values of Σ and S, the gain factor can therefore (in principle) achieve the value of about 10^3, which does not exceed the ratio θ/τ. By way of example, we indicate that, for the pulsed fast-neutron reactor IBR-2, the value of θ/τ is about 500.

The idea of F.L. Shapiro has yet to be implemented, because arranging a locking gate near a converter involves considerable technical difficulties. Moreover, the converter and the accumulating vessel are usually located rather far from each other and are connected by a neutron guide a few meters long. The neutron guide is included in the vessel volume, but this reduces significantly the storage time for a number of reasons. Only for sources with a low repetition frequency is it useful to arrange the locking gate near the trap [4] because, in this case, the scatter of the time of UCN arrival at the trap is about one second. For the majority of pulsed sources, this exceeds substantially both the burst duration τ and the interval θ between the bursts.

Time focusing removes these difficulties, making it possible to arrange the gate in close proximity to the trap, the effective burst duration being changed insignificantly (by a factor of M). The position of the lens, the time magnification associated with this, and the interval of the velocities of the neutrons to be focused can be chosen on the basis of practical considerations. In this case, the time lens plays a role similar to the role of the optical lighter in a conventional microscope. It permits matching the object under study with the image of the light source, while the source itself (lamp) cannot be matched with the object.

Let us consider the possible construction of the time lens. Generally, it is necessary to analyze all mechanisms capable of changing the neutron energy.

Methods based on the Doppler effect in the processes of neutron reflection [5] or diffraction [6] can hardly be operative because of the need for rapidly changing the scatterer (mirror or crystal) velocity.

Changing the neutron energy by means of time-dependent quantum effects [7, 8] is an attractive possibility, albeit it may seem bizarre at first glance. In this case, a quantum modulator can play the role of a focusing device. By a modulator, we mean a device that affects periodically the amplitude or the phase of the initial plane wave, so that the wave function at small distances from the modulator assumes the form

$$\Psi(x, t) \cong f(t)e^{i(kx - \omega t)}, \quad k^{-1} < x \ll vT, \qquad f(t) = f(t + T). \tag{5}$$

The state in the right half-space represents a time-dependent superposition of waves with energies $\hbar\omega_n$ and the corresponding wave numbers k_n; that is,

$$\Psi(x, t) = \sum_{n=-\infty}^{\infty} a_n e^{i(k_n x - \omega_n t)}, \quad x > 0, \tag{6}$$

where the amplitudes a_n are the Fourier coefficients for the modulation function $f(t)$, and

$$\omega_n = \omega + n\Omega, \quad k_n = k\left(1 + n\frac{\gamma}{2}\right), \qquad \gamma = \frac{\Omega}{\omega} \ll 1, \quad \Omega = \frac{2\pi}{T}, \tag{7}$$

T being the period. In a sense, a modulator appears to be a time analog of a diffraction grating.

Since a modulator generates neutrons whose energies differ from the original value (by quantities that are integral multiples of $\hbar\Omega$), such a device appears to be a good candidate for a time lens. In order to satisfy the focusing conditions, the modulator frequency must be changed with time in just the same way as, in optics, the space frequency of focusing devices (zone plates) is made to change with coordinates. If we restrict our considerations to the focusing of the waves of the first diffraction order, the frequency $\Omega(t) = E(t)/\hbar$ will change with time according to (2). It is necessary that these changes obey the adiabaticity condition

$$\frac{d\Omega}{dt} \ll \Omega^2. \tag{8}$$

Figure 2 displays the frequency of the time modulator, $f(t) = \Omega(t)/2\pi$, as a function of the time of flight for UCN velocities and a neutron-guide length chosen quite arbitrarily, but within realistic limits.

For a purely phase π modulator that changes the phase of the neutron wave by π for each half-period, the intensity of the wave corresponding to the first order of diffraction is about 0.4 of the initial wave intensity.

Since we are interested only in changes in the particle energy, the modulation phase can be arbitrary at each point of the beam cross section. For a phase modulator, we can use a conventional phase grating having a variable step and moving across the beam [9]. The characteristic modulation frequency is then determined by the ratio V/d, where V is the grating velocity and d is the space period of the grating. If d is about a few microns, which is quite feasible for modern technologies, the required modulation frequency is ensured by neutron velocities on the order of a few tens of meters per second.

[2] In UCN physics, a thin moderator located inside the reactor core is referred to as a converter.

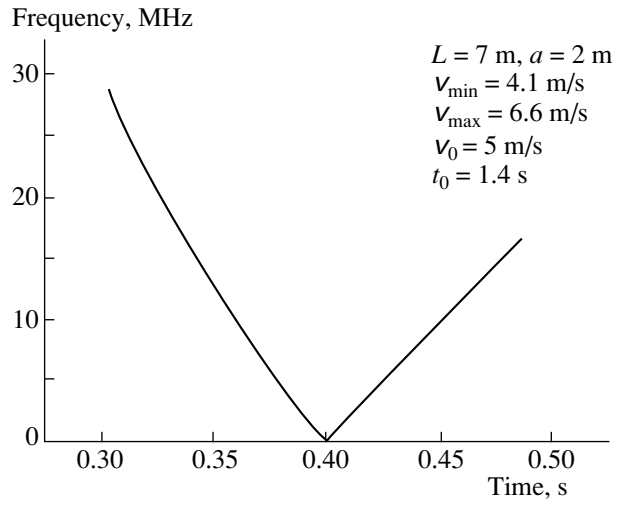

Fig. 2. Frequency of a quantum modulator as a function of time after the source burst.

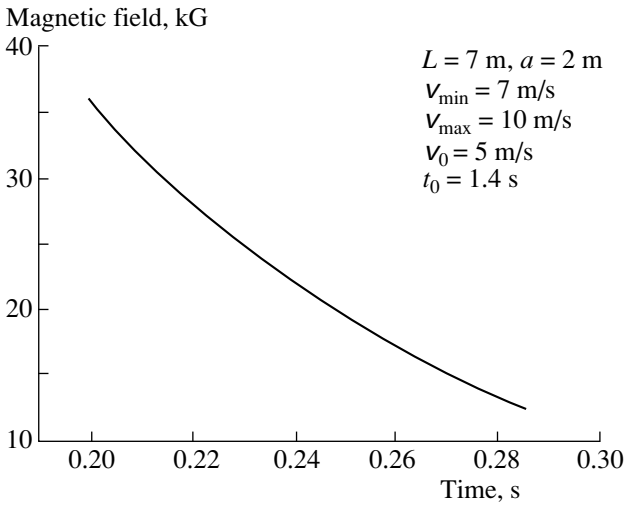

Fig. 3. Magnetic field as a function of time for the resonance moderation of neutrons.

Another attractive possibility is based on resonance neutron-spin flip in a magnetic field [10]. Upon traversing a volume where there are a slowly changing field $B(t)$ and a radio-frequency field orthogonal to it and where the resonance condition ensuring spin flip is permanently satisfied, neutrons change energy by $\hbar\omega_r(t)$, where $\omega_r(t)$ is the frequency of the radio-frequency field.

An implementation of this method in practice will probably be simplified if, in contrast to the case illustrated in Figs. 1 and 2, the quantity $v_0 = L/t_0$ does not lie in the interval of the velocities of the neutrons to be focused. In particular, all neutrons can be moderated by the lens used. In this case, the magnetic field $B(t)$ does not take zero value in the process of focusing, whereby permanent fulfillment of the resonance condition is facilitated. For the case being discussed, Fig. 3 shows the magnetic field as a function of time. The position of the time focus t_0 and the geometric parameters of the neutron guide are identical to those in Fig. 2, but the initial neutron velocities are increased.

The efficiency of the resonance lens for unpolarized neutrons is 50%. In this case, only neutrons with one value of the spin projection are focused. The possibility of accumulating polarized neutrons in a trap can contribute significantly to solving the problem of a fast pulsed gate. For this, we can use, for example, a magnetic film whose magnetization is reversed with a rather high frequency [11].

ACKNOWLEDGMENTS

A. I. Frank is indebted to the late M.V. Kazarnovsky for stimulating discussions on the results presented here and some other related topics.

REFERENCES

1. F. L. Shapiro, *Neutron Studies* (Nauka, Moscow, 1976), p. 229.
2. J. M. Pendelbury, Annu. Rev. Nucl. Part. Sci. **43**, 687 (1993).
3. V. P. Alfimenkov, V. V. Nesvizhevsky, A. P. Serebrov, *et al.*, Pis'ma Zh. Éksp. Teor. Fiz. **55**, 92 (1992) [JETP Lett. **55**, 84 (1992)].
4. Yu. N. Pokotilovskii, Nucl. Instrum. Methods Phys. Res., Sect. A **356**, 412 (1995).
5. A. Steyerl, H. Nagel, F.-X. Schriber, *et al.*, Phys. Lett. A **116**, 347 (1986).
6. T. O. Brun, J. M. Carpenter, V. E. Krohn, *et al.*, Phys. Lett. A **75**, 223 (1980).
7. J. Felber, R. Gähler, and R. Golub, Physica B **151**, 135 (1988).
8. A. I. Frank and V. G. Nosov, Yad. Fiz. **57**, 1029 (1994) [Phys. At. Nucl. **57**, 968 (1994)].
9. A. I. Frank and V. G. Nosov, Phys. Lett. A **118**, 120 (1994).
10. B. Alefeld, G. Badurek, and H. Rauch, Z. Phys. B **41**, 231 (1981).
11. M. I. Novopoltsev, Yu. N. Pokotilovskii, and I. G. Shelkova, Nucl. Instrum. Methods Phys. Res., Sect. A **264**, 318 (1988).

Translated by M. Kobrinsky

Physics of Atomic Nuclei, Vol. 63, No. 4, 2000, pp. 548–550. Translated from Yadernaya Fizika, Vol. 63, No. 4, 2000, pp. 609–612.

IN MEMORIAM OF F. L. SHAPIRO

Temperature Dependence of Inelastic Ultracold-Neutron Scattering at Low Energy Transfer

E. V. Lychagin, A. Yu. Muzychka, V. V. Nesvizhevsky[1)], G. V. Nekhaev, R. R. Tal'daev[2)], and A. V. Strelkov

Joint Institute for Nuclear Research, Dubna, Moscow oblast, 141980 Russia

Received November 2, 1999

Abstract—The temperature dependence of inelastic ultracold-neutron scattering on beryllium and copper surfaces at low energy transfers (about 10^{-7} eV) is investigated, and the results of this investigation are presented. The recorded flux of neutrons inelastically scattered by these surfaces at liquid-nitrogen temperature is less than that at room temperature by a factor of about two. © *2000 MAIK "Nauka/Interperiodica".*

This article reports on an investigation into the properties of ultracold neutrons (UCN). This realm owes its existence to F.L. Shapiro, who initiated, in 1968, the first observation of UCNs in Dubna. He supervised the pioneering experiments devoted to UCN generation, propagation, and confinement in closed vessels. The physics of UCNs was Shapiro's favorite topic during the last years of his life, and he was able to contribute greatly to the development of this realm, laying its foundations, which have suffered virtually no changes since then. A slight heating of UCNs, which was observed in recent years, is probably the only effect that stands out in this respect, since it does not fit in the conventional pattern of UCN interaction with matter.

1. INTRODUCTION

The present-day view of inelastic UCN interaction with matter assumes that the energies of scattered neutrons lie predominantly in the region corresponding to the temperature of the walls of the vessel containing UCNs. In [1, 2], however, a UCN scattering process was found where an energy transfer of about 10^{-7} eV occurs with a probability exceeding that which is predicted theoretically by many orders of magnitude [3, 4]. In the following, we will refer to this type of scattering as a slight heating of UCNs, in contrast to the well-known heating of UCNs to energies of the thermal region [5, 6], and to neutrons heated in this way as excited UCNs (EUCN). The nature of this process has yet to be clarified. Knowing the temperature dependence of the probability of slight heating at the surfaces of various substances, we could constrain the range of possible mechanisms of this phenomenon.

2. EXPERIMENTAL SETUP

Our measurements were performed with the aid of a gravitational UCN spectrometer shown schematically in Fig. 1 (this facility and the experimental procedure used are described in greater detail elsewhere [7, 8]). A Steyerl turbine at the reactor of the Laue–Langevin Institute (Grenoble) was used as a source of UCDs. Ultracold neutrons from this source arrived at the spectrometer representing a vertically arranged cylindrical vessel (*1*) 180 cm in height and 20 cm in diameter. In this vessel, which was made from copper, neutrons could be confined with the aid of a shutter (*2*). A slide

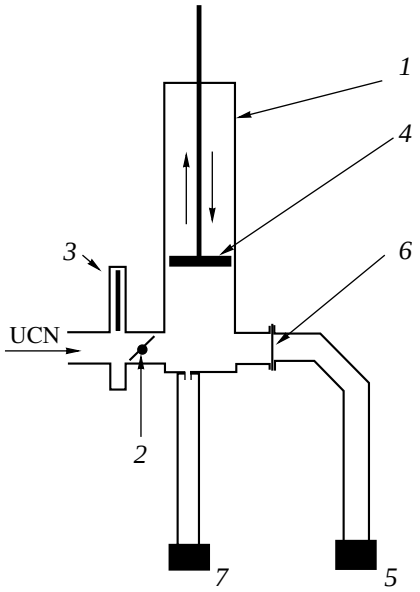

Fig. 1. Layout of the experimental setup: (*1*) storage vessel, (*2*) inlet shutter, (*3*) slide valve, (*4*) UCN absorber, (*5*) UCN detector, (*6*) aluminum foil, and (*7*) monitoring detector.

[1)] Laue–Langevin Institute, Grenoble, France.

[2)] Petersburg Nuclear Physics Institute, Russian Academy of Sciences, Gatchina, 188350 Russia.

1063-7788/00/6304-0548$20.00 © 2000 MAIK "Nauka/Interperiodica"

valve (*3*), impermeable to UCNs when latched, was arranged in front of the shutter.

The spectrum of stored UCNs was cut off from above by a polyethylene absorber (*4*) installed at a certain altitude. (The kinetic energy of a neutron that rises at an altitude of 1 cm in the gravitational field of the Earth is reduced by about 1 neV.)

In order to ensure an investigation of UCN storage in the temperature range between about 80 and 750 K, a coil for pumping liquid nitrogen and an electric heater were fastened to the outer surface of the storage vessel along its full height.

The samples under study were placed on the bottom of the spectrometer. At low temperatures, thermal contact between the sample and the spectrometer walls was ensured by supplying ^{4}He to the spectrometer (at a pressure of $P \approx 1$ mbar), which was removed before the measurements.

The whole storage vessel, together with the neutron inlets, was enclosed in a vacuum chamber, which was evacuated with an oil-free turbo-molecular pump to a pressure of about 10^{-4}–10^{-5} mbar.

A UCD detector (*5*) was connected to the spectrometer by a curved neutron guide and was separated from the storage vessel by an aluminum foil (*6*).

The UCN flux in the spectrometer was measured by a monitoring detector (*7*), which was similar to the main detector (*5*). Ultracold neutrons from the storage vessel penetrated into the monitor through a small hole (of area about 5 mm^2) in the vessel bottom.

The two UCN detectors (*5*) and (*7*) represented proportional counters of the same design and performance; either was filled with ^{3}He (at a pressure of $P \approx 3$ mbar) and had an aluminum window of thickness 100 μm and area about 60 cm^2. The detectors were positioned about 1 m below the spectrometer bottom, so that neutrons accelerated in the gravitational field could penetrate through the inlet aluminum windows of the detectors with a higher probability. The half-width of the peak of the pulse-height distribution for the reaction ^{3}He(n, p)t was about 6 to 7%; by recording only pulses from this pulse-height bin, we were able to reduce substantially the background from pulses that were not associated with neutrons. The background over the entire pulse-height spectrum was $(4.0 \pm 0.3) \times 10^{-3}$ s^{-1}, while the background within the bin was $(3.0 \pm 0.7) \times 10^{-4}$ s^{-1}, which was much less than the recorded EUCN flux.

3. MEASUREMENTS AND RESULTS

An aluminum foil (*6*) 12 μm thick was positioned in the neutron guide, covering its cross-sectional area entirely (Fig. 1). In order to eliminate the possible leakage of UCNs into the detector, the foil was gasketed along the perimeter with polyethylene rings (efficient UCN absorbers) on both sides. Thus, only UCNs whose energy was in excess of the endpoint energy of the aluminum spectrum (about 52 neV) could penetrate through the foil into the detector. Prior to filling the spectrometer with UCNs, the absorber was arranged at an altitude of 48.5 cm. After the inlet shutter was closed, all UCNs whose kinetic energy was sufficient for reaching the absorber, efficiently left the storage vessel, the time constant for their escape being about 3 s. Some of the neutrons escaping from the vessel with energies above the endpoint energy of the aluminum spectrum penetrated through the aluminum foil and were recorded by the UCN detector. Thus, the removal of UCNs with such energies from the stored-neutron spectrum can be traced by monitoring the variation of the detector counting rate. After a lapse of some 40 s since the latching of the slide valve, the detector counting rate must decrease to background values; however, a sharp dropout gives way to a smooth reduction whose characteristic time coincides with the storage time constant for UCNs with energies below the endpoint energy of the aluminum spectrum (about 100 s). In this case, the detector counting rate is much greater than the background value. If the absorber is raised at that moment, the counting rate in the UCN detector will increase sharply to some maximal value, but it then again begins to follow the UCN storage curve recorded by the monitoring detector.

Thus, the observed neutrons penetrating through the aluminum foil were slightly heated UCNs (EUCN) that were unceasingly produced throughout the storage period. Some of them had hit the detector even before the absorber was raised; once the absorber had been raised, however, EUCNs perished in it no longer: accumulated in the vessel, almost all of them arrived at the detector, whereby the counting rate increased sharply.

The results of the measurements can be conveniently represented as the time dependence of the ratio of the flux of recorded EUCNs to the monitor counting rate. Figure 2 shows such dependences for a beryllium sample and the empty copper spectrometer at room temperature and those at 100 K. This sample consisted of separate plates 0.1 and 0.3 mm thick made from rolled beryllium and separated on average by about 0.5 mm; it was 12 cm in height, and its total cross-sectional area was 2.6 m^2. The sample was placed on the vessel bottom. The absorber was raised after a lapse of 55 s since the inlet shutter had been closed (it was the 95th second from the beginning of the cycle). The solid curves in Fig. 2 represent results obtained from fits to experimental data. Before the absorber was raised, the fitting was performed in terms of the sum of a decreasing exponential with a time constant of about 3 s and a constant that corresponds to the EUCN flux recorded when the absorber was in the lower position. When the absorber was in the upper position, the fitted function was $A - B\exp\left(-\frac{t-t_0}{\tau}\right)$, where the constant A corresponds to the EUCN flux recorded when the absorber was in the upper position, the constant $\tau \approx 20$ s is close to the time constant for EUCN escape through the foil to the detector, and t_0 is the instant at which the absorber is raised.

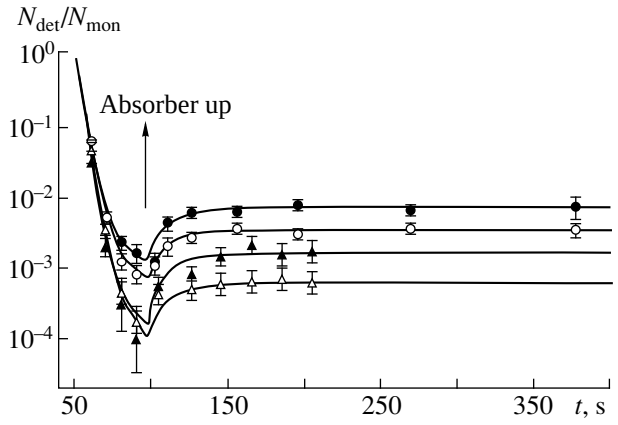

Fig. 2. Ratio of the EUCN flux to the monitor counting rate versus time: (●) results for rolled beryllium (S = 2.6 m^2) at 298 K; (○) results for the same sample at 100 K; and (▲ and △) results for the walls of the empty copper spectrometer (S = 0.2 m^2) at 298 K and 100 K, respectively.

The experimental setting in question gives no way to determine the total probability of EUCN generation because the spectrometer is sensitive only to a rather narrow bin in the spectrum of heated neutrons. From above, this bin is limited by the fact that neutrons with energies exceeding the endpoint energy of the copper spectrum are not stored in the spectrometer; from below, the boundary is determined by the impossibility of observing neutrons whose energies are slightly above the endpoint of the aluminum spectrum since such neutrons are readily reflected by the separating aluminum foil or are absorbed within it. These boundaries are somewhat uncertain, a determination of the lower boundary being complicated by coherent elastic scattering within the foil [9]. In view of these methodological difficulties, we cannot state that the probability of a slight heating per hit also changes upon cooling, since the reduction of the recorded EUCN flux may result from changes in the EUCN spectrum.

The cooling of the sample from room temperature to (100 ± 5) K led to the reduction of the detector counting rate by a factor of about two both in measurements with the empty spectrometer and in measurements with a beryllium sample within it. This can be caused by a decrease in the probability of slight heating and by changes in the spectrum of EUCNs. If we assume that the spectrum of EUCNs remains unchanged and consider that, as the vessel is cooled, the storage time increases, which results in that a greater fraction of EUCNs hit the detector, the observed variations in the counting rate correspond to the reduction of the probability of a slight heating of neutrons by a factor of 2.5 ± 0.2 for beryllium samples and by a factor of 2.4 ± 0.5 for the empty copper spectrometer.

4. CONCLUSION

Irrespective of the method used to obtain the UCN spectrum, this spectrum always features EUCNs—that is, neutrons that have energies in excess of the endpoint energy and which are generated from neutrons with energies below the endpoint energy. This irremovable admixture of EUCNs in the spectrum of stored neutrons causes a systematic error in precision experiments studying UCN storage—for example, in the measurements of the free-neutron lifetime.

The observed temperature dependence of the EUCN flux is compatible with the presumed linear temperature dependence of EUCN generation [10], but it is much weaker than that for conventional phonon heating to thermal energies [5, 6], which is substantially suppressed at liquid-nitrogen temperatures.

We note that the very presence of the temperature dependence makes it possible to disprove the popular point of view that it is not UCN heating that we observe, but faster neutrons from the initial spectrum that do not reach the absorber for some reason or another (for instance, they can be captured into ring trajectories under the absorber). In the last case, the process would be independent of temperature.

ACKNOWLEDGMENTS

The experiment was performed at the high-flux reactor installed at the Laue–Langevin Institute (Grenoble, France). We are grateful to the staff of the ILL, especially to P. Geltenbort, J. Butterworth, and T. Brenner, who were responsible for the beam, for their continuous and high-qualified assistance.

This work was supported by the Russian Foundation for Basic Research (project no. 99-02-16621).

REFERENCES

1. V. V. Nesvizhevsky, A. V. Strelkov, P. Geltenbort, *et al.*, ILL Annual Report (1997), p. 62.
2. V. V. Nesvizhevsky, A. V. Strelkov, P. Geltenbort, *et al.*, Yad. Fiz. **62**, 832 (1999) [Phys. At. Nucl. **62**, 776 (1999)]; Preprint No. R3-98-79, JINR (Joint Institute for Nuclear Research, Dubna, 1998).
3. V. K. Ignatovich, *The Physics of Ultracold Neutrons* (Nauka, Moscow, 1986).
4. R. Golub, D. J. Richardson, and S. K. Lamoreaux, *Ultracold Neutrons* (Adam Hilger, Bristol, 1991).
5. A. V. Strelkov and M. Hetzelt, Zh. Éksp. Teor. Fiz. **74**, 23 (1978) [Sov. Phys. JETP **47**, 11 (1978)].
6. A. D. Stoica, A. V. Strelkov, and M. Hetzelt, Z. Phys. B **29**, 349 (1978).
7. P. Geltenbort, V. V. Nesvizhevsky, D. G. Kartashov, *et al.*, Pis'ma Zh. Éksp. Teor. Fiz. **70**, 175 (1999) [JETP Lett. **70**, 170 (1999)].
8. P. Geltenbort, D. G. Kartashov, E. V. Lychagin, *et al.*, Preprint No. R3-99-91, JINR (Joint Institute for Nuclear Research, Dubna, 1999).
9. A. Steyerl and H. Vonach, Z. Phys. **250**, 166 (1972).
10. A. L. Barabanov and C. T. Belyaev, Yad. Fiz. **62**, 824 (1999) [Phys. At. Nucl. **62**, 769 (1999)].

Translated by E. Kozlovskiĭ

Physics of Atomic Nuclei, Vol. 63, No. 4, 2000, pp. 551–561. Translated from Yadernaya Fizika, Vol. 63, No. 4, 2000, pp. 613–624.

IN MEMORIAM OF F. L. SHAPIRO

Theoretical Approaches to Studying Protonic Decays of Nuclei and Interpretation of Experimental Data

S. G. Kadmensky

Voronezh State University, Universitetskaya pl. 1, Voronezh, 394693 Russia

Received June 11, 1999; in final form, October 25, 1999

Abstract—A comparison of various theoretical approaches to describing deep-subbarrier protonic decays of nuclei leads to the conclusion that the multiparticle theory of protonic decays of nuclei that is based on the use of an integral formula for decay widths is quite correct and general. A theoretical scheme for computing the protonic widths of odd–odd deformed nuclei is developed. The dependence of the fine structure in the protonic spectrum of the ^{141}Ho nucleus on the type of the odd-proton orbital is investigated. It is shown that the nuclear-deformation parameters as extracted from the analysis of protonic decays are consistent with analogous parameters predicted in some compilations. *© 2000 MAIK "Nauka/Interperiodica".*

1. INTRODUCTION

Investigation of protonic decays of ground and isomeric states of nuclei [1], which has been vigorously continued over the past years, makes it possible to determine protonic widths and the energies of emitted protons for a wide range of nuclei lying in the vicinity of the proton drip line, which determines the boundaries of the existence of nuclei in nature. By comparing the experimental values of protonic widths with the corresponding widths computed on the basis of modern theories of protonic decay, we can deduce unique information about the structure of the states involved and about the shapes of parent and daughter nuclei. Contrasting this information against the predictions of various compilations, we can verify the consistency of nuclear physics concepts based on studying the properties of nuclei from the vicinity of the beta-stability band.

The first theoretical calculations [2–6] of half-lives assumed the spherical shape of proton-decay nuclei and relied on the single-particle formula for the protonic width in the semiclassical approximation. To the best of my knowledge, the only calculation that deals with a protonic width [7] and which takes account of the multiparticle character of the protonic-decay process was performed for an isomeric state of the ^{53}Co nucleus, but this calculation was based on some unrealistic approximations—in particular, on the resonance approximation for the wave function of the emitted proton.

A multiparticle theory of the protonic decay of nuclei was constructed in [8, 9] on the basis of the integral formula for decay widths that was derived for the first time in [10–12] and which was used in studying the alpha decay of spherical nuclei [13–15]. Within this theory, protonic transitions were classified according to the degree of their diagonality, and protonic spectroscopic factors were introduced that take into account the effect of multiparticle states of the parent and daughter nuclei on protonic-decay probabilities. Within the multiparticle theory of protonic decays, it proved possible to describe successfully widths of spherical nuclei with respect to protonic decays not only from the ground states [1, 8, 16] but also from multiquasiparticle isomeric states [9]. A high-spin excited state of the ^{53}Co nucleus provides a typical example of the latter case. The decay of this state was detected experimentally [17] long before the discovery of the protonic decay of nuclei from the ground states [3, 4].

Later on, it was shown in [18] that by no means can we explain the features of the protonic decays of the ^{109}I and ^{113}Cs nuclei without going beyond the assumption that these nuclei are spherical. At the same time, it follows from the compilations presented in [19–21] that the ^{109}I and ^{113}Cs nuclei, as well as some other nuclei lying in the vicinity of the proton drip line, are characterized by significant deformations. In this connection, it became necessary to develop a multiparticle theory of protonic decays for deformed nuclei.

This theory was constructed in [22–24] on the basis of the formalism that was used previously to describe the alpha decay of deformed nuclei [25–27] and which also relies on the integral formula for decay widths. In contrast to *R*-matrix theory [28, 29], where there arises the problem of choosing decay-channel radii dependent on angles, this version of the multiparticle theory of protonic decays is free from such difficulties; owing to this, it provided an appropriate framework for successfully describing [22–24, 30, 31] the protonic-decay widths of some deformed nuclei, including the ^{147}Tm, ^{147m}Tm, and ^{151}Lu nuclei, which were assumed to be spherical in the first calculations [3–5, 8].

In recent years, there have appeared new methods [16, 32–35] for computing the single-particle features of protonic decays of spherical and deformed nuclei. Presently, these methods are used to analyze experi-

1063-7788/00/6304-0551$20.00

mental data. The objective of the present study is to compare the capabilities of various theoretical approaches to describing protonic decays of nuclei and to investigate, on the basis of the aforementioned multiparticle theory, the protonic decay of deformed odd–even and odd–odd nuclei and the fine structure of proton spectra.

2. STUDYING CONDITIONS UNDER WHICH THE INTEGRAL FORMULA FOR PROTONIC-DECAY WIDTHS OF NUCLEI IS APPLICABLE

By using methods developed in constructing the theories of protonic and alpha-particle radioactivity [8–15], we will investigate the deep-subbarrier protonic decay of a parent nucleus having an atomic weight A and a charge number Z and occurring in a state described by the wave function $\Psi_{\sigma_i}^{J_i M_i \pi_i}$ characterized by a nuclear spin J_i, its projection M_i, a parity π_i, and other quantum numbers σ_i. This function represents a quasistationary state of the parent nucleus in question and satisfies the Schrödinger equation

$$(H - E_i)\Psi_{\sigma_i}^{J_i M_i \pi_i} = 0, \qquad (1)$$

where H is the Hamiltonian of the A nucleus, while $E_i = E_i^0 - i\Gamma_i/2$ is a complex energy, whose imaginary part is related to the total decay width Γ_i of the state under study. That this state is quasistationary implies that its lifetime $T_i = \hbar/\Gamma_i$ is much greater than the characteristic periods of the single-particle and collective modes of intranuclear motion that determine this state. As a result, the total width Γ_i appears to be the sum $\Gamma_i = \sum_\lambda \Gamma_{i\lambda}$ of the partial widths $\Gamma_{i\lambda}$ with respect to all possible open decay channels λ, including the α, β, and γ channels, as well as the channel of protonic decay. Since the parent-nucleus state considered here is quasistationary, an analysis of various channels of its decay and, hence, a calculation of various partial widths $\Gamma_{i\lambda}$ can be performed independently. It follows that, for the wave function of the nucleus, $\Psi_{\sigma_i}^{J_i M_i \pi_i}$, the boundary condition at the absolute value of the relative coordinate $\mathbf{r}$ of the centers of mass of the emitted proton and the daughter nucleus in excess of the proton-channel radius R_0 [in which case all terms in the potential V_{pA-1} of the interaction between the emitted proton and the daughter nucleus, with the exception of the long-range Coulomb potential $V_0^{\mathrm{Coul}}(r) = (Z-1)e^2/r$, are negligibly small] can be taken in the form of the Gamow condition, which involves diverging spherical waves for all open channels c ($c \equiv J_f \pi_f \sigma_f j_p l_p$) of protonic decay:

$$\Psi_{\sigma_i}^{J_i M_i \pi_i} = \sum_c N_c \hat{A}\left[U_c \frac{G_{l_p}(k_c r) + iF_{l_p}(k_c r)}{r}\right], \quad r \geq R_0. \qquad (2)$$

Here, $\hat{A}$ is the operator of antisymmetrization between the emitted proton and the protons of the daughter nucleus [this operator acts on the bracketed functions in (2)]; $Q_c = \hbar^2 k_c^2/2m = E_i^0 - E_f^0$, where $m = M_p M_{A-1}/M_A$ is the reduced mass of the system formed by the emitted proton and the daughter nucleus, is the energy of relative motion in this system; $G_l(kr)$ and $F_l(kr)$ are, respectively, the irregular and the regular radial Coulomb function; and U_c is the channel function given by

$$U_c = \{\Psi_{\sigma_f}^{J_f M_f \pi_f} \Phi_{j_p l_p m_p}(\Omega_{\mathbf{r}}, \boldsymbol{\sigma}_p)\}_{J_i M_i}, \qquad (3)$$

where $\Phi_{j_p l_p m_p}$ is its spin–orbit component and where the braces correspond to the vector composition of the total spin J_f of the daughter nucleus and the total spin j_p of the emitted proton.

We will further make use of the continuity equation following from equation (1), the boundary condition (2), and the condition requiring that the function $\Psi_{\sigma_i}^{J_i M_i \pi_i}$ be normalized to unity within a multidimensional sphere specified by the equation $r \leq R_1$ in the configuration space τ of all coordinates of the parent-nucleus nucleons, where the radius R_1 lies in the deep-subbarrier region, considerably exceeding the proton-channel radius R_0, so that we additionally have the condition $G_{l_p}(k_c R_1) \gg F_{l_p}(k_c R_1)$. The constants N_c in (2) can then be expressed in terms of the partial widths Γ_{ipc} with respect to protonic decay through the channel c as $N_c = \sqrt{k_c \Gamma_{ipc}/2Q_c}$. It should be emphasized that a decaying-nucleus state is quasistationary only if its wave function $\Psi_{\sigma_i}^{J_i M_i \pi_i}$ is not sensitive, over the entire region $r \leq R_1$, to the presence of open decay channels and, hence, to the emergence of an imaginary part that the energy of the nucleus develops in this case. For protonic decay channels, this implies that, in the region $R_0 \leq r \leq R_1$, the function $F_{l_p}(k_c r)$ can be disregarded against $G_{l_p}(k_c r)$ in (2) owing to the fact that protonic decay is a deep-subbarrier process. As a result, the boundary condition (2) becomes real:

$$(\Psi_{\sigma_i}^{J_i M_i \pi_i})_0 = \sum_c \sqrt{\frac{k_c \Gamma_{ipc}}{2Q_c}} \hat{A}\left[U_c \frac{G_{l_p}(k_c r)}{r}\right]. \qquad (4)$$

In this case, the wave function $\Psi_{\sigma_i}^{J_i M_i \pi_i}$ coincides, in the region $r \leq R_1$, with the function that satisfies the

Schrödinger equation (1) and the boundary condition (4) and which corresponds to the stationary-state wave function $(\Psi_{\sigma_i}^{J_iM_i\pi_i})_0$ for the real-valued energy $E_i^0 = \mathrm{Re}E_i$.

Let us now consider the wave function $\Phi_{c_0}^{J_iM_i\pi_i}$ that satisfies the time-independent Schrödinger equation with a Hamiltonian H and which describes proton scattering on the daughter nucleus at energies E close to the quasistationary-state energy E_i^0, in which case the input channel corresponds to the channel function U_{c_0} (3). In the external region $R_0 \le r$, this function normalized to the delta function of energy satisfies the boundary condition

$$\Phi_{c_0}^{J_iM_i\pi_i} = \sum_c \frac{i}{2r}\sqrt{\frac{k_c}{\pi Q_c}} \times \hat{A}[U_c((G_c - iF_c)\delta_{cc_0} - \tilde{S}_{cc_0}(G_c + iF_c))], \quad (5)$$

where the quantity $\tilde{S}_{cc_0}$ is related to the exact S matrix by the simple equation

$$S_{cc_0} = \tilde{S}_{cc_0}\exp[i(\delta_c^{\mathrm{Coul}} + \delta_{c_0}^{\mathrm{Coul}})], \quad (6)$$

with δ_c^{Coul} being the Coulomb phase shift. Since the proton involved in the reaction being considered occurs in the deep-subbarrier region, we can disregard the contribution to the $\tilde{S}$ matrix from the direct mechanisms of elastic and inelastic proton scattering on the daughter nucleus that are due to the nuclear and the nonpointlike Coulomb component of the potential V_{pA-1}, restricting our consideration to the only mechanism that is of importance in the case being studied, a resonance reaction mechanism. In the vicinity of an isolated resonance at $E \approx E_i^0$, the matrix $\tilde{S}_{cc_0}$ can then be represented as [15]

$$\tilde{S}_{cc_0} = \delta_{cc_0} - i\frac{\Gamma_{ipc_0}^{1/2}\Gamma_{ipc}^{1/2}}{E - E_i^0 + i\Gamma_i/2}. \quad (7)$$

If we make use of this formula and if, in the region $R_0 \le r \le R_1$, we disregard the functions F_c in equation (5) against the functions G_c because of a deep-subbarrier character of the process, it can be shown that the function in (5) obeys the asymptotic condition

$$\Phi_{c_0}^{J_iM_i\pi_i} = \sum_c \frac{\Gamma_{ipc_0}^{1/2}\Gamma_{ipc}^{1/2}}{E - E_i^0 + i\Gamma_i/2}\sqrt{\frac{k_c}{4\pi Q_c}}\hat{A}\left[U_c\frac{G_c(r)}{r}\right]. \quad (8)$$

The functions $(\Psi_{\sigma_i}^{J_iM_i\pi_i})_0$ and $\Phi_{c_0}^{J_iM_i\pi_i}$ satisfy the Schrödinger equation with the same Hamiltonian H and correspond to close energies; in addition, they obey the boundary conditions (4) and (8), which differ by a constant factor. From all this, it follows that, within the sphere $r \le R_1$ of the configuration space τ, these functions are related by the equation

$$\Phi_{c_0}^{J_iM_i\pi_i} = \sqrt{\frac{\Gamma_{ipc_0}}{2\pi}}\frac{1}{E - E_i^0 + i\Gamma_i/2}(\Psi_{\sigma_i}^{J_iM_i\pi_i})_0. \quad (9)$$

By using the methods developed in [10–15], we can express the matrix $\tilde{S}_{cc_0}$ in terms of the relevant T-matrix element as

$$\tilde{S}_{cc_0} = \delta_{cc_0} - 2\pi i\left\langle \hat{A}\left[\frac{\tilde{F}_cU_c}{r}\middle|(V_{pA-1} - V_0^{\mathrm{Coul}})\right]\middle|\Phi_{c_0}^{J_iM_i\pi_i}\right\rangle, \quad (10)$$

where $\tilde{F}_c = \sqrt{k_c/\pi Q_c}F_c$ is the regular radial Coulomb function normalized to the delta function of energy. By substituting (9) into (10) and comparing the resulting expression with that in (7), we can obtain an integral expression for the partial width Γ_{ipc} in the form

$$\Gamma_{ipc} = 2\pi|B_{ipc}|^2, \quad (11)$$

where the amplitude B_{ipc} for the protonic decay of the parent nucleus through the channel c is given by

$$B_{ipc} = \int \hat{A}\left[\frac{\tilde{F}_{l_p}(k_cr)U_c}{r}(V_{pA-1} - V_0^{\mathrm{Coul}}(r))\right] \times (\Psi_{\sigma_i}^{J_iM_i\pi_i})_0 d\tau, \quad (12)$$

integration in (12) being performed over the multidimensional sphere $r \le R_1$ in the configuration space τ.

From the above derivation, it follows that the integral formula (12) is quite accurate, provided that $F_c(r)/G_c(r) \ll 1$ for $r \le R_1$, whence we immediately find that the condition $\Gamma_{ip}/Q_c \ll 1$, under which the decaying-nucleus state is quasistationary, holds automatically. The above formula has nothing to do with perturbation theory in the potential V_{pA-1} of interaction between the decay fragments; in contrast to the statement of Aberg *et al.* [16], it does not therefore represent the distorted-wave Born approximation (DWBA). Indeed, the wave function $(\Psi_{\sigma_i}^{J_iM_i\pi_i})_0$ of the quasistationary state of the parent nucleus generally takes into account the potential V_{pA-1} in all orders of perturbation theory.

To conclude this section, we note that the developed multiparticle theory of protonic decay is free from the difficulties of the R-matrix theory [28, 29] that are associated with the choice of the decay-channel radii; this theory is quite general, which makes it possible to investigate, within a unified conceptual framework, protonic transitions between various states of both spherical and deformed parent and daughter nuclei.

3. CLASSIFICATION OF TYPES OF PROTONIC DECAYS OF NUCLEI

The multidimensional integral in (12), which determines the protonic-decay amplitude, can be represented as the sum of integrals over the internal (shell), intermediate, and external regions specified, respectively, as $r \le R_{sh}$, $R_{sh} \le r \le R_0$, and $R_0 \le r \le R_1$. As was shown in [8], the main contribution to the integral in question comes from the internal region, where the wave function $(\Psi_{\sigma_i}^{J_i M_i \pi_i})_0$, which describes a quasistationary state of the parent nucleus, coincides with the function $(\Psi_{\sigma_i}^{J_i M_i \pi_i})_0^{sh}$. By analogy with the wave functions of bound nuclear states, the latter is computed on the basis of the generalized model of the nucleus [36], a model that relies on the multiparticle shell model and which takes into account normal and superfluid correlations, as well as collective modes of motion—for instance, a rotational mode for deformed nuclei. In this case, protonic decays of nuclei can be classified by the degree of their diagonality [8, 9].

The case of diagonal protonic decays of nuclei is realized when the radial shell form factor $\varphi_{ic}^{sh}(r) \equiv \langle \hat{A}\{\delta(r - r_1)U_c/r\}|(\Psi_{\sigma_I}^{J_i M_I \pi_I})_0^{sh}\rangle$ is dominant for the decay channel c under study. This corresponds to the situation where the dominant contribution to the decay-width amplitude (12) is due to that matrix element $V_{pA-1}^0(r)$ of the potential V_{pA-1} which is diagonal in the channel functions U_c. The form factor $\varphi_{ic}^{sh}(r)$ can be represented as [8]

$$\varphi_{ic}^{sh}(r) = Z_{ic}^{1/2}\chi_{j_p l_p}(r), \tag{13}$$

where Z_{ic} is the proton spectroscopic factor, while $\chi_{j_p l_p}(r)$ is the radial shell-model wave function for the proton in the $j_p l_p$ state. The protonic width Γ_{ipc} is then given by [8]

$$\Gamma_{ipc} = Z_{ic}\Gamma_{j_p l_p}, \tag{14}$$

where $\Gamma_{j_p l_p}$ is the effective single-particle decay width of the proton shell state characterized by the radial wave function $\chi_{j_p l_p}(r)$. This width has the form (11), where the amplitude is given by

$$B_{j_p l_p} = \int_0^{R_{sh}} \tilde{F}_{l_p}(k_c r)[V_{pA-1}^0(r) - V_0^{Coul}(r)]\chi_{j_p l_p}(r)dr. \tag{15}$$

The diagonal case is realized for protonic transitions from the ground states of spherical nuclei to the ground states of daughter nuclei. Owing to this, the experimental protonic width for such transitions can be successfully described within the formalism developed above [8].

The case of nondiagonal protonic decays is possible if the shell form factor $\varphi_{ic}^{sh}(r)$ for the decay channel c being studied is negligibly small. The width Γ_{ipc} is then nonzero either owing the intermediate and external regions for the amplitude in (12), where the form factor $\varphi_{ic}(r)$ is nonzero, or owing to the effect of those components of the potential V_{pA-1} of interaction between the emitted proton and the daughter nucleus that are nondiagonal in the channel function U_c. The case of nondiagonal protonic decay is realized if the contribution of the intermediate and external regions to the amplitude in (12) is small. This occurs if the core of the daughter nucleus is strongly rearranged in the decay process. The situation in question is exemplified by protonic decays of multiquasiparticle isomeric states of parent nuclei into the ground states of daughter nuclei and by protonic decays of the ground states of parent nuclei into collective vibrational and multiquasiparticle states of daughter nuclei. In [9], the protonic decay of a high-spin three-quasiparticle isomeric state of the spherical nucleus ^{53}Co was successfully explained within the formalism described here.

Finally, the intermediate case is realized when transitions that are diagonal in the potential V_{pA-1} and those that are nondiagonal in this potential both play an important role. This is peculiar to protonic transitions from the ground states of deformed nuclei to levels of the ground-state rotational bands of daughter nuclei.

4. COMPARISON OF VARIOUS APPROACHES TO DESCRIBING PROTONIC DECAYS OF DEFORMED NUCLEI

Here, the potential of the multiparticle theory of protonic decays [8, 9, 22–24] and the potential of some new approaches [16, 32–35] will be considered by applying them to protonic decays of the ground and single-quasiparticle isomeric states of odd–even deformed nuclei to levels of the ground-state rotational bands of even–even daughter nuclei. We will assume that the deformation parameters of the parent and the daughter nucleus are close. We introduce the complete orthonormalized basis of the shell-model nucleon wave functions $f_k(\mathbf{r}', \boldsymbol{\sigma}')$ in the intrinsic coordinate frame of a deformed axisymmetric nucleus, where the subscript k stands for the form $k^{\pi_k}[NN_z\Lambda]$ involving, according to the Nilsson classification [36], the projection k of the total nucleon spin onto the symmetry axis of the nucleus, the parity π_k, and asymptotic quantum numbers—the principal quantum number N, the number N_z of quanta corresponding to the motion of the nucleon along the symmetry axis z of the nucleus, and the projection of the nucleon orbital angular momentum Λ onto the z axis. The quantity $\Sigma = k - \Lambda$ then determines the projection of the nucleon spin onto the z axis. The function $f_k(\mathbf{r}', \boldsymbol{\sigma}')$ corresponding to the energy ε_k appears to be a solution to the single-particle Schrödinger equa-

tion describing the motion of a nucleon in the nonspherical shell-model potential $V^0(\mathbf{r}', \boldsymbol{\sigma}')$. In the case of protons, this potential is equal to the sum of the nonspherical nuclear, nonspherical Coulomb, and nonspherical spin–orbit potentials. The nuclear potential $V_p^{\text{nucl}}(\mathbf{r}')$ can be represented as

$$V_p^{\text{nucl}}(\mathbf{r}') = -V_0\left[1 + \exp\left(\frac{r - R_A(\theta')}{a}\right)\right]^{-1}, \quad (16)$$

where

$$R_A(\theta') = r_0 A^{1/3}\left\{1 + \beta_0 + \sum_{\lambda = 2, 4}\beta_\lambda Y_{\lambda 0}(\theta')\right\}, \quad (17)$$

β_λ being the deformation parameters of the nucleus. The nonspherical Coulomb potential $V_p^{\text{Coul}}(\mathbf{r}')$ is given by

$$V_p^{\text{Coul}}(\mathbf{r}') = V_0^{\text{Coul}} + \sum_{\lambda = 2, 4}\frac{Q'_\lambda}{r^{\lambda+1}}\sqrt{\frac{4\pi}{2\lambda+1}}Y_{\lambda 0}(\theta'), \quad (18)$$

where Q'_λ are the intrinsic electric multipole moments of the nucleus.

The wave function $f_k(\mathbf{r}', \boldsymbol{\sigma}')$ can generally be represented as an expansion in spin–orbit functions as

$$f_k(\mathbf{r}', \boldsymbol{\sigma}') = \sum_{jl}\frac{\chi^k_{jl}(r)}{r}\Phi_{jlk}(\Omega_{\mathbf{r}'}, \boldsymbol{\sigma}'). \quad (19)$$

The radial function $\chi^k_{jl}(r)$ in turn can be expanded in a series in radial spherical shell-model functions $R_{njl}(r)$ as

$$\chi^k_{jl}(r) = \sum_n a^k_{njl}R_{njl}(r). \quad (20)$$

In the strong-coupling approximation [36], the multiparticle shell-model wave functions of the deformed parent and daughter nuclei can be represented as

$$(\Psi^{J_i M_i \pi_i}_{\sigma_i})^{\text{sh}}_0 = \left(\frac{\hat{J}_i}{16\pi^2}\right)^{1/2} \times \{D^{J_i}_{M_i k_i}(\omega)\chi^i_{k_i} + (-1)^{J_i + k_i}D^{J_i}_{M_i - k_i}(\omega)\chi^i_{\bar{k}_i}\}, \quad (21)$$

$$(\Psi^{J_f M_f \pi_f}_{\sigma_f})^{\text{sh}}_0 = \left(\frac{\hat{J}_f}{8\pi^2}\right)^{1/2}D^{J_f}_{M_f 0}(\omega)\chi^f_0, \quad (22)$$

where $D^J_{Mk}(\omega)$ is the generalized spherical function dependent on the Euler angles ω, $\hat{J} \equiv 2J + 1$, and $\chi^i_{k_i}$ and χ^f_0 are the intrinsic wave functions of the parent and daughter nucleus. Within the superfluid model of the nucleus, we can make use of the formulas $\chi^i_{k_i} = \chi^{ip}_{k_i}\chi^{in}_0$ and $\chi^f_0 = \chi^{fp}_0\chi^{fn}_0$, which are obtained on the basis of the Bogolyubov method of u–v transformations [37]. In these formulas, the intrinsic wave functions of the proton and neutron subsystems of the parent and the daughter nucleus in the second-quantization representation are given by

$$\chi^{ip}_{k_i} = a^+_{k_i}\prod_{k \neq k_i}(u^i_k + v^i_k a^+_k a^+_{-k})|0\rangle, \quad (23)$$

$$\chi^{fp}_0 = \prod_k (u^f_k + v^f_k a^+_k a^+_{-k})|0\rangle, \quad (24)$$

where a^+_k is the operator creating a proton in the shell state k.

From (23) and (24), it follows that, for the protonic transitions being studied, the structure of the wave function χ^f_0 of the daughter-nucleus core undergoes virtually no changes. For this reason, we can make use of the approximation where the potential V_{pA-1} is diagonal in the intrinsic wave function χ^f_0 of the daughter nucleus and replace this potential by the shell-model potential $V^0_p(\mathbf{r}', \boldsymbol{\sigma}')$. In this case, the shell-model proton form factor $\varphi^{\text{sh}}_{k_i}(\mathbf{r}', \boldsymbol{\sigma}')$ given by

$$\varphi^{\text{sh}}_{k_i}(\mathbf{r}', \boldsymbol{\sigma}') = \langle \hat{A}\{\delta(\mathbf{r}' - \mathbf{r})\delta(\boldsymbol{\sigma}' - \boldsymbol{\sigma})\chi^f_0\}\big|\chi^i_{k_i}\rangle \quad (25)$$

appears in expression (12) for the amplitude of the protonic width.

In order to take into account the antisymmetrization operator in expression (25), we can go over to the second-quantization representation, where the wave functions $\chi^i_{k_i}$ and χ^f_0 are given by (23) and (24) and where the completeness condition for the set of the shell-model wave functions $f_k(\mathbf{r}', \boldsymbol{\sigma}')$,

$$\delta(\mathbf{r}' - \mathbf{r}'_1)\delta(\boldsymbol{\sigma}' - \boldsymbol{\sigma}'_1) = \sum_k f_k(\mathbf{r}', \boldsymbol{\sigma}')f^*_k(\mathbf{r}'_1, \boldsymbol{\sigma}'_1), \quad (26)$$

makes it possible to represent the product of delta functions in the form

$$\delta(\mathbf{r}' - \mathbf{r}'_1)\delta(\boldsymbol{\sigma}' - \boldsymbol{\sigma}'_1) = \sum_k f^*_k(\mathbf{r}', \boldsymbol{\sigma}')a_k.$$

To a high accuracy, the proton form factor (25) can then be approximated as [22]

$$\varphi^{\text{sh}}_{k_i}(\mathbf{r}', \boldsymbol{\sigma}') = u^f_{k_i}f_k(\mathbf{r}', \boldsymbol{\sigma}'). \quad (27)$$

Let us express the function $\Phi_{j_p l_p k}(\Omega_{\mathbf{r}}, \boldsymbol{\sigma})$ in terms of intrinsic coordinates. We have

$$\Phi_{j_p l_p k}(\Omega_{\mathbf{r}}, \boldsymbol{\sigma}) = \sum_k D^{j_p}_{m_p k}(\omega)\Phi_{j_p l_p k}(\Omega_{\mathbf{r}'}, \boldsymbol{\sigma}'). \quad (28)$$

By taking into account the addition theorem for D functions [36], the channel function U_c (3) can be reduced to the form

$$U_c = \left(\frac{\hat{J}_f}{8\pi^2}\right)^{1/2} \sum_k C^{J_i k}_{J_f j_p 0 k} D^{J_i}_{M_i k}(\omega)\chi_0 \Phi_{j_p l_p k}(\Omega_{\mathbf{r}'}, \boldsymbol{\sigma}'). \quad (29)$$

Upon integration with respect to the Euler angles, the amplitude B_{ipc} (12) can be written as

$$B_{ipc} = Z^{1/2}_{ipc} B^0_{ipc}, \quad (30)$$

where the amplitude of the proton spectroscopic factor is given by

$$Z^{1/2}_{ipc} = \left(\frac{2\hat{J}_f}{\hat{J}_i}\right)^{1/2} C^{J_i k_i}_{J_f j_p 0 k_i} u^f_{k_i}, \quad (31)$$

while the amplitude B^0_{ipc} for the protonic decay of the single-particle proton state described by the wave function $f_k(\mathbf{r}', \boldsymbol{\sigma}')$ can be represented in the form

$$B^0_{ipc} = \left\langle \frac{\tilde{F}_{l_p}(k_c r)\Phi_{j_p l_p k_i}(\mathbf{r}', \boldsymbol{\sigma}')}{r} \middle| V^0_p(\mathbf{r}', \boldsymbol{\sigma}') - V^{\mathrm{Coul}}_0 \middle| f_k(\mathbf{r}', \boldsymbol{\sigma}') \right\rangle. \quad (32)$$

The expression for the partial protonic-decay width Γ_{ipc} can then be recast into a form similar to that of (14); that is,

$$\Gamma_{ipc} = Z_{ipc}\Gamma^0_{ipc}, \quad (33)$$

where the effective single-particle width Γ^0_{ipc} of the quasistationary state described by the wave function $f_k(\mathbf{r}', \boldsymbol{\sigma}')$ with respect to the protonic decay through the channel characterized by the quantum numbers $j_p l_p$ has the form (11) with the amplitude B^0_{ipc} given by expression (32). Since the problem of protonic decays of nuclei is of a multiparticle character, the width Γ^0_{ipc} differs substantially from the decay width $\Gamma^0_{j_p l_p}$ of the single-particle quasistationary state characterized by the wave function $f_k(\mathbf{r}', \boldsymbol{\sigma}')$. If the function $f_k(\mathbf{r}', \boldsymbol{\sigma}')$ is represented in the form (19), it can be shown that, in the asymptotic region $r \geq R_0$, the functions $\chi_{jl}(r)$ satisfy a boundary condition similar to the boundary condition (2); that is,

$$\chi_{jl}(r) = \sum_{jl} \sqrt{\frac{\Gamma^0_{jl} k^0_i}{2\varepsilon_{k_i}}} \left(\frac{G_l(k^0_i r) + iF_l(k^0_i r)}{r}\right), \quad (34)$$

where $k^0_i = \sqrt{2m\varepsilon_{k_i}/\hbar^2}$ is the nucleon wave vector corresponding to the shell energy ε_{k_i}. Since protonic decay is a deep subbarrier process, we can disregard the Coulomb functions $F_l(k^0_i r)$ and obtain a boundary condition that is similar to that in (4) and which leads to a real energy ε_{k_i} of the proton shell state described by the wave function $f_k(\mathbf{r}', \boldsymbol{\sigma}')$. In general, this energy, ε_{k_i}, differs substantially from the proton separation energies $Q_c = E^0_i - E^0_f$ for all channels of parent-nucleus decay, since the energies of the parent and the daughter nucleus, E^0_i and E^0_f, include not only shell energies of nucleons but also effects caused by nucleon–nucleon correlations of the normal and superfluid types, as well as by the finiteness of nuclear dimensions and by collective modes of nuclear motion that are associated with it—for example, rotational modes. For this reason, the amplitude $B^0_{j_p l_p}$ of the width $\Gamma^0_{j_p l_p}$ differs from the amplitude B^0_{ipc} (32) of the width Γ^0_{ipc} in that the former features the Coulomb functions $\tilde{F}_{l_p}(r)$ corresponding to the emitted-proton energy ε_{k_i} rather than the energy Q_c. Since the Coulomb functions depend greatly on the proton energy in the deep-subbarrier region, the widths Γ^0_{ipc} differ significantly in magnitude from the widths $\Gamma^0_{j_p l_p}$. An attempt at improving the situation can be made by varying the well depth in order that the energy ε_{k_i} of the proton shell state described by the wave function $f_k(\mathbf{r}', \boldsymbol{\sigma}')$ become the energy Q_c dependent on the decay channel under study, whereby we would arrive at the modified widths $\tilde{\Gamma}^0_{j_p l_p}$. Even in this case, however, the absolute values of the widths $\tilde{\Gamma}^0_{j_p l_p}$ can differ from the values Γ^0_{ipc} obtained within the consistent theoretical scheme because the function $f_k(\mathbf{r}', \boldsymbol{\sigma}')$ is modified in the internal region $r \leq R_0$ of the parent nucleus as we go over from the energy ε_{k_i} to Q_c.

A new method for calculating the partial widths with respect to protonic transitions from the ground or single-quasiparticle states of deformed odd–even parent nuclei to the ground states of the even–even daughter nuclei was developed in [33–35], where formula (33), with the spectroscopic factor Z_{ipc} (31) obtained in [22], was used for the protonic partial width. In the case of $J_f = 0$, this spectroscopic factor takes the value $\frac{2}{\hat{J}_i}(u^f_{k_i})^2 \delta_{j_p J_i}$. As to the effective single-particle width Γ^0_{ipc}, it was replaced there by the width $\tilde{\Gamma}^0_{j_p l_p}$ with respect to the protonic decay of the quasistationary state that is described by the wave function $f_k(\mathbf{r}', \boldsymbol{\sigma}')$ and which occurs at an energy ε_{k_i} whose real part was fitted, by varying the well depth, to the experimental energy Q_{c_0} for the channel c_0 of parent-nucleus decay into the ground ($J_f = 0$) state of the daughter nucleus. The following method was used to compute the quanti-

ties $\tilde{\Gamma}^0_{j_p l_p}$. The Schrödinger equation with the potential $V^0_p(\mathbf{r}', \boldsymbol{\sigma}')$ for the function $f_k(\mathbf{r}', \boldsymbol{\sigma}')$ was solved on the basis of the representation in (19) by using the Gamow boundary conditions (34), and the imaginary part of the energy was determined as $\mathrm{Im}\varepsilon_{k_i} = \tilde{\Gamma}^0_p/2$, where $\tilde{\Gamma}^0_p$ is the total protonic-decay width of the state being studied: $\tilde{\Gamma}^0_p = \sum_{jl}\tilde{\Gamma}^0_{jl}$. Further, the width $\tilde{\Gamma}^0_{j_p l_p}$ was found with the aid of the relation

$$\tilde{\Gamma}^0_{j_p l_p} = -2\mathrm{Im}\varepsilon_{k_i}\frac{\beta^2_{l_p j_p}}{\sum_{jl}\beta^2_{jl}}, \quad \beta^2_{jl} = \frac{\chi^2_{jl}(r)}{F^2_l(r) + G^2_l(r)}, \quad (35)$$

which follows from the condition in (34). Here, the radius r was chosen in the asymptotic region $r > R_0$. Aberg *et al.* [16] used a similar procedure to describe protonic decays of spherical nuclei.

It should be noted that, even for modern supercomputers, the method of those studies leads to formidable difficulties because it is necessary to calculate the imaginary part of the energy, $\mathrm{Im}\varepsilon_{k_i}$, a quantity whose absolute value can prove to be 20 orders of magnitude less than the real part of the energy Q_{c_0}. However, this method can be simplified substantially without spoiling the accuracy of the calculations. To do this, it is sufficient to recall that, in the deep-subbarrier region for $R_0 \le r \le R_1$, the condition $G_l(r) \gg F_l(r)$ holds for all channels of the decay of the quasistationary state described by the wave function $f_k(\mathbf{r}', \boldsymbol{\sigma}')$. In the asymptotic condition (34), we can therefore discard the functions $F_l(r)$ and solve the corresponding problem for a stationary state that is described by the wave function $f^0_k(\mathbf{r}', \boldsymbol{\sigma}')$ and which has the real-valued energy Q_{c_0} by fitting the well depth as is described above and by using, for $R_0 \le r \le R_1$, the boundary condition

$$\chi^0_{jl}(r) = \sum_{jl}\sqrt{\frac{\tilde{\Gamma}^0_{jl}k^0_i}{Q_{c_0}}}\left(\frac{G_l(r)}{r}\right), \quad (36)$$

which is similar to (4).

Within this simplified approach, the partial decay width $\tilde{\Gamma}^0_{j_p l_p}$ can be calculated by the formula

$$\tilde{\Gamma}^0_{j_p l_p} = \frac{\hbar^2 k_{c_0}(\chi^0_{j_p l_p}(r))^2}{mG^2_{l_p}(r)}, \quad (37)$$

which is similar to the formulas of *R*-matrix theory.

It should be noted that the method used in [32–35] to calculate the shell-model wave functions $f^0_k(\mathbf{r}', \boldsymbol{\sigma}')$ corresponding to arbitrary real negative and positive (for subbarrier case) energies ε_{k_i} relies on the representation in (19) and on the coupling-channel method for determining the functions $\chi^0_{jl}(r)$ over a vast basis of the spin–orbit functions Φ_{jlk_i}. This makes it possible to improve considerably the accuracy in evaluating the functions $f^0_k(\mathbf{r}', \boldsymbol{\sigma}')$ in the surface region of the nucleus in relation to what is obtained by using a representation of the type in (20) with a set of shell-model spherical harmonics that are discrete in energy.

From the above, it can be concluded that, in contrast to the multiparticle theory of protonic decays [8, 9, 22–24], the methods that were developed in [16, 32–35] and which made it possible—albeit they involve extremely cumbersome calculations—to obtain some interesting results are approximate, as was indicated above in discussing the relationship between the widths Γ^0_{ipc} and $\tilde{\Gamma}^0_{j_p l_p}$ in the case of protonic transitions between the ground states of the parent and daughter nuclei. Hence, these methods are less accurate than the multiparticle theory of protonic decays and show little promise for extensions to the case of nondiagonal protonic decays.

5. PROTONIC DECAYS OF ODD–EVEN NUCLEI

With the aid of expressions (30)–(32), we can calculate the half-lives of odd–even deformed nuclei with respect to protonic decays, $T_{p1/2}$. Since these half-lives are highly sensitive both to values of the deformation parameter β_2 and to the type of proton orbitals, a comparison of the results of calculations for $T_{p1/2}$ with corresponding experimental data may furnish information about β_2 and about the structural features of the parent and the daughter nuclei.

The $T_{p1/2}$ values as computed in [8, 35] are in agreement with data on the ^{109}I nucleus at $\beta_2 = 0.14$ for the $(1/2)^+$ [420] proton orbital and with data on the ^{113}Cs nucleus at $\beta_2 = 0.1$–0.15 for the $(3/2)^+$ [421] proton orbital. In [34], it was shown that experimental data on ^{113}Cs can also be described by using the value of $\beta_2 = 0.12$ and the $(1/2)^+$ [420] proton orbital, for which the half-life $T_{p1/2}$ exhibits an anomalous dependence on the deformation parameter β_2. The β_2 values obtained from the aforementioned calculations comply well with the compilations presented in [19–21].

On the basis of these compilations, we can also expect sizable equilibrium deformations in the ^{147}Tm, ^{147m}Tm, and ^{151}Lu nuclei, which were first treated as spherical nuclei [3, 4]. For these nuclei, the experimental values of $T_{p1/2}$ were reproduced [24] at $\beta_2 = 0.1$–0.2, which is consistent with the compilation presented in [21]. The corresponding proton orbitals are $(7/2)^-$ [523] and $(7/2)^+$ [404] for the ^{147}Tm nucleus, $(1/2)^+$ [411] for the ^{147m}Tm nucleus, and $(7/2)^-$ [523] and $(7/2)^+$ [404] for the ^{151}Lu nucleus. It should be recalled that more recent compilations from [19, 20] predict sizable negative deformation parameters [$\beta_2 = -(0.15$–$0.25)$] for the ^{147}Tm, ^{150}Lu, and ^{151}Lu nuclei. In view of this, it would

be of interest to calculate anew the half-lives of these nuclei with respect to protonic decays under the assumption that they are oblate.

It was shown in [30–32, 35] that, at a deformation-parameter value of $\beta_2 \approx 0.3$, the $T_{p1/2}$ values calculated for the ^{131}Eu, ^{141}Ho, and ^{141m}Ho nuclei are compatible with relevant experimental data and with compilations presented in [19–21], the corresponding proton orbitals being $(3/2)^+$ [411] and $(5/2)^+$ [413], $(7/2)^-$ [523] and $(5/2)^-$ [532], and $(1/2)^+$ [411], respectively.

Thus, we can see that, for the deformation parameter β_2 in even–odd nuclei undergoing protonic decays, the values that are extracted from half-life calculations agree fairly well with the compilations presented in [19–21]. This indicates that, by and large, the basic concepts of modern nuclear physics are self-consistent.

6. FINE STRUCTURE OF PROTON SPECTRA

The problem of discovering the fine structure of the proton spectra is of extreme interest to experimenters investigating the protonic radioactivity of nuclei. (That such a structure can be observed was demonstrated in [38].) The point is that the protonic decay of a parent nucleus can result in the population of not only the ground state of the daughter nucleus but also its excited states. As a result, the spectrum of emitted protons involves several groups differing in energy. Of particular interest is the situation that arises in the protonic decay of an odd–even parent nucleus, in which case proton emission leads to the formation of an even–even daughter nucleus. If this nucleus is characterized by a sizable deformation—say, $\beta_2 \approx 0.3$—the spin–parity is $J_f^\pi = 0^+$ in its ground state and $J_f^\pi = 2^+$ in the first excited state. For $A \approx 140$ nuclei, the latter corresponds to the rotation of the nucleus as a discrete unit at a sufficiently low excitation energy of $\Delta E = E_{2^+} - E_{0^+} \approx 120$ keV. In this case, protonic transitions can occur, with a sizable probability, not only to the ground state of the daughter nucleus but also to its first excited state. Owing to this, the proton spectrum develops a second line corresponding to the emitted-proton energy E_p that differ from the energy of the main line by ΔE. From (14) and (15), it follows that the partial width $\Gamma_{ip0j_p^0l_p^0}$ with respect to protonic decay to the ground state of the daughter nucleus is related to fixed values of the total spin $j_p^0 = J_i = k_i$ and of the orbital angular momentum l_p^0 of the emitted proton whose parity coincides with the parity of the state of the emitted proton in the parent nucleus, the orbital-angular-momentum values corresponding to this parity being $l_p^0 = j_p^0 \pm 1/2 = k_i \pm 1/2$. As to the total width Γ_{ip2} with respect to protonic decay to the 2^+ state of the daughter nucleus, it is given by the sum $\Gamma_{ip2} = \sum_{j_pl_p} \Gamma_{ip2j_pl_p}$ of four partial widths $\Gamma_{ip2j_pl_p}$ corresponding to the following values of j_p and l_p: j_p^0, l_p^0; $j_p^0 + 1$, l_p^0; $j_p^0 + 1$, $l_p^0 + 2$; and $j_p^0 + 2$, $l_p^0 + 2$. On the basis of these data, we can find the branching fraction α_2 for protonic decays to the 2^+ state: $\alpha_2 = \Gamma_{ip2}/(\Gamma_{ip0} + \Gamma_{ip2})$. An especially favorable situation for protonic decay into the 2^+ state is realized under the condition that the contribution to the shell-model proton wave function $f_k(\mathbf{r}', \boldsymbol{\sigma}')$ (19) from the $j = j_p^0 + 1$, $l = l_p^0$ spherical component is much greater than the contribution from the $j = j_p^0$, $l = l_p^0$ spherical component. In this case, the main contribution to the width Γ_{ip2} comes from the partial width $\Gamma_{ip2j_p^0+1l_p^0}$, which is much greater than the partial width $\Gamma_{ip2j_p^0l_p^0}$. Such a situation is realized in the ^{131}Eu nucleus for the $(3/2)^+$ [411] protonic configuration since the squared coefficient $(a_{njl}^k)^2$ in the spherical-harmonic expansion (20) of its wave function is 0.04 for the $j = j_p^0$, $l = l_p^0$ $d_{3/2}$ state and 0.6 for the $j = j_p^0 + 1$, $l = l_p^0$ $d_{5/2}$ state. A still more interesting situation is realized for the $(5/2)^-$ [532] proton configuration in the ^{141}Ho nucleus, in which case $(a_{njl}^k)^2$ is close to zero for the $j = j_p^0$, $l = l_p^0$ $f_{5/2}$ state and is 0.13 for the $j = j_p^0 + 1$, $l = l_p^0$ $f_{7/2}$ state.

But in the case where the $l = l_p^0 + 2$ spherical configuration is dominant in the wave function (19), the enhancement of the partial amplitude $B_{ip2j_pl_p^0+2}$ (32) in relation to the amplitude $B_{ip0j_p^0l_p^0}$ is compensated by a substantial reduction of the amplitude of the radial Coulomb function $F_{l_p}(R)$ in the subbarrier region when l_p is changed from l_p^0 to $l_p^0 + 2$, so that the partial widths corresponding to $l = l_p^0 + 2$ do not contribute substantially to the width Γ_{ip2}. A similar situation is realized for the $(5/2)^+$ [413] proton orbital in the ^{131}Eu nucleus and for the $(7/2)^-$ [523] proton orbital in the ^{141}Ho nucleus.

The calculation of α_2 for ^{131}Eu protonic decay into the ground state of the daughter nucleus yields the values of $\alpha_2 = 0.25$ and 0.03 for, respectively, $(3/2)^+$ [411] and $(5/2)^+$ [413] odd-proton configurations (see [30–32, 35]). That the value of α_2 is sizable for the $(3/2)^+$ [411] configuration in the ^{131}Eu nucleus gives sufficient grounds to hope that a second proton line will be detected, which will furnish information about the energy ΔE and refine the odd-proton configuration in this nucleus.

Let us consider in greater detail the fine structure of the proton spectrum for the decay of the ^{141}Ho nucleus.

Table 1. Ratio $\alpha_2 = \Gamma_{2^+}/(\Gamma_{0^+} + \Gamma_{2^+})$ for transitions to the first excited state of the even–even nucleus ^{140}Dy in the protonic decays of the odd–odd nucleus ^{141}Ho versus the structure of the odd-proton orbital

p	$J_i = k_i$	J_f	j_p	l_p	$Z_{J_f j_p l_p}$	$\frac{\Gamma_{J_f j_p l_p}(Q_c)}{\Gamma_{0 j_p^0 l_p}(Q_{c0})}$	α_2, %
7/2⁻ [523]	7/2	0	$j_{p0} = 7/2$	3	0.125	1	
7/2⁻ [523]	7/2	2	7/2	3	0.29	0.11	10
5/2⁻ [532]	5/2	0	$j_{p0} = 5/2$	3	0.073	1	
5/2⁻ [532]	5/2	2	5/2	3	0.13	0.08	73
5/2⁻ [532]	5/2	2	7/2	3	0.13	2.54	

From Table 1, it can be seen that, for the $(7/2)^-$ [523] proton configuration of the parent nucleus, α_2 is equal to 0.1 if a value of 120 keV is used for the energy ΔE. This gives reason to hope that a second line in the proton spectrum can be detected. As to the $(5/2)^-$ [532] proton configuration of the same nucleus, the corresponding width Γ_{ip2} with respect to protonic decay to the 2^+ excited state of the daughter nucleus is 2.6 times as great as the width with respect to analogous decay to the ground state of this nucleus, in which case we have $\alpha_2 = 0.73$. The total width $\Gamma_{ip} = \Gamma_{ip0} + \Gamma_{ip2}$ with respect to the protonic decay of the ^{141}Ho nucleus then exceeds the width Γ_{ip0} with respect to its decay to the ground state of the daughter nucleus by a factor of 3.6. The calculated half-life $T_{p1/2}$ corresponding to Γ_{ip0} is 8 ms, which is twice as great as the value of $T_{p1/2} = 4$ ms, the ^{141}Ho half-life observed experimentally. If we consider that uncertainties in the computational scheme that are associated with the choice of specific form for the potential $V^0(\mathbf{r}', \boldsymbol{\sigma}')$ are estimated within a factor of two, it will become clear that so great a value obtained theoretically for Γ_{ip2} does not contradict experimental data. It would be interesting to continue detailed investigations of the shape of the proton spectrum for the ^{141}Ho nucleus.

Presently, the first experiments aimed at observing the fine structure of proton spectra have been completed at the Argonne National Laboratory (USA). Having accumulated vast statistics, the authors of [39] were able to reveal a second proton line in the spectrum of ^{131}Eu decay. They found that it is shifted by $\Delta E \approx 120$ keV with respect to the main line. Upon introducing corrections for the conditions of the experiment in question, the experimental result for α_2 proved to be 0.24 ± 0.05, which is in good agreement with the theoretical value of $\alpha_2 = 0.25$ derived in [39] for the $(3/2)^+$ [411] proton configuration. Thereby, the assumption that the shape of the ^{131}Eu nucleus deviates strongly from that of a sphere was confirmed, and the structure of the proton orbital was established; concurrently, it was demonstrated once again that the multiparticle theory of protonic decay is applicable to deformed nuclei.

Searches for the fine structure of proton spectra for strongly deformed nuclei such as the odd–even nucleus ^{141}Ho and the odd–odd nucleus ^{140}Ho are of great topical interest. Investigations along these lines could prove promising in this respect for Tm and Lu isotopes as well, where we can expect strong negative deformations of $\beta_2 \approx -(0.15–0.25)$ (see above).

7. PROTONIC DECAYS OF ODD–ODD DEFORMED NUCLEI

Let us now address the case of protonic decays of odd–odd deformed nuclei. In the strong-coupling approximation [36], the wave function of the ground state of an odd–odd nucleus can be represented in the form (21), where k_i takes two values—these are $(k_i)_1 = k_{ip} + k_{in}$ (k_{ip} and k_{in} are the positive definite projections of the total angular momenta of, respectively, the odd proton and the odd neutron onto the symmetry axis of the nucleus) with $\chi_{k_i} = \chi^p_{k_{ip}}\chi^n_{k_{in}}$ and $(k_i)_2 = k_{ip} - k_{in}$ with $\chi_{k_i} = \chi^p_{k_{ip}}\chi^n_{-k_{in}}$. For the $(k_i)_1$ and $(k_i)_2$ states, the Gallagher–Moszkovski rule [40] says that, of these two, that in which the projection of the spin of the odd proton onto the z axis is parallel to the analogous projection of the odd-neutron spin has the lower energy. This rule is not fulfilled only for the $(k_i)_2^{\pi_i} = 0^-$ state.

The wave function of states belonging to the ground-state rotational band of the even–odd daughter nucleus can also be represented in the form (21), but we must replace there k_i by $+k_{in}$ and χ_{k_i} by $\chi_0^{fp}\chi^n_{k_{in}}$ for the case of the parent nucleus in the $(k_i)_1 = k_{ip} + k_{in}$ state and k_i by $-k_{in}$ and χ_{k_i} by $\chi_0^{fp}\chi^n_{-k_{in}}$ for the case of the parent nucleus in the $(k_i)_2 = k_{ip} - k_{in}$ state.

Further, we can make use of the technique developed above for describing the protonic decay of odd–even nuclei. Within this framework, the partial width with respect to the protonic decay of an odd–odd nucleus can be represented in the form (33), where the proton spectroscopic factor Z_{ipc} is given by

$$Z_{ipc} = \frac{\hat{J}_f}{\hat{J}_i}(C^{J_i k_i}_{J_f j_p k_f k_{ip}})^2 (u^f_{k_{ip}})^2 \qquad (38)$$

Table 2. Ratio δ of the protonic-decay half-lives of the ^{140}Ho and ^{141}Ho nuclei versus the structure of the odd-proton orbital and the odd-neutron orbital in the ^{140}Ho nucleus

p	n	$J_i = k_i$	$J_f = k_{ni}$	j_p, l_p	δ^{theor}	δ^{expt}
$7/2^-$ [523]	$9/2^-$ [514]	8^+	9/2	7/2, 3	2.26–5.53	0.75–2.25
$7/2^-$ [523]	$5/2^+$ [402]	6^-	5/2	7/2, 3	2.9–7.1	0.75–2.25
$5/2^-$ [532]	$9/2^-$ [514]	7^+	9/2	7/2, 3	0.76–1.88	0.75–2.25
$5/2^-$ [532]	$5/2^+$ [402]	5^-	5/2	7/2, 3	0.92–2.27	0.75–2.25

for two possible sets of k_i and k_f values: (i) $(k_i)_1 = k_{ip} + k_{in}$ and $(k_f)_1 = k_{in}$; (ii) $(k_i)_2 = k_{ip} - k_{in}$ and $(k_f)_2 = -k_{in}$. For the protonic transitions between the ground states of the odd–odd parent nucleus and even–odd daughter nucleus, in which case $J_i = |k_i|$ and $J_f = |k_f|$, it follows from the properties of the Clebsch–Gordan coefficient in (38) that the total angular momentum of the emitted proton, j_p, satisfies the following conditions: (i) $k_{ip} \le j_p \le k_{ip} + 2k_{in}$ for the first set of k_i and k_f values; (ii) $k_{ip} \le j_p \le -k_{ip} + 2k_{in}$ if $k_{ip} \le k_{in}$ and $j_p = k_{ip}$ if $k_{ip} \ge k_{in}$ for the second set of k_i and k_f values. A comparison with the case of protonic transitions from the ground states of odd–even deformed nuclei to the ground states of even–even daughter nuclei, where the selection rule $j_p = k_{ip}$ follows from equation (31), shows that, although the odd neutron plays the role of a spectator in the transition being considered, its state can affect the decay width of the odd–odd nucleus through the law requiring the conservation of the total spin of the system.

By using equations (33) and (38) and the Gallagher–Moszkovski rule, we will now analyze the protonic decay of the odd–odd nucleus ^{140}Ho, for which the values of $T_{p1/2} = 6 \pm 3$ ms and $E_p = 1086 \pm 10$ keV for, respectively, the half-life and the emitted-proton energy are known from experiments [20, 21]. Concurrently, we will compare the features of this decay with those of the protonic decay of the odd–even nucleus ^{141}Ho, for which the experimental values of the half-life and of the emitted-proton energy are, respectively, $T_{p1/2} = 3.9 \pm 0.5$ ms and $E_p = 1169 \pm 8$ keV [20, 21]. In Table 2, the calculated values of the ratio $\delta = T_{p1/2}(^{141}\text{Ho})/T_{p1/2}(^{140}\text{Ho})$ for ^{140}Ho and ^{141}Ho half-lives are displayed for the case of the $(7/2)^-$ [523] and $(5/2)^-$ [532] odd-proton configurations, which were established in studying the protonic decay of the ^{141}Ho nucleus. In these calculations, the $(9/2)^-$ [514] and $(5/2)^+$ [402] orbitals occurring near the Fermi surface were used for the odd proton in the ^{140}Ho nucleus [31] at the deformation-parameter value of $\beta_2 \approx 0.3$, which was also fixed in analyzing the protonic decay of the ^{141}Ho nucleus. Uncertainties in the δ values are associated with the errors in the measured energies of protons emitted from ^{140}Ho and ^{141}Ho decays, as well as with the errors in the measured half-life of the ^{140}Ho nucleus. It can be seen from Table 2 that, for the $(7/2)^-$ [523] proton configuration, the admissible interval of theoretical δ values only borders on the upper boundary of the corresponding experimental interval. At the same time, the intervals of the experimental and theoretical δ values overlap almost completely for the $(5/2)^-$ [532] proton configuration, which leads to a substantial contribution to the protonic-decay width of the ^{141}Ho nucleus from transitions to the first excited state of the daughter nucleus (see above). At the same time, either of the $(9/2)^-$ [514] and $(5/2)^+$ [402] neutron configurations is consistent with experimental data.

In the future, I am going to continue the calculation of protonic-decay half-lives for odd–odd nuclei, especially for the cases where there are sizable deviations from a spherical shape.

8. CONCLUSION

A comparison of various approaches to describing the protonic decays of nuclei that has been presented above confirms the viability of the multiparticle theory of protonic radioactivity and demonstrates the potential of this theory in determining the deformation parameters of odd–even and odd–odd nuclei capable of undergoing protonic decays, as well as in establishing the fine structure of proton spectra for such nuclei. That the deformation parameters as extracted from the analysis of the protonic decays of deformed nuclei occurring in the vicinity of the proton drip line are similar to those parameters predicted by modern compilations indicates that the fundamental concepts of modern nuclear physics are self-consistent.

ACKNOWLEDGMENTS

This work was supported in part by the Russian Foundation for Basic Research (project no. 99-02-16546).

REFERENCES

1. P. J. Woods and C. N. Davids, Annu. Rev. Nucl. Part. Sci. **47**, 541 (1997).
2. B. S. Dzhelepov, Izv. Akad. Nauk SSSR, Ser. Fiz. **15**, 496 (1951).
3. S. Hofmann *et al.*, Z. Phys. A **305**, 111 (1982).
4. O. Klepper *et al.*, Z. Phys. A **305**, 125 (1982).
5. W. F. Feix and E. R. Hilf, Phys. Lett. B **120**, 14 (1983).
6. T. Faestermann *et al.*, Phys. Lett. B **137**, 23 (1984).
7. L. K. Peker *et al.*, Phys. Lett. B **36**, 6 (1971).

8. V. P. Bugrov, S. G. Kadmensky, V. I. Furman, *et al.*, Yad. Fiz. **41**, 1123 (1985) [Sov. J. Nucl. Phys. **41**, 717 (1985)].
9. V. P. Bugrov, V. E. Bunakov, S. G. Kadmensky, *et al.*, Yad. Fiz. **42**, 57 (1985) [Sov. J. Nucl. Phys. **42**, 34 (1985)].
10. S. G. Kadmensky and V. E. Kalechits, Yad. Fiz. **12**, 70 (1970) [Sov. J. Nucl. Phys. **12**, 37 (1970)].
11. S. G. Kadmensky, V. E. Kalechits, and A. A. Martynov, Yad. Fiz. **14**, 1174 (1971) [Sov. J. Nucl. Phys. **14**, 654 (1971)].
12. S. G. Kadmensky and V. G. Khlebostroev, Yad. Fiz. **18**, 980 (1973) [Sov. J. Nucl. Phys. **18**, 505 (1973)].
13. S. G. Kadmensky, V. E. Kalechits, and A. A. Martynov, Yad. Fiz. **16**, 717 (1972) [Sov. J. Nucl. Phys. **16**, 400 (1972)].
14. S. G. Kadmensky, Z. Phys. A **312**, 113 (1983).
15. S. G. Kadmensky and V. I. Furman, *Alpha Decay and Related Nuclear Reactions* (Énergoatomizdat, Moscow, 1985).
16. S. Aberg, P. B. Semmes, and W. Nazarevicz, Phys. Rev. B **56**, 1762 (1997).
17. J. Cerny *et al.*, Phys. Lett. B **33**, 281 (1970).
18. S. Hofmann, Preprint No. GSI 87-30 (Darmstadt, 1987).
19. S. Liran and N. Zeldes, At. Data Nucl. Data Tables **17**, 1 (1976).
20. P. Moller *et al.*, At. Data Nucl. Data Tables **59**, 185 (1995).
21. R. Bengtsson *et al.*, Phys. Scr. **28**, 402 (1984).
22. V. P. Bugrov and S. G. Kadmensky, Yad. Fiz. **49**, 1562 (1989) [Sov. J. Nucl. Phys. **49**, 967 (1989)].
23. D. D. Bogdanov, V. P. Bugrov, and S. G. Kadmensky, Yad. Fiz. **52**, 358 (1990) [Sov. J. Nucl. Phys. **52**, 229 (1990)].
24. S. G. Kadmensky and V. P. Bugrov, Yad. Fiz. **59**, 424 (1996) [Phys. At. Nucl. **59**, 399 (1996)].
25. S. G. Kadmensky, V. E. Kalechits, and A. A. Martynov, Yad. Fiz. **14**, 343 (1971) [Sov. J. Nucl. Phys. **14**, 193 (1971)].
26. S. G. Kadmensky and S. D. Kurgalin, Izv. Akad. Nauk SSSR, Ser. Fiz. **44**, 1955 (1980).
27. S. G. Kadmensky, S. D. Kurgalin, and V. I. Furman, Yad. Fiz. **49**, 1562 (1989) [Sov. J. Nucl. Phys. **49**, 967 (1989)].
28. H. J. Mang and J. O. Rasmussen, Mat. Fys. Medd. K. Dan. Vidensk. Selsk. **2** (3) (1962).
29. O. Fromen, Mat. Fys. Medd. K. Dan. Vidensk. Selsk. **1** (3) (1957).
30. C. N. Davids *et al.*, Phys. Rev. Lett. **80**, 1849 (1998).
31. J. C. Batchelder, C. R. Bingham, *et al.*, ENAM-98 (Woodbury, New York, 1998), p. 264.
32. K. Rykaczevski, J. C. Batchelder, *et al.*, Preprint Oak-Ridge Nat. Lab. Phys. and Astron., Feb. 16, 1999.
33. E. Maglione, R. J. Liotta, and T. Vertse, Nucl. Phys. A **584**, 13 (1995).
34. E. Maglione, L. S. Ferreira, and R. J. Liotta, Phys. Rev. Lett. **81**, 538 (1998).
35. E. Maglione, L. S. Ferreira, and R. J. Liotta, Phys. Rev. C **59**, 589 (1999).
36. A. Bohr and B. R. Mottelson, *Nuclear Structure* (Benjamin, New York, 1969, 1975; Mir, Moscow, 1971, 1977), Vols. 1, 2.
37. V. G. Soloviev, *Theory of Atomic Nucleus* (Énergoatomizdat, Moscow, 1981).
38. S. G. Kadmensky, ENAM-98 (Woodbury, New York, 1998), p. 672.
39. A. A. Sonzogni, C. N. Davids, *et al.*, Preprint No. PHY-9348-H1-99 (Argonne Nat. Lab., 1999).
40. G. J. Gallagher and S. A. Moszkovski, Phys. Rev. **111**, 1282 (1958).

Translated by A. Isaakyan

Physics of Atomic Nuclei, Vol. 63, No. 4, 2000, pp. 562–569. Translated from Yadernaya Fizika, Vol. 63, No. 4, 2000, pp. 625–632.

NUCLEI
Experiment

Elastic Scattering of ^{3}He Nuclei on ^{13}C Nuclei at 50 and 60 MeV and *V–W* Ambiguity in Choosing Optical Potentials

N. Burtebaev[1)], A. Duĭsebaev[1)], B. A. Duĭsebaev[1)], and S. B. Sakuta*

Russian Research Centre Kurchatov Institute, pl. Kurchatova 1, Moscow, 123182 Russia

Received April 15, 1999

Abstract—At energies of 50 and 60 MeV, the elastic scattering of ^{3}He nuclei on ^{13}C nuclei is investigated at laboratory angles in the range 10°–170°. The measured differential cross sections are analyzed on the basis of the optical model of the nucleus by using Woods–Saxon potentials, including both volume and surface absorption. The potential parameters are determined by fitting the computed cross sections to experimental data. It is found that, even in the region of sensitivity, the values of the real and imaginary parts of the potentials (*V* and *W*, respectively) show considerable scatter, with extreme values differing by a factor greater than two. This scatter is explained by the existence of a *V–W* ambiguity in choosing optical potentials. © *2000 MAIK "Nauka/Interperiodica".*

1. INTRODUCTION

Two types of scattering that represent the extreme cases of the same process—diffractive scattering and rainbowlike scattering—can be singled out at energies above the Coulomb barrier, in which case nuclear forces play the most important role. As is well known, the type of scattering depends on the effect of absorption in it. By way of example, we indicate that, in the case of strong absorption—this is realized most often in heavy-ion collisions—scattering shows virtually no sensitivity to the behavior of the real potential within the nucleus involved, so that the cross-section value is affected by quite a few partial waves corresponding to peripheral collisions. In this case, the observed angular distributions are well described by a diffraction at an absorbing sphere—they show a pronounced oscillating structure covering the entire range of angles. A determination of the real part of the potential from such experimental data is highly ambiguous; that is, any potential capable of reproducing phase-shift values for a limited set of partial waves is appropriate for describing angular distributions. Under certain constraints imposed on the imaginary part of the potential, the ambiguity in choosing its real part manifests itself in the discrete form as well.

In the weak-absorption case, which is usually realized for light projectiles at sufficiently high energies, the character of scattering is totally different. Oscillations observed at small angles give way to a broad maximum at larger angles, which is followed by a sharp exponential fall. It was shown in [1] for the first time that this behavior of the cross sections is associated with refractive properties of the potential and with the existence of the angle of maximal deflection in the attractive nuclear field, a feature peculiar to rainbow scattering. The observed rainbowlike structure corresponds to small impact-parameter values. This suggests a sufficiently high nuclear transparency and, hence, a sensitivity of cross sections to the real interaction potential at small distances. By analyzing elastic alpha-particle scattering measured over a wide angular range, Goldberg and Smith [1] and Goldberg *et al.* [2] were able to show that, in the case of a rainbowlike angular distribution, the problem of a discrete ambiguity in choosing the real part of the optical potential can indeed be removed. This conclusion was confirmed by numerous subsequent investigations. We note, however, that investigations leading to this conclusion relied on standard Woods–Saxon potentials featuring volume absorption, which fix rather tightly the radial dependence of the imaginary part of the potential. At the same time, it has long since been known that there is a strong correlation between the real (*V*) and imaginary (*W*) parts of the potential. We mean here that changes in the real part can be compensated by the corresponding changes in the imaginary part (and vice versa) without spoiling the quality of description of experimental cross sections.

A strong correlation between the parameters of the real and imaginary parts of the potential was discovered in [3]. There, an analysis of a conventional Woods–Saxon potential describing the scattering of 50.5-MeV alpha particles on ^{64}Zn nuclei revealed that by no means are the factors $K_{a_V r_{0W}}$ and $K_{a_V a_W}$ measuring the correlation between the parameters of its real and imaginary parts less than the factor $K_{V r_{0V}}$, which is responsible for the well-known continuous ambiguity in determining the real part of the potential.

[1)] Institute of Nuclear Physics, National Nuclear Center of Republic of Kazakhstan, Almaty, 480082 Republic of Kazakhstan.
* e-mail: sakuta@dni.polyn.kiae.su

1063-7788/00/6304-0562$20.00 © 2000 MAIK "Nauka/Interperiodica"

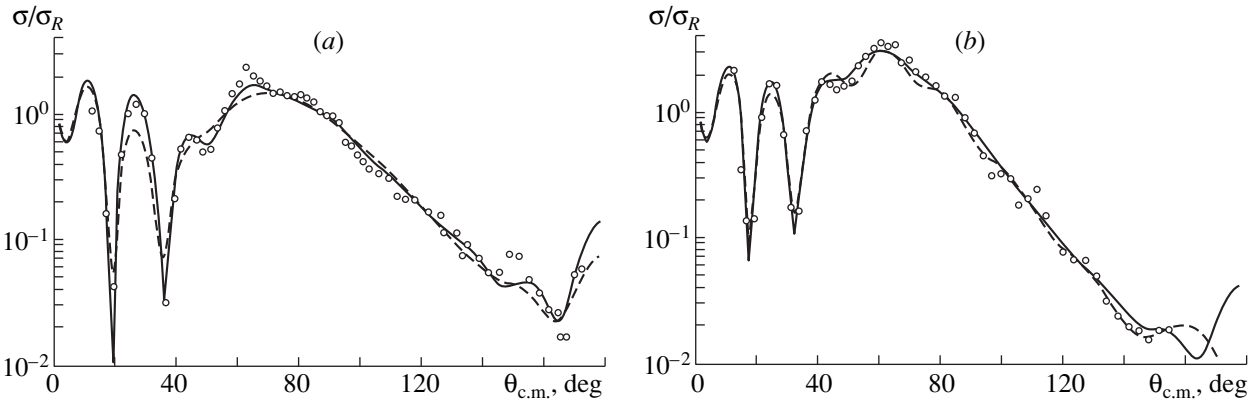

Fig. 1. Differential cross sections for the elastic scattering of (*a*) 50- and (*b*) 60-MeV ^{3}He nuclei on ^{13}C nuclei. The solid and dashed curves represent the results of the optical-model calculations with potentials nos. 1 and 5 (Tables 1, 2), respectively.

The interrelation between the shapes of *V* and *W* was found by Freindl *et al.* [4] in describing the scattering of 40- and 99.5-MeV alpha particles on a ^{90}Zr nucleus. On this basis, they arrived at the conclusion that, in the optical model, there exists an ambiguity of a new type.

In a model-independent analysis of alpha-particle scattering on ^{50}Ti nuclei, Roberson [5] was unable to find a clear-cut χ^2 minimum in fitting the depth of the real part of a potential belonging to a family characterized by the volume integral of $J_V/4A \sim 300$ MeV fm^3, because variations in the real part of the potential could be compensated by the corresponding changes in its imaginary part.

Brandan *et al.* [6], who analyzed the angular distributions of elastic ^{12}C + ^{12}C and ^{12}C + ^{16}O scattering at a few hundred MeV, showed that, even in the case of conventional Woods–Saxon potentials, whose real and imaginary parts have strongly different geometric characteristics, there arises a new type of discrete ambiguities.

The latest investigations of the *V*–*W* correlations were performed in [7–9] on the basis of data on the elastic scattering of 40- and 72-MeV ^{3}He nuclei on ^{12}C, ^{13}C, and ^{14}C nuclei. These investigations, which employed potentials featuring both volume and surface absorption, revealed that, despite the manifestation of effects associated with nuclear rainbow scattering, a discrete ambiguity in choosing the real part of the potential still remains. Specifically, three potential families characterized by volume-integral values of about 200, 300, and 400 MeV fm^3 were found to describe the experimental cross sections equally well.

Thus, a correlation between the real and imaginary parts of the potential leads to ambiguities in their determination even when a nuclear rainbow is observed, in which case differential cross sections are sensitive to the interaction at small distances. In this context, investigations of the *V*–*W* correlation gains in importance, especially in the case where data from a phenomenological analysis of elastic scattering are used to deduce information about the distribution of nuclear matter or about the matter radii of nuclei.

In the present article, we report on an investigation of the elastic scattering of 50- and 60-MeV ^{3}He nuclei on ^{13}C nuclei. The corresponding differential cross sections measured in a full angular interval are analyzed within the optical model of the nucleus by using Woods–Saxon potentials that involve both volume and surface absorption. The main objective of our analysis is to deduce information about the correlations between the radial dependences of the real and imaginary parts of the optical potentials.

2. EXPERIMENTAL PROCEDURE

Our experiment was conducted in ^{3}He beams extracted from the isochronous cyclotron installed at the Institute of Nuclear Physics, National Nuclear Center (Republic of Kazakhstan). The energies of the accelerated ions were 50 and 60 MeV. For a target, we used a self-supporting carbon film of thickness 1.2 mg/cm^2 enriched in the ^{13}C isotope to 86%. Charged reaction products were recorded by a ΔE–E telescope of silicon counters whose thicknesses were about 100 μm for ΔE and 2 mm for E. The particles were identified via a computer-aided two-dimensional analysis. The total energy resolution was 500–600 keV; it was determined primarily by the energy spread in the beam and by the target thickness. The differential cross sections for elastic scattering were measured for laboratory angles in the range 10°–170° for $E_{^3\mathrm{He}} = 50$ MeV and for laboratory angles in the range 10°–150° for $E_{^3\mathrm{He}} = 60$ MeV. The absolute error of the measurements was about 10–15%, while the statistical error did not exceed 5%.

3. ANALYSIS OF EXPERIMENTAL RESULTS AND DISCUSSION

Figure 1 shows the angular distributions for the elastic scattering of 50- and 60-MeV ^{3}He nuclei on ^{13}C

Table 1. Potential parameters found from an analysis of the elastic scattering of 50-MeV ^{3}He nuclei on ^{13}C nuclei

no.	$-V$, MeV	r_V, fm	a_V, fm	$-W$, MeV	r_W, fm	a_W, fm	W_D, MeV	r_D, fm	a_D, fm
1	126.6	1.00	0.82				13.39	1.21	0.92
2	159.4	0.78	0.86	1.53	1.32	0.03	12.29	1.05	1.06
3	136.5	0.97	0.82	1.75	1.10	0.35	12.76	1.37	0.82
4	105.8	1.12	0.71	12.22	1.780	0.97	4.09	1.33	0.50
5	149.3	0.76	0.83	5.44	2.31	0.95	8.94	1.08	0.47
6	118.6	1.0	0.73	4.10	2.36	0.95	10.02	1.24	0.58
7	106.2	1.15	0.74	6.00	2.15	0.90	9.43	1.43	0.47
8	106.7	1.19	0.77	1.39	1.33	0.57	14.65	1.42	0.70

no.	V_{so}, MeV	r_{so}, fm	a_{so}, fm	$J_V/3A$, MeV fm^3	$J_I/3A$, MeV fm^3	χ^2/N
1	2.98	1.45	0.58	390	171	4.6
2	5.00	1.29	0.85	335	170	4.6
3	0.12	1.18	0.89	394	174	5.8
4	0.23	1.67	0.84	355	174	9.2
5	5.18	1.25	0.87	288	160	7.2
6	5.39	1.25	0.91	322	170	7.8
7	3.57	1.25	0.65	392	178	5.6
8	3.35	1.45	0.54	439	176	8.0

nuclei. These distributions exemplify manifestations of effects associated with nuclear rainbow scattering. The region of Fraunhofer oscillations at small angles (less than 50°) is followed successively by a broad maximum around 60° and then by an exponential fall. A comparison with data obtained in [7, 8] at energies of 40 and 72 MeV reveals that the position of this maximum varies in inverse proportion to energy: $\theta \sim 1/E$. This dependence is peculiar to rainbow scattering [10].

The angular distributions in question were computed within the optical model of the nucleus as implemented on the basis of SPI-GENOA code [11]. In addition to volume absorption, the optical potentials used involved surface absorption and a spin–orbit term; that is,

$$U(r) = V f_V(r) + i\left(W f_W(r) + 4a_D W_D \frac{d f_D(r)}{dr}\right)$$

$$+ V_{so}\left(\frac{h}{m_\pi c}\right)^2 \frac{1}{r}\frac{d}{dr} f_{so}(r)(L\sigma) + V_{Coul}(r),$$

where $f_i(r) = [1 + \exp(r - r_i A^{1/3})/a_i]^{-1}$ is the Woods–Saxon form factor, while $V_{Coul}(r)$ is the Coulomb potential of a uniformly charged sphere of radius $R_{Coul} = 1.3A^{1/3}$ fm.

The potential parameters were determined by fitting the theoretical cross sections to experimental values. For an input potential, we took that from the study of Trost *et al.* [12], who proposed empirical expressions for the central potential involving purely surface absorption, the parameters of this potential being dependent on the ^{3}He energy and on the target-nucleus mass. The potential in question describes well ^{3}He scattering on nuclei from beryllium to lead in the energy range between 10 and 220 MeV. Other input parameter values were borrowed from [8, 9]. The results of fitting via a χ^2 minimization are quoted in Tables 1 and 2. For each energy value, we obtained eight potentials describing experimental data equally well. Some examples of the resulting description are displayed in Fig. 1. As can be seen from the tables, the volume integrals of the real parts of the potential (J_V) per pair of interacting particles show a considerable scatter, from 200 to 430 MeV fm^3. As to the analogous integrals for the imaginary part ($J_I = J_W + J_D$), they change only slightly. By way of example, we indicate that $J_I = 172 \pm 7$ MeV fm^3 at 50 MeV and $J_I = 153 \pm 13$ MeV fm^3 at 60 MeV.

With an eye to the ensuing discussion, it is advisable to specify the regions where the results show the highest sensitivity to the real and imaginary parts of the potential. For this purpose, we performed a series of calculations with potential no. 6 from Table 2. The values of this potential were specified on a grid of radii with a step of 0.1 fm. For the potentials $V(r)$ and $W(r)$, we determined intervals such that no more than 20% changes could be induced in χ^2/N by variations in the potentials within these intervals, established individually for each point lying between 0 and 7.5 fm. The resulting ratios V'/V and W'/W versus r are displayed in Fig. 2*a*. It can be seen that the region of the highest sensitivity to the real potential is between 0.5 and 5 fm. For the imaginary part, it is somewhat narrower, occurring between 2.5 and 5.5 fm. The calculations reveal that, in region of sensitivity, changing $V(r)$ and $W(r)$ by about

Table 2. Potential parameters found from an analysis of the elastic scattering of 60-MeV ^{3}He nuclei on ^{13}C nuclei

no.	$-V$, MeV	r_V, fm	a_V, fm	$-W$, MeV	r_W, fm	a_W, fm	W_D, MeV	r_D, fm	a_D, fm
1	135.6	0.95	0.84				13.85	1.26	0.80
2	127.7	0.80	0.78	0.45	1.52	0.04	11.93	1.00	1.04
3	136.9	0.97	0.82	7.43	1.10	0.35	12.24	1.39	0.72
4	111.5	1.08	0.72	7.26	1.83	0.95	8.50	1.29	0.58
5	142.6	0.67	0.81	3.95	2.58	0.42	6.35	1.10	0.48
6	113.0	1.06	0.73	4.28	2.23	0.84	13.43	1.17	0.48
7	109.5	1.15	0.74	3.38	2.29	0.73	13.32	1.43	0.47
8	112.0	1.15	0.78	2.33	1.33	0.26	14.59	1.39	0.69

no.	V_{so}, MeV	r_{so}, fm	a_{so}, fm	$J_V/3A$, MeV fm^3	$J_I/3A$, MeV fm^3	χ^2/N
1	2.75	1.29	0.58	390	156	3.5
2	18.20	0.65	1.16	245	147	6.7
3	0.09	1.76	0.89	395	158	4.4
4	2.23	1.69	0.80	350	157	4.5
5	6.84	0.38	1.24	215	128	3.0
6	3.98	1.48	0.89	344	153	6.1
7	2.18	1.15	0.56	404	166	3.4
8	2.62	1.39	0.56	433	166	5.3

10% only at one point increases χ^2/N by 20%. In the central and the peripheral region, only a more than two-fold change in the potential values can generate a similar growth of χ^2.

The real and imaginary parts of the resulting potentials from Table 2 are displayed in Fig. 2*b*. It can be seen that, even in the region of the highest sensitivity, the extreme values of $V(r)$ differ by a factor greater than two. The scatter decreases for $r < 2.0$ exclusively—that is, in the region where the imaginary part of the potential affects insignificantly cross-section values—and only there can we deem that the potential is determined almost unambiguously. In the overlap of regions of the highest sensitivity to V and W, the imaginary parts of the potentials also differ significantly. Only in the region of values that exceed somewhat 5 fm and which are close to the strong-absorption radius, where V has a less pronounced effect on cross-section values, are they close, which ensures the identity of the diffraction structure for all potentials found here. In all probability, this is reason why the volume integrals of the imaginary parts of the potentials have a comparatively small scatter, so that they can be determined quite reliably from scattering data (see above). All that was said here in connection with the data in Fig. 2 applies equally well to the potentials from Table 1.

A considerable scatter of the V and W values in the region of the highest sensitivity can be explained by the interrelation between the potentials V and W, which makes it possible to compensate even quite sizable changes in the real part by the corresponding changes in the imaginary part (and vice versa) without changing the computed cross sections. Figure 3*a*, which displays the values of V and W at a radius of 4 fm, provides a good illustration of the V–W interrelation. From this figure, it can be seen that the real and the imaginary part of each potential from Tables 1 and 2 are related as $V(r = 4\text{ fm}) \simeq 1.5W(r = 4\text{ fm})$. The relation between V and W holds in the region $r = 2.5$–5 fm, as is suggested by close radial dependences of the ratio V/W for the potentials from Tables 1 and 2 (see Fig. 3*b*, where these dependences are depicted for the case of $E_{^3\text{He}} = 50$ MeV). Figure 3*b* shows that, over the interval $r = 2.5$–5 fm, the mean value of the ratio in question changes smoothly from 4 to 1.

Although all the potentials found here reproduce experimental data equally well, the scattering matrices corresponding to them can differ strongly. By way of example, the complex scattering-matrix elements (S_l) associated with potentials no. 2, 3, and 5 from Table 2 are displayed in Fig. 4 for partial waves making the largest contributions to the cross section. As can be seen from this figure, the potentials in question do not yield identical phase shifts; hence, they do not belong to families associated with conventional discrete and continuous ambiguities. It is well known that potentials from those families are nearly phase-equivalent ones.

In order to answer the question of whether there is some degree of ambiguity—and to assess this degree, if any—in extracting the volume integrals of the real part of the potential from scattering data, we performed more detailed calculations in which we studied the quality of fitting versus J_V. These calculations were per-

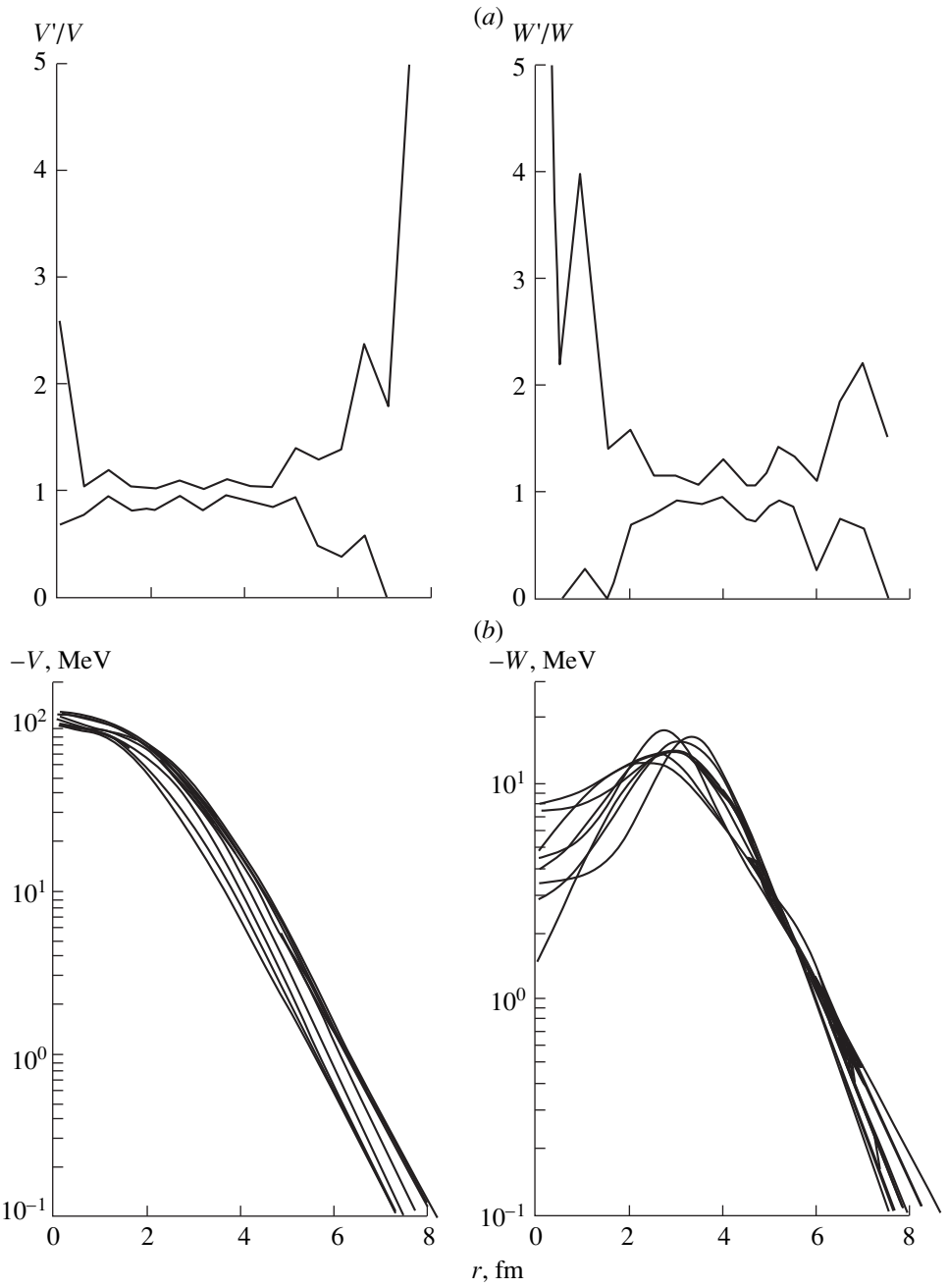

Fig. 2. (*a*) Relative changes that must be introduced in the real and the imaginary part of the potential at r in order that χ^2 grow by 20%. (*b*) Radial dependences of the real and imaginary parts of the potentials found at E = 60 MeV (Table 2).

formed for a grid of fixed radii in the vicinity of their tabular values for each potential from Table 2. The remaining parameters, with the exception of the parameters of the spin–orbit interaction, were sought by fitting the cross sections calculated theoretically to the corresponding experimental values. Since the spin–orbit component is operative only at the largest angles, it was sufficient to perform fitting within 120° in order to eliminate its effect on the results of our analysis. The resulting dependence of χ^2/N on J_V is illustrated in Fig. 5. Naturally, this is not the only possible dependence of this type—as a matter of fact, it is determined by the input values of the potentials and by the procedure of searches itself. The calculations only indicate that a satisfactory description of the experimental data in question can be obtained at almost any value of J_V from the interval 200–450 MeV fm^3. Thus, the volume integral of the real part of the optical potential cannot be determined unambiguously from scattering data without imposing additional constraints on the poten-

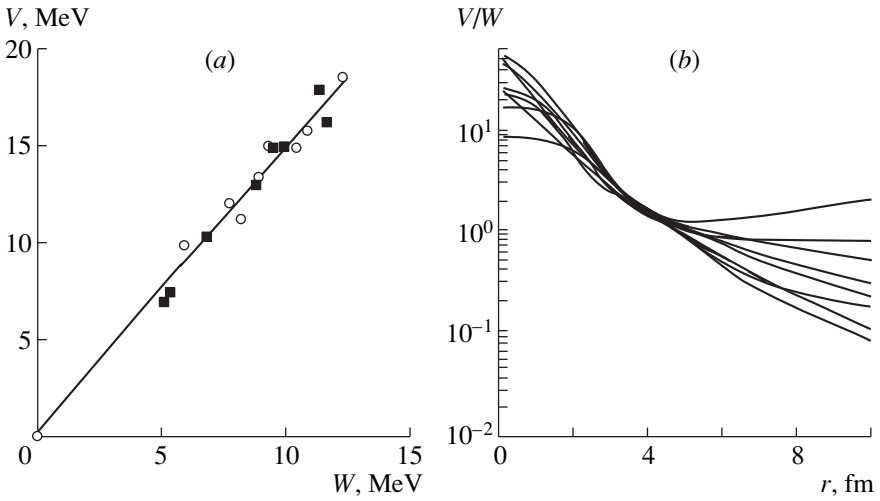

Fig. 3. (*a*) Values found for the optical potentials at $r = 4$ fm for the energy values of E = (○) 50 and (■) 60 MeV. (*b*) Radial dependence of the ratio $V(r)/W(r)$ at an energy of 50 MeV.

tial parameters. By no means do relatively higher values of χ^2/N for potentials with $J_V \simeq 250$–300 MeV fm^3 imply that, among other potentials having J_V values in this range, there are none that describe angular distributions. In support of this, we note that, at an energy of 50 MeV, there are potentials with $J_V \simeq 290$ and 320 MeV fm^3 (see Table 1) that provide quite a satisfactory description.

Our analysis confirms that the special features of angular distributions are explained by nuclear-rainbow effects. Indeed, it can be shown that, for all potentials, classical deflection functions yield limiting angles less than 180°. For an energy of 60 MeV, they lie in the range 80°–100°. Since the rainbow bump observed in the angular distribution is due to the refraction properties of the nuclear potential—that is, to its real part—this bump must be reproduced in the far cross-section component corresponding to scattering at negative angles on the far edge of the nucleus under the effect of the nuclear attractive field [13]. The expansion of the cross section into the far and the near component is shown in Fig. 6 for potential no. 5 from Table 2. It can be seen that the far component makes a dominant contribution to the cross section in the angular range between 40° and 100°, completely saturating the maximum in the vicinity of 60°. The oscillating structure at small angles results from the interference of the amplitudes of the far and the near component. The calculation for the far component with zero imaginary part clarifies the pattern still further, demonstrating that the maximum proper and the fall that follows it are due to the refracting properties of the nuclear field and that absorption leads only to an overall reduction of the cross sections. The analogous calculation with potential no. 8—the results of this calculation are shown by the dashed curve in Fig. 6—leads to strongly different cross sections. For this potential, the classical angle of the maximal deflection θ_R is shifted toward larger angles by 20°. Nonetheless, an appropriate choice of

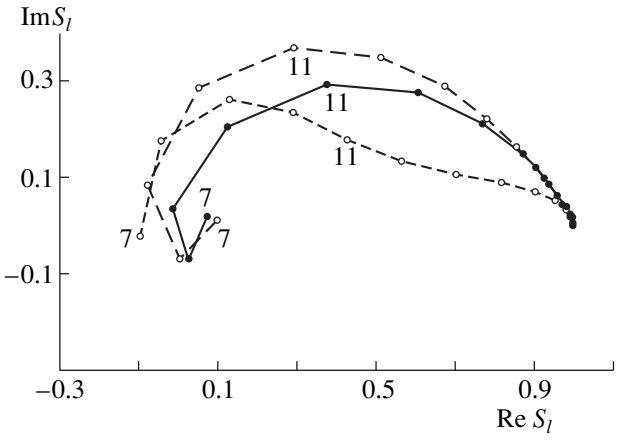

Fig. 4. Complex elements of the scattering matrix for potentials nos. 2, 3, and 5 from Table 2. The figures on the curves indicate the angular momenta of contributing partial waves.

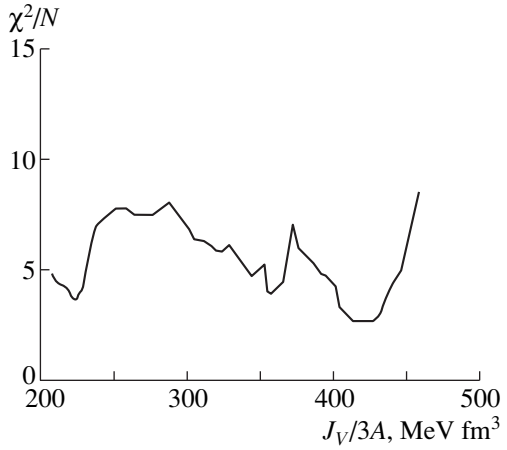

Fig. 5. χ^2/N as a function of the volume integral of the real part of the potential.

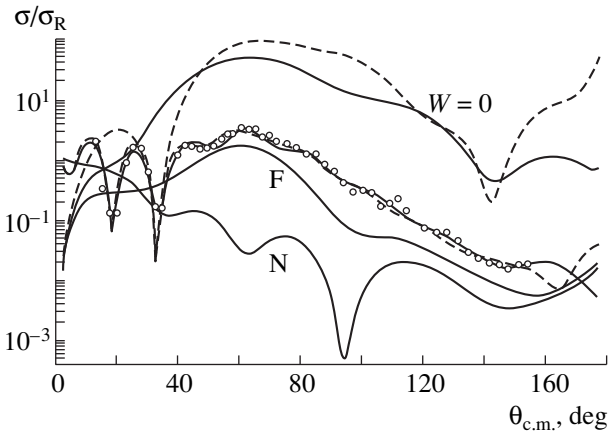

Fig. 6. Ratio of the differential cross section for the elastic scattering of 60-MeV ^{3}He nuclei on ^{13}C nuclei to the corresponding Rutherford cross section: (solid curves) results based on the optical model with potential no. 5 from Table 2; (dashed curves) results obtained with potential no. 8; (curves labeled with uppercase F and N) results for, respectively, the far and the near component of the cross section; (two upper curves) results for the far components of the cross section at $W = 0$.

the imaginary part of the potential compensates for this distinction to such an extent that the calculated angular distributions are virtually indiscernible up to an angle of 160°.

Thus, we conclude that, despite the observation of a distinct rainbow in the scattering of 50- and 60-MeV ^{3}He nuclei, an unambiguous determination of the optical potential on the basis of a phenomenological analysis of the experimental cross sections cannot be performed even in the region of the highest sensitivity to this potential. The ambiguity in the choice of potential stems from the interrelation between its real and imaginary parts. This complies with the results of the analyses performed by Ershov *et al.* [7] and Demyanova *et al.* [8], who studied the scattering of 40- and 72-MeV ^{3}He nuclei on carbon isotopes.

4. CONCLUSION

We have investigated the elastic scattering of 50- and 60-MeV ^{3}He nuclei on ^{13}C nuclei. The differential cross sections measured over a broad angular range (up to 160°–170°) have been analyzed within the optical model of the nucleus by using Woods–Saxon potentials including both volume and surface absorption. The potential parameters have been determined phenomenologically by fitting the computed cross sections to experimental data. For each energy value, we have found eight potentials that describe experimental data over the full angular range equally well. Their volume integrals for the real parts show a considerable scatter from 200 to 450 MeV fm^3. Our analysis has revealed that, in the region of the highest sensitivity, the values of both the real and the imaginary parts of the potentials can differ by a factor greater than two. The observed scatter is explained by a strong correlation between V and W. Because of this correlation, even considerable variations in the real part can be compensated by the corresponding variations in the imaginary part (and vice versa). This indicates that there is a V–W ambiguity in choosing optical potentials. This type of ambiguity complicates, despite clear-cut manifestations of nuclear-rainbow effects in the scattering processes being discussed, the extraction of information about the distribution of nuclear matter or about the matter radii from data of phenomenological analyses.

Data on ^{3}He and alpha-particle scattering are sufficient for drawing a more general conclusion. Although the broad maximum observed in the angular distributions and the exponential fall that follows it are due to refraction effects—that is, eventually to the behavior of the real part of the potential at small distances—it is hardly possible at present to make use of this circumstance for deducing unambiguous information about the radial dependence of this real part. Here, the ambiguity is associated with a strong correlation between the real and the imaginary part of the potential. The situation here is aggravated by the fact that the modern theory of the nucleus is unable to compute the imaginary part of the potential on the basis of first principles. In practice, this part is treated phenomenologically, which creates a vicious circle: from scattering data, we cannot determine the real part of the potential because we do not know its imaginary part, and vice versa.

This brings about the natural question of whether it is possible to extrapolate these results to heavier projectiles such as ^{12}C and ^{16}O. Considerable advances have recently been made in understanding the dynamics of collisions between such ions (for an overview, see [14] and references therein). Among other things, it was shown that, at energies in excess of 10 MeV per projectile nucleon, the angular distributions for ^{12}C + ^{12}C and ^{16}O + ^{16}O elastic scattering exhibit refraction effects—in particular, a nuclear rainbow. These effects manifest themselves despite an almost complete absorption (the values of the scattering-matrix elements for the inner region are $|S_l| < 0.3$). No high penetrability is required in order to trace a signal from the inner region of the potential at large angles. A few-percent amplitude of scattering off this region or even a smaller value is quite sufficient. An analysis of such angular distributions made it possible to determine basic features of optical potentials and, in many cases, to remove ambiguities in the depth of the real parts of the potentials. In the light of data obtained for the elastic scattering of ^{3}He nuclei and alpha particles, it is interesting, however, to consider the effect of V–W correlations on the results of the phenomenological analyses of ^{12}C + ^{12}C, ^{16}O + ^{16}O, and ^{12}C + ^{16}O scattering under the conditions of limited transparency.

ACKNOWLEDGMENTS

We are grateful to A. A. Ogloblin and V. Z. Goldberg for stimulating discussions.

REFERENCES

1. D. A. Goldberg and S. M. Smith, Phys. Rev. Lett. **29**, 500 (1972).
2. D. A. Goldberg, S. M. Smith, and G. F. Burdzik, Phys. Rev. C **10**, 1362 (1974).
3. K. B. Baktybaev, A. D. Duisebaev, and A. B. Kabulov, Izv. Akad. Nauk Kaz. SSR, Ser. Fiz.–Mat., No. 6, 68 (1974).
4. L. Freindl, H. Dabrowski, K. Grotowski, *et al.*, Raport No. 1059/PL IFJ (Kraków, 1979).
5. P. L. Roberson, Phys. Rev. C **22**, 482 (1980).
6. M. E. Brandan, S. H. Fricke, and K. V. McVoy, Phys. Rev. C **38**, 673 (1988).
7. S. N. Ershov, F. A. Gareev, R. S. Kurmanov, *et al.*, Phys. Lett. B **227**, 315 (1989).
8. A. S. Demyanova, A. A. Ogloblin, S. N. Ershov, *et al.*, Phys. Scr. **32**, 89 (1990).
9. V. V. Adodin, N. T. Burtebaev, and A. D. Duisebaev, Yad. Fiz. **55**, 577 (1992) [Sov. J. Nucl. Phys. **55**, 319 (1992)].
10. J. Knoll and R. Schaeffer, Ann. Phys. **97**, 307 (1976).
11. F. Perey, SPI-GENOA an optical model search code (unpublished).
12. H.-J. Trost, P. Lezoch, and U. Strohbusch, Nucl. Phys. A **462**, 333 (1987).
13. R. C. Fuller, Phys. Rev. C **12**, 1561 (1975).
14. M. E. Brandan and G. R. Satchler, Phys. Rep. **285**, 143 (1997).

Translated by A. Isaakyan

Physics of Atomic Nuclei, Vol. 63, No. 4, 2000, pp. 570–573. Translated from Yadernaya Fizika, Vol. 63, No. 4, 2000, pp. 633–637.

NUCLEI
Theory

Relation between *E*2-Transition Probabilities for Nuclei That Are Soft with Respect to β Vibrations

R. V. Jolos and Yu. V. Palchikov*

Joint Institute for Nuclear Research, Dubna, Moscow oblast, 141980 Russia

Received March 19, 1999; in final form, June 3, 1999

Abstract—For collective even–even nuclei, a relation between the *E*2-transition probabilities, which characterize the decay properties of 0_2^+- and 2_γ^+ states, are obtained. This relation features no free parameters; it is applicable to describing nuclei that are soft with respect to β vibrations. The ^{152}Sm and ^{154}Gd nuclei are considered as examples illustrating the application of the aforementioned relation. © *2000 MAIK "Nauka/Interperiodica".*

1. INTRODUCTION

A description of ground nuclear states is a challenging problem for spectroscopic nuclear calculations. This is so both within phenomenological models like interacting-boson models (IBM) and within shell-model calculations. The reason is that configuration spaces of various models used are insufficiently wide. The quantity that is taken to be a ground-state wave function in some model calculation may in fact saturate only a small part of its norm [1].

At the same time, it is well known from experimental data that the application of the quadrupole-moment operator or of the magnetic-dipole-moment operator to the ground state of a nucleus yields, respectively, the first 2^+ state or the collective 1^+ state. These examples suggest that, with the aid of the ground-state wave function, it is possible to reproduce faithfully the wave functions of collective excited states by applying appropriately chosen single-particle operators to the ground state. This approach underlies the scheme of *Q* phonons [2–6], which was developed to describe collective quadrupole excitations of nuclei. The basic idea of the approach is as follows. Let $|0_1^+\rangle$ be the state vector for the ground state of a nucleus. The state vectors for nuclear excitations above this ground state are then constructed in terms of the basis

$$|I^+, M, n\rangle = \mathcal{N}^{(I,n)}(Q_2 \ldots Q_2)_{IM}|0_1^+\rangle, \quad (1)$$

where Q_2 is the quadrupole-moment operator, while $\mathcal{N}^{(I,n)}$ is a normalization factor. Investigations revealed that states of interest for experiments can be described by invoking one to two components of the basis in (1). (It is important to note that this simple form of collective-state vectors can be retained over the entire range of the IBM parameters—that is, in going over from spherical through transition nuclei to deformed ones.) For example, the first 2^+ state can be represented as

$$|2_1^+\rangle = \mathcal{N}^{(2,1)}Q_2|0_1^+\rangle, \quad (2)$$

the accuracy of the description being about 90%. By taking into account the component involving two quadrupole operators, the accuracy in describing the 2_1^+ state can be improved up to 98% [5].

That simple expressions featuring no more than one free parameter can be used for the wave functions of collective states makes it possible to demonstrate that *E*2-transition probabilities satisfy definite relations depending only on quantities that can be determined experimentally [7, 8]. This proves possible because the state vectors in question are constructed in terms of the transition quadrupole-moment operator.

It was shown in [6] that, irrespective of whether the nucleus being considered is spherical, transition, or deformed, the wave function of the first excited ($I^\pi = 0^+$) state—it is common practice to denote it by $|0_2^+\rangle$—can be approximated, to a high accuracy, as a superposition of two components; that is,

$$|0_2^+\rangle = \cos\varphi|0_{QQ}^+\rangle + \sin\varphi|0_{QQQ}^+\rangle, \quad (3)$$

where

$$|0_{QQ}^+\rangle = \mathcal{N}_{QQ}((QQ)_0 - \langle 0_1^+|(QQ)_0|0_1^+\rangle)|0_1^+\rangle, \quad (4)$$

$$|0_{QQQ}^+\rangle = \mathcal{N}_{QQQ}((QQQ)_0 - \langle 0_1^+|(QQQ)_0|0_1^+\rangle)|0_1^+\rangle \quad (5)$$

with

$$\mathcal{N}_{QQ}^{-2} = \langle 0_1^+|(QQ)_0(QQ)_0|0_1^+\rangle - \langle 0_1^+|(QQ)_0|0_1^+\rangle^2,$$

$$\mathcal{N}_{QQQ}^{-2} = \langle 0_1^+|(QQQ)_0(QQQ)_0|0_1^+\rangle - \langle 0_1^+|(QQQ)_0|0_1^+\rangle^2.$$

For γ-soft nuclei—within the generalized model of the nucleus, these are described by a potential that is inde-

* e-mail: plchkv@thsun1.jinr.ru

pendent of γ—the second component is dominant, while, for β-soft nuclei, which include those from the beginning of the rare-earth region (say, for ^{150,152}Sm and ^{152,154}Gd), the first component prevails.

In recent years, considerable advances have been made in experimental investigations of the decays of 0_2^+ and 2_γ^+ states [9]. In the future, such investigations promise a considerable extension of a database that can be used as a testing ground for various theoretical models. For this reason, it is of interest to derive equations that would relate transition probabilities and which would feature no free parameters.

The objective of this study is to obtain a relation for the probabilities of $E2$ transitions from excited 0_2^+ states of β-soft nuclei. In such nuclei, 0_2^+ states are of particular interest since they have comparatively low excitation energies.

2. RELATION FOR $B(E2)$

Let us consider the reduced probabilities of $E2$ transitions between the 0_1^+, 0_2^+, 2_1^+, 2_γ^+, and 4_1^+ collective states. The expressions for the 2_1^+, 2_γ^+, and 4_1^+ state vectors in terms of the Q-phonon basis are given by [2, 3, 5, 8]

$$|2_1^+,\mu\rangle = \frac{1}{\sqrt{1+R_1}}|2_\mu^+,Q\rangle + \mathrm{sgn}(\langle 0_1^+|(QQQ)_0|0_1^+\rangle)\sqrt{\frac{R_1}{1+R_1}}|2_\mu^+,QQ\rangle, \quad (6)$$

$$|2_\gamma^+,\mu\rangle = -\mathrm{sgn}(\langle 0_1^+|(QQQ)_0|0_1^+\rangle)\sqrt{\frac{R_1}{1+R_1}}|2_\mu^+,Q\rangle + \frac{1}{\sqrt{1+R_1}}|2_\mu^+,QQ\rangle, \quad (7)$$

$$|4_1^+,\mu\rangle = \frac{(QQ)_{4\mu}}{\sqrt{\frac{1}{3}\langle 0_1^+|((QQ)_4(QQ)_4)_0|0_1^+\rangle}}|0_1^+\rangle, \quad (8)$$

where

$$|2_\mu^+,Q\rangle = \frac{1}{\sqrt{\frac{1}{\sqrt{5}}\langle 0_1^+|(QQ)_0|0_1^+\rangle}}Q_{2\mu}|0_1^+\rangle, \quad (9)$$

$$|2_\mu^+,QQ\rangle = \left(\frac{1}{\sqrt{5}}\left(\langle 0_1^+|((QQ)_2(QQ)_2)_0|0_1^+\rangle - \frac{\langle 0_1^+|(QQQ)_0|0_1^+\rangle^2}{\langle 0_1^+|(QQ)_0|0_1^+\rangle}\right)\right)^{-1/2} \times\left((QQ)_{2\mu} - \frac{\langle 0_1^+|(QQQ)_0|0_1^+\rangle}{\langle 0_1^+|(QQ)_0|0_1^+\rangle}Q_{2\mu}\right)|0_1^+\rangle, \quad (10)$$

$$R_1 = \frac{B(E2;\,2_2^+ \longrightarrow 0_1^+)}{B(E2;\,2_1^+ \longrightarrow 0_1^+)}. \quad (11)$$

The sign of $\langle 0_1^+|(QQQ)_0|0_1^+\rangle$ coincides with the sign of the quadrupole moment in the 2_1^+ state. Since we consider only β-soft nuclei that are comparatively stiff with respect to γ vibrations, the 0_2^+ state vector can be represented as

$$|0_2^+\rangle = |0_{QQ}^+\rangle, \quad (12)$$

where $|0_{QQ}^+\rangle$ is given by (4).

By means of direct calculations based on the above expressions for the state vectors involved, it can be shown that the reduced matrix elements of the quadrupole-moment operator $Q_{2\mu}$ can be represented as

$$\langle 2_\gamma^+\|Q\|0_2^+\rangle = -\mathrm{sgn}(\langle 0_1^+|(QQQ)_0|0_1^+\rangle)\sqrt{\frac{R_1}{1+R_1}}\sqrt{A} + \frac{5^{1/4}}{\sqrt{1+R_1}}\frac{(T-1)B}{\sqrt{N_1N_2}}, \quad (13)$$

$$\langle 2_\gamma^+\|Q\|0_1^+\rangle = -\mathrm{sgn}(\langle 0_1^+|(QQQ)_0|0_1^+\rangle) \times\sqrt{\frac{R_1}{1+R_1}}\sqrt{\sqrt{5}\langle 0_1^+|(QQ)_0|0_1^+\rangle}, \quad (14)$$

where

$$T = \frac{\langle 0_1^+|(QQQ)_0(QQ)_0|0_1^+\rangle\langle 0_1^+|(QQ)_0|0_1^+\rangle}{\langle 0_1^+|(QQ)_0^2|0_1^+\rangle\langle 0_1^+|(QQQ)_0|0_1^+\rangle},$$

$$A = \sqrt{5}\left(\frac{\langle 0_1^+|(QQ)_0^2|0_1^+\rangle}{\langle 0_1^+|(QQ)_0|0_1^+\rangle} - \langle 0_1^+|(QQ)_0|0_1^+\rangle\right),$$

$$B = \frac{\langle 0_1^+|(QQ)_0^2|0_1^+\rangle\langle 0_1^+|(QQQ)_0|0_1^+\rangle}{\langle 0_1^+|(QQ)_0|0_1^+\rangle}, \quad (15)$$

$$N_1 = \frac{2\sqrt{5}}{7}\langle 0_1^+|(QQ)_0^2|0_1^+\rangle - \frac{\langle 0_1^+|(QQQ)_0|0_1^+\rangle^2}{\langle 0_1^+|(QQ)_0|0_1^+\rangle},$$

$$N_2 = \langle 0_1^+|(QQ)_0^2|0_1^+\rangle - \langle 0_1^+|(QQ)_0|0_1^+\rangle^2.$$

By using expression (14) and (15), we can recast the ratio of one pair of reduced matrix elements into the form

$$\frac{\langle 2_\gamma^+\|Q\|0_2^+\rangle}{\langle 2_\gamma^+\|Q\|0_1^+\rangle} = \sqrt{\bar{K}_4 - 1} - \frac{T-1}{\sqrt{R_1}}\bar{K}_4 \times\left(\frac{7}{2\sqrt{5}}\frac{\langle 0_1^+|(QQQ)_0|0_1^+\rangle^2}{\langle 0_1^+|(QQ)_0|0_1^+\rangle^3}\right)^{1/2} \times\left[(\bar{K}_4-1)\left(\bar{K}_4 - \frac{7}{2\sqrt{5}}\frac{\langle 0_1^+|(QQQ)_0|0_1^+\rangle^2}{\langle 0_1^+|(QQ)_0|0_1^+\rangle^3}\right)\right]^{-1/2}, \quad (16)$$

where

$$\bar{K}_4 = \frac{\langle 0_1^+|(QQ)_0^2|0_1^+\rangle}{\langle 0_1^+|(QQ)_0|0_1^+\rangle^2}. \quad (17)$$

In a similar way, the other ratio of the reduced matrix elements can be expressed as

$$\frac{\langle 2_1^+\|Q\|0_2^+\rangle}{\langle 2_1^+\|Q\|0_1^+\rangle} = \sqrt{\bar{K}_4 - 1} + (T-1)\sqrt{R_1}\bar{K}_4 \times\left(\frac{7}{2\sqrt{5}}\frac{\langle 0_1^+|(QQQ)_0|0_1^+\rangle^2}{\langle 0_1^+|(QQ)_0|0_1^+\rangle^3}\right)^{1/2} \times\left((\bar{K}_4-1)\left(\bar{K}_4 - \frac{7}{2\sqrt{5}}\frac{\langle 0_1^+|(QQQ)_0|0_1^+\rangle^2}{\langle 0_1^+|(QQ)_0|0_1^+\rangle^3}\right)\right)^{-1/2}. \quad (18)$$

In [7, 8], it was shown that the ratio $\bar{K}_4$ can be approximated as

$$\bar{K}_4 = 0.7\frac{B(E2; 4_1^+ \longrightarrow 2_1^+)}{B(E2; 2_1^+ \longrightarrow 0_1^+)}. \quad (19)$$

By comparing (16) and (18), we arrive at the relation

$$\frac{\langle 2_\gamma^+\|Q\|0_2^+\rangle}{\langle 2_\gamma^+\|Q\|2_1^+\rangle} = \sqrt{\bar{K}_4 - 1} - \frac{1}{R_1}\left(\left|\frac{\langle 2_1^+\|Q\|0_2^+\rangle}{\langle 2_1^+\|Q\|0_1^+\rangle}\right| - \sqrt{\bar{K}_4 - 1}\right), \quad (20)$$

which involves only experimentally measurable quantities. In terms of the $E2$-transition probabilities, the last relation can be rewritten as

$$R_1\sqrt{\frac{B(E2; 2_\gamma^+ \longrightarrow 0_2^+)}{B(E2; 2_\gamma^+ \longrightarrow 0_1^+)}} = (1+R_1)\sqrt{0.7\frac{B(E2; 4_1^+ \longrightarrow 2_1^+)}{B(E2; 2_1^+ \longrightarrow 0_1^+)} - 1} - \sqrt{\frac{B(E2; 2_1^+ \longrightarrow 0_2^+)}{B(E2; 2_1^+ \longrightarrow 0_1^+)}}. \quad (21)$$

3. COMPARISON WITH EXPERIMENTAL DATA

Because of large experimental uncertainties in the measured values of

$$0.7\frac{B(E2; 4_1^+ \longrightarrow 2_1^+)}{B(E2; 2_1^+ \longrightarrow 0_1^+)} - 1,$$

the use of relation (21) involves some difficulties in a comparison with experimental data. We will now transform it, considering that, to within 10–15%, the $E2$-transition probabilities as computed on the basis of the IBM model obey the relation

$$1 + \frac{B(E2; 2_1^+ \longrightarrow 0_2^+)}{B(E2; 2_1^+ \longrightarrow 0_1^+)} = 0.7\frac{B(E2; 4_1^+ \longrightarrow 2_1^+)}{B(E2; 2_1^+ \longrightarrow 0_1^+)}. \quad (22)$$

The validity of relation (22) was checked by using the Hamiltonian [10, 11]

$$H = \epsilon\sum_\mu d_\mu^+ d_\mu^+ - \kappa\sum_\mu (-1)^\mu Q_{2\mu}Q_{2-\mu}, \quad (23)$$

where

$$Q_{2\mu} = d_\mu^+ s + s^+\tilde{d}_\mu - \chi(d^+\tilde{d})_{2\mu}. \quad (24)$$

Let us compare relation (22) with experimental data for nuclei such that the wave function of the 0_2^+ state can be represented by the approximation in (12). The required information is available for Pd isotopes [12–16]. The results of this comparison are presented in the table. It can be seen that relation (22) is compatible with the data for Pd isotopes.

Substituting (22) into (21), we arrive at

$$\sqrt{\frac{B(E2; 2_\gamma^+ \longrightarrow 0_2^+)}{B(E2; 2_\gamma^+ \longrightarrow 0_1^+)}} = \sqrt{\frac{B(E2; 2_1^+ \longrightarrow 0_2^+)}{B(E2; 2_1^+ \longrightarrow 0_1^+)}}. \quad (25)$$

We emphasize once again that relation (25) was obtained under the assumption that the wave function of the 0_2^+ state is given by (12). It follows that relation (25) can prove to be valid for a small number of nuclei such that 0_2^+ states for them are purely β-vibrational states. It is interesting to note that relation (25) can also

be inferred from the Davydov–Chaban model, within which it was obtained many years ago [17], albeit on the basis of a totally different formalism.

Let us now consider experimental data. The required information is available for the ^{152}Sm and ^{154}Gd nuclei [9]. We have

$$\sqrt{\frac{B(E2;\,2^+_\gamma \longrightarrow 0^+_2)}{B(E2;\,2^+_\gamma \longrightarrow 0^+_1)}} = 0.22 \pm 0.01,$$

$$\sqrt{\frac{B(E2;\,2^+_1 \longrightarrow 0^+_2)}{B(E2;\,2^+_1 \longrightarrow 0^+_1)}} = 0.21 \pm 0.01$$

for ^{152}Sm and

$$\sqrt{\frac{B(E2;\,2^+_\gamma \longrightarrow 0^+_2)}{B(E2;\,2^+_\gamma \longrightarrow 0^+_1)}} = 0.46 \pm 0.06,$$

$$\sqrt{\frac{B(E2;\,2^+_1 \longrightarrow 0^+_2)}{B(E2;\,2^+_1 \longrightarrow 0^+_1)}} = 0.26 \pm 0.02$$

for ^{154}Gd.

For the ^{172}Yb nucleus, which is not soft with respect to β vibrations, so that relation (12) does not hold for it, we have

$$\sqrt{\frac{B(E2;\,2^+_\gamma \longrightarrow 0^+_2)}{B(E2;\,2^+_\gamma \longrightarrow 0^+_1)}} = 1.35 \pm 0.09,$$

$$\sqrt{\frac{B(E2;\,2^+_1 \longrightarrow 0^+_2)}{B(E2;\,2^+_1 \longrightarrow 0^+_1)}} = 0.058 \pm 0.008,$$

and the ratio of the expression on the left-hand side of equation (25) to that on the right-hand side of it is equal to 23. Thus, relation (25) is quite a sensitive criterion for β-soft nuclei.

It should be noted that, within the present approach, the smallness of the quantity on the left-hand side of (25)—this point was discussed in [9]—is explained by the fact that, by virtue of the hypothesis that the 0^+_2 state is of a beta-vibrational origin, it coincides with the quantity that appears on the right-hand side of (25) and which is small for all nuclei.

4. CONCLUSION

For collective even–even nuclei, we have obtained a relation between the $E2$-transition probabilities characterizing the decay properties of the 0^+_2 and 2^+_γ states. The relation is applicable to nuclei that are soft with respect to β vibrations. A comparison with experimental data has revealed that this relation is quite a sensitive criterion for β-soft nuclei that are sufficiently stiff in γ.

Experimental values of $1 + \dfrac{B(E2;\,2^+_1 \longrightarrow 0^+_2)}{B(E2;\,2^+_1 \longrightarrow 0^+_1)}$ and $0.7\dfrac{B(E2;\,4^+_1 \longrightarrow 2^+_1)}{B(E2;\,2^+_1 \longrightarrow 0^+_1)}$ for the $^{104\text{–}110}$Pd isotopes

Isotope	$1 + \dfrac{B(E2;\,2^+_1 \longrightarrow 0^+_2)}{B(E2;\,2^+_1 \longrightarrow 0^+_1)}$	$0.7\dfrac{B(E2;\,4^+_1 \longrightarrow 2^+_1)}{B(E2;\,2^+_1 \longrightarrow 0^+_1)}$
^{104}Pd	1.08 ± 0.01	1.02 ± 0.10
^{106}Pd	1.20 ± 0.06	1.18 ± 0.21
^{108}Pd	1.21 ± 0.05	1.04 ± 0.20
^{110}Pd	1.10 ± 0.01	1.14 ± 0.01

ACKNOWLEDGMENTS

This work was supported in part by the Russian Foundation for Basic Research (project nos. 97-02-16030 and 96-15-96729).

REFERENCES

1. H. Feshbach, in *International Conference on Perspectives for the Interacting Boson Model, Padova, Italy, 1994*, Ed. by R. F. Casten *et al.* (World Sci., Singapore, 1994), p. 693.
2. N. Pietralla, P. von Brentano, R. F. Casten, *et al.*, Phys. Rev. Lett. **73**, 2962 (1994).
3. N. Pietralla, P. von Brentano, T. Otsuka, *et al.*, Phys. Lett. B **349**, 1 (1995).
4. T. Otsuka and K.-M. Kim, Phys. Rev. C **50**, 1768 (1994).
5. N. Pietralla, T. Mizusaki, P. von Brentano, *et al.*, Phys. Rev. C **57**, 150 (1998).
6. Yu. V. Palchikov, P. von Brentano, and R. V. Jolos, Phys. Rev. C **57**, 3026 (1998).
7. R. V. Jolos and P. von Brentano, Phys. Lett. B **381**, 1 (1996).
8. R. V. Jolos, P. von Brentano, N. Pietralla, *et al.*, Nucl. Phys. A **618**, 126 (1997).
9. M. Wilhelm, E. Radermacher, R. F. Casten, *et al.*, Phys. Rev. C **57**, R1553 (1998).
10. D. D. Warner and R. F. Casten, Phys. Rev. Lett. **48**, 1385 (1982).
11. P. O. Lipas, P. Tiovonen, and D. D. Warner, Phys. Lett. B **155**, 295 (1985).
12. J. Blachot, Nucl. Data Sheets **64**, 1 (1991).
13. D. de Frenne and E. Jacobs, Nucl. Data Sheets **72**, 1 (1994).
14. L. E. Svenson, C. Fahlander, L. Hasselgren, *et al.*, Nucl. Phys. A **584**, 547 (1995).
15. J. Blachot, Nucl. Data Sheets **64**, 803 (1991).
16. D. de Frenne and E. Jacobs, Nucl. Data Sheets **67**, 809 (1992).
17. A. S. Davydov, V. S. Rostovsky, and A. A. Chaban, Nucl. Phys. **27**, 134 (1961).

Translated by A. Isaakyan

Physics of Atomic Nuclei, Vol. 63, No. 4, 2000, pp. 574–581. Translated from Yadernaya Fizika, Vol. 63, No. 4, 2000, pp. 638–645.

NUCLEI
Theory

Three-Body Scattering at Positive Energies: Solving the Problem of Moving Logarithmic Singularities

N. Zh. Takibayev

Institute of Nuclear Physics, National Nuclear Center of the Republic of Kazakhstan, Almaty, Republic of Kazakhstan

Received January 11, 1999; in final form, May 5, 1999

Abstract—For three-body scattering at positive total energies, integral equations are obtained whose kernels have no logarithmic singularities on the contour of integration. The corresponding singularities that are present in original integral equations can be circumvented by shifting a part of the contour of integration from the real axis to the complex plane. This is done only for a special auxiliary solution appearing to be an analytic function in this region. The physical amplitude proper is found as one of the solutions to the resulting set of equations. In contrast to conventional techniques, an additional analysis is therefore not required here, so that numerical solutions can be obtained within standard computational schemes. *© 2000 MAIK "Nauka/Interperiodica".*

1. INTRODUCTION

Some time ago, the problem of moving singularities hindered significantly the development of methods for numerical calculations of three-body scattering at positive total energies. In this region, the logarithmic singularities of the kernels of relevant integral equations occur on the real axis of the complex plane of momentum variables—that is, on the contour of integration itself. That these singularities move along the real axis in response to variations in momentum variables, including those that determine the functional form of sought solutions is the main reason behind the aforementioned difficulties. As a result, it becomes difficult to obtain numerical solutions directly and to control the accuracy of the relevant calculations [1–3].

The problem of moving singularities was solved by Hetherington and Schick [4] and by Sohre and Ziegelmann [5], who proposed a method for sidestepping these difficulties by deforming the contour of integration. Essentially, the method consisted in shifting the contour of integration to the region of complex momentum values. This led to a new equation whose numerical solutions could be obtained straightforwardly within standard computational schemes. That constructing the scattering amplitude at physical momentum values required, within this method, a continuation of the resulting solutions back to the real axis created, however, difficulties of another kind. These could be overcome only via a dedicated analysis of the analytic properties of the solutions and additional numerical calculations [1, 2, 4, 5].

At the same time, the advent of modern supercomputers made it possible to perform direct calculations by using, for example, spline functions or a finer (or a variable-step) grid in the region of moving singularities [1, 3].

Thus, we can say that the problem has been solved in principle, but specific applications call for some refinements, including a simplification or a unification of relevant computational schemes and an extension of the approaches in question to more involved problems of few-body physics.

In the present study, a new method is proposed for solving the problem of moving singularities. This method, which can prove useful in performing practical calculations, combines two well-known techniques, that of the theory of scattering on two potentials and that of a deformation of the contour of integration. In the region of moving singularities, the proposed procedure involves isolating a compensating potential that contains these singularities explicitly. Solutions in the compensating potential are of an auxiliary character. From the equation with the compensating potential, we further find solutions that are analytic either in the upper or in the lower half-plane of complex momenta. It is for this purpose that we shift the contour of integration. At the same time, the equation for the scattering amplitude in the physical region is parametrized from the outset in terms of real momentum values—that is, without shifting the contour of integration. The latter equation, together with the equations for the auxiliary solutions, gives a complete solution to the problem. It is important that the kernels of the resulting equations have no singularities on the corresponding contours of integration. As a result, we arrive at a closed set of equations that features an equation that determines directly the physical amplitude.

The ensuing exposition is organized as follows. In Section 2, we briefly discuss the properties of the basic equation for the three-body scattering problem—the equation that describes the elastic scattering of one particle on the bound pair of the other particles. This equation plays a special role in three-body physics. Some

1063-7788/00/6304-0574$20.00

general information about moving singularities is given in this section as well. The properties of the compensating potential are presented in Section 3. Solutions that are analytic on the upper or on the lower half-disks of the complex plane of momenta and equations governing these solutions are also obtained in Section 3. Section 4, where a method is developed for transforming the basic equation into a set of equations whose kernels are free from moving singularities, is a key one in this study.

2. BASIC EQUATION FOR THREE-BODY SCATTERING AND PROBLEM OF LOGARITHMIC SINGULARITIES

Omitting the details concerning the three-body problem, which is expounded consistently and rigorously in classical monographs and textbooks (see, for example, [1, 6, 7]), we focus here on a key result of the theory, the equation for quasi-two-particle transitions. Such equations (we refer to them as basic equations) were obtained in [8] by the method of Alt–Grassberger–Sandhas transformations of basic Faddeev equations (for T matrices or wave functions [6]) into equations for the matrices of quasi-two-particle transitions. These equations can also be obtained within the effective-potential approach, which represents a modification of the Alt–Grassberger–Sandhas method [9]. Here, it is important that, if solutions to the basic equation are known, all other transitions, including breakup processes and $3 \longrightarrow 3$ scattering, can be determined independently—that is, by using integral relations rather than by solving the basic integral equation.

Since we analyze here the problem of moving singularities—a problem common to all situations in three-body physics for $E \geq 0$—we can maximally simplify it, retaining only the main ingredient of this problem, moving singularities and all other things that are related to them.

For the sake of simplicity, we will henceforth assume that the particles involved are identical ($m_1 = m_2 = m_3 = m = 1$) and spinless and that their pair interaction is short-range, yielding only one bound state (at energy ε).

We note, however, that a generalization to the case of nonidentical particles and the inclusion of multichannel transitions and of the spin–isospin and other dependences are straightforward. In this case, it is necessary to treat the original equation as a matrix equation whose rank is equal to the number of channels and to introduce summation over spin–isospin quantum numbers and other quantum numbers involved. There remains, however, the main problem, that of developing a procedure for overcoming difficulties associated with moving singularities.

Under the adopted simplifying assumptions, the amplitude of the quasi-two-particle elastic scattering of a particle on a bound pair of the other two particles, $f(\mathbf{k}_i, \mathbf{k}_j; E)$, appears to be a solution to the equation

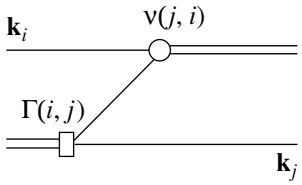

Fig. 1. Diagram corresponding to the Born term in the expansion of the potential $V(k_i, k_j; E)$.

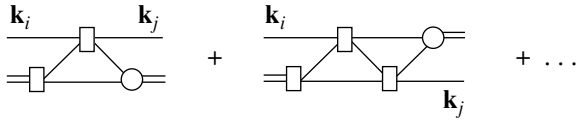

Fig. 2. Diagrams corresponding to higher order terms in the expansion of the potential $V(k_i, k_j, E)$.

$$f(\mathbf{k}_i, \mathbf{k}_j; E) = -V(\mathbf{k}_i, \mathbf{k}_j; E) + \int d\mathbf{k}_s V(\mathbf{k}_i, \mathbf{k}_s; E) \frac{f(\mathbf{k}_s, \mathbf{k}_j; E)}{E - E_s + i\gamma}, \quad (1)$$

where $E = 3k_0^2/4 - \varepsilon$, $E_s = 3k_s^2/4 - \varepsilon$ is the energy of the quasi-two-particle intermediate state, $\mathbf{k}_s$ is the momentum of the relative motion of the free particle in the c.m. frame, and $\gamma \longrightarrow 0_+$.

In contrast to the conventional two-body problem, the potential $V(\mathbf{k}_i, \mathbf{k}_j; E)$ is complex-valued here and is dependent on the energy E. A determination of its exact form is a separate problem [8, 9]. It is important, however, that moving singularities in this effective potential are generated by the lowest order (Born) term in its expansion in nonrepeated pair forces—that is, by the exchange diagram (see Fig. 1). In this figure, a circle labeled with the symbol $\nu(j, i)$ corresponds to the transition of a pair of free particles into a bound state, while the square vertex $\Gamma(i, j)$ represents the effective (dressed) value for the inverse of such a transition in the space of three particles [as a matter of fact, this vertex is equal to the product of $\nu(i, j)$ and the residue of the pair T_i matrix at the pole). Higher order terms in this expansion, which are represented by the diagrams in Fig. 2, do not involve the moving singularities in question (because they are averaged upon summation over additional intermediate states).

This is in accord with the obvious circumstance that moving singularities are of a kinematical origin—they are related to the character of pair forces only indirectly, to the extent that such forces are necessary for the existence of pair bound states. In particular, the region where such singularities exist and their behavior depend only on kinematical variables like the total energy, the wave numbers, and the ratios of the particle masses. By way of example, we can investigate separa-

ble pair forces, in which case the effective potential has a compact form since only one exchange diagram in Fig. 1 corresponds to it. However, all problems associated with moving singularities survive in that case completely.

From equation (1) for the partial-wave components of the amplitude, we obtain

$$f_{i,0} = -V_{i,0} + \frac{2}{3\pi^2}\int_0^\infty k_s^2 dk_s \frac{V_{i,s} f_{s,0}}{(k_0^2 - k_s^2 + i\gamma)}. \qquad (2)$$

For the sake of simplicity, we have introduced here the notation $f_{i,0} = f_L(k_i, k_0; E)$, $V_{i,j} = V_L(k_i, k_j; E)$, and so on.

Let us present the lowest order general expression for $V_{i,j}$ corresponding to the exchange diagram in Fig. 1. We have

$$V^{\mathrm{B}}_{i,j} = \frac{1}{2}\int_{-1}^{+1} dx P_L(x) \frac{\Gamma(i,j)\nu(j,i)}{E - k_i^2 - k_j^2 - k_i k_j x + i\gamma}, \qquad (3)$$

where $P_L(x)$ is a Legendre polynomial of the first kind. It is the Green's function for three free particles in this expression that generates moving logarithmic singularities. Indeed, $V^{\mathrm{B}}_{i,j}$ is proportional to $Q_L(x_0 + i\gamma)$, where x_0 is determined by the condition

$$E - k_i^2 - k_j^2 - k_i k_j x_0 = 0. \qquad (4)$$

If all the variables involved are real-valued, this equality holds for $-1 \le x_0 \le +1$ only when $E \ge 0$ and k_i^2, $k_j^2 \le 4E/3$.

It is well known that the Legendre polynomial of the second kind can be represented in the form

$$Q_L(x_0) = \frac{1}{2} P_L(x_0) \ln\left\{\frac{1+x_0}{1-x_0}\right\} - W_{L-1}(x_0), \qquad (5)$$

where

$$W_{L-1}(x) = \sum_{l=1}^{L} \frac{1}{l} P_{l-1}(x) P_{L-l}(x),$$

which is a regular function.

Obviously, the logarithmic term, whose singularities change positions in the k_i plane in response to changes in the other variable, k_j, is hazardous.

Logarithmic singularities were analyzed in a number of monographs devoted to the three-body problem (see, for example, [1, 2]). Here, we will dwell on the basic points of these analyses.

Let us introduce an auxiliary variable k_Z that is defined by the condition $E = 3k_Z^2/4 \ge 0$. Normalizing the momentum variables to it, we denote

$$y_i = k_i/k_Z, \quad y_j = k_j/k_Z. \qquad (6)$$

The region on the real axis where the logarithmic singularities manifest themselves at real values of the above variables is specified by the conditions $y_i^2 \le 1$ and $y_j^2 \le 1$.

Let us investigate this region of $y_{i,j}$ values in some detail. We recast the logarithmic term in (5) into the form

$$\ln\left\{\frac{1+x_0}{1-x_0}\right\} - i\pi = -\ln\left\{\frac{(y_i + a_1^j + i\gamma)(y_i + a_2^j - i\gamma)}{(y_i - a_1^j - i\gamma)(y_i - a_2^j + i\gamma)}\right\}. \qquad (7)$$

The quantities a_1 and a_2 are given by [10]

$$a_1^j = y_j/2 + b_j, \quad a_2^j = y_j/2 - b_j, \qquad (8)$$

where $b_j = \frac{\sqrt{3}}{2}\sqrt{1 - y_j^2}$. The auxiliary functions a_1 and a_2 possess the following symmetry properties:

$$a_1(-y) = -a_2(y), \quad a_2(-y) = -a_1(y). \qquad (9)$$

For these functions, we also present transformation formulas. Upon the formal change of variables according to $y = a_1(t)$, we obtain

$$\begin{aligned} a_1(y) &= t, \quad t \ge 0.5, \\ a_2(y) &= -a_2(t), \quad t \ge 0.5, \\ a_1(y) &= -a_2(t), \quad t \le 0.5, \\ a_2(y) &= t, \quad t \le 0.5. \end{aligned} \qquad (10)$$

For $y = a_2(t)$, the corresponding results are

$$\begin{aligned} a_1(y) &= t, \quad t \ge -0.5, \\ a_2(y) &= -a_1(t), \quad t \ge -0.5, \\ a_1(y) &= -a_1(t), \quad t \le -0.5, \\ a_2(y) &= t, \quad t \le -0.5. \end{aligned} \qquad (11)$$

It is noteworthy that the logarithmic term on the right-hand side of (7) can be represented as the sum

$$\ln\left\{\frac{y_i + a_1^j + i\gamma}{y_i - a_2^j + i\gamma}\right\} + \ln\left\{\frac{y_i + a_2^j - i\gamma}{y_i - a_1^j - i\gamma}\right\}. \qquad (12)$$

It is important that, if y_i is taken to be real-valued and if $|y_{i,j}| \le 1$, the first (second) term is analytic in y_j in the upper (lower) unit half-disk.

These analytic properties, as well as the symmetry properties of $a_{1,2}$, will be used below in transforming the basic equation (2).

3. TRANSFORMATION OF THE BASIC EQUATION IN THE SINGULAR REGION

As a matter of fact, we have already broken down the entire interval of the momentum variables into two regions, $k \le k_Z$ and $k > k_Z$. In order to distinguish between solutions in these regions, we introduce the notation

$$\begin{aligned} f_L(k_i, k_0; E) &= \varphi_L(y_i) = \varphi_i, \quad k_i \le k_Z, \\ f_L(k_i, k_0; E) &= f_L(y_i) = f_i, \quad k_i > k_Z, \end{aligned} \tag{13}$$

where the variables k_0 and E are omitted for the sake of simplicity. It should noted that $k_0 > k_Z$ by definition—that is, $y_0 = k_0/k_Z > 1$.

From equation (2), it follows that the function φ ($y_i \le 1$) satisfies the equation

$$\begin{aligned} \varphi_i &= -V_{i,0} + \frac{2k_Z}{3\pi^2}\int_0^1 y_s^2 dy_s V_{i,s}\frac{\varphi_s}{\omega_s} \\ &\quad + \frac{2k_Z}{3\pi^2}\int_1^\infty y_s^2 dy_s V_{i,s}\frac{f_s}{\omega_s}, \end{aligned} \tag{14}$$

where $\omega_s = (y_0^2 - y_s^2 + i\gamma)$.

For f_i ($y_i > 1$), we have

$$\begin{aligned} f_i &= -V_{i,0} + \frac{2k_Z}{3\pi^2}\int_0^1 y_s^2 dy_s V_{i,s}\frac{\varphi_s}{\omega_s} \\ &\quad + \frac{2k_Z}{3\pi^2}\int_1^\infty y_s^2 dy_s V_{i,s}\frac{f_s}{\omega_s}. \end{aligned} \tag{15}$$

It can easily be seen that only the kernel of the first integral term in (14) has logarithmic singularities since the inequalities $y_i, y_s \le 1$ hold for it. The kernels of the remaining integral terms in (14) and (15) have no such singularities on the contour of integration since at least one of the variables or both exceed unity. Therefore, our transformations will be applied only to the integral term featuring the singular kernel.

Let us introduce the compensating potential $V_L^0(y_i, y_j)$ in the form

$$V_{i,j}^0 = \frac{1}{k_Z}\frac{Q_L(x_0 + i\gamma)}{y_i y_j} Z_{i,j}, \tag{16}$$

where the variables satisfy the conditions $y_i, y_j \le 1$ and where $Z_{i,j} \equiv Z_{i,j}(x_0) = Z_{i,j}(x)|_{x = x_0}$ with

$$Z_{i,j}(x) = \frac{1}{k_Z}\Gamma(i, j)\nu(j, i). \tag{17}$$

Let us assume that the functions $Z_{i,j}$ and $Z_{i,j}(x)$ are analytic within the unit disk $|y_i|, |y_j| \le 1$. For problems featuring only short-range pair forces, this is indeed so, as follows from the analytic properties of the relevant pair solutions.

Let us now consider the difference

$$\Delta V_{i,j} = V_{i,j} - V_{i,j}^0 \tag{18}$$

in the singular region (that is, for $y_i, y_j \le 1$). This difference does not involve logarithmic singularities because, in the lowest (hazardous) approximation, we have

$$\Delta V_{i,j}^{\mathrm{B}} = \frac{1}{2k_Z}\int_{-1}^{+1} dx P_L(x)\frac{Z_{i,j}(x) - Z_{i,j}}{3/4 - y_i^2 - y_j^2 - y_i y_j x + i\gamma}. \tag{19}$$

Representing the integrand in (19) as a series, we arrive at

$$\begin{aligned} \Delta V_{i,j}^{\mathrm{B}} &= -\frac{1}{2k_Z}\frac{1}{y_i y_j} \\ &\quad \times \int_{-1}^{+1} dx P_L(x)\left\{ Z'_{i,j} + \frac{1}{2}(x - x_0)Z''_{i,j} + \ldots \right\}, \end{aligned} \tag{20}$$

where

$$Z'_{i,j} = \left\{\frac{d}{dx}Z_{i,j}(x)\right\}\Big|_{x = x_0},$$

$$Z''_{i,j} = \left\{\frac{d^2}{dx^2}Z_{i,j}(x)\right\}\Big|_{x = x_0},$$

$$\ldots .$$

That the series in (20) is convergent follows from the properties of the pair vertex form factors.

Equation (14) can be rewritten in the form ($y_i \le 1$)

$$\varphi_i = \frac{2}{y_i}\Omega_i + \frac{2k_Z}{3\pi^2}\int_0^1 y_s^2 dy_s V_{i,s}^0\frac{\varphi_s}{\omega_s}, \tag{21}$$

where

$$\begin{aligned} \frac{2}{y_i}\Omega_i &= -V_{i,0} + \frac{2k_Z}{3\pi^2}\int_0^1 y_s^2 dy_s \Delta V_{i,s}\frac{\varphi_s}{\omega_s} \\ &\quad + \frac{2k_Z}{3\pi^2}\int_1^\infty y_s^2 dy_s V_{i,s}\frac{f_s}{\omega_s}. \end{aligned} \tag{22}$$

The kernel of equation (21) still remains singular, but some important transformations can be performed owing to its simple structure. The kernels of the integral terms in Ω_i (22) have no logarithmic singularities.

Let us represent V^0 in the form

$$V_{i,j}^0 = \frac{1}{k_Z}Z_{i,j}\{\lambda^+ + \lambda^-\}\frac{1}{y_i y_j}, \tag{23}$$

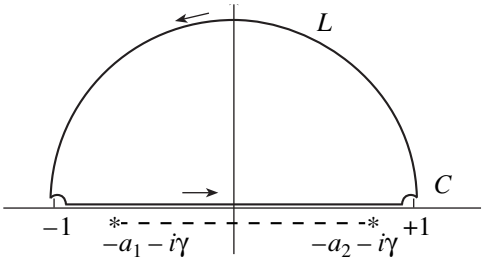

Fig. 3. Contour C consisting of the segment (–1, +1) and the unit semicircle L closing it from above. The extreme points of the segment are circumvented along circles of infinitely small radius ($\delta \longrightarrow 0$). The dashed line indicates the cut.

where

$$\lambda^+ = \lambda^+(y_i, y_j) = -\frac{1}{2}P_L(x_0)\ln\left\{\frac{y_i + a_1^j + i\gamma}{y_i - a_2^j + i\gamma}\right\} + \frac{1}{2}W_{L-1}(x_0), \quad (24)$$

$$\lambda^- = \lambda^-(y_i, y_j) = -\frac{1}{2}P_L(x_0)\ln\left\{\frac{y_i + a_2^j - i\gamma}{y_i - a_1^j - i\gamma}\right\} + \frac{1}{2}W_{L-1}(x_0). \quad (25)$$

The functions in (24) and (25) have the following symmetry properties:

$$\lambda^+(-y_i, y_j) = (-1)^{L+1}\lambda^-(y_i, y_j), \quad \lambda^-(-y_i, y_j) = (-1)^{L+1}\lambda^+(y_i, y_j) \quad (26)$$

$$\lambda^+(y_i, -y_j) = (-1)^{L+1}\lambda^+(y_i, y_j), \quad \lambda^-(y_i, -y_j) = (-1)^{L+1}\lambda^-(y_i, y_j). \quad (27)$$

In accordance with the decomposition in (23), we seek the solution φ in the form of the sum

$$\varphi = \frac{1}{y_i}\{r^+ + r^-\}, \quad (28)$$

whose components satisfy the equations

$$r_i^+ = \Omega_i + \frac{2}{3\pi^2}\int_0^1 y_s dy_s Z_{i,s}\lambda_{i,s}^+\frac{\varphi_s}{\omega_s}, \quad (29)$$

$$r_i^- = \Omega_i + \frac{2}{3\pi^2}\int_0^1 y_s dy_s Z_{i,s}\lambda_{i,s}^-\frac{\varphi_s}{\omega_s}. \quad (30)$$

These components possess the following symmetry properties:

$$r^+(-y_i) = (-1)^{L+1}r^-(y_i), \quad r^-(-y_i) = (-1)^{L+1}r^+(y_i). \quad (31)$$

By taking into account the above symmetry properties, it can be shown that the set of equations (29) and (30) decouples into the following independent equations for r^+ and r^-:

$$r_i^+ = \Omega_i + \frac{2}{3\pi^2}\int_{-1}^1 dy_s Z_{i,s}\lambda_{i,s}^+\frac{r_s^+}{\omega_s}, \quad (32)$$

$$r_i^- = \Omega_i + \frac{2}{3\pi^2}\int_{-1}^1 dy_s Z_{i,s}\lambda_{i,s}^-\frac{r_s^-}{\omega_s}. \quad (33)$$

We note that the solutions r^+ and r^- are the analytic functions in, respectively, the upper and the lower unit half-disk in the complex plane of y_i.

On the real axis, these functions are related by simple transformations [see equations (31)]. In order to obtain a complete solution to the problem in question, it is therefore sufficient to determine one of these functions—for example, r^+.

4. SET OF EQUATIONS TO BE SOLVED

By using the analytic properties of the function $r \equiv r^+$, the argument values y_i in equation (32) can be chosen on the semicircle $y_i = \exp(i\xi_i)$ in the interval $0 \le \xi_i \le \pi$ (see Fig. 3). It is obvious that the logarithmic singularities will then be circumvented and that the equation itself will relate the values $r(\exp(i\xi_i))$ on the upper semicircle (left-hand side of the equation) to the values $r(y_s)$ on the real-axis segment $-1 \le y_s \le +1$ [integral term on the right-hand side of (32)]. In order to obtain a closed set of equations, equation (32) must now be supplemented with the inverted equation that determines the values $r(y_i)$ on the real-axis segment $-1 \le y_i \le +1$ in terms of the values $r(y_s = \exp(i\phi))$ on the semicircle where $0 \le \phi \le \pi$.

In order to derive this equation, the integral

$$I_L = i\frac{2}{3\pi^2}\int_0^\pi d\phi\left\{y_s Z_{i,s}\lambda_{i,s}^+\frac{r_s}{\omega_s}\right\}\Bigg|_{y_s = \exp(i\phi)}, \quad (34)$$

where L is the semicircle shown in Fig. 3 and where y_s are real-valued, is subtracted from and added to the expression on the right-hand side of equation (32). For the sake of brevity, we introduce the notation

$$M_{i,s} = Z_{i,s}P_L(x_0)\frac{r_s}{\omega_s}. \quad (35)$$

Equation (32) then reduces to the form

$$r_i = \Omega_i - I_L + I_C, \quad (36)$$

where the integral

$$I_C = -\frac{1}{3\pi^2}\oint_C dy_s M_{i,s}\ln\left\{\frac{y_i + a_1^j + i\gamma}{y_i - a_2^j + i\gamma}\right\} \quad (37)$$

is taken over the closed contour C going along the real axis from –1 to +1 and along the semicircle L in the inverse direction.

First, we consider the integral along the semicircle, I_L. At real values in the range $-1 \le y_i \le 1$ and at $y_s = \exp(i\phi)$, where $0 \le \phi \le \pi$, the quantity $\lambda^+(y_i, y_s)$ is finite—that is, it features no singularities. This is not so only for the extreme points of the semicircle L (see Fig. 3), where $\arg(x_s) = 0$ or π. However, a circumvention of these points along circles of infinitely small radius δ yields a contribution proportional to $\delta\ln\delta$; therefore, this contribution can be disregarded.

It is important that the integral I_L involves the function r_s defined on the semicircle L, whereby the closure problem is solved.

We now proceed to estimate the integral I_C for real y_i values satisfying the condition $y_i \le 1$. This integral can be evaluated by conventional methods of the theory of analytic functions by taking into account the important circumstance that the function $M_{i,s}$ is analytic everywhere inside the contour C and on the contour itself. Further, the logarithmic function that appears on the right-hand side of (24) and which generates the difficulties studied here can be represented in the form

$$\ln\left\{\frac{y_i + i\gamma + a_1^s}{y_i + i\gamma - a_2^s}\right\} = \ln\left\{\frac{1/2 + i\gamma + a_1^s}{1/2 + i\gamma - a_2^s}\right\} - \int_{y_i}^{1/2} dt\left\{\frac{1}{t + i\gamma + a_1^s} - \frac{1}{t + i\gamma - a_2^s}\right\}. \quad (38)$$

It should be noted that the first term on the right-hand side of (38) makes zero contribution to I_C because its branch points are situated outside the contour C. In other words, the singularities of the function $\lambda^+(y_i, y_s)$ in y_s do not belong to the contour C if $y_i > 1/2$. The singularities are determined by the second term for $y_i \le 1/2$. Here, the situation is more intricate because the singular points at complex values of y_s are within the contour C, occurring immediately above the real axis. Let us represent the contribution of this term as

$$I_C = \frac{1}{3\pi^2}\oint_C dy_s M_{i,s} \times \int_{y_i}^{1/2} dt\left\{\frac{1}{t + i0 + a_1(y_s)} - \frac{1}{t + i0 - a_2(y_s)}\right\} \quad (39)$$

and change the order of integrations. This is quite legitimate because, in the integration along the contour C near the point of singularity, the contribution to the integral from the interval $(-\delta, +\delta)$ for $\delta \to 0$ is proportional to $\delta\ln\delta$; therefore, this contribution can be disregarded.

The integral I_C can be represented as

$$I_C = \frac{1}{3\pi^2}\int_{x_i}^{1/2} dt\{J_1 - J_2\}, \quad (40)$$

where

$$J_1 = \oint_C dy_s \frac{M_{i,s}}{t + i0 + a_1^s}, \quad (41)$$

$$J_2 = \oint_C dy_s \frac{M_{i,s}}{t + i0 - a_2^s}. \quad (42)$$

The integrals in (41) and (42) can be simplified. For example, the expression for J_1 can be recast into the form

$$J_1 = \oint_C dy_s M_{i,s}\frac{t + i0 + a_2^s}{(t + i0 + a_1^s)(t + i0 + a_2^s)} = \oint_C dy_s M_{i,s}\frac{t + i0 + a_2}{(y_s + a_1(t + i0))(y_s + a_2(t + i0))}, \quad (43)$$

where we have used the obvious equality

$$(t + i0 + a_1^s)(t + i0 + a_2^s) = (t + i0)^2 + (t + i0)y_s + y_s^2 - 3/4 = [y_s + a_1(t + i0)][y_s + a_2(t + i0)]. \quad (44)$$

From the expression for J_1, it can be seen that the singularities of the integrand in the complex variable y_s are fixed by the variable t. The two singularities occur within the contour C: one is at $y_s = -a_1(t)$ for $t \le 1/2$, while the other is at $y_s = -a_2(t)$ for $t \le -1/2$.

We note that, at the point $y_s = -a_1(t)$, the residue involves the factor

$$t + i0 + a_2(-a_1(t)) = t + i0 - a_1(a_1(t)) = t + i0 - t$$

[see the transformations given by (10) and (11)]; that is, it is equal to zero. The residue at the other singular point, $y_s = -a_2(t)$, involves the factor

$$t + i0 + a_2(-a_2(t)) = t + i0 - a_1(a_2(t)) = t + i0 + a_1(t),$$

which is different from zero.

Thus, we conclude that $J_1(t) = 0$ for $-1/2 < t < 1$ and that

$$J_1 = \pi i\frac{t + a_1(t)}{b_t}\{M_{i,s}\}\big|_{y_s = -a_2(t)} = 2\pi i a_2'(t)\{M_{i,s}\}\big|_{y_s = -a_2(t)} \quad (45)$$

for $-1 \le t \le -1/2$.

For the integral J_2, we similarly obtain $J_2(t) = 0$ for $1/2 < t \le 1$ and

$$J_2 = \pi i \frac{t + a_2(t)}{b_t} \{M_{i,s}\}\Big|_{y_s = a_1(t)} = -2\pi i a_1'(t) \{M_{i,s}\}\Big|_{y_s = a_1(t)} \quad (46)$$

for $-1 \le t \le 1/2$.

Eventually, we have the following results:

(a) for $1/2 < y_i \le 1$,

$$I_C = 0; \quad (47)$$

(b) for $-1/2 \le y_i \le 1/2$,

$$I_C = \frac{2i}{3\pi} \int_{a_1^i}^{1} dt Z_{i,t} P_L(x_0) \frac{r_t}{\omega_t}; \quad (48)$$

(c) for $-1 \le y_i \le -1/2$,

$$I_C = \frac{2i}{3\pi} \left\{ \int_{a_1^i}^{1} + \int_{-a_2^i}^{1} \right\} dt Z_{i,t} P_L(x_0) \frac{r_t}{\omega_t}. \quad (49)$$

We note that the integrand in I_C involves the function r_t specified at real values of the argument t. All the remaining quantities [$Z_{i,t}$, $P_L(x_0)$, etc.] also involve real momentum variables (y_i and t instead of y_s).

Let us summarize our results. For the problem of three-body scattering at positive total energies of the system, we have derived a closed set of equations whose kernels feature no moving singularities on the contour of integration; that is, the problem in question can be solved within conventional computational schemes.

We will now present this set of equations in an eventual form.

(i) For $|y_i| \le 1$, where $y_i = \exp(i\xi_i)$ ($0 \le \xi_i \le \pi$), the function $r(\xi_i) \equiv r(y_i = \exp(i\xi_i))$ satisfies the equation

$$r(\xi_i) = \Omega_i + \frac{2}{3\pi^2} \int_{-1}^{1} dy_s Z_{i,s} \lambda_{i,s}^{+} \frac{r_s}{\omega_s}. \quad (50)$$

At real y_i satisfying the condition $-1 \le y_i \le 1$, the equation for r_i takes the form

$$r_i = \Omega_i - i \frac{2}{3\pi^2} \int_0^{\pi} d\phi r(\phi) \left\{ y_s Z_{i,s} \frac{\lambda_{i,s}^{+}}{\omega_s} \right\}\Big|_{y_s = \exp(i\phi)} + I_C, \quad (51)$$

where Ω_i is given by

$$\frac{2}{y_i}\Omega_i = -V_{i,0} + \frac{2k_Z}{3\pi^2} \int_{-1}^{1} y_s dy_s \Delta V_{i,s} \frac{r_s}{\omega_s} + \frac{2k_Z}{3\pi^2} \int_1^{\infty} y_s^2 dy_s V_{i,s} \frac{f_s}{\omega_s}, \quad (52)$$

while I_C is defined in (47)–(49).

(ii) In the region $y_i > 1$, the equation for the scattering amplitude has a nearly conventional form:

$$f_i = -V_{i,0} + \frac{2k_Z}{3\pi^2} \int_{-1}^{1} y_s dy_s V_{i,s} \frac{r_s}{\omega_s} + \frac{2k_Z}{3\pi^2} \int_1^{\infty} y_s^2 dy_s V_{i,s} \frac{f_s}{\omega_s}. \quad (53)$$

Here, all momentum variables are real-valued.

Equation (50) relates the function $r[y_i = \exp(i\xi_i)]$ specified on the semicircle L to its values on the real axis—that is, to $r(y_s)$, where $-1 \le y_s \le 1$. Equation (51) defines the inverse dependence—it expresses the function specified on the real axis in terms of the function on the semicircle. Finally, equation (53) determines the scattering amplitude in the region $y_i > 1$—that is, the physical amplitude (at the point $y_i = y_0$).

Thus, instead of two equations (14) and (15) corresponding to one original equation (2) with a singular kernel, we have obtained a set of three equations whose kernels feature no singularities.

We note that only on the real segment $-1 \le y_{i,s} \le +1$ can we relate the same values r^+ by the same equation, but this is achieved through a singular kernel [see equation (32)]. The values r^+ defined on any other contour—for example, on the semicircle L—cannot be related by one equation. This is because the contour of the integral I_C always circumvents moving branch points, which occur within the contour C for any complex values of y.

In the case considered above, singular points penetrate into the region circumvented by the contour C and occur immediately above the real axis. The curve in question, which corresponds to a circumvention of the moving branch points in I_C, then proves to be adjacent to the real y_s axis from above, and the new values r^+ involved will be coincident with the old ones—that is, with the values on the real axis proper. Thus, the set of equations obtained in the present study becomes closed.

REFERENCES

1. V. B. Belyaev, *Lectures on the Theory of Few-Body Systems* (Énergoatomizdat, Moscow, 1986).

2. E. W. Schmid and H. Ziegelmann, *The Quantum Mechanical Three-Body Problem* (Nauka, Moscow, 1979; Pergamon, Oxford, 1974).
3. *Proceedings of the XIV European Conference on Few-Body Problems in Physics, Amsterdam, 1993*, in Few-Body Syst. Suppl., Vol. 7 (Springer-Verlag, Vienna, 1994).
4. J. Hetherington and L. H. Schick, Phys. Rev. B **137**, 935 (1965).
5. F. Sohre and H. Ziegelmann, Phys. Lett. B **34**, 579 (1971).
6. L. D. Faddeev, Tr. Mat. Inst. im. V. A. Steklova, Akad. Nauk SSSR **69** (1963).
7. S. P. Merkuriev and L. D. Faddeev, *Quantum Scattering Theory for Few-Body Systems* (Nauka, Moscow, 1985).
8. E. O. Alt, P. Grassberger, and W. Sandhas, Nucl. Phys. B **2**, 167 (1967).
9. F. M. Pen'kov and N. Zh. Takibayev, Yad. Fiz. **56** (7), 97 (1993) [Phys. At. Nucl. **56**, 911 (1993)].
10. N. Zh. Takibayev and A. C. Liventsova, Preprint No. 7, INP NRC RK (Institute of Nuclear Physics, National Research Center, Republic of Kazakhstan, Almaty, 1998).

Translated by A. Isaakyan

Physics of Atomic Nuclei, Vol. 63, No. 4, 2000, pp. 582–587. Translated from Yadernaya Fizika, Vol. 63, No. 4, 2000, pp. 646–651.

NUCLEI
Theory

Simple Local *NN* Potentials Involving Forbidden States and Polarization in *ed* Scattering

S. B. Dubovichenko* and I. I. Strakovsky[1), **]

Kazakh State University, ul. Timiryazeva 46, Almaty, 480121 Republic of Kazakhstan,
and Institute for Physics and Technology, National Academy of Sciences of Kazakhstan, Almaty, Republic of Kazakhstan

Received November 16, 1998

Abstract—A simple *NN* potential is proposed in an analytic form. The parameters of this potential are fixed by fitting the effective range, the scattering length, and the deuteron binding energy. The phase shifts for *np* scattering at energies ranging up to 500 MeV and the properties of the deuteron are calculated with the resulting parameters. The effect of the πNN coupling constant on the potential parameters and on the accuracy in describing various properties of *NN* interaction is explored. The results of the present calculations are found to be in good agreement with experimental data, with available results from *NN* partial-wave analyses, and with the results of calculations with Nijmegen potentials. The tensor polarization t_{20} in elastic electron–deuteron scattering is analyzed by using some *NN* interactions. © *2000 MAIK "Nauka/Interperiodica".*

A phenomenological triplet *NN* potential involving a tensor component and the one-pion-exchange potential (OPEP) was proposed in [1]. This potential provides a good description of phase shifts for energies up to 500 MeV and of the properties of the deuteron, including form factors $A(q)$ and $B(q)$ for momentum transfers $q < 6$ fm^{-1}. The wave functions calculated with it for the deuteron and for *np* scattering have a node at a distance of about 0.52 fm in the *S* wave and are nodeless in the *D* wave. The parameters of the potential involving a forbidden state were fixed by fitting only the scattering length, the effective range, and the deuteron binding energy, all other properties of the deuteron being calculated with the parameters obtained in this way. It was shown that the potential in question provides a more accurate description of all the above features of *NN* scattering than the Gaussian and the exponential versions of deep interaction (see [2] and [3], respectively), which lead to wave functions that have nodes both in the *S* and in the *D* wave.

The approach based on the concept of forbidden states [4] assumes that the deuteron ground state corresponds to the {42} orbital symmetry consistent with the orbital-angular-momentum values of $L = 0$, 2 and that the first bound state of {6} orbital symmetry is forbidden. This means that the triplet interaction potential involves a low-lying forbidden state and that the deuteron ground state corresponds to the second bound state in this potential. Therefore, the wave function of the deuteron ground state must have a node only in the *S* wave.

The πNN coupling constant $f^2 = 0.0776$ determined in [5] from an analysis of the features of *NN* scattering was used in [1] to specify the deep *NN* potential. At the same time, other values of this constant are also known—for example, the values of $f^2 = 0.074$ and $f^2 = 0.076$ were obtained in [6] and [7], respectively.

In view of this, it is of interest to establish the dependence of the parameters of deep potentials involving forbidden states on the πNN coupling constant and to study the sensitivity of the description of the results obtained from *NN* partial-wave analyses to variations in this coupling constant. Following [1], we use here the *NN* local potential

$$V(r) = V_c(r) + V_t(r)S_{12},$$

where the tensor operator S_{12} has the conventional form $S_{12} = 3(n\sigma_1)(n\sigma_2) - (\sigma_1\sigma_2)$ [8] and

$$V_c(r) = -V_0\exp(-\alpha r) + V_{oc}(r)g(r),$$

$$V_t(r) = V_{ot}(r)[g(r)]^{20}.$$

In accordance with [1–3], the central and tensor components of the OPEP are written, respectively, as

$$V_{oc}(r) = -V_1\exp(-\mu r)/(\mu r)$$

and as

$$V_{ot}(r) = -V_1[1 + 3/(\mu r) + 3/(\mu r)^2]\exp(-\mu r)/(\mu r),$$

where the function $g(r) = 1 - \exp(-\alpha r)$ cuts off the tensor component at small distances. As in [1–3], the average mass of the pions is set to $m_\pi = 138.03$ MeV, which leads to $\mu = m_\pi/\hbar c = 0.6995$ fm^{-1} ($\hbar c = 197.327$ MeV fm).

[1)] Petersburg Nuclear Physics Institute, Russian Academy of Sciences, Gatchina, St. Petersburg, 188350 Russia, and George Washington University, Washington, DC, USA.

* e-mail: serg@lorton.com

** e-mail: igor@gwis2.circ.gwu.edu

1063-7788/00/6304-0582$20.00

In our calculations, we also use the value of $\hbar^2/m_N = 41.47$ MeV fm^2. The depth of the OPE potential is related to the πNN coupling constant f^2 as $V_1 = m_\pi f^2$ [1, 3].

For each f^2 value, the potential parameters were determined by fitting the effective range r_0, the scattering length a_0, and the deuteron binding energy E_d; after that, the *np* phase shifts for energies up to 500 MeV, mixing parameters, and the properties of the deuteron were calculated with the parameter values found in this way. The results of recent *NN* partial-wave analyses are presented in [6, 9], while the properties of the deuteron can be found in [5, 6]. Various features of the deuteron and of *np* scattering that were calculated here for the resulting versions of *NN* potentials are presented in the table versus f^2 values, along with the potential-parameter values. It can be seen that all features under consideration are faithfully reproduced in all cases and that, with increasing f^2, the quadrupole moment value somewhat decreases, falling between the results obtained in [5] and in [6]. At $f^2 = 0.0776$, the parameters of the singlet-interaction potential were found to be $\alpha = 3.30$ fm^{-1} and $V_0 = 3170.72$ MeV. The scattering length a_s and the effective range r_0 calculated with these α and V_0 values, $a_s = -23.716$ fm and $r_0 = 2.732$ fm, are in good agreement with the results presented in [5], $a_s = -23.715(15)$ fm and $r_0 = 2.73(3)$ fm.

The power-law exponent of the cutoff function in the tensor component of the OPEP was set to $N = 20$ in order to avoid the emergence of a node in the *D* wave. Small values of $N = 3$–5 do not remove the node [2, 3]; only by increasing N to 15 can we eventually get rid of a node. As a matter of fact, variations in the power-law exponent of the cutoff function affect only slightly the results of our calculations, and we can choose this exponent in the range $N \simeq 15$–30. A further increase in this exponent spoils the description of the *np* phase shifts, but the general shape of the deuteron wave function remains virtually intact.

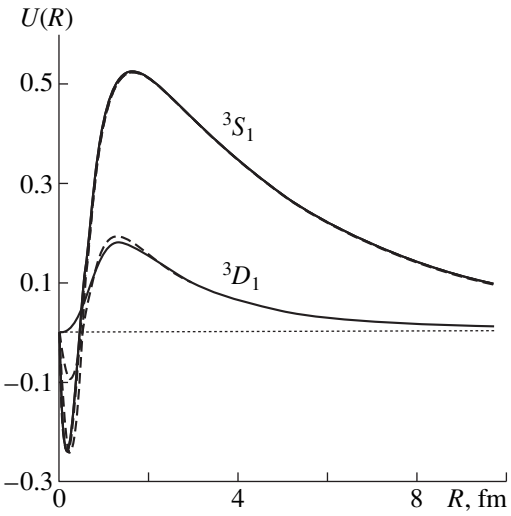

Fig. 1. Deuteron wave function calculated for various *NN* potentials. The meaning of the curves is explained in the main body of the text.

For any version of the *NN* potential, the deuteron wave function has a node in the *S* wave at a distance in the range 0.50–0.52 fm; as to the *D* wave, it has no nodes. These statements are illustrated by the solid curves in Fig. 1, which were calculated for $f^2 = 0.074$.

Properties of the deuteron and of *np* scattering for various versions of *NN* potentials

Version of the *NN* potential	E_d, MeV	Q_d, fm^2	P_D, %	A_S	$\eta = A_S/A_D$	a_t, fm	r_t, fm	R_d, fm	V_1, MeV	$f^2_{\pi NN}$	α, fm^{-1}	V_0, MeV
LP1	2.2246	0.271	5.62	0.884(1)	0.0253 (1)	5.417	1.753	1.965	10.076	0.0730	3.68	3495.641
LP2	2.2246	0.274	5.75	0.884(1)	0.0256 (1)	5.417	1.753	1.966	10.214	0.0740	3.72	3524.172
LP3	2.2246	0.279	6.00	0.884(1)	0.0261 (1)	5.419	1.754	1.967	10.490	0.0760	3.80	3575.435
LP4	2.2246	0.285	6.23	0.884(1)	0.0266 (1)	5.417	1.751	1.968	10.710	0.0776	3.90	3652.860
LP5	2.2246	0.290	6.56	0.884(1)	0.0273 (1)	5.419	1.752	1.968	11.080	0.0803	4.05	3744.980
Nijm93 [6]	2.224575 (9)	0.271 (1)	5.67	0.8845 (8)	0.0253 (2)	5.4194 (20)	1.7536 (25)	1.9676(10)	–	0.074	–	–
CERN [5]	2.224579 (9)	0.2859 (3)	–	0.8802 (20)	0.0271 (4)	5.419 (7)	1.754(8)	1.9560(68)	10.71 (12)	0.0776	–	–

Note: The abbreviation LP denotes local potentials.

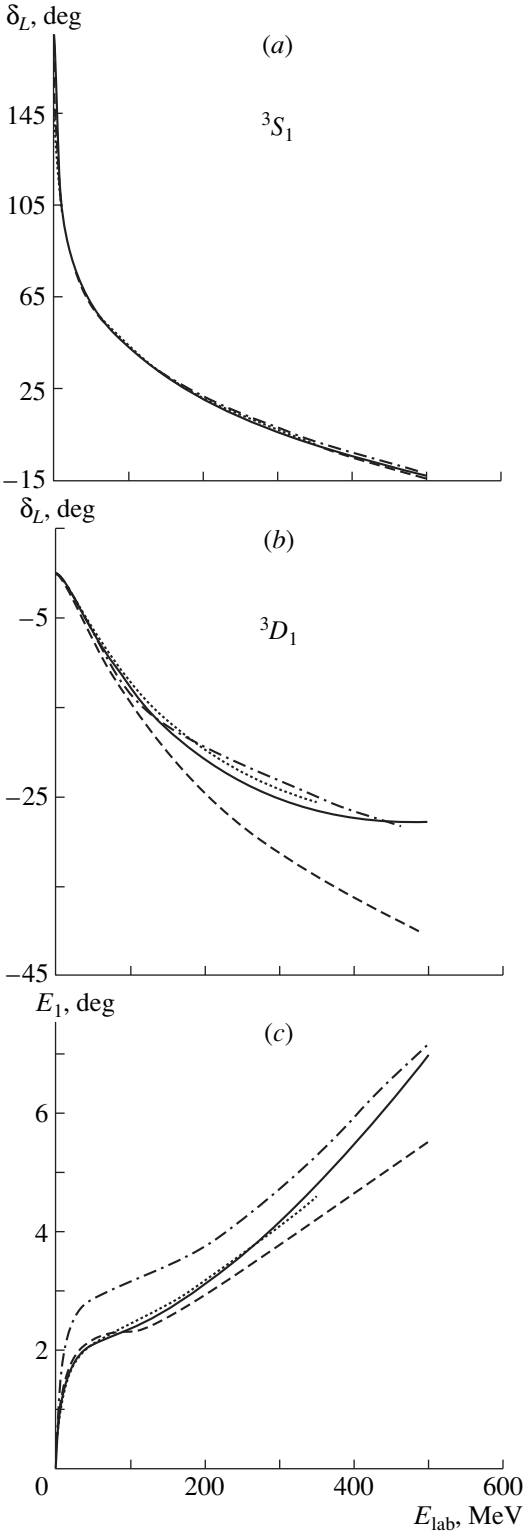

Fig. 2. (*a*, *b*) Triplet phase shifts and (*c*) mixing parameter for *NN* scattering.

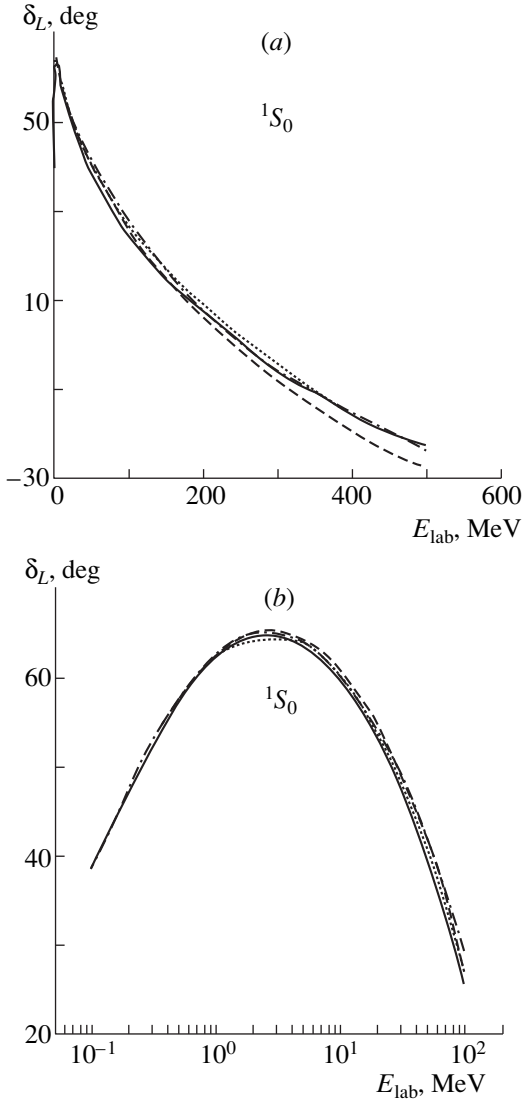

Fig. 3. Singlet phase shifts for *NN* scattering.

The dashed curves in Fig. 1 represent the wave functions obtained in [2] with a Gaussian potential.

Figures 2 and 3 show the phase shifts and mixing parameter calculated with the parameter values presented in the table for $f^2 = 0.074$ (solid curves), the results of SM97 partial-wave analysis from [9] (dash-dotted curves), the phase shifts obtained in [6] (dotted curves), and the phase shifts calculated with the potential presented in [2] (dashed curves).

The accuracy in describing the triplet phase shifts for $f^2 > 0.076$—in particular, for f^2 in the range 0.0776–0.0803 [5, 10]—is much poorer. For example, the *D*-wave phase shift decreases faster than in the partial-wave analysis. This is clearly illustrated in Fig. 2*b*, where the dashed curve calculated for the Gaussian potential from [2] at $f^2 = 0.07745$ shows a much steeper decrease. The value of 0.074 proposed in [6] for the πNN coupling constant is preferable for describing more precisely the *D*-wave phase shift.

Figure 4 presents the deuteron form factors calculated with the ground-state wave function for the exponential interaction at $f^2 = 0.074$ (solid curves) and the

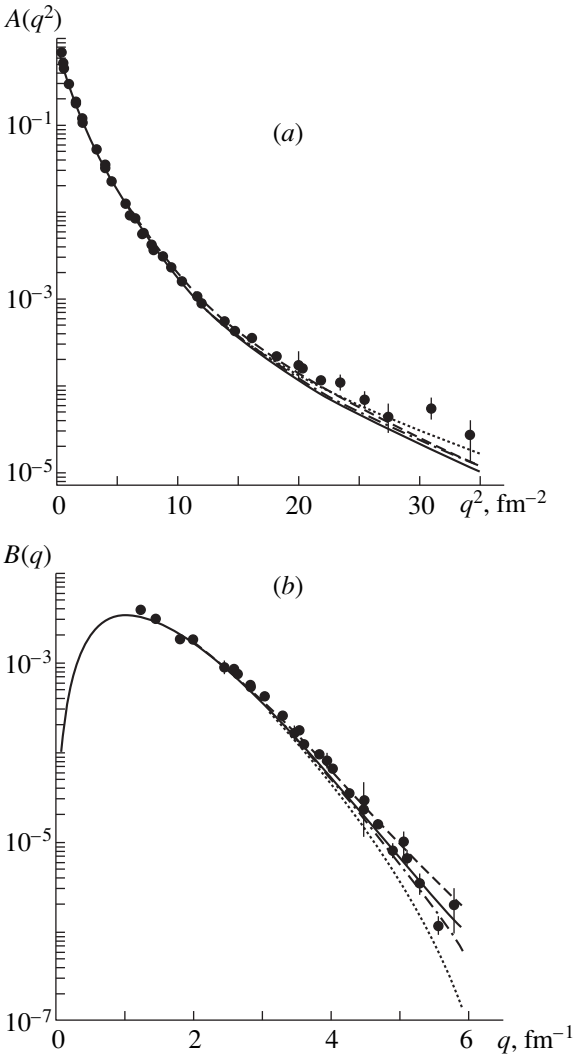

Fig. 4. Deuteron form factors calculated for various *NN* potentials.

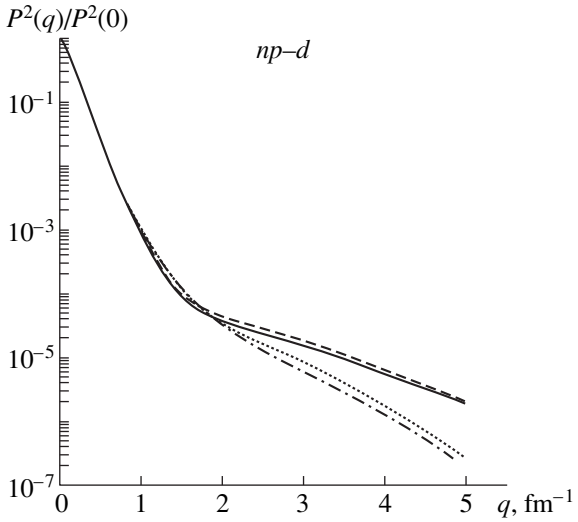

Fig. 5. Momentum distributions of nucleons in the deuteron.

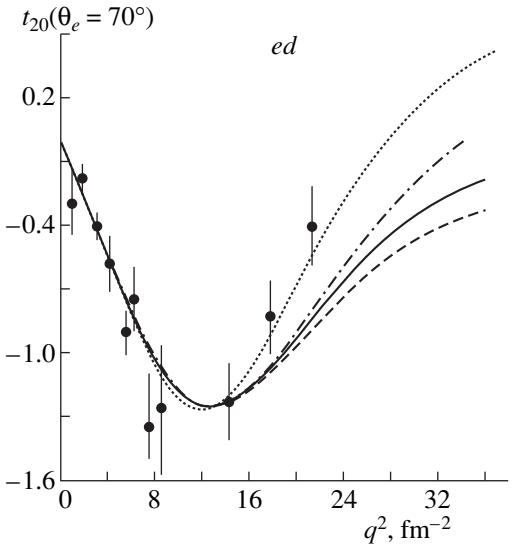

Fig. 6. Tensor polarization t_{20} in *ed* scattering.

results obtained with the potential from [2] (dashed curves), with the Reid potential [8] (dotted curves), and with the Nijmegen potential Nijm93 [11] (dash-dotted curves). Experimental data were taken from [12].

The form factors were calculated on the basis of nonrelativistic expressions from [2, 12]. This is justified by a comparison drawn in [13] between relativistic and nonrelativistic computational procedures as implemented with the Paris and Argonne potentials. It turned out that, in the momentum-transfer range q = 3.5–4.0 fm^{-1}, there is no significant difference between the results. Relativistic effects become sizable for higher momentum transfers of q = 4.0–6.0 fm^{-1}, but they do not considerably affect the shape of the form factors and do not play a dominant role. Relativistic corrections were also considered in [14], where it was demonstrated that they do not make a crucial contribution in the momentum-transfer region extending to 5 or 6 fm^{-1}, nor do their values exceed the experimental errors.

Figure 5 shows the momentum distributions of nucleons in the deuteron for f^2 = 0.074 (solid curve); for a momentum transfer of $q \sim 3$ fm^{-1}, they are approximately 1.5–2 times less than those for the potential leading to a node in the *D* wave [2] (dashed curve). The dotted and dash-dotted curves in Fig. 5 represent the results for, respectively, the Reid potential and the Nijm93 potential [11].

It was shown in [15] that the potentials that were presented in [2] and which lead to a node in the *D* wave yield strongly overestimated cross sections for proton-induced deuteron disintegration and for backward *pd* scattering at high momentum transfers. It is commonly

believed that this is due to comparatively large momentum distributions for potentials that lead to two nodes in the wave function. That the momentum distributions at momentum transfers of about 3 fm^{-1} are less for interactions leading to a node only in the S wave can improve the theoretical description of the cross sections for elastic *pd* scattering and deuteron disintegration.

With the potentials obtained here, we also considered the tensor polarization observables for elastic *ed* scattering that are defined as (see, for example, [13, 16])

$$d\sigma/d\Omega = S(d\sigma/d\Omega)_{\text{Mott}},$$

$$S = A(q) + B(q)\tan^2(\theta_e/2),$$

$$A(q) = G_c^2(q) + (8\eta^2/9)G_q^2(q) + (2\eta/3)G_m^2(q),$$

$$B(q) = (4\eta/3)(1+\eta)G_m^2(q),$$

$$t_{20} = -(S/\sqrt{2})\{(8\eta/3)G_cG_q + (8\eta^2/9)G_q^2 + (\eta/3)[1+2(1+\eta)\tan^2(\theta_e/2)]G_m^2\},$$

where $A(q)$ and $B(q)$ are the deuteron form factors; η is the Coulomb parameter; and G_c, G_q, and G_m are the structure functions defined in terms of the wave functions in [13, 16].

Figure 6 displays the polarization t_{20} calculated for $f^2 = 0.074$ (solid curve) and the corresponding results obtained for the potential from [2] (dashed curve), for the Nijmegen potential Nijm I [11] (dash-dotted curve), and for the Reid potential [8] (dotted curve). Experimental data were taken from [13, 16]. It can be seen that, at low momentum transfers, the results obtained by using the different potentials are virtually coincident. The difference between the results corresponding to the potentials involving a repulsive core and those corresponding to the potentials involving forbidden states becomes pronounced for $q > 15$ fm^{-1}. However, no definitive conclusion in favor of a specific interaction type can be drawn at present because of the absence of data at high momentum transfers and because of large experimental uncertainties. But even at this stage, we can see that the potential from [2] leads to an underestimated value of t_{20} for $q^2 > 20$ fm^{-2}. The potential version with $f^2 = 0.074$ yields somewhat better results, but they also fall significantly short of the experimental data. For the tensor observables t_{21} and t_{22}, available experimental data are scanty, the uncertainties in them being so large that no decision in favor of one potential type or another can be made.

In summary, it can be seen that all properties of the *np* system that have been considered here can be successfully described on the basis of a simple two-parameter deep potential leading to a node only in the S wave. For the proposed interaction form, as well as for the Nijmegen potentials [11], small values of the πNN coupling constant are preferable, because they provide a better description of available experimental data on the deuteron and on *np* scattering.

ACKNOWLEDGMENTS

We are grateful to V.I. Kukulin and V.S. Parke for stimulating discussions on some specific points of the problem considered in this study; to D. Phillips for a discussion on relativistic corrections and for placing experimental data on the deuteron form factors at our disposal; and to M. Garson, S.V. DeYager, and D.M. Nikolenko for providing access to data on tensor polarizations.

This work was supported in part by grant no. DE-FG02-95ER4090138 from the Department of Energy of the USA and by a grant from the National Academy of Sciences of Kazakhstan.

REFERENCES

1. S. B. Dubovichenko, in *Proceedings of XVI European Conference on Few-Body Problems in Physics, Autrans, France, 1998*, p. 49; in *Nuclear Spectroscopy and Nuclear Structure* (St. Petersburg, 1998), p. 115; nucl-th/9803005; nucl-th/9805030.
2. V. I. Kukulin, V. N. Pomerantsev, V. M. Krasnopol'sky, *et al.*, Phys. Lett. B **135**, 20 (1984); **165**, 7 (1985); V. I. Kukulin, V. N. Pomerantsev, A. Faessler, *et al.*, Phys. Rev. C **57**, 535 (1998).
3. S. B. Dubovichenko, Yad. Fiz. **60**, 704 (1997) [Phys. At. Nucl. **60**, 621 (1997)]; in *Proceedings of 12th International Symposium on High Energy Spin Physics, Amsterdam, 1996*, p. 250; nucl-th/9803001.
4. V. G. Neudatchin, I. T. Obukhovsky, V. I. Kukulin, *et al.*, Phys. Rev. C **11**, 128 (1975); V. G. Neudatchin, I. T. Obukhovskii, and Yu. F. Smirnov, Phys. Lett. B **43**, 13 (1973); in *Proceedings of International Conference on Cluster Structures in Nuclear Physics, Chester, England, 1985*, p. 353.
5. T. E. O. Ericson, Nucl. Phys. A **416**, 281 (1984); T. E. O. Ericson and M. Rosa-Clot, Nucl. Phys. A **405**, 497 (1983).
6. J. J. de Swart, C. P. F. Terheggen, and V. G. J. Stoks, in *Proceedings of 3rd International Symposium "Dubna-Deuteron 95," Dubna, Russia, 1995* (JINR, Dubna, 1996); V. Stoks, R. Timmermans, and J. J. de Swart, Phys. Rev. C **47**, 512 (1993); V. G. J. Stoks, R. A. M. Klomp, M. C. M. Rentmeester, *et al.*, Phys. Rev. C **48**, 792 (1993).
7. R. A. Arndt, I. I. Strakovsky, R. L. Workman, *et al.*, Phys. Rev. C **52**, 2120 (1995).
8. R. V. Reid, Ann. Phys. **50**, 411 (1968).
9. R. A. Arndt, C. H. Oh, I. I. Strakovsky, *et al.*, Phys. Rev. C **56**, 3005 (1997).
10. G. Hohler, in *Landoldt-Bornstein: Pion–Nucleon Scattering*, Ed. by H. Schopper (Springer-Verlag, 1983), Vol. I/9b2.
11. V. G. J. Stoks, R. A. M. Klomp, C. P. F. Terheggen, *et al.*, Phys. Rev. C **49**, 2950 (1994); J. J. de Swart, R. A. M. Klomp, M. C. M. Rentmeester, *et al.*, Few-Body Syst., Suppl. **8**, 43 (1995).

12. D. J. Drickey and L. N. Hand, Phys. Rev. Lett. **9**, 521 (1962); C. D. Buchanan and M. R. Yearian, Phys. Rev. Lett. **15**, 303 (1965); J. F. Elias, J. I. Friedman, G. C. Hartmann, *et al.*, Phys. Rev. **177**, 2075 (1969); R. G. Arnold, B. T. Chertok, E. B. Dally, *et al.*, Phys. Rev. Lett. **35**, 776 (1975); G. G. Simon, Ch. Schmitt, and V. H. Walther, Nucl. Phys. A **364**, 285 (1981); R. Cramer *et al.*, Z. Phys. C **29**, 513 (1985); S. Platchkov, A. Amroun, S. Auffret, *et al.*, Nucl. Phys. A **508**, 343 (1990); S. Auffret, J. M. Cavedon, J. C. Clemens, *et al.*, Phys. Rev. Lett. **54**, 649 (1985).

13. M. Garson, J. Arvieux, D. H. Beck, *et al.*, Phys. Rev. C **49**, 2516 (1994).

14. D. R. Phillips, S. J. Wallace, and N. K. Devine, Phys. Rev. C **58**, 2261 (1998).

15. C. F. Perdrisat and V. Punjabi, Phys. Rev. C **42**, 1899 (1990); O. Imambekov, Yu. M. Uzikov, and L. V. Schevchenko, Z. Phys. A **332**, 349 (1989).

16. M. Ferro-Luzzi, M. Bouwhuis, E. Passonier, *et al.*, Phys. Rev. Lett. **77**, 2630 (1996); V. F. Dmitriev, D. M. Nikolenko, S. G. Popov, *et al.*, Phys. Lett. B **157**, 143 (1985); B. B. Voĭtsekhovskiĭ, D. M. Nikolenko, K. T. Ospanov, *et al.*, Pis'ma Zh. Éksp. Teor. Fiz. **43**, 567 (1986) [JETP Lett. **43**, 733 (1986)]; R. Gilman, R. J. Holt, E. R. Kinney, *et al.*, Phys. Rev. Lett. **65**, 1733 (1990); M. E. Schulze, D. Beck, M. Farkhonden, *et al.*, Phys. Rev. Lett. **52**, 597 (1984); I. The, J. Arvieux, D. H. Beck, *et al.*, Phys. Rev. Lett. **67**, 173 (1991).

Translated by R. Tyapaev

Physics of Atomic Nuclei, Vol. 63, No. 4, 2000, pp. 588–593. Translated from Yadernaya Fizika, Vol. 63, No. 4, 2000, pp. 652–658.

ELEMENTARY PARTICLES AND FIELDS
Experiment

Investigation of the Narrow Structure *K*(1630) Decaying into the $K_S^0\pi^+\pi^-$ System

V. M. Karnaukhov, C. Coca[1)], and V. I. Moroz

Joint Institute for Nuclear Research, Dubna, Moscow oblast, 141980 Russia

Received June 22, 1998; in final form, April 23, 1999

Abstract—The narrow structure *K*(1630) is singled out in the effective-mass spectrum of the $K_S^0\pi^+\pi^-$ system originating from π^-p collisions at 16 GeV/*c*. This structure is predominantly formed in inelastic collisions accompanied by high momentum transfers. For events from the *K*(1630) region, kinematical distributions show special features that may be associated with spin manifestations and with correlations between the products arising from the decays of the hypothesized exotic resonance state. Experimental observations of narrow hadronic structures formed at high momentum transfers are reviewed. © *2000 MAIK "Nauka/Interperiodica".*

1. INTRODUCTION

Experimental data collected with a 2-m hydrogen bubble chamber at CERN indicate that, in the effective-mass spectrum of the $K_S^0\pi^+\pi^-$ system formed in π^-p collisions at 16 GeV/*c*, there is a narrow enhancement characterized by the mass and width values of $M = 1629 \pm 7$ MeV/c^2 and $\Gamma = 16^{+19}_{-16}$ MeV/c^2, respectively, and referred to as *K*(1630) (see Fig. 1*a*, which illustrates the data for four-prong events each featuring a detected K_S^0 meson). The enhancement is not sensitive to variations in the bin width of the effective-mass spectrum within 50 MeV/c^2, nor could it be explained by kinematical reflections from any known resonances [1].

In the same data sample, the effective-mass spectra of the neutral systems $K^+\pi^+\pi^-\pi^-$, $K^-\pi^-\pi^+\pi^+$, and $K_S^0\pi^+\pi^+\pi^-\pi^-$ showed narrow enhancements near 1.63 GeV/c^2 (see Fig. 1*b*). Likewise, the effective-mass spectra of $K^+\pi^+\pi^-$ and $K^+\pi^-\pi^-$ (exotic system) from four-prong events each featuring a detected Λ hyperon proved to be weakly enhanced near the same mass of 1.63 GeV/c^2 [2] (see Fig. 1*c*).

In analyzing the *K*(1630) structure, we were able to reveal kinematical distinctions between the groups of events populating the central and sideband regions of this structure in the effective mass of the $K_S^0\pi^+\pi^-$ system. The origin of these distinctions appears to be systematic rather than purely statistical. The structure *K*(1630) is manifested predominantly in events characterized by high momentum transfers from the primary π^- meson to the secondary one accompanying *K*(1630) production [1, 2], $t' > 0.8$ (GeV/c)^2, where $t' = |t - t_{\min}|$, t being the square of the 4-momentum transfer.

Available data on the formation of $K\pi\pi$ resonances were obtained primarily by studying quasi-two-body reactions. That these reactions are characterized by relatively low momentum transfers effectively suppresses the yield of *K*(1630) with respect to fragmentation processes if this hypothetical state is indeed formed at high momentum transfers. As a result, the statistics of an individual experiment prove to be insufficient for detecting the effect being discussed. The procedure used in [2] to push down statistical uncertainties that

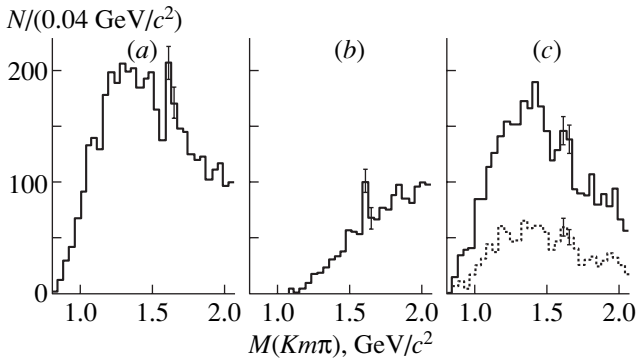

Fig. 1. Effective-mass distributions of weighted $Km\pi$ systems formed in π^-p collisions at 16 GeV/*c*: (*a*) distribution of the $K_S^0\pi^+\pi^-$ system for events each featuring a detected K_S^0 meson, (*b*) distribution of the $K^+\pi^+\pi^-\pi^- + K^-\pi^-\pi^+\pi^+ + K_S^0\pi^+\pi^+\pi^-\pi^-$ systems in events each featuring a detected K_S^0 meson, and (*c*) distribution of the $K^+\pi^+\pi^-$ and $K^+\pi^-\pi^-$ systems for events each featuring a detected Λ hyperon (the contribution of the exotic system $K^+\pi^-\pi^-$ is shown by the dashed histogram).

[1)] Institute of Atomic Physics, PO Box MG-6, R-76900 Bucharest, Romania.

1063-7788/00/6304-0588$20.00

are due to enhanced statistics involved combining the data from different bubble-chamber experiments [3, 4] for each $K\pi\pi$ channel that were included in the table presented in [5]. This procedure was justified by the fact that, in each of them, the mean event weight was close to unity. The combined effective-mass spectra, which are illustrated in Fig. 2, show a prominent peak associated with the known resonance $K_2^*(1430)$ and a narrow enhancements near 1.63 GeV/c^2.

Beyond the realm of bubble-chamber experiments, the formation of broad resonances in the reaction $K^-p \longrightarrow \bar{K}^0\pi^+\pi^-n$ at an incident-kaon momentum of 10 GeV/c was investigated with the broad-aperture spectrometer OMEGA at CERN [6]. Again, the effective-mass spectrum of the $\bar{K}^0\pi^+\pi^-$ system revealed, in addition to the peaks associated with the known broad resonances $K_2^*(1430)$ and $K_3^*(1780)$, a narrow enhancement occurring near 1.63 GeV/c^2 and reaching a level of some four standard deviations above the background. Of all $M(\bar{K}^0\pi^+\pi^-) < 2$ GeV/c^2 events detected in [6], about 10% are characterized by the squares of the 4-momentum transfers from the proton to the neutron, $t'(p \longrightarrow n)$, in excess of 0.8 (GeV/c)^2. The electron experiments that were reported in [7] and which applied the selections $t'(p \longrightarrow n) < 0.2$ and 0.3 (GeV/c)^2 to the same reaction at primary K^--meson momenta of 6 and 11 GeV/c [7] failed to detect a peak near 1.63 GeV/c^2 in the corresponding effective-mass spectra.

The emergence of exotic narrow resonances in multiparticle final states of high-momentum-transfer interactions was predicted theoretically in a number of studies (see, for example, [8]).

2. SELECTING THE $K(1630) \longrightarrow K_S^0\pi^+\pi^-$ SIGNAL

For π^-p interactions at 16 GeV/c that are detected in the 2-m hydrogen bubble chamber, an estimate of ionization in hydrogen along the tracks of secondaries indicates that the hypothesized resonance $K(1630) \longrightarrow K_S^0\pi^+\pi^-$ is predominantly formed along with a secondary π^- meson [2]. The transition that reveals the above resonance structure can be represented as

$$\pi_I^- p_I \longrightarrow (K_S^0\pi_1^+\pi_1^-)h_2^+\pi_2^-X^0, \qquad (1)$$

where the subscript I labels primary particles; π_1^+ and π^- are the pions that enter into the resonance structure being discussed, $K_S^0\pi^+\pi^-$; and h_2^+ (not necessarily identified) and π_2 are the extra charged secondaries; and X^0 stands for neutral secondaries that escaped detection in the bubble chamber. The assumption that π_2^- is of a resonance origin is not supported by the data.

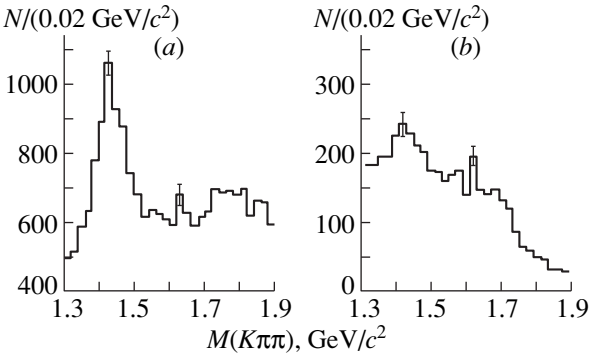

Fig. 2. Combined data of different experiments for the effective masses of various $K\pi\pi$ systems: (*a*) distribution of the $\bar{K}^0\pi^+\pi^-$ system formed in the reaction $K^-p \longrightarrow \bar{K}^0\pi^+\pi^-n$ at incident-kaon momenta of 3.9–16.0 GeV/c [3] and (*b*) distribution of the $K^0\pi^+\pi^- + K^+\pi^-\pi^0$ system formed in the reactions $\pi^-p \longrightarrow \Lambda K^0\pi^+\pi^-$ and $\pi^-p \longrightarrow \Lambda K^+\pi^-\pi^0$ at incident momenta of 3.8–6.0 GeV/c [4].

In an inelastic reaction featuring no charge exchange, a secondary identical to the projectile may provide a measure of inelasticity [9, 10]. In $K(1630)$-formation reactions of the type in (1), such a secondary (π_2^-) is predominantly emitted into the target hemisphere in the collision c.m. frame, picking up a high momentum from the projectile: $t'(\pi_I^- \longrightarrow \pi_2^-) > 0.8$ (GeV/c)^2 [1, 2]. In other words, the hypothetical state $K(1630)$ is predominantly formed in highly inelastic collisions, where the projectile invests the bulk of its energy in the emission of other secondaries, eventually appearing in the final state as a soft π^- meson. In accordance with this qualitative picture, such processes can be isolated by using the momentum of a π_2^- meson (or the angle of its deflection from the beam direction) in the laboratory frame. (Note that this kind of event selection may prove useful in a dedicated electron experiment.) Indeed, the resonance $K(1630)$ is predominantly formed in the kinematical region specified by inequalities

$$p(\pi_2^-) < 1800 \text{ MeV/}c, \quad \theta(\pi_I^-, \pi_2^-) \geq 0.24 \text{ rad}. \qquad (2)$$

For the case of these selections, the effective-mass spectrum of the $K_S^0\pi^+\pi^-$ system is illustrated in Fig. 3*a*. By the method of least squares, sections of the spectrum that were symmetric with respect to the peak were fitted either to

$$\text{BG}(M) = C(3) + C(1)M + C(2)M^2, \qquad (3)$$

or to

$$\text{BG}(M) = (M - M_{\text{sum}})^{C(3)}(C(1)M + C(2)M^2), \qquad (4)$$

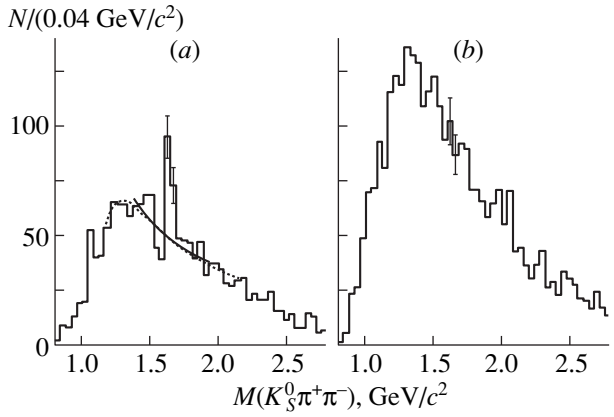

Fig. 3. Effective-mass distributions of weighted $K_S^0\pi^+\pi^-$ systems selected according to (*a*) (2) and (*b*) (5). In Fig. 3*a*, the solid and the dotted curve represent fits of the relevant distribution to the forms (3) and (4) over, respectively, the range 1.36–1.92 GeV/c^2 and the range 1.12–2.16 GeV/c^2, not including the peak region 1.60–1.68 GeV/c^2.

where M is the effective mass of the $K_S^0\pi^+\pi^-$ system, M_{sum} stands for the sum of the K_S^0, π^+, and π^- masses, and $C(i)$ are adjustable parameters.

Treating the enhancement in the range 1600–1680 MeV/c^2 as a statistical fluctuation and fitting the mass distribution over the interval 1360–1920 MeV/c^2, including the peak region, to the regular form (3), we arrive at a confidence level (C.L.) of only 0.00004. Excluding the peak region from the fit, we obtain C.L. = 0.14 (in Fig. 3*a*, the latter fit is depicted by the solid curve).

Fitting the mass spectrum in question over the entire interval 1120–2160 MeV/c^2 to the alternative form (4), we arrive at C.L. = 0.003. The fit without the peak region 1600–1680 MeV/c^2 yields 0.76. The latter fit, which is depicted by the dotted curve in Fig. 3*a*, yields a signal of 72.5 combinations, the background being constituted by 96.3 combinations. In the case of the null hypothesis treating the peak as a statistical fluctuation [11], its magnitude reaches 7.4 standard deviations.

Since the width of $K(1630)$ is small, the statistical significance of the peak is not totally immune to changing the interval of fitting the effective-mass distribution. In particular, a mass shift of 20 MeV/c^2 results in the least significant peak observed in the interval 1580–1700 MeV/c^2. Fitting the mass spectrum over the entire interval 1340–1940 MeV/c^2 to the form (3), we obtain C.L. = 0.002 in this case. When the peak region is excluded from the fit, the result is C.L. = 0.12. According to such estimates, the significance of the effect amounts to 5.5 standard deviations, the signal-to-background ratio being 0.5.

For the selections

$$p(\pi_2^-) \geq 1800 \text{ MeV}/c \quad \text{or} \quad \theta(\pi_I^-, \pi_2^-) < 0.24 \text{ rad}, \quad (5)$$

in which case at least one of the conditions in (2) is violated, we obtain the $K_S^0\pi^+\pi^-$ mass spectrum illustrated in Fig. 3*b*. Treating this distribution as a background to the distribution in Fig. 3*a* and normalizing it by area to the latter, we find an excess of 8.3 standard deviations above the background in the enhancement region.

A relatively high multiplicity of secondaries in reactions of the type in (1) implies high inelasticity and high 4-momentum transfers from the primary to the secondary particles. The conditions in (2) are aimed at selecting those collisions that are characterized by high momentum transfers from the primary π^- meson to the secondary π_2^- meson. The processes in question can be represented as

$$\pi_I^- p_I \longrightarrow (K_S^0\pi_1^+\pi_1^-)\pi_2^- B^+, \quad (6)$$

where B^+ stands for the baryonic system that is formed by the nonidentified positively charged secondary h_2^+ and the undetected neutral secondaries X^0. For the events populating the peak interval 1600–1680 MeV/c^2 of the mass spectrum in Fig. 3*a* (Fig. 3*b*), the mean values of $t'(\pi_I^- \longrightarrow K_S^0\pi_1^+\pi_1^-)$, $t'(\pi_I^- \longrightarrow \pi_2^-)$, and $t'(p_I \longrightarrow B^+)$ are 2.93 ± 0.27 (3.64 ± 0.30), 3.69 ± 0.20 (1.18 ± 0.11), and 3.85 ± 0.31 (2.04 ± 0.19) (GeV/c)^2, respectively. We can see that the values of $\langle t'(\pi_I^- \longrightarrow K_S^0\pi_1^+\pi_1^-)\rangle$ do not differ significantly, but that the values of $\langle t'(\pi_I^- \longrightarrow \pi_2^-)\rangle$ and $\langle t'(p_I \longrightarrow B^+)\rangle$ are much greater for the distributions showing the structure in Fig. 3*a*.

The degree of inelasticity of a $\pi^- p$ collision is measured by the inelasticity factor $K = (E(0) - E(\pi^-))/E(0)$, where $E(0)$ is the total collision energy in the target frame, while $E(\pi^-)$ is the energy of the secondary π^- meson (the energy of the leading one if the multiplicity of π^- mesons in the process is greater than unity)—that is, the inelasticity factor has the meaning of the total-energy fraction invested in the formation of all secondaries other than the leading π^- meson [10]. For the events populating the peak interval 1600–1680 MeV/c^2 of the $K_S^0\pi_1^+\pi_1^-$ mass spectrum in Fig. 3*a*, the mean value of K is estimated at 0.955 ± 0.002 if we use the energy of the π_2^- meson accompanying the hypothesized-resonance production and at 0.839 ± 0.010 if we use the energy of the fastest secondary π^- meson. Similar estimates for the spectrum in Fig. 3*b* are 0.798 ± 0.010 and 0.766 ± 0.010. We can see that criteria (2) isolate events characterized by a high degree of inelasticity; for $\pi^- p$ collisions producing the resonance $K(1630) \longrightarrow K_S^0\pi_1^+\pi_1^-$, the mean inelasticity factor is close to 0.955 ± 0.002 [here, the smallness of the quoted uncertainty reflects the fact that the K distribution of events selected according to (2) is relatively nar-

row owing to the softness of π_2^-). For the sake of comparison, we indicate that, in $\pi^- p$ collisions at 40 GeV/c [10], the mean values of the inelasticity factor for six-, eight-, ten-, and twelve-prong events were estimated at 0.76 ± 0.01, 0.77 ± 0.01, 0.81 ± 0.02, and 0.80 ± 0.02, respectively.

3. POSSIBLE SPIN MANIFESTATIONS

For the hypothesis of the $K_S^0\pi^+\pi^-$ resonance, we analyzed the distribution of events with respect to the cosine of the angle formed by the normal to the plane of the decay of the resonance (in its rest frame) and the direction of its motion in the $\pi^- p$ c.m. frame [$\cos\theta(\mathbf{n}_{K_S^0\pi^+\pi^-}, \mathbf{p}_{K_S^0\pi^+\pi^-})$]. For a strongly decaying state, such distributions can be described by the sum of Legendre polynomials of even degrees not exceeding $2J$, where J is the resonance spin [12]. For zero spin, the distribution in question must be isotropic.

Figure 4 shows the $\cos\theta(\mathbf{n}_{K_S^0\pi^+\pi^-}, \mathbf{p}_{K_S^0\pi^+\pi^-})$ distributions for events that were selected according to the criteria in (2) and which populate the peak region (1600–1680 MeV/c^2) and various sideband regions of the effective-mass spectrum in Fig. 3*a*. The distribution of peak events in Fig. 4*c* differs from the corresponding distributions of events from the sidebands (Figs. 4*a*, 4*b*): the distribution for the peak region is not isotropic—the hypothesis of isotropy leads to C.L. = 0.01—while the distributions for the sidebands 1520–1600, 1680–1760, 1440–1600, and 1680–1840 MeV/c^2 are nearly flat, fits to them for the hypothesis of isotropy yielding high confidence levels of 0.45, 0.34, 0.58, and 0.65, respectively. That the peak events are not uniformly distributed suggests the formation of a resonance with a nonzero spin. The background distribution either can be assumed to be uniform or can be estimated from the data as a weighted mean of the distributions for the two 80-MeV/c^2-wide sidebands between 1520 and 1600 MeV/c^2 and between 1680 and 1760 MeV/c^2 (see the dashed histogram in Fig. 4*c* for the latter estimate). The background estimated by either method is then subtracted from the central distribution (see Fig. 4*d*), and the difference is fitted to the sum of Legendre polynomials of maximum degrees $2J = 0$, 2, 4, and 6. For the former (latter) estimate of the background, these fits are characterized by confidence levels of 0.01 (0.03), 0.01 (0.20), 0.42 (0.48), and 0.73 (0.29), respectively.

The above distribution of events from the peak region of the effective-mass spectrum that is plotted in Fig. 3*a* and which corresponds to the selections in (2) differs from the analogous distribution of events from the peak region of the effective-mass spectrum in Fig. 3*b*. The latter distribution is more isotropic (under the assumption of isotropy, we obtain C.L. = 0.13). The distributions in question for the peak regions of the mass spectra in Figs. 3*a* and 3*b* are compared in Fig. 4*e* (the latter, shown by the dashed histogram, was normalized to 96.3 events—see Section 2). Again, the result (Fig. 4*f*) obtained by subtracting the background from the central distribution was fitted to the sum of Legendre polynomials of maximum degrees $2J = 0$, 2, 4, and 6, whereby we arrived at confidence levels of 0.04, 0.40, 0.79, and 0.59, respectively.

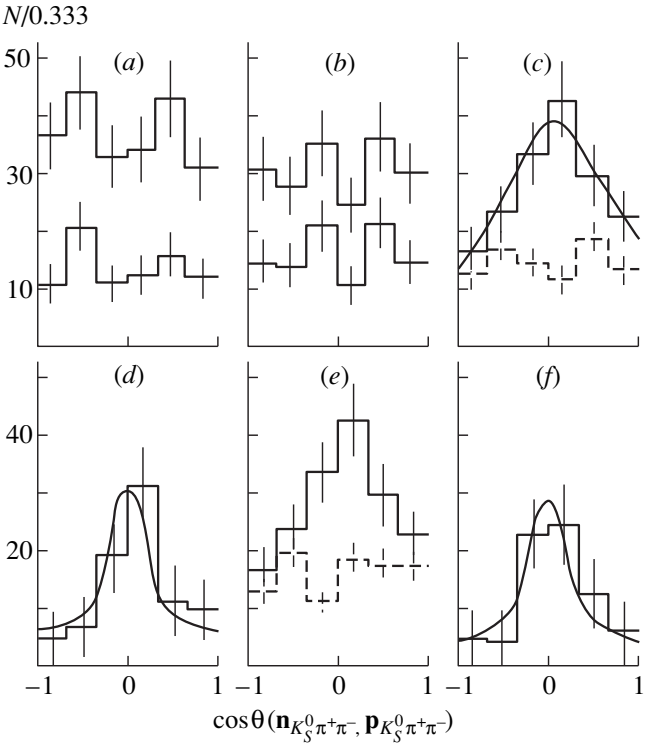

Fig. 4. Distributions of events from the effective-mass spectrum in Fig. 3*a* with respect to the cosine of the angle between the normal to the plane of hypothesized-resonance decay in the resonance rest frame and the direction of resonance motion in the $\pi^- p$ c.m. frame: (*a*) distributions for the sidebands 1.44–1.60 and 1.52–1.60 GeV/c^2, (*b*) distributions for the sidebands 1.68–1.84 and 1.68–1.76 GeV/c^2, (*c*) distributions for the peak region 1.60–1.68 GeV/c^2 (the dashed histogram represents the weighted mean distribution for events from the sidebands 1.52–1.60 and 1.68–1.76 GeV/c^2), (*d*) difference of the distributions shown in Fig. 4*c*, (*e*) distribution for events from the interval 1.60–1.68 GeV/c^2 of the spectrum in Fig. 3*a* (the dashed histogram represents the distribution obtained for events from the interval 1.60–1.68 GeV/c^2 of the spectrum in Fig. 3*b* and normalized to the number of background combinations in the region of the hypothesized resonance—see main body of the text), (*f*) difference of the distributions shown in Fig. 4*e*. Also displayed in this figure (solid curves) are fits to some distributions in terms of Legendre polynomials of maximal degrees six (Fig. 4*c*) and four (Figs. 4*d*, 4*f*).

Thus, the above analysis of the angular distributions strongly suggests that the resonance state $K(1630)$ possesses a nonzero spin.

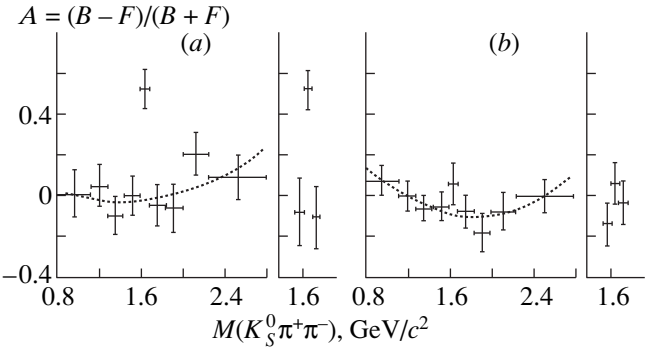

Fig. 5. Asymmetry $A = (B - F)/(B + F)$ (see main body of the text) as a function of the effective mass of the $K_S^0\pi^+\pi^-$ system for events contributing to the mass spectra in Figs. (*a*) 3*a* and (*b*) 3*b*. Dotted curves represent fits of the distributions to the regular form (3) over intervals not including the peak region 1.60–1.68 GeV/c^2. The value of A for the peak region is also shown along with its values for the sideband regions of the same size (plots on the right of Figs. 5*a* and 5*b*).

4. CORRELATIONS BETWEEN THE DECAY PRODUCTS

In contrast to known broad resonances, the $K(1630) \longrightarrow K_S^0\pi^+\pi^-$ candidate events show no resonance substructures in the two-body subsystems $\pi\pi$ and $K\pi$. This, together with the extremely small width of $K(1630)$ in relation to known $K\pi\pi$ resonances and unusual properties of the production processes, is in line with some theoretical predictions for multiquark states. By way of example, we indicate that, according to the color-cluster model [13], the small width (large lifetime) of a multiquark system is due to a centrifugal barrier between two color quark clusters bound together by color exchanges. (However, the analyses in [13] did not pave ways to seek experimentally internal clustering in such states and possibilities for breaking them down into two constituent clusters.)

We performed searches for angular correlations between the products of $K(1630)$ decays. For events from the peak region of the $K_S^0\pi^+\pi^-$ mass spectrum in Fig. 3*a*, we analyzed the angular variable

$$\delta\theta_T = \theta_T(K_S^0\pi_1^-, \pi_1^+) - \theta_T(K_S^0\pi_1^+, \pi_1^-) \qquad (7)$$

{for events not subjected to the selections in (2), a similar analysis was performed in [1]}, where $\theta_T(K_S^0\pi_1^-, \pi_1^+)$ is the angle between the transverse momenta of the $K_S^0\pi_1^-$ system and the π_1^+ meson, $\theta_T(K_S^0\pi_1^+, \pi_1^-)$ is the angle between the transverse momenta of the $K_S^0\pi_1^+$ system and the π_1^- meson, and π_1^+ and π_1^- are the two charged pions from the $K_S^0\pi_1^+, \pi_1^-$ combination considered in the mass spectrum. In contrast to what is observed in the sideband regions, events from the peak region of the mass spectrum in Fig. 3*a* are characterized by negative values of the difference $\delta\theta_T$. Yet another variable that is sensitive to grouping the decay products into two different parts is

$$\delta M_T = [M_T(K_S^0\pi_1^-) + M_T(\pi_1^+)] - [M_T(K_S^0\pi_1^+) + M_T(\pi_1^-)], \qquad (8)$$

where $M_T = (M^2 + p_T^2)^{1/2}$ is the so-called transverse mass. We found that the region of the enhancement near 1.63 GeV/c^2 in the mass spectrum shown in Fig. 3*a*, unlike the sideband regions of the same spectrum, is largely populated by events for which $\delta M_T < 0$.

Combining the two variables (7) and (8), we define F (B) as the weighted number of $K_S^0\pi_1^+, \pi_1^-$ systems with $\delta\theta_T \geq 0$ and $\delta M_T \geq 0$ ($\delta\theta_T < 0$ and $\delta M_T < 0$) and then consider the asymmetry $A = (B - F)/(B + F)$. For the two groups of events contributing to the mass spectra in Figs. 3*a* and 3*b*, the asymmetry A is plotted as a function of $M(K_S^0\pi_1^+, \pi_1^-)$ in Figs. 5*a* and 5*b*, respectively. Either excluding or including the peak region in fitting the distribution in Fig. 5*a* to the regular form (3), we obtained $\chi^2(5) = 4.13$ at C.L. = 0.53 or $\chi^2(6) = 27.88$ at C.L. = 9×10^{-5}, respectively. Similar fits of the distribution in Fig. 5*b* yielded $\chi^2(5) = 1.02$ at C.L. = 0.96 for the case where the peak region is excluded and $\chi^2(6) = 2.97$ at C.L. = 0.81 for the case where the peak region is included. From Fig. 5*a*, we can see that events populating the peak region show a much greater asymmetry than the events populating the sideband regions of the same width: the deviation is characterized by the value of $\chi^2(1) = 16.83$ at C.L. = 4×10^{-5}. For the distribution in Fig. 5*b*, we have $\chi^2(1) = 1.39$ at C.L. = 0.24.

Kinematically, the observed anomalous behavior of the asymmetry A (Fig. 5*a*) is not correlated with the enhancement in the mass spectrum shown in Fig. 3*a*; therefore, it provides an extra means for isolating the effect. Conceivably, the feature that we revealed in the distributions of the invariant quantities $\delta\theta_T$ and δM_T [correlation between the color-singlet products of $K(1630)$ decay] may reflect the underlying dynamics of color clusters that, according to [13], form exotic states. Probing the spatial separation of two color clusters will require further theoretical and experimental studies.

5. CONCLUSION

The effective-mass spectrum of the $K_S^0\pi^+\pi^-$ system formed in π^-p collisions at 16 GeV/c shows a narrow resonance that occurs near 1.63 GeV/c^2 and which is referred to as $K(1630)$. This state originates predominantly from inelastic collisions characterized by high

momentum transfers. For events from the peak region, we have revealed anomalies in kinematical distributions. These anomalies are probably associated with manifestations of the spin of the hypothesized exotic resonance and of correlations between its decay products.

Previous searches for exotic resonances in the $K\pi\pi$ system were largely performed in peripheral collisions featuring low momentum transfers. However, more favorable conditions for the formation of such states may be offered by high momentum transfers that are expected to excite the internal color degrees of freedom more efficiently [8]. Indeed, the formation of two narrow baryonic resonances $N(3520)$ and $\Sigma(3170)$ (possible candidates for exotic states) [14], whose decay products also feature strange particles, were observed in the region of high momentum transfers as well.

The $N(3520)$ state, which reveals itself as an enhancement, with width $\Gamma = 6^{+21}_{-6}$ MeV/c^2, in the mass spectrum of the $K^0_S K^+ p\pi^-\pi^-$ system, is largely formed in quasi-two-body reactions [15]. That the enhancement is not a statistical fluctuation is supported by specific kinematical features of candidate events. In the $\pi^- p$ c.m. frame, the majority (ten standard deviations) of the resonance combinations in question travel in the hemisphere of the primary π^- meson, the mean square of the momentum transfer being $\langle t'(p_I \longrightarrow K^0_S K^+ p\pi^-\pi^-)\rangle = 6.3 \pm 0.6$ (GeV/c)^2.

The formation of the $\Sigma(3170)$ state, with $\Gamma < 20$ MeV/c^2, was observed in quasi-two-body $K^- p$ interactions at 6.5 and 8.25 GeV/c [16]. This baryonic resonance decays to final states that, apart from several pions, include either $\Sigma K\bar{K} + (\geq)2\pi$, or $\Lambda K\bar{K} + (\geq)2\pi$, or $\Xi K + (\geq)3\pi$ [16]. In the $K^- p$ collision frame, the resonance system being discussed is predominantly emitted into the hemisphere of K^-, picking up a high momentum transfer from the primary proton.

The formation of the exotic states $K(1630)$, $N(3520)$, and $\Sigma(3170)$ may be best investigated in hadronic collisions occurring at relatively low energies and involving high 4-momentum transfers ($t > M_p^2$). A high momentum transfer implies that, in the target rest frame, the secondaries are emitted at a large angle with respect to the projectile momentum [2, 15]. Therefore, the bulk of the signal can be lost in a spectrometer having a limited angular acceptance for secondaries. In view of this, the specific kinematics of the signal dictates either the 4π geometry of the detector or a specially designed trigger.

ACKNOWLEDGMENTS

We wish to thank the CERN authorities for allowing us to process the data collected with the 2-m hydrogen bubble chamber. We are grateful to N.S. Angelov, F.A. Gareev, A.P. Ierusalimov, V.L. Lyuboshitz, and V.V. Uzhinskiĭ for stimulating discussions.

REFERENCES

1. V. M. Karnaukhov, C. Coca, and V. I. Moroz, Yad. Fiz. **61**, 252 (1998) [Phys. At. Nucl. **61**, 203 (1998)].
2. V. M. Karnaukhov, Soobshch. Ob'edin. Inst. Yad. Issled. No. R1-95-293 (Dubna, 1995); V. M. Karnaukhov, C. Coca, and V. I. Moroz, Soobshch. Ob'edin. Inst. Yad. Issled. No. R1-95-187 (Dubna, 1995); No. R1-96-76 (Dubna, 1996); No. R1-98-169 (Dubna, 1998).
3. F. Schweingruber *et al.*, Phys. Rev. **166**, 1317 (1968); D. C. Colley *et al.*, Nuovo Cimento A **59**, 519 (1969); M. Aguilar-Benítez *et al.*, Phys. Rev. D **4**, 2583 (1971); Phys. Rev. Lett. **30**, 672 (1973); M. Spiro *et al.*, Phys. Lett. B **60**, 389 (1976); H. Grassler *et al.*, Nucl. Phys. B **125**, 189 (1977); B. Jongejans *et al.*, Nucl. Phys. B **139**, 383 (1978); M. Baubillier *et al.*, Nucl. Phys. B **202**, 21 (1982).
4. O. I. Dahl *et al.*, Phys. Rev. **163**, 1377 (1967); D. J. Crennell *et al.*, Phys. Rev. D **6**, 1220 (1972); S. Rodeback *et al.*, Z. Phys. C **9**, 9 (1981).
5. Particle Data Group, Phys. Lett. B **111**, 1 (1982); **170**, 1 (1986).
6. W. Beusch *et al.*, Phys. Lett. B **74**, 282 (1978).
7. A. Etkin *et al.*, Phys. Rev. D **22**, 42 (1980); D. Aston *et al.*, Nucl. Phys. B **247**, 261 (1984); **292**, 693 (1987).
8. J. L. Rosner, Phys. Rev. Lett. **21**, 950 (1968); M. Jacob and J. Weyers, Nuovo Cimento A **69**, 521 (1970); Ya. Ya. Balitskiĭ, D. I. D'yakonov, and A. V. Yung, Yad. Fiz. **35**, 1300 (1982) [Sov. J. Nucl. Phys. **35**, 761 (1982)].
9. R. G. Roberts, in *Proceedings of the Seventh School in Physics, Loma-Koli, Finland, 1972*, p. 119; I. M. Dremin and K. Quigg, Usp. Fiz. Nauk **124**, 535 (1978) [Sov. Phys. Usp. **21**, 265 (1978)].
10. A. U. Abdurakhimov *et al.*, Yad. Fiz. **20**, 954 (1974) [Sov. J. Nucl. Phys. **20**, 507 (1975)].
11. W. T. Eadie *et al.*, *Statistical Methods in Experimental Physics* (North-Holland, Amsterdam, 1971).
12. S. M. Berman and M. Jacob, Phys. Rev. B **139**, 1023 (1965).
13. H. Hogaasen and P. Sorba, Nucl. Phys. B **145**, 119 (1978); M. De Grombrugghe, H. Hogaasen, and P. Sorba, Nucl. Phys. B **156**, 347 (1979).
14. Particle Data Group, Phys. Rev. D **54**, 573, 659 (1996).
15. V. M. Karnaukhov *et al.*, Phys. Lett. B **281**, 148 (1992); V. M. Karnaukhov, Soobshch. Ob'edin. Inst. Yad. Issled. No. R1-93-375 (Dubna, 1993); V. M. Karnaukhov *et al.*, Yad. Fiz. **57**, 841 (1994) [Phys. At. Nucl. **57**, 790 (1994)]; **58**, 860 (1995) [**58**, 796 (1995)].
16. J. Amirzadeh *et al.*, Phys. Lett. B **89**, 125 (1979); J. B. Kinson *et al.*, in *Proceedings of Physics Conference, Toronto, Canada, 1980*, p. 263.

Translated by A. Asratyan

Physics of Atomic Nuclei, Vol. 63, No. 4, 2000, pp. 594–605. Translated from Yadernaya Fizika, Vol. 63, No. 4, 2000, pp. 659–671.

ELEMENTARY PARTICLES AND FIELDS
Theory

Resonance Chiral Theory for Low-Energy ππ Scattering

E. P. Shabalin

Institute of Theoretical and Experimental Physics, Bol'shaya Cheremushkinskaya ul. 25, Moscow, 117259 Russia

Received November 21, 1998; in final form, July 2, 1999

Abstract—The scattering of a pion on a pion in the energy region $\sqrt{s} \leq 1$ GeV is successfully described on the basis of pole diagrams featuring spinless, spin-1, and spin-2 intermediate particles, provided that the properties of these particles and of their interactions are deduced from the basic principles of QCD and from the requirements of chiral theory. © *2000 MAIK "Nauka/Interperiodica".*

1. INTRODUCTION

Quantum chromodynamics (QCD), which is used to describe high-energy hadronic processes, loses its predictive potential upon going over to low energies. This is because the coupling constant increases fast there, invalidating perturbation theory. In view of this, low-energy processes are described by means of effective Lagrangians that reflect more or less the properties of the fundamental QCD interaction. Another way is to employ an effective Lagrangian including all possible covariant combinations of pseudoscalar fields and their derivatives up to a certain order p^n in the meson momentum. The latter approach is realized in chiral perturbation theory (ChPT). In the case of mesons, the relevant Lagrangian involves ten terms in the p^4 approximation [1], the coefficients of these terms being determined predominantly from a comparison of theoretical predictions with experimental data.

This approach is quite general, but it is not free from some substantial disadvantages:

(i) It does not take fully into account the nature of physical phenomena leading to specific values for the coefficients of various meson-matrix combinations.

(ii) Chiral perturbation theory can be employed to evaluate the amplitudes only near the threshold. Its application in the energy region $\sqrt{s} > m_K$ is not quite correct because resonances emerging there cannot be described by the function $p^2 + ap^4$ and because corrections of higher orders in p^2 cannot be evaluated in practice. To illustrate this statement, it is sufficient to recall that, even in the p^6 order, the effective Lagrangian includes 111 combinations of meson matrices not featuring $\varepsilon_{\mu\nu\sigma\tau}$ and 32 terms involving this antisymmetric tensor, all the coefficients being unknown [2].

(iii) Chiral perturbation theory, which is based on a nonlinear realization of chiral symmetry, is incapable of determining the features of scalar partners of the mesons from the pseudoscalar nonet, thus providing no way to interpret the features of the existing scalar resonances.

In an attempt at advancing toward higher energies, it was found in [3, 4] that the theory that employs only the p^2 part of the effective Lagrangian and which elicits terms of order p^4 from the expansion of the propagators of resonances added to the theory leads to a set of constants that is virtually identical to that which is provided by ChPT. In this case, however, the use of a nonlinear realization of chiral symmetry leads to terms of order p^2 that are not associated with any particular internal structure of interaction. In view of this, it is impossible to specify the function whose expansion leads to terms of order p^2, and the underlying physics cannot therefore be understood conclusively.

Moreover, some other problems were not solved in [4]. In particular, the authors of [4] could not explain why the g_ρ value as determined from data on the decay process $\rho \longrightarrow \pi\pi$ differed from that extracted from data on the charged-pion form factor, nor were they able to reproduce the experimental behavior of the phase shift $\delta_0^0(s)$ for $\sqrt{s} > 0.85$ GeV and the experimental behavior of the phase shift $\delta_0^2(s)$ for $\sqrt{s} > m_K$.

In my opinion, there were two reasons behind these failures: (i) The approach to the problem of specifying the form of interaction between the resonances under study and the pions was oversimplified in [4]. (ii) The relations established in chiral theory between pseudoscalar and scalar particles were not taken into account there.

In many studies, the behavior of phase shifts is analyzed in terms of some resonance and a repulsive core that is postulated in an ad hoc manner and which ensures a negative background (see [5] and references therein). It will become clear from the following, however, that the negative background is due to the exchanges of scalar sigma particles and rho mesons in the t and u reaction channels. For this reason, the background contribution cannot be treated as an adjustable function in fitting a theoretical description to experimental data.

1063-7788/00/6304-0594$20.00

The above list of unresolved problems and problems solved unsatisfactorily, which includes, above all, the problem of extrapolating chiral theory from the near-threshold region, where the use of ChPT is quite legitimate, to the resonance region gave me an incentive to revising all basic ideas and conclusions of the theory of low-energy pion–pion scattering.

The result of the present analysis is that the phase shifts δ_0^0, δ_0^2, δ_1^1, δ_2^0, and δ_2^2 in the energy range from the threshold to $\sqrt{s} \leq 1$ GeV can be described quite satisfactorily within a theory that takes into account only exchanges of intermediate low-lying spinless, spin-1, and spin-2 resonances, provided that the properties of the resonances and of their interactions are compatible with QCD and with the principles underlying the construction of chiral theory.

2. SPECIFYING THE FORM OF LOW-ENERGY THEORY ADEQUATELY REFLECTING THE PROPERTIES OF QCD

In the chiral-symmetry limit (that is, at $m_q = 0$), the QCD Lagrangian

$$L^{\mathrm{QCD}} = -\frac{1}{4}G^a_{\mu\nu}G^a_{\mu\nu} + \sum_q \bar{q}\left[i\gamma_\mu\left(\partial_\mu + i\frac{g}{\sqrt{2}}G^a_\mu t^a\right) - m_q\right]q \tag{1}$$

is invariant under independent transformations of the left- and the right-handed quarks:

$$q_{\mathrm{L}} \longrightarrow q_{\mathrm{L}}\exp(-i\hat{\varepsilon}_{\mathrm{L}}/\sqrt{2}),$$
$$q_{\mathrm{R}} \longrightarrow q_{\mathrm{R}}\exp(-i\hat{\varepsilon}_{\mathrm{R}}/\sqrt{2}). \tag{2}$$

Here, $\hat{\varepsilon}_{\mathrm{L,R}}$ are independent 3×3 matrices in flavor space,

$$\hat{\varepsilon}_{\mathrm{L,R}} = \varepsilon^a_{\mathrm{L,R}}t^a, \quad t^0 = \frac{1}{\sqrt{3}}\mathbf{1}, \quad t^{1\text{–}8} = \frac{1}{\sqrt{2}}\lambda^{1\text{–}8}, \tag{3}$$

$\varepsilon^a_{\mathrm{L,R}}$ being c numbers.

Within QCD, the construction $\bar{q}_{\mathrm{R}}t^a q_{\mathrm{L}}$ and its Hermitian conjugate correspond to the simplest spinless states. In constructing a Lagrangian satisfying the principles of QCD, we must therefore invoke a non-self-conjugate matrix featuring opposite parity fields,

$$\hat{U} = \hat{\sigma} + i\hat{\pi}, \tag{4}$$

where σ^a and π^a are, respectively, the scalar and the pseudoscalar members of the meson-field nonet. According to (2), the transformation properties of the matrix U under independent chiral rotations of the left- and the right-handed quarks are given by

$$\hat{U} \longrightarrow \exp(i\hat{\varepsilon}_{\mathrm{R}}/\sqrt{2})\hat{U}\exp(-i\hat{\varepsilon}_{\mathrm{L}}/\sqrt{2}). \tag{5}$$

This transformation converts scalars into pseudoscalars, and vice versa:

$$\hat{\sigma} \longrightarrow \hat{\sigma} - \frac{i}{\sqrt{2}}[\hat{\sigma}, \hat{\varepsilon}_V]_- + \frac{1}{\sqrt{2}}\{\hat{\pi}, \hat{\varepsilon}_A\}_+,$$
$$\hat{\pi} \longrightarrow \hat{\pi} - \frac{i}{\sqrt{2}}[\hat{\pi}, \hat{\varepsilon}_V]_- - \frac{1}{\sqrt{2}}\{\hat{\sigma}, \hat{\varepsilon}_A\}_+. \tag{6}$$

Since the transformations in (2) do not change the number of quarks, σ^a and π^a appear to be the chiral partners constructed from the same number of quarks. Consequently, QCD dictates the presence of diquark scalar states. Formally, however, we can eliminate scalar mesons from our consideration by choosing the matrix U in the form

$$\hat{U} = \frac{F_\pi}{\sqrt{2}}\exp(i\sqrt{2}\hat{\pi}/F_\pi), \tag{7}$$

which corresponds to the nonlinear realization of chiral symmetry and which means that the chiral partner to the pseudoscalar field π is a combination of even powers of the same field. Since two pions represent a four-quark system, the above choice results in the loss of physical states corresponding to a scalar combination of two quarks; hence, we can no longer, in this case, treat observable scalar resonances as chiral partners to pseudoscalar mesons.

Actually, the choice of the form (7) for the matrix U is equivalent to the assumption that the masses of the scalar mesons are either infinite or so great that the corresponding quantum excitations are absent at low energies. From what follows, it will be seen that a transition to the limit of an infinite mass m_σ is not forbidden from a formal mathematical point of view, but this transition leads to unphysical values for the parameters of the theory that control m_σ.

Thus, the use of a nonlinear realization of chiral symmetry—it should be emphasized that this simplifies considerably the calculation of amplitudes in the leading order in p^2—involves rejecting the principle of detailed conformity between theory and nature, in which case some part of information contained in QCD is lost.

According to QCD, the Lagrangian of spinless fields must be constructed by employing the matrix U, and this will therefore be the sigma-model Lagrangian.

For spin-1 fields, the principle of detailed conformity between the properties of QCD objects and the real world implies that such fields must be associated with the quark combination $\frac{\partial}{\partial x_\nu}\bar{q}_{\mathrm{R}}\sigma_{\mu\nu}t^a q_{\mathrm{L}}$ and its conjugate rather than with the combinations $\bar{q}_{\mathrm{L}}\gamma_\mu t^a q_{\mathrm{L}}$ and $\bar{q}_{\mathrm{R}}\gamma_\mu t^a q_{\mathrm{R}}$, as was often assumed. This circumstance affects substantially the character of vector-meson interaction with the system of two spinless mesons.

In order to describe $\pi\pi$ scattering up to $\sqrt{s} \le 1$ GeV, it is also necessary to take into account effects associated with the scalar resonance $f_0(980)$, which does not fit in the simple $\bar{q}q$ two-quark picture, and those associated with the spin-2 resonance $f_2(1270)$. These objects will be included in our consideration, and the form of their coupling to the pions is matched with the requirements of chiral theory.

We now return, however, to the scalar mesons of chiral theory.

3. SPINLESS FIELDS AND THEIR INTERACTIONS

The simplest Lagrangian of the system of $0^{\pm}$ fields has the form

$$\begin{aligned} L(0^{\pm}) &= \frac{1}{2}\mathrm{tr}\{\partial_\mu U \partial_\mu U^\dagger\} - c\,\mathrm{tr}\{UU^\dagger - A^2 t_0^2\}^2 \\ &- c\xi(\mathrm{tr}\{UU^\dagger - A^2 t_0^2\})^2 + \frac{F_\pi}{2\sqrt{2}}\mathrm{tr}\{\hat{m}(U + U^\dagger)\} \\ &+ \frac{\Delta m_P^2 F_\pi^2}{12}\left(\frac{i}{2}\mathrm{tr}\left\{\ln\left(\frac{U}{U^\dagger}\right)\right\}\right)^2, \end{aligned} \tag{8}$$

where the first three terms possess, in just the same way as the Lagrangian in (1) at $m_q = 0$ does, left–right global symmetry—that is, they are invariant under the transformations in (5). The parameter A induces a spontaneous breakdown of symmetry via a nonzero vacuum expectation value $\langle\bar{q}q\rangle$ in QCD. The matrix $\hat{m} \sim \mathrm{diag}\{m_u, m_d, m_s\}$ secures a hard breakdown of chiral symmetry. The last term in (8) solves the $U(1)$ problem in the pseudoscalar-meson sector by shifting the mass of the isosinglet π_0 meson with respect to the masses of the π_{1-8} mesons belonging to the octet. This shift is due to the mixing of the quark state $i\bar{q}\gamma_5 t^0 q$ with the pseudoscalar gluonium state $\left(\frac{\alpha_s}{\pi}G^a_{\mu\nu}\tilde{G}^a_{\mu\nu}\right)$ [6]. A similar effect occurs in the case of the quark state $\bar{q}\,t^0 q$, whose mixing with the scalar gluonium state $\left(\frac{\alpha_s}{\pi}G^a_{\mu\nu}G^a_{\mu\nu}\right)$ shifts the mass of the isosinglet scalar meson σ_0 with respect to the masses of the scalar mesons σ_{1-8} belonging to the octet. In the case of processes involving no more than four pseudoscalar mesons, this effect is taken into account through that term in Lagrangian (8) which is proportional to ξ.

From the analysis presented in [7], it follows that, for processes featuring an arbitrary number of pseudoscalar mesons, the third term in (8) must be replaced by

$$-c\xi\left(\mathrm{tr}\left\{A^2 t_0^2 \ln\left(\frac{UU^\dagger}{A^2 t_0^2}\right)\right\}\right)^2. \tag{9}$$

Since 0^+ and 0^- mesons enter into the matrix U on an equal footing, the masses of the octet $0^{\pm}$ mesons and their coupling constants are expressed in terms of the same parameters c, A, and $\hat{m}$. This implies that they can be related to the parameters of the 0^- mesons by simple equations. For example, we have (see [8])

$$\begin{aligned} m^2_{\sigma_\pi} - \mu^2 &= (m_K^2 - \mu^2)[(R-1)(2R-1)]^{-1}, \\ m^2_{\sigma_K} - m_K^2 &= (m_K^2 - \mu^2)(R-1)^{-1}, \end{aligned} \tag{10}$$

where $\mu^2 \equiv m_\pi^2$ and

$$R \equiv \frac{F_K}{F_\pi}, \tag{11}$$

F_K and F_π being given by

$$\begin{aligned} &\left\langle 0\left|\bar{q}\gamma_\mu\gamma_5\frac{\lambda^a}{2}q\right|\pi^b(k)\right\rangle \\ &= i\delta^{ab}\begin{pmatrix} F_\pi k_\mu, & a = 1, 2, 3 \\ F_K k_\mu, & a = 4, 5, 6, 7 \end{pmatrix}. \end{aligned} \tag{12}$$

From (10) and (11), it follows that, although a transition to the limit $m_\sigma \longrightarrow \infty$ is admissible in the theory from the purely mathematical standpoint, this would correspond either to $(m_K^2 - \mu^2) \longrightarrow \infty$ or to $F_K \longrightarrow F_\pi$. This possibility is not realized, and the masses of the octet scalar mesons are on the order of 1 GeV, enabling us to identify these mesons with the scalar resonances in the same mass region.

For the isosinglet scalar mesons, the mass formulas are more complicated than those in (10), since σ_0 is mixed with the scalar gluonium state and since σ_0 is mixed with σ_8 owing to the breakdown of $SU(3)$ symmetry. The expressions for the masses of the physical isoscalar–scalar mesons

$$\begin{aligned} \sigma_{\eta'} &= \sigma_0\cos\theta_S + \sigma_8\sin\theta_S, \\ \sigma_\eta &= -\sigma_0\sin\theta_S + \sigma_8\cos\theta_S \end{aligned} \tag{13}$$

can be found in [8, 9].

In just the same way as the parameter δm_P^2, the parameter ξ is not specified in the theory; it can be determined by fitting theoretical predictions to experimental data.

Since the widths of scalar mesons are on the same order of magnitude as their masses and since the interpretation of data for wide resonances is rather intricate, comparatively reliable information on the mass of the lightest scalar meson is extracted from data on the decay $K^+ \longrightarrow \pi^+\pi^- e^+\nu$ [9]. The analysis of the relevant experimental results yielded

$$m_{\sigma_{\eta'}} = 650 \pm 20 \text{ MeV}. \tag{14}$$

Within three standard deviations, this value agrees with that found in the present study from an analysis of the phase shifts for $\pi\pi$ scattering as functions of energy in the region $\sqrt{s} \le 1$ GeV:

$$m_{\sigma_{\eta'}} \cong 700 \text{ MeV}. \tag{15}$$

The exchange of scalar mesons $\sigma_1 \equiv \sigma_{\eta'}$ and $\sigma_2 \equiv \sigma_\eta$, in addition to the contact interaction $\pi^4(x)$ appearing in Lagrangian (8), leads to the amplitude

$$\begin{aligned} T_\sigma &= \left\langle \pi_k(p_1')\pi_l(p_2') \middle| \pi_i(p_1)\pi_j(p_2) \right\rangle_\sigma \\ &= \delta_{ij}\delta_{kl}\left[G_1 \frac{s-\mu^2}{m_{\sigma_1}^2 - s} + G_2 \frac{s-\mu^2}{m_{\sigma_2}^2 - s} \right] \\ &+ \delta_{ik}\delta_{jl}\left[G_1 \frac{t-\mu^2}{m_{\sigma_1}^2 - t} + G_2 \frac{t-\mu^2}{m_{\sigma_2}^2 - t} \right] \\ &+ \delta_{il}\delta_{jk}\left[G_1 \frac{u-\mu^2}{m_{\sigma_1}^2 - u} + G_2 \frac{u-\mu^2}{m_{\sigma_2}^2 - u} \right], \end{aligned} \tag{16}$$

where

$$s = (p_1 + p_2)^2, \quad t = (p_1 - p_1')^2, \quad u = (p_1 - p_2')^2, \tag{17}$$

$$G_1 = \frac{g_{\sigma_1\pi\pi}^2}{m_{\sigma_1}^2 - \mu^2}, \quad G_2 = \frac{g_{\sigma_2\pi\pi}^2}{m_{\sigma_2}^2 - \mu^2}. \tag{18}$$

By virtue of the properties of chiral theory and according to the results of the soft-pion approximation, the quantities G_1 and G_2 are related by the equation

$$\frac{G_1}{m_{\sigma_1}^2 - \mu^2} + \frac{G_2}{m_{\sigma_2}^2 - \mu^2} = \frac{1}{F_\pi^2}, \quad F_\pi \cong 93 \text{ MeV}. \tag{19}$$

Although G_j and m_{σ_j} depend on the parameter ξ, relation (19) holds for any value of this parameter. In the leading order in p^2, equation (16) then yields, irrespective of the masses of intermediate scalar sigma mesons, the well-known result [10] of the current algebra and of the soft-pion approximation:

$$\begin{aligned} T_\sigma^{(p^2)} &= \frac{1}{F_\pi^2} \\ &\times [\delta_{ij}\delta_{kl}(s-\mu^2) + \delta_{ik}\delta_{jl}(t-\mu^2) + \delta_{il}\delta_{jk}(u-\mu^2)]. \end{aligned} \tag{20}$$

That the near-threshold amplitude is associated with sigma-meson exchanges enables us to trace the evolution of T_σ with increasing s. In doing this, it is necessary to take into account not only the dependence fixed by (16) but also the fact that the quantities $G_{1,2}$ satisfy relation (19) only in the soft-pion approximation—that is, for $s, t, u \longrightarrow \mu^2$. A more general form of T_σ violating neither the properties of chiral theory nor the requirements of crossing symmetry is then given by

$$\begin{aligned} T_\sigma &= \sum_{n=1,2}\left[\delta_{ij}\delta_{kl} G_n(s) \frac{s-\mu^2}{m_{\sigma_n}^2 - s} \right. \\ &\left. + \delta_{ik}\delta_{jl} G_n(t) \frac{t-\mu^2}{m_{\sigma_n}^2 - t} + \delta_{il}\delta_{jk} G_n(u) \frac{u-\mu^2}{m_{\sigma_n}^2 - u} \right]. \end{aligned} \tag{21}$$

This form actually considers that the $\sigma\pi\pi$ vertex may involve the form factor. With the exception of the condition

$$G_n(s = \mu^2) = G_n(t = \mu^2) = G_n(u = \mu^2) \tag{22}$$

and of the fact that the form factor shows identical functional dependences on s, t, and u, our theory can say nothing about the form factor. In our analysis, we employ the form factor given by

$$G_n(x) = G_n(x = \mu^2)\exp[-k(x-\mu^2)], \quad k > 0. \tag{23}$$

In addition to the resonances σ_1 and σ_2, which are chiral partners to the η' and η mesons, the resonance $f_0(980)$ plays an important role in the region $\sqrt{s} <$ 1 GeV. The features of this resonance do not fit in the simple $\bar{q}q$ pattern. According to chiral theory, it interacts with the π mesons through coupling to derivatives:

$$\left\langle \pi^a(p_1)\pi^b(p_2) \middle| f_0(q) \right\rangle = -\frac{g_{f_0}}{M_{f_0}} p_{1\mu} p_{2\mu} \delta^{ab}. \tag{24}$$

The contribution of this resonance to the amplitude of $\pi\pi$ scattering is given by

$$\begin{aligned} T_{f_0} &= \left\langle \pi_k(p_1')\pi_l(p_2') \middle| \pi_i(p_1)\pi_j(p_2) \right\rangle_{f_0} \\ &= \frac{g_{f_0}^2}{4M_f^2}\left[\delta_{ij}\delta_{kl}\frac{(s-2\mu^2)^2}{M_f^2 - s} \right. \\ &\left. + \delta_{ik}\delta_{jl}\frac{(t-2\mu^2)^2}{M_f^2 - t} + \delta_{il}\delta_{jk}\frac{(u-2\mu^2)^2}{M_f^2 - u} \right], \end{aligned} \tag{25}$$

where

$$g_{f_0}^2 = \frac{128\pi M_f^3 \Gamma(f_0 \longrightarrow 2\pi)}{3(M_f^2 - 2\mu^2)^2\sqrt{1 - 4\mu^2/M_f^2}}. \tag{26}$$

In (25), we disregarded the possible additional dependence of g_{f_0} on momentum transfers, assuming that this dependence is very weak for $\sqrt{s} < 1$ GeV.

4. SPIN-1 FIELDS AND THEIR INTERACTIONS

A conventional way to include spin-1 fields in chiral theory is to supplement the Lagrangian in (8) with the

Lagrangian of left- and right-handed Yang–Mills fields [11],

$$L_0(1^\pm) = \frac{1}{8}\mathrm{tr}\{\hat{F}^{\mathrm{L}}_{\mu\nu}\hat{F}^{\mathrm{L}}_{\mu\nu} + \hat{F}^{\mathrm{R}}_{\mu\nu}\hat{F}^{\mathrm{R}}_{\mu\nu}\} + \frac{1}{4}M_V^2\mathrm{tr}\{\hat{A}^{\mathrm{L}}_\mu\hat{A}^{\mathrm{L}}_\mu + \hat{A}^{\mathrm{R}}_\mu\hat{A}^{\mathrm{R}}_\mu\}, \quad (27)$$

and to replace the derivative ∂_μ in (8) by the covariant derivative

$$D_\mu\hat{U} = \partial_\mu\hat{U} + \frac{ig}{\sqrt{2}}\hat{U}\hat{A}^{\mathrm{R}}_\mu - \frac{ig}{\sqrt{2}}\hat{A}^{\mathrm{L}}_\mu\hat{U}. \quad (28)$$

In the above formulas, we have introduced the notation

$$A^{\mathrm{L}}_\mu = V_\mu + A_\mu, \quad A^{\mathrm{R}}_\mu = V_\mu - A_\mu, \quad (29)$$

$$F^{\mathrm{L},a}_{\mu\nu} = \partial_\mu A^{\mathrm{L},a}_\nu - \partial_\nu A^{\mathrm{L},a}_\mu + g f^{abc}A^{\mathrm{L},b}_\mu A^{\mathrm{L},c}_\nu,$$
$$F^{\mathrm{R},a}_{\mu\nu} = \partial_\mu A^{\mathrm{R},a}_\nu - \partial_\nu A^{\mathrm{R},a}_\mu + g f^{abc}A^{\mathrm{R},b}_\mu A^{\mathrm{R},c}_\nu. \quad (30)$$

Within this approach, the Hermitian fields $A^{\mathrm{L},a}_\mu$ and $A^{\mathrm{R},a}_\mu$ are associated with the Hermitian quark currents

$$i\bar{q}_{\mathrm{L}}\gamma_\mu\frac{\lambda^a}{2}q_{\mathrm{L}}, \quad i\bar{q}_{\mathrm{R}}\gamma_\mu\frac{\lambda^a}{2}q_{\mathrm{R}}. \quad (31)$$

However, this procedure does not define correctly the correspondence between the features of physical spin-1 mesons and the quark structures associated with them. This becomes obvious when we consider that spin-1 fields—both vector ones V_μ and axial-vector ones A_μ—must satisfy the transversality condition

$$k_\mu V^a_\mu(k) = 0, \quad k_\mu A^a_\mu(k) = 0, \quad (32)$$

which eliminates the spinless component from these fields. For the vector combination of the quark currents (31), this condition is not satisfied at $a = 4$, 5, 6, and 7; for the axial-vector combination, it is satisfied at no value of a. Quark constructions that satisfy the condition in (32) are given by

$$A^a_\nu \sim i\frac{\partial}{\partial x_\mu}\bar{q}_{\mathrm{R}}\sigma_{\mu\nu}\lambda^a q_{\mathrm{L}}, \quad A^{a\dagger}_\nu \sim (-i)\frac{\partial}{\partial x_\mu}\bar{q}_{\mathrm{L}}\sigma_{\mu\nu}\lambda^a q_{\mathrm{R}}. \quad (33)$$

This suggests that physical fields associated with vector and axial-vector mesons are determined by the divergences of tensor and pseudotensor quark currents, respectively. The assumption that spin-1 fields could be associated with the divergence of tensor currents was put forth previously in [12, 14]. However, our statement in (33) follows from different considerations—namely, from the requirement of one-to-one correspondence between the properties of physical objects and quark–gluon constructions. Thus, our theory leads to the relation

$$\boldsymbol{\rho}_\mu \sim \frac{\partial}{\partial x_\nu}(\bar{q}_{\mathrm{R}}\sigma_{\nu\mu}\boldsymbol{\tau}q_{\mathrm{L}} + \bar{q}_{\mathrm{L}}\sigma_{\nu\mu}\boldsymbol{\tau}q_{\mathrm{R}}) = \frac{\partial}{\partial x_\nu}\mathbf{t}_{\nu\mu}(x), \quad (34)$$

which possesses a remarkable feature: the $\rho\pi\pi$ vertex vanishes at zero value of the squared rho-meson momentum. Indeed, relation (34), used in conjunction with the reduction technique, means that

$$\left\langle \rho^a_\mu(q)\pi^b(p_2)\middle|\pi^c(p_1)\right\rangle = (M_\rho^2 - q^2) \times \int e^{iqx}d^4x\left\langle \pi^b(p_2)\middle|\rho^a_\mu(x)\middle|\pi^c(p_1)\right\rangle \sim -iq_\nu(M_\rho^2 - q^2) \times \int e^{iqx}d^4x\left\langle \pi^b(p_2)\middle|t^a_{\mu\nu}(x)\middle|\pi^c(p_1)\right\rangle.$$

The most general form of the integral of the relevant matrix element is

$$\int e^{iqx}d^4x\left\langle \pi^b(p_2)\middle|t^a_{\mu\nu}(x)\middle|\pi^c(p_1)\right\rangle = \epsilon^{abc}F(q^2)(P_\nu q_\mu - P_\mu q_\nu),$$

where $P = p_1 + p_2$ and $q = p_1 - p_2$. Thus, we have

$$\left\langle \rho^a_\mu(q)\pi^b(p_2)\middle|\pi^c(p_1)\right\rangle_{q^2\to 0} \sim i\epsilon^{abc}q^2M_\rho^2F(q^2)P_\mu. \quad (35)$$

In the absence of massless hadrons, the function $F(q^2)$ does not feature a pole at $q^2 = 0$; physically, this is equivalent to a shift of the rho meson with respect to the pion for $q^2 \longrightarrow 0$. This circumstance can be taken into account by choosing a phenomenological Lagrangian of interaction between spin-1 fields and the system of two spinless mesons in the form

$$L(1^\pm; 0^\pm; 0^\pm) = \frac{ig_V}{\sqrt{2}M_V^2} \times \mathrm{tr}[\hat{A}_{\mu\nu}\partial_\mu\hat{U}\partial_\nu\hat{U}^\dagger - \hat{A}^\dagger_{\mu\nu}\partial_\nu\hat{U}\partial_\mu\hat{U}^\dagger] = -\frac{g_V}{M_V^2}f^{abc}[V^c_{\mu\nu}(\partial_\mu\sigma^a\partial_\nu\sigma^b + \partial_\mu\pi^a\partial_\nu\pi^b) + A^c_{\mu\nu}(\partial_\mu\sigma^a\partial_\nu\pi^b - \partial_\mu\pi^a\partial_\nu\sigma^b)], \quad (36)$$

where

$$\hat{A}_{\mu\nu} = \hat{V}_{\mu\nu} + i\hat{A}_{\mu\nu}, \quad (37)$$

while $V^c_{\mu\nu}$ and $A^c_{\mu\nu}$ are antisymmetric tensors of the vector and the axial-vector field, respectively.

In the case of Lagrangian (36), the use of the propagators of the antisymmetric tensors $V_{\mu\nu}$ and $A_{\mu\nu}$,

$$D(k)_{\mu\nu,\rho\sigma} = \frac{i}{M^2_{V,A} - k^2 - i\varepsilon} \times [(\delta_{\mu\rho}\delta_{\nu\sigma} - \delta_{\nu\rho}\delta_{\mu\sigma})(M^2_{V,A} - k^2) + \delta_{\mu\rho}k_\nu k_\sigma - \delta_{\mu\sigma}k_\nu k_\rho - \delta_{\nu\rho}k_\mu k_\sigma + \delta_{\nu\sigma}k_\mu k_\rho], \quad (38)$$

from the outset provides a convenient framework for an analysis of processes featuring intermediate spin-1 particles.

This approach to taking into account the contribution of vector exchange to ππ scattering was employed in [1, 3, 4]. We will follow it here.

For the amplitude caused by rho-meson exchange, the use of relations (35), (36), and (38) yields

$$\begin{aligned} T_\rho &= \left\langle \pi_k(p_1')\pi_l(p_2') \middle| \pi_i(p_1)\pi_j(p_2) \right\rangle_\rho \\ &= \frac{1}{M_\rho^2}\Bigg(\delta_{ij}\delta_{kl}\left[g^2(u)\frac{(s-t)u}{M_\rho^2-u} + g^2(t)\frac{(s-u)t}{M_\rho^2-t}\right] \\ &\quad + \delta_{ik}\delta_{jl}\left[g^2(s)\frac{(t-u)s}{M_\rho^2-s} + g^2(u)\frac{(t-s)u}{M_\rho^2-u}\right] \\ &\quad + \delta_{il}\delta_{jk}\left[g^2(s)\frac{(u-t)s}{M_\rho^2-s} + g^2(t)\frac{(u-s)t}{M_\rho^2-t}\right]\Bigg), \end{aligned} \tag{39}$$

where s, t, and u are specified by relations (17) and

$$g^2(s = M_\rho^2) \equiv g_\rho^2 = \frac{48\pi\Gamma(\rho \longrightarrow 2\pi)}{M_\rho(1-4\mu^2/M_\rho^2)^{3/2}}. \tag{40}$$

If the conditions $g(s) = g(t) = g(u) = g_\rho = \text{const}$ are satisfied, the requirements of chiral symmetry lead to the validity of expressions of the type (39) for T_ρ both in the approach based on the theory specified by Lagrangian (27) and in the approach where vector fields are included in the theory according to (28) [15, 16]. But for processes where it is not the pion current but some other source (for example, weak current) that is responsible for ρ-meson production, the presence of the additional factor $q^2F(q^2)$ in the matrix element (35) leads to results that are different from those predicted in the standard approach.

Moreover, our result in (39) for the amplitude of ππ scattering differs drastically from those obtained in [1, 3, 4], where no account was taken of the fact that, according to (35), $g(s) \neq g(t) \neq g(u)$. Although the explicit form of the $x = s, t, u$ dependence of g is not specified by our theory, phenomenological considerations suggest that

$$g(x) = g_\rho \exp\left(0.7855\left[\frac{x}{2M_\rho^2} - \left(\frac{x}{2M_\rho^2}\right)^2\right]\right). \tag{41}$$

The result in (41) solves a number of problems:

(i) In accordance with the constraints imposed by unitarity in going over to high energies, the near-threshold growth of the ππ-scattering amplitude is moderated.

(ii) The contradiction (indicated in [1, 4]) between the g_ρ value determined from data of the decay $\rho \longrightarrow \pi\pi$ and that deduced from the electromagnetic form factor for the charged pion is removed.

(iii) For the vector form factor $f_\pi(s)$ of the pion at $s = M_\rho^2$, the present result—in contrast to the prediction of the vector-dominance model (VDM)—yields a value close to that measured experimentally.

(iv) In contrast to what is obtained in [4], the s dependence obtained here for the phase shift δ_0^2 agrees with experimental data for $\sqrt{s} > 0.5$ GeV.

The statement in (i) immediately follows from the form of $g(x)$. The statement in (ii) resolves the problem of theoretically reproducing the well-known experimental result according to which the root-mean-square charge radius of the $\pi^\pm$ mesons virtually coincides with that predicted on the basis of the VDM. Within our theory, the vector form factor for the pion is given by the expression

$$f_\pi(s) = 1 + \frac{F_\rho g(s)s}{M_\rho[M_\rho^2 - s - i\sqrt{s}\Gamma_\rho(s)]}. \tag{42}$$

In order to derive it, we made use of the relation

$$\langle 0 \left| V_\mu^i \right| \rho_\nu^k(\rho) \rangle = \delta^{ik}\delta_{\mu\nu}F_\rho M_\rho. \tag{43}$$

Within the VDM, we have

$$f_\pi^{\text{VDM}}(s)\big|_{s\to 0} = 1 + \frac{s}{M_\rho^2 - s}. \tag{44}$$

The condition

$$\left.\frac{df_\pi(s)}{ds}\right|_{s=0} = \left.\frac{df_\pi^{\text{VDM}}(s)}{ds}\right|_{s=0} \tag{45}$$

is equivalent to the requirement

$$g(0) = M_\rho/F_\rho \cong 5. \tag{46}$$

The second equality in (46) corresponds to the choice of $M_\rho = 770$ MeV and to the value of $F_\rho = 154$ MeV, which was fitted to the $\rho \longrightarrow e^+e^-$ decay width. For Γ_ρ, we used the value of 153 MeV. All the above values are within 1σ around the world-average experimental values. The relation (40) yields

$$g(M_\rho^2) = 6.085, \tag{47}$$

which is in accord with (41).

To demonstrate that the statement in (iii) is correct, we indicate that

$$\left|f_\pi(s = M_\rho^2)\right|^2 = 1 + \left(\frac{F_\rho g(M_\rho^2)}{\Gamma_\rho}\right)^2 = 38.5, \tag{48}$$

which is much closer to the experimental value of 43.95 ± 1.78 from [17] than the value of 26.35 predicted by the VDM.

The role of t and u dependences of g in calculating the phase shift $\delta_0^2(s)$ will be clarified in Section 7.

5. SPIN-2 FIELDS AND THEIR INTERACTIONS

The gauge-invariant form of the vertex describing the interaction of a spin-2 particle with two π mesons (see, for example, [18]) is

$$\begin{aligned}&\left\langle \pi^a(p_1)\pi^b(p_2)\middle|\varphi_{\mu\nu}(q)\right\rangle\\ &= \mathcal{F}_T(q^2)\left(p_{1\mu}p_{2\nu}+p_{1\nu}p_{2\mu}-\frac{1}{2}q^2\delta_{\mu\nu}\right).\end{aligned} \tag{49}$$

However, this vertex and the amplitude of ππ scattering via a tensor meson do not satisfy Adler's self-consistency condition [19], according to which the amplitude must vanish when one of the meson 4-momenta is zero. In order to satisfy this condition, the φππ vertex must have the form

$$[a(q^2)(p_{1\mu}p_{2\nu}+p_{2\mu}p_{1\nu})-b(q^2)(p_1p_2)\delta_{\mu\nu}]\varphi_{\mu\nu}(q).$$

In conjunction with the requirement of gauge invariance and the requirement that there be no pole at $q^2 = 0$, this yields

$$\mathcal{F}_T(q^2) = \frac{2g_T(q^2)}{M_T}\frac{q^2-2\mu^2}{M_T^2-2\mu^2}, \tag{50}$$

where $g_T(q^2)$ is a slowly varying function of q^2; in the limit of $q^2 = M_T^2$, it becomes

$$g_T^2(q^2=M_T^2) = \frac{40\pi\Gamma(\varphi\longrightarrow 2\pi)}{M_T(1-4\mu^2/M_T^2)^{5/2}}. \tag{51}$$

The form in (50) means that, within chiral theory, the φππ vertex is of order p^4 and not of order p^2, as might have been expected. Recall that a similar situation occurs in the case of the ρππ vertex—within chiral theory, it appeared to be of order p^3 instead of p^1 expected intuitively.

The tensor-meson propagator has the form [20]

$$\begin{aligned}D_{\mu\nu,\,\alpha\beta}(q) &= \left(d_{\mu\alpha}d_{\nu\beta}+d_{\nu\alpha}d_{\mu\beta}-\frac{2}{3}d_{\mu\nu}d_{\alpha\beta}\right)\\ &\times(M_T^2-q^2)^{-1},\end{aligned} \tag{52}$$

where

$$d_{\mu\nu} = \delta_{\mu\nu}-q_\mu q_\nu/M_T^2. \tag{53}$$

Tensor-meson exchange is responsible for the ππ-scattering amplitude of the form

$$\begin{aligned}T_T = \left\langle \pi_k(p_1')\pi_l(p_2')\middle|\pi_i(p_1)\pi_j(p_2)\right\rangle_T &= \frac{2}{M_T^2(M_T^2-2\mu^2)^2}\\ &\times\left[\delta_{ij}\delta_{kl}g_T^2(s)(s-2\mu^2)^2\frac{(u-t)^2-\frac{1}{3}(s-4\mu^2)^2}{M_T^2-s}\right.\\ &+\delta_{ik}\delta_{jl}g_T^2(t)(t-2\mu^2)^2\frac{(s-u)^2-\frac{1}{3}(t-4\mu^2)^2}{M_T^2-t}\\ &\left.+\delta_{il}\delta_{jk}g_T^2(u)(u-2\mu^2)^2\frac{(s-t)^2-\frac{1}{3}(u-4\mu^2)^2}{M_T^2-u}\right].\end{aligned} \tag{54}$$

In the ensuing analysis, we set $g_T(x)$ to

$$g_T(x) = g_T(M_T^2)\frac{1+M_T^4/m^4}{1+x^2/m^4}. \tag{55}$$

6. FORMALISM FOR DESCRIBING ππ SCATTERING

6.1. Partial-Wave Expansion

Each amplitude associated with resonance exchange is given by

$$\begin{aligned}T_n(ij\longrightarrow kl) &= \delta_{ij}\delta_{kl}A_n\\ &+\delta_{ik}\delta_{jl}B_n+\delta_{il}\delta_{jk}C_n,\end{aligned} \tag{56}$$

where the subscript $n = \sigma$, f_0, ρ, and φ specifies a relevant resonance. The crossing symmetry of the amplitude implies that B_n and C_n are obtained from A_n by means of the substitutions ($s\longrightarrow t$, $t\longrightarrow s$) and ($s\longrightarrow u$, $u\longrightarrow s$), respectively.

For the case of a fixed total isospin of the system of initial (final) pions, the expressions for the amplitudes are given by [21]

$$T^{(0)} = 3A+B+C, \tag{57}$$

$$T^{(1)} = B-C, \tag{58}$$

$$T^{(2)} = B+C. \tag{59}$$

The amplitudes for various charged channels are expressed in terms of $T^{(a)}$ as

$$\begin{aligned}T(\pi^+\pi^+\longrightarrow\pi^+\pi^+) &= T(\pi^-\pi^-\longrightarrow\pi^-\pi^-) = T^{(2)},\\ T(\pi^+\pi^0\longrightarrow\pi^+\pi^0) &= T(\pi^-\pi^0\longrightarrow\pi^-\pi^0)\\ &= \frac{1}{2}(T^{(2)}+T^{(1)}),\\ T(\pi^+\pi^-\longrightarrow\pi^0\pi^0) &= \frac{1}{3}(T^{(0)}-T^{(2)}),\\ T(\pi^+\pi^-\longrightarrow\pi^+\pi^-) &= \frac{1}{3}T^{(0)}+\frac{1}{2}T^{(1)}+\frac{1}{6}T^{(2)},\end{aligned} \tag{60}$$

$$T(\pi^0\pi^0 \longrightarrow \pi^0\pi^0) = \frac{1}{3}(2T^{(0)} + T^{(2)}).$$

The decomposition of the isotopic amplitudes into amplitudes corresponding to fixed values of the orbital angular momentum is given by

$$T^{(I)} = 32\pi\sum_{l=0}^{\infty}(2l+1)t_l^I(s)P_l(\cos\theta), \qquad (61)$$

where θ is the scattering angle in the c.m. frame of primary mesons. It follows from (61) that the partial-wave amplitude t_l^I is

$$t_l^I(s) = \frac{1}{64\pi}\int_{-1}^{1}T^{(I)}P_l(\cos\theta)d\cos\theta. \qquad (62)$$

The near-threshold behavior of the partial-wave amplitudes is described by the expansion

$$\mathrm{Re}t_l^I(s) = q^{2l}[a_l^I + b_l^I q^2 + O(q^4)], \qquad (63)$$

where

$$q^2 = \frac{1}{4}s - \mu^2 \qquad (64)$$

and where the quantities a_l^I are referred to as scattering lengths. However, phase shifts as functions of energy are of greater interest than the low-energy parameters a_l^I and b_l^I, because the former control the scattering cross sections. Since the partial-wave amplitudes t_l^I grow with energy, unitarization of the amplitudes is an important element of scattering theory. We address this point immediately below.

6.2. Unitarization Procedure and Phase Shifts

In calculating phase shifts, it is necessary that operations with the amplitudes $t_l^I(s)$ not violate the unitarity of the S matrix. In other words, we must ensure fulfillment of the condition $SS^\dagger = 1$ for the S matrix constructed from the transformed amplitudes.

If there are a number of resonances at $\sqrt{s} = m_{R_1}$, m_{R_2}, … in a channel specified by fixed values of I and l and if, in addition, there is potential scattering, the expression for the S matrix in the region of elasticity can be represented in the form

$$S = e^{2i\delta^I_{R_1}}e^{2i\delta^I_{R_2}}\ldots e^{2i\delta^I_{l,\mathrm{bg}}}, \qquad (65)$$

where

$$e^{2i\delta^I_{R_j}} = \frac{1+i\rho t^I_{R_j}}{1-i\rho t^I_{R_j}}, \quad e^{2i\delta^I_{l,\mathrm{bg}}} = \frac{1+i\rho t^I_{l,\mathrm{bg}}}{1-i\rho t^I_{l,\mathrm{bg}}}. \qquad (66)$$

Here, the subscript bg labels the potential-scattering amplitude, while

$$\rho = \sqrt{1-4\mu^2/s}. \qquad (67)$$

From (65) and (66), it immediately follows that the resonance phase shifts are given by

$$\delta^I_{R_j}(s) = \arctan(\rho t^I_{R_j}). \qquad (68)$$

The same formula, featuring, however, $t^I_{l,\mathrm{bg}}$ is valid for the potential-scattering phase shift. Obviously, the total phase shift in a channel characterized by fixed I and l is given by

$$\delta^I_l(s) = \sum_j(\delta^I_{R_j}(s)) + \delta^I_{l,\mathrm{bg}}(s). \qquad (69)$$

In our theory, the phase shift $\delta^I_{l,\mathrm{bg}}$ for potential scattering is controlled by the diagrams involving the exchanges of spinless, spin-1, and spin-2 particles in the t and u channels. This very contribution determines that part of the amplitude which is referred to as a repulsive core.

In a conventional analysis of experimental data (see, for example, [5]), such a core is introduced as an adjustable function. In our case, however, this core is determined by formulas (21), (25), (39), and (54), which admit only variations in vertex form factors and in some constants (the masses of the scalar mesons σ and their coupling constants, as well as the constant g_f for the f meson).

7. RESULTS FOR PHASE SHIFTS

In this section, we present the results for the S-, P-, and D-wave phase shifts calculated for a specific set of the parameters of our theory. This set provides a satisfactory description of the functions $\delta_0^0(s)$, $\delta_0^2(s)$, $\delta_1^1(s)$, $\delta_2^0(s)$, and $\delta_2^2(s)$ in the energy range from the threshold for the generation of two pions to $\sqrt{s} = 1$ GeV.[1)] In the present article, we restrict our consideration to the above energy values in order to avoid complications associated with a need for taking into account the production of $\bar{K}K$ systems.

The results for the phase shifts are presented in Figs. 1–4. Listed below are the parameter sets used to obtain these results. For the scalar sigma mesons, we set

$$m_{\sigma_1} = 697.6\ \mathrm{MeV}, \quad m_{\sigma_2} = 1374\ \mathrm{MeV}, \quad G_1 = 50.043, \quad G_2 = 15.365, \qquad (70)$$

[1)]Searches for different parameter sets that could provide a better description of the entire body of experimental data on $\pi\pi$ scattering would be rather interesting, but this requires a cooperation with experimentalists since those features of interactions that are dictated by chiral theory were often disregarded in previous data analyses.

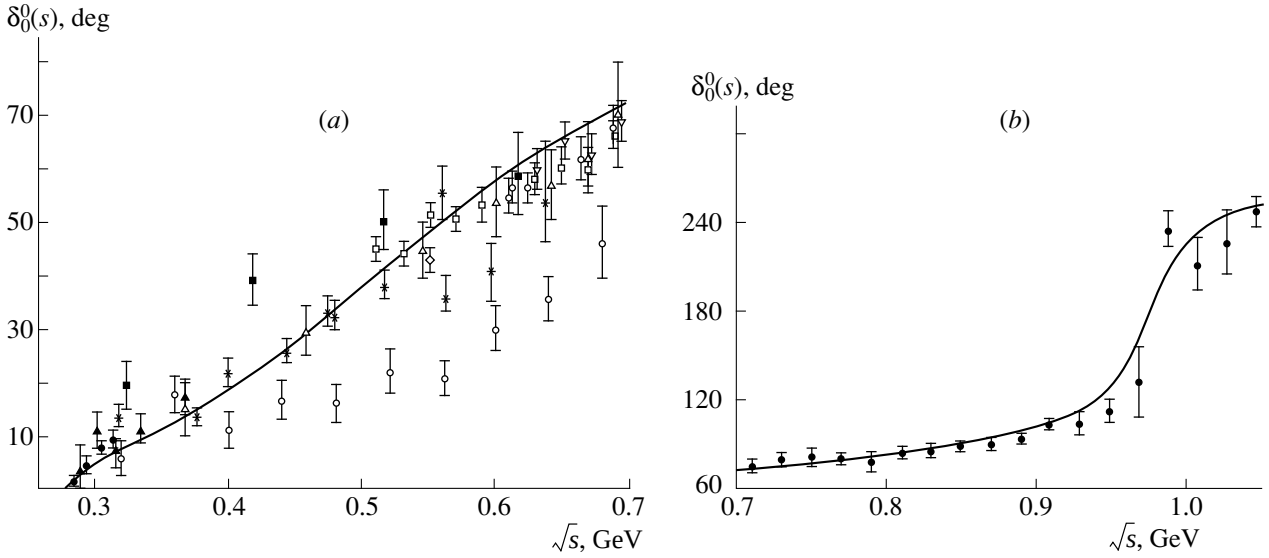

Fig. 1. Phase shift $\delta_0^0(s)$ for (*a*) $\sqrt{s} \le 0.7$ GeV and (*b*) 0.7 GeV $\le \sqrt{s} \le 1.1$ GeV. The curve represents the predictions of the present theory with the parameters specified in Sections 4 and 7. The compilation of experimental data was borrowed from [4].

which corresponds to the mixing angle of $\theta_S = 19.8°$ in (13). For the form factor (23), we used the value of $k = 0.5/(\text{GeV})^2$. For the isosinglet scalar resonance $f_0(980)$ having a width in the range $\Gamma_{f_0}^{\text{expt}} = 40$–$100$ MeV [25], we chose the value of $g_{f_0}^2 = 7.62$, which corresponds to the total width of $\Gamma_{f_0} \cong 63$ MeV.

The parameters of the rho-meson form factor were specified in Section 4.

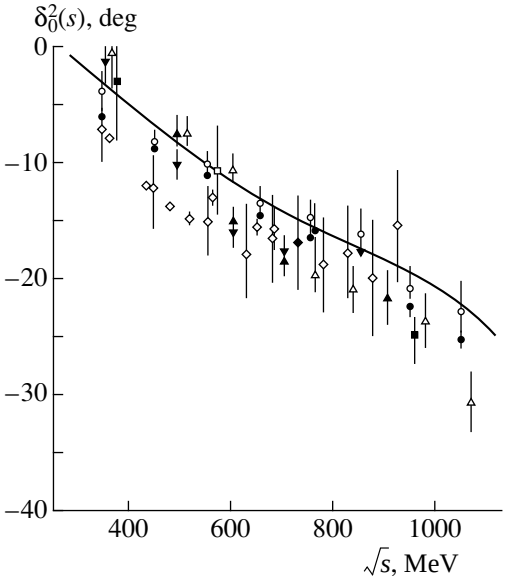

Fig. 2. Phase shift $\delta_0^2(s)$ for $\sqrt{s} \le 1.1$ GeV. The curve represents the predictions obtained within the present theory. The compilation of experimental data was borrowed from [22].

For the tensor meson $f_2(1270)$, we took the values

$$M_T = 1.27 \text{ GeV}, \quad \Gamma(f_2 \longrightarrow 2\pi) = 159 \text{ MeV}, \quad m^4 = 0.839 \text{ (GeV)}^4. \tag{71}$$

Although this resonance is off the energy range under consideration, it has a pronounced effect on the *D*-wave phase shifts since its coupling constant is rather large ($g_{f_2}^2 = 17.8$), its relatively small width being due to the presence of the factor $(2J+1)^{-1} = 1/5$ in the expression for the decay probability.

7.1. Phase Shift δ_0^0

In order to clarify the question of why the scalar resonance σ_1 of mass about 700 MeV does not lead to the phase shift of $\delta_0^0 = \pi/2$ at $\sqrt{s} = m_{\sigma_1}$, it is reasonable to consider the relation between δ^{res} and δ^{bg} in expression (69) for the total phase shift. Table 1 lists terms contributing to the total phase shift δ_0^0. Recall that, according to the discussion in Subsection 6.2, we have

$$\delta^{\text{bg}} = \arctan[\rho(t_{\sigma_1+\sigma_2}^{\text{bg}} + t_{f_0}^{\text{bg}} + t_\rho^{\text{bg}} + t_{f_2}^{\text{bg}})]. \tag{72}$$

Among other things, the data in Table 1 indicate that, although the phase shift for resonance scattering takes the value of $\pi/2$ for $\sqrt{s} < 0.7$ GeV, the total phase δ_0^0 assumes this value in the energy range $0.8 < \sqrt{s} < 0.9$ GeV (more precisely, at $\sqrt{s} = 0.845$ GeV), which complies well with available experimental data (see Fig. 1*b*). The compilation of data on the phase shift δ_0^0

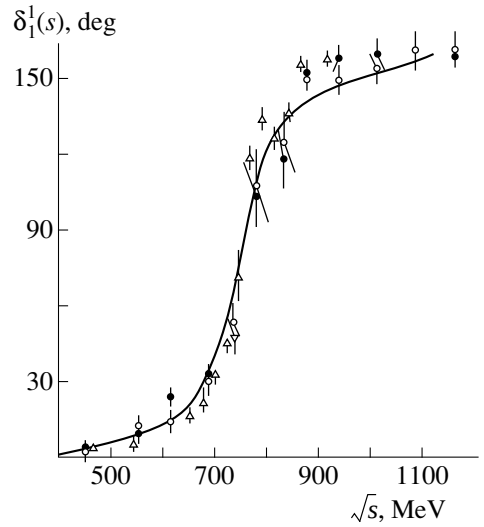

Fig. 3. Phase shift $\delta_1^1(s)$ for $\sqrt{s} \leq 1.1$ GeV. The curve represents the results obtained within the theory proposed here. The compilation of experimental data was borrowed from [23].

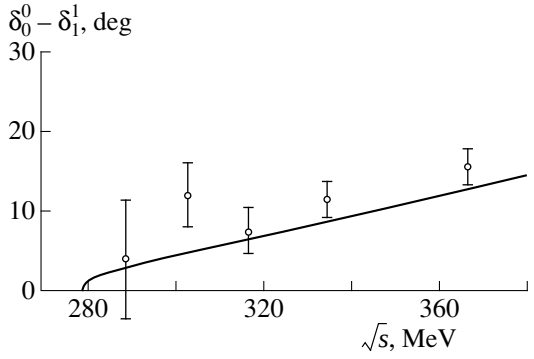

Fig. 4. Phase-shift difference $\delta_0^0(s) - \delta_1^1(s)$ for s values characteristic of K_{e_4} decays. The curve represents the results obtained within the theory proposed here. Experimental data were borrowed from [24].

in Figs. 1*a* and 1*b* was borrowed from [4], where the reader can also find references to relevant experimental studies.

7.2. Phase Shift δ_0^2

In the absence of exotic resonances, the phase shift δ_0^2 is caused by purely potential scattering. The phase shift δ_0^2 differs from $\delta_{0,\,\mathrm{bg}}^0$ in that the rho-meson contribution appears in δ_0^2 with a factor of –1/2; hence, this contribution is opposite in sign to the sigma-meson contribution. Had the condition $g(t) = g(u) = \mathrm{const}$ been satisfied for the rho meson, a fast growth of the rho-meson contribution with energy would have resulted in a sharp rise of the δ_0^2 curve in Fig. 2 from $\sqrt{s} \approx m_K$, an effect that was indeed obtained in [4], but which is at odds with experimental data. This flaw is remedied, however, by taking into account the dependence of g on t and u, as is demonstrated by the present result.

The compilation of data on δ_0^2 was borrowed from the article of Ishida *et al.* [22], who also present references to relevant experimental studies.

For the difference $(\delta_0^0 - \delta_0^2)_{\sqrt{s} = m_K}$, which is of interest for verifying *CP* and *CPT* invariance in $K \longrightarrow 2\pi$ decays, we obtained

$$(\delta_0^0 - \delta_0^2)_{\sqrt{s} = m_K} = 44.85^\circ. \tag{73}$$

Relevant experiments yield

$$(\delta_0^0 - \delta_0^2)_{\sqrt{s} = m_K} = \begin{cases} 41.4^\circ \pm 8.1^\circ & [26] \\ 47^\circ \pm 6^\circ (\mathrm{data}) & [27] \\ 44^\circ \pm 3^\circ (\mathrm{data + BFP}) & [27]. \end{cases} \tag{74}$$

Table 1. Contributions of resonance and potential scattering to δ_0^0 (the resonance contribution comes from the exchange of $\sigma_{1,2}$ and f_0 particles in the s channel, while the potential contribution comes from the exchange of all scalar mesons, a vector particle, and a tensor particle in the t and u channels)

$\sqrt{s}$, GeV	$\delta_{\sigma_{1+2}}^{\mathrm{res}}$	$\delta_{f_0}^{\mathrm{res}}$	$\delta_0^{0,\,\mathrm{bg}}$	$\delta_0^{0,\,\mathrm{tot}}$	$\sqrt{s}$, GeV	$\delta_{\sigma_{1+2}}^{\mathrm{res}}$	$\delta_{f_0}^{\mathrm{res}}$	$\delta_0^{0,\,\mathrm{bg}}$	$\delta_0^{0,\,\mathrm{tot}}$
0.3	5.72	0.0037	–1.21	4.52	0.7	96.89	1.3445	–26.14	72.09
0.4	24.7	0.0444	–5.9	18.84	0.8	112.54	3.5781	–32.34	83.78
0.5	49.95	0.1763	–12.07	38.05	0.9	125.38	12.54	–37.44	100.48
0.6	76.07	0.5151	–19.13	57.45	1.0	137.43	127.03	–41.64	222.82

Note: All phase-shift values are given here in angular degrees.

Table 2. Comparison of the results obtained in this study for δ_2^0 and δ_2^2 with those evaluated on the basis of Roy's dispersion relations

$\sqrt{s}$, GeV	δ_2^0, deg		δ_2^2, deg	
	present result	result from Roy's relations [29]	present result	result from Roy's relations [29]
0.3	0.00065	–	0.00012	–
0.4	0.057	0.07 ± 0.01	0.0052	0.00 ± 0.01
0.5	0.28	–	−0.00095	–
0.6	0.78	0.9 ± 0.1	−0.065	-0.1 ± 0.1
0.7	1.765	–	−0.237	–
0.8	3.51	3.5 ± 0.5	−0.535	-0.5 ± 0.2
0.9	6.42	–	−0.92	–
1.0	11.35	11 ± 2	–1.3	-1.0 ± 0.6

Table 3. Low-energy parameters of $\pi\pi$ scattering

	Experiment [31]	Standard ChPT [1, 32]	Generalized $ChPT_1$ [33]	Generalized $ChPT_2$ [33]	Present theory
a_0^0	0.26 ± 0.05	0.20 ± 0.01	0.27	0.28	0.186
b_0^0	0.25 ± 0.03	0.25	0.26	0.28	0.255
$-10a_0^2$	0.28 ± 0.12	0.42	0.23	0.28	0.43
$-10b_0^2$	0.82 ± 0.08	0.72	0.79	0.75	0.79
$10a_1^1$	0.38 ± 0.02	0.37	0.39	0.38	0.324
$100b_1^1$		0.48	0.48	0.28	0.126
$100a_2^0$	0.17 ± 0.03	Input	0.18	0.21	0.154
$10^3a_2^2$	0.13 ± 0.31	″	0.24	0.57	0.515

Note: A comparison of the predictions of the present theory with experimental data from [31] and with the predictions of standard ChPT [1, 32] and of two versions of generalized ChPT [33] that correspond to setting $r = 10$ and $10^3L_3 = -3.5$ or $10^3L_3 = -2$.

7.3. Phase Shift δ_1^1

Our result for $\delta_1^1(s)$ is presented in Fig. 3. The compilation of experimental data was borrowed from [23]. In Fig. 4, our result for $(\delta_0^0 - \delta_1^1)$ in the range $2\mu \le \sqrt{s} \le 0.38$ GeV is presented along with data on K_{e_4} decays.

7.4. Phase Shifts δ_2^0 *and* δ_2^2

Information about the *D*-wave phase shifts δ_2^0 and δ_2^2 from [23, 28] is incomplete and may involve large uncertainties. Moreover, it is desirable that the procedure for extracting this information from experimental data take into account the effect of the $f_2(1270)$ resonance, whose role has yet to be clarified conclusively, as can be seen from our study. In the dispersion approach, this is not very important. Therefore, it seems preferable to compare the present results with those obtained in [29] by using Roy's dispersion relations. The results of this comparison are illustrated in Table 2.

8. BRIEF COMMENTS ON THE SCATTERING LENGTHS

For the sake of completeness, our results for the scattering lengths calculated according to (64) are presented in Table 3 along with the scattering-length val-

ues that were extracted from experimental data, as well as the values predicted within various modifications of ChPT. It can be seen that our value of $a_0^0 = 0.186$ for the length is somewhat larger than $(a_0^0)_W = 0.157$, but the current-algebra prediction

$$\frac{2a_0^0 - 5a_0^2}{18a_1^1} = 1 \qquad (75)$$

is satisfied to within 0.6%.

9. CONCLUSION

From the study presented here, it follows that the dynamics of low-energy $\pi\pi$ scattering is controlled by the exchanges of spinless, spin-1, and spin-2 particles having the lowest masses. The near-threshold behavior of the phase shifts is determined primarily by the exchanges of scalar sigma mesons, chiral partners of η' and η mesons. In order to reproduce, within the concept of single-particle exchange, experimental data on the phase shifts δ_0^0, δ_0^2, and δ_1^1 and the predictions of Roy's dispersion relations for the *D*-wave phase shifts, it is necessary consider that the $\sigma\pi\pi$, $\rho\pi\pi$, and $f_{0,2}\pi\pi$ vertex functions depend on the square q^2 of the momentum transfer. Although the structure of these vertices for either $q^2 \longrightarrow 0$ or $q^2 \longrightarrow \mu^2$ is fixed by the requirements of chiral theory—and by the requirement of gauge invariance as well for ρ and f_2—the expressions for the form factors far off the threshold are not specified completely within the theory. An example of the form-factor type for scalar, vector, and tensor $\pi\pi$ interactions that provides a satisfactory description of five phase shifts as functions of energy in the energy range from the threshold for two-pion generation to $\sqrt{s} = 1$ GeV has been given in this study.

According to the present analysis, the lightest scalar sigma meson has a mass of $m_\sigma \approx 700$ MeV and a width of $\Gamma \approx 725$ MeV.

The approach developed here may prove useful in constructing a theory for other low-energy hadronic processes as well.

REFERENCES

1. J. Gasser and H. Leutwyler, Ann. Phys. **158**, 142 (1984); Nucl. Phys. B **250**, 465, 517, 539 (1985).
2. H. W. Fearing and S. Scherer, Phys. Rev. D **53**, 315 (1996).
3. G. Ecker *et al.*, Nucl. Phys. B **321**, 311 (1989).
4. V. Bernard, N. Kaiser, and U.-G. Meissner, Nucl. Phys. B **364**, 283 (1991).
5. S. Ishida *et al.*, Prog. Theor. Phys. **95**, 745 (1996).
6. C. Rosenzweig, J. Schechter, and G. Trahern, Phys. Rev. D **21**, 3388 (1980); P. Di Vecchia and G. Veneziano, Nucl. Phys. B **171**, 253 (1980).
7. J. Schechter, Phys. Rev. D **21**, 3393 (1980).
8. E. Shabalin, Nucl. Phys. B **409**, 87 (1993).
9. E. Shabalin, Yad. Fiz. **49**, 588 (1989) [Sov. J. Nucl. Phys. **49**, 365 (1989)].
10. S. Weinberg, Phys. Rev. Lett. **17**, 616 (1966).
11. B. W. Lee and H. T. Nieh, Phys. Rev. **166**, 1507 (1968); A. K. Bhargava and T. Dass, Phys. Rev. D **1**, 649 (1970); D. P. Majumdar, Phys. Rev. D **1**, 684 (1970).
12. W. Krolikowski, Nuovo Cimento A **42**, 435 (1966).
13. M. Ademolo *et al.*, Phys. Lett. **22**, 521 (1966).
14. D. G. Galdi and H. Pagels, Phys. Rev. D **14**, 809 (1976).
15. S. Weinberg, Phys. Rev. **166**, 1568 (1968).
16. M. Bando, T. Kugo, and K. Yamawaki, Phys. Rep. **164**, 218 (1988).
17. L. M. Barkov *et al.*, Nucl. Phys. B **256**, 365 (1985).
18. V. I. Zakharov, Zh. Éksp. Teor. Fiz. **48**, 303 (1965) [Sov. Phys. JETP **21**, 199 (1965)].
19. S. L. Adler, Phys. Rev. B **137**, 1022 (1965).
20. M. Fierz, Helv. Phys. Acta **12**, 3 (1939).
21. J. L. Petersen, Preprint No. 77-04, CERN (Geneva, 1977).
22. S. Ishida *et al.*, Prog. Theor. Phys. **98**, 1005 (1997).
23. E. A. Alekseeva *et al.*, Zh. Éksp. Teor. Fiz. **82**, 1007 (1982) [Sov. Phys. JETP **55**, 591 (1982)].
24. L. Rosselet *et al.*, Phys. Rev. D **15**, 574 (1977).
25. Particle Data Group, Eur. Phys. J. C **3**, 1 (1998).
26. T. J. Devlin and J. O. Dickey, Rev. Mod. Phys. **51**, 237 (1979).
27. W. Ochs, Preprint No. MPI-Ph/ph 91-35 (1991).
28. W. Hoogeland *et al.*, Nucl. Phys. B **69**, 266 (1974); M. J. Losty *et al.*, Nucl. Phys. B **69**, 185 (1974); N. B. Durosoy *et al.*, Phys. Lett. B **45**, 517 (1973); D. Cohen *et al.*, Phys. Rev. D **7**, 662 (1973); W. Hoogland *et al.*, Nucl. Phys. B **157**, 250 (1979).
29. J. L. Basdevant, C. D. Froggat, and J. L. Petersen, Nucl. Phys. B **72**, 413 (1974).
30. S. M. Roy, Phys. Lett. B **36**, 353 (1971).
31. O. Dumbrajs *et al.*, Nucl. Phys. B **216**, 227 (1983).
32. J. Gasser and H. Leutwyler, Phys. Lett. B **125**, 321, 325 (1983).
33. M. Knecht, B. Moussallam, and J. Stern, in *The Second DAΦNE Physics Handbook*, Ed. by L. Maiani, G. Pancheri, and N. Paver (INFN–LNF, 1995), p. 221.

Translated by O. Chernavskaya

Physics of Atomic Nuclei, Vol. 63, No. 4, 2000, pp. 606–616. From Yadernaya Fizika, Vol. 63, No. 4, 2000, pp. 672–682.

ELEMENTARY PARTICLES AND FIELDS
Theory

Distribution of Charmed Constituent Quarks in Hadrons*

Yu. A. Golubkov

Institute of Nuclear Physics, Moscow State University, Vorob'evy gory, 119899 Russia

Received November 12, 1998; in final form, April 29, 1999

Abstract—By using a statistical approach within noncovariant perturbation theory, the distributions of light and charmed quarks in hadrons are derived with allowance for the charmed-quark mass. The parameters of the model are extracted from a comparison with NA3 data on the hadroproduction of J/ψ particles. A reanalysis of EMC data on charm production in muon–nucleon scattering is performed. In relation to the conventional source of charmed quarks from photon–gluon fusion, the EMC data are found to suggest the presence of an additional contribution from deep-inelastic scattering on charmed quarks at large x. The resulting admixture of Fock states that contain charmed quarks in the decomposition of the proton wave function is about 1%. The approach presented for the excitation of Fock states involving charmed quarks can also be applied to states featuring beauty quarks, as well as to the hadronic component of the virtual photon (resolved photon component). © *2000 MAIK "Nauka/Interperiodica".*

1. INTRODUCTION

The production of heavy flavors in lepton–hadron and hadron–hadron collisions is a very important tool for a quantitative test of QCD and for searches for new physics. Due to the presence of a pointlike probe particle (lepton) and the possibility of controlling the QCD scale of hard subprocess, deep-inelastic scattering (DIS) has a number of advantages in relation to hadronic reactions in the analysis of charm production. The QCD-based parton model has been remarkably successful in describing a wide variety of high-energy processes involving energy scales much greater than the masses of known particles and of the partons themselves. Many analyses of charm production that were performed within the parton model assume that hadrons consist only of massless or approximately massless partons (gluons and *u*, *d*, and *s* quarks). The heavy quarks (charm and bottom ones) are treated as massive objects external to hadrons. In DIS neutral-current reactions, this kind of consideration leads naturally to the $O(\alpha_s^{(1)})$ "photon–gluon fusion" (PGF) mechanism $\gamma g \longrightarrow c\bar{c}$ as a dominant mechanism of heavy-quark production. In hadronic collisions, analogous "parton–parton fusion" processes, $gg \longrightarrow c\bar{c}$ and $q\bar{q} \longrightarrow c\bar{c}$, are expected to contribute. These parton-fusion processes are flavor-creating (FC) since heavy flavor is created by the interaction with a light constituent of a hadron.

Existing experimental data on μp collisions [1] show some irregularities that are inconsistent with PGF predictions. The experimental observation of a deviation of the charm distribution at large pseudorapidities (that is, charm production close to the direction of the proton beam) from conventional predictions in *ep* scattering were also reported by the ZEUS experiment at the HERA collider [2]. In hadronic collisions, the interpretation of data on open-charm production within the standard parton–parton fusion scheme followed by the hadronization of charmed quarks runs into problems for charmed particles at large x_F. In this region, the charm distributions are harder than the predictions of the factorization approach. Furthermore, the yield of charmed particles containing the valence quarks of the projectile significantly exceeds the yield of their antiparticles. Models considering the recombination of the newly created charmed quark with one of the valence quarks of the projectile [3, 4] or string fragmentation [5] can improve the situation with open-charm production. In both approaches, a part of the proton-remnant momentum is imparted to the final-state charmed particle, increasing its momentum and improving the agreement with experimental observations. However, these models have problems with describing J/ψ and double-J/ψ production, as well as with the *A* dependence of the charm-production cross section in hadron–nucleus collisions at large x_F [6–8].

A part of the discrepancies between data and models can be resolved by introducing the flavor-excitation (FE) scheme, which assumes that heavy quarks can also be constituents of hadrons. We note that a consideration of heavy quarks as those that are external to hadrons is appropriate when the characteristic scale of the process (μ) is less than or on the order of the heavy-quark mass—that is, $\mu \lesssim m_Q$. This condition holds for *c* and *b* quarks for the majority of fixed-target experiments. The HERA *ep* collider provides an opportunity to investigate heavy-quark production at Q^2 scales much greater than $4m_Q^2$. At such scales, it seems justified to consider charm (and bottom) quarks as light objects.

* This article was submitted by the author in English.

The so-called variable-flavor-number scheme proposed in [9–11] combines the FC and FE schemes and ensures a "soft" transition between the two production mechanisms. A more sophisticated approach for the FC mechanism performs an effective resummation of large logarithms of the type $[\alpha_s(\mu)\ln(\mu^2/m_Q^2)]^n$, which limit the validity of the conventional FC mechanism to the region $\mu \sim O(m_Q)$. It was shown in those studies that the contribution from scattering on a charmed constituent quark of the proton [process of order $O(\alpha_s^{(0)})$] becomes more important than PGF for $x \gtrsim 0.1$ at surprisingly low $Q^2 \gtrsim 20$–30 GeV^2. The authors used splitting functions and standard distributions for massless partons, including heavy flavors, and introduced the "slow-rescaling" variable $x \longrightarrow x[1 + (m_Q/Q)^2]$ to take into account the charmed-quark mass. However, perturbative QCD requires the scale μ to be large and needs, as inputs, the initial parton distributions for their evolution. The initial distributions of heavy quarks are not necessarily similar to the distributions of light partons because of the nonzero quark mass, which is commensurate with the QCD scale. This kind of consideration is closely related to the old question of which type of high-order QCD corrections must be assigned to the matrix element and which is due to QCD evolution of the parton distributions. So far, we have no clear answer to this question.

The authors of [12] proposed a procedure for obtaining the distribution of massive charmed quarks in hadrons. They considered the proton-wave-function decomposition that may contain the Fock state component $|uudc\bar{c}\rangle$ called "intrinsic charm" (IC). Such a state may appear as a quantum fluctuation of the hadron wave function and may become free in interactions featuring substantial momentum transfers. In this case, the proton is described as a decomposition in terms of color-singlet eigenstates of the free Hamiltonian: $|uud\rangle$, $|uudg\rangle$, $|uudq\bar{q}\rangle$, …. Over a sufficiently short time, the proton can contain Fock states of arbitrary complexity, including pairs of charmed quarks. In the proton rest frame, the lifetime τ of such fluctuations is on the order of the nuclear time about R_h, where R_h is the hadronic size. On average, there are extra partons (gluons and $q\bar{q}$ pairs) in addition to valence quarks. In the infinite-momentum frame, a partonic fluctuation will be "frozen" and can be observed, for example, in lepton–hadron scattering. Charmed quarks are heavy objects, and their lifetime is much smaller than those of light partons. On average, the admixture of heavy-quark pairs is expected to be small, about $(m_q/m_Q)^2$. Because quantum fluctuations in the initial proton are determined by the self-interaction of the color field, the structure of the Fock states of the proton can be considered independently of hard interaction, providing the initial nonperturbative parton distributions. These distributions will evolve in hadron–hadron or lepton–hadron collisions owing to high momentum transfers.

In the present paper, we modify and generalize the statistical approach to the Fock state hadron structure with heavy quarks, suggested in [12–14], within noncovariant perturbation theory. We obtain scaling expressions for the heavy- and light-parton distributions in the infinite-momentum frame. We calculate the charmed structure function of the proton, $F_2^{(c)}(x, Q^2)$, taking into account QCD radiative corrections of order $\alpha_s^{(1)}$, as well as mass corrections caused by the nonzero values of the c-quark and the proton mass. We use the experimental data for $\pi A \longrightarrow J/\psi X$ [7] and $\mu p \longrightarrow \mu c\bar{c} X$ [1] to evaluate the parameters of the model and present the relative contributions of the PGF and the IC mechanism to the charm structure function of the proton. Note that we use the terms FE and IC for the charm-production mechanisms involving the charmed constituent quarks of the proton.

2. DESCRIPTION OF THE MODEL

2.1. General Features

In QCD, high-energy hadrons are coherent superpositions (Fock state vectors) of quarks and gluons. Note that the lifetime of a fluctuation, $\Delta t \sim 1/\Delta E \approx 2P_h/(M^2 - m^2)$ (P_h is the hadron momentum, m is the hadron mass, and M is the mass of the fluctuation), can be sufficiently large at high energies even for large mass values of the fluctuation.

Based on the above picture of the proton, Kuti and Weisskopf [13], who used the statistical approach, achieved a good description of the proton structure function. In [14], I presented a statistical consideration of the hadron structure and obtained noninvariant (that is, frame-dependent) expressions for parton distributions. In principle, the frame dependence can take place at sufficiently low energies, while, in the infinite-momentum frame, one expects invariant expressions.

We take all partons on the mass shell and use noncovariant perturbation theory. Thus, we consider a hadron as a statistical system that consists of N quarks carrying quantum numbers of the hadron, two charmed quarks c and $\bar{c}$, and a system of n light partons (gluons and quarks) carrying, in total, the quantum numbers of the vacuum.

In noncovariant perturbation theory, the probability of producing an m-particle final state in the case of an instantaneous interaction has the form [15]

$$dW^{(m)} \sim \frac{|H_{\text{int}}|^2}{(E_{\text{fin}} - E_h)^2}\delta(P_{\text{fin}} - P_h)d\Phi_{\text{fin}}^{(m)}, \qquad (1)$$

where $d\Phi_{\text{fin}}^{(m)}$ is an element of the m-particle phase space; $m = N + 2 + n$; P_h and E_h are, respectively, the

momentum and the energy of the hadron being considered; $P_{\rm fin}$ and $E_{\rm fin}$ are, respectively, the momentum and the energy of the final-state partonic fluctuation; and $d\Phi_{\rm fin}^{(m)}$ describes the Lorentz invariant phase space,

$$d\Phi_{\rm fin}^{(m)} = \prod_{k=1}^{m}\frac{d^3p_k}{\varepsilon_k}. \tag{2}$$

The delta function in (1) ensures the conservation of the total 3-momentum.

Due to a sharp cutoff on the transverse momenta of partons, it is sufficient to consider only the longitudinal phase space; that is,

$$\frac{d^3p}{\varepsilon} \longrightarrow \frac{d\xi}{\sqrt{\xi^2+\mu^2}}, \tag{3}$$

where $\xi = p_z/P_h$ and $\mu = m_\perp/P_h$, $m_\perp$ being the transverse mass of the parton.

Following the parton model, we assume an independent primordial distribution of each parton and make the substitution

$$|H_{\rm int}|^2 d\Phi_{\rm fin}^{(m)} \longrightarrow \prod_{k=1}^{m}\rho_k(\xi_k)d\xi_k, \tag{4}$$

where $\rho(\xi)$ is the probability density for observing a parton with a momentum fraction ξ. Therefore, the probability of observing an m-parton Fock state has the form

$$W^{(m)} = \int_0^1\prod_{k=1}^{m}d\xi_k\rho_k(\xi_k)\delta\left(1-\sum_{j=1}^{m}\xi_j\right). \tag{5}$$

The omitted common factors will be incorporated in the general normalization. Integration with respect to m parton momenta can be performed [13] by using the following integral representation of the delta function:

$$2\pi\delta(x) = \int_{-\infty}^{+\infty}d\nu e^{i\nu x}. \tag{6}$$

Upon integration with respect to all ξ_k, we obtain

$$W^{(m)} = \frac{1}{2\pi}\int_{-\infty}^{+\infty}d\nu e^{i\nu}\prod_{k=1}^{m}\rho_k(\nu). \tag{7}$$

Here, integration with respect to ξ could be extended to infinity owing to the presence of the fast-oscillating exponential, and the Fourier transform of the parton density $\rho_k(\xi)$ was defined by

$$\rho_k(\nu) = \int_0^\infty d\xi\rho_k(\xi)e^{-i\nu\xi}.$$

Following [13], we introduce different probability densities for valence quarks, charmed quarks, gluons, and light sea quarks: ρ_v, ρ_c, ρ_g, and ρ_q, respectively. Because all light sea partons of the same type have the same distributions, we have to perform summation over all possible permutations of the n light sea partons (gluons and $q\bar q$ pairs separately). For the probability of observing a Fock state featuring N valence quarks, one $c\bar c$ pair, n_g gluons, and n_q pairs of light sea quarks ($n = n_g + 2n_q$), we arrive at the expression

$$W_N^{(n)} = \frac{1}{2\pi}\int_{-\infty}^{+\infty}d\nu e^{i\nu}[\rho_v(\nu)]^N\rho_{c\bar c}(\nu) \times\sum_{n_g+2n_q=n}\frac{\rho_g(\nu)^{n_g}}{n_g!}\frac{\rho_q(\nu)^{2n_q}}{(2n_q)!}, \tag{8}$$

where $\rho_{c\bar c}$ is the probability of creating a $c\bar c$ pair.

The factors $1/n_g!$ and $1/(2n_q)!$ take into account the indistinguishability of gluons and quarks, respectively. In order to obtain the total probability for all Fock states containing a $c\bar c$ pair, we must perform summation over $0 < n < \infty$. This summation can be carried out by using the properties of binomial sums:

$$\sum_{n_g+2n_q=n}\frac{\rho_g^{n_g}}{n_g!}\frac{\rho_q^{2n_q}}{(2n_q)!} = \frac{1}{2}\left[\frac{\rho_+^n}{n!}+\frac{\rho_-^n}{n!}\right], \qquad \rho_\pm = \rho_g\pm\rho_q. \tag{9}$$

The general form of the partition function is [16]

$$Z_N^{(c)} = \sum_{n=0}^{\infty}W_N^{(n)} = \frac{1}{2\pi}\int_{-\infty}^{+\infty}d\nu e^{i\nu}[\rho_v(\nu)]^N \times\rho_{c\bar c}(\nu)\exp[\rho_g(\nu)]\cosh[\rho_q(\nu)]. \tag{10}$$

It is clear from (5) that the distribution $P_k(\xi)$ for the kth parton can be obtained by omitting integration with respect to the momentum of precisely this parton. In general, one- or many-particle distributions can be derived from the partition function by taking the functional derivative of the required function(s) [16]. Thus, the inclusive distribution of light partons and the distribution of the $c\bar c$ pair are given by

$$P_k(\xi) = \frac{1}{Z_N^{(c)}}\rho_k(\xi)\frac{\delta Z_N^{(c)}}{\delta\rho_k} \equiv \frac{1}{Z_N^{(c)}}\rho_k(\xi)C_k(1-\xi),$$

$$P_{c\bar c}(\xi_c,\xi_{\bar c}) = \frac{1}{Z_N^{(c)}}\rho_{c\bar c}(\xi_c,\xi_{\bar c})\frac{\delta Z_N^{(c)}}{\delta\rho_{c\bar c}} \equiv \frac{1}{Z_N^{(c)}}\rho_{c\bar c}(\xi_c,\xi_{\bar c})C_{c\bar c}(1-\xi_c-\xi_{\bar c}), \tag{11}$$

where $C_k(1-\xi)$ and $C_{c\bar{c}}(1-\xi_c-\xi_{\bar{c}})$ are correlation functions that ensure momentum conservation and where normalization to unity is implied.

2.2. Probability Densities and Parton Distributions

The origin of the $c\bar{c}$ pair is the same as that of light-sea-quark pairs—namely, the splitting of a gluon into a virtual $c\bar{c}$-pair, $g \longrightarrow c\bar{c}$. At sufficiently low energies, where $\xi_c P_h \leq m_{\perp c}$, one can in principle expect $\rho_c \approx$ const, but, in the limit $P_h \longrightarrow \infty$, one has $\xi \gg \mu_c$; therefore, the situation is similar to that for light sea quarks. We will compare the model with data from fixed-target experiments, neglecting the transverse mass of the charmed quarks for the projectile hadron. Following [13], we can then represent the probability densities $\rho(\xi)$ as

$$\begin{aligned}\rho_v(\xi) &\propto \frac{\xi^\alpha}{\sqrt{\xi^2+\mu_v^2}} \approx \xi^{\alpha-1},\\ \rho_g(\xi) &= \frac{a_g}{\sqrt{\xi^2+\mu_g^2}},\\ \rho_q(\xi) &= \frac{a_q}{\sqrt{\xi^2+\mu_q^2}},\end{aligned} \tag{12}$$

and

$$\rho_c(\xi) \propto \frac{1}{\sqrt{\xi^2+\mu_c^2}} \approx \frac{1}{\xi}$$

for valence quarks, gluons, light sea quarks, and charmed quarks, respectively, with a_g and a_q being unknown constants.

In the infinite-momentum frame, we neglected the transverse mass in the probability densities (12) for the valence and charmed quarks. At the same time, we retain temporarily, for sea partons, the term μ in the denominators to perform the Fourier transformations later. In the final expressions, we will go over to the limit $\mu \longrightarrow 0$.

From experiments, we know that the momentum distribution of valence quarks at small ξ is approximately proportional to $1/\sqrt{\xi}$—that is, $\alpha = 0.5$. We will use this value in our comparison with experimental data, but, in the formulas, we use the general expression (12).

Let us consider the energy denominator in (1). Taking into account the momentum-conservation equation $P_h = \sum_i p_i$ and using the light-cone expansion in the infinite momentum frame, we obtain

$$E_{\text{fin}} - E_h \approx \frac{1}{P_h}\left(M_h^2 - \sum_{k=1}^{m}\frac{m_{\perp k}^2}{\xi_k}\right). \tag{13}$$

Because the transverse mass of the charmed quark is much larger than M_h (the hadron mass) and than the transverse mass of the light partons, $m_{\perp k}$, we have [12]

$$\frac{1}{(E_{\text{fin}}-E_{\text{in}})^2} \propto \frac{\xi_c^2\xi_{\bar{c}}^2}{(\xi_c+\xi_{\bar{c}})^2}. \tag{14}$$

The validity of the light-cone expansion of the energy denominator for Fock states featuring heavy quarks was considered in [14].

Substituting expression (14) into the definition of the probability density $\rho_{c\bar{c}}$ for observing the pair $c\bar{c}$, we arrive at

$$\rho_{c\bar{c}}(\xi_c,\xi_{\bar{c}}) \equiv \frac{\xi_c^2\xi_{\bar{c}}^2}{(\xi_c+\xi_{\bar{c}})^2}\rho_c(\xi_c)\rho_{\bar{c}}(\xi_{\bar{c}}) = \frac{\xi_c\xi_{\bar{c}}}{(\xi_c+\xi_{\bar{c}})^2}.$$

In just the same way as in the case of valence quarks, we will use a more general form for $c\bar{c}$ probability density in the formulas that are given below:

$$\rho_{c\bar{c}}(\xi_c,\xi_{\bar{c}}) = \frac{\xi_c^\beta\xi_{\bar{c}}^\beta}{(\xi_c+\xi_{\bar{c}})^2}. \tag{15}$$

We have introduced in this formula the phenomenological parameter β to take into account a possible deviation of the charm distribution from the phase-space-approximation expression (12) at moderate energies or momentum transfers. In analytic expressions, we use the generalized formula (15); in numerical calculations and in a comparison with data, we go over to the phase-space approximation, setting $\beta = 1$.

For the partition functions of Fock states featuring a $c\bar{c}$ pair and for that of Fock states featuring no such pairs ($Z_N^{(c)}$ and Z_N, respectively), the expressions that are obtained from (10) in the limit $\mu \longrightarrow 0$ are then given by

$$\begin{aligned}Z_N^{(c)} &= \frac{1}{2\pi}\int_{-\infty}^{+\infty} d\nu e^{i\nu}\left[\frac{\Gamma(\alpha)}{\nu^\alpha}\right]^N \frac{1}{\nu^g}\frac{\Gamma(2\beta)f_c(\beta)}{\nu^{2\beta}},\\ Z_N &= \frac{1}{2\pi}\int_{-\infty}^{+\infty} d\nu e^{i\nu}\left[\frac{\Gamma(\alpha)}{\nu^\alpha}\right]^N \frac{1}{\nu^g},\end{aligned} \tag{16}$$

where $\Gamma(x)$ is the gamma function and $g = a_g + a_q$ is the unknown model parameter characterizing the level of the sea in the hadron being considered.

Note here that the integral for light sea partons is proportional to $1/\mu^g$ and diverges logarithmically in the limit $\mu \longrightarrow 0$, but this divergence can be incorporated in the general normalization, as can be seen from (11), and is not important.

The analytic expressions for the partition functions

with and without a $c\bar{c}$ pair are

$$Z_N^{(c)} = \frac{[\Gamma(\alpha)]^N \Gamma(2\beta) f_c(\beta)}{\Gamma(\alpha N + 2\beta + g)},$$

$$Z_N = \frac{[\Gamma(\alpha)]^N}{\Gamma(\alpha N + g)}, \quad (17)$$

$$f_c(\beta) = \int_0^{\pi/2} d\varphi \frac{(\sin\varphi\cos\varphi)^\beta}{(\sin\varphi + \cos\varphi)^{2\beta+2}}.$$

For integer β, the function $f_c(\beta)$ takes the values of $f_c(0) = 1$, $f_c(1) = 1/6$, $f_c(2) = 1/30$, and $f_c(3) = 1/140$. For arbitrary values of β, integration can be performed numerically.

For the parton momentum distributions of valence quarks, sea partons, and charmed quarks, we obtain

$$V(\xi) = \frac{Z_{N-1}^{(c)}}{Z_N^{(c)}} \xi^{\alpha-1}(1-\xi)^{\alpha(N-1)+2\beta+g-1},$$

$$S(\xi) = g\xi^{-1}(1-\xi)^{\alpha N+2\beta+q-1},$$

$$P_{c\bar{c}}(\xi_c;\xi_{\bar{c}}) = \frac{\xi_c^\beta \xi_{\bar{c}}^\beta}{(\xi_c+\xi_{\bar{c}})^2}(1-\xi_c-\xi_{\bar{c}})^{\alpha N+q-1}, \quad (18)$$

$$c(\xi) = \frac{Z_N}{Z_N^{(c)}} \xi^\beta (1-\xi)^{\alpha N+\beta+g} J_N^{(c)}(\xi),$$

$$J_N^{(c)}(\xi) = \int_0^1 dy \frac{y^\beta (1-y)^{\alpha N+g-1}}{[\xi+(1-\xi)y]^2}.$$

The valence-quark and c-quark distributions are normalized to unity, $\int_0^1 d\xi\, P(\xi) = 1$.

Although the charmed-quark mass does not appear directly in the final expression for the probability of the Fock state, we see from (18) that, due to the factor ξ^β with $\beta > 0$, the distribution of charmed quarks is much harder than the distribution of light sea partons. This hardness stems from the large value of the charmed-quark mass. This effect must be taken into account by any phenomenological parametrization of the initial (not QCD-evolved) charmed-quark distribution.

If $SU(3)$ symmetry in the sea is broken, one can introduce a suppression factor λ_s for strange quarks and obtain

$$S_u(\xi) = S_{\bar{u}}(\xi) = S_d(\xi) = S_{\bar{d}}(\xi) = \frac{1}{4+2\lambda_s} S(\xi),$$
$$S_s(\xi) = S_{\bar{s}}(\xi) = \frac{\lambda_s}{4+2\lambda_s} S(\xi). \quad (19)$$

Since the total probability of the excitation of a $c\bar{c}$ pair in a hadron is unknown, we assumed normalization to unity. The final result can be obtained via multiplication by the factor N_c to be extracted from experimental data. In the sections that follow, the model is compared with experimental data in order to evaluate the free parameters N_c and g.

A comment on the excitation of states featuring beauty quarks is in order here. If we consider b quarks within this approach, we again obtain expressions (15) and (18), neglecting the charmed-quark mass against the much larger mass of the beauty quark. In this case, charmed quarks must be treated as massless partons of the sea.

This model can also be applied to the excitation of the heavy flavors in the virtual photon ("resolved photon") in e^+e^- annihilation or in photoproduction. In order to obtain the required distributions, it is sufficient to omit the term $[\rho_V(\nu)]^N$ in (10) because the photon does not obviously contain valence quarks.

3. COMPARISON OF THE MODEL WITH J/ψ HADROPRODUCTION

It was noted in the Introduction that there exist a number of hadronization mechanisms that describe more or less successfully the inclusive open-charm yield at large x_F. These schemes incorporate some aspects of the hadronization process, but there is no commonly accepted mechanism that is based on a well-founded theoretical approach and which describes the entire body of available data. The uncertainties in the existing hadronization models are too large to perform a direct evaluation of the parameters of the model for the charm-quark distribution presented here from the experimental data on open-charm production.

On the other hand, the data from NA3 collaboration [7] on the production of J/ψ particles in hadron–platinum collisions suggest an unusual production mechanism. Badier *et al.* [7] identified two different components in the x_F distribution of J/ψ mesons: a hard component with the usual A dependence $\sigma_A \sim A\sigma_N$ and a diffractive component with a weaker A dependence—namely, $\sigma_A \sim A^{0.77}\sigma_N$ for incident pions and $\sigma_A \sim A^{0.71}\sigma_N$ for incident protons. The relative contributions of the diffractive component are about 0.20 and 0.30 for pion and proton projectiles, respectively. The hard component, as was shown in [7], can be described well by the conventional QCD parton–parton fusion mechanism. The linear A dependence agrees well with the predictions of the QCD factorization theorem valid for hard processes.

The unusual A dependence of the diffractive component can naturally be described within the intrinsic-charm model [12] and within the model [6] based on the Gribov approach to particle interactions with nuclei. It can be shown in [6] that, for J/ψ production at NA3 energies, $p_{lab} \approx 150$–300 GeV, a deviation from the A^1 behavior for inclusive spectra is present only for those components of the initial partonic configuration

that contain a heavy state. Therefore, we can attribute the diffractive component in J/ψ distribution, as is seen in the NA3 experiment, to the interaction of the hadronic Fock state containing a $c\bar{c}$ pair and use these data to evaluate the parameters of our model.

In order to estimate the longitudinal distribution of J/ψ particles, we use the recombination model [17]. In this model, the differential cross section for J/ψ production can be written as

$$\frac{d\sigma}{dx_F} = \sigma_{tot}\int d\xi_1 d\xi_2 S_{c\bar{c}}(\xi_c, \xi_{\bar{c}}) R(\xi_c, \xi_{\bar{c}}; x_F), \qquad (20)$$

where $S_{c\bar{c}}(\xi_c, \xi_{\bar{c}})$ is the two-particle distribution of c and $\bar{c}$ quarks with momentum fractions x_c and $x_{\bar{c}}$, respectively, while $R(\xi_c, \xi_{\bar{c}}; x_F)$ is the recombination function describing the probability for two quarks to coalesce in the final J/ψ meson with a momentum fraction x_F. In the simplest case, we have

$$R(\xi_c, \xi_{\bar{c}}; x_F) = \delta(x_F - \xi_c - \xi_{\bar{c}}),$$

which ensures longitudinal-momentum conservation. For charmed particles, the primordial transverse momenta of the initial c quarks can in principle reach large values (in excess of 1 GeV), so that they must be taken into account (see, for example, [4]). This is not important, however, for the purposes of the present paper. Since we consider only longitudinal distributions, integration over transverse momenta is included in the total normalization of the experimental data. As a result, the following expression is obtained from (18) and (20) for the x_F distribution of J/ψ particles:

$$\frac{d\sigma(J/\psi)}{dx_F} = \sigma_{tot}^{expt}\frac{Z_N}{Z_N^{(c)}}\frac{[\Gamma(\beta+1)]}{\Gamma(2\beta+2)} \times x_F^{2\beta-1}(1-x_F)^{\alpha N+g-1}. \qquad (21)$$

For a fit, we used only πN data from [7], assuming that the number of valence quarks is $N = 2$. We do not use $pp \longrightarrow J/\psi$ data because we actually do not know the probability for the $c\bar{c}$ pair to form a J/ψ meson. This probability can be different for incoming π mesons and protons. Therefore, expression (21) has two free parameters, the total normalization and the parameter g characterizing the level of sea partons in the π meson. The fit yielded

$$g = 1.35 \pm 0.09, \qquad (22)$$

with χ^2/NDF being approximately equal 0.9. It should be borne in mind that the parameters α and β have been fixed at $\alpha = 0.5$ and $\beta = 1$. The results are shown in Figs. 1*a*–1*d*.

In order to rescale the predictions of our model to the NA3 data on $pA \longrightarrow J/\psi$, we must set $N = 3$ in (21) and replace the normalization σ_{tot}^{expt} found for pion data by $W_{p\pi}\sigma_{tot}^{expt}$, where $W_{p\pi} = \sigma_{tot}(pp \longrightarrow J/\psi)/\sigma_{tot}(\pi p \longrightarrow J/\psi)$. To estimate the ratio $W_{p\pi}$, we neglect any dynamical effects and use a combinatorial consideration based on the following simple assumptions. We consider only fast quarks—that is, the valence and c quarks of the beam particle. Each massless quark has two spin states and three color states (we neglect masses for fast c quarks). In order to form a color-singlet, spin-1 final J/ψ meson, we must take c and $\bar{c}$ quarks with parallel spins in the color-singlet state. It is clear that the probability of choosing at random a $c\bar{c}$ pair with the necessary quantum numbers is given by the binomial coefficients C_2^n, where n is the total number of states in the beam particle. The statistical weight of the final state takes the same value for both beam particles and cancels in the ratio. In the π mesons, we have four fast quarks ($u\bar{d}c\bar{c}$) and, consequently, $n_\pi = 3 \times 2 \times 4 = 24$ states. In the proton, we have five fast quarks ($uudc\bar{c}$) and $n_p = 3 \times 2 \times 5 = 30$ states. Thus, we arrive at $W_{p\pi} = C_2^{24}/C_2^{30} = 92/145$, in good agreement with data.

In Fig. 1*e*, we plotted the resulting distribution $d\sigma/dx_F(J/\psi)$ for pp interactions. We can see from Fig. 1*e* that the model provides a satisfactory description for J/ψ production in pp collisions as well. This allows us to use the same parameter g for the analysis of EMC data on charm production in muon–proton scattering.

There are some irregularities in J/ψ distributions in Figs. 1*a*–1*c* around $x_F \approx 0.8$–0.9. By way of example, we indicate that, in Fig. 1*c*, the point at $x_F \approx 0.85$ is about one order of magnitude higher than the theoretical curve. If this is not a statistical fluctuation in data, this discrepancy can be easily understood within the model developed in [6], which predicts that, for very large A and $x_F \longrightarrow 1$, the production cross section can have an $A^{1/3}$ dependence if there is final-state interaction between the product J/ψ particle and nuclear matter. In this case, we would obtain an additional factor of $195^{1/3} \approx 5.8$, in good agreement with Fig. 1*c*.

In Fig. 1*f*, we also present the distributions $xq(x)$ for charmed and valence quarks in the model and the distribution of the valence u quark from the MRS(G) parametrization.

4. CHARM ELECTROPRODUCTION

4.1. IC Structure Function and Subleading Corrections

The cross section for charm production in deep-inelastic muon–proton scattering is given by

$$\frac{d\sigma}{dxdQ^2} \approx \frac{2\pi\alpha^2[1+(1-y)^2]}{xQ^4}F_2^{(c)}(x, Q^2), \qquad (23)$$

where $x = Q^2/2(Pq)$ is the Bjorken variable and $y = Q^2/sx$ is the muon-momentum fraction carried by the

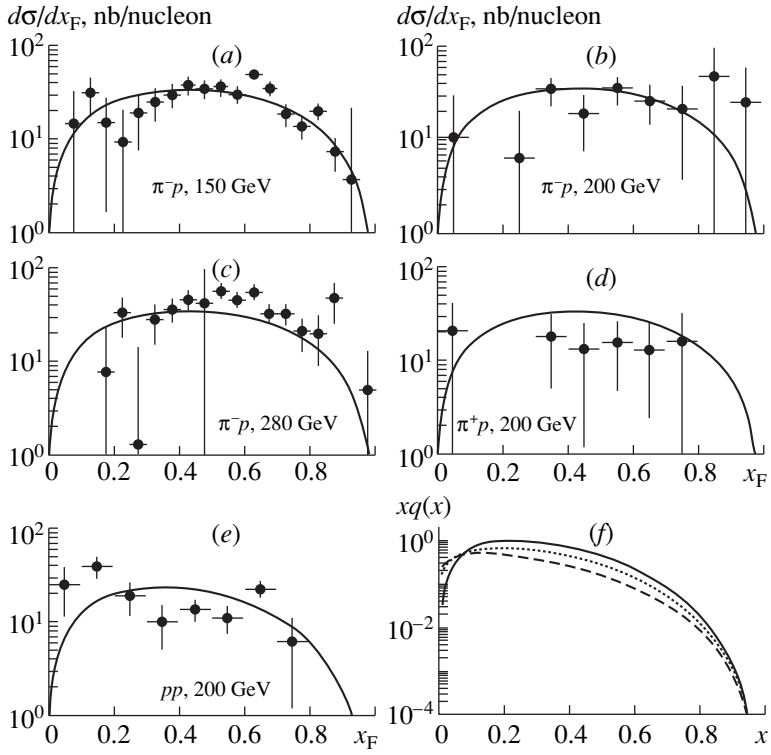

Fig. 1. (*a*–*e*) Results of a fit to the NA3 data on J/ψ production in πp and pp interactions using the model described in the main body of the text. The fit was performed only for πN collisions. (*f*) $xq(x)$ distributions in the proton of the (solid curve) c and (dashed curve) valence u quarks in the model and (dotted curve) MRS(G) parametrization for valence u quarks.

virtual photon (we neglected the contribution from the longitudinal structure function F_L).

In the approach developed here, the charm structure function of the proton can be represented as the sum of two terms; that is,

$$F_2^{(c)}(x, Q^2) = F_2^{(\mathrm{PGF})}(x, Q^2) + N_c F_2^{(\mathrm{IC})}(x, Q^2), \quad (24)$$

where N_c is an unknown normalization constant to be found from a comparison with experimental data. The first term in (24) describes the conventional photon–gluon fusion $\mu g \longrightarrow \mu c\bar{c}$ (Fig. 2*a*), while the second term represents the direct scattering of the muon on the constituent charmed quark of the proton, $\mu + c \longrightarrow \mu + c$ (Fig. 2*b*).

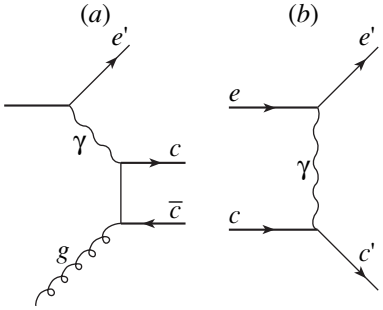

Fig. 2. Diagrams for (*a*) photon–gluon fusion and (*b*) scattering on the intrinsic charmed quark.

Within the naive parton model, the IC structure function is related to the momentum distribution $c(x, Q^2)$ of the charmed quark in the proton as

$$F_2^{(\mathrm{IC})}(x, Q^2) = 2e_c^2 x c(x, Q^2), \quad (25)$$

where $e_c = 2/3$ is the electric charge of the c quark.

The PGF charm structure function is given by [18]

$$F_2^{(\mathrm{PGF})}(x, Q^2) = \int_{\sqrt{1+4\lambda x}}^{1} \frac{d\xi}{\xi} G(\xi, Q^2) f_2\left(\frac{x}{\xi}, Q^2\right), \quad (26)$$

where

$$f_2(z, Q^2) = \frac{\alpha_s(\hat{s})}{\pi} e_c^2 \pi z$$

$$\times \left\{ V_c \left[-\frac{1}{2} + 2z(1-z)(2-\lambda) \right] \right. \quad (27)$$

$$\left. + [1 - 2z(1-z) + 4\lambda z(1-3z) - 8\lambda^2 z^2] \ln \frac{1+V_c}{1-V_c} \right\}.$$

In the above expressions, $\hat{s} = Q^2(1 - z)/z$, while $V_c(\hat{s}) = \sqrt{1 - 4m_c^2/\hat{s}}$ is the c-quark velocity in the (γg) c.m. system.

In order to compare the model with the experimental data, we must take into account the dependence of $c(x)$ on the momentum transfer squared Q^2. This dependence originates from two sources [19]. The first is associated with the nonzero masses of the proton and the c quark. The second source is represented by the first-order QCD radiative corrections (Fig. 3).

To take into account effects of the nonzero masses, we replaced the variable x by the variable ζ [19, 20],

$$x \longrightarrow \zeta(x) = \frac{\sqrt{1 + 4\lambda} + 1}{1 + \sqrt{1 + 4\rho x^2}} x, \tag{28}$$

and, for the distribution $c(x)$, used the substitution

$$c(x) \longrightarrow c(\zeta, \hat{\zeta}) = c\left(\frac{\zeta}{\hat{\zeta}}\right), \quad 0 \le \zeta \le \hat{\zeta}. \tag{29}$$

The parameters ρ, $\hat{x}$, λ, and $\hat{\zeta}$ are then given by

$$\begin{gathered} \rho = \frac{m_p^2}{Q^2}, \quad \lambda = \frac{m_c^2}{Q^2}, \\ x_{\max} = \frac{1}{1 + 4\lambda - \rho}, \quad \hat{\zeta} = \zeta(x_{\max}). \end{gathered} \tag{30}$$

The first-order correction to the structure function $F_2^{(c,0)}(x, Q^2)$ can be represented as a convolution of the c-quark distribution $c(\zeta, \hat{\zeta})$ with the radiative corrections. As a result, the IC structure function, including the radiative corrections, has the form [19]

$$\begin{aligned} F_2^{(c)}(x, Q^2) &= 2e_c^2 \zeta c(\zeta, \hat{\zeta}) \\ &+ 2e_c^2 \zeta \int_\zeta^{\hat{\zeta}} \frac{dy}{y} c(y, \hat{\zeta}) \sigma_2^{(1)}\left(\frac{\zeta}{y}, \lambda\right). \end{aligned} \tag{31}$$

The expression for the first-order radiative corrections $\sigma_2^{(1)}(z, \lambda)$ is given in the Appendix.

In this paper, we do not consider the QCD evolution of the charmed-constituent-quark distributions and assume that the QCD radiative corrections to the matrix element of virtual-photon absorption give a correct description of $\alpha_s^{(1)}$ effects. At large Q^2, this point requires a more careful study. There is also the problem of correctly describing the QCD evolution of the heavy-quark distributions for intermediate momentum transfers, where the mass of the heavy partons cannot be neglected.

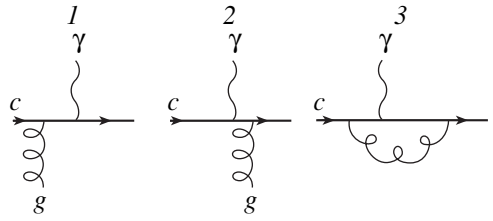

Fig. 3. $O(\alpha_s)$ corrections to the intrinsic-charm structure function: (*1*, *2*) gluon bremsstrahlung and (*3*) virtual gluon corrections.

4.2. Comparison with EMC Data

In order to evaluate the contribution to the charm part $F_2^{(c)}$ of the proton structure function F_2 from scattering on charmed constituent quarks (also called intrinsic-charm quarks), we used the data on charm production that were obtained by the EMC collaboration [1] in μp collisions at $E_\mu = 200$ GeV. The EMC collaboration presented data on $\sigma(\gamma^* p \longrightarrow c\bar{c} + X)$. Thus, it is necessary to extract $F_2^{(c)}(x, Q^2)$ from the data by taking into account both the difference in the definitions used for the virtual-photon flux in (23) and in the EMC study [21] and the finite size of the experimental bins in (x, Q^2) plane.

According to the equivalent-photon approximation (EPA) [22], the cross section for muon–proton scattering can be represented as

$$d\sigma(\mu p \longrightarrow c\bar{c}X) = \sigma(\gamma^* p \longrightarrow c\bar{c}X) dn_\gamma, \tag{32}$$

where dn_γ is the differential flux of equivalent photons. The definition of the equivalent-photon flux is arbitrary to some extent. The conventional expression used in (23) for $Q^2/E^2 \ll 1$ has the form

$$dn_\gamma = \frac{\alpha}{2\pi}[1 + (1 - y)^2]\frac{dx}{x}\frac{dQ^2}{Q^2}. \tag{33}$$

The EMC collaboration employed a slightly different definition for the photon flux [21]; it includes the additional factor $(1 - x)$ on the right-hand side of (33). Taking into account this factor and approximating the differential flux $dn_\gamma/dxdQ^2$ by $\Delta n/\Delta x \Delta Q^2$ [where $(\Delta\nu, \Delta Q^2)$ is the experimental-bin size], we can relate the structure function to the experimentally measured γp cross section $\sigma_{\gamma p}^{\text{expt}}$ for charm production as

$$\begin{aligned} F_2^{(c)}(x, Q^2) &= \frac{\Delta n_y}{\Delta\nu Q^2} \\ &\times \frac{\nu Q^4}{4\pi\alpha[1 + (1 - y)^2]} \sigma_{\gamma p}^{\text{expt}}(\nu, Q^2). \end{aligned} \tag{34}$$

The value of Δn_γ is found by integrating the expression for the photon flux over each experimental bin

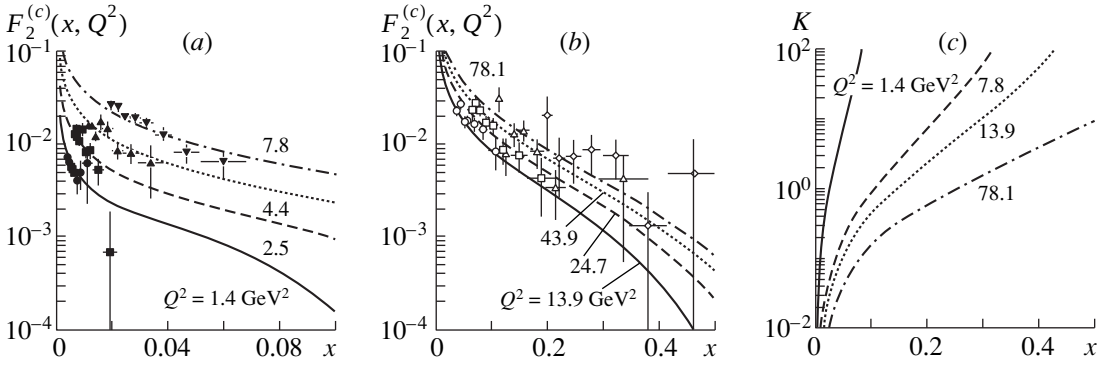

Fig. 4. (*a*, *b*) Results of the fit of the PGF + IC sum to the EMC data at Q^2 = (closed circles) 1.4, (closed boxes) 2.5, (closed triangles) 4.4, and (inverted closed triangles) 7.8 GeV^2 in Fig. 4*a* and Q^2 = (open circles) 13.9, (open boxes) 24.7, (open triangles) 43.9, and (open diamonds) 78.1 GeV^2 in Fig. 4*b*; (*c*) ratio $K = F_2^{(\mathrm{IC})}/F_2^{(\mathrm{PGF})}$ of the contributions from intrinsic charm and photon–gluon fusion.

$(\Delta\nu, \Delta Q^2)$. Defining $\Delta\nu = \nu_2 - \nu_1$ and $\Delta Q^2 = Q_1^2 - Q_2^2$, we obtain

$$\Delta n_\gamma(\nu, Q^2) = \frac{\alpha}{2\pi}\left\{\ln\left(\frac{Q_2^2}{Q_1^2}\right)\right.$$

$$\times\left[2\ln\frac{\nu_2}{\nu_1} - \frac{2}{E}(\nu_2 - \nu_1) + \frac{\nu_2^2 - \nu_1^2}{2E^2}\right] \qquad (35)$$

$$\left. - \frac{Q_2^2 - Q_1^2}{s}\left[2E\left(\frac{1}{\nu_1} - \frac{1}{\nu_2}\right) - 2\ln\frac{\nu_2}{\nu_1} + \frac{\nu_2 - \nu_1}{E}\right]\right\}.$$

The mass corrections for IC structure functions were used in the form of ζ scaling (29). The radiative corrections (see Appendix) were also taken into account. The strong-coupling constant $\alpha_s(Q^2)$ and the QCD scale Λ_{QCD} were chosen according to the PDFLIB parametrization [23].

To perform a fit to the EMC data, we used expression (24) for the charmed structure function with two free parameters: N_c, the normalization of $F_2^{(\mathrm{IC})}$, and m_c, the charmed-quark mass, which enters into the PGF structure function and both the radiative and the mass corrections. For the gluon distribution, we took the MRS(G) parametrization, which is the default one for PDFLIB 7.09 [23].

The results of our fit to the EMC data are shown in Figs. 4*a* and 4*b*. The fit yields

$$N_c = (0.9 \pm 0.2)\%$$

for the admixture from scattering on the charmed constituent quark and

$$m_c = 1.43 \pm 0.01 \text{ GeV}$$

for the charmed-quark mass. We have also used other PDFLIB parametrizations and, within the errors, obtained similar values.

Figure 4*c* presents the ratio $F_2^{(\mathrm{IC})}/F_2^{(\mathrm{PGF})}$ versus x for some values of Q^2. We see that, at large x ($x > 0.1$), a 1% IC component dominates charm production for $Q^2 \lesssim 10$–12 GeV^2.

5. CONCLUSION

We have modified and generalized the statistical approach to the Fock state hadron structure with heavy quarks, using the framework of noncovariant perturbation theory. We have obtained scaling expressions for heavy- and light-parton distributions in the infinite-momentum frame. We have calculated the charmed structure function of the proton, $F_2^{(c)}(x, Q^2)$, taking into account the QCD radiative corrections of order $\alpha_s^{(1)}$, as well as the mass corrections to the structure function that are caused by the nonzero masses of the c quark and of the proton. We have used the experimental data on $\pi A \longrightarrow J/\psi X$ and $\mu p \longrightarrow \mu c\bar{c} X$ to evaluate the parameters of the model and presented the relative contributions of the photon–gluon fusion mechanism and of direct scattering on the charmed constituent quark (intrinsic charm) to the charmed structure function of the proton.

We have found that, in πA collisions, the so-called diffractive component of J/ψ can be well described by the coalescence of c and $\bar{c}$ constituent quarks. This success supports, in my opinion, Gribov's spacetime picture of hadron interaction with nuclei, as well as the presence of long-lived heavy-quark fluctuations in hadrons (intrinsic charm). The results also show that the longitudinal distribution of the constituent heavy quarks is harder than that for light sea partons and has a shape like that of the valence-quark distributions.

From a comparison with charm production by muons at $E_\mu = 200$ GeV, we have estimated the contribution from scattering on charmed constituent quarks to total charm production. This contribution is about 1% and is expected to grow with increasing beam energy. At large values of the Bjorken variable, $x \gtrsim 0.1$, scattering on the charmed constituent quark dominates forward charm production in deep-inelastic lepton–proton collisions.

The approach adopted here to consider the excitation of Fock states containing heavy quarks can also be applied to states featuring beauty quarks in hadrons, as well as to the hadronic component of the virtual photon (resolved photon).

Finally, we want to emphasize that the HERA *ep* collider is well suited to investigating heavy-flavor production mechanisms over a wide kinematical region of (x, Q^2) that is inaccessible at other existing facilities.

ACKNOWLEDGMENTS

I am indebted to Prof. G. Wolf for illuminating discussions and exceptionally useful remarks. I am grateful to Dr. B. Harris for mutual a cross-check of the codes for calculating radiative corrections.

This work was supported in part by DESY.

APPENDIX

The expression for the first-order radiative corrections $\sigma_2^{(1)}(z, \lambda)$ to the charmed structure function has the form

$$\sigma_2^{(1)}(z,\lambda) = \frac{2\alpha_s}{3\pi}\delta(1-z)\left\{4\ln\lambda - 2 + \sqrt{1+4\lambda}L\right.$$
$$+\frac{1+2\lambda}{\sqrt{1+4\lambda}}\left[3L^2 + 4L + 4\mathrm{Li}_2\left(\frac{-d}{a}\right)\right.$$
$$\left.\left.+2L\ln\lambda - 4L\ln(1+4\lambda) + 2\mathrm{Li}_2\left(\frac{d^2}{a^2}\right)\right]\right\}$$
$$+\frac{\alpha_s}{3\pi}\frac{1}{(1+4\lambda z^2)^2}\left\{\frac{1}{[1-(1-\lambda)z]^2}\right.$$
$$\times[(1-z)(1-2z-6z^2+8z^4)$$
$$+6\lambda z(1-z)(3-15z-2z^2+8z^3)$$
$$+4\lambda^2z^2(8-77z+65z^2-2z^3)$$
$$+16\lambda^3z^3(1-21z+12z^2)-128\lambda^4z^5]$$
$$-\frac{2\hat{L}}{\sqrt{1+4\lambda z^2}}[(1+z)(1+2z^2)$$
$$-2\lambda z(2-11z-11z^2)-8\lambda^2z^2(1-9z)]$$
$$\left.-\frac{8z^4(1+\lambda)^2}{(1-z)_+}-\frac{4z^4(1+2\lambda)(1+4\lambda)^2\hat{L}}{\sqrt{1+4\lambda z^2}(1-z)_+}\right\}, \quad \text{(A.1)}$$

where

$$\hat{L} = \ln\frac{4\lambda z[1-(1-\lambda)z]}{(1+2\lambda z+\sqrt{1+4\lambda z^2})^2},$$
$$a = \frac{\sqrt{1+4\lambda}+1}{2}, \quad d = a-1, \quad \text{(A.2)}$$
$$L = \ln\frac{a}{d}, \quad \mathrm{Li}_2 = -\int_0^x dz\frac{\ln(1-z)}{z}.$$

REFERENCES

1. European Muon Collab. (J. J. Aubert *et al.*), Phys. Lett. B **110**, 73 (1982); Nucl. Phys. B **213**, 31 (1983).
2. ZEUS Collab., *XXIX International Conference on High Energy Physics (ICHEP'98), Vancouver, 1998*.
3. V. G. Kartvelishvili, A. K. Likhoded, and S. R. Slabospitsky, Yad. Fiz. **33**, 832 (1981) [Sov. J. Nucl. Phys. **33**, 434 (1981)]; A. K. Likhoded, S. R. Slabospitsky, and M. V. Suslov, Yad. Fiz. **38**, 727 (1983) [Sov. J. Nucl. Phys. **38**, 433 (1983)].
4. Yu. A. Golubkov, R. V. Konoplich, and Yu. P. Nikitin, Preprint No. 245 (Rome, 1981); Yad. Fiz. **35**, 417 (1982) [Sov. J. Nucl. Phys. **35**, 239 (1982)]; Yu. A. Golubkov, A. V. Zhilin, and Yu. P. Nikitin, Yad. Fiz. **48**, 1104 (1988) [Sov. J. Nucl. Phys. **48**, 702 (1988)].
5. T. Sjøstrand, Comput. Phys. Commun. **82**, 74 (1994).
6. K. Boreskov, A. Capella, A. Kaidalov, *et al.*, Phys. Rev. D **47**, 919 (1993); A. B. Kaidalov, in *Proceedings of the 138th WE-Heraeus Seminar*, Ed. by J. G. Körner and P. Kroll (World Sci., Singapore, 1994), p. 171.
7. J. Badier *et al.*, Z. Phys. C **20**, 101 (1983).
8. R. Vogt, S. J. Brodsky, and P. Hoyer, Nucl. Phys. B **360**, 67 (1991).
9. F. I. Olness and W.-K. Tung, Nucl. Phys. B **308**, 813 (1988).
10. M. A. G. Aivazis, F. I. Olness, and W.-K. Tung, Phys. Rev. D **50**, 3085 (1994); M. A. G. Aivazis, J. C. Collins, F. I. Olness, *et al.*, Phys. Rev. D **50**, 3102 (1994).
11. F. I. Olness and S. T. Riemersma, Phys. Rev. D **51**, 4746 (1995).
12. S. J. Brodsky, P. Hoyer, C. Peterson, *et al.*, Phys. Lett. B **93**, 451 (1980); S. J. Brodsky and C. Peterson, Phys. Rev. D **23**, 2745 (1981).
13. J. Kuti and V. F. Weisskopf, Phys. Rev. D **4**, 3418 (1971).
14. Yu. A. Golubkov, Preprint No. 96-30/437 INP MSU (Institute of Nuclear Physics, Moscow State University, 1996); hep-ph/9609492.

15. L. D. Landau and E. M. Lifshitz, *Quantum Mechanics: Non-Relativistic Theory* (Russ. original 4th ed., Nauka, Moscow, 1989; 3rd ed., Pergamon, Oxford, 1977).
16. E. Takasugi and X. Tata, Preprint No. 3992-378 (Univ. Texas, ORO, 1979); E. Takasugi, X. Tata, C. B. Chiu, *et al*., Phys. Rev. D **20**, 211 (1979).
17. K. P. Das and R. C. Hwa, Phys. Lett. B **68**, 459 (1977).
18. M. Glück, in *Proceedings of the HERA Workshop, Hamburg, 1987*, Ed. by R. D. Peccei, p. 119.
19. E. Hoffmann and R. Moore, Z. Phys. C **20**, 71 (1983).
20. R. Barbieri, J. Ellis, M. K. Gaillard, *et al*., Nucl. Phys. B **117**, 50 (1976).
21. L. N. Hand, Phys. Rev. **129**, 1834 (1963).
22. P. Kessler, Acta Phys. Austriaca **41**, 141 (1975); V. M. Budnev *et al*., Phys. Rep. **15**, 181 (1975).
23. H. Plothow-Besh, *PDFLIB version 7.09*, 1997.

Physics of Atomic Nuclei, Vol. 63, No. 4, 2000, pp. 617–622. Translated from Yadernaya Fizika, Vol. 63, No. 4, 2000, pp. 683–688.

ELEMENTARY PARTICLES AND FIELDS
Theory

Representation of the Propagator of a Massive Spinning Particle as a BFV–BRST Path Integral

V. G. Zima* and S. A. Fedoruk[1), **]

Kharkov State University, pl. Svobody 4, Kharkov, 310077 Ukraine

Received October 2, 1998; in final form, August 2, 1999

Abstract—In the index-spinor approach, the transition amplitude for a free massive particle of arbitrary spin is obtained by calculating the relevant path integral in the BFV–BRST formalism. The calculation is performed without any renormalization of the measure in the path integral. The result coincides with the Weinberg propagator in the index-free representation. It is shown that the type of representation for the particle spin—a holomorphic or an antiholomorphic one—is determined by the choice of boundary conditions for the index spinor. *© 2000 MAIK "Nauka/Interperiodica".*

A spin can be described by either commuting or anticommuting variables, which can be used independently or on equal terms within supersymmetric theories. Boson, as well as fermion, variables can be adequately included in spin theory in the form of spinors. In this case, there exists a nontrivial "classical limit" of the spin; hence, all what is needed for quantization is to pinpoint ordering constants. Until recently, spinors involving boson variables have been used quite rarely in spin theory, primarily as twistor-type variables for resolving the mass constraint in the massless case. There are, however, other fields of application for such variables. By way of example, we indicate that, in a theory featuring index spinors [1], there is, at least at the classical level, an elementary solution to the problem of an infinite reducibility of fermion κ symmetry. This suggests the existence of subtler geometric and group-theoretical aspects.

In dealing with massive spinning particles, the quantization procedure combining Batalin–Fradkin–Vilkovisky and Becchi–Rouet–Stora–Tyutin approaches (BFV–BRST quantization [2]) has attracted little attention. In a few studies devoted to this subject [3], a consideration was restricted to making use of Grassmann vectors in the case of spin-1/2 particles. In these models, the derivation of the propagator does not amount to calculating the original path integral, requiring some additional steps associated with choosing a representation for spin operators.

In the present study, we apply the BFV–BRST quantization procedure to a massive particle of arbitrary spin in the conventional spacetime dimension. Our description of the spin in terms of index spinors [1] is readily applicable to the massless case in higher spacetime dimensions. Thus, our study here merely provides a test of the efficiency of the method.

Within modern approaches to quantization, this is the first consideration of the above type. Apart from extending our approach to higher spins, it was for the first time that full advantage was taken of the Hamiltonian formalism in similar problems, whereby it became possible to calculate the path integral without resort to an indeterminate renormalization of the functional measure. The resulting propagator coincides with that obtained previously in conventional field theory within the $(2J + 1)$-component formalism [4].

In $D4$, a spinning particle can be described in terms of commuting coordinates $(z^A) = (x^\mu, \zeta^\alpha, \bar{\zeta}^{\dot{\alpha}})$, where x is a spacetime vector and ζ is a Weyl index spinor. Within the first-order formalism, the Lagrangian for such a particle has the form

$$L = p\dot{\omega} - \frac{e}{2}(p^2 + m^2) - \lambda(\zeta\hat{p}\zeta - j), \qquad (1)$$

where $\omega \equiv \dot{\omega}\,d\tau = dx - id\zeta\sigma\zeta + i\zeta\sigma d\zeta$ is the boson superform. The kinetic term $p\dot{\omega}$ is the sum of the conventional kinetic term for a spinless particle, $p\dot{x}$ (p_μ is the auxiliary energy–momentum vector), and a spin term that takes a standard oscillator form in the rest frame. As a consequence, ω coincides with the superform of $N = 1$ SUSY, provided that the Grassmann spinor in $N = 1$ SUSY is replaced by the index spinor. It should be emphasized that this coincidence is something other than the result of some naive or straightforward generalization of the well-known expression of supersymmetric theory. In fact, it is a manifestation of a characteristic feature common to descriptions of the spin in terms of commuting and anticommuting variables—namely, the two descriptions emerge from an extension of the known representations of the small

[1)] Ukrainian Engineering Pedagogical Academy, Universitetskaya ul. 16, Kharkov, 310003 Ukraine.

* e-mail: zima@postmaster.co.uk

** e-mail: fed@postmaster.co.uk

group by, respectively, c and a numbers to the relativistic case; that is, these descriptions are associated with the respective induced representations of the Poincaré group. A transition to these induced representations naturally leads to the boson or fermion supersymmetry of the kinetic terms. Unfortunately, boson supersymmetry is broken because the boson configuration space is restricted by the spin constraint $\zeta\hat{p}\bar{\zeta} - j \approx 0$ [1]; in the relativistic form, this constraint enters into the Lagrangian in (1) with a Lagrange multiplier.

In the Lagrangian (1), the coefficients e and λ are Lagrange multipliers, while j is the classical spin, whose sign determines the sign of energy. The action functional $A = \int_{\tau_i}^{\tau_f} L\, d\tau$ is correctly defined both in the massive and in the massless case. In the present study, however, we restrict our consideration to the massive case. In the absence of the last term in the Lagrangian specified by (1), our action functional coincides with that of Casalbuoni, Brink, and Schwarz [5], provided that ζ is assumed to be a Grassmann spinor.

Upon going over to the Hamiltonian form of the theory [6], we obtain, in addition to the mass constraint $T \equiv \frac{1}{2}(p^2 + m^2) \approx 0$ and the spin constraint $\zeta\hat{p}\bar{\zeta} - j \approx 0$, which appear explicitly in the action functional, the spinor Bose constraints

$$d_\zeta \equiv ip_\zeta - \hat{p}\bar{\zeta} \approx 0, \quad \bar{d}_\zeta \equiv -i\bar{p}_\zeta - \zeta\hat{p} \approx 0. \tag{2}$$

On the constraint surface, the spin constraint is equivalent to the constraint

$$S \equiv S_\zeta - j \equiv \frac{i}{2}(\zeta p_\zeta - \bar{p}_\zeta\bar{\zeta}) - j \approx 0, \tag{3}$$

since $S \equiv \frac{1}{2}(\zeta d_\zeta + \bar{d}_\zeta\bar{\zeta}) + (\zeta\hat{p}\bar{\zeta} - j)$.

The constraint algebra was described in detail elsewhere [1]. The constraints $(F_a) = (F_1, F_2) \equiv (T, S)$ are first-class constraints, while the spinor constraints $(G_i) = (d_{\zeta\alpha}, \bar{d}_{\zeta\dot{\alpha}})$ are second-class constraints ($\hat{p}\tilde{p} = m^2 > 0$).

The mass constraint generates the conventional reparametrizations $\delta x^\mu = p^\mu\epsilon$, $\delta p_\mu = 0$, and $\delta e = \dot{\epsilon}$. The spin constraint (3) generates phase transformations of the spinor components,

$$\delta\zeta^\alpha = \frac{i}{2}\zeta^\alpha\varphi, \quad \delta p_{\zeta\alpha} = -\frac{i}{2}p_{\zeta\alpha}\varphi \text{ and c.c.}; \quad \delta\lambda = \dot{\varphi}.$$

The corresponding variation of the action functional,

$$\delta A = \frac{1}{2}(p^2 - m^2)\epsilon\big|_{\tau_i}^{\tau_f} + j\varphi\big|_{\tau_i}^{\tau_f},$$

vanishes only when $\epsilon(\tau_i) = \epsilon(\tau_f) = 0$ and $\varphi(\tau_i) = \varphi(\tau_f)$. For this reason, only those relativistic gauges featuring derivatives are admissible that express $\dot{e}$ in terms of the other quantities from this action functional [7, 8].

The constant j in Lagrangian (1) is referred to as a classical spin because, on the constraint surface, the Pauli–Lubanski vector $w = (\zeta\hat{p}\bar{\zeta})p - p^2(\zeta\sigma\bar{\zeta})$ satisfies the relation $w^2 = m^2j^2$.

To obtain the quantum spectrum of the system whose behavior is controlled by the Lagrangian in (1), we must perform operator quantization. Since the second-class constraints can be divided into two complex-conjugate groups so that all constraints within each group commute with one another, we can employ the Gupta–Bleuler procedure. According to this procedure, all first-class constraints and half of the second-class constraints chosen in such a way that they weakly commute with one another are imposed on the states involved, so that all expectation values of these constraints vanish. Of course, the above choice of second-class constraints is not unambiguous. This ambiguity does not affect the spectrum, but a specific choice determines the realization of the Hilbert space of the states. There are two essentially different options referred to as a holomorphic and an antiholomorphic representation, the respective constraints being $\bar{d}_\zeta$ and d_ζ.

In the representation diagonal in ζ, in which case $p_\zeta = -i\partial/\partial\zeta$ and $\bar{p}_\zeta = -i\partial/\partial\bar{\zeta}$, the wave function satisfying the condition $\bar{d}_\zeta\Psi = 0$ ($d_\zeta\Psi = 0$) has the form $\Psi = \exp(\mp\zeta\hat{p}\bar{\zeta})\Phi_\pm$, where the field $\Phi_\pm$ is (anti)holomorphic: $\partial\Phi_+/\partial\bar{\zeta} = 0$ ($\partial\Phi_-/\partial\zeta = 0$).

In the quantum operator $(\zeta\partial/\partial\zeta - \bar{\zeta}\partial/\partial\bar{\zeta})/2 - J$, which corresponds to the classical quantity $S_\zeta - j$, the constant J represents the classical spin j renormalized by the ordering constant. Since the wave function is single-valued, J can take only half-integer and integral values, $2J \in Z$. The spin constraint imposed on Ψ implies that the (anti)holomorphic field $\Phi_\pm$ must be homogeneous of degree $\pm 2J$ in ζ ($\bar{\zeta}$). The requirement that the wave function Ψ be bounded both at the origin of the complex plane C^2 of the index spinor ζ and at infinity implies that the function $\Phi_\pm$ is holomorphic or antiholomorphic, depending on the sign of J and the sign of energy: in the holomorphic representation, $J \geq 0$ and $p^0 \geq m$, while, in the antiholomorphic representation, $J \leq 0$ and $p^0 \leq m$. The field $\Phi_\pm$ is then a homogeneous polynomial of degree $2|J|$ in ζ ($\bar{\zeta}$)—that is, it appears to be a contraction of the conventional field carrying $2|J|$ undotted (dotted) spinorial indices with $2|J|$ spinor factors ζ ($\bar{\zeta}$). The conventional field is irreducible (symmetric in spinor indices), satisfies the Klein–Gordon equation (obeys the mass constraint T), and describes spin-$|J|$ particles (antiparticles).

Thus, the wave function naturally acquires an index-spinor dependence in our approach. This dependence is equivalent, in a sense, to equipping a conventional field

with an index associated with a finite-dimensional representation of the Lorentz group. It is precisely this circumstance that is concealed behind the term "index spinor."

It should be emphasized that our field does not transform according to any elementary representation of the $SL(2C)$ group over index (this notion was introduced in [10]); hence, it is not a polynomial in the index spinor. A field that is transformed according to an elementary representation generally corresponds an infinite-dimensional representation of the $SL(2C)$ group over index. A finite-dimensional representation may be contained in such an infinite-component field, together with an infinite-dimensional representation, provided that the homogeneity index takes an "integral" value [11], in which case the representation is reducible.

The BFV–BRST approach provides a consistent formalism for calculating the transition amplitudes for a constrained system [2]. For each first-class constraint F_a, the coordinates of the original phase space are supplemented, in this approach, with the "dynamical" Lagrange multipliers $(\lambda^a) \equiv (\lambda_T, \lambda_S)$ and the corresponding canonically conjugate momenta π_a, as well as with the ghost variables, including the ghosts C^a and the antighosts $\tilde{C}_a$, together with the quantities $\tilde{\mathcal{P}}_a$ and $\mathcal{P}^a$ canonically conjugate to the ghosts and antighosts, respectively.

Upon going over to the Dirac bracket, the algebra of the first-class constraints F_a remains Abelian, so that the rank of the BRST charge is zero:

$$\Omega = F_a C^a + \pi_a \mathcal{P}^a. \tag{4}$$

In the expression for the transition amplitude,

$$Z_\Psi = \int D[z, p_z; \lambda, \pi; C, \tilde{\mathcal{P}}; \mathcal{P}, \tilde{C}] \prod_{i,\tau} \delta(G_i) \times \prod_\tau (2\pi)^2 |\det\{G_i, G_j\}|^{1/2} \exp(iA_{\text{eff}}), \tag{5}$$

we make use of the Liouville measure for integration with respect to both Bose and Fermi variables. In terms of conventional integrals used in a finite-dimensional approximation of the path integral, this means that each product of the differentials of two canonically conjugate real-valued Bose variables in the measure is divided by 2π. In accordance with the boundary conditions being considered, the differential of each variable that has no canonically conjugate partner is also divided by 2π. The boundary conditions [see equations (7) and (9) below] are chosen in such a way that this concerns the variables p_μ and λ^a. In the Hamiltonian approach, the measure does not feature factors that correspond to the Jacobian of the transformation from the complex variables to the real ones.

In expression (5), fulfillment of the second-class constraints (2) is ensured by the functional delta function; upon going over to real-valued variables, the factors that correspond to the Jacobian of this transition do not appear in the product $\prod_i \delta(G_i)$. The measure is normalized by the determinant $\det\{G_i, G_j\} = (4p^2)^2$ of the matrix of the Poisson brackets for the real second-class constraints. For each instant of time τ, a factor of 2π must be additionally introduced in the measure for each pair of canonically conjugate real second-class Bose constraints.

In the effective Hamiltonian action

$$A_{\text{eff}} = \int_{\tau_i}^{\tau_f} (p\dot{x} + \dot{\zeta} p_\zeta + p_\zeta \dot{\bar{\zeta}} + \pi\dot{\lambda} + \tilde{\mathcal{P}}\dot{C} + \tilde{C}\dot{\mathcal{P}} - H_\Psi) d\tau + A_{\text{b.t.}} \tag{6}$$

of the theory being considered, the Hamiltonian H_Ψ is defined as the BRST derivative of a gauge fermion Ψ: $H_\Psi = \{\Omega, \Psi\}$. The transition amplitude is independent of the choice of a gauge fermion, provided that the path integral is taken along trajectories from the same coset with respect to BRST transformations. This coset is specified by an appropriate choice of gauge and boundary conditions. With $\Psi = \tilde{\mathcal{P}}_a \lambda^a$, we obtain the relativistic gauge with derivatives for the Lagrange multipliers ($\dot{\lambda}^a = 0$), in which case we have $H_\Psi = F_a\lambda^a + \tilde{\mathcal{P}}_a \mathcal{P}^a$. We do not simplify the expression for Ψ further by eliminating some terms, because this would require infinite renormalizations of the integration measure [12].

We calculate the transition amplitude by using the boundary conditions

$$x^\mu(\tau_i) = x_i^\mu, \quad x^\mu(\tau_f) = x_f^\mu; \tag{7}$$

$$\zeta^\alpha(\tau_1) = \zeta_1^\alpha, \quad \bar{\zeta}^{\dot{\alpha}}(\tau_2) = \bar{\zeta}_2^{\dot{\alpha}}, \tag{8}$$

where the labels (1, 2) on the spinors stand for (f, j) in the case of the holomorphic representation and for (i, f) in the case of the antiholomorphic representation; we also have

$$\pi_a(\tau_i) = \pi_a(\tau_f) = 0, \quad C^a(\tau_i) = C^a(\tau_f) = 0, \quad \tilde{C}_a(\tau_i) = \tilde{C}_a(\tau_f) = 0. \tag{9}$$

The boundary values of the remaining variables are not fixed. These boundary conditions are BRST-invariant and ensure that the BRST charge vanishes at the boundary. The conditions in (8) determine a covariant solution compatible with the fact that, by virtue of the second-class constraints, the quantities ζ and $\bar{\zeta}$ are canonically conjugate to each other. This solution is not unique. There are an infinitely large number of covariant boundary conditions for the index spinor. All of

these are essentially equivalent to each other, each specifying an individual realization of the Hilbert space of spin states. Here, we restrict our consideration to two basic types of (8) described in the literature [1].

For the boundary conditions (8) to be compatible with the variational principle, we must introduce the boundary term [8]

$$A_{\text{b.t.}} = \frac{-\varepsilon_\zeta}{2}(\zeta_i p_{\zeta i} + \zeta_f p_{\zeta f} - \bar{p}_{\zeta i}\bar{\zeta}_i - \bar{p}_{\zeta f}\bar{\zeta}_f), \qquad (10)$$

where the values of $\varepsilon_\zeta = +1$ and -1 correspond to the holomorphic and the antiholomorphic representation, respectively.

In the gauge under consideration, the path integral (5) factorizes to become

$$Z_\Psi = ZZ_{\text{gh}}. \qquad (11)$$

The integral with respect to the ghost variables, Z_{gh}, has a simple Gaussian form. We break down the interval of variation of the evolution parameter τ into N equal parts, setting $T_\tau = \tau_f - \tau_i$ and $\Delta\tau = T_\tau/N$. By induction, it can easily be proven that, prior to evaluating the limit of the expression for Z_{gh}, it is independent of N. For zero boundary values of C and $\tilde{C}$ (8), we obtain $Z_{\text{gh}} = -T_\tau^2$.

Integration with respect to π_a yields the delta function $\delta(\dot{\lambda}^a)$, so that the expression for Z_Ψ involves only conventional integrals over zero modes of λ^a. Below, the domain of integration with respect to these variables is determined more precisely, which plays a key role.

Integration with respect to x leads to the delta function $\delta(\dot{p})$; therefore, the path integral with respect to p in (11) reduces to the standard integral over the zero modes, with the integral $\int p\dot{x}\,d\tau$ in the exponent of the exponential function in the integrand being replaced by the expression $ip(x_f - x_i)$.

The second-class constraints (2) are resolved for the spinor momenta p_ζ and $\bar{p}_\zeta$. This makes it possible to perform integration with respect to these variables by using the functional delta functions in the expression for the measure.

The remaining integral with respect to the index spinor factorizes to become

$$Z_\zeta = \int\prod_\tau d^2\zeta d^2\bar{\zeta}|p^2| \times \exp\left\{i\int_{\tau_i}^{\tau_f}(-i\dot{\zeta}\hat{p}\bar{\zeta} + i\zeta\hat{p}\dot{\bar{\zeta}} - \lambda_S\zeta\hat{p}\bar{\zeta})d\tau + i\tilde{A}_{\text{b.t.}}\right\}, \qquad (12)$$

where $\tilde{A}_{\text{b.t.}} = -i\varepsilon_\zeta(\zeta_i\hat{p}\,\bar{\zeta}_i + \zeta_f\hat{p}\,\bar{\zeta}_f)$. The exponential factor in the expression resulting from the evaluation of the Gaussian integral (12) can be found by the saddle-point method. The equations of motion for ζ and $\bar{\zeta}$ have the form $2i\dot{\zeta}\,\hat{p} + \lambda_S\zeta\hat{p} = 0$ and c.c.; therefore, a nontrivial contribution to the ultimate result comes only from the boundary term $\tilde{A}_{\text{b.t.}}$. The equations of motion can readily be solved. Taking into account equation (8) and the relations $\zeta\hat{p} = e^{\frac{i}{2}\lambda_S(\tau-\tau_1)}\zeta_1\hat{p}$ and $\hat{p}\,\bar{\zeta} = e^{-\frac{i}{2}\lambda_S(\tau-\tau_2)}\hat{p}\,\bar{\zeta}_2$, we obtain

$$Z_\zeta = \exp\{2\varepsilon_\zeta\zeta_1\hat{p}\bar{\zeta}_2 e^{-i\varepsilon_\zeta\lambda_S T_\tau/2}\}. \qquad (13)$$

The preexponential factor in (13) is equal to unity; it can be evaluated as follows. We break the range of the evolution parameter τ into small segments and then determine the integral in (12) as the limit $Z_\zeta = \lim_{N\to\infty} Z_\zeta[\zeta_1,\ \bar{\zeta}_2;\ T_\tau,\ N]$. It is straightforward to derive the relation

$$Z_\zeta[\zeta_1, \bar{\zeta}_2; T_\tau, N] = \left[1 + \left(\frac{\varepsilon_\zeta\lambda_S T_\tau}{2N}\right)^2\right]^{-N} \times \exp\left\{2\varepsilon_\zeta\zeta_1\hat{p}\bar{\zeta}_2\left(1 + i\varepsilon_\zeta\lambda_S\frac{T_\tau}{2N}\right)^{-N}\right\},$$

which goes over to (13) in the limit $N \longrightarrow \infty$.

Now, all functional integrations have been performed and the expression for Z_Ψ takes the form

$$Z_\Psi = -T_\tau^2\int\frac{d^2p}{(2\pi)^4}e^{ip(x_f-x_i)}\frac{d\lambda_T d\lambda_S}{(2\pi)^2} \times \exp\left\{-i\frac{T}{2}\lambda_T(p^2 + m^2) + i\lambda_S T_\tau J\right\}Z_\zeta. \qquad (14)$$

The appearance of the quantum spin J in this formula means that the classical spin j from formula (1) can be redefined by using the ordering constant that arises in going over from classical theory to the corresponding quantum theory.

The orbits of the gauge group are characterized by the Teichmüller parameters

$$C_T = \frac{1}{2}\int_{\tau_i}^{\tau_f}\lambda_T(\tau)d\tau,\ \ C_S = \frac{1}{2}\int_{\tau_i}^{\tau_f}\lambda_S(\tau)d\tau, \qquad (15)$$

where C_T is the proper time [7]. In the theory under consideration, the quantities C_S arise from the classical description of the intrinsic quantum numbers (spin,

charge, etc.) in terms of the topological characteristics of paths on a torus.

If the parameters of gauge transformations satisfy the boundary conditions, the quantities C_T and C_S are invariant under such transformations because $\delta\lambda_T = \dot{\epsilon}$ and $\delta\lambda_S = \dot{\varphi}$. The fact that the gauge $\dot{\lambda}_T = \dot{\lambda}_S = 0$ is admissible implies that there is one-to-one correspondence between the orbits and the zero modes of the Lagrange multipliers. For the latter, we have

$$C_T = \lambda_T \times T_\tau/2, \quad C_S = \lambda_S \times T_\tau/2. \tag{16}$$

Only those reparametrizations are admissible that correspond to monotonic functions [7]. Therefore, the reparametrization group is broken down into two connected components: the subgroup conserving orientation of the world line and the set of reparametrizations changing orientation. The corresponding modular group is $\mathscr{L}_2$. BFV–BRST quantization involves only those gauge transformations that are continuously connected with the identical transformation. For this reason, integration must be performed over the fundamental domain of the modular group in the Teichmüller space. If the fundamental domain for the parameter C_T is defined as that where $C_T > 0$, positive-energy particles propagate forward in time, and the transition amplitude (5) appears to be a causal propagator.

The fundamental domain of the modular group for the phase transformations of index spinors is determined by expression (14) for the amplitude. Since the integrand is a periodic function of C_S at half-integer values of J, any interval of length equal to the period (say, $[0, 2\pi]$) can be taken for the fundamental domain. The corresponding modular group is $\mathscr{L}$.

We can consider the modular invariance of the transition amplitude as the condition on the quantum theory resulting from the classical theory through the calculation of the path integral. In this case, the boundary conditions on the parameter φ are relaxed to take the form $\varphi(\tau_f) - \varphi(\tau_i) = 2\pi n$, $n \in \mathscr{L}$, in which case the requirement that the transition amplitude be a single-valued function leads to a quantization of the spin J (a similar consideration can be found in [13]).

Integration with respect to C_T in (14) can be performed by using the relation

$$\int_0^\infty dC_T \exp\{-iC_T(p^2 + m^2)\} = -i/(p^2 + m^2 - i0).$$

Thus, the above choice of the fundamental domain corresponds to a conventional prescription for the circumvention of poles in the integral representation of the causal propagator.

The integral with respect to C_S can be calculated by the Cauchy formula for the nth derivative of an analytic function of a single complex variable z.

The ultimate result for the transition amplitude,

$$Z_\Psi = \frac{-i}{(2J\varepsilon_\zeta)!}\int \frac{d^4p}{(2\pi)^4} e^{ip(x_f - x_i)} \frac{(2\varepsilon_\zeta \zeta_1 \hat{p} \bar{\zeta}_2)^{2J\varepsilon_\zeta}}{p^2 + m^2 - i0}, \tag{17}$$

is an index-free representation of the Weinberg propagator [1]. In the holomorphic case, $J \geq 0$ [1] and the particles are described by symmetric spinors carrying $(2J + 1)$ undotted indices; in the antiholomorphic case, $J \leq 0$ and the particles are described by spinors carrying dotted indices. The connection between the sign of J and the sign of energy indicates [7] that the change in the boundary conditions (8) is equivalent to the change in the definition of the particles and antiparticles.

The spin-dependent factor in the integrand on the right-hand side of (17) can be represented in the form $(2\varepsilon_\zeta \zeta_1 \hat{p}\, \bar{\zeta}_2)^{2|J|}/(2|J|)! = (2\varepsilon_\zeta \zeta_1 \hat{p}\, \bar{\zeta}_2)^{2|J|}/\Gamma(2|J| + 1)$, which is valid for all spin values. This formula can be analytically continued in J to the entire complex plane; this is important for the theory of moving Regge poles and for string theory.

Our result can be compared with the propagator from [4] as follows. The Wigner wave function $u(p, \zeta; \sigma)$ is determined by first quantization [1]. It obeys the spin constraint $(\hat{S}_\zeta - J)u = 0$ and, in the holomorphic case, the constraint $\hat{\bar{d}}_\zeta u = 0$. In the representation diagonal in the index spinor, this wave function has the form [1] $u(p, \zeta; \sigma) = e^{-\zeta \hat{p} \bar{\zeta}} [\zeta]^{J, \sigma}$, where $[\zeta]^{J, \zeta}$ is a homogeneous polynomial in ζ of degree $2J$ and σ is the spin projection.

The wave function for an arbitrary momentum p can be obtained from the wave function for the standard momentum $\mathring{p} = (m, 0)$ by transforming the index spinor as $u(p, \zeta; \sigma) = u(\mathring{p}, \zeta B_p; \sigma)$, where $B_p = B_p^+$ is the Wigner operator.

In the rest frame, we have $(\hat{M}_3 - \sigma)u(\mathring{p}, \zeta; \sigma) = 0$, where $\hat{M}_3$ is the spinor part of the third component of the angular momentum. This equation determines the degree $(J \mp \sigma)$ of the component $[\zeta]^{J,\sigma}$ of the index spinor in the expression

$$[\zeta]^{J,\sigma} = N_J \begin{pmatrix} 2J \\ J - \sigma \end{pmatrix}^{1/2} (\zeta^1)^{J-\sigma} (\zeta^2)^{J+\sigma},$$

where $\begin{pmatrix} 2J \\ J - \sigma \end{pmatrix}$ is a binomial coefficient and N_J is a normalization factor.

For functions polynomial in ζ, a conventional sesquilinear form in the space of holomorphic functions of the index spinor induces the scalar product

$$(\varphi, \psi) = N\int d^2\zeta d^2\bar{\zeta} e^{-2\zeta \hat{p} \bar{\zeta}} \bar{\varphi}\psi. \tag{18}$$

For homogeneous functions of degree J, we obtain

$$(\varphi^J, \psi^J) = \frac{2^{-(2J+2)}}{(2J)!m^{4J}}\left(\frac{\partial}{\partial\zeta}\hat{p}\frac{\partial}{\partial\bar{\zeta}}\right)^{2J}\overline{\varphi^J}\psi^J N\frac{4\pi^2}{m^2} \quad (19)$$

(see also [10], where the common factor is not fixed). The orthonormality condition $([\zeta]^{J',\sigma'}, [\zeta]^{J,\sigma}) = \delta_{J'J}\delta_{\sigma'\sigma}$ determines the norm of basic symmetric spinors. The factor N can be found from the condition requiring that N_J be equal to unity at $J = 0$.

Multiplying the integrand in (17) by $[\zeta_i]^{J,\sigma}[\bar{\zeta}_f]^{J,\sigma'}$ and integrating this product with the measure from formula (18) with respect to the initial (ζ_i) and final (ζ_f) index spinors, we obtain the Weinberg propagator

$$G^J_{\sigma'\sigma}(x) = -im^{-2J}\Pi^J_{\sigma'\sigma}(i\partial)\Delta^C(x),$$

where $\Delta^C(x) = (2\pi)^{-4}\int d^4p e^{ipx}/(p^2 + m^2 - i0)$ is the causal Green's function for the scalar field, while Π^J is determined by the formula

$$\frac{1}{(2J)!}(2\zeta_f\hat{p}\bar{\zeta}_i)^{2J} = \frac{1}{(2J)!}((\zeta_f B_p)2\hat{p}(B_p\bar{\zeta}_i))^{2J}$$

$$\equiv [\zeta_f B_p]^{J,\sigma'}\Pi^J_{\sigma'\sigma}(p)[B_p\bar{\zeta}_i]^{J,\sigma} = [\zeta_f]^{J,\sigma'}\Pi^J_{\sigma'\sigma}(p)[\bar{\zeta}_i]^{J,\sigma}.$$

The properties of Π^J are listed in [4]; it is important that $\Pi_{\sigma'\sigma}(\overset{\circ}{p}) = m^{2J}\delta_{\sigma'\sigma}$.

In comparing our propagator with that obtained in [4], we must consider that the factors π^{-1} and $2i$ reflect the difference between our and Weinberg's descriptions of the spin and the difference between the ways in which the pole factor was introduced in the integrand here and in [4].

ACKNOWLEDGMENTS

We are grateful to I.A. Bandos, D.P. Sorokin, and A.Yu. Nurmagambetov for the hospitality at the Kharkov Institute for Physics and Technology and for stimulating discussions. Thanks are also due to E.A. Ivanov and S.O. Krivonos for the hospitality extended to us at the Joint Institute for Nuclear Research (Dubna) and to A.I. Pashnev for providing us with necessary references. V.G. Zima is indebted to A.A. Kapustnikov for a discussion on κ symmetry.

REFERENCES

1. V. G. Zima and S. A. Fedoruk, Pis'ma Zh. Éksp. Teor. Fiz. **61**, 241 (1995) [JETP Lett. **61**, 251 (1995)].
2. E. S. Fradkin and G. A. Vilkovisky, Phys. Lett. B **55**, 224 (1975); I. A. Batalin and G. A. Vilkovisky, Phys. Lett. B **69**, 309 (1977); E. S. Fradkin and T. E. Fradkina, Phys. Lett. B **72**, 343 (1978); I. A. Batalin and E. S. Fradkin, in *Group Theoretical Methods in Physics: Proceedings of International Seminar, Zvenigorod* (1979), Vol. 2.
3. S. Monaghan, Phys. Lett. B **181**, 101 (1986); S. Batlle, J. Gomis, and J. Roca, Phys. Rev. D **40**, 1950 (1989).
4. S. Weinberg, Phys. Rev. **133**, 1318 (1964).
5. R. Casalbuoni, Nuovo Cimento A **35**, 377 (1976); L. Brink and J. H. Schwarz, Phys. Lett. B **100**, 310 (1981).
6. P. A. M. Dirac, *Lectures on Quantum Mechanics* (Mir, Moscow, 1968; Yeshiva University, New York, 1964).
7. C. Teitelboim, Phys. Rev. D **25**, 3159 (1982).
8. M. Henneaux, C. Teitelboim, and J. D. Vergara, Nucl. Phys. B **387**, 391 (1992).
9. W. Kalau, Int. J. Mod. Phys. A **8**, 391 (1993).
10. N. N. Bogolyubov, A. A. Logunov, A. I. Oksak, and I. T. Todorov, *General Principles of Quantum Field Theory* (Nauka, Moscow, 1987).
11. I. M. Gel'fand, M. I. Graev, and N. Ya. Vilenkin, *Integral Geometry and Representation Theory* (Fizmatgiz, Moscow, 1962; Academic, New York, 1966).
12. I. Bandos, A. Maznytsia, I. Rudychev, *et al*., Int. J. Mod. Phys. A **12**, 3259 (1997).
13. I. A. Bandos, Pis'ma Zh. Éksp. Teor. Fiz. **52**, 837 (1990) [JETP Lett. **52**, 205 (1990)].

Translated by R. Rogalyov

Physics of Atomic Nuclei, Vol. 63, No. 4, 2000, pp. 623–628. From Yadernaya Fizika, Vol. 63, No. 4, 2000, pp. 689–694.

VIII INTERNATIONAL CONFERENCE ON SYMMETRY METHODS IN PHYSICS

Symmetry and Some Consequences for Spin-Particle Reactions*

M. P. Chavleishvili

Joint Institute for Nuclear Research, Dubna, Moscow oblast, 141980 Russia; International University, Dubna, Russia

Abstract—On the basis of general spacetime and crossing symmetry, the general structure for amplitudes describing spin-particle binary reactions is considered. Using the knowledge of the kinematic structure of helicity amplitudes in the dynamical amplitude approach, we can get as model-independent general consequences about observable quantities, as some asymptotic relations between polarization parameters on the basis of a "kinematic hierarchy" assumption. *© 2000 MAIK "Nauka/Interperiodica".*

1. SYMMETRY AND SPIN

Symmetry means harmony, beauty, and order.

In physics, symmetry has three levels:

(i) Coordinate systems and frames (spherical system, inertial systems);

(ii) Variables (for example, for binary processes, we have two independent variables, energy and angle, or invariant variables, s and t);

(iii) Functions. If we consider reactions with particles with spin

$$s_1 + s_2 \longrightarrow s_3 + s_4, \tag{1}$$

we have $N = (2s_1 + 1)(2s_2 + 1)(2s_3 + 1)(2s_4 + 1)$ functions to describe the process, and we must choose the optimal set of these functions.

In particle physics one can consider three types of symmetry [1]:

(i) Spacetime symmetries;

(ii) Intrinsic symmetries;

(iii) "Intermediate" symmetry: crossing.

The language of symmetry is the mathematical theory of groups and their representations. We have rotation, Lorentz and Poincaré invariance, and the corresponding groups with their representations. The Poincaré invariance has two Kasimir operators, or two invariants. These invariants are connected with two fundamental properties of elementary particles: mass and spin. Their existence is connected with symmetry. Mass is both a classical and a quantum quantity, whereas spin is a pure quantum object.

Symmetry is connected with fundamental conservation rules—conservation of energy, momentum, and angular momentum (the latter is the sum of spin and orbital momentum).

Thus, in elementary particle physics, we have a particle with mass m, spin s, energy E, and momentum p. It is often convenient to consider helicity as well, the projection of spin onto the direction of motion.

We have two types of symmetry: global and local (gauge). If we suggest symmetry (Lorentz) and the spin of the particle, we can write a free particle Lagrangian L_0. If we suggest the gauge symmetry for a free particle Lagrangian, we necessarily obtain a particle that takes interactions (photon, gauge W and Z bosons, gluon) and even the interaction Lagrangian L_{Int}.

Generalization of the spin onto the "intrinsic" direction is isospin [2]. The isospin is connected with the group $SU(2)$. Wigner [3] suggests first generalization of $SU(2)$ and $SU(4)$. A revolution in physics was made by suggesting $SU(3)$ and quarks [4], color [5], unified theory of electroweak interactions, and quantum chromodynamics.

Due to the symmetry in particle physics (quantum field theory), we have a Lagrangian of a definite form that depends on a small number of masses and interaction constants. This is in sharp contrast with quantum mechanics where interactions are considered as arbitrary functions (potentials) for every pair of particles. Symmetry does not admit arbitrary functions. Today, we have the following succession:

Symmetry $\longrightarrow$ group $\longrightarrow$ particle interaction.

Thus, $SU_c(3)$ symmetry and the corresponding group give us quantum chromodynamics, and symmetry and group $U(1) \times SU(2)$ give us electroweak interactions. We have the standard $1 \times 2 \times 3$ model and other unification schemes. These unifications are realized at very high energies, which occurred at the earliest stages of our Universe in the Big Bang theory, so symmetry gives us the key to the Universe.

Symmetry between fermions and bosons creates supersymmetry, a theory that predicts new particles—supersymmetric partners of the old ones. These particles are the gravitino (with spin 3/2), photino, and so on.

Thus, symmetry gives us the characteristics of particles (mass, spin momentum, and so on), the particles that carry interactions (gauge particles), and the interaction Lagrangian. This, in principle, must be the full theory.

* This article was submitted by the author in English.

1063-7788/00/6304-0623$20.00 © 2000 MAIK "Nauka/Interperiodica"

However, today we have no full and final theory for the time being. Thus, there exists a problem that has its own history: the problem of direct investigation of processes with elementary particles based on the general symmetry principles and independent of the explicit form of the Lagrangian—spin kinematics (or amplitude kinematics).

2. SPIN AND PARTICLE REACTIONS

Most particles have a nonzero spin. We are going to consider binary reactions with particles of arbitrary spins. The spin-particle reactions are convenient to describe in the helicity amplitude formalism [6]. Helicity amplitudes $f_{\lambda_3,\lambda_4;\lambda_1,\lambda_2}(s,t)$ have a clear physical meaning, and observables are expressed by them in a simple way. Helicity amplitudes contain all the information about the considered process. But helicity amplitudes have kinematic singularities.

Scattering of spinless particles is described by one amplitude. Considering this amplitude as a function of invariant variables, we have the function $A(s, t)$. This amplitude has some singularities. They are called dynamical singularities. The analytic properties of the amplitude are connected with causality and unitarity, and this amplitude obeys dispersion relations.

For spin particles, the process is described by several functions, several helicity amplitudes. And they have additional, so-called kinematic, singularities. Thus, helicity amplitudes do not fulfill simple dispersion relations. It is necessary to find and separate kinematic singularities. Thus, helicity amplitudes are expressed via a set of other amplitudes without kinematic singularities. For a lowest spin, it is convenient to introduce invariant amplitudes.

Let us consider the simplest nontrivial reaction: π–N scattering, elastic scattering of a spin-zero particle with the mass μ on a spin-1/2 particle of mass m. Using the Dirac equation, we can find the following connection between the helicity and invariant amplitudes (in standard designation):

$$f^s_{0,\lambda_4;0,\lambda_2}(s,t) = \bar{u}^{\lambda_4}(p_4)\{A(s,t) + \hat{Q}B(s,t)\}u^{\lambda_2}(p_2). \quad (2)$$

Here $A(s, t)$ and $B(s, t)$ are invariant amplitudes. Properly defined invariant amplitudes have no kinematic singularities.

For the general case of scattering of particles with spins s_i, we have

$$f_{\lambda_3,\lambda_4,\lambda_1,\lambda_2}(s,t) = \sum_{n=1}^{N} a^n_{\lambda_3,\lambda_4,\lambda_1,\lambda_2}(s,t)A_n(s,t). \quad (3)$$

Kinematic singularities of $f_{\lambda_3,\lambda_4,\lambda_1,\lambda_2}(s,t)$ are contained in the coefficient functions $a^n(s, t)$.

This procedure is nice for low spins. It is difficult to construct such an expansion for high spins. For all $s_i = 3/2$, we have $N = 256$, and for $s_i = 11/2$, we have $N \simeq 20000$. Besides, the main difficulty is in finding such a decomposition in a way that coefficients of invariant amplitudes do not contain "secret singularities" rather than in dimensions. Thus, in describing the Compton effect, for several years people used a decomposition suggested in [7], but then it appeared that those invariant amplitudes had additional singularities, and later a more complicated decomposition [8] was suggested.

Besides technical difficulties for spins greater than unity, a nontrivial question of uniqueness of such a decomposition arises, and, since for higher spins the invariant amplitude decomposition is not unique, the "secret" singularities and additional and noncontrollable kinematic constraints appear.

There exists another way that uses symmetry principles and is connected with the use of representations of a rotation group—Wigner's d functions. If we use d functions in the s channel, then using d functions in the t channel and finally connecting channels also by d functions, we can obtain a result much more convenient than (3).

The helicity amplitudes in the center-of-mass system of the s channel obey rotation symmetry (this symmetry is connected with the conservation of angular momentum). Because of this symmetry, it is convenient to expand helicity amplitudes over the representation of a rotation group, over Wigner's functions:

$$f^s_{\lambda_3,\lambda_4,\lambda_1,\lambda_2}(s,t) = \sum_J (2J+1) f^J_{\lambda_3,\lambda_4,\lambda_1,\lambda_2}(s) d^J_{\lambda\mu}(\cos\theta). \quad (4)$$

Here, we have infinite summation. Wigner's functions have the form

$$d^J_{\lambda\mu}(\cos\theta) = g\left(\sin\frac{\theta}{2}\right)^{|\lambda-\mu|}\left(\cos\frac{\theta}{2}\right)^{|\lambda+\mu|} P^{|\lambda-\mu|,|\lambda+\mu|}_{J-M}(\cos\theta), \quad (5)$$

where $P^{mn}_k(\cos\theta)$ are Jacobi polynomials (see, for example, [9]),

$$g = \sqrt{\frac{(J+M)!(J-M)!}{(J+N)!(J-N)!}}$$

with $M = \max(|\lambda|, |\mu|)$ and $N = \min(|\lambda|, |\mu|)$.

The crossing relations between the s- and t-channel helicity amplitudes appear as follows [10]:

$$f_{\lambda_3,\lambda_4,\lambda_1,\lambda_2}(s,t) = \alpha \sum_{\mu_1\mu_2\mu_3\mu_4} d^{s_1}_{\lambda_1\mu_1}(\chi_1) d^{s_2}_{\lambda_2\mu_2}(\chi_2) \times d^{s_3}_{\lambda_3\mu_3}(\chi_3) d^{s_4}_{\lambda_4\mu_4}(\chi_4) f^t_{\mu_3\mu_4,\mu_1\mu_2}(s,t). \quad (6)$$

The crossing relations also contain the Wigner functions. Here, the summation is over helicity values, and it is restricted (α is some phase factor).

3. SPIN KINEMATICS AND DYNAMICS

A lot of people have worked in this direction by considering spin kinematics and decomposition of helicity amplitudes in terms of other sets of amplitudes [11]. Combining some approaches and modifying others, we suggest a new variant of formalism that has all the advantages of different approaches, differs from all of them, is based on the symmetry and conservation laws, and is general and simple.

Symmetry imposes restrictions on amplitudes. When one has additional symmetries in definite directions, the number of independent amplitudes in such "symmetrical directions" is reduced. Such situations occur for forward and backward scattering.

Consider the reaction in the *s* channel described by the helicity amplitudes. Introduce the quantities $\lambda = \lambda_1 - \lambda_2$ and $\mu = \lambda_3 - \lambda_4$. Two particles in the center-of-mass system move in opposite directions, and thus λ and μ are projections of the total spin onto the directions of motion prior to and after collision. Owing to the conservation of the projection of the total angular momentum, the amplitudes in the forward direction, $\theta_s \longrightarrow 0$, should vanish in all cases except for $\lambda = \mu$. Analogously, for backward scattering, $\theta_s \longrightarrow \pi$, the amplitudes should vanish for the same reasons in all cases except for $\lambda = -\mu$. For forward scattering, we have

$$f^{\text{forward}}_{\lambda_3\lambda_4,\lambda_1,\lambda_2} = \begin{cases} f_{\lambda_3\lambda_4,\lambda_1,\lambda_2}, & \text{when} \quad \lambda = \mu \\ 0, & \text{when} \quad \lambda \neq \mu, \end{cases} \tag{7}$$

whereas for backward scattering,

$$f^{\text{backward}}_{\lambda_3\lambda_4,\lambda_1,\lambda_2} = \begin{cases} f_{\lambda_3\lambda_4,\lambda_1,\lambda_2}, & \text{when} \quad \lambda = -\mu \\ 0, & \text{when} \quad \lambda \neq -\mu. \end{cases} \tag{8}$$

Two questions arise:

Can the helicity amplitudes be parametrized so as to satisfy the conditions (7) and (8) automatically?

Can kinematic singularities of helicity amplitudes be found and separated in a simple way?

The answer is "yes."

Using (4), for the spinless case, we get the decomposition via the Legendre polynomials, depending on $\cos\theta$. By definition, in the spinless case, we have no kinematic singularities.

In the nonzero spin case, helicity amplitudes are split into two parts: one part is defined by the symmetry properties and enters into the functions $d^J_{\lambda\mu}(\cos\theta)$ that make the conservation laws of the angular momentum valid, and the other part has a dynamic nature and enters into the partial helicity amplitudes $f^J_{\lambda_3\lambda_4,\lambda_1,\lambda_2}(s)$.

In (4), all the *t* dependence is contained in *d* functions via $\cos\theta_s$. At the points $\cos\theta_s = \pm 1$, the *d* function has kinematic singularities on the *t* variable, which can be separated explicitly.

These singularities do not depend on *J*, and we can separate the common singular factors. The rest of the sum will contain decomposition by polynomials on the *t* variable. Therefore, we can define dispersion amplitudes for any binary process:

$$f^s_{\lambda_3\lambda_4,\lambda_1,\lambda_2}(s,t) = A^{|\lambda-\mu|}B^{|\lambda+\mu|}\bar{f}^s_{\lambda_3\lambda_4,\lambda_1,\lambda_2}(s,t). \tag{9}$$

Here,

$$A = \frac{\sqrt{L^2 - a^2}}{(m_1+m_2)(m_3+m_4)},$$

$$B = \frac{\sqrt{L^2 + a^2}}{(m_1+m_2)(m_3+m_4)},$$

$$L^2 = \{[s-(m_1+m_2)][s-(m_1-m_2)]$$

$$\times [s-(m_3+m_4)][s-(m_3-m_4)]\}^{1/2},$$

$$a^2 = 2st + s^2 - s\sum m_k^2 + (m_1^2 - m_2^2)(m_3^2 - m_4^2).$$

The mass factors in the denominators make *A* and *B* dimensionless without introducing additional singularities in the variable *s*. Under this parametrization, the conditions (7) and (8) are fulfilled automatically. All kinematic singularities in the variable *t* are separated explicitly, and no false singularities in *s* are introduced. The amplitudes $\bar{f}^s_{\lambda_3\lambda_4,\lambda_1,\lambda_2}(s,t)$ are well suited to studying the analytic properties of the amplitudes at fixed *s* because they obey dispersion relations. Therefore, we call them the dispersion amplitudes [12]. They may still have the kinematic singularities in the variable *s*.

Dispersion amplitudes resemble reduced amplitudes [11], but they have no additional *s*-variable false singularities.

For *t*-channel processes, the corresponding dispersion amplitudes are free from kinematic singularities in the variable *s*. Expressing the dispersion amplitudes of the *s* channel in terms of the dispersion amplitudes on the annihilation channel, we obtain the connection between the amplitudes having kinematic singularities in *s* with the amplitudes that are free from them. Thus, kinematic singularities of the *s*-channel helicity amplitudes are in crossing coefficients in crossing relations between *s*- and *t*-channel amplitudes. The number of coefficients is restricted, and we do know the singularities of these coefficients; indeed, these coefficients are Wigner's functions and we do know their singularities!

Therefore, using crossing symmetry, we can find kinematic singularities of the *s*-channel dispersion

amplitudes also in the variable s. Separating these singularities, we determine a new set of functions describing binary processes—dynamical amplitudes. Dynamical amplitudes for elastic processes ($m + \mu \longrightarrow m + \mu$) have the following relations with the helicity amplitudes [13]:

$$f_{\lambda_3\lambda_4,\lambda_1,\lambda_2}(s,t) = \left(\frac{\sqrt{-t}}{m+\mu}\right)^{-|\lambda-\mu|}\left(\frac{\sqrt{L^2+st}}{(m+\mu)^2}\right)^{-|\lambda+\mu|} \times \left(\frac{L}{(m+\mu)^2}\right)^{-2(s_1+s_2)} D_{\lambda_3\lambda_4,\lambda_1,\lambda_2}(s,t). \quad (10)$$

Dynamical amplitudes are in fact modified regularized helicity amplitudes, and they differ from the reduced amplitudes by dimensions: all dynamical amplitudes have the same dimensions, whereas the dimensions of regularized amplitudes depend on spins and helicities.

4. OBSERVABLES

The dynamical amplitude formalism is interesting for studying the general characteristics of particle reaction theory, and it also suitable for exploring concrete processes. This approach provides an analysis where kinematics is fully taken into account and is clearly separated from dynamics. The observable quantities are simply expressed via the helicity amplitudes.

As we have already mentioned, the helicity amplitudes have a clear physical meaning, and physical observables (polarization cross sections, asymmetries, etc.) are simply expressed via them. As for elastic processes, the connection between the helicity and dynamical amplitudes is one-to-one and every helicity amplitude for elastic scattering is expressed in terms of one dynamical amplitude. Hence, it follows that all attractive features of the helicity amplitudes—a clear physical meaning, simple relations with observables, and equal dimensions—are also inherent in the dynamical amplitudes. The formalism of dynamical amplitudes is simple for low spins and remains so for higher spins as well: the formalism is simple for any spins.

The differential cross section for elastic scattering, when one measures the helicity of each particle, is expressed via helicity, invariant, and dynamical amplitudes in the following form:

$$\frac{d\sigma}{dt}(\lambda_3\lambda_4,\lambda_1\lambda_2) \sim \left|f_{\lambda_3\lambda_4,\lambda_1\lambda_2}(s,t)\right|^2 = \left|\sum_1^N a^n_{\lambda_3\lambda_4,\lambda_1\lambda_2}(s,t)A_n(s,t)\right|^2 = \left|\left(\frac{\sqrt{-t}}{m+\mu}\right)^{-|\lambda-\mu|} \times \left(\frac{\sqrt{L^2+st}}{(m+\mu)^2}\right)^{-|\lambda+\mu|}\left(\frac{L}{(m+\mu)^2}\right)^{-2(s_1+s_2)} D_{\lambda_3\lambda_4,\lambda_1\lambda_2}(s,t)\right|^2. \quad (11)$$

The first relation in outward appearance is the simplest, but helicity amplitudes contain kinematic singularities, and the conservation laws are not fulfilled automatically, so kinematics and dynamics are not separated. Here, we have one term. In the second equation, there is a sum of all invariant amplitudes. Here, we have N terms. For the spins equal to 3/2, there are 256; and for the spins equal to 11/2, more than 20000 terms. In each term, we have kinematic–dynamical separation, but there are so many such terms. In the parametrization via dynamical amplitudes, we have no summation! The differential cross section is expressed only via one dynamical amplitude with the kinematic factors that contain all kinematic singularities. We have only one term.

Other quantities such as P, A_{nn}, A_{ll}, and A_{ss} in terms of the helicity amplitudes have the form [14]

$$\frac{\sum c_{mn} f_m f_n^*}{\sum |f_m|^2}.$$

Here, m and n represent sets of helicity indices, $c_{mn} = \pm 1$. The sum is taken for all values of helicities. Obviously, the expressions will be most convenient in terms of dynamical amplitudes.

5. KINEMATIC HIERARCHY

In the framework of the general spin formalism based on the symmetry properties ("dynamical amplitude" approach), obligatory kinematic factors arise in the expressions of observables. These spin structures for high energies give a small parameter that orders the contributions of helicity amplitudes to observables. Such a "kinematic hierarchy" predicts for pp elastic scattering at high energies and a large fixed angle (90°) a simple connection between asymmetry parameters and even numerical values for them [15].

Dynamical amplitudes in some sense are a generalization of form factors: in both cases, we separate kinematics. Dynamics of the processes containing matrix elements of the electromagnetic current operator (three-point functions) are described by form factors. After separation of kinematics and dynamics, it is convenient to express physical observables in terms of form factors. Analogously, dynamics of binary reactions (four-point functions) are contained in dynamical amplitudes (it is the reason they are so called). After separation of kinematics and dynamics, it will be convenient to express observables in terms of dynamical amplitudes.

In the dynamical amplitude approach, obligatory kinematic factors arise in the expressions of observables. These spin structures for high energies give a

small parameter that orders the contributions of helicity amplitudes to observables.

In studying the binary processes at fixed scattering angles and high energies, it is convenient to represent kinematic factors in the definition of dynamical amplitudes as functions of the scattering angle θ in the center-of-mass system and invariant variable *s*. Kinematic factors expressed in terms of θ and *s* are factorizable, and we can write

$$f_{\lambda_3\lambda_4,\,\lambda_1\lambda_2} = P_{\lambda_3\lambda_4,\,\lambda_1\lambda_2}(s)\varphi_{\lambda_3\lambda_4,\,\lambda_1\lambda_2}(\theta)D_{\lambda_3\lambda_4,\,\lambda_1\lambda_2}. \quad (12)$$

At high energies when $s \longrightarrow \infty$, we get the small kinematic factor

$$P_{\lambda_3\lambda_4,\,\lambda_1\lambda_2}(s) \sim \left(\frac{m}{\sqrt{s}}\right)^{l(\lambda_3\lambda_4,\,\lambda_1\lambda_2)}. \quad (13)$$

For different values of helicities *l* changes, $l_{\min} \le l(\lambda_3\lambda_4, \lambda_1\lambda_2) \le l_{\max}$.

In observables, some of the contributions of the amplitudes are kinematically increased (such amplitudes will give leading contributions), whereas others are suppressed (and can be neglected in the first approximation). Thus, we have the "kinematic hierarchy"—the helicity amplitudes are divided into classes giving the leading contribution, the first corrections, second corrections, and so on. The kinematic hierarchy also gives definite relations between various observables.

We have five independent helicity amplitudes:

$$f_1 = f_{1/2,\,1/2;\,1/2,\,1/2}, \quad f_2 = f_{1/2,\,1/2;\,-1/2,\,-1/2},$$
$$f_3 = f_{1/2,\,-1/2;\,1/2,\,-1/2}, \quad f_4 = f_{1/2,\,-1/2;\,-1/2,\,1/2}, \quad (14)$$
$$f_5 = f_{1/2,\,1/2;\,1/2,\,-1/2}.$$

For asymmetry parameters, we have [10]

$$\frac{d\sigma}{dt}A_{nn} = -\mathrm{Re}[f_3 f_4^* - f_1 f_2^* - 2|f_5|^2],$$
$$\frac{d\sigma}{dt}A_{ss} = \mathrm{Re}[f_1 f_2^* + f_3 f_4^*], \quad (15)$$

$$\frac{d\sigma}{dt}A_{ll} = -\frac{1}{2}\{|f_1|^2 + |f_2|^2 - |f_3|^2 - |f_4|^2\}. \quad (16)$$

For nucleon–nucleon scattering, the connection between helicity and dynamical amplitudes at fixed angles and asymptotics has the following form:

$$f_1(s,t) = \left(\frac{m}{\sqrt{s}}\right)^2 D_1(s,t), \quad f_2(s,t) = \left(\frac{m}{\sqrt{s}}\right)^2 D_2(s,t),$$
$$f_3(s,t) = \cos^2\frac{\theta_s}{2}D_3(s,t),$$
$$f_4(s,t) = \sin^2\frac{\theta_s}{2}D_4(s,t), \quad (17)$$
$$f_5(s,t) = \frac{\sqrt{s}}{2m}\sin\theta_s D_5(s,t).$$

In the high-energy large-fixed-angle region, we have the small parameter $(m/\sqrt{s}) \ll 1$, and helicity amplitudes are split into three classes in the order of smallness determined by the kinematic factors:

$$f_{1/2,\,1/2;\,1/2,\,-1/2} \gg f_{1/2,\,-1/2;\,1/2,\,-1/2} \sim f_{1/2,\,-1/2;\,-1/2,\,1/2}$$
$$\gg f_{1/2,\,1/2;\,1/2,\,1/2} \sim f_{1/2,\,1/2;\,-1/2,\,1/2}. \quad (18)$$

Here "$a \gg b$" means that the contribution of *b* is suppressed relative to the contribution of *a* in the observables.

For proton–proton scattering at $\theta_{\mathrm{c.m.}} = 90°$, we have from the *s*–*u* crossing symmetry that $f_{1/2,\,1/2;\,1/2,-1/2}(90°) = 0$ and $f_{1/2,\,-1/2;\,1/2,\,-1/2}(90°) = -f_{1/2,\,-1/2;\,-1/2,\,1/2}(90°)$.

Taking into account the dominating amplitudes, we obtain for asymmetries

$$A_{nn} = -A_{ss} = A_{ll}$$
$$= \frac{2\mathrm{Re}\, f_{1/2,\,-1/2;\,1/2,\,-1/2} f^*_{1/2,\,-1/2;\,-1/2,\,1/2}}{|f_{1/2,\,-1/2;\,1/2,\,-1/2}|^2 + |f_{1/2,\,-1/2;\,-1/2,\,1/2}|^2} \longrightarrow 1. \quad (19)$$

Recent developments in acceleration of polarized protons using the so-called Siberian snakes now allow the achievement of polarized proton–proton collisions at new accelerators. New possibilities will be open for studying spin effects at high energies [16, 17], and it will be possible to check our predictions. Existing data show growth of $A_{nn}(p_\perp^2\,(\mathrm{GeV}^2))$ [18]: $A_{nn}(3.81) = 0.26$, $A_{nn}(4.79) = 0.52$, and $A_{nn}(5.56) = 0.59$.

Another interesting process is the reaction *proton* + *antiproton* $\longrightarrow$ *photino* + *antiphotino*. The process is interesting because, at new accelerators, we will have a chance to discover particles predicted by theories based on supersymmetry, in particular, photino. Dynamical amplitudes for inelastic reaction with massive particles of masses $m + m \longrightarrow M + M$ are expressed by binary combinations of helicity amplitudes (kinematic factors are considered as functions of the variables *s* and θ) [19]:

$$D^{s,\pm}_{\lambda_3\lambda_4,\,\lambda_1,\,\lambda_2} = \left(\frac{\sqrt{s}}{m+M}\right)^a \left(\frac{\sqrt{s-4m^2}}{m+M}\right)^b \left(\frac{\sqrt{s-4M^2}}{m+M}\right)^c$$
$$\times\left\{\left(\sin\frac{\theta}{2}\right)^{-|\lambda-\mu|}\left(\cos\frac{\theta}{2}\right)^{-|\lambda+\mu|} F_{\lambda_3\lambda_4,\,\lambda_1,\,\lambda_2}\right.$$
$$\left. \pm \left(\sin\frac{\theta}{2}\right)^{-|\lambda+\mu|}\left(\cos\frac{\theta}{2}\right)^{-|\lambda-\mu|} F_{\lambda_3\lambda_4,\,-\lambda_1,\,-\lambda_2}\right\}. \quad (20)$$

We have helicity amplitudes

$$F_1 = F_{1/2,\,1/2;\,1/2,\,1/2}, \quad F_2 = F_{1/2,\,1/2;\,-1/2,\,-1/2},$$
$$F_3 = F_{1/2,\,-1/2;\,1/2,\,-1/2}, \quad F_4 = F_{1/2,\,-1/2;\,-1/2,\,1/2}, \quad (21)$$
$$F_5 = F_{1/2,\,1/2;\,1/2,\,-1/2}, \quad F_6 = F_{1/2,\,-1/2;\,1/2,\,1/2}.$$

For asymmetry parameters, we have [14]

$$\frac{d\sigma}{dt}A_{nn} = \mathrm{Re}[F_1F_2^* - F_3F_4^* - F_5F_5^* - F_6F_6^*], \quad (22)$$

$$\frac{d\sigma}{dt}A_{ss} = \mathrm{Re}[F_1F_2^* + F_3F_4^* + F_5F_5^* - F_6F_6^*], \quad (23)$$

$$\frac{d\sigma}{dt}A_{ll} = \frac{1}{2}\{|F_1|^2 + |F_2|^2 - |F_3|^2 - |F_4|^2 + 2|F_5|^2 - 2|F_6|^2\}. \quad (24)$$

In these equations,

$$\frac{d\sigma}{dt} = \frac{1}{2}\{|F_1|^2 + |F_2|^2 + |F_3|^2 + |F_4|^2 + 2|F_5|^2 + 2|F_6|^2\}. \quad (25)$$

Using the explicit form of connection between helicity and dynamical amplitudes and smallness of the kinematic factor that appears, we have a "kinematic hierarchy" for the discussed reaction. Helicity amplitudes are split into three classes in the order of smallness determined by the kinematic factors.

$$F_5, F_6 \gg F_3, \quad F_4 \gg F_1, F_2. \quad (26)$$

If we take into account only the dominating amplitudes, we get asymmetries (for some other reasons, for example, for *s*–*u* symmetry and at definite angles, there can be additional restrictions, which have not been taken into account here).

Thus, we have two results.

(i) Hierarchy relation: $A_{ll} = A_{ss}$.

(ii) Numerical value for asymmetry parameter: $A_{nn} = -1$.

6. OTHER APPLICATIONS

Spin kinematics allows one to obtain the low-energy theorems for photon–hadron processes [20] and gravitino scattering on a spin-0 target. For the latter process at low energies, the helicity amplitudes up to $O(E^3)$ are determined by their *t*-channel Born terms with the photon exchange [21].

The dynamical amplitudes, or more simply the *t*-channel dispersion amplitudes, can be used to prove mode-independent dispersion inequalities for the Compton effect on the pion and nucleon target, including the case of polarized photon scattering [22].

Here, we have mentioned other possible applications of dynamical amplitudes. These are the dispersion relations for individual helicity amplitudes for any elastic scattering and sum rules (especially dual sum rules), also for any elastic scattering.

REFERENCES

1. E. P. Wigner, *Symmetries and Reflection* (Indiana Univ. Press, Bloomington, 1970).
2. W. Heisenberg, Z. Phys. **77**, 1 (1932).
3. E. P. Wigner, Phys. Rev. **51**, 105 (1937).
4. M. Gell-Mann, Phys. Rev. **125**, 1067 (1962); Y. Neeman, Nucl. Phys. **26**, 222 (1961).
5. N. N. Bogoliubov, B. V. Struminsky, and A. N. Tavkhelidze, Preprint No. D-1968, JINR (Dubna, 1965); M. Y. Han and Y. Nambu, Phys. Rev. **139**, 1006 (1965); H. Fritzsch, and M. Gell-Mann, in *Proceedings of the XVI International Conference on High Energy Physics, Chicago, 1972*, Vol. 2, p. 135.
6. M. Jacob and G. C. Wick, Ann. Phys. (N.Y.) **7**, 404 (1959).
7. A. C. Hern and E. Leader, Phys. Rev. **126**, 789 (1962).
8. W. A. Bardeen and Wu-Ki Tung, Phys. Rev. **173**, 1423 (1968).
9. D. A. Warshalovich *et al.*, *Quantum Theory of Angular Momentum* (Nauka, Leningrad, 1975).
10. Ya. A. Smorodinsky, Preprint No. E-1227, JINR (Dubna, 1963); T. L. Trueman and G. C. Wick, Ann. Phys. (N.Y.) **26**, 322 (1964); Y. Hara, Phys. Rev. B **136**, 507 (1964).
11. H. Joos, Fortschr. Phys. **10**, 65 (1962); D. N. Williams, Preprint No. UCRL-11113, UCRL (Berkeley, California, 1963); M. Gell-Mann *et al.*, Phys. Rev. B **133**, 145 (1964); L. L. Wang, Phys. Rev. **142**, 1187 (1966); G. Cohen-Tannoudji, A. Morel, and H. Navelet, Ann. Phys. (N.Y.) **46**, 239 (1968); J. P. Ader, M. Capdeville, and H. Navelet, Nuovo Cimento A **56**, 315 (1968); T. L. Trueman, Phys. Rev. **173**, 1684 (1968).
12. M. P. Chavleishvili, *Proceedings of the International Symposium on Polarization Dynamics in Nuclear and Particle Physics, Trieste, 1992*; Preprint No. LMU-02-93, Ludwig-Maximilian University (Munich, 1993).
13. M. P. Chavleishvili, Preprint No. LMU-03-93, Ludwig-Maximilian University (Munich, 1993); Sov. J. Nucl. Phys. **40**, 155 (1984); **41**, 678 (1985).
14. C. Bourrely, E. Leader, and J. Soffer, Phys. Rep. **59**, 96 (1980).
15. M. P. Chavleishvili, *Proceedings of the 8th International Symposium on High Energy Spin Physics, Minneapolis, 1988*, Ed. by K. J. Heller (New York, 1989), Vol. 1, p. 123; Preprint No. LMU-05-93, Ludwig-Maximilian University (Munich, 1993).
16. A. D. Krish, Phys. Rev. Lett. **63**, 1137 (1989).
17. G. Bunce *et al.*, Particle World **3**, 1 (1992).
18. E. A. Crosbie *et al.*, Phys. Rev. D **23**, 1137 (1981).
19. M. P. Chavleishvili, Symmetry and Spin in Binary Processes (Review), Phys. Part. Nucl. (to be published).
20. R. M. Muradyan and M. P. Chavleishvili, Sov. Theor. Math. Phys. **8**, 639 (1971); M. P. Chavleishvili, Preprint No. P2-88-179, JINR (Dubna, 1988).
21. M. P. Chavleishvili, Preprint No. E2-87-69, JINR (Dubna, 1987); *Proceedings of the 9th International Symposium on High Energy Spin Physics, Bonn, 1990*, Ed. by K.-H. Althoff and W. Meyer (Springer-Verlag, Berlin, 1991), Vol. 1, p. 489.
22. M. P. Chavleishvili, Sov. J. Nucl. Phys. **37**, 405 (1983); **43**, 247 (1986).

Physics of Atomic Nuclei, Vol. 63, No. 4, 2000, pp. 629–634. From Yadernaya Fizika, Vol. 63, No. 4, 2000, pp. 695–700.

VIII INTERNATIONAL CONFERENCE ON SYMMETRY METHODS IN PHYSICS

The Conditions of Existence of First Integrals and Hamiltonian Structures of Lotka–Volterra and Volterra Systems*

V. M. Dubovik, A. G. Galperin[1)], V. S. Richvitsky[2)], and S. K. Slepnyov[2)]

Bogolubov Laboratory of Theoretical Physics, Joint Institute for Nuclear Research, Dubna, Moscow oblast, 141980 Russia

Abstract—A study of a certain subset of Volterra equations has revealed that some statements about time-independent constants of motion, Hamiltonian functions, and Poisson structure matrices appearing in the Lotka–Volterra equations, either regarded as proven or of the sort that could be proven, are not valid, in fact. Particular cases are given as examples to explain the reasons for the occurring phenomena. © *2000 MAIK "Nauka/Interperiodica".*

1. INTRODUCTION

The Lotka–Volterra equations (LVE) are systems of ordinary nonlinear differential equations of the form

$$\dot{x}_i = x_i y_i, \quad i = 1, \ldots, N, \quad \text{where} \quad \mathbf{y} = A\mathbf{x} + \mathbf{b}. \tag{1}$$

The Volterra equations (VE) are a special case of the LVE [1], when there exist $\beta_i \neq 0$ such that

$$\beta_i a_{ij} = -\beta_j a_{ji}. \tag{2}$$

In the odd-dimensional case of the VE, the matrix A is degenerate. Initially even-dimensional systems were studied with variables coupled in predator–prey pairs, admitting a classical Hamiltonian approach (see [2]) with nondegenerate symplectic structure. The classical approach, however, cannot be applied in a straightforward way for odd-dimensional systems, or in even dimensions when the equation for the central equilibrium point $\mathbf{p}$,

$$A\mathbf{p} = -\mathbf{b}, \tag{3}$$

gives $p_i = 0$ for at least one i. In the biological implementations, the dependent variables x_i are regarded as real positive numbers, representing populations of species i; the components of the vector $\mathbf{b}$ are called linear growth rates, or Malthusian terms; and A is called the interaction matrix, the diagonal terms describing self-interaction of species and the off-diagonal terms being responsible for interactions between different species. The terms of interaction matrix A and the Malthusian terms $\mathbf{b}$ are arbitrary real numbers in the case of the general LVE. In the case of the VE, the terms of the interaction matrix are not completely arbitrary; for instance, the self-interaction (diagonal) terms are all equal to zero.

The Volterra lattice model, usually written as $\frac{d}{dt}N_i = N_i(N_{i+1} - N_{i-1})$, studied with the Hamiltonian methods in [3], known for close relations to the Toda lattice model and the Korteveg–de Vries (KdV) equation (see [4, 5]), and cited by Gümral and Nutku [6] as the Faddeev–Takhtajan system, turns into different subcases of the VE under different boundary conditions. For example, the 3D case of periodic boundary conditions (22) complies with the form of "*ABC* matrix" (4) used in [6–8], while the conditions used in [4] do not. Both are subcases of the general antisymmetric interaction matrix studied in [9], which in turn is a subcase ($\beta_i = 1$, $\forall i$; $\mathbf{b} = 0$) of the VE; and the latter are a subset (2) of the LVE (1). We classify the systems with multiple pairwise interactions, called LVE in [10], as Volterra equations.

To make things clear, we use the definition of the LVE and the VE complying with that given in [11, 12], the works that we cite most extensively. But, in contradistinction to [11, 12], we do not assume the "natural" $x_i > 0$ conditions.

2. BI-HAMILTONIAN STRUCTURE

The first example of a bi-Hamiltonian structure for an LVE system of a special form was given by Nutku [8]. For the system studied earlier by Grammatikos *et al*. [7] with the "*ABC*" interaction matrix

$$A = \begin{pmatrix} 0 & C & 1 \\ 1 & 0 & A \\ B & 1 & 0 \end{pmatrix}, \quad \mathbf{b} = \begin{pmatrix} \lambda \\ \mu \\ \nu \end{pmatrix}, \tag{4}$$

on the conditions

$$ABC + 1 = 0, \quad \nu = \mu B - \lambda AB,$$

* This article was submitted by the authors in English.

[1)] Laboratory of High Energy, Joint Institute for Nuclear Research, Dubna, Moscow oblast, 141980 Russia.

[2)] Laboratory Comp. Tech. Automat., Joint Institute for Nuclear Research, Dubna, Moscow oblast, 141980 Russia.

1063-7788/00/6304-0629$20.00 © 2000 MAIK "Nauka/Interperiodica"

and for the constants of motion

$$H_1 = AB\ln x_1 - B\ln x_2 + \ln x_3,$$
$$H_2 = ABx_1 + x_2 - Ax_3 + \nu\ln x_2 - \mu\ln x_3, \quad (5)$$

Nutku has written Hamiltonian equations as

$$\dot{x}^i = J_1^{ik}\nabla_k H_2 = J_2^{ik}\nabla_k H_1 \quad (6)$$

with the antisymmetric Poisson structure matrices J_1 and J_2, which we represent here by the corresponding vectors $\mathbf{j}_1$ and $\mathbf{j}_2$, so that $\mathbf{j}_i = ((J_i)^{23}, -(J_i)^{13}, (J_i)^{12})^T$:

$$\mathbf{j}_1 = (-x_2x_3, -BCx_1x_3, Cx_1x_2)^T, \quad (7)$$

$$\mathbf{j}_2 = (x_1x_2x_3, -Cx_1x_3(x_2+\nu), Cx_1x_2(Ax_3+\mu))^T \quad (8)$$

satisfy the Jacobi identity,

$$J^k[^m\nabla_k J^{np}] = 0, \quad (9)$$

where the square brackets denote symmetrization in the indices m, n, p.

In the $3D$ case, the Jacobi identity for the Poisson structure matrix J, represented by vector $\mathbf{j}$, becomes

$$(\mathbf{j}, \mathrm{rot}\,\mathbf{j}) \equiv 0, \quad (10)$$

which is recognizably the condition of the theorem of Frobenius on the integrability of Pfaff's form, this fact being more than a mere coincidence, and subsequently substantially used in [6]. However, the "*ABC* matrix," on the terms of the constraints used, is a very special case of the interaction matrix of a Volterra type.

3. THE PRIMARY INVARIANTS OF CAIRÓ AND FEIX

The invariants of motion for the LVE of the most general form were studied in [11, 13] by means of the generalized Carleman embedding method. These invariants come together with certain constraints and have been classified by Cairó and Feix [11] into primary invariants of three types, secondary invariants, and those deduced by rescaling.

If and only if $\det(A) = 0$, the primary invariant type I

$$\mathcal{J}_\mathrm{I} = \prod_{i=1}^N x_i^{\alpha_i} e^{st} \quad (11)$$

exists with α_i and s satisfying

$$A^T\boldsymbol{\alpha} = \mathbf{0}, \quad s = -(\boldsymbol{\alpha}, \mathbf{b}). \quad (12)$$

Defining the auxiliary matrix D and the vectors $\mathbf{n}$ and $\overrightarrow{\mathrm{diag}}\,(A)$ according to

$$d_{ij} = a_{ij} - a_{jj}, \quad \mathbf{n} = (1, 1, \ldots, 1)^T,$$
$$\overrightarrow{\mathrm{diag}}(A) = (a_{11}, a_{22}, \ldots, a_{NN})^T, \quad (13)$$

the conditions for the existence of the primary invariant type II are $(N-1)(N-2)/2$ equations

$$\bar{R}_{ijk} = d_{ij}d_{jk}d_{ki} + d_{ji}d_{kj}d_{ik} = 0, \quad (14)$$

together with the conditions

$$b_1 = b_2 = \ldots = b_N = b_0, \quad \text{that is} \quad \mathbf{b} = b_0\mathbf{n}. \quad (15)$$

The form of the invariant type II is

$$\mathcal{J}_\mathrm{II} = \prod_{i=1}^N x_i^{\alpha_i}\left(-x_1 + \sum_{l=2}^N \frac{d_{1l}}{d_{l1}}x_l\right)e^{st}, \quad (16)$$

where α_i and s are found from the equations

$$A^T\boldsymbol{\alpha} = -\overrightarrow{\mathrm{diag}}(A), \quad s = -b_0(1 + (\boldsymbol{\alpha}, \mathbf{n})). \quad (17)$$

Considering the time dependence, Cairó and Feix state that $s = 0$ when N is odd. This statement is based on the assumption $\mathrm{rank}(A) = N$, which does not appear among the conditions, but is used in the proof of their theorem, and becomes invalid when $\det(A) = 0$. Here is an example that makes this clear:

$$A = \begin{pmatrix} 3 & 4 & 5 \\ 2 & 3 & 4 \\ 1 & 2 & 3 \end{pmatrix}, \quad \mathbf{b} = \begin{pmatrix} 3 \\ 3 \\ 3 \end{pmatrix}, \quad (18)$$

$$\mathcal{J}_\mathrm{II} = x_2^{-3}x_3^3(-x_1 - x_2 - x_3)e^{-3t}.$$

The primary invariant type III of Cairó and Feix

$$\mathcal{J}_\mathrm{III} = \prod_{i=1}^N x_i^{\alpha_i}\left(1 + \sum_{l=1}^N \frac{a_{ll}}{b_l}x_l\right)e^{st} \quad (19)$$

exists on $N(N-1)/2$ conditions

$$R_{ij} = \frac{a_{ii}}{b_i}d_{ij} + \frac{a_{jj}}{b_j}d_{ji} = 0. \quad (20)$$

For this invariant, $\boldsymbol{\alpha}$ and s are defined from

$$A^T\boldsymbol{\alpha} = -\overrightarrow{\mathrm{diag}}(A), \quad s = -(\boldsymbol{\alpha}, \mathbf{b}). \quad (21)$$

There is a certain correspondence between invariants II and III in the neighboring odd and even dimensions that Cairó and Feix have discovered. However, for the primary invariant III, their statement is that $s = 0$ for even N. The controversial example for the latter statement is the same as (18), with an additional equation

$$\dot{x}_4 = x_4(-3 - 3x_4),$$
$$\mathcal{J}_\mathrm{III} = x_2^{-3}x_3^2x_4^{-1}(1 + x_1 + x_2 + x_3 + x_4)e^{-3t}.$$

Considering the classical Volterra invariant, Cairó and Feix use a procedure for obtaining a limit of invariant III when the diagonal terms of the interaction matrix tend to zero. They have managed to obtain it for $N = 2$, but in the case of the "*ABC* matrix" (4), their result for

the Volterra invariant is H_1, which is not correct, since the expression for the Volterra invariant should contain the coordinates of the central equilibrium point, or stable population levels; thus, the correct expression should be H_2. This is a consequence of the fact that the generalized Carleman ansatz does not contain logarithmic terms additively to the linear ones.

4. BI-HAMILTONIAN TECHNIQUE VERSUS RESCALING

Gümral and Nutku [6] studied the Poisson structures of dynamical systems with three degrees of freedom from the point of view of the theorem of Frobenius on the integrability of Pfaff's equation. Among others, they used the same "*ABC*-matrix" example (4) and Faddeev–Takhtajan system closed modulo 3

$$A = \begin{pmatrix} 0 & 1 & -1 \\ -1 & 0 & 1 \\ 1 & -1 & 0 \end{pmatrix}, \quad \mathbf{b} = \mathbf{0} \tag{22}$$

as its particular case. Although the bi-Hamiltonian structures for the LVE given in [6] are the same as in [8], the general considerations on the forms of the bi-Hamiltonian structures are important. Namely, the Poisson structures include, in general, the terms of the order from 0 to 3 in the powers of x_i. The Poisson 1-forms corresponding to the Poisson structures should be compatible, so a conformal factor should be used to add two of them. In a certain case, the equations of motion can be written in a manifestly bi-Hamiltonian form through the exterior product of the gradients of two Hamiltonians. It was also pointed out in [6] that a ratio of components of Poisson structure functions obeys a partial differential equation, which could be quite a manageable one. An analogous idea was also used in [14, 15].

In [14], a representative set of three-dimensional autonomous systems was studied, the LVE being the last and the most difficult case. The procedure implemented therein included rescaling of the vector field and using the Jacobi identities for the Poisson structure matrix as partial differential equations to obtain one of its components. The idea was that every particular solution of these equations should identically satisfy both the Hamiltonian form of the rescaled equations and the Jacobi identities. However, to find a particular solution in the case of the LVE with primary invariant I as the Hamiltonian function, an additional constraint

$$d_{32}(a_{23}a_{11} - a_{13}a_{21}) = d_{31}(a_{23}a_{12} - a_{13}a_{22}) \tag{23}$$

was imposed. In [15], the same idea was used but two constraints were imposed. The common feature of both works [14, 15] is that no numerical examples are given, so a consistency check is still to be performed. On our part, we have found that the formulas from [15] do not reproduce the Malthusian terms $\mathbf{b}$ for $s = 0$. The Poisson structure functions obtained in [14] are also not applicable if $s = 0$, although the constraint (23) and the two constraints imposed in [15] are satisfied with matrices (32) given in Section 6. The correct Poisson structures in this case are given in Section 7.

5. HAMILTONIAN STRUCTURES BY PLANK

Plank studied generalized Hamiltonian structures in the LVE [12] using time-independent constants of motion as Hamiltonian functions and quadratic Poisson structure functions

$$j_{il} = c_{il}x_i x_l, \tag{24}$$

where c_{il} are the matrix elements of a constant skew-symmetric matrix C. To the usual items of the definition of the generalized Hamiltonian system, "(i) $\dot{\mathbf{x}} = J\nabla H$ is the vector field with smooth real-valued Poisson structure matrix J and Hamiltonian function H defined on an open subset G of R^N, and (ii) the Jacobi identities for the skew-symmetric J are satisfied," he added the third item, "(iii) The matrix of linearization at every fixed point can be written as a product of a symmetric and a skew-symmetric matrix."

The forms for the Hamiltonian functions were deduced by Plank from the explicitly solved case $N = 2$:

$$H(x) = \sum_{i=1}^{N} \beta_i(x_i - p_i \ln x_i); \tag{25}$$

$$H(x) = \prod_{i=1}^{N} x_i^{\alpha_i}\left(1 + \sum_{l=1}^{N} B_l x_l\right), \quad B_l \neq 0; \tag{26}$$

$$H(x) = \prod_{i=1}^{N} x_i^{\alpha_i}\left(\sum_{l=1}^{N} B_l x_l\right), \quad B_l \neq 0; \tag{27}$$

$$H(x) = \sum_{i=1}^{N} \alpha_i \ln x_i + \frac{B_0 + \sum_{l=1}^{N} B_l x_l}{x_k}, \quad B_k = 0. \tag{28}$$

Cairó and Feix [16] regard the constant of motion of the form (28) as a limiting case of their primary invariant type III. The following example shows that this is not so:

$$A = \begin{pmatrix} 3 & -1 & 1 \\ -3 & -1 & -2 \\ 0 & 2 & 1 \end{pmatrix}, \quad \mathbf{b} = \begin{pmatrix} 0 \\ 1 \\ -1 \end{pmatrix}, \tag{29}$$

$$H(x) = \ln\frac{x_1 x_2}{x_3^2} + \frac{1 - x_2 - x_3}{x_1},$$

because the equations for $\boldsymbol{\alpha}$ (21) give $\alpha_2 = \alpha_3$ for $\mathcal{J}_{\mathrm{III}}$ in contrast to $\alpha = 1$, $\alpha_3 = -2$ in the example.

However, all of Plank's theorems, with the exception of that on the Volterra invariant, in the case $N > 2$ are not valid for the part of the proof that the first part of the definition of a Hamiltonian system fulfills. Calculating the Hamiltonian vector field $\dot{\mathbf{x}} = J\nabla H$, the author [12] obtains the correct expressions

$$\dot{x}_i = g(x)x_i\left(b_i + \sum_{i=1}^{N} a_{ij}x_j\right), \tag{30}$$

where $g(x) = 1$ for (25), $g(x) = \prod_{i=1}^{N} x_i^{\alpha_i}$ for (26) and (27), and $g(x) = x_k^{-1}$ for (28). The proofs of the mentioned Plank theorems end with the following similar words: "Since the factor $g(x)$ is positive in the first orthant, it can be dropped without altering the phase portrait of the differential equation QED." All these words are true except for the last three letters "QED," because the definition point (i) demands *the differential equation itself* to be written in the Hamiltonian form, *not* the phase portrait. Thus, Plank has discovered, or rather, constructed, Hamiltonian systems with quadratic Poisson structure matrices having the same phase portrait as certain LVE in the first orthant. For the pure LVE, another form of Poisson structure matrices should be used with Plank's Hamiltonian functions:

$$j_{il} = \frac{1}{g(x)}c_{il}x_ix_l. \tag{31}$$

In three dimensions, the Jacobi identities with this form of Poisson structure matrices are satisfied. When $N = 4$, additional constraints arise from the closure of the Jacobi identities: $\boldsymbol{\alpha} = \mathbf{b} = \mathbf{0}$ when $\det(C) \neq 0$, or $\det(C) = \det(A) = 0$. Of course, when $N > 4$, still more additional constraints will appear. However, the open subset G in which the Hamiltonian system should be defined may be extended now, in certain cases, to the entire R^N, excluding the subspaces $x_i = 0$.

6. DEGENERACIES WITH 3*D* PLANK STRUCTURES

The puzzling absence of the analog of Cairó and Feix's primary invariant type I among Plank's Hamiltonian functions can be explained by comparing Nutku's example (8), with cubic terms, and Plank's ansatz (24), without cubic terms in the Poisson structure matrices. But, in fact, all of Plank's Hamiltonian functions (26)–(28) imply the degeneracy of interaction matrices in three dimensions, which is easily proved by straightforward calculations of the vector fields through $J\nabla H$. The following formulas (32) and (33) are the results of such calculations. Defining $\boldsymbol{\gamma}$ as the vector dual to the matrix C and introducing $B_0 = 1$ for (26) and $B_0 = 0$ for (27), we have for the cases of Hamiltonian functions (26) and (27)

$$A = \begin{pmatrix} \lambda_1 B_1 & (\lambda_1 + \gamma_3)B_2 & (\lambda_1 - \gamma_2)B_3 \\ (\lambda_2 - \gamma_3)B_1 & \lambda_2 B_2 & (\lambda_2 + \gamma_1)B_3 \\ (\lambda_3 + \gamma_2)B_1 & (\lambda_3 - \gamma_1)B_2 & \lambda_3 B_3 \end{pmatrix}, \tag{32}$$

$$\mathbf{b} = B_0\begin{pmatrix} \lambda_1 \\ \lambda_2 \\ \lambda_3 \end{pmatrix},$$

where $\boldsymbol{\lambda} = C\boldsymbol{\alpha} \equiv [\boldsymbol{\alpha}, \boldsymbol{\gamma}]$. In the same notation, for the case of Hamiltonian function (28), with $k = 1$ we have

$$A = \begin{pmatrix} \lambda_1 & \gamma_3 B_2 & -\gamma_2 B_3 \\ \lambda_2 & \gamma_3 B_2 & (\gamma_1 + \gamma_3)B_3 \\ \lambda_3 & -(\gamma_1 + \gamma_2)B_2 & -\gamma_2 B_3 \end{pmatrix}, \tag{33}$$

$$\mathbf{b} = \begin{pmatrix} 0 \\ \gamma_3 B_0 \\ -\gamma_2 B_0 \end{pmatrix}.$$

The determinants of these matrices are

$$\det(A) = B_1B_2B_3(\mathbf{n}, \boldsymbol{\gamma})(\boldsymbol{\lambda}, \boldsymbol{\gamma}) \equiv 0 \tag{34}$$

for (32) and

$$\det(A) = B_2B_3(\mathbf{n}, \boldsymbol{\gamma})(\boldsymbol{\lambda}, \boldsymbol{\gamma}) \equiv 0 \tag{35}$$

for (33). They are identical to zero because $(\boldsymbol{\lambda}, \boldsymbol{\gamma}) \equiv ([\boldsymbol{\alpha}, \boldsymbol{\gamma}], \boldsymbol{\gamma}) \equiv 0$. This means that primary invariants type I should exist in both cases. Moreover, $\boldsymbol{\gamma}$ is a solution of the equations for this invariant with $s = 0$. The corresponding equations in Plank's form are $A^T\boldsymbol{\gamma} = \mathbf{0}$; $(\boldsymbol{\gamma}, \mathbf{b}) = 0$ for the constant of motion

$$K(x) = \prod_{i=1}^{3} x_i^{\gamma_i}. \tag{36}$$

7. THE "MANIFESTLY BI-HAMILTONIAN" EQUATIONS

With the invariant (36), we can write, using Gümral and Nutku's expression, the "manifestly bi-Hamiltonian form" of the equations of motion of the system as

$$\dot{\mathbf{x}} = m(x)[\nabla H, \nabla K], \tag{37}$$

so that

$$\mathbf{j}_H = m(x)\nabla K \quad \text{and} \quad \mathbf{j}_K = -m(x)\nabla H, \tag{38}$$

where the scalar function $m(x)$ is defined from (37) using a component of the vector field:

$$m(x) = \prod_{i=1}^{3} x_i^{1-\gamma_i-\alpha_i} \quad \text{for} \quad (26), (27)$$

and

$$m(x) = x_1 \prod_{i=1}^{3} x_i^{1-\gamma_i} \quad \text{for} \quad (28). \qquad (39)$$

Along this line, we get the correct form of Poisson structure matrices with Plank's Hamiltonian functions in the dual representation

$$\mathbf{j}_H = m(x) \prod_{i=1}^{3} x_i^{\gamma_{i-1}} (\gamma_1 x_2 x_3, \gamma_2 x_1 x_3, \gamma_3 x_1 x_2)^T, \quad (40)$$

which is equivalent to (31), containing quadratic terms due to their origin from ∇K. The Poisson structure matrices for the time-independent case of the invariant $\mathcal{J}_{\mathrm{I}}$ of Cairó and Feix contain only cubic terms when this invariant exists together with Plank's Hamiltonian function (27), and with Hamiltonian functions (26) and (28), the quadratic terms are also included. In the dual representation, the expressions for the Poisson structure matrices corresponding to the invariants (26) and (27) are

$$\mathbf{j}_K = -\prod_{i=1}^{3} x_i^{-\gamma_i} \begin{pmatrix} (\alpha_1 L + B_1 x_1) x_2 x_3 \\ (\alpha_2 L + B_2 x_2) x_1 x_3 \\ (\alpha_3 L + B_3 x_3) x_1 x_2 \end{pmatrix} \qquad (41)$$

with

$$L = B_0 + \sum_{l=1}^{3} B_l x_l,$$

and for the invariant (28),

$$\mathbf{j}_K = -\prod_{i=1}^{3} x_i^{-\gamma_i} \begin{pmatrix} (\alpha_1 x_1 - B_0 - B_2 x_2 - B_3 x_3) x_2 x_3 \\ (\alpha_2 x_1 + B_2 x_2) x_1 x_3 \\ (\alpha_3 x_1 + B_3 x_3) x_1 x_2 \end{pmatrix}. \quad (42)$$

These should be compared with the results of Haas and Goedert, since the additional constraints imposed in [15] are satisfied for interaction matrices (32) when $B_1 = B_2 = B_3$.

8. NONDEGENERATE 3*D* INTERACTION MATRICES

The degeneracy of interaction matrices (32) in the case of Plank's Hamiltonian function (26) is implied in the three-dimensional case by the conditions of the corresponding theorem $C\boldsymbol{\alpha} = \mathbf{b}$, $a_{il} = B_l(b_i + c_{il})$. However, in the case of Plank's theorem for the Hamiltonian function (27), the conditions $\mathbf{b} = \mathbf{0}$, $A^T\boldsymbol{\alpha} = -\overrightarrow{\mathrm{diag}}(A)$, and $B_i d_{ik} = -B_k d_{ki}$ do not imply the degeneracy of A. In the latter case, if a row $\epsilon(B_1, B_2, B_3)$ is added to each row of a degenerate interaction matrix $\tilde{A}$, the corresponding matrix D (13) remains the same. The determinant of the new interaction matrix A is nonzero; thus, the invariant $K(x)$ ceases to exist for the new system. The phenomenon appearing in such a case is clear from the following example with $\epsilon = 1$ and $\mathbf{b} = \mathbf{0}$:

$$\tilde{A} = \begin{pmatrix} -2 & 1 & 0 \\ 1 & 0 & -1 \\ 0 & -1 & 2 \end{pmatrix} \longrightarrow A = \begin{pmatrix} 1 & 0 & 3 \\ 4 & -1 & 2 \\ 3 & -2 & 5 \end{pmatrix}, \qquad (43)$$

with the constant of motion

$$\tilde{H}(x) = x_1^{-3/4} x_2^{1/2} x_3^{-3/4} (3x_1 - x_2 + 3x_3) \qquad (44)$$

common to both systems. It is a Hamiltonian function of the type (26) for $\tilde{A}$, but it is not for the new system with the interaction matrix A, since the values of the components of the vector field coincide for these two matrices only in the invariant plane $\bar{P}: 3x_1 - x_2 + 3x_3$ of the invariant $\mathcal{J}_{\mathrm{II}}$, defined in [11]. Thus, the conditions of Plank's theorem for this case are not sufficient to reproduce even the phase portrait of the differential equation.

However, all the known examples of Hamiltonian structures for LVE up to this moment have been of degenerate interaction matrices for the case $N = 3$. Here follows an example with a nondegenerate interaction matrix with a bi-Hamiltonian structure of Lie–Poisson form:

$$A = \begin{pmatrix} -\alpha & \beta & \gamma \\ \alpha & -\beta & \gamma \\ \alpha & \beta & -\gamma \end{pmatrix}, \quad \mathbf{b} = \mathbf{0}, \qquad (45)$$

$$H_1 = x_1(\beta x_2 - \gamma x_3), \quad H_2 = x_2(\alpha x_1 - \gamma x_3); \quad (46)$$

$$\mathbf{j}_{H_1} = -\frac{1}{\gamma} \begin{pmatrix} \alpha x_2 \\ \alpha x_1 - \gamma x_3 \\ -\gamma x_2 \end{pmatrix}, \qquad \mathbf{j}_{H_2} = \frac{1}{\gamma} \begin{pmatrix} \beta x_2 - \gamma x_3 \\ \beta x_1 \\ -\gamma x_1 \end{pmatrix}. \qquad (47)$$

Equations (45) were derived by Brenig [17] from the equations of an asymmetric top and resonant three-wave interaction system. The Hamiltonian functions (46) could be thought of as secondary invariants of

Cairó and Feix, since Plank's Hamiltonian function of the type (27) must have all coefficients $B_l \neq 0$ in the linear polynomial expression. The Poisson structures (47) are not equal to those given in [6] for Euler's top, but are of the same linear type.

9. CONCLUSIONS

The conditions of Plank's theorems on the Hamiltonian systems for LVE with Hamiltonian functions of the types (26)–(28) are not sufficient to reproduce the vector field of LVE with quadratic Poisson structure matrix (24). For (27), the conditions are not sufficient to reproduce even the phase portrait of LVE (43). A modified Poisson structure matrix (31) should be used, and an additional constraint $\det(A) = 0$ is implied in the $3D$ case of the Hamiltonian function (27).

In the $3D$ case, the interaction matrices (32) and (33) are identically degenerate, implying the existence of the second Hamiltonian function (36) and allowing the Poisson structure matrices to be obtained using the gradients of the two Hamiltonians.

In three dimensions, Lie–Poisson-type structures may appear in the cases when secondary linear polynomial invariants of Cairó and Feix exist.

Plank's conditions for the absence of time dependence of the constants of motion are more exact than those of Cairó and Feix. The existence of a sufficient number of time-independent constants of motion is important, since it makes possible a direct application of a bi-Hamiltonian [6] or, more generally, multi-Hamiltonian [18, 19] formulation, thus leading to complete integrability.

With the exception of the case of the Volterra invariant, the correct forms of Poisson structure matrices include the product of certain powers of dependent variables, which give their contributions to the left-hand sides of the Jacobi identities, implying some additional constraints when $N > 3$. For instance, in the case of $N = 4$, either the Poisson structure matrix and the interaction matrix are both degenerate, or the Hamiltonian function is linear.

NOTE ADDED IN PROOF

The work by M. Plank "Bi-Hamiltonian Systems and Lotka–Volterra Equations: A Three-Dimensional Classification" [M. Plank, Nonlinearity **9**, 887 (1996)], which contains, in particular, some results to those in Section 7, was not available to us when this report was submitted.

REFERENCES

1. V. Volterra, *Léçons sur la théorie mathematique de la lutte pour la vie* (Gauthier Villars, Paris, 1931).
2. E. H. Kerner, J. Math. Phys. **38**, 1218 (1997).
3. L. D. Faddeev and L. A. Takhtajan, *Hamiltonian Method in the Theory of Solitons* (Springer-Verlag, Berlin, 1987; Nauka, Moscow, 1988).
4. P. Damianou, Phys. Lett. A **155**, 126 (1991).
5. O. Bogoyavlensky, Phys. Lett. A **134**, 34 (1988).
6. H. Gümral and Y. Nutku, J. Math. Phys. **34**, 5691 (1993).
7. B. Grammatikos, J. Moulin-Ollagnier, A. Ramani, *et al.*, Physica A **163**, 683 (1990).
8. Y. Nutku, Phys. Lett. A **145**, 245 (1990).
9. A. G. Galperin, V. M. Dubovik, and V. S. Richvitsky, *CMCP96, Book of Abstracts*, D5, 11-96-300 (JINR, Dubna, 1996), p. 69; Preprint No. R4-97-340, JINR (Dubna, 1997); V. M. Dubovik, A. G. Galperin, V. S. Richvitsky, *et al.*, Preprint Nos. E4-97-416, E4-97-417, JINR (Dubna, 1997); V. S. Richvitsky, A. G. Galperin, and V. M. Dubovik, Preprint No. R4-98-42, JINR (Dubna, 1998).
10. A. Nagai and J. Satsuma, J. Phys. Soc. Jpn. **64**, 3669 (1995).
11. L. Cairó and M. R. Feix, J. Math. Phys. **33**, 2440 (1992).
12. M. Plank, J. Math. Phys. **36**, 3520 (1995).
13. L. Cairó, M. R. Feix, and J. Goedert, Phys. Lett. A **140**, 421 (1989).
14. J. Goedert, F. Haas, D. Hua, *et al.*, J. Phys. A **27**, 6495 (1994).
15. F. Haas and J. Goedert, Phys. Lett. A **199**, 173 (1995).
16. L. Cairó and M. R. Feix, J. Math. Phys. **37**, 3644 (1996).
17. L. Brenig, Phys. Lett. A **133**, 378 (1988).
18. J. Hietarinta, J. Phys. A **30**, L27 (1997).
19. R. Chatterjee, Lett. Math. Phys. **36**, 117 (1996).

Physics of Atomic Nuclei, Vol. 63, No. 4, 2000, pp. 635–641. From Yadernaya Fizika, Vol. 63, No. 4, 2000, pp. 701–707.

VIII INTERNATIONAL CONFERENCE ON SYMMETRY METHODS IN PHYSICS

Semiclassical Model of Atomic Collisions: Stopping and Capture of Heavy Charged Particles and Exotic Atom Formation*

W. A. Beck

MicroSound Systems, Issaquah, WA 98027, USA

Abstract—The semiclassical approach to modeling atomic collision systems lies between the easy classical model, which is most useful for simple systems in which quantum effects can be neglected, and the full quantum mechanical description, which is generally too difficult for more than simple systems. By adding a mathematical model of quantum-mechanical effects to a classical Hamiltonian, the calculational simplicity of the many-bodied classical model can be extended to the quantum realm; the validity of this approach can be measured by the degree to which the semiclassical model can replicate experimental data. Evolving from earlier work by Kirschbaum and Wilets, our model uses momentum-dependent pseudopotentials to exclude particles from quantum mechanically forbidden regions of phase space: a Heisenberg pseudopotential stabilizes the system by preventing atomic electrons from collapsing into the nucleus, while a Pauli pseudopotential holds identical electrons apart in phase space, structuring the electron configuration. This semiclassical model of an atom is then used as a target in collision simulations with a heavy projectile, which is itself treated classically. Collision cross sections are calculated from a series of simulation runs with Monte Carlo target orientations and impact parameters. The model is dialed in to match published experimental proton stopping powers, then applied to other systems of interest. Here, we present stopping and capture cross sections for antiprotons colliding with our semiclassical model of He. Antiproton stopping on He is compared with the results reported recently by the OBELIX group, and initial capture states are discussed in some detail, including a comparison with the quantum-mechanical calculations originally presented by Yamazaki and Ohtsuki and the later paper by Shimamura; among the differences: (1) In our calculations, the angular momentum of captured antiprotons obeys the classical limit $l = n$, and (2) the angular momentum distribution of our $He^+\bar{p}$ states extends beyond that of the quantum calculations. It should be emphasized that our calculations are for times much shorter than the metastable lifetimes. © *2000 MAIK "Nauka/Interperiodica".*

1. INTRODUCTION

Classical Trajectory Monte Carlo (CTMC) calculations of charged particle collisions, in which individual collisions are calculated microscopically and then averaged over an ensemble of initial conditions, have long been used to model collision processes in simple systems. The lack of any quantum mechanics in the CTMC approach, however, apparently limited it to systems in which quantum effects played a small role, e.g., single heavy charged particle collisions with very simple targets such as H and He^+, or in which one active electron was treated classically in the mean field of the rest of the target; in classical models of multielectron atoms, outer electrons evaporate, while inner electrons collapse into the nucleus.

Following the approach of Kirschbaum and Wilets [1], our semiclassical trajectory Monte Carlo (STMC) method uses momentum-dependent pseudopotentials of the general form

$$V = \frac{\xi^2\hbar^2}{4\alpha r^2}\exp\{\alpha[1-(rp/\xi\hbar)^4]\} \quad (1)$$

to exclude electrons from forbidden regions of phase space; $\xi\hbar$ is the size of the forbidden region, and α is the hardness of the exclusion. Effective use of this approach requires an understanding of how these parameters determine the static and dynamic behavior of the atomic model [2].

2. THE SEMICLASSICAL MODEL OF AN ATOM

With atomic units $\hbar = e = m_e = 1$, the semiclassical N-electron atom of atomic number Z is described by

$$H_{sc} = T + V_z + V_{ij} + V_H + V_P \quad (2)$$
$$= \sum_{i=1}^{N}\left[\frac{p_i^2}{2} - \frac{Z}{r_i} + V_H(r_i, p_i)\right] + \sum_{i<j}\left[\frac{1}{r_{ij}} + V_P(r_{ij}, p_{ij})\right],$$

where $\mathbf{r}_i$ and $\mathbf{p}_i$ are the positions and momenta of the atomic electrons relative to the fixed nucleus and r_{ij} and p_{ij} are the relative coordinates of electron pairs;

$$V_H(r_i, p_i) = \frac{\xi_H^2}{4\alpha_H r_i^2}\exp\{\alpha_H[1-(r_i p_i/\xi_H)^4]\} \quad (3)$$

is the Heisenberg pseudopotential which prevents collapse of electrons into the nucleus;

* This article was submitted by the author in English.

1063-7788/00/6304-0635$20.00 © 2000 MAIK "Nauka/Interperiodica"

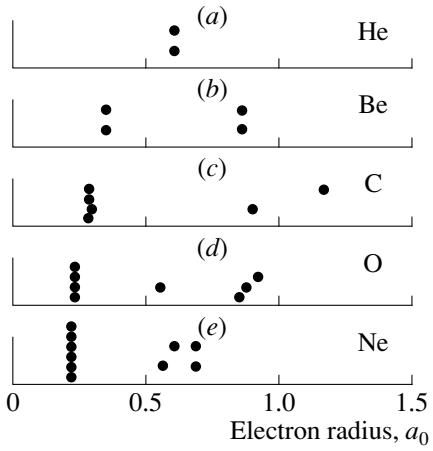

Fig. 1. Radial distribution of semiclassical ground-state electrons for (*a*) He, (*b*) Be, (*c*) C, (*d*) O, and (*e*) Ne.

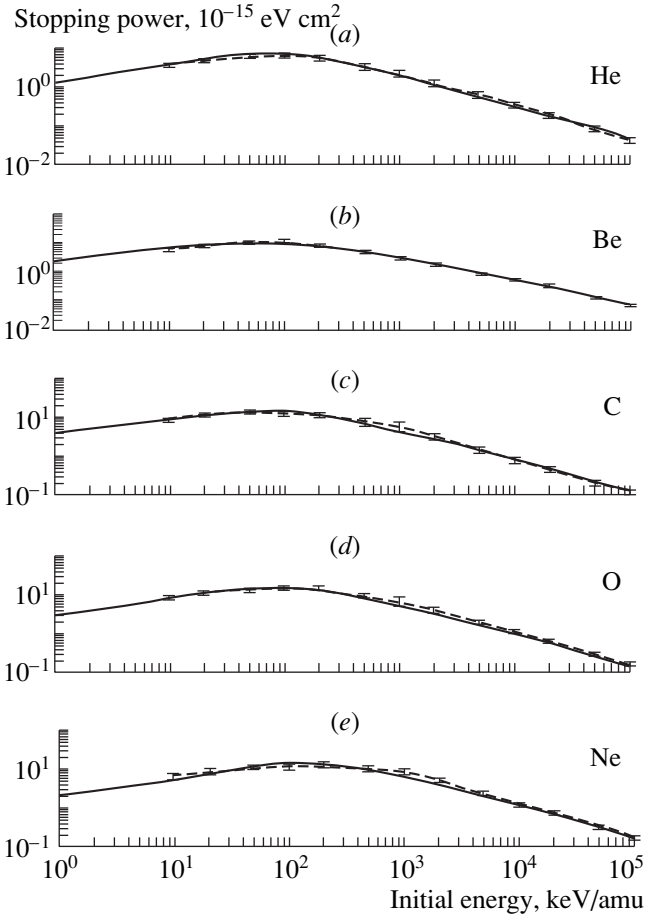

Fig. 2. Semiclassical vs experimental proton stopping powers for (*a*) He, (*b*) Be, (*c*) C, (*d*) O and (*e*) Ne.

$$V_P(r_{ij}, p_{ij}) = \frac{\xi_P^2}{4\alpha_P r_{ij}^2}\exp\{\alpha_P[1-(r_{ij}p_{ij}/\xi_P)^4]\}\delta_{s_i s_j} \quad (4)$$

is the Pauli pseudopotential, separates identical electron pairs (electron spin $s_i = s_j$), resulting in an electron structure in the ground state atom.

This semiclassical model of an atom is minimized to find a stable ground state in which the electrons, while at rest, have nonzero momenta in the presence of momentum-dependent pseudopotentials. Proper choice of the parameters α_H, ξ_H, α_P, and ξ_P is essential to provide a physically reasonable ground state model which will not distort collision dynamics. Figure 1 illustrates the radial distribution of ground-state electrons for our semiclassical models from He to Ne. While all of these ground states have the correct total binding energy, the electron configurations were not chosen to meet any particular detail of real atomic ground states, e.g., first ionization potentials or mean electron radii, but were chosen as reasonable overall approximations of ground state conditions for use in collision studies.

3. SEMICLASSICAL COLLISION MODELING; STOPPING POWER

The total Hamiltonian for a proton colliding with a fixed nucleus of a semiclassical atom is given by

$$H_{sc+p} = H_{sc} + \frac{P^2}{2M} - \frac{Z}{R} - \sum_{i=1}^{N}\frac{1}{|\mathbf{r}_i - \mathbf{R}|}, \quad (5)$$

where **R** and **P** are the coordinates of the proton relative to the nucleus. To model collisions, the classical equations of motion for this system,

$$\frac{dx_i}{dt} = \frac{\partial H}{\partial p_i}, \quad \frac{dp_i}{dt} = -\frac{\partial H}{\partial x_i}, \quad (6)$$

are solved for $\mathbf{r}_i$, $\mathbf{p}_i$ and **R**, **P** over time. Note that there is no pseudopotential term $V_{H,p}(|\mathbf{r}_{i,p}|, |\mathbf{p}_{i,p}|)$ between the projectile and the target electrons; V_H is used only to stabilize the target system, and all interactions between the target and the projectile are via the Coulomb forces.

Quantum uncertainty is rolled into the model by averaging over a sequence of collision calculations using Monte Carlo initial conditions: target distributions are generated by separate, solid body rotation and parity inversion of the electron positions and momenta, and impact parameters are randomized with equal areas πdb^2 up to some b_{max}. The same Monte Carlo seed is used for sequences of collisions allowing calculation of collision cross sections from repeatable ensembles of initial conditions. For *N* collisions starting with such initial conditions, the total energy-loss cross section or stopping power, $\sigma\Delta E$, is calculated from the average proton-energy loss as

$$\sigma\Delta E(E_0) = \pi b_{max}^2 \frac{1}{N}\sum_{i=1}^{N}\Delta E_i(E_0) \quad (7)$$

with an uncertainty

$$\delta(\sigma\Delta E) = \pi b_{max}^2\left[\frac{1}{N}(\langle(\Delta E_i)^2\rangle - \langle\Delta E_i\rangle^2)\right]^{1/2}. \quad (8)$$

Figure 2 shows the semiclassical stopping powers calculated for the semiclassical He to Ne targets depicted above in Fig. 1; with correct design of the target systems, good agreement with the experimental data is obtained [2].

4. STOPPING AND CAPTURE OF NEGATIVELY CHARGED PARTICLES

To first order, the atomic stopping of positive and negative particles is equivalent, as is shown in the first-order treatment of the Born approximation [3]. The Barkas effect [3–5] is the reduction in the atomic stopping of negative particles relative to positive particles at lower projectile energies, around the region of maximum stopping. In concept, the Barkas effect is fairly straightforward: as the projectile slowly approaches the atomic target, at a velocity on the order of the electron velocities, it will have time to interact with the electron cloud, and Coulomb forces deform the electron cloud toward or away from the projectile, increasing or decreasing the interaction between the electrons and the projectile, thus splitting the (primarily electron) stopping of the atomic target for projectiles of opposite charge.

Theoretical analyses of this effect remain fairly complicated [5, 6], but it is understood that higher order terms, including electron–electron correlations, play a significant role. In the Born approximation, the first-order term in the energy loss of heavy charged particles is proportional to Z_1^2, where Z_1 is the charge of the projectile; the next higher order Born term is proportional to Z_1^3; thus, a change of sign in the projectile charge changes the contribution of this term [3]. The unique advantage of the STMC approach to collision modeling is its simultaneous treatment of all particles in the collision system, thus incorporating all of the higher order terms due to multiple particle interactions, terms which are not well handled by methods which must average over a large number of particles in order to make their calculations tractable. This advantage shows up in calculation of the stopping powers of negatively charged particles.

In our initial study of antiproton stopping on He, we used the technique described above for proton stopping, averaging the results of 5000 collision calculations performed at a series of fixed initial energies, each time using the same ensemble of initial conditions for target configuration and impact parameter. We extended our calculations down to 0.01 keV/amu, allowing us to rough out the behavior of our model when applied to antiprotons, particularly in the lower velocity region of interest for antiproton capture. Figure 3 plots these STMC antiproton stopping powers against the recent antiproton stopping powers of the OBELIX group [7]; the proton experimental values are shown for comparison. Our results differ somewhat from the OBELIX values, but the differences are comparable to those obtained from the current (and much more complicated) state of the art in quantum approximations to this problem, the atomic orbital method of Schiwietz and Grande, which involves calculation of several hundred atomic orbital base states [8]. As shown in Fig. 4, which details the ionization and capture cross sections for these collisions, capture begins

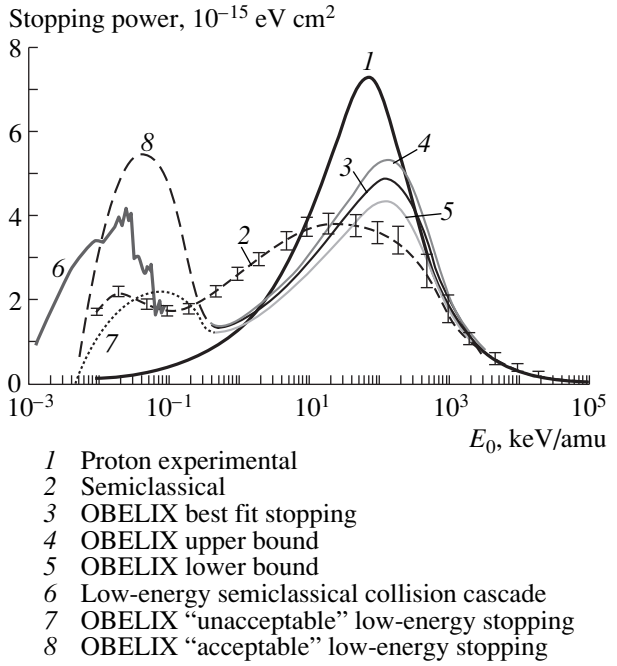

Fig. 3. Low-energy, semiclassical collision cascade antiproton stopping powers compared to the higher energy semiclassical results calculated from discrete initial energies and compared with the recent experimental results of the OBELIX group.

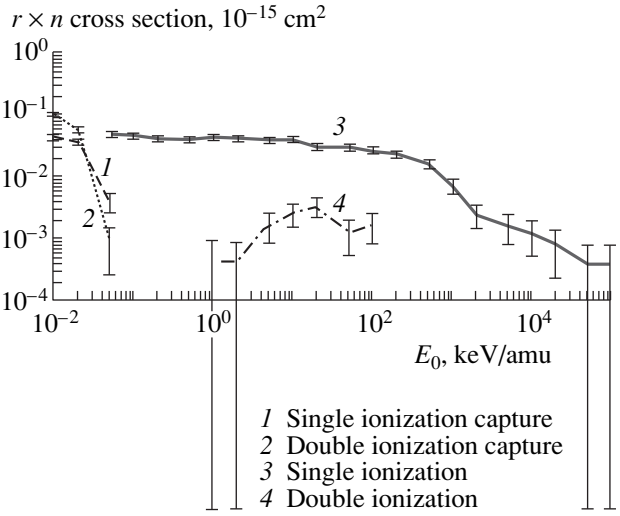

Fig. 4. Semiclassical cross sections for antiproton single and double ionization of the He target and for antiproton capture onto the He target via single and double ionization.

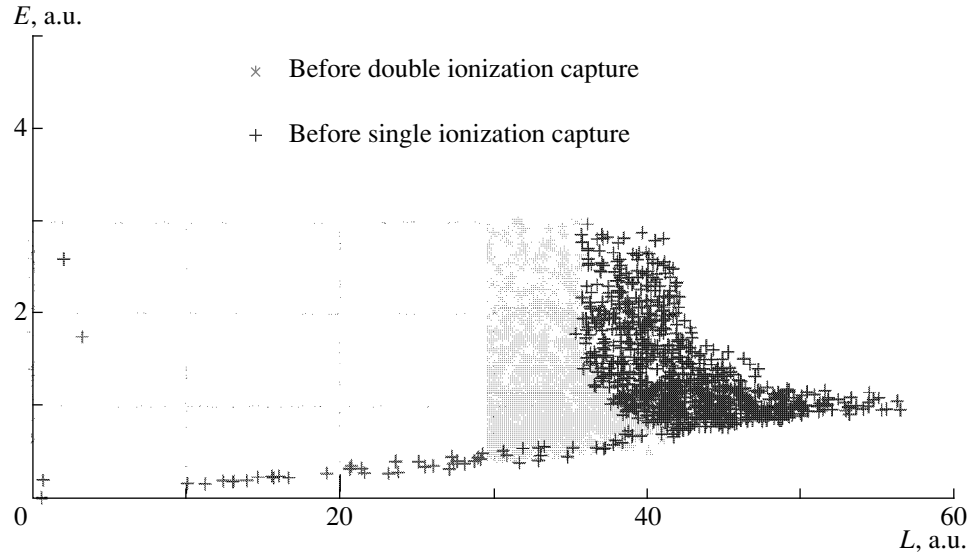

Fig. 5. Antiproton energies and angular momenta at the start of the collisions leading to capture on helium at the end of the collision cascade.

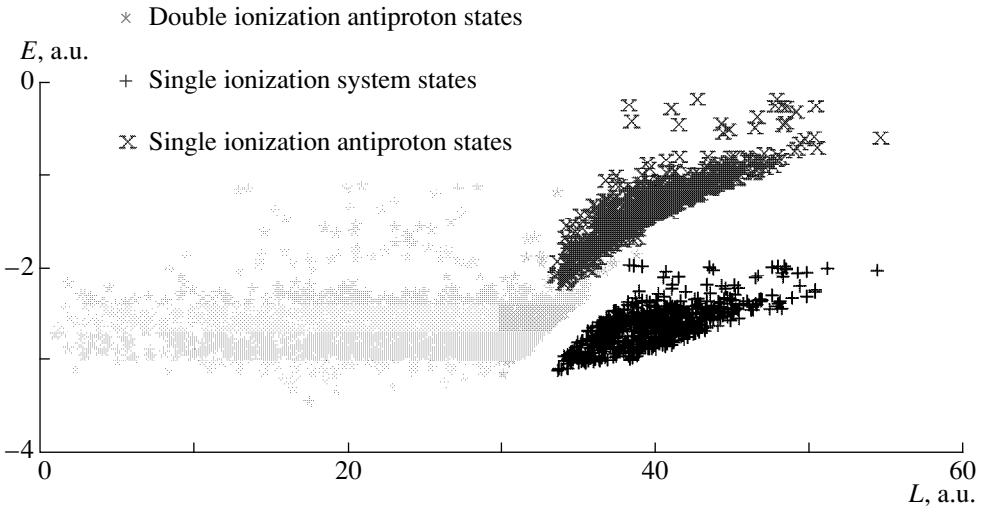

Fig. 6. Energies and angular momenta of antiprotons captured at the end of the collision cascade via single and double ionization; total system energy and angular momentum for the neutral $\bar{p}He^+$ system.

near the low-energy end of this data set, at an energy roughly equal to that observed experimentally; capture via single ionization into the neutral $\bar{p}\,He^+$ is much less frequent than the double ionization capture into $\bar{p}\,He^{++}$; the large error bars result from the small number of capture and ionization events in this approach.

To obtain a more realistic picture of the capture process, we developed a collision cascade [9], in which antiprotons were started with an energy above the onset of capture, then followed as they slowed via a sequence of collisions until capture occurred. Figure 3 shows that our cascade stopping powers fall between the OBELIX "acceptable" and "unacceptable" estimates. Given the current state of experimental knowledge, the fact that the STMC method yields results in the right ball park, particularly at the lower energies, where capture begins to occur and the experimental uncertainties remain quite high [7, 10, 11], is more reassuring than the specific disagreements with experiment are disquieting; even in this difficult low-velocity region, where the projectiles are actually stopped and capture processes begin to predominate, the STMC approach remains a reasonable approximation to the imperfectly understood experimental situation.

The larger number of capture events resulting from the collision cascade provided a better picture of the capture process; most captured antiprotons would quickly annihilate, but the distribution of those cap-

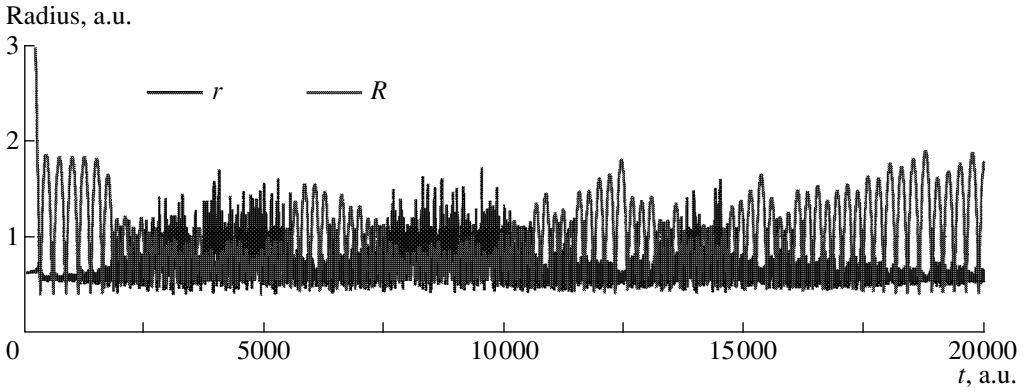

Fig. 7. Typical antiproton–electron dynamics after capture via single ionization; the high-velocity electron trajectory (r) is aliased from undersampling.

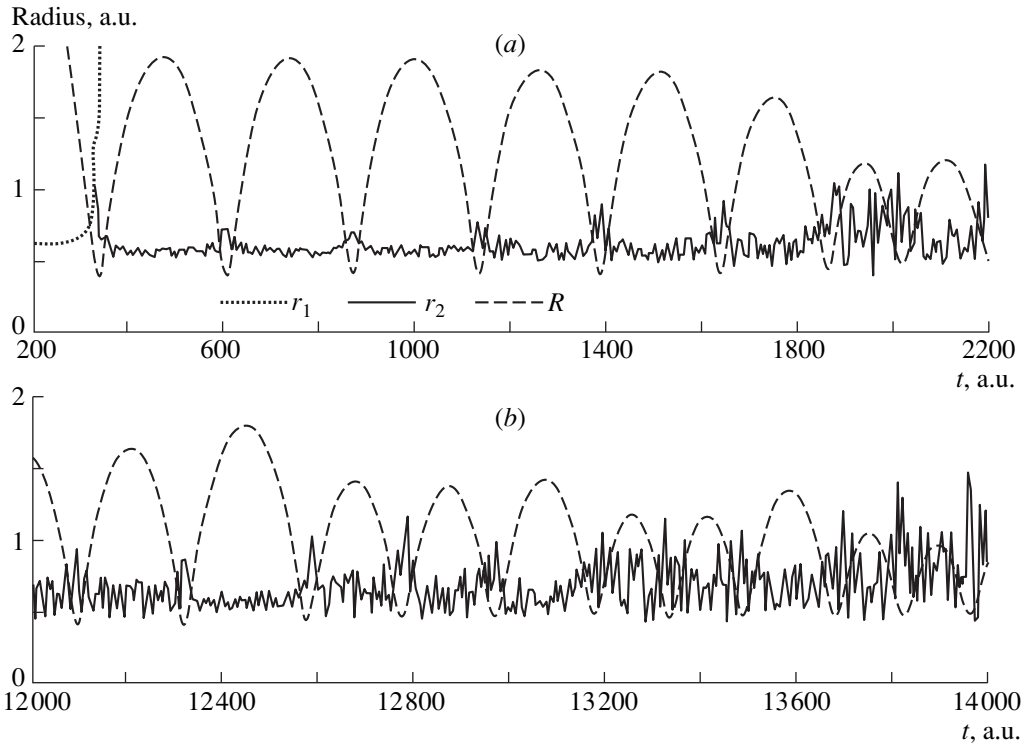

Fig. 8. Expanded view of antiproton–electron dynamics (a) immediately after antiproton capture and (b) after t = 12000 a.u.; the electron trajectory (r_2) is again aliased due to undersampling.

tured by single ionization into the potentially metastable Condo–Russell states could then be studied in greater detail.

5. CAPTURE ANALYSIS

Figure 5 shows the distribution of antiproton energies and angular momenta at the start of the last stage of the collision cascade, just prior to capture; due to the limited amount of energy and angular momentum that can be exchanged by the massive antiproton and the bound electrons of the He atom, antiproton energies and angular momenta which result in capture fall into a fairly narrow range. Figure 6 shows the energies and angular momenta of the states into which antiprotons were captured at the end of the collision cascade. The continuous distribution of antiprotons prior to capture has split into separate, distinct distributions of energy and angular momentum; the higher energy, higher angular momentum antiprotons have only been able to ionize a single electron during the capture process and have been captured into the higher energy and angular momentum states of Fig. 6.

Of the 4000 collision cascades followed until capture, 916, or about 23%, ended with capture via single

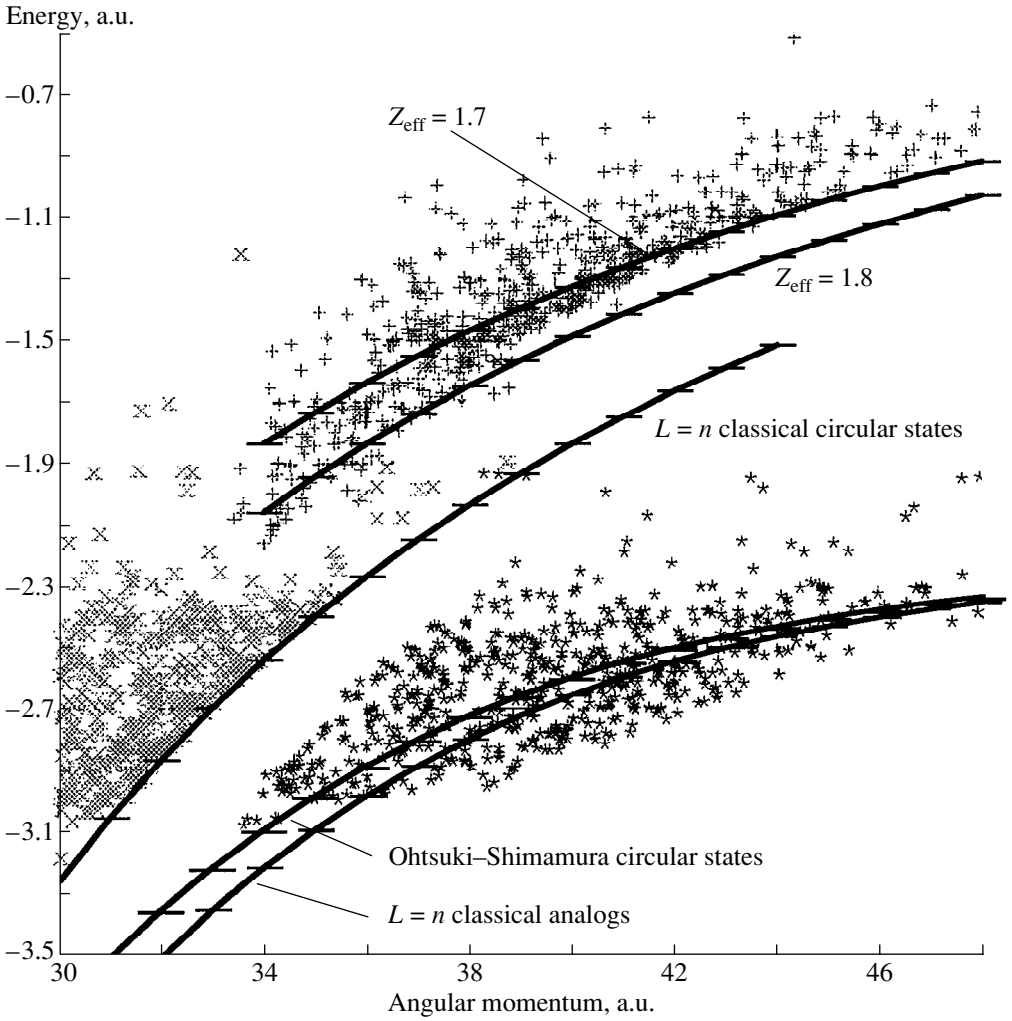

Fig. 9. Comparison of the center of the capture distributions of Fig. 6 with calculated antiproton states.

electron ionization into the neutral exotic $\bar{p}\,He^+$, while the remaining 77% resulted in capture via double ionization into a positively charged $\bar{p}\,He^{++}$. While significantly larger than the observed metastable fraction of 3.6%, the value of our primary population of neutral antiprotonic helium is comparable to that obtained by Korenman, who used a semiclassical calculation for coupled two-particle and three-particle channels to estimate the primary population of antiprotons captured into high l orbitals by an isolated helium atom at 30% [12, 13] and reasoned that the higher lying states would be quickly destroyed by collisions with other atoms in the target medium.

In our model, after capture via single ionization, the antiproton continues to interact and exchange energy and angular momentum with the remaining electron, so each of the single ionization antiproton states plotted in Fig. 6 represents a time average of the antiproton configurations. The (constant) total sum of the antiproton and electron energy and angular momentum in these neutral antiprotonic helium atoms are the quantities used by Yamazaki and Ohtsuki in their original analysis of the metastability [14].

Figure 7, showing the changing electron and antiproton radii after antiproton capture, is an example of the overall nature of antiproton–electron dynamics in a typical $\bar{p}\,He^+$ system; because of the much higher velocity of the electron relative to the antiproton, the electron trajectory is unavoidably undersampled and aliased. This antiproton is initially captured into a fairly eccentric orbit with $R \simeq 0.5$–2, from which it has little interaction with the electron until about $t = 1800$, at which time its orbit begins to tighten and become less eccentric, and the antiproton–electron interaction increases, as shown by the increased eccentricity of the electron orbit from $t \simeq 2000$ to 5500; the amount of antiproton–electron interaction continues to vary over the time, with the final conditions at $t = 20000$ similar to those existing shortly after initial capture of the antiproton.

Figure 8 provides expanded views of the system dynamics of Fig. 7. Figure 8*a* depicts the initial dynamics after capture, including the immediate ionization of e_1, the initial stability of e_2, and the change in system dynamics as the antiproton–electron interaction begins to increase for $t > \sim 1800$. Figure 8*b* illustrates the continuing variation in the amount of antiproton–electron interaction as the antiproton and electron continue exchanging angular momentum as the system evolves after capture.[1)]

Figure 9 overlays the expanded view of the central portion of the capture distributions of Fig. 6 with calculated antiprotonic states: The antiprotons in the doubly ionized $\bar{p}He^{++}$ stack up against the classical $L = n$ circular states, while antiprotons in the singly ionized $\bar{p}He^{+}$ stack up against the $L = n_{\text{eff}}$ circular states for $Z_{\text{eff}} \simeq 1.7$–$1.8$. Note that the $\bar{p}He^{+}$ system states extend well beyond the $E_{0,j}$ circular boundary calculated by Shimamura [15], which is essentially the $L = n - 1$ circular boundary of Ohtsuki [14]; this results from the excitation of the remaining electron to higher angular momentum states during the capture process. As discussed in our original paper on this topic [9], this is an entirely reasonable result: because of the infinite range of the Coulomb potential, the total system energy level diagram of $E(L)$ should extend further to the right than the Ohtsuki–Shimamura circular boundaries, since electrons in hydrogenic states of arbitrarily small energy and arbitrarily large angular momentum can be added to any of the simple $\bar{p}He^{++}$ states. It appears that neither Ohtsuki nor Shimamura located these states, because neither included electron base states of $l > 1$ in their quantum-mechanical calculations of the system; in the semiclassical system, it is clear that the antiproton can transfer angular momentum to the electron during the capture process and can continue to exchange angular momentum as it interacts with the electron after capture into $\bar{p}He^{+}$, as shown in Figs. 7 and 8.

6. SUMMARY AND CONCLUSIONS

The good agreement obtained to experimental proton stopping power values with our semiclassical model, in particular, in the difficult region of maximum stopping, where the proton collides with a velocity on the order of the Bohr velocity, resulting in complex, many-body interactions with the target electrons, allows us to apply the model with greater confidence to less well-defined experimental problems such as antiproton capture on helium.

The semiclassical description allows a detailed examination of the antiproton capture process, including the continuing exchange of energy and angular momentum between the antiproton and the electron after initial capture, and a prediction of antiproton capture states with higher total angular momentum than have been found in the more complicated treatments of this system. Whether or not these states actually exist remains an open question, but this treatment of antiproton capture on helium provides a good example of the "less is more" nature of the semiclassical method: by approximating a complex quantum-mechanical system with a more manageable model, calculations can proceed further than is possible in a more rigorous treatment, offering a greater, albeit approximate, insight into the overall nature of the system.

[1)]As in Fig. 7, undersampling of the much faster electron results in aliasing of the electron orbit, more visible on the expanded time scale of Fig. 8.

REFERENCES

1. C. L. Kirschbaum and L. Wilets, Phys. Rev. A **21**, 834 (1980).
2. W. A. Beck and L. Wilets, Phys. Rev. A **55**, 2821 (1997).
3. G. Basbas, Nucl. Instrum. Methods Phys. Res., Sect. B **232**, 227 (1984).
4. W. Barkas, J. Dyer, and H. Heckman, Phys. Rev. Lett. **11**, 26 (1963).
5. E. Uggerhoj, Nucl. Phys. A **558**, 665c (1993).
6. H. Knudsen and J. F. Reading, Phys. Rep. **212**, 107 (1992).
7. M. Agnello *et al.*, Phys. Rev. Lett. **74**, 371 (1995).
8. G. Schiwietz *et al.*, J. Phys. B **29**, 307 (1996).
9. W. A. Beck, L. Wilets, and M. A. Alberg, Phys. Rev. A **48**, 2779 (1993).
10. A. Adamo *et al.*, Phys. Rev. A **47**, 4517 (1993).
11. A. Adamo *et al.*, Nucl. Phys. A **558**, 665c (1993).
12. G. Y. Korenman, Primary Populations of Antiprotonic Helium (invited talk at the Workshop on Metastable Hadronic States in Helium, Balatonfured, Hungary, Jan. 26–28, 1995).
13. G. Y. Korenman, Primary Populations of Antiprotonic Helium and Effects of Collisions on Metastable States (invited talk at the ITAMP Workshop on Exotic Atoms, Cambridge, MA, July 11–13, 1996).
14. T. Yamazaki and K. Ohtsuki, Phys. Rev. A **45**, 7782 (1992).
15. I. Shimamura, Phys. Rev. A **46**, 3776 (1992).

Physics of Atomic Nuclei, Vol. 63, No. 4, 2000, pp. 642–647. From Yadernaya Fizika, Vol. 63, No. 4, 2000, pp. 708–713.

VIII INTERNATIONAL CONFERENCE ON SYMMETRY METHODS IN PHYSICS

Relativistic Theory of Atom–Laser Interactions at Very High Laser Intensities*

A. M. Ermolaev

Université Libre de Bruxelles, Belgium

Abstract—The high-frequency approximation of Kristić and Mittleman is considered in detail as a basis for the relativistic theory of atom–laser interactions. The properties of the 3*D* potentials are discussed. Within a one-dimensional model similar to that employed by Kylstra, Ermolaev, and Joachain in *ab initio* calculations on the time-dependent Dirac equation, the electron mass-shift due to dressing by a superstrong laser field is investigated. In the full domain of the laser parameters, the frequency ω and the peak field strength $\mathcal{E}_0$, the 1*D* bound states exhibit remarkable features. The numerical calculations show the existence of a very wide intermediate range of the field strengths where, in the zeroth order of the high-frequency approximation, the binding is stabilized by the field. © *2000 MAIK "Nauka/Interperiodica"*.

1. INTRODUCTION

The nonrelativistic theory of interactions between atoms and high-frequency, high-intensity laser fields is well developed in several complementary forms, all of which assume the dipole approximation. Theories based on the Floquet method include the high-frequency Floquet theory [1], the Sturmian–Floquet method [2], and the *R*-matrix Floquet theory [3]. An alternative approach is offered by *ab initio* time-dependent calculations carried out on atomic hydrogen [4, 5], as well as more recently on helium, particularly in [6], although at somewhat lower intensities. Recent accounts of work done in the nonrelativistic field can be found, e.g., in reviews [1, 7, 8].

The numerical studies of relativistic interactions between atoms and classical fields are more limited, although the full QED treatment of the problem was considered in the case of multiphoton ionization (MPI) some time ago [9]. The time-dependent Dirac equation for an atomic electron in the presence of a classical laser field has been solved only very recently. Kylstra *et al.* [10] considered a one-dimensional model, and Rathe *et al.* [11] examined a two-dimensional model. Prior to that, several classical and quantal models were considered in [12–15].

The high-frequency approach that was so fruitful in the nonrelativistic domain, particularly in the studies of atomic stabilization by strong laser fields, has not yet been explored in relativistic conditions, although the problem was formulated some time ago [16–18] and the general equations were presented. This talk draws attention to the high-frequency theory of Kristić–Mittleman (KM) [17] and presents some results obtained in the numerical solution of a 1*D* model problem.

* This article was submitted by the author in English.

2. RELATIVISTIC HIGH-FREQUENCY APPROXIMATION

The theory of Kristić–Mittleman [17] is a relativistic generalization of the zeroth order of Gavrila's nonrelativistic high-frequency theory described in detail in [1]. The unitary transformation U, $\Psi = U\Phi$, where Ψ is the wave function in the laboratory frame and Φ is the wave function in the relativistic Kramers–Henneberger (KH) frame, is obtained in the form

$$U(\mathbf{r}, \mathbf{r}', t) = \sum_q \Psi_q(\mathbf{r}, t)\chi_q^*(\mathbf{r}', t). \tag{1}$$

In equation (1), Ψ_q is the relativistic Volkov state, χ_q is a relativistic (Dirac) free state of an electron with the mass m^* dressed by the laser field, and summation in electron momentum q is extented to all components of the relativistic spinors. Generally, the expression is very complicated, and the resulting operator is nonlocal. However, it can be made local and considerably simplified if it is assumed that the wave functions contain only values of q that are small compared to mc. In the approximation of Kristić–Mittleman, the contribution from large q is neglected, only terms linear in q are retained in the phase, and only terms of order q^0 are retained in the prefactors of the matrix U. Then the matrix U is local and gives a time-dependent local potential $\mathcal{U} = U^{-1}VU$, where V is the nonrelativistic atomic potential.

The time-dependent Dirac equation in the relativistic KH frame takes the form (in atomic units used throughout)

$$i\frac{\partial\Phi}{\partial t} = [c\boldsymbol{\alpha}\cdot\mathbf{p} + \beta\mu c^2 + \mathcal{U}(\mathbf{r}, t)]\Phi, \tag{2}$$

where

$$\mathcal{U}(\mathbf{r}, t) = V(\mathbf{r}) - \beta_0 \sin\phi\boldsymbol{\gamma}(\phi) \tag{3}$$

1063-7788/00/6304-0642$20.00 © 2000 MAIK "Nauka/Interperiodica"

and

$$\boldsymbol{\gamma}(\phi) = \hat{\mathbf{e}}_x - \frac{1}{2}\hat{\mathbf{e}}_z \eta_0 \cos\phi. \quad (4)$$

In equation (3), it is assumed that the electric field $\mathscr{E}_0$ is directed along the x axis, the propagation vector $\mathbf{k}$ is directed along the z axis, and the parameters β_0 and η_0 are defined below by equation (8). On account of retardation, the total phase ϕ is defined as $\phi = \omega t - kz'(z)$, with $z'(z)$ to be obtained by inverting the transcendental equation

$$z = z' - \gamma_0 \sin 2\phi, \quad (5)$$

where $\gamma_0 = \beta_0\eta_0/4$.

$\mathcal{U}$ can be compared with the potential in the nonrelativistic KH frame. In both cases, the potentials have all harmonics, and further simplification is achieved by introducing the high-frequency approximation. As usual, the zeroth order is obtained by averaging the time-dependent KH potential over the laser period. In the relativistic case, however, this averaging procedure must take retardation into account.

Equation (2) provides a convenient model for the studies of coupling with the negative energy states in the presence of a superintense laser field. By reducing this equation to the Pauli form, the spin effects may be accounted for in a simpler form.

Further approximations in the main equation (2) are possible. Within the large-component approximation, which will be considered in this work, equation (2) for an atom in an intense, linearly polarized laser field takes the form of a Schrödinger equation with a static potential $\mathcal{U}_0$; thus,

$$[\mathbf{p}^2/2\mu + \mathcal{U}_0(\mathbf{r})]\Phi(\mathbf{r}) = W\Phi(\mathbf{r}), \quad (6)$$

where $\mathbf{p} = -i\nabla$ is the momentum operator, W is the nonrelativistic bound energy, and μ is the averaged electron mass dressed by the laser field [18]. For a monochromatic wave, the invariant time-averaged mass μ is given by

$$\mu = \sqrt{1 + \alpha_0^2\omega^2/2c^2}. \quad (7)$$

In equation (7), $\alpha_0 = \mathscr{E}_0/\omega^2$ is the classical quiver amplitude of a nonrelativistic electron oscillating in a laser field of frequency ω and field strength $\mathscr{E}_0$, and $c \approx 137$ is the velocity of light. Using the parameters

$$\beta_0 = \alpha_0/\mu, \quad \eta_0 = \omega\beta_0/2c, \quad (8)$$

the relativistic atomic potential of Kristić and Mittleman averaged over a cycle of the laser field is

$$\mathcal{U}_0(\mathbf{r}) = \frac{1}{2\pi}\int_{-\pi}^{\pi}(1 + \eta_0^2\cos 2\phi)\mathcal{U}(\mathbf{r}, \phi)d\phi, \quad (9)$$

where $\mathcal{U}$ is given by equation (3).

The zeroth-order equation (5) contains two laser parameters, $\mathscr{E}_0$ and ω (or β_0 and η_0), instead of a single parameter α_0 of the nonrelativistic high-frequency theory. The parameter β_0 is the quiver amplitude of the relativistic motion of the electron under the influence of the electric field of the laser. The parameter η_0 is of the same order of magnitude as the ratio of the quiver amplitude (i.e., the characteristic size of the atom in the laser field) to the wavelength of the laser field. The condition $\eta_0 \ll 1$ corresponds to the physical domain where the dipole approximation is justified. Beyond this approximation, the retardation correction is given by the $\eta_0^2\cos 2\phi$ term in equation (9), and the magnetic field enters equation (3). The curve defined by it is the classical figure-eight trajectory in the xz plane, and it corresponds to the electron motion in the reference frame where the average momentum is zero. The ratio of the amplitudes of the x and z oscillations is given by $\rho_0 = \frac{1}{4}\eta_0$. For a Coulomb potential V, the KM potential $\mathcal{U}_0$ has a logarithmic singularity on this curve [17].

We observe from equation (7) that the dressed mass μ scales as α_0 at ultrastrong field strengths $\mathscr{E}_0$. Hence, both β_0 and η_0 remain bound at a given laser frequency ω, and the potential (9) does not depend on the field $\mathscr{E}_0$ in this limit. The full domain of the parameter values is

$$0 \le \beta_0 \le \sqrt{2}c/\omega \approx 0.225cT, \quad 0 \le \eta_0 \le 1/\sqrt{2}, \quad 0 \le \rho_0 \le \sqrt{2}/8, \quad (10)$$

where T is the laser period. During one cycle, the electron travels a distance along x with a speed that does not exceed the velocity of light c whatever the magnitude of $\mathscr{E}_0$ may be. Consequently, the quiver amplitude β_0 is always finite. In the high-intensity limit, $\rho_0 = 0.1768$, and it does not depend on either amplitude or frequency of the field.

The upper panels of Fig. 1 show xz plots of the $y = 0$ cross section of the KM potential for the field strength of $\mathscr{E}_0 = 175$ a.u. and for two laser frequencies $\omega = 1$ and 2 a.u. The graphs $|\mathcal{U}_0|$ in Fig. 1 are for the Coulomb potential in the hydrogen atom. Note that, by taking a coarse grid, the singularities of the KM potential have been smoothed near the discontinuities.

Several general features can be seen in Fig. 1. The trace of the classical figure-eight trajectory on the potential surface can be clearly observed as a ridge. The dimensions of the ridges in Fig. 1 are those given by equation (8). The distortion of the potential surface in the vicinity of the origin is quite significant. The ridge of the potential formed all along the figure-eight line replaces the simpler picture of the Gavrila potential. In the latter, nonrelativistic, case and for linear polarization, the potential is square-root singular near the turning points and has a logarithmic singularity on the line connecting the turning points. This produces a distinctive dichotomic structure of the nonrelativistic potential

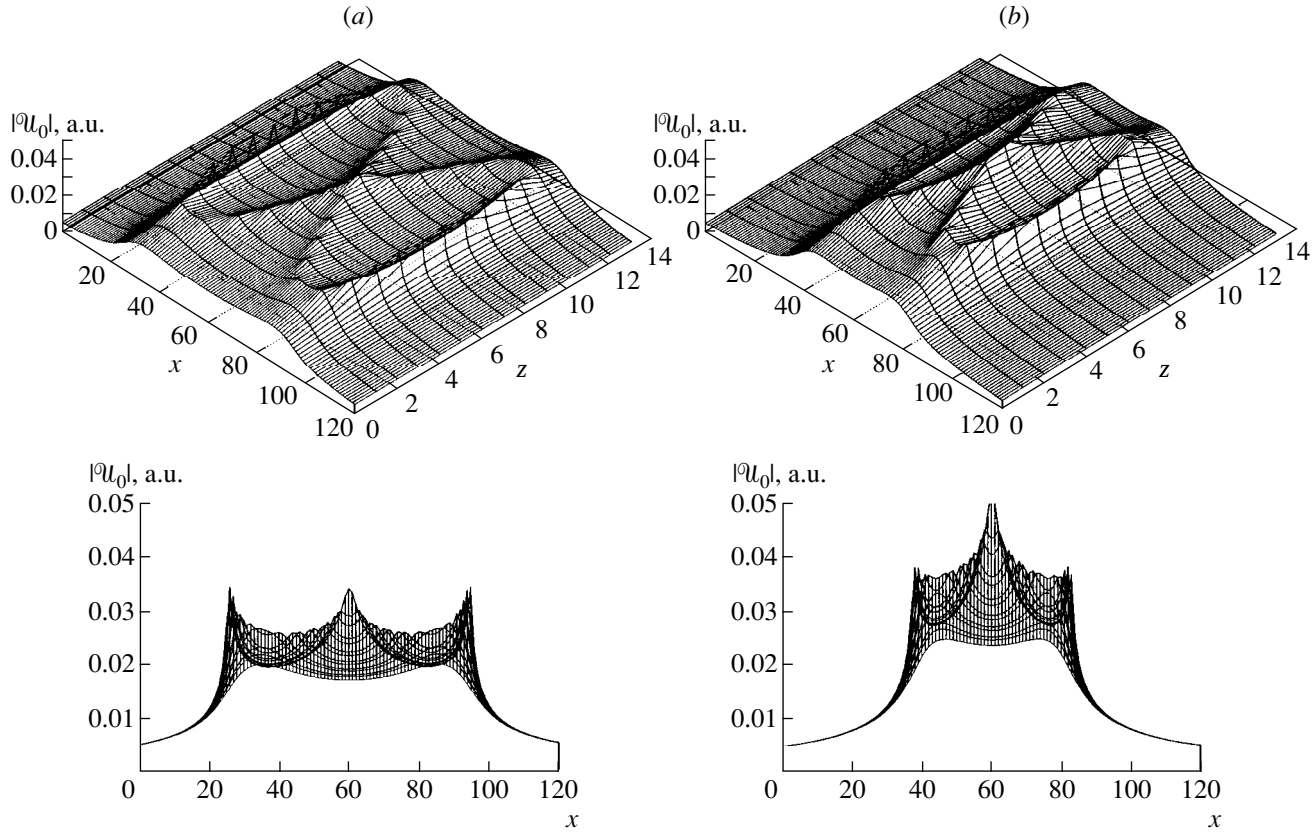

Fig. 1. The upper panel: *xz* plots of the 3*D* potential of Kristić and Mittelman, $|\mathcal{U}_0(x, 0, z)|$ (a.u.) for $\mathcal{E}_0$ = 175 a.u. The base areas correspond to $-225 \le x \le 225$, $-40 \le z \le 40$ (a.u.). (*a*): $\omega = 1$ a.u. ($\mu = 1.347$, $\beta_0 = 129.9$ a.u., $\eta_0 = 0.474$, $\rho_0 = 0.118$); (*b*): $\omega = 2$ a.u. ($\mu = 1.097$, $\beta_0 = 39.9$ a.u., $\eta_0 = 0.291$, $\rho_0 = 0.073$). The potential has been smoothed out. The ridges along the figure-eight curves represent a logarithmic singularity of varied strength. The lower panel: frontal views of the plots in the upper panel in the *z* (propagation) direction. Apart from the potential wells representing the turning points, there is a central potential well which becomes more prominent as the laser frequency ω increases.

and the ground state wave function in the KH frame. Kristić and Mittleman have suggested [17] that the dichotomy of the relativistic wave function may disappear in the high-intensity limit. Figure 1 shows that, even at such a high field strength as 175 a.u., it does not yet happen. The lower panels in Fig. 1 present the frontal view of the *xz* plots in the direction of propagation, with distinctive potential wells near the turning points and at the origin. This structure persists at the higher field strengths up to 1000 a.u. investigated in the present work.

The three-dimensional KM theory accounts for relativistic effects due to dressing of the electron mass by the laser field and the averaged motion in the magnetic field, as well as due to retardation. However, some other important effects are left unaccounted for. Among those, spin interactions were later discussed by the same authors in [19] within the same approximations. Coupling with the negative energy states can be studied in an approximate way within the present theory if the KM potential is included in the Dirac equation, as is done in (2). However, the dynamical effects due to the magnetic field [12, 20] including the switching on and off of the pulse are beyond the scope of the present static model, which also assumes a monochromatic external field. Such QED effects as, for example, pair creation [21] are also not considered.

3. THE 1*D*-MODEL PROBLEM

An application of the full theory is a difficult problem. However, as seen from Fig. 1, some essential features of the theory can be recognized in a one-dimensional model that accounts for only motion of the electron along the direction *x* of the electric field and where the retardation term in (9) is dropped. The corresponding 1*D* time-dependent Dirac equation has been recently solved numerically by Kylstra *et al*. [10]. In this work, we report a complete numerical solution for this model in the high-frequency approximation. The time-averaged potentials $\mathcal{U}_0(x)$, the binding energies W_n, and the wave functions $\Psi_n(x)$ have been obtained for the ground and a few low-lying excited states. As in [10], in these calculations, a "soft" potential $V(x)$,

$$V(x) = -Z(\exp(-\varepsilon|x|) - \exp(-|x|))/|x|, \qquad (11)$$

which is finite at the origin, has been used with $Z = 1$ and $\varepsilon = 0.001$. Its binding energy W_1 is –0.60149 a.u. Generally, this potential is similar to the smooth so-called Rochester potential used, for instance, in [15]. The main reason for preferring the present form was that the Fourier transform of (11) required in the momentum space calculations [10] could be carried out analytically.

For a given $\mathscr{E}_0$, the 1*D* solution of (2) was obtained by a finite-difference method. The Hamiltonian was discretized on a uniform *N*-point grid, $\Delta x = 0.005$–0.015 a.u., with $N \approx 10^5$. This allowed the box size of 500–1500 a.u. to be used. The averaging of the potential, equation (11), was carried out at each point of the *x* grid by using an *M*-point ϕ grid. Typically, $M \approx 400$ had to be taken for good averaging at high α_0 in the range considered. Computations have been carried out on the Cray J916 at the Université Libre de Bruxelles.

4. RESULTS AND DISCUSSION

Figure 2 shows the binding energy W_1 of the ground state with the potential (9)–(11) as a function of α_0 and ω. For low field strengths $\mathscr{E}_0$, the binding always depends on a single parameter α_0, so that the upper curve in Fig. 2 represents W_1 for any ω in the nonrelativistic limit considered by Gavrila [1].

As the field strength increases, the dependence of W_1 on ω develops, and at larger $\mathscr{E}_0$, the binding shows a rapid change and a deviation from the nonrelativistic curve. Whereas the nonrelativistic binding decreases and asymptotically approaches the free-field ionization limit, the relativistic binding exhibits quite a different pattern of behavior. For low field intensities, it follows the nonrelativistic pattern, but at some intermediate intensity, it departs from the nonrelativistic curve and, for a given laser frequency ω, is practically independent of the field strength. At higher intensities, the binding gradually increases, although at a very slow rate. For the ground state, for example, the rate is 3×10^{-6} at $\alpha_0 = 1000$ a.u. In a wide region of field strengths that stretches out well beyond the graph, the binding as a function of $\mathscr{E}_0$ is practically constant, although it is remarkably different at different ω. This can be characterized by a parameter $\overline{W_1} = W_1(\overline{\alpha_0}, \omega)$, where $\overline{\alpha_0}$ is chosen to be 300 a.u. The dependence of the binding $\overline{W_1}$ on ω is shown in the insert to Fig. 2.

It is interesting to compare these results with the estimates obtained by Kristić and Mittleman [17]. Using a one-state variational function, they obtained an estimate $\tilde{W}_1$ for the binding energy at ultrahigh intensities as follows:

$$\tilde{W}_1 = -\omega(3/8)^{1/2}\frac{\alpha_F}{4\pi}(\ln(\alpha_0/a_0) - 4.23), \qquad (12)$$

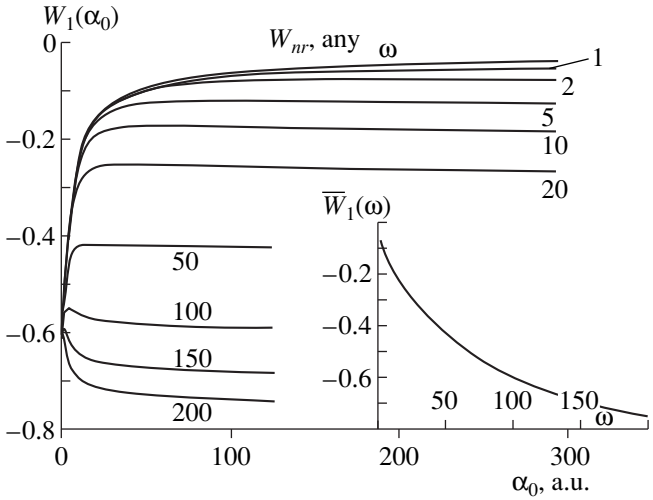

Fig. 2. Plot of the relativistic ground state energy $W_1(\alpha_0, \omega)$ as a function of α_0 at a fixed laser frequency ω. The numbers at the curves are values of ω in a.u. The upper curve W_{nr}, which asymptotically approaches the free-field ionization threshold, is the nonrelativistic ground state term. Insert: $\overline{W_1}$ defined in the text as a function of ω.

where α_F is the fine-structure constant. According to their result, the binding slowly increases with α_0 and the dependence of the binding on ω is strictly linear. The present calculations show that the change of the binding $\overline{W_1}(\omega)$ with ω is faster than linear at lower frequencies but is better represented by a linear function as the laser frequency increases.

As an example, the potential $\mathscr{U}_0(x)$ and the corresponding probability densities $|\Psi_1(x)|^2$ in the ground state are displayed in Fig. 3 for the case of $\omega = 1$ a.u. and increasing field strengths $\mathscr{E}_0$, up to 1000 a.u. For this laser frequency, the relativistic effects in the potential $\mathscr{U}_0$ and those in the probability density are not significant at field strengths below 50 a.u. However, as the classical quiver amplitude α_0 increases with the field, the dichotomy of the relativistic potential tends to saturate and the relativistic probability densities tend to peak at the relativistic quiver values, $x_0 = \pm\beta_0$. For $\omega = 1$ a.u., the value of β_0 is limited by $\sqrt{2}\,c/\omega \approx 193$ a.u., whereas the corresponding nonrelativistic densities peak at ever increasing distances $x_0 = \pm\alpha_0$. There is exact agreement between this and the results obtained from the dynamical treatment [10].

In the nonrelativistic case, the spatial variables scale as $\alpha_0^{-1/3}$, and the width of the dichotomy peaks around the end points $x = \pm\alpha_0$ increases as $\alpha_0^{1/3}$ [1]. The scaling is different in the relativistic case. We now have to take into account the variable dressed mass of the electron, μ, in equation (1). Then, one finds that the width of the relativistic peaks around the end points $x = \pm\beta_0$

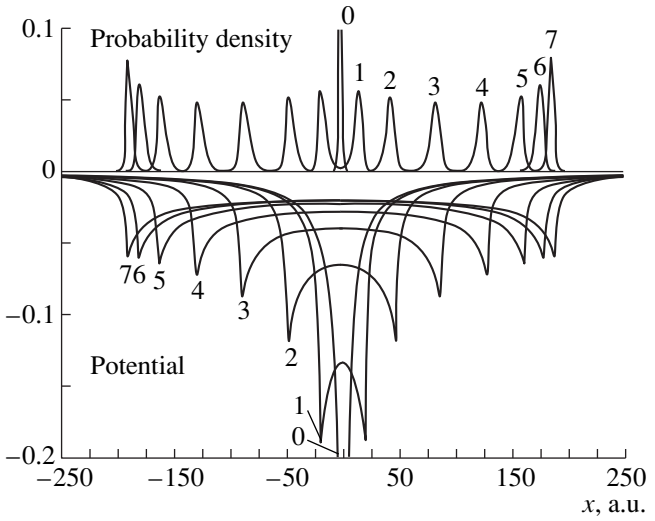

Fig. 3. The 1*D* relativistic high-frequency model. The potential $^{0}u_0$ is obtained by taking the $z = 0$ cross section of the potential in Fig. 1. Dichotomy of the relativistic ground state as a function of α_0 at $\omega = 1$ a.u. Upper panel: probability density $|\Psi(x)|^2$. Lower panel: the corresponding potential $^{0}u_0$. The numbers 0 through 7 at the curves denote nonrelativistic classical excursion amplitudes α_0 of 0, 20, 50, 100, 175, 300, 500, and 1000 a.u. Note that the relativistic excursion amplitude, β_0, tends to 193 a.u.

decreases as $\mathscr{E}_0^{-1/6}$ with increasing field strength. Transition from a nonrelativistic to the relativistic case is clearly seen in the variation of the peak widths and heights in Fig. 3 at α_0 around 100 a.u.

It is also useful to compare our *ab initio* calculations [10] and the present results with the relativistic Schrödinger treatment of Protopapas *et al.* [15]. Their time-dependent, relativistic KH potential is obtained by replacing the quiver amplitude α_0 in the nonrelativistic KH potential by the relativistic amplitude β_0. Consequently, they also observe a contraction of the relativistic potential due to the mass shift. In comparison with the KM equation (2), it is clear that other square-root differential terms in the relativistic Schrödinger equation [15] are just to account for the mass shift in the kinetic term of (6). Therefore, we would expect that their method should be close to solving a time-dependent equation with the 1*D* Hamiltonian (6) (see also [22]).

The present 1*D* results may suggest that it is justified, for $\omega = 1$ a.u., to use the Schrödinger equation (instead of fully relativistic equations) at field strengths $\mathscr{E}_0$ up to 100 a.u. However, for a three-dimensional atom with a full potential (9) presented in Fig. 1, the relativistic treatment may become necessary at lower field strengths. The calculations of Latinne *et al.* [5] on atomic hydrogen beyond the dipole approximation (time-dependent Schrödinger and Pauli equations) show that the relativistic corrections for the ionization rates are still small at $\mathscr{E}_0 \approx 10$–20 a.u. However, the classical Monte Carlo calculations of Keitel and Knight [12] and the quantal calculations of Bugacov *et al.* [23] carried out at higher field strengths both appear to suggest that, for $\omega = 1$ a.u., the magnetic field must be included in the atom–laser interactions at a relatively low $\mathscr{E}_0 \approx 50$ a.u.

Finally, we note that the localization of the wave packets away from the nucleus as the laser field is applied is usually considered as the reason for the stabilization of the atom against ionization. Since the size of the atom remains finite according to equation (7), some inhibition of stabilization may be generally expected in the relativistic regime. However, this may occur at intensities well above the nonrelativistic stabilization region. This question will be addressed elsewhere.

ACKNOWLEDGMENTS

This work was supported by the ECHCM Program under contracts ERBCHBGCT 940552 and ERBCHRXCT 940470, and by the Belgian Institut Interuniversitaire des Sciences Nucléaires (IISN). The author also acknowledges a grant from the NSF that enabled him to visit ITAMP, Harvard.

REFERENCES

1. M. Gavrila, Adv. At. Mol. Opt. Phys., Suppl. 1, 435 (1992) (and references therein).
2. R. M. Potvliege and R. Shakeshaft, Adv. At. Mol. Opt. Phys., Suppl. 1, 373 (1992).
3. P. G. Burke, P. Francken, and C. J. Joachain, Europhys. Lett. **13**, 617 (1990); J. Phys. B **24**, 761 (1991).
4. C. K. Kulander, K. J. Schafer, and J. L. Krause, Phys. Rev. Lett. **66**, 2601 (1991).
5. O. Latinne, C. J. Joachain, and M. Dorr, Europhys. Lett. **26**, 333 (1994).
6. A. Scrinzi and B. Piraux, Phys. Rev. A **56**, R13 (1997).
7. C. J. Joachain, in *Multiphoton Processes*, Ed. by P. Lambropoulos and H. Walther (Inst. of Physics, Bristol, 1997), p. 46.
8. M. Protopapas, C. H. Keitel, and P. L. Knight, Rep. Prog. Phys. **60**, 389 (1997).
9. D.-S. Guo and T. Aberg, J. Phys. A **21**, 4577 (1988) (and earlier references therein).
10. N. J. Kylstra, A. M. Ermolaev, and C. J. Joachain, J. Phys. B **30**, L449 (1997).
11. U. W. Rathe, C. H. Keitel, M. Protopapas, *et al.*, J. Phys. B **30**, L531 (1997).
12. C. H. Keitel and P. L. Knight, Phys. Rev. A **51**, 1420 (1995).
13. F. H. M. Faisal and T. Radozycki, Phys. Rev. A **47**, 4464 (1993).

14. F. H. M. Faisal and T. Radozyski, Phys. Rev. A **48**, 554 (1993).
15. M. Protopapas, C. H. Keitel, and P. L. Knight, J. Phys. B **30**, L591 (1997).
16. J. Kaminski, Z. Phys. D **16**, 153 (1990).
17. P. S. Kristić and M. H. Mittleman, Phys. Rev. A **42**, 4037 (1990).
18. L. S. Brown and T. W. B. Kibble, Phys. Rev. **133**, A705 (1964).
19. P. S. Kristić and M. H. Mittleman, Phys. Rev. A **45**, 6514 (1992).
20. T. Katsouleas and W. B. Mori, Phys. Rev. Lett. **70**, 1561 (1993).
21. G. Mainfray and C. Manus, Rep. Prog. Phys. **54**, 1333 (1991).
22. A. M. Ermolaev, J. Phys. B **31**, L65 (1998).
23. A. Bugacov, M. Pont, and R. Shakeshaft, Phys. Rev. A **48**, 4027 (1993).

Physics of Atomic Nuclei, Vol. 63, No. 4, 2000, pp. 648–656. From Yadernaya Fizika, Vol. 63, No. 4, 2000, pp. 714–722.

VIII INTERNATIONAL CONFERENCE ON SYMMETRY METHODS IN PHYSICS

Symmetry as a Source of Hidden Coherent Structures in Quantum Physics: General Outlook and Examples*

V. P. Karassiov

Lebedev Institute of Physics, Russian Academy of Sciences, Leninskiĭ pr. 53, Moscow, 117924 Russia

Abstract—A general algebraic approach incorporating both invariance groups and dynamical symmetry algebras is developed to reveal hidden coherent structures (closed complexes and configurations) in quantum many-body physics models due to symmetries of their Hamiltonians *H*. Its general ideas are manifested on some recent new examples: (1) G-invariant biphotons and a related *SU*(2)-invariant treatment of unpolarized light; (2) quasispin clusters in nonlinear models of quantum optics; and (3) construction of composite particles and (para)fields from *G*-invariant clusters due to internal symmetries. © *2000 MAIK "Nauka/Interperiodica".*

1. INTRODUCTION: GENERAL REMARKS

Symmetry methods have been widely used in quantum physics from the time of its origin and up to now because they yield powerful epistemological and computational tools for examining many physical problems (see, e.g., [1–14] and literature cited therein). In particular, invariance principles provide formulations of dynamical laws and classifications of quantum states which are most adequate to reveal different physical phenomena [1, 2], whereas the formalism of groups and Lie algebras, especially generalized coherent states and related techniques, yield simple and elegant solutions to spectral and evolution problems [9, 13]. From the spectroscopic point of view, one distinguishes two (exploiting, as a rule, independently) types of physical symmetries depending on the behavior of Hamiltonians *H* under study with respect to symmetry transformations [5]. One of them, associated with invariance groups $G_i(H)$ ($[G_i, H]_- = 0$) of Hamiltonians, describes (nonaccidental) degeneracies of energy spectra within fixed irreducible representations (irreps) of $G_i(H)$, while another one, connected with so-called dynamical symmetry (or spectrum generating) algebras g^D ($[g^D, H]_- \subseteq g^D \neq 0$) [5], enables one to determine such spectra within fixed irreps of g^D and to give spectral decompositions of Hilbert spaces $L(H)$ of quantum systems in g^D-invariant subspaces $L(\lambda)$ (with λ being labels of g^DirrepsD^λ) which describe certain (macroscopic) coherent structures (CS), i.e., stable sets of states (shells, (super)multiplets, configurations, phases, etc. [3–12]) evolving in time independently under actions of *H*.

Applications of these methods are especially fruitful in examining many-body problems whose Hamiltonians *H* and quantum state spaces $L(H)$ are given in terms of boson–fermion operators: $H = H(a_i, a_i^+, b_j, b_j^+)$, $L(H) \subseteq L_F(n; m) \equiv Span\left\{\prod_{i=1}^{n}(a_i^+)^{\eta_i}\prod_{j=1}^{m}(b_j^+)^{\mu_j}|0\rangle\right\}$ ($[a_i, a_j^+]_- = \delta_{ij} = [b_i, b_j^+]_+$). Indeed, various (originating from [16]) boson–fermion mappings *f*,

$$(a_i, a_i^+, b_j, b_j^+) \overset{f}{\mapsto} F_\alpha,$$
$$[F_\alpha, F_\beta]_\mp \equiv F_\alpha F_\beta \mp F_\beta F_\alpha = \sum_{\gamma=1}^{d} c_{\alpha\beta}^{\gamma} F_\gamma \equiv \psi_{\alpha\beta}(\{F_\alpha\}), \quad (1)$$

enable us to introduce generators F_β of $d(<\infty)$-dimensional Lie algebras (or superalgebras [11]) as (super)symmetry operators of both types and collective dynamical variables of problems under study in whose terms one gets reformulations of *H*, $L(H)$ facilitating solutions of many, mainly spectroscopic, many-body tasks [3–12]. On the other hand, within many-body models, due to composite structures of their "elementary" coupled microobjects (quasiparticles, clusters, etc.), one can reveal in a natural manner deep (although hidden) interrelations between both symmetry types above; therefore, a study of one of them automatically yields information about the other one [16]. A consequent realization of this standpoint, being complemented by an "invariant confinement principle" (for constituents), leads to a unified "invariant-dynamical" approach (IDA) to reveal new cooperative effects and phenomena in many-body physics on both micro- and macrolevels [14]; from the methodological point of view, it may be considered as a specification of the general natural philosophical principle (used at the intuitional level by Kepler and explicitly realized by Weyl and Wigner within modern physics [1, 2]): symmetry generates (induces) the formation of CS (coherent configurations) in sets of interacting objects.

Note that single (mostly formal) aspects of IDA were implemented in quantum physics long ago, beginning with the use of binary *SU*(2) invariants to describe

* This article was submitted by the author in English.

1063-7788/00/6304-0648$20.00 © 2000 MAIK "Nauka/Interperiodica"

bipolar molecular valent bonds in 1931 [18] and with group-theoretical studies of complex atomic spectra by Racah between 1942 and 1949 [19]. Specifically, these were fruitfully developed later in nuclear, atomic, and molecular physics [3, 4, 6, 12] and have led to exact definitions of two basic concepts of IDA [13, 20]: dynamical symmetry algebras (see [4, 5] and references therein) and complementarity of groups [20]. The most complete (although implicit) implementations of IDA were given in superfluidity/superconductivity theories by introducing $U(1)$-invariant Bogolyubov–Cooper pairs and the $SU(1,1)/SU(2)$ canonical transformations [22] and in particle physics [interrelations between "color" and "flavor" $SU(n)$ symmetries] [10]. However, until recently, an explicit mathematical formulation of IDA summing up such implementations was absent, which prevented its systematic application. The aim of this paper is to give (destined for physicists) mathematical grounds of IDA [13, 23] and to manifest its efficiency and physical meaning on some recently examined examples in quantum optics [20, 24–27] and in the theory of composite particles and fields with internal symmetries [13, 23].

The paper is dedicated to the memory of Academician N.N. Bogolyubov, whose ideas and works promoted the formulation of IDA, and of Prof. Ya.A. Smorodinsky, discussions with whom stimulated the developments presented below.

2. MATHEMATICAL GROUNDS: *G*-INVARIANT JORDAN MAPPINGS AND WEYL–HOWE DUAL PAIRS IN MANY-BODY PHYSICS

The mathematical formulation of IDA is based on a synthesis of vector invariant theory [1, 28] and extensions [13, 20] of the concept of complementary groups and of Jordan mapping [15].

As is known, the original Jordan mapping given by equations (1) with quadratic functions f introduces collective dynamical variables $F_\alpha(t)$ related to generators F_α of certain Lie (super)algebras g_0^D of dynamical symmetry and reduces quadratic (in field operators) Hamiltonians $H_0(a_i, a_i^+, b_j, b_j^+)$ describing free and linear (in the Heisenberg picture) dynamics to the form

$$H_0 = \sum_\alpha \lambda_\alpha F_\alpha + C, \quad [F_\alpha, C]_- = 0, \qquad Span\{F_\alpha\} = g_0^D, \tag{2}$$

where λ_α are c-number coefficients; herewith algebras g_0^D for particular H are subalgebras of certain "maximal" (in a sense) finite-dimensional Lie superalgebras g_0^{DM} which act on $L_F(n; m)$ irreducibly and are semidirect products of the superalgebras $osp(2n|2m)$ (with the even part $sp(2n, R) \otimes o(2m)$ and the Weyl–Heisenberg superalgebras $w(n, m) = Span(a_i, a_i^+, b_j, b_j^+)$ [5, 11–13].

Suppose now that H_0 has (both continuous and discrete) invariance groups $G_i(H_0) = G_i^0$ and that field operators form sets of vectors $a_i^+ = (a_{ki}^+)$ and $b_j^+ = (b_{kj}^+)$ which are transformed with respect to some (e.g., fundamental) irreps of the groups G_i^0. Then, $F_\alpha \in g_0^D$ are quadratic vector G_i^0 invariants, and, in addition, there is the characteristic equation $[g_0^D, G_i^0]_- = 0 \Leftrightarrow G_i^0 g_0^D G_i^{0-1} = g_0^D$ entailing functional connections between G_i and g_0^D invariant (Casimir and class [3]) operators $C_k(G_i)$ and $C_k(g_0^D)$ and specifications of their eigenvalues on spaces $L(H)$ by common sets $[l_i] \equiv [l_0, l_1, \ldots]$ of invariant quantum numbers l_i which determine irreps of both G_i and g_0^D and label their common extremal (usually lowest) vectors $|[l_i]\rangle$ [23]. All that, in turn, yields spectral decompositions

$$L(H) = \sum_{[l_i]} \sigma([l_i]) L([l_i]), \qquad L([l_i]) = Span\{D^{[l_i]}(G_i^0) \otimes D^{[l_i]}(g_0^D)|[l_i]\rangle\} \tag{3}$$

of spaces $L(H)$ in direct sums of the subspaces $L([l_i])$, which are invariant with respect to joint actions $D(g_0^D) \otimes D(G_i^0)$ of algebras g_0^D and groups G_i^0 being carrier spaces of so-called isotypic components (factor representations) [5] of both these algebraic structures; i.e. $L([l_i])$ contains carrier spaces of equivalent irreps $D^{[l_i]}(G_i^0)(D^{[l_i]}(g_0^D))$ with multiplicities being equal to dimensions of irreps $D^{[l_i]}(g_0^D)$ $(D^{[l_i]}(G_i^0))$. In the case of suitable [for given H and $L(H)$] groups G_i^0, decompositions (3) have the simple spectra $\sigma([l_i]) = 1$ and then pairs (G_i^0, g_0^D) [or (G_i^0, G_0^D), $G_0^D = \exp(g_0^D)$, $G_i^0 \otimes G_0^D \subset G_0^{DM}$] are said to act complementarily [21, 29] on $L(H)$ and to form the Weyl–Howe dual pairs [28], since pairs ($G_i^0 = S_N$, $G_0^D = U(n)$) of permutation and unitary groups were first considered within quantum mechanics by Weyl [1], and their explicit mathematical characterization for pairs $(O(n), Sp(2m, R))$ of orthogonal and symplectic groups was given by Howe [28] (from here on, indices i, 0, and D are omitted whenever it is of no importance). Note that implicitly such Weyl–Howe dual pairs were used in different fields of many-body physics (see, e.g., [20, 29] and references therein); without dwelling on a review of these applica-

tions, we mention some of the known examples: pairs $SU(n)$, $SU(m)$) in particle physics [10]; ($U(1)$, $su(1, 1) \subset sp(2m, R)$) ($m \longrightarrow \infty$) in superfluidity theory [9]; and (C_2, $SU(1, 1)$) in describing so-called squeezed light [30].

The constructions above are generalized in a natural manner when extending quadratic Hamiltonians H_0 by G_i^I ($\subseteq G_i^0$)-invariant polynomials $H_I(a_i, a_i^+, b_j, b_j^+)$ of higher degrees, which describe essentially nonlinear interactions [13, 31] [and, often, with enlarging Hilbert spaces $L(H)$]. In general, such extensions lead to dual pairs where dynamical algebras g^D are infinite-dimensional graded Lie (super)algebras $g^D = \sum_{r=-\infty}^{\infty} g_r$, $[g_r, g_s] \subset g_{r+s}$ enlarging Lie algebras g_0^D and embedded into enveloping algebras $\mathcal{U}(w(n; m))$ of algebras $w(n; m)$ (from here on, we omit the subscript "$\pm$" in $[,]_\pm$ whenever it is unnecessary) [17]. However, G_i invariance of H enables us to obtain generalized dual pairs (G_i^I, $g^D = \hat{g}$) where dynamical symmetry is described by finite-dimensional nonlinear (polynomial) Lie (super)algebras $\hat{g} = g_0^D + y_+ + y_-$ extending Lie algebras g_0^D and having an independent meaning. These algebras $\hat{g}$ are introduced with the help of G_i^I-invariant polynomial Jordan mappings, which, in the simplest case, when $H_I(\ldots)$ are homogeneous polynomials in a_i, a_i^+, b_j, and b_j^+, has the form $\tilde{f}$ [13, 16],

$$\begin{gathered}(a_i, a_i^+, b_j, b_j^+) \overset{\tilde{f}}{\mapsto} (F_\alpha, Y_\lambda, Y_\lambda^+) \in \hat{g}, \\ [g_0^D, y] \subseteq y, \quad [y, y] \subset \mathcal{U}(g_0^D), \quad y = y_+ + y_-,\end{gathered} \tag{4}$$

where generators $Y_\lambda \in y_-$ and $Y_\lambda^+ \in y_+$ are simultaneously elementary vector G_i invariants [1] and components of two mutually conjugate g_0^D-irreducible tensor operators Y and Y^+. In practice, Hamiltonians H_0 and H_I may be inhomogeneous polynomials in a_i, a_i^+, b_j and b_j^+ and, in addition, contain other g_0^D-covariant operators that lead to modifications of equation (4) [20, 26]. The first example of using the mapping (4) in physical problems was given (implicitly) in [30] for extending the unitary algebra $u(1)$ by its G_n-invariant symmetric tensors; later, such constructions were introduced explicitly in [17, 20] for extending algebras $u(m)$ by their C_n-invariant symmetric and $SU(n)$-invariant skew-symmetric tensor operators (see Section 5), as well as for extending the symplectic algebras $sp(2m, R)$ by $SO(n)$-invariant skew-symmetric tensors.

Without dwelling on a complete analysis of the algebras $\hat{g}$, we outline some of their features. As is seen from equations (4), algebras $\hat{g}$ resemble in their structure so-called q-deformed Lie algebras (widely used over the last time [14]) and have the coset structure (generalizing the Cartan decomposition for real semisimple algebras [5]) that enables us to construct irreps of $\hat{g}$ starting from g_0^D modules. However, unlike usual (linear) Lie algebras, exponentials $\exp(\hat{g})$ generate only pseudogroup structures rather than finite-dimensional Lie groups (cf. [32]), which impedes direct extensions of standard group-theoretical techniques for solving physical tasks [23]. Nevertheless, using generalizations [20]

$$\begin{gathered}(F_\alpha, Y_\lambda, Y_\lambda^+) \overset{\tilde{f}}{\mapsto} (F_\alpha^0 = F_\alpha, F_\alpha'^+, F_\alpha') \in h, \\ F_\alpha'^+ = (F_\alpha')^+ = \sum_\lambda Y_\lambda^+ f_{\alpha,\lambda}(\{F_\beta\}), \quad [h, h] \subseteq h\end{gathered} \tag{5}$$

of the Holstein–Primakoff mappings [15] [with h being usual Lie (super)algebras and "coefficients" $f_{\alpha,\beta}(\ldots)$ determined from sets of finite-difference equations], one can construct some finite-dimensional Lie subgroups $\exp(h) \subset \exp(\hat{g})$ which are useful for physical applications [23].

Let us now sketch some of the physical aspects of the formal constructions above to elucidate the heuristic meaning of IDA. The key role here belongs to the decomposition (3), which describes "kinematical" premises of arising CS in $L(H)$ due to the G_i symmetry. Indeed, subspaces $L([l_i])$ consist of the "g^D layers" $L([l_i]; \nu) = Span\{|[l_i]; \mu; \nu\rangle = \mathcal{P}_\nu^{[l_i];\, D}(F_\alpha^+, Y_\lambda^+)|[l_i]; \mu\rangle\}$ obtained by actions of polynomials in the g^D positive weight-shift generators on basic vectors $|[l_i]; \mu\rangle = \mathcal{P}_\mu^{[l_i];\, i}|[l_i]\rangle$ of the irreps $D^{[l_i]}(G_i)$, which are simultaneously specific (degenerated) "pseudovacuum" vectors with respect to g^D: $Y_\lambda|[l_i]; \mu\rangle = F_\alpha|[l_i]; \mu\rangle = 0$. Thus, G_i invariance plays a "synergetic" role and yields "potential (kinematical) forms" for CS which may be formed in $L(H)$ and are described by subspaces $L([l_i])$ at the macroscopic level and by g^D-cluster variables F_α^+ and Y_α^+ at the microscopic level. Note that, generally, the decompositions (3) contain the "particular" (G_i scalar) subspaces $L([0])$ "consisting" only of g^D clusters, whereas other spaces $L([l_i])$ "contain" fixed (determined by the "signatures" $[l_i]$) numbers of uncoupled or partially coupled "primary particles." "Physical" realizations of these hidden CS are implemented dynamically in their "pure" or "mixed" kinematical forms determined by concrete G_i-invariant Hamiltonians H_I [containing or not G_i-covariant coupling parameters (fields) "mixing" different $L([l_i])$] and initial states $|\psi(0)\rangle$. "Pure" realizations lead to superselection rules for quantum numbers l_i (cf. [5]), whereas "mixed" ones imply possibilities of critical ("thresh-

old") phenomena and spontaneous symmetry breaking (cf. [7]). And now, we turn to some recent examples of explicit IDA applications, focusing our attention only on key points.

3. *G*-INVARIANT BIPHOTONS AND THE *SU*(2)-INVARIANT TREATMENT OF UNPOLARIZED LIGHT

The first examples of applications of IDA to be examined deal with quantum-optical parametric models with m spatiotemporal and two polarization ($\pm$) light field modes whose Hamiltonians

$$H^2 = H_f + H_p^2, \quad H_f = \sum_{i=1}^{m} \omega_i \sum_{\alpha=+,-} a_{\alpha i}^+ a_{\alpha i},$$
$$H_p^2 = \sum_{i=1}^{m} \sum_{\alpha,\beta=+,-} [g_{ij}^{\alpha\beta} a_{\alpha i}^+ a_{\beta j}^+ + g_{ij}^{\alpha\beta *} a_{\alpha i} a_{\beta j}] \quad (6)$$

are quadratic in field operators and c numbers $g_{ij}^{\alpha\beta}$ determine concrete parametric processes [13, 20, 24]. Their simplest one-mode version [$m = 1$, $\alpha = +(-)$] has the invariance group $G_i^0 = C_2 = \{c_{k2} = \exp(i\pi k a^+ a), k = 0, 1\}$ acting on the Fock space $L_F(1) \equiv L_F(1; 0) = L(H^2)$ as follows: $a^+ \longrightarrow c_{k2} a^+$. The dual pair is ($G_i = C_2$, $g^D = su(1, 1) = Span\{Y_0 = a^+a/2 + 1/4, Y^+ = a^{+2}/2, Y = a^2/2\} \sim Sp(2, R)$), and the decomposition (3) is trivial: $L_F(1) = L(0) + L(1/2)$, where the eigenvalue $l_0 = \kappa/2$ of the operator $R_0 = a^+a/2 - [a^+a/2]$ ([x] is the "entire part" of x), connected with the lowest weights k of the $su(1, 1)$ irreps realized on L_F (1) : $\kappa = 2k - 1/2$, determines the number $N_{up} = \kappa$ of unpaired photons in $L(l_0) = Span\{(Y^+)^\mu (a^+)^\kappa |0\rangle\}$. The "particular" space $L(0)$ consists of biphotons Y^+ and contains states $|\beta\rangle = \exp(\beta Y^+ - \beta^* Y)|0\rangle$ of the so-called "squeezed vacuum" light [30]. However, more interesting examples of CS in quantum optics due to symmetry have been found recently by using a specific polarization invariance of light fields.

Indeed, the free field Hamiltonian H_f in (6) is invariant with respect to the group $G_i^0 = \prod_{i=1}^m U^i(2) \subset Sp(4m, R)$, where $U^i(2) = \{\exp(i\gamma N_i + i\eta_0 P_0(i) + \eta_1 P_+(i) - \eta_1^* P_-(i))\}$, $N_i = \sum_{\alpha=+,-} N_{\alpha i}$ ($N_{\alpha i} = a_{\alpha i}^+ a_{\alpha i}$) is the photon number operator of the ith spatiotemporal mode, and $P_0(i) = [N_{+i} - N_{-i}]/2$, $P_\pm(i) = a_{\pm i}^+ a_{\mp i}$ are generators of the $SU(2)_p^i \subset U(2)^i$ subgroups defining the polarization $P(i)$ quasispins (related to the polarization Stokes vector operators of single spatiotemporal modes) [24]. The group G_i^0 contains the $SU(2)_p$ subgroup generated by the total P-quasispin operators $P_\alpha = \sum_{i=1}^m P_\alpha(i)$ and enabled us to reveal hidden CS and to examine new collective phenomena connected with "polarization clusterizations" of light field modes [13, 24].

Really, the $SU(2)_p$ group acts on $L_F(2m) \equiv L_F(2m; 0)$ complementarily to the $so^*(2m)$ algebra generated by operators $E_{ij} \equiv \sum_{\alpha=\pm} a_{\alpha i}^+ a_{\alpha j} \in u(m)$ and $SU(2)_p$ invariants $X_{ij}^+ = a_{+i}^+ a_{-j}^+ - a_{-i}^+ a_{+j}^+ : [P_\alpha, X_{ij}^+] = 0$, $\alpha = 0, \neq, -$, $X_{ij} = (X_{ij}^+)^+$. The decomposition (3) of $L(H) = L_F(2m)$ with respect to the dual pair ($G_i^p = SU(2)_p$, $g^D = so^*(2m)$) contains an infinite number of the $SU(2)_p \otimes SO^*(2m)$-invariant subspaces $L(l_0 = p) = L(p) = Span\{|p; \mu; \nu\rangle\}$ labeled by values p of the total P quasispin, which also determine the Casimir operator values of the $so^*(2m)$ irreps realized on $L_F(2m)$ and are measured in experiments with "polarization noises" [13, 24]. Basic vectors $|p; \mu; \nu \equiv [n_i, p_j]\rangle$, specified by the P_0 eigenvalue μ (helicity), photon numbers n_i, and "intermediate" cluster quasispins p_j, have, in general, the form $|p; \mu; \nu\rangle = \mathcal{P}_\nu^{p;\, so^*(2m)}(X_{ij}^+)|p; \mu\rangle$, where the $so^*(2m)$ "pseudovacuum" vectors $|p; \mu\rangle = \mathcal{P}_\mu^{p;\, su(2)_p}(a_{\pm i}^+, Y_{ij}^+)|0\rangle$ are given by polynomials in $a_{\pm i}^+$ and P_0-invariant operators $Y_{ij}^+ = (a_{+i}^+ a_{-j}^+ + a_{-i}^+ a_{+j}^+)/2$, $[P_0, Y_{ij}^+] = 0$, which are direct analogs of Bogolyubov pairs in superfluidity. The operators Y_{ij}^+, $Y_{ij} = (Y_{ij}^+)^+$ extend the algebra $so^*(2m)$ to the algebra $u(m, m)$ acting on $L_F(2m)$ complementarily to the polarization subalgebra $u(1)_p = Span\{P_0\}$. From the physical point of view, quantities X_{ij}^+, Y_{ij}^+ may be interpreted, respectively, as creation operators of P-scalar and P_0-scalar biphoton kinematical clusters determining, in fact, two classes of unpolarized light (UL) associated, respectively, with the "particular" subspaces $L(0) \equiv L(p = 0)$ and $L'(0) \equiv L'(\mu = 0) = Span\{|p; \mu = 0; \nu\rangle\}$ [24].

Indeed, in [24], we proved that quantum states $|\rangle \in L(0)$, $L'(0)$ satisfy the familiar definition of UL, $\mathcal{P} \propto [\langle P_0\rangle^2 + \langle P_1\rangle^2 + \langle P_2\rangle^2]^{1/2} = 0$ [$\mathcal{P}$ is the light polarization degree, $P_\pm = (P_1 \pm iP_2)$, and the symbol $\langle\ldots\rangle$ denotes both statistical and quantum averages] and, in addition, extra (polarization "classicality" and "squeezing") conditions

$$\text{(a)}\ \left\langle \left| P_{i=1,2,0}^s \right| \right\rangle = 0, \quad \forall s \geq 2, \quad |\rangle \in L(0);$$
$$\text{(b)}\ \left\langle \left| P_0^s \right| \right\rangle = 0, \quad \forall s \geq 2, \quad |\rangle \in L'(0). \quad (7)$$

States $|\rangle \in L(0)$, $|\rangle \in L'(0)$ (P- and P_0-scalar light in terminology [24]) are natural [and "particular" due to equations (7)] representatives of two (introduced in [33] and named as P- and P_0-invariant light in [24]) kinds of UL which obey general invariance conditions used in [33, 34] (in different forms) for stronger (in

comparison with the above familiar) definitions of UL retaining some features of the natural (thermal) UL. Namely, states of P-invariant light satisfy the conditions

$$\begin{aligned}(a)\ \ \mathrm{tr}[S\rho S^{\dagger}A(\{P_\alpha\})] &= \mathrm{tr}[\rho A(\{P_\alpha\})] \\ \equiv \langle A(\{P_\alpha\})\rangle \Leftrightarrow (b)\ \ S\rho S^{\dagger} &= \rho\end{aligned} \tag{8}$$

for arbitrary P_α-dependent observables $A(\{P_\alpha\})$ of field density operators ρ (and appropriate quasiprobability functions) with any $S = \exp(ib_0P_0 + b_1P_+ - b_1^*P_-) \in SU(2)_p$, while states of P_0-invariant light obey equations (8) with $S = \exp(ib_0P_0)\exp(i\pi P_2) \in SU(2)_p$. We emphasize, however, that P_0- and P-scalar types of UL are due to strong phase correlations between photons, unlike familiar states of UL generated by randomizing mechanisms. Note also that, in fact, the usual definition of arbitrary UL states ($\mathcal{P} = 0$) can be given in the form (8a) with any $S \in SU(2)_p$ if one takes in it only linear functions $A(\{P_\alpha\})$ [25]. All these observations lead to a new treatment of (quantum and classical) UL states based on their $SU(2)_p$ invariance properties and to a natural division of UL into two classes: (i) weak UL having a characteristic property (8a) with any $S \in SU(2)_p$ only for first moments $\langle P_\alpha\rangle$ (measured in standard polarization experiments) and (ii) strong UL possessing invariance properties (8) for higher moments and including P_0- and P-invariant light.

Thus, taking into account only the $SU(2)_p$ invariance of H_f, we have found in $L_F(2m)$ hidden kinematical CS ("polarization domains") described by subspaces $L(p)$ and $L'(\mu)$, which, according to the general remarks in Section 2, can be realized "physically" with the help of G_i^p-invariant interaction Hamiltonians H_I of two kinds: (i) $H_I = H_I^{X,Y}$ depending only on biphoton variables Y_{ij}, Y_{ij}^+, X_{ij}, and X_{ij}^+, and G_i^p-scalar coupling constants; (ii) $H_I = H_I^{\mathrm{cov}}$ containing "free" photon operators $a_{\pm i}^+$ and G_i^p-covariant coupling parameters describing (phenomenologically) the chiral $SU(2)$ symmetry of the matter (which, perhaps, is realized in some of biophysical models) [24]. The simplest examples of $H_I^{X,Y}$ are obtained from equations (6) by imposing the conditions $g_{ij}^{+-} = \mp g_{ij}^{-+} = \tilde{g}_{ij}$ and $g_{ij}^{\alpha\beta} = 0$ otherwise in H_f; actually, their (X_{ij}, X_{ij}^+)-independent versions were used to produce P_0-scalar light (as states $\exp(\beta Y_{11}^+ - \beta^* Y_{11})|0\rangle$ of the "two-mode squeezed vacuum" [30]), while the problem of an experimental production of P-scalar light is not yet solved [24].

4. COHERENT CLUSTERS IN NONLINEAR MODELS OF QUANTUM OPTICS

The examples of applications of IDA using generalized Weyl–Howe dual pairs $(G_i, \hat{g})$ are yielded by generalizations of models (6) describing multiphoton scattering processes and quantum matter–radiation interactions [20]; their simplest versions are given by Hamiltonians

$$\begin{aligned}H_{mp} &= \sum_{i=1}^{m}\omega_i a_i^+ a_i + \omega_0 a_0^+ a_0 \\ &+ \sum_{1\le i_1\le i_2\ldots\le i_n\le m}[g_{i_1}\ldots(a_{i_1}^+\ldots a_{i_n}^+)a_0 + g_{i_1}^*\ldots(a_{i_1}\ldots a_{i_n})a_0^+], \\ n &\ge 2,\end{aligned} \tag{9}$$

where polarization labels are omitted in subscripts i and nonquadratic parts of H_{mp} describe, in particular, higher harmonics generation ($H_{mp} = H_{hg}$ when $m = 1$) and frequency conversions ($H_{mp} = H_{fc}$ when $m = n$ and only $g_{12\ldots n} \neq 0$), whereas models of matter–radiation interactions are obtained via replacing in equation (9) the "pump" mode a_0^+ by "atomic" operators [20, 26].

The general Hamiltonians (9) have the invariance groups $G_i^{mp} = C_n = \{\exp(i2\pi k a^+ a/n),\ k = 0, 1, \ldots, n-1\} \subset \prod_j U^j(1) = \exp(i\lambda_j a_j^+ a_j) = G_i^0$, whereas their specifications may have extra factors $\exp(i\beta_j R_j)$ related to dynamical constants (integrals of motion) $R_j \in Span\{N_i = a_i^+ a_i\}$ describing additional interaction symmetries; for instance, models H_{hg} have dynamical constants $R_1 = (N_1 + nN_0)/(1 + n)$. Groups G_i^{mp} form on the Fock spaces $L_F(m+1)$ the generalized dual pairs $[G_i^{mp}, g_{mp}^D = \hat{g}^Y(m, n; 1)]$ together with polynomial Lie algebras $\hat{g}^Y(m, n; 1) = s(u(m) + u(1)) + y(n; 1)$ obtained via the mapping (4) as extensions of the Lie algebras $u(n+1) = Span\{E_{ij} = a_i^+ a_j\}$ by coset spaces $y(n; 1) = Span\{Y_{i_1\ldots i_n;\,0}^0 = a_{i_1}^+\ldots a_{i_n}^+ a_0,\ Y_{i_1\ldots i_n;\,0} = (Y_{i_1\ldots i_n;\,0}^+)^+\}$; herewith commutators $[Y_{i_1\ldots i_n;\,0}, Y_{j_1\ldots j_n;\,0}^+]$ are polynomials in E_{ij} [17]. Such an introduction of G_i^{mp}-invariant collective variables E_{ij}, $Y_{\ldots;\,0}^+$, $Y_{\ldots;\,0}$ enables us to rewrite Hamiltonians H_{mp} in the linear form (2) with respect to E_{ij}, $Y_{\ldots;\,0}$, $Y_{\ldots;\,0}^+$ and to apply the $\hat{g}^Y(m, n; 1)$ formalism for revealing hidden CS and examining collective dynamical peculiarities in models (9), which slip off within standard studies [13, 27].

In order to elucidate basic ideas of such applications, we restrict our analysis to models with Hamiltonians H_{hg} when $\hat{g}^{Y}(m, n; 1)$ are reduced to the polynomial Lie algebras $su_{pd}(2) = Span\{Y_0 = (N_1 - N_0)/(1 + n), Y_+ = (a_1^+)^n a_0, Y_- = (Y_+)^+\}$ with commutation relations

$$\begin{aligned} [Y_0, Y_\pm] &= \pm Y_\pm, \\ [Y_-, Y_+] &= \Phi(Y_0; R_1) \\ &\equiv \Psi(Y_0 + 1; R_1) - \Psi(Y_0; R_1), \quad [Y_\alpha, R_1] = 0 \end{aligned} \tag{10}$$

resembling those for $su(2)$ but with polynomial structure functions $\Psi(Y_0; R_1) = (R_1 - Y_0 + 1)(nY_0 + R_1)^{(n)}$ ($A^{(n)} \equiv A(A - 1)\ldots(A - n + 1)$) [26]; note that the R_1 dependence of $\Phi(Y_0; R_1)$, in fact, "intertwines" $G_i^{hg} = C_n \otimes \exp(i\beta R_1)$ and $g^D = su_{pd}(2)$ in an algebraic object resembling the semidirect product of groups (cf. [3, 5]). Then, Hamiltonians H_{hg} are expressed by linear functions

$$\begin{aligned} H_{hg} &= aY_0 + bY_+ + b^*Y_- + cR_1, \\ a &= n\omega_1 - \omega_0, \quad b = g_{1\ldots1}, \quad c = (\omega_1 + \omega_0) \end{aligned} \tag{11}$$

in the generators Y_α and dynamical constant R_1, and the decomposition (3) of $L(H) = L_F(n + 1)$ with respect to $(G_i^{hg}, su_{pd}(2))$ contains an infinite number of the $su_{pd}(2)$-irreducible s-dimensional subspaces $L([l_i]) = Span\{(Y_+)^\eta |[l_0]\rangle, |[l_0]\rangle = (a_1^+)^\kappa (a_0^+)^s |0\rangle, \kappa = 0, \ldots, n - 1, s \geq 0\}$ labeled by eigenvalues $l_0 = (\kappa - s)/(1 + n)$, $l_1 = (\kappa + ns)/(1 + n)$ of R_i, where R_0 is determined from the identity $\Psi(R_0; R_1) \equiv \Psi(Y_0; R_1) - Y_+Y_-$ defining the $su_{pd}(2)$ Casimir operator [27].

This "$su_{pd}(2)$-cluster" formulation of models entails a dimension reduction of physical tasks and an explicit "geometrization" of model dynamics manifested at the classical level of examination. Thus, e.g., the decomposition (3) implies the representation of model phase spaces C^{n+1} as fiber bundles: $C^{n+1} = \bigcup_{[l_i]} \mathcal{A}([l_i])$, where $su_{pd}(2)$-invariant dynamical manifolds $\mathcal{A}([l_i])$ correspond to spaces $L([l_i])$ and are in the mean-field approximation Abelian varieties given in dynamical variables $\bar{Y}_\alpha = \langle Y_\alpha \rangle$ as follows: $\mathcal{A}([l_i]) = \{\bar{Y}_\alpha : \bar{Y}_+\bar{Y}_- + \bar{Y}_-\bar{Y}_+ = \Psi(\bar{Y}_0; l_1) + \Psi(\bar{Y}_0 + 1; l_1)\}$. Then, states belonging to a fixed manifold $\mathcal{A}([l_i])$ {or $\mathcal{A}([\bar{R}_i])$ in the general case} will evolve in it under the action of Hamiltonian flows with Hamiltonian functions $\mathcal{H} = a\bar{Y}_0 + b\bar{Y}_+ + b^*\bar{Y}_- + c\bar{R}_1$. Herewith, (approximate) dynamical trajectories are determined as intersections of manifolds $\mathcal{A}([\bar{R}_i])$ with energy planes $\mathcal{H} = E$, which enables us to determine some features of model dynamics [27].

These considerations become more transparent if "quasispin" reformulations of the models (11) are used in terms of the $su(2)$ generators V_α connected with Y_α via the mapping (5): $V_0 = Y_0 - R_0 - J$, $V_+ = Y_+[\varphi(V_0)]^{1/2}$, $\varphi(V_0) = (J + V_0 + 1)(J - V_0)/\Psi(Y_0 + 1; R_1)$, $Y_- = (Y_+)^+$ [J is the $su(2)$ highest weight operator with eigenvalues $j = s/2$] [20]. Then, the Hamiltonians (11) are represented by nonlinear functions

$$\begin{aligned} H &= aV_0 + bV_+[\varphi(V_0)]^{-1/2} + b^*[\varphi(V_0)]^{-1/2}V_- \\ &\quad + cR_1 + a(R_0 + J) \end{aligned} \tag{12}$$

in the "$su(2)$-cluster" variables V_α, and fiber-bundle representations of phase spaces C^{n+1} contain $SU(2)$-invariant "Bloch spheres" S_j^2, $\bar{V}_0^2 + \bar{V}_1^2 + \bar{V}_2^2 = j^2$ instead of $su_{pd}(2)$-invariant manifolds $\mathcal{A}([l_i])$, while energy planes are replaced by nonlinear energy surfaces $\langle H \rangle = E$. Furthermore, these "quasispin" reformulations enable us to obtain new (in comparison with those obtained earlier) $su(2)$-cluster semiclassical solutions of spectral and evolution tasks using techniques of the $SU(2)$ coherent states $|\phi_0; \alpha\rangle = S_V(\alpha)|\phi_0\rangle \in L(H)$, $S_V(\alpha) = \exp(\alpha V_+ - \alpha^* V_-)$, which can be of "spinlike" type {when $|\phi_0\rangle \in L([l_i])$} or $su(2)$-reducibile [when $|\phi_0\rangle \in L(H)$] [27].

For example, energy eigenstates $|E([l_i]; v)\rangle$ and spectra $\{E([l_i]; v)\}$ can be approximated by means of standard variational schemes using $SU(2)$ coherent states $S_V(\xi)\mathcal{N}([l_i]; v)V_+^v |[l_i]\rangle = |[l_i]; v; \xi\rangle$ as trial functions. Namely, we find approximate eigenstates $|E^{qc}([l_i]; v)\rangle = |[l_i]; v; \xi\rangle$ and eigenergies $E^{qc}([l_i]; v) = \langle [l_i]; v; \xi | H | [l_i]; v; \xi \rangle$, where values of the parameter $\xi = r\exp(-i\theta)$ are determined by the stationarity conditions for the energy functional $\mathcal{H}([l_i]; v; \xi)$:

$$\begin{aligned} &\frac{\partial \mathcal{H}([l_i]; v; \xi)}{\partial \theta} = 0, \quad \frac{\partial \mathcal{H}([l_i]; v; \xi)}{\partial r} = 0, \\ &\mathcal{H}([l_i]; v; \xi) = \langle [l_i]; v; \xi | H | [l_i]; v; \xi \rangle. \end{aligned} \tag{13}$$

In fact, in such a way, we obtain $\exp(-i\theta) = b/|b|$ and a whole series of competitive potential solutions for values r; their final selection may be made with the help of a "quality criterion" using the "energy error" functionals introduced in [20]. Similarly, an appropriate semiclassical dynamics is described by the classical Hamiltonian equations [27]

$$\begin{aligned} \dot{q} &= \frac{\partial \mathcal{H}}{\partial p}, \quad \dot{p} = -\frac{\partial \mathcal{H}}{\partial q}, \\ \mathcal{H} &= \langle \phi_0; z(t) | H | \phi_0; z(t) \rangle, \\ q &= \theta, \quad p \equiv \langle \phi_0; z(t) | Y_0 | \phi_0; z(t) \rangle, \end{aligned} \tag{14}$$

for "motion" of the canonical parameters p and q of the $SU(2)$ coherent states $|\phi_0; z(t)\rangle = S_V(z(t))|\phi_0\rangle$ [$z = -r\exp(i\theta)$] as trial functions in the time-dependent

Hartree–Fock variational scheme. Note that solutions of equations (13) and (14) smoothly approximate exact ones and catch explicitly quantum cooperative features of models at semiclassical levels [27].

5. GENERALIZED DUAL PAIRS IN THE THEORY OF COMPOSITE FIELDS

Another area of "natural" appearance of generalized dual pairs (G_i, $g^{DS} = \hat{g}$) is the algebraic analysis [13, 23] of composite fields with internal (gauge) symmetries [5], which generalizes basic ideas of the paraquantization [8, 35] and implements in a sense the method of fusion of de Broglie [36]. Actually, the simplest example of such an analysis (but without introducing dual pairs and nonlinear Lie algebras $\hat{g}$) was given in [31] by means of using n-boson one-mode versions

$$H^n = \omega_1 a_1^+ a_1 + gY_{1\ldots}^+ + g^* Y_{1\ldots}, \quad Y_{1\ldots}^+ = a_1^+ \ldots a_1^+ = (a_1^+)^n \tag{15}$$

of Hamiltonians (6) to describe resonance states in particle physics; later, it was generalized on multimode cases to study multiphoton processes in quantum optics (see [13] and references therein).

Specifically, in [31], it was shown that operators $Y^+ \equiv Y_{1\ldots}^+$ describe n-particle kinematical clusters which display unusual (para)statistics and correspond to generalized asymptotically free fields realized on the Fock space $L_F(1)$. In fact, the operators Y^+, $Y = (Y^+)^+$, $Y_0 = a_1^+ a_1/n \equiv E_{11}/n$ satisfy [13] (noncanonical) commutation relations (10) of the $su_{pd}(1, 1)$ algebra with the structure polynomial $\Psi(Y_0) = (E_{11})^{(n)}$ and, in addition, extra multilinear relations $ad_Y^{n+1} Y^+ = ad_Y^n (ad_Y Y^+) = 0$, $ad_Y Y^+ \equiv [Y, Y^+]$, generalizing (for $n \geq 3$) trilinear parastatistical Green's relations [8, 35]. Thus, we obtain an action of the generalized dual pair ($G_i = C_n = \{\exp(i \times 2\pi k a_1^+ a_1)/n\}$, $\hat{g} = su_{pd}(1, 1)$) on the space L_F (1). The appropriate decomposition (3) contains the subspaces $L([l_0 = \kappa/n]) = Span\{(Y^+)^\eta |[l_0]\rangle, |[l_0]\rangle = (a^+)^\kappa |0\rangle\}$, $\kappa = 0, 1, \ldots, n-1$, describing coherent mixtures of constant numbers κ of uncoupled bosons a_1^+ and of numbers varying in time N_Y of Y clusters. However, operators N_Y have no standard [for (para)fields] forms bilinear in Y and Y^+ [8], but they can be expressed [due to the evident identity $\Psi(Y_0) = Y^+ Y$ on $L_F(1)$] as nonlinear functions in the bilineals Y^+Y and YY^+ [13]: $N_Y = (E_{11} - nR_0)/n = [a_1^+ a_1/n] = [E_{11}/n]$, $E_{11} = \varphi(Y^+Y) \equiv n\Psi^{-1}(Y_0)$, as is the case for algebras $A(K)$ describing nonstandard statistics [35]. Therefore, at best, the quantities Y^+ and Y can be set in correspondence only to parafield (when $n = 2$) quanta [8, 35] rather than to certain asymptotically free particles [13]. Nevertheless, one can construct from them operators $W^+ = W^+(\{Y_i\})$, $W = (W^+)^+$ obeying canonical commutation relations $[W, W^+] = 1$, having the standard number operators $N_W = W^+W$ ($=N_Y$) and corresponding to quanta of asymptotically free multiboson fields {which can be realized in subspaces $L([0])$ in "pure forms"}. Actually, two equivalent forms [13, 20, 31],

$$W^+ = Y^+ \sum_{r \geq 0} c_r (Y^+)^r (Y)^r = Y^+ [(Y_0 - R_0 + 1)/(E_{11} + n)^{(n)}]^{1/2}, \quad W = (W^+)^+, \tag{16}$$

were found for such W^+ and W, where the second one is a specification of the mapping (5).

The analysis above has been generalized [18] by means of (i) using "m"-mode extensions of models (15) with C_n-invariant interaction Hamiltonians $\sum_{1 \leq i_1 \ldots \leq m} [g_{i_1\ldots} Y_{i_1\ldots}^+ + g_{i_1\ldots}^* Y_{i_1\ldots}]$, $Y_{i_1\ldots}^+ = a_{i_1}^+ \ldots a_{i_n}^+$; (ii) considering their analogs with non-Abelian groups $G_i = SU(n)$ [whose Hamiltonians are obtained by the substitutions $a_i^+ a_i \longrightarrow (\mathbf{a}_i^+ \cdot \mathbf{a}_i) \equiv \sum_{j=1}^n a_{ji}^+ a_{ji}$, $Y_{i_1\ldots}^+ \longrightarrow X_{i_1\ldots}^+ \equiv \sum_{(j_k)} \epsilon_{j_1\ldots j_n} a_{j_1 i_1}^+ \ldots a_{j_n i_n}^+$ ($\epsilon_{j_1\ldots j_n}$ is the totally antisymmetric tensor)]; and (iii) involving both boson and fermion variables. These procedures yield a variety of generalized dual pairs. For instance, when using the first two, we get dual pairs C_n, $osc^Y(m; (n))$ and $(SU(n), osc^X(m; 1^n))$, where $osc^Y(m; (n))$ and $osc^X(m; 1^n)$ are extensions of the unitary algebras $u(m) = Span\{E_{ij}, E_{ij} = a_i^+ a_j$ and $E_{ij} = (\mathbf{a}_i^+ \cdot \mathbf{a}_i)\}$ by their symmetric $(Y_{\ldots}^+, Y_{\ldots})$ and skew-symmetric $(X_{\ldots}^+, X_{\ldots})$ tensor operators [17, 23]. The operators $X_{\ldots}^+$, $X_{\ldots}$, $Y_{\ldots}^+$, and $Y_{\ldots}$ satisfy noncanonical commutation relations whose right-hand sides depend on E_{ij} [and on the $SU(n)$ Casimir operators for $osc^X(m; 1^n)$] and obey (due to the invariant theory [1, 29]) certain extra "bootstrap" relations of the type $Y_{1\ldots 1} Y_{2\ldots 2} = Y_{21\ldots 1} Y_{12\ldots 2}$ [13, 17], which are similar to those occurring in quantum field theories with constraints [5, 8] and in nonstandard quantization schemes discussed in [35]. All this entails unusual statistical and other features of G_i-invariant clusters associated with $X_{\ldots}^+$ and $Y_{\ldots}^+$ and complicated extensions of the one-mode analysis above [17]. Specifically, the task of obtaining m-mode generalizations

$$W_a^+ = \sum_{i_1\ldots i_n} (Y_{i_1\ldots i_n}^+ / X_{i_1\ldots i_n}^+) f_{i_1\ldots i_n}^a (\{E_{ij}\}), \quad [W_a, W_b^+] = \delta_{ab}, \quad W_a = (W_a^+)^+ \tag{17}$$

of the mapping (16) is, in general, fairly difficult owing to "syzygies" between Y/X clusters (and resembles the "reducibility problem" for algebras $A(K)$ [35]).

When determining explicit expressions for $f_{\dots}(\dots)$ in equations (17) [and in their generalizations, e.g., for constructing $W_a^+ \in A(K)$], we obtain an effective tool for analyzing composite field models with internal G_i symmetries at the algebraic and quasiparticle levels (including a new insight into some "old problems," such as, quark confinement [3, 10]). Furthermore, examining the limit "$m \longrightarrow \infty$" and taking spatiotemporal variables and symmetries into consideration, one can also construct in terms of "quanta" W_a appropriate "physical" (asymptotically free) composite fields [13] and then develop standard theories for them, including nonlinear (due to Hamiltonian forms) evolution equations and their soliton/instanton solutions [7]; herewith, discrete quantum numbers l_i labeling subspaces $L([l_i])$ in (3) may display themselves as specific topological charges. In particular, in such a way, using suitable analogs of equations (16) for P/P_0-scalar biphotons [24], we answer in the affirmative within quantum optics the problem of the existence of UL waves posed by Fresnel at the beginning of the nineteenth century and having a negative solution within the framework of classical electrodynamics due to the vector nature of the Maxwell equations [4, 6].

6. CONCLUSION

Thus, we have formulated mathematical grounds of IDA and have shown its physical meaning "in action." In conclusion, we briefly discuss some ways of applying and developing the results obtained.

The general constructions of Sections 2 and 5 may be applied to the systematic search for hidden CS within different areas of quantum many-body physics by using known dual pairs [20, 28] and to developing field theories with "hidden quantum variables" and unusual statistics [8, 13, 35] (including the problem of consistency of the Poincaré symmetry with dynamic ones [7, 11, 13]). On the other hand, they are useful in solving appropriate "inverse problems" [16] to display hidden symmetries G_i and "preparticles" from analyzing spectroscopic data for complex systems associated with irreps of certain dynamic algebras g^D (that is of great importance when interaction Hamiltonians are determined phenomenologically). For this aim, it is worthwhile to enlarge lists of dual pairs used by taking new classes of groups G_i and q-deformed oscillators into consideration [23].

More concrete results of Sections 3 and 4, firstly, can be used as general patterns for applying IDA in G_i-invariant many-body models and, secondly, to open new lines of investigation in quantum optics. For example, the above $SU(2)_p$-invariant treatment of UL stimulates experiments on producing new states of quantum UL (especially, of P-scalar light); studies of interactions of these states with material media [13]; and their applications in communication theory, spectroscopy of anisotropic media, and biophysics [24]. At the same time, "quasispin" formulations and $su(2)$-cluster semiclassical approximations in models (9) outline (related to geometric quantization schemes [32]) ways of "geometrization" of dynamics in models of strongly interacting subsystems and, simultaneously, can be used to reveal new collective phenomena in such models, including topological features of Hamiltonian flows determined by equations (14) at the different semiclassical levels [27].

ACKNOWLEDGMENTS

The author thanks G.S. Pogosyan for his interest and attention to the work and V.P. Bykov, R.N. Faustov, and S.M. Chumakov for useful discussions.

Support of this work from the Russian State Research and Technology Program "Fundamental Spectroscopy" and the Russian Foundation for Basic Research (project no. 96-02-18746a) is acknowledged.

REFERENCES

1. H. Ewyl, *Gruppentheorie und Quantenmechanik* (Hirzel, Leipzig, 1931); *Classical Groups: Their Invariants and Representations* (Princeton Univ. Press, Princeton, 1939); *Symmetry* (Nauka, Moscow, 1968).
2. E. P. Wigner, *Group Theory and Its Application to the Quantum Mechanics of Atomic Spectra* (Academic, New York, 1959); *Symmetries and Reflections* (Indiana Univ. Press, Bloomington, 1970).
3. J. P. Elliott, and P. G. Dawber, *Symmetry in Physics* (Macmillan, London, 1979).
4. H. J. Lipkin, *Quantum Mechanics: New Approaches to Selected Topics* (North-Holland, Amsterdam, 1973); H. J. Lipkin, N. Meshkov, and A. J. Glick, Nucl. Phys. **62**, 188 (1965).
5. A. O. Barut and R. Racka, *Theory of Group Representations and Applications* [PWN (Polish Sci. Publ.), Warsaw, 1977].
6. L. C. Biedenharn, and J. D. Louck, *Angular Momentum in Quantum Physics: Theory and Applications* (Addison-Wesley, Reading, 1981).
7. R. Rajaraman, *Solitons and Instantons* (North-Holland, Amsterdam, 1982).
8. A. B. Govorkov, Fiz. Élem. Chastits At. Yadra **14**, 1229 (1983).
9. A. M. Perelomov, *Generalized Coherent States and Their Applications* (Springer-Verlag, Berlin, 1986).
10. L. B. Okun, *Elementary Particle Physics* (Nauka, Moscow, 1988).
11. V. I. Ogievetsky and L. Mezinchesku, Usp. Fiz. Nauk **117**, 637 (1975).
12. E. G. Nadjakov, Fiz. Élem. Chastits At. Yadra **21**, 467 (1990).

13. V. P. Karassiov, J. Sov. Laser Res. **12**, 147 (1991); Tr. Fiz. Inst. im. P.N. Lebedeva, Ross. Akad. Nauk **208**, 18 (1992).
14. *Symmetry Methods in Physics*, Ed. by N. A. Sissakian and G. S. Pogosyan (JINR, Dubna, 1996).
15. P. Z. Jordan, Z. Phys. **94**, 531 (1935); T. Holstein and H. Primakoff, Phys. Rev. **58**, 1098 (1940); F. Dyson, Phys. Rev. **192**, 1217 (1956).
16. V. P. Karassiov and L. A. Shelepin, Yad. Fiz. **8**, 615 (1968); V. P. Karassiov, Tr. FIAN **70**, 147 (1973); Ya. A. Smorodinsky and L. A. Shelepin, Usp. Fiz. Nauk **196**, 3 (1972).
17. V. P. Karassiov, Kratk. Soobshch. Fiz., No. 9, 3 (1988); Lect. Notes Phys. **382**, 493 (1991); J. Phys. A **25**, 392 (1992); Preprint No. 65, FIAN (Moscow, 1992).
18. G. Rumer, E. Teller, and H. Weyl, Nachr. Ges. Wiss. Goettingen, Math.-Phys. Kl. (1932), p. 499.
19. G. Racah, Phys. Rev. **62**, 437 (1942); **63**, 368 (1949); **76**, 1352 (1949).
20. V. P. Karassiov, Teor. Mat. Fiz. **95**, 3 (1995); J. Phys. A **27**, 153 (1994).
21. M. Moshinsky and C. Quesne, J. Math. Phys. **11**, 1631 (1970); **12**, 1772 (1971).
22. N. N. Bogolyubov, Izv. Akad. Nauk SSSR, Ser. Fiz. **11**, 77 (1947); JETP **34**, 58 (1958).
23. V. P. Karassiov, Rep. Math. Phys. **40** (2), 235 (1997).
24. V. P. Karassiov, J. Phys. A **26**, 4345 (1993); Phys. Lett. A **190**, 387 (1994).
25. V. P. Karassiov, Kratk. Soobshch. Fiz. FIAN, No. 9–10, 13 (1996).
26. V. P. Karassiov and A. B. Klimov, Phys. Lett. A **189**, 43 (1994); **191**, 117 (1994).
27. V. P. Karassiov, *Symmetry Methods in Physics*, Ed. by N. A. Sissakian and G. S. Pogosyan (JINR, Dubna, 1996), vol. 1, p. 306; Phys. Lett. A **238**, 19 (1998).
28. R. Howe, Remarks on Classical Invariant Theory, Preprint of Yale Univ. (1976).
29. S. I. Ališauskas, Fiz. Élem. Chastits At. Yadra **14**, 1336 (1983) [Sov. J. Part. Nucl. **14**, 563 (1983)].
30. D. F. Smirnov and A. S. Troshin, Usp. Fiz. Nauk **153**, 233 (1987); V. P. Bykov, Usp. Fiz. Nauk **161**, 145 (1991).
31. R. A. Brandt and O. W. Greenberg, J. Math. Phys. **10**, 1168 (1969).
32. S. L. Woronowicz, Commun. Math. Phys. **111**, 613 (1987); M. V. Karasev and V. P. Maslov, *Nonlinear Poisson Brackets. Geometry and Quantization* (Nauka, Moscow, 1991).
33. J. Lehner, U. Leonhardt, and H. Paul, Phys. Rev. A **53**, 2727 (1996).
34. H. Prakash and N. Chandra, Phys. Rev. A **4**, 796 (1971).
35. S. A. Balashova, V. V. Kuryshkin, and E. E. Entralgo, Fiz. Élem. Chastits At. Yadra **20**, 965 (1989); O. W. Greenberg, Phys. Rev. Lett. **64**, 705 (1990).
36. L. De Broglie, *Theorie générale des particules à spin: Methode à fusion* (Gauthier Villars, Paris, 1954).

Physics of Atomic Nuclei, Vol. 63, No. 4, 2000, pp. 657–660. From Yadernaya Fizika, Vol. 63, No. 4, 2000, pp. 723–726.

VIII INTERNATIONAL CONFERENCE ON SYMMETRY METHODS IN PHYSICS

Supersymmetry of the Nonstationary Schrödinger Equation and Time-Dependent Exactly Solvable Quantum Models*

B. F. Samsonov and L. A. Shekoyan

Tomsk State University, Tomsk, 634050 Russia

Abstract—New, exactly solvable time-dependent quantum models are obtained with the help of the supersymmetric extension of the nonstationary Schrödinger equation. © *2000 MAIK "Nauka/Interperiodica".*

1. INTRODUCTION

An essential ingredient of the conventional supersymmetric quantum mechanics (for reviews see [1]) is the well-known Darboux transformation [2] for the stationary Schrödinger equation. This transformation permits us to construct new, exactly solvable stationary potentials from the known ones. Similar constructions may be developed for the time-dependent Schrödinger equation [3].

Our approach to the Darboux transformation is based on a general notion of the transformation operator introduced by Delsart [4]. In terms of this notion, Darboux [2] studied differential first-order transformation operators for the Sturm–Liouville problem. This is a reason, in our opinion, to call every differential transformation operator a *Darboux transformation operator*. A different approach to the Darboux transformation is presented in the monograph [5]. It is worthwhile mentioning that our approach, in contrast to that of [5], leads to real potential differences. This property is crucial for constructing the supersymmetric extension of the nonstationary Schrödinger equation.

2. FORMALISM

In this section, we briefly review the basic constructions leading to the supersymmetry of the nonstationary Schrödinger equation established in [3].

Consider two time-dependent Schrödinger equations:

$$(i\partial_t - h_0)\psi(x, t) = 0, \quad h_0 = -\partial_x^2 + V_0(x, t), \quad (1)$$

$$(i\partial_t - h_1)\varphi(x, t) = 0, \quad h_1 = -\partial_x^2 + V_1(x, t). \quad (2)$$

We assume the potential $V_0(x, t)$ and the solutions of equation (1), called *the initial Schrödinger equation*, to be known. By definition, the transformation operator denoted by L transforms solutions $\psi(x, t)$ into solutions $\varphi(x, t) = L\psi(x, t)$. It is obvious that this condition is fulfilled if L participates in the following intertwining relation: $L(i\partial_t - h_0) = (i\partial_t - h_1)L$. In the simplest case of a first-order differential operator L this equation can readily be solved with respect to operator L and potential difference $A(x, t)$:

$$L = L_1(t)[-u_x(x, t)/u(x, t) + \partial_x],$$

$$L_1(t) = \exp[2\int dt \mathrm{Im}(\log u)_{xx}],$$

$$A(x, t) = V_1(x, t) - V_0(x, t) = -[\log|u(x, t)|^2]_{xx}.$$

Note that the operator L and the new potential $V_1(x, t)$ are completely defined by a function $u(x, t)$ called *the transformation function*. This function is a particular solution to the initial Schrödinger equation (1) subject to the condition $(\log u/\bar{u})_{xxx} = 0$, called *the reality condition of the new potential*.

Operator $L^+ = -L_1(t)[\bar{u}_x(x, t)/\bar{u}(x, t) + \partial_x]$, which is Laplace adjoint to L, realizes the transformation in the inverse direction, i.e., the transformation from the solutions of equation (2) to the ones of equation (1). The product L^+L is a symmetry operator for equation (1), and LL^+ is a similar one for equation (2).

With the help of the transformation operators L and L^+, we build up the time-dependent nilpotent supercharge operators

$$Q = \begin{pmatrix} 0 & 0 \\ L & 0 \end{pmatrix}, \quad Q^+ = \begin{pmatrix} 0 & L^+ \\ 0 & 0 \end{pmatrix}, \quad (3)$$

which commute with the Schrödinger superoperator $iI\partial_t - H$, where $H = \mathrm{diag}\{h_0, h_1\}$ is the time-dependent super-Hamiltonian and I is the unit 2×2 matrix. In general, the super-Hamiltonian is not the integral of motion for the quantum system guided by the matrix Schrödinger equation

$$(iI\partial_t - H)\Psi(x, t) = 0. \quad (4)$$

Two-component function $\Psi(x, t)$ belongs to the linear space defined over the complex number field and spanned by the basis $\Psi_+ = \psi e_+$, $\Psi_- = L\psi e_-$, where $e_+ = (1, 0)^T$ and $e_- = (0, 1)^T$. The sign "T" stands for the transposition.

The operators (3) are integrals of motion for equation (4). Using the symmetry operators L^+L and LL^+, we

* This article was submitted by the authors in English.

1063-7788/00/6304-0657$20.00 © 2000 MAIK "Nauka/Interperiodica"

can construct the other integral of motion for this equation: $S = \mathrm{diag}\{L^+L, LL^+\}$. The operators Q, Q^+, and S realize the well-known superalgebra $sl(1/1)$

$$[Q, S] = [Q^+, S] = 0, \quad \{Q, Q^+\} = S - \alpha I,$$

where, instead of the Hamiltonian, we see another symmetry operator. In general, the operators S, Q, and Q^+ depend on time; consequently, we have obtained the *time-dependent superalgebra*.

3. HARMONIC OSCILLATOR WITH A TIME-VARYING FREQUENCY

Consider the Hamiltonian

$$h_0 = -\partial_x^2 + \omega^2(t)x^2. \tag{5}$$

The variety of potentials we can obtain by the technique described above depends on the variety of solutions of the initial Schrödinger equation suitable for use as transformation functions. A wide class of solutions can be found with the help of the method of *R separation of variables* [6] based on the orbit structure of the symmetry algebra with respect to the adjoint representation of the corresponding group symmetry. The symmetry algebra of the Schrödinger equation with Hamiltonian (5) is the well-known Schrödinger algebra G_2 [6]. The following representation of this algebra is suitable for our purpose:

$$K_1 = a - a^+, \quad K_{-1} = -i(a + a^+), \quad K_0 = i,$$

$$K_{-2} = -i(a + a^+)^2, \quad K_2 = -i(a - a^+)^2,$$

$$K^0 = -2[a^2 - (a^+)^2],$$

$$a = \varepsilon\partial_x - i\dot{\varepsilon}x/2, \quad a^+ = -\bar{\varepsilon}\partial_x + i\dot{\bar{\varepsilon}}x/2,$$

$$aa^+ - a^+a = 1/4,$$

where $\varepsilon = \varepsilon(t)$ is a (complex) solution to the classical equation of motion for the oscillator $\ddot{\varepsilon}(t) + 4\omega^2(t)\varepsilon(t) = 0$.

Five orbits are known for this algebra which give four nonequivalent solutions to the Schrödinger equation in *R*-separated variables with respect to transformations from the Schrödinger group. Below is a summary of all suitable transformation functions and corresponding potentials.

(1) Two orbits with the representatives $J_1 = K_1$ and $J_1 = K_2$:

$$u(x, t) = u_\lambda + u_{\bar{\lambda}} = \gamma^{-1/2}\cosh\left(\frac{\nu x}{8\gamma} + \mu\nu\frac{\delta}{32\gamma}\right)$$

$$\times \exp\left[\frac{ix^2\dot{\gamma}}{4\gamma} - \frac{i\mu x}{8\gamma} + i(\nu^2 - \mu^2)\frac{\delta}{64\gamma}\right],$$

$$\lambda = -\mu - i\nu, \quad L_1(t) = \gamma = (\varepsilon + \bar{\varepsilon})/2,$$

$$V_1(x, t) = \omega^2(t)x^2 - \frac{\nu^2}{32\gamma^2}\cosh^{-2}\left(\frac{\nu x}{8\gamma} + \mu\nu\frac{\delta}{32\gamma}\right).$$

(2) The orbit with representative $J_2 = K_2 - K_1$:

$$\psi_\lambda(x, t) = \delta^{-1/2}\exp\left(ix^2\frac{\dot{\delta}}{4\delta} - ix\frac{\gamma}{2\delta^2} + i\frac{\gamma^3}{6\delta^3} + i\lambda\frac{\gamma}{\delta}\right)$$

$$\times Q\left(2^{-1/2}\left(\frac{x}{\delta} - \frac{\gamma^2}{2\delta^2}\right) - 2^{2/3}\lambda\right),$$

where $\gamma = \varepsilon + \bar{\varepsilon}$, $i\delta = \varepsilon - \bar{\varepsilon}$, λ is a separation constant, and $Q(z)$ is an Airy function defined by the equation $Q''(z) = zQ(z)$. An exactly solvable potential is expressed in this case through the Airy function $Ai(z)$. It is an easy exercise to show that a regular on full real axis potential can be obtained with the help of the second-order Darboux transformation operator with transformation functions ψ_λ and $\psi_{\bar{\lambda}}$.

(3) The orbit with the representative $J_3 = K_2 - K_{-2}$ gives several classes of potentials. First, we may choose solutions which form a discrete basis in the Hilbert space of states [7] as transformation functions

$$u_n(x, t) = N_n\gamma^{-1/4}\left(\frac{\bar{\varepsilon}}{\varepsilon}\right)^{n/2 + 1/4}\exp\left(\frac{2i\dot{\gamma} - 1}{16\gamma}x^2\right)He_n\left(\frac{x}{2\sqrt{\gamma}}\right),$$

$$\gamma = \varepsilon\bar{\varepsilon},$$

where $He_n(z) = 2^{-n/2}H_n(z/\sqrt{2})$ are the Hermite polynomials. The second-order Darboux transformation with transformation functions u_n and u_{n+1} produces potentials

$$V_n(x, t) = \omega^2(t)x^2 - \frac{1}{2\gamma}\left[\frac{J_n''(z)}{J_n(z)} - \left(\frac{J_n'(z)}{J_n(z)}\right)^2 - 1\right],$$

$$z = x/(2\sqrt{\gamma}),$$

$$J_n(z) = \sum_{k=0}^{n}\frac{\Gamma(n+1)}{\Gamma(k+1)}He_k^2(z) = kJ_{k-1}(z) + He_k^2(z).$$

Second, we may use a general solution to the quantization equation for the operator J_3,

$$u(x, t) = \bar{\varepsilon}^{-1/2}\exp\left(\frac{2i\dot{\gamma} + 1}{16\gamma}x^2\right)\left[C + \mathrm{erf}\left(\frac{x}{2\sqrt{2\gamma}}\right)\right].$$

This leads to potentials that, in the case of $\omega(t) = \mathrm{const}$, reduce to the well-known isospectral potentials

$$V(x, t) = \omega^2(t)x^2$$

$$-\frac{1}{4\gamma}[1 - 2zQ^{-1}(z)e^{-z^2/2} - 2Q^{-2}(z)e^{-z^2}],$$

$$Q(z) = \sqrt{\frac{\pi}{2}}\left[C + \mathrm{erf}\left(\frac{z}{\sqrt{2}}\right)\right], \quad z = \frac{x}{2\sqrt{\gamma}}, \quad |C| > 1.$$

Other cases are similar to those described in [3] for the free particle Schrödinger equation, so they are omitted here.

4. THE DEPENDENT SINGULAR OSCILLATOR

Consider now the following Hamiltonian:

$$h_0 = -\partial_x^2 + \omega^2(t)x^2 + gx^{-2}.$$

The symmetry algebra of the Schrödinger equation with this Hamiltonian is $su(1, 1) \sim sl(2, R)$. We use the following representation for this algebra:

$$K_+ = 2[(a^+)^2 - \bar{\varepsilon}^2 g x^{-2}], \quad K_- = 2[a^2 - \varepsilon^2 g x^{-2}],$$

$$K_0 = \frac{1}{2}(K_- K_+ - K_+ K_-) = \frac{1}{2}[K_-, K_+].$$

Consider solutions of the Schrödinger equation which are eigenstates of K_0: $K_0\varphi_\lambda(x, t) = \lambda\varphi_\lambda(x, t)$. When $\lambda = n + k$, $n = 0, 1, 2, \ldots$, we have a discrete basis of the Hilbert space,

$$\varphi_n(x, t) = 2^{1/2-3k}\sqrt{\frac{n!}{\Gamma(n+2k)}}\gamma^{-k}\left(\frac{\bar{\varepsilon}}{\varepsilon}\right)^{n+k} x^{2k-1/2}$$

$$\times \exp\left[i\frac{x^2\dot{\gamma}}{8\gamma} - \frac{x^2}{16\gamma}\right]L_n^{2k-1}\left(\frac{x^2}{8\gamma}\right),$$

$$k = \frac{1}{2} + \frac{1}{4}\sqrt{1+4g}, \quad \gamma = \varepsilon\bar{\varepsilon}.$$

To construct a model with spontaneously broken supersymmetry, we need transformation functions $u(x, t)$ such that neither $u(x, t)$ nor $u^{-1}(x, t)$ are not from the Hilbert space and $u(x, t)$ is nodeless for all real values of t and $x > 0$. These conditions are fulfilled for the functions

$$u_p(x, t) = \gamma^{-k}\left(\frac{\bar{\varepsilon}}{\varepsilon}\right)^{-p-k} x^{2k-1/2}$$

$$\times \exp\left[i\frac{x^2\dot{\gamma}}{8\gamma} + \frac{x^2}{16\gamma}\right]L_p^{2k-1}\left(-\frac{x^2}{8\gamma}\right),$$

$$K_0 u_p(x, t) = -(p+k)u_p(x, t).$$

These transformation functions create the following exactly solvable family of potential differences $A(x, t) = \omega^2(t)x^2 + gx^{-2} - V_1(x, t)$:

$$A(x, t) = A_p(x, t) = \frac{1}{4\gamma} - \frac{4k-1}{x^2} - \frac{1}{8}\left(\frac{xL_{p-1}^{2k}(z)}{\gamma L_p^{2k-1}(z)}\right)^2$$

$$+ \frac{x^2 L_{p-2}^{2k+1}(z) + 4\gamma L_{p-1}^{2k}(z)}{8\gamma^2 L_p^{2k-1}(z)}, \quad z = -\frac{x^2}{8\gamma}.$$

To construct a model with exact supersymmetry, we need transformation functions $u(x, t)$ such that $u^{-1}(x, t)$ is a square integrable on semiaxis $x \geq 0$ and satisfies the zero boundary condition at the origin for all values of t. The following solution of the Schrödinger equation may be chosen in this case:

$$u_p(x, t) = \gamma^{k-1}\left(\frac{\bar{\varepsilon}}{\varepsilon}\right)^{k-p-1} x^{3/2-2k}$$

$$\times \exp\left[i\frac{x^2\dot{\gamma}}{8\gamma} + \frac{x^2}{16\gamma}\right]L_p^{1-2k}\left(-\frac{x^2}{8\gamma}\right),$$

$$K_0 u_p(x, t) = (k-p-1)u_p(x, t).$$

It is not difficult to establish the possible values of p. If p is even, it may take the values $p < 2k - 1$ and $p = [2k] + 1, [2k] + 3, \ldots$. For odd p values, we may use only $p = [2k], [2k] + 2, \ldots$, where $[2k] \equiv \text{entire}(2k)$. For regular potential differences we obtain

$$A_p(x, t) = \frac{1}{4\gamma} + \frac{4k-3}{x^2} - \frac{1}{2}\left(\frac{xL_{p-1}^{2-2k}(z)}{2\gamma L_p^{1-2k}(z)}\right)^2$$

$$+ \frac{x^2 L_{p-2}^{3-2k}(z) + 4\gamma L_{p-1}^{2-2k}(z)}{8\gamma^2 L_p^{1-2k}(z)}.$$

5. CONCLUSION

The supersymmetry of the time-dependent Schrödinger equation based on the nonstationary Darboux transformation is very useful for obtaining a wide class of exactly solvable nonstationary quantum models. With the help of the Darboux transformation operator, we may obtain solutions for transformed equations. In particular, if we know the coherent states for the initial system, then by applying to them the Darboux transformation operator we obtain coherent states for the transformed quantum system [8]. The coherent states are known [7] for the systems considered here. Next step is to obtain and investigate coherent states for the transformed systems. Corresponding results will be presented elsewhere.

ACKNOWLEDGMENTS

One of the authors (BFS) would like to thank the organizers of the VIII International Conference "Symmetry Methods in Physics" for their kind invitation to this meeting.

This work was supported in part by the Russian Foundation for Basic Research (project no. 97-02-16279).

REFERENCES

1. J. Junker, *Supersymmetric Methods in Quantum and Statistical Physics* (Springer-Verlag, Berlin, 1996); F. Coo-

per, A. Khare, and U. Sukhatme, Phys. Rep. **251**, 267 (1995).

2. G. Darboux, C. R. Acad. Sci. (Paris) **94**, 1343, 1456 (1882); E.L. Ince, *Ordinatory Differential Equations* (Dover, New York, 1927).
3. V. G. Bagrov, B. F. Samsonov, and L. A. Shekoyan, Izv. Vyssh. Uchebn. Zaved., Fiz. **7**, 59 (1995); V. G. Bagrov and B. F. Samsonov, Phys. Lett. A **210**, 60 (1996); Fiz. Élem. Chastits At. Yadra **28**, 951 (1997).
4. J. Delsart, C. R. Acad. Sci. (Paris) **206**, 178 (1938); Colloque Int. Nancy (1956), p. 29.
5. V. B. Matveev and M. A. Salle, *Darboux Transformations and Solutions* (Springer-Verlag, Berlin, 1995).
6. W. Miller, *Symmetry and Separation of Variable* (Addison-Wesley, Massachusetts, 1977).
7. I. A. Malkin and V. I. Man'ko, *Dynamical Symmetries and Coherent States of Quantum Systems* (Nauka, Moscow, 1979).
8. B. F. Samsonov, Phys. At. Nucl. **59**, 720 (1996); V. G. Bagrov and B. F. Samsonov, J. Phys. A **29**, 1011 (1996); B. F. Samsonov, J. Math. Phys. (in press).

Physics of Atomic Nuclei, Vol. 63, No. 4, 2000, pp. 661–663. From Yadernaya Fizika, Vol. 63, No. 4, 2000, pp. 727–729.

VIII INTERNATIONAL CONFERENCE ON SYMMETRY METHODS IN PHYSICS

Solutions to the Time-Dependent Schrödinger Equations by Inversion Methods*

E. P. Velicheva[1)]

Joint Institute for Nuclear Research, Dubna, Moscow oblast, 141980 Russia

Abstract—Time-dependent potentials and wave functions are constructed in terms of time-independent ones on the basis of the parametric inverse scattering problem in the adiabatic representation. © *2000 MAIK "Nauka/Interperiodica".*

Consider the system evolving according to the Schrödinger equation

$$i\hbar\frac{d|\Psi(t)\rangle}{dt} = H(x(t))|\Psi(t)\rangle. \quad (1)$$

If $|\psi_n(x(t); y)\rangle$ are solutions to the equation

$$H(x(t))|\psi_n(x(t); y)\rangle = \mathscr{E}_n(x(t))|\psi_n(x(t); y)\rangle \quad (2)$$

and form a complete orthonormal set

$$|\psi_n(x; y)\rangle\langle\psi_n(x; y')| = \delta(y - y'), \langle\psi_n(x; y)|\psi_m(x; y)\rangle = \delta_{nm}$$

for $\forall x$, with elements depending on $x = x(t)$ parametrically, the solution of equation (1) is sought in the form of expansion over eigenstates $|\psi_n(x(t); y)\rangle$ of the self-adjoint parametric Hamiltonian $H(x(t))$ [1],

$$|\Psi(x(t), y)\rangle = \sum_n \mathcal{U}_n(x(t)) \times \exp\left(-\frac{i}{\hbar}\int_0^t \mathscr{E}_n(x(t'))dt'\right)|\psi_n(x(t); y)\rangle. \quad (3)$$

Taking into account (3) in (1), we find that the system of equations for $\mathcal{U}_n(t)$ can be written in the form

$$\partial_t \mathcal{U}_n(t) = \sum_m B_{nm}(x(t)) \times \exp\left[-\frac{i}{\hbar}\int_0^t (\mathscr{E}_n(t') - \mathscr{E}_m(t'))dt'\right]\mathcal{U}_m(t). \quad (4)$$

The matrix elements of the exchange interaction $B_{nm}(x(t))$ are generated by the basis functions $|n\rangle = \psi_n(x; y)$ of the "instantaneous" Hamiltonians (2)

$$B_{nm}(x(t)) = \langle n|\dot{m}\rangle = A_{nm}(x(t))\dot{x}(x), \quad A_{nm}(x) = \langle\psi_n(x; y)|\nabla_x|\psi_m(x; y)\rangle, \quad (5)$$

where the dot denotes the time derivative. Thus, the initial problem is formulated by consistently reducing it to the parametric one (2) and the multichannel system of equation (4). Here, we assume that $H(x(t))$ is real, limited, and continuous in t. Since the eigenfunctions are real-valued and orthonormal for each t, the nonadiabatic couplings $B_{nm} = -B_{mn}$ in (5) are real and antisymmetric in n and m. The transitions from an initial state $\Psi(t_0) = \psi(x(t_0))$ to a final state $\Psi(x(t))$ are determined by the matrix elements of the evolution operator $\mathcal{U}(t, t_0)$ that satisfies the integral equation

$$\mathcal{U}_{nm}(t, t_0) = \delta_{nm} + \sum_{m'}\int_{t_0}^t B_{nm'}(x(s)) \times \exp\left[-\frac{i}{\hbar}\int_{t_0}^s (\mathscr{E}_n(t') - \mathscr{E}_{m'}(t'))dt'\right]\mathcal{U}_{m'm}(s, t_0)ds. \quad (6)$$

One can solve this equation by iteration,

$$\mathcal{U}_{nm}(t, t_0) = \delta_{nm} + \int_{t_0}^t B_{nm}(x(s)) \times \exp\left[-\frac{i}{\hbar}\int_{t_0}^s (\mathscr{E}_n(t') - \mathscr{E}_m(t'))dt'\right]ds + \dots . \quad (7)$$

The transition amplitudes in this case are defined by the matrix elements $B_{nm}(x(t))$ of the exchange interaction (5), which can be calculated in terms of the basis functions $\psi_n(x(t), y)$. The inversion method permits one to construct a wide class of potentials and corresponding solutions of the parametric equation (2) in a closed analytic form. After that, the obtained exact solutions $\psi_n(x(t), y)$ are applied to calculate the matrix elements of the nonadiabatic coupling determining the exchange interaction. Note that the first procedure is an algebraic one, but that the second one is, in general, numerical; therefore, the method is semianalytical.

Transform the procedure of the inverse problem to straightforwardly express the time-dependent potential and solutions of the parametric equation (2) in terms of time-independent ones. Note that this statement is par-

* This article was submitted by the author in English.

[1)] Gomel State University, Gomel, Belarus.

1063-7788/00/6304-0661$20.00 © 2000 MAIK "Nauka/Interperiodica"

ticularly convenient for the investigation of systems with slowly varying spectral functions of time. The solution of this problem is achieved in two stages. At the first stage, one can reconstruct the time-independent potentials $\overset{\circ}{V}(x, y)$ and corresponding solutions $\overset{\circ}{\phi}(k, x, y)$ within the ordinary procedure. After that, the potential and solutions parametrically depending on time through $x(t)$ can be defined from the generalized relations of the parametric inverse problem [2] by using the above-obtained solutions $\overset{\circ}{\phi}(k, x, y)$ as the initial ones. In complete analogy with the procedure [2], when parametric Jost functions are chosen to be rational,

$$f(x(t); k) = \overset{\circ}{f}(k)\prod\frac{k - i\alpha(x(t))}{k + i\beta(x(t))}, \tag{8}$$

the integral equations of the inverse problems are reduced to a set of algebraic equations parametrically depending on the dynamical variables $x(t)$ through the dependence of spectral parameters on these variables. The parametric Jost function (8) has N curves $k = -i\beta_j(x(t))$ of simple poles and N curves of simple zeros $k = i\alpha_j(x(t))$ defined as functions of the parametric variable $x = x(t)$. In this case, the scattering matrix and the spectral function assume the form

$$\mathcal{S}(x; k) = \overset{\circ}{\mathcal{S}}(k)\prod\frac{(k + i\alpha(x))(k + i\beta(x))}{(k - i\beta(x))(k - i\alpha(x))},$$

$$\rho(x; k) = \overset{\circ}{\rho}(k)\prod\frac{(k - i\beta(x))(k + i\beta(x))}{(k + i\alpha(x))(k - i\alpha(x))}.$$

For this type of $\mathcal{S}(x; k)$ and $\rho(x; k)$, the kernels of the integral equations of the parametric inverse problem can be represented as the sums of terms with a factorized dependence on the fast variable y: $Q(x; y, y') = \sum_i^N B_i(x; y)B_i(x; y')$. When the kernel Q is inserted into the base parametric equation of the inverse problem

$$K(x(t); y, y') + Q(x(t); y, y') + \int_{y(0)}^{\infty(y)} K(x(t); y, y'')Q(x(t); y'', y')dy' = 0, \tag{9}$$

it is evident that the kernel of the generalized shift $K(x; y, y')$ also becomes degenerate. As a consequence, the system of integral equations of the inverse problem is reduced to a system of algebraic equations. Potentials and Jost solutions are determined from $K(x; y, y')$, with respect to which the linear integral equation (9) is solved for every fixed x. The parametric dependence of the scattering data $\{\mathcal{S}(x, k), M^2(x), \mathcal{E}(x)\}$ or the spectral data $\{\rho(x, k), N^2(x), \mathcal{E}(x)\}$ reflects the peculiarity of the nonstandard parametric inverse problem. Specifying this dependence and employing the algebraic methods of the inverse scattering problem, one can present a wide class of parametric Hamiltonians for which one can construct exactly solvable models and, consequently, derive solutions in a closed analytic form [3].

For instance, for the reflectionless potentials $\mathcal{S}^{\text{ref}}(k) = 0$, the kernel $Q(x(t); y, y')$ is obtained from the potential curves $\mathcal{E}_n(x(t_0))$ and $\mathcal{E}_n(x(t))$ and the normalizing functions $\gamma_n^2(x(t_0))$ and $\gamma_n^2(x(t))$ corresponding to the potentials $\overset{\circ}{V}(y)$ and $V(x(t); y)$, respectively:

$$\begin{aligned} &Q(x(t); y, y') \\ &= \sum_n^N \gamma_n^2(x(t))\overset{\circ}{\phi}(i\kappa_n(x(t)), y)\overset{\circ}{\phi}(i\kappa_n(x(t)), y') \\ &- \sum_n^N \gamma_n^2(x(t_0))\overset{\circ}{\phi}(i\kappa_n(x(t_0)), y)\overset{\circ}{\phi}(i\kappa_n(x(t_0)), y') \\ &= \overset{\circ}{\Phi}{}^T(x(t), y)\hat{\Gamma}(x(t))\overset{\circ}{\Phi}(x(t), y'). \end{aligned} \tag{10}$$

Here, $\overset{\circ}{\phi}(x(t), y) = |\overset{\circ}{\phi}_n(x(t), y)\rangle$ is the $2N$ vector, the N components of which are taken at $k = i\kappa_n(x(t))$, $n = 1, 2, \ldots, N$ and the other N components are taken at $k = i\kappa_n(x(t_0))$, $n = N + 1, N + 2, \ldots, 2N$. The diagonal $2N \times 2N$ matrix $\hat{\Gamma}$ is combined from two block matrices, each also being diagonal: $\Gamma(x(t)) = \gamma_j(x(t))\hat{I}$ and $\overset{\circ}{\Gamma}(x(t_0)) = \gamma_j(x(t_0))\hat{I}$,

$$\hat{\Gamma}(x(t)) = \begin{pmatrix} \Gamma(x(t)) & 0 \\ 0 & -\overset{\circ}{\Gamma}(x(t_0)) \end{pmatrix}.$$

The kernels $K(x(t); y, y')$ obtained from (9) with $Q(x(t); y, y')$ determined by (10) are presented in the matrix form as

$$K(x(t); y, y') = -\Phi^T(x(t), y)\hat{\Gamma}(x(t))\overset{\circ}{\Phi}(x(t), y'). \tag{11}$$

Here, $\Phi(x(t), y) = |\phi_n(x(t), y)\rangle$ is the $2N$ vector, the N components of which are taken at $k = i\kappa_n(x(t))$, $\phi_n(x(t), y) = \phi(i\kappa_n(x(t)), y)$, $n = 1, 2, \ldots, N$ and the other N components are taken at $k = i\kappa_n(x(t_0))$, $n = N + 1, N + 2, \ldots, 2N$. If the spectral data are defined as $\kappa_n(x(t_0)) = \kappa_n$ and $\gamma_n(x(t_0)) = \gamma_n$, then $\phi_n(i\kappa_n(x(t_0)), y) = \overset{\circ}{\phi}(i\kappa_n, y)$. Substituting the vector $\overset{\circ}{\Phi}(x(t), y)$ and the kernel $K(x(t); y, y')$ (11) into (9), we obtain the following equation for the sought solution $\Phi(x(t), y)$:

$$\Phi(x(t), y) = \overset{\circ}{\Phi}{}^T(x(t), y)P^{-1}(x(t), y), \tag{12}$$

or in an alternative form,

$$\phi(i\kappa_n(x(t)), y) = \sum_m^{2N}\overset{\circ}{\phi}(i\kappa_m(x(t)), y)P_{mn}^{-1}(x(t), y).$$

Here, the functions $\overset{\circ}{\phi}(k, y)$ are taken at $k = i\kappa_n(x(t))$. This is possible, since the functions $\overset{\circ}{\phi}(k, y)$ are deter-

mined for any k. The matrix $P(x(t), y)$ is

$$P(x(t), y) = \hat{I} + \Gamma(x(t)) \int_{y(0)}^{\infty(y)} \overset{\circ}{\Phi}{}^{T}(x(t), y')\overset{\circ}{\Phi}(x(t), y')dy'. \quad (13)$$

Now the potential can be obtained in the following form:

$$V(x(t); y) = \overset{\circ}{V}(y) \mp 2\frac{d^2}{dy^2}\ln|\det P(x(t), y)|. \quad (14)$$

The normalized eigenfunctions $\psi_n(x(t); y) = \gamma_n(x(t)) \times \phi(i\kappa_n(x(t)), y)$ can be determined by using (12). It is evident that at $t = t_0$, we have $\psi_n(x(t_0); y) = \overset{\circ}{\psi}_n(y)$.

Now the matrix elements $B_{nm}(x(t))$ (5) can be written in terms of the exact time-independent solutions $\overset{\circ}{\phi}(i\kappa_n(x(t)), y)$ taken at $k = i\kappa_n(x(t))$ and for the parametric spectral data $\{\mathscr{E}_n(x(t)), \gamma_n(x(t))\}$. Note that $\phi(i\kappa_n(x(t)), y)$ can be obtained analytically in terms of free solutions by the ordinary procedure of Darboux or Bargmann transformations performed at each moment of time [3–6]. Nevertheless, in both cases, the matrix elements $B_{nm}(x(t))$ (5) should be obtained in terms of exact solutions by numerical calculation, although it is straightforward. However, for the investigation of adiabatically driven systems, the statement where $\phi(i\kappa_n(x(t)), y)$ is expressed in terms of $\overset{\circ}{\phi}(i\kappa_n(x(t)), y)$ is preferable. The matrix elements (6) of the evolution operator $\mathcal{U}_{nm}(t, t_0)$ should be calculated numerically by using $B_{nm}(x(t))$ within the iteration procedure. In many cases when spectral functions $i\kappa_n(x(t))$ and $\gamma_n(x(t))$ are slowly and smoothly varying functions of time through the dependence of the adiabatic variable on time, $x(t) = xg(t)$, it is possible to make the following replacement in (5):

$$B_{nm}(x(t)) \longrightarrow \langle\gamma_n(x(t))\overset{\circ}{\phi}(i\kappa_n(x(t)), y)|\partial_t|\gamma_m(x(t))\overset{\circ}{\phi}(i\kappa_m(x(t)), y)\rangle.$$

The parametric dependence of the matrix elements $B_{nm}(x(t))$ can be factorized,

$$B_{nm}(x(t)) = \overset{\circ}{A}_{nm}(x)\partial_t g(t),$$

where $g(t)$ is a slowly varying function of time. After that, the transition matrix takes a very simple form,

$$\mathcal{U}_{nm}(t_0, t) = \delta_{nm} + \overset{\circ}{A}_{nm}(x)\int_{t_0}^{t}\partial_s g(s)\exp\left[-\frac{i}{\hbar}\int_{t_0}^{s}(\mathscr{E}_n(t') - \mathscr{E}_m(t'))dt'\right]ds. \quad (15)$$

In principle, it is not difficult to take into account the exact functions $\psi_n(x(t); y)$, but calculating $\mathcal{U}_{nm}(t_0, t)$ becomes cumbersome. The transition amplitude for the concrete smooth behavior of $x(t) = \overset{\circ}{x}(1 + a\exp(-1/t))$ was investigated in [7].

It is quite evident that one can choose a different dependence of the adiabatic variables on time and different spectral data with the prescribed properties. In particular, for a special case of parametric variation, the spectral characteristics may be taken in a factorized form, $\mathscr{E}_n(x) = x^2\tilde{\mathscr{E}}_n$, where $\tilde{\mathscr{E}}_n$ are eigenvalues of the initial problem (see, e.g., [8]). Some examples of the reconstruction of time-dependent and time-independent two-dimensional potentials and the corresponding solutions were considered in [3–6].

CONCLUSIONS

The method presented permits one to construct a wide class of potentials and corresponding solutions of the parametric equation (2) in a closed analytic form and, after that, calculate the matrix elements of the exchange interaction and the transition matrix. The first procedure is an algebraic one, but the second step is, in general, numerical. Therefore, the method is semianalytic. We have constructed time-dependent potentials and wave functions in terms of time-independent ones on the basis of the parametric inverse scattering problem in the adiabatic representation. This statement is suggested for investigating adiabatically driven systems.

ACKNOWLEDGMENTS

The authors are grateful to Prof. H. von Geramb, Dr. M. Sander, and Dr. L. Jade for valuable discussions.

REFERENCES

1. J. T. Hwang and Ph. Pechukas, J. Chem. Phys. **67**, 4640 (1977).
2. A. A. Suzko, Phys. Part. Nucl. **24**, 485 (1993); in *Proceedings of the International Conference on Quantum Inversion Theory and Applications*, Ed. by H. V. von Geramb, Ser. "Lecture Notes in Physics" (Springer-Verlag, Heidelberg, 1993), Vol. 427, p. 67.
3. A. A. Suzko and E. P. Velicheva, Phys. Part. Nucl. **27**, 379 (1996).
4. A. A. Suzko and E. P. Velicheva, Preprint No. E4-97-200, JINR (Dubna, 1997).
5. A. A. Suzko and E. P. Velicheva, in *Proceedings of the International Conference on Inverse and Algebraic Quantum Scattering Theory, Lake Balaton, Balatonfoldvar*, Ser. "Lecture Notes in Physics" (Springer-Verlag, Heidelberg, 1997), Vol. 488, p. 342.
6. A. A. Suzko, in *Proceedings of the International Conference on Inverse and Algebraic Quantum Scattering Theory, Lake Balaton, Balatonfoldvar*, Ser. "Lecture Notes in Physics" (Springer-Verlag, Heidelberg, 1997), Vol. 488, p. 314.
7. A. A. Kvitsinsky and S. Putterman, Phys. Rev. A **42**, 6303 (1990).
8. V. Spiridonov, Phys. Rev. A **52**, 1909 (1995).

Physics of Atomic Nuclei, Vol. 63, No. 4, 2000, pp. 664–665. From Yadernaya Fizika, Vol. 63, No. 4, 2000, pp. 730–731.

VIII INTERNATIONAL CONFERENCE ON SYMMETRY METHODS IN PHYSICS

SU(2) Skyrme Vortices*

Yu. P. Rybakov, A. M. Tarabay, and I. G. Chugunov

Department of Theoretical Physics, Russian University of Peoples' Friendship, ul. Miklukho-Maklaya 6, Moscow, 117198 Russia

Abstract—A regular method for constructing vortexlike solutions with cylindrical symmetry to the equations of the *SU*(2) Skyrme chiral model is proposed. A numerical estimate for the length density of mass is given. *© 2000 MAIK "Nauka/Interperiodica".*

The Skyrme model [1] has proven its efficiency in modeling the structure of baryons [2] and nuclei [3] since the appearance of Witten's analysis of the quark confinement problem [4, 5]. The model considers pions as Goldstone bosons and uses the Lagrangian density

$$\mathcal{L} = -\frac{1}{4\lambda^2}\mathrm{tr}(l_\mu l^\mu) + \frac{\varepsilon^2}{16}\mathrm{tr}([l_\mu, l_\nu][l^\mu, l^\nu]), \qquad (1)$$

constructed from the chiral current $l_\mu = U^+\partial_\mu U$, $U \in SU(2)$. The energy in the model is estimated from below through the topological charge

$$Q = -\frac{1}{24\pi^2}\varepsilon^{ijk}\int d^3x\,\mathrm{tr}(l_i l_j l_k),$$

which takes integer values and can be interpreted as the baryon number. In particular, the nucleon emerges as an absolutely stable state with minimal energy in the first homotopic class ($Q = 1$) [6]. Unfortunately, the corresponding hedgehog configuration cannot be described analytically due to the complexity of the nonlinear equations for the chiral field. The situation is aggravated for the higher homotopic classes in view of nonseparability of radial and angular variables. To overcome these difficulties, we propose to approximate the configuration with higher charges by closed vortices. As a first step in this direction, we consider in the present paper the simplest static vortex configurations given by the matrix

$$U = \exp(i\tau\Theta(\rho)), \quad \tau = \begin{bmatrix} 0 & e^{-i\varphi} \\ e^{i\varphi} & 0 \end{bmatrix}, \qquad (2)$$

with ρ and φ being cylindrical coordinates. The configuration (2) appears to be equivariant under the group $G = T(z) \otimes \mathrm{diag}[SO(2)_I \otimes SO(2)_S]$ including the translation along the vortex and combined isotropic-space rotations around its axis.

Substituting (2) into (1) amounts to the radial Lagrangian density for the chiral angle $\Theta(\rho)$:

$$\mathcal{L} = -\frac{1}{2\lambda^2}\left(\Theta'^2 + \frac{\sin^2\Theta}{\rho^2}\right) - \varepsilon^2\Theta'^2\frac{\sin^2\Theta}{\rho^2}.$$

After the change of variable $\rho = \lambda\sqrt{2}\,e^t$, $-\infty \le t \le +\infty$, we obtain the mechanical problem given by the action functional

$$I[\Theta] = \int_{-\infty}^{+\infty} dt[\dot\Theta^2(1 + \varepsilon^2 e^{-2t}\sin^2\Theta) + \sin^2\Theta], \qquad (3)$$

where the dimensionless parameter ε^2 is reserved for technical purposes.

From (3), we derive the canonical momentum

$$p = 2\dot\Theta(1 + \varepsilon^2 e^{-2t}\sin^2\Theta) = \partial_\Theta S \qquad (4)$$

and the Hamilton–Jacobi equation

$$\partial_t S + \frac{1}{4}(\partial_\Theta S)^2(1 + \varepsilon^2 e^{-2t}\sin^2\Theta)^{-1} - \sin^2\Theta = 0. \qquad (5)$$

Now, we search for the solution to equation (5) as a formal series

$$S(t, \Theta) = \sum_{n=0}^{\infty}\varepsilon^{2n}S_n(t, \Theta). \qquad (6)$$

Inserting (6) into (5), we get the recurrence relation

$$\frac{1}{4}\sum_{l=0}^{n}\partial_\Theta S_l\partial_\Theta S_{n-l} + \partial_t S_n + \partial_t S_{n-1}e^{-2t}\sin^2\Theta = \delta_{n0}\sin^2\Theta + \delta_{n1}e^{-2t}\sin^4\Theta \qquad (7)$$

with the evident particular solution for $n = 0$,

$$S_0 = W_0(\Theta) = 2\cos\Theta. \qquad (8)$$

In order to satisfy (7), we set for $n > 0$

$$S_n(t, \Theta) = e^{-2nt}W_n(\Theta). \qquad (9)$$

From (7)–(9), we derive for $n = 1$ the equation

$$\sin\Theta W_1' + 2W_1 + \sin^4\Theta = 0$$

with the two different solutions (two branches) corresponding to the ranges $\pi/2 \le \Theta \le \pi$ and $0 \le \Theta \le \pi/2$,

* This article was submitted by the authors in English.

respectively:

$$W_1^+(\Theta) = \frac{1}{3}(1+\cos\Theta)^2\left(\frac{4}{1-\cos\Theta}+3-\cos\Theta\right), \quad (10)$$

$$W_1^-(\Theta) = -\frac{1}{3}(1-\cos\Theta)\sin^2\Theta. \quad (11)$$

For $n > 1$, we deduce from (7)–(9) the equation

$$\sin\Theta W_n' + 2nW_n = \frac{1}{4}\sum_{l=1}^{n-1} W_l' W_{n-l}' - 2(n-1)\sin^2\Theta W_{n-1}$$

with the solution

$$W_n^{\pm}(\Theta) = \tan^{-2n}(\Theta/2)\int_{a_\pm}^{\Theta}\frac{d\Theta}{\sin\Theta}\tan^{2n}(\Theta/2) \times\left[\frac{1}{4}\sum_{l=1}^{n-1} W_l' W_{n-l}' - 2(n-1)\sin^2\Theta W_{n-1}\right], \quad (12)$$

where $a_+ = \pi$ and $a_- = 0$. Formulas (10)–(12) determine the recurrent procedure for constructing the solution to the Hamilton–Jacobi equation (5). Inserting this solution into the right-hand side of equation (4), we can find the canonical momentum p for the two branches of the solution:

$$p = 2\dot{\Theta}(1+\varepsilon^2 e^{-2t}\sin^2\Theta) = \sum_{n=0}^{\infty}\varepsilon^{2n}e^{-2nt}W_n'(\Theta). \quad (13)$$

For matching these branches at the point $\Theta = \pi/2$, $t = t_0$, we deduce from (13) the algebraic equation

$$\sum_{n=1}^{\infty}\varepsilon^{2n}e^{-2nt_0}[W_n^{+\prime}(\pi/2) - W_n^{-\prime}(\pi/2)] = 0. \quad (14)$$

In particular, within the scope of the $n = 2$ approximation, we obtain from (14) the effective development parameter

$$\xi = \frac{1}{3}\varepsilon^2 e^{-2t_0} = 2(16\ln 2 - 37/15)^{-1} \approx 0.232,$$

which permits us to calculate the mass of the vortex (its length density):

$$M = \frac{\pi}{\lambda^2}I = \frac{\pi}{\lambda^2}[S^-(+\infty, 0) - S^-(t_0, \pi/2) + S^+(t_0, \pi/2) - S^+(-\infty, \pi)]$$

$$= \frac{4\pi}{\lambda^2}[1 + 2\xi + \xi^2(41/15 - 8\ln 2) + O(\xi^3)] \approx \frac{4\pi}{\lambda^2}\times 1.31.$$

In conclusion, we note that the function $\Theta(t)$ defining the radial distribution of matter inside the vortex can be found from equation (13), which is represented in the integral form

$$\tan\frac{\Theta}{2} = e^{t_0 - t}\exp\left\{\int_{t_0}^{t} dt(1+\varepsilon^2 e^{-2t}\sin^2\Theta)^{-1} \times\left(\varepsilon^2 e^{-2t}\sin^2\Theta + \frac{1}{2}\sum_{n=1}^{\infty}\varepsilon^{2n}e^{-2nt}\frac{W_n'}{\sin\Theta}\right)\right\}.$$

REFERENCES

1. T. H. R. Skyrme, Nucl. Phys. **31**, 556 (1962).
2. G. S. Adkins, Ch. R. Nappi, and E. Witten, Nucl. Phys. B **228**, 552 (1983).
3. R. M. Nikolayeva, V. A. Nikolayev, and O. G. Tkachov, Fiz. Élem. Chastits At. Yadra **23**, 542 (1992) [Sov. J. Part. Nucl. **23**, 239 (1992)].
4. E. Witten, Nucl. Phys. B **223**, 422 (1983).
5. E. Witten, Nucl. Phys. B **223**, 433 (1983).
6. Yu. P. Rybakov, *VINITI Series: Classical Field Theory and Gravitational Theory*, Vol. 2: *Gravitation and Cosmology* (VINITI, Moscow, 1991), p. 56.

Physics of Atomic Nuclei, Vol. 63, No. 4, 2000, pp. 666–667. From Yadernaya Fizika, Vol. 63, No. 4, 2000, pp. 732–733.

VIII INTERNATIONAL CONFERENCE ON SYMMETRY METHODS IN PHYSICS

The Riemann Surface of a Static Dispersion Model and Regge Trajectories*

V. A. Meshcheryakov

Joint Institute for Nuclear Research, Dubna, Moscow oblast, 141980 Russia

Abstract—The S matrix in the static limit of a dispersion relation is a matrix of a finite order N of meromorphic functions of energy ω in the plane with cuts $(-\infty, -1]$ and $[+1, +\infty)$. In the elastic case, it reduces to N functions $S_i(\omega)$ connected by the crossing-symmetry matrix A. The scattering of a neutral pseudoscalar meson with an arbitrary angular momentum l at a source with spin 1/2 is considered ($N = 2$). The Regge trajectories of this model are explicitly found. *© 2000 MAIK "Nauka/Interperiodica".*

The analytic structure of physical amplitudes in gauge theories with confinement was investigated in [1]. It was shown that the analytic structure of hadron physical amplitudes established in old proofs of dispersion relations remains valid in QCD. It is well known [2] that the static limit of a dispersion relation is equivalent to the system of nonlinear integral equations [3]. Below, we will study this type of equations, reducing them to a nonlinear boundary-value problem [4]. It consists of the following series of conditions on S_i, S-matrix elements:

$$S_i(z) \text{ are meromorphic functions in the complex plane } z \text{ with cuts } (-\infty, -1], [+1, +\infty), \tag{1a}$$

$$S_i^*(z) = S_i(z^*), \tag{1b}$$

$$|S_i(\omega + i0)|^2 = 1 \text{ at } \omega \geq 1; \quad S_i(\omega + i0) = \lim_{\epsilon \to +0} S_i(\omega + i\epsilon), \tag{1c}$$

$$S_i(-z) = \sum_{j=1}^{N} A_{ij} S_j(z). \tag{1d}$$

Real values of the variable z represent the total energy ω of a relativistic particle scattered at a fixed center. The requirement that function $S_i(z)$ be meromorphic results from the static limit of the scattering problem [5]. The elastic condition of unitarity (1c) is valid only on the right cut of the plane z. On the left cut, functions $S_i(z)$ are given by the conditions of crossing symmetry (1d). The matrix of crossing symmetry A is defined by the group under which the S matrix is invariant (see, for instance, [4]). Let us write conditions (1a)–(1c) in matrix form. To this end, we introduce the column $S^{(0)}(z) = [S_1(z), S_2(z), \ldots, S_N(z)]$, where the upper index denotes the physical sheet of the Riemann surface of the S matrix. Conditions (1a), (1b), and (1d) refer to the physical sheet, while the unitarity condition (1c) can be extended to complex values of ω, being of a componentwise form, $S_i^{(0)}(z)S_i^{(1)}(z) = 1$. The matrix form of the unitarity condition (1c) is derived by the nonlinear operation of inversion I according to the formula $IS(z) = [1/S_1(z), 1/S_2(z), \ldots, 1/S_N(z)]$. As a result, conditions (1a)–(1d) assume the form

$$S^{(0)}(z) \text{—a column of meromorphic functions in the complex plane } z \text{ with cuts } (-\infty, -1] \text{ and } [+1, +\infty), \tag{2a}$$

$$S^{(0)*}(z) = S^{(0)}(z^*), \tag{2b}$$

$$S^{(1)}(z) = IS^{(0)}(z), \tag{2c}$$

$$S^{(0)}(-z) = AS^{(0)}(z). \tag{2d}$$

Analytic continuation onto unphysical sheets will be defined as follows [6]:

$$S^{(p)}(z) = (IA)^p S^{(0)}(z(-1)^p). \tag{3}$$

By using definition (3), we can easily continue the unitarity condition (2c) and crossing-symmetry condition (2d) onto unphysical sheets

$$IS^{(p)}(z) = S^{(1-p)}(z), \quad AS^{(p)}(z) = S^{(-p)}(-z) \tag{4}$$

and we arrive at the formula

$$(IA)^q S^{(p)}(z) = S^{(q+p)}(z(-1)^q). \tag{5}$$

For example, the scattering of a neutral pseudoscalar pion at a fixed nucleon with spin 1/2 is defined by the condition (1) and the two-row matrix

$$A = \frac{1}{2l+1}\begin{pmatrix} -1 & 2l+2 \\ 2l & 1 \end{pmatrix}, \quad l \in N. \tag{6}$$

Let us introduce the function $X = S_1/S_2$ and consider it for $z = 0$. Then, the continuation of X onto the first

* This article was submitted by the author in English.

1063-7788/00/6304-0666$20.00 © 2000 MAIK "Nauka/Interperiodica"

unphysical sheet is determined by the rule

$$X^{(1)} = \frac{2lX^{(0)} + 1}{-X^{(0)} + (2l + 2)},$$

and, together with the crossing-symmetry conditions (4), gives the following expression for $X^{(n)}$:

$$X^{(n)} = \frac{n - (l + 1)}{n + l}, \quad X^{(0)} = -(1 + 1/l). \tag{7}$$

Thus, on any unphysical sheet n, the ratio S_1/S_2 is defined at $z = 0$, and, in order to construct S_1 and S_2, it is sufficient to find any of them. Let us denote S_2 by $\varphi = S_2$. This function is determined by the system of functional equations

$$\varphi^{(n)}\varphi^{(1-n)} = 1, \tag{8}$$

$$\frac{\varphi^{(n)}}{\varphi^{(-n)}} = \frac{n + l}{n - l}, \tag{9}$$

which follows from the unitarity and the crossing symmetry conditions (4) on the unphysical sheets. Here, only those equalities are used from (4) which were not used for derivation of equation (7). Equation (8) has an obvious solution in the ring of meromorphic functions

$$\varphi^{(n)} = G(n)/G(1 - n), \tag{10}$$

where $G(n)$ is an entire function. Solution (10) can be represented in another form $\varphi^{(n)} = g(n - 1/2)$, where $g(n - 1/2)$ is any odd function of its argument. That form of $\varphi^{(n)}$ is convenient for the solution to equation (9), which is now of the form

$$g(n + 1) + g(n) = \ln\frac{n + 1/2 + l}{n + 1/2 - l}.$$

A partial solution to this nonhomogeneous difference equation can be found by subsequent substitutions of unknown functions according to the formulas

$$g_m(n) = g_{m+1}(n) + \ln\frac{n + (-1)^m\alpha_{m+1}}{n - (-1)^m\alpha_{m+1}},$$

where $\alpha_k = 1/2 + l - k$ and $g_0(n) = g(n)$. The function g_k obeys the equation

$$g_k(n + 1) + g_k(n) = \ln\frac{n + 1/2 + (-1)^k(l - k)}{n + 1/2 - (-1)^k(l - k)}.$$

It is clear that

$$g_l(n + 1) + g_l(n) = 0 \tag{11}$$

and a general solution to this equation gives a trivial solution to the problem (1), which does not depend on l. Therefore, we obtain [5]

$$\varphi^{(n)} = \prod_{m=1}^{l}\frac{n - 1/2 - (-1)^m(1/2 + l - m)}{n - 1/2 + (-1)^m(1/2 + l - m)}. \tag{12}$$

We have an infinite product in formulas (12) for noninteger $l \in R$. Now, equation (11) is of the form

$$g(n + 1) + g(n) = \ln(-1). \tag{13}$$

In this case, we have instead of equation (12)

$$\varphi^{(n)} = \psi(n)\frac{\Gamma\left[-\frac{n + l}{2} + 1\right]\Gamma\left[\frac{n - l}{2}\right]}{\Gamma\left[\frac{n - 1 - l}{2} + 1\right]\Gamma\left[-\frac{n - 1 + l}{2}\right]}, \tag{14}$$

where $\psi(n)$ is a general solution of equation (13) with properties

$$\psi(n + 1)\psi(n) = -1, \quad \psi(n)\psi(-n) = 1. \tag{15}$$

Until now, one of the unitarity conditions (1c) was not used, and it gives the following result:

$$n(z) = 1/\pi \times \arcsin z + i\sqrt{z^2 - 1}\beta(z), \tag{16}$$

where $\beta(z) = -\beta(-z)$ is a meromorphic function. Equation (16) shows that the Riemann surface of the model has algebraic branch points at $z = \pm 1$ and a logarithmic one at infinity. Now, formulas (7), (14)–(16) give the general solution to the problem (1) for matrix (6). The function ψ can be determined from the requirement that equation (14) turn into equation (12) for integer l. This gives $\psi(n) = -\cot n \times \pi/2$ for l even and $\psi(n) = -\tan n \times \pi/2$ for l odd.

Let us recall that, in equation (14), $l \in R$, but it is clear that this relation can be continued to $l \in C$ and allows explicit determination of the Regge trajectories with definite signature $l_k^{\pm}(z)$. The common part of the set of Regge trajectories for $J_{\pm} = l \pm 1/2$ is of the form $l^{\pm}(z) = \{2 - n(z) + 2k, n(z) + 2k|_{k=0,1,2,\ldots}\}$. The Regge trajectories for $J_- = l - 1/2$ contain one additional trajectory $l_{J_-}^{\pm}(z) = -n(z)$. All the Regge trajectories of the model depend on one function $\beta(z)$.

REFERENCES

1. R. Oehme, Phys. Rev. D **42**, 4209 (1990); Phys. Lett. B **252**, 14 (1990); Int. J. Mod. Phys. A **10**, 1995 (1995).
2. G. Chew *et al.*, Phys. Rev. **106**, 1337 (1957).
3. F. Low, Phys. Rev. **97**, 1932 (1955); G. Chew and F. Low, Phys. Rev. **101**, 1570 (1956); R. Oehme, Phys. Rev. **102**, 1174 (1956).
4. V. A. Meshcheryakov, JINR Commun., No. R-2369 (Dubna, 1965); V. I. Zhuravlev and V. A. Meshcheryakov, Fiz. Élem. Chastits At. Yadra **5**, 173 (1974).
5. V. A. Meshcheryakov, Sov. Phys. JETP **26**, 120 (1968).
6. V. A. Meshcheryakov, Int. J. Mod. Phys. A **12**, 249 (1997).

Physics of Atomic Nuclei, Vol. 63, No. 4, 2000, pp. 668–671. From Yadernaya Fizika, Vol. 63, No. 4, 2000, pp. 734–737.

VIII INTERNATIONAL CONFERENCE ON SYMMETRY METHODS IN PHYSICS

Direct Mode Summation for the Casimir Energy of a Spherical Shell and a Compact Ball*

V. V. Nesterenko and I. G. Pirozhenko

Joint Institute for Nuclear Research, Dubna, Moscow oblast, 141980 Russia

Abstract—A simple method for calculating the Casimir energy for a sphere and a compact ball is developed on the basis of a direct mode summation by means of contour integration in a complex plane of eigenfrequencies. © *2000 MAIK "Nauka/Interperiodica".*

1. INTRODUCTION

The Casimir effect can be generally defined as an influence of the boundedness of the configuration space on the physical characteristics of the quantum field system.

When considering the Casimir effect, different methods are used: Green's function formalism, the stress-tensor method, multiple scattering expansion, the zeta regularization technique, and the heat-kernel series [1]. In all the approaches to calculation of the Casimir effect, a vague point is the procedure of unique separation and subsequent removal of the divergences. The lack of a universal mathematically rigorous prescription for this purpose leads, in some problems, to different results when different methods are applied.

With allowance for all this, the simplest, from the mathematical point of view, method of direct mode summation [2] has an obvious advantage because it right away allows one to reveal the difficulties generated by divergences. The main goal of this paper is to show the simplicity and efficiency of this method when calculating the Casimir energy for a perfectly conducting and infinitely thin spherical shell and for a solid ball placed in an infinite medium. This approach is completely based on using the classical frequencies of the quantum field system concerned, and the main tool employed is the Cauchy theorem from complex analysis.

2. PERFECTLY CONDUCTING SPHERICAL SHELL

The starting point of our approach is the following definition of the Casimir energy:

$$E = \frac{1}{2}\sum_s(\omega_s - \bar{\omega}_s). \qquad (1)$$

Here, ω_s are the eigenfrequencies of the system under consideration, and $\bar{\omega}_s$ are those of the same system when the parameters determining its boundaries take on some limiting values. There are two modes of oscillations of the electromagnetic field inside and outside the perfectly conducting sphere with radius a: transverse-electric and transverse-magnetic modes (TE modes and TM modes, respectively). The eigenfrequencies of the TE modes are defined by the equations [3]

$$j_l(\omega a) = 0, \quad h_l^{(1)}(\omega a) = 0, \qquad (2)$$

and the eigenfrequencies for the TM modes are given by

$$\frac{d}{dr}[rj_l(\omega r)]\big|_{r=a} = 0, \quad \frac{d}{dr}[rh_l^{(1)}(\omega r)]\big|_{r=a} = 0. \qquad (3)$$

In formulas (2) and (3), $j_l(z)$ and $h_l^{(1)}(z)$ are the spherical Bessel functions [4],

$$j_l(z) = \sqrt{\frac{\pi}{2z}}J_{l+1/2}(z), \quad h_l^{(1)}(z) = \sqrt{\frac{\pi}{2z}}H_{l+1/2}^{(1)}(z), \qquad (4)$$

and $l = 1, 2, \ldots$. Only positive roots of these equations $\omega_{nl} > 0$, $n = 1, 2, \ldots$, should be considered. The first (second) equations (2) and (3) specify the frequencies of the electromagnetic oscillations inside (outside) the sphere [3].

In the case of a spherical boundary, the sum $\sum_s$ in (1) can be written as

$$\frac{1}{2}\sum_s\omega_s = \frac{1}{2}\sum_{l=1}^{\infty}\sum_{m=-l}^{l}\sum_{n=1}^{\infty}\omega_{nl} = \sum_{l=1}^{\infty}(l+1/2)S_l, \qquad (5)$$

where $S_l = \sum_{n=1}^{\infty}\omega_{nl}$, and each frequency equations (2) and (3) generates its own partial sum S_l^{α}, $\alpha = 1, \ldots, 4$, so that $\sum_{\alpha=1}^{4}S_l^{(\alpha)}$.

For the partial sums $S_l^{(\alpha)}$, we use the integral representation that follows from the Cauchy theorem [4]:

$$S_l^{(\alpha)} = \frac{1}{2\pi i}\oint_C dz z\frac{d}{dz}\ln f^{(\alpha)}(z, a). \qquad (6)$$

* This article was submitted by the author in English.

1063-7788/00/6304-0668$20.00 © 2000 MAIK "Nauka/Interperiodica"

Here, $f^{(\alpha)}(z, a)$ are the functions defining the frequency equations (2), (3) in the form $f^{(\alpha)}(\omega, a) = 0$, $\alpha = 1, 2, 3, 4$. The contour C encloses counterclockwise positive roots of these equations and consists of the segment $[-i\Lambda, i\Lambda]$ of the imaginary axis and a semicircle of radius Λ with $\Lambda \longrightarrow \infty$ in the right half-plane. When Λ is fixed, the contour integral (6) gives the regularized value of corresponding frequency sum. For negative values of the argument ω, the functions $f^{(\alpha)}(\omega, a)$ have to be defined by a condition $f^{(\alpha)}(-\omega, a) = f^{(\alpha)}(\omega, a)$, $\omega > 0$.

In accordance with definition (1), it is necessary to perform subtraction in order to obtain a finite (observable) value of the Casimir energy. As usual, we shall subtract the contribution of the Minkowski space that corresponds to the limit $a = \infty$ in equation (6). Letting $\bar{S}_l^{(\alpha)}$ represent the value of the partial sum $S_l^{(\alpha)}$, which is to be subtracted from (6), we get

$$S_l^{(\alpha)} - \bar{S}_l^{(\alpha)} = \frac{1}{\pi}\int_0^\infty dy \ln\left[\frac{f^{(\alpha)}(iy, a)}{f^{(\alpha)}(iy, a \longrightarrow \infty)}\right]. \quad (7)$$

Integration along the semicircle of radius Λ does not contribute to difference (7) when $\Lambda \longrightarrow \infty$. Now we proceed to substitute into equation (7) the concrete expressions for the functions $f^{(\alpha)}$ defined by frequency equations (2) and (3). From equation (2), we obtain

$$\frac{f^{(1)}(iy, a)}{f^{(1)}(iy, a \longrightarrow \infty)} = \frac{J_\nu(iya)}{\lim\limits_{a\to\infty} J_\nu(iya)} = \frac{I_\nu(ay)}{\lim\limits_{a\to\infty} I_\nu(ay)} = \sqrt{2\pi ay}e^{-ay}I_\nu(ay), \quad (8)$$

$$\frac{f^{(2)}(iy, a)}{f^{(2)}(iy, a \longrightarrow \infty)} = \frac{H_\nu^{(1)}(iya)}{\lim\limits_{a\to\infty} H_\nu^{(1)}(iya)} = \frac{K_\nu(ay)}{\lim\limits_{a\to\infty} K_\nu(ay)} = \sqrt{\frac{2ay}{\pi}}e^{ay}K_\nu(ay). \quad (9)$$

Here, $I_\nu(z)$ is the modified Bessel function $J_\nu(iz) = i^\nu I_\nu(z)$ and $H_\nu^{(1)} = J_\nu(z) + iN_\nu(z)$ is the Hankel function of the first kind. We have used here the asymptotic expressions for the functions $I_\nu(z)$ and $K_\nu(z)$ for a fixed value of ν and large z [4].

In the same way, we deduce from the frequency equation (3)

$$\frac{f^{(3)}(iy, a)}{f^{(3)}(iy, a \longrightarrow \infty)} = \frac{J_\nu/2 + iyaJ_\nu'}{\lim\limits_{a\to\infty}[J_\nu/2 + iyaJ_\nu']} = \sqrt{\frac{2\pi}{ay}}e^{-ay}[I_\nu/2 + ayI_\nu'], \quad (10)$$

$$\frac{f^{(4)}(iy, a)}{f^{(4)}(iy, a \longrightarrow \infty)} = \frac{K_\nu/2 + ayK_\nu'}{\lim\limits_{a\to\infty}[K_\nu/2 + ayK_\nu']} = -\sqrt{\frac{2}{\pi ya}}e^{ay}[K_\nu/2 + ayK_\nu']. \quad (11)$$

The prime over the Bessel functions $I_\nu(ay)$ and $K_\nu(ay)$ means differentiation with respect to their arguments.

Finally, summing up the contributions of the TE and TM modes to the Casimir energy, we obtain from (1), (5), (7)–(11)

$$E = \frac{1}{\pi a}\sum_{l=1}^\infty \left(l + \frac{1}{2}\right)\int_0^\infty dy \ln[1 - (\sigma_l'(y))^2] \equiv \frac{1}{a}\sum_{l=1}^\infty Q_l, \quad (12)$$

where the notation $\sigma_l'(y)$ is introduced for the derivative of the function $\sigma_l(y) = yI_\nu(y)K_\nu(y)$, $\nu = l + 1/2$. The integral in (12) converges. This follows from the asymptotic behavior of $\sigma_l'(y)$ for large y and fixed $\nu = l + 1/2$ [4]. To carry out the summation with respect to l in (12), one needs the asymptotic behavior of the integral Q_l at large l. Applying the uniform (with respect to z) asymptotic expressions for the modified Bessel functions at large ν [1, 4],

$$I_\nu(\nu z)K_\nu(\nu z) \simeq \frac{1}{2\nu}\frac{1}{(1 + z^2)^{1/2}}, \quad (13)$$

we obtain from (12)

$$Q_l \simeq \frac{\nu^2}{\pi}\int_0^\infty dz \ln\left[1 - \frac{1}{4\nu^2(1 - z^2)^3}\right] \simeq -\frac{1}{4\pi}\int_0^\infty \frac{dz}{(1 + z^2)^3} = -\frac{3}{64}, \quad l \longrightarrow \infty. \quad (14)$$

Thus, the sum (12) at large l diverges as $\sum_{l=1}^\infty (l + 1/2)^0$. To determine the finite value for this sum, we rewrite (12) in the following way:

$$E = \frac{1}{a}\sum_{l=1}^\infty \left[Q_l + \frac{3}{64} - \frac{3}{64}\right] = \frac{1}{a}\sum_{l=1}^\infty \bar{Q}_l - \frac{3}{64a}\sum_{l=1}^\infty \left(l + \frac{1}{2}\right)^0, \quad (15)$$

where $\bar{Q}_l = Q_l + 3/64$.

The sum $\sum_{l=1}^\infty \bar{Q}_l$ converges because $\bar{Q}_l = -9/(16384\nu^2) + O(\nu^{-4})$ at large l. The last divergent sum

in (15) can be defined by using the Hurwitz zeta function $\zeta(z, q)$ [4] as

$$-\frac{3}{64a}\sum_{l=1}^{\infty}\left(l+\frac{1}{2}\right)^0 = -\frac{3}{64a}(\zeta(0, 1/2)-1) = \frac{3}{64a} \quad (16)$$

since $\zeta(0, 1/2) = 0$.

Finally, we obtain

$$E = \frac{1}{a}\sum_{l=1}^{\infty}\bar{Q}_l + \frac{3}{64a}. \quad (17)$$

The sum $\sum_l \bar{Q}_l$ can be estimated with allowance for the asymptotics of $\bar{Q}_l$ at large l:

$$\sum_{l=1}^{\infty}\bar{Q}_l \simeq -\frac{9}{16\,384}\sum_{l=1}^{\infty}\frac{1}{(l+1/2)^2} = -\frac{9}{2^{14}}[\zeta(2, 1/2)-4] = -0.000514\ldots. \quad (18)$$

Thus, the main contribution to (17) is given by the second term, and to a good approximation one can put for the Casimir energy $E \simeq 3/(64a) = 0.046875/a$. Taking into account (18), we get, with greater accuracy, $E \simeq 0.046361/a$. It is worth comparing our calculations with those using other methods [1].

3. SOLID BALL IN AN INFINITE MEDIUM WHEN $\varepsilon\mu = 1$

Let us consider the Casimir effect for a ball made of a material with dielectric constant ε_1 and magnetic constant μ_1. The ball is assumed to be surrounded by an infinite medium with dielectric and magnetic constants ε_2 and μ_2, respectively.

The central role in our consideration is again played by the equations defining the eigenfrequencies of the electromagnetic oscillations [3]. The TE modes are determined by the equation

$$\frac{[\omega_1 r j_l(\omega_1 r)]'}{\mu_1 j_l(\omega_1 r)} = \frac{[\omega_2 r h_l^{(1)}(\omega_2 r)]'}{\mu_2 h_l^{(1)}(\omega_2 r)}, \quad r = a, \quad (19)$$

where $\omega_i = \sqrt{\varepsilon_i\mu_i}\,\omega$, $i = 1, 2$. The prime means differentiation with respect to the arguments of the Bessel functions $\omega_i r$, $i = 1, 2$. For the TM oscillations, we have the analogous frequency equations

$$\frac{[\omega_1 r j_l(\omega_1 r)]'}{\varepsilon_1 j_l(\omega_1 r)} = \frac{[\omega_2 r h_l^{(1)}(\omega_2 r)]'}{\varepsilon_2 h_l^{(1)}(\omega_2 r)}, \quad r = a. \quad (20)$$

The parameter l in equations (19) and (20) takes the values 1, 2, … . Under the exchange $\varepsilon_i \longleftrightarrow \mu_i$, equation (19) turns into equation (20) and vice versa.

If the characteristics of the media ε_i, μ_i, $i = 1, 2$, satisfy the condition $\varepsilon_i\mu_i = 1$, $i = 1, 2$, the frequency equations are considerably simplified. With allowance for this condition, equations (19) and (20) can be written as follows:

$$[\omega a j_l(\omega a)]' h_l^{(1)}(\omega a) - \mu^{\pm 1} j_l(\omega a)[\omega a h^{(1)}(\omega a)]' = 0, \quad (21)$$

where $\mu = \mu_1/\mu_2$. Following the calculations in the previous section, we obtain the Casimir energy of a solid ball in the form

$$E_{\text{ball}} = \frac{1}{\pi a}\sum_{l=1}^{\infty}(l+1/2)\int_0^{\infty} dx \ln\frac{\xi_\nu^+(x)\xi_\nu^-(x)}{\xi_\nu^-(\infty)\xi_\nu^+(\infty)}, \quad \nu = l + 1/2, \quad (22)$$

where

$$\xi_\mu^{\pm}(x) = \left(xI_\nu' + \frac{1}{2}I_\nu(x)\right)K_\nu(x) - \mu^{\pm 1} I_\nu(x)\left(xK_\nu'(x) + \frac{1}{2}K_\nu(x)\right). \quad (23)$$

Using the asymptotic behavior of the modified Bessel functions $I_\nu(x)$ and $K_\nu(x)$ for large x and fixed ν, we arrive at $\xi^{\pm}(\infty) = (1 + \mu^{\pm 1})/2$. In view of this, equation (22) assumes the form

$$E_{\text{ball}} = \frac{1}{\pi a}\sum_{l=1}^{\infty}\left(l+\frac{1}{2}\right)Q_l, \quad (24)$$

where

$$Q_l = \frac{1}{\pi}\int_0^x dx \ln\left[\frac{4\mu}{(1+\mu)^2}\xi_\nu^+(x)\xi_\nu^-(x)\right].$$

The formula for Q_l can be rewritten in the compact form

$$Q_l = \frac{1}{\pi}\int_0^{\infty} dx \ln[1-(\eta\sigma_l'(x))^2], \quad \eta = (1-\mu)/(1+\mu) \quad (25)$$

with the same function $\sigma_l'(x)$ as in equation (12). Thus the only difference from the case of a perfectly conducting sphere is the multiplier η in front of $\sigma_l'(x)$. We find the sum over l in (24) again by making use of the Hurwitz zeta-function technique. It gives

$$E_{\text{ball}} = \frac{1}{a}\sum_{l=1}^{\infty}\bar{Q}_l + \frac{3}{64a}\eta^2, \quad (26)$$

where

$$\bar{Q}_l = Q_l + 3\eta^2/64\ldots.$$

By the taking into account the uniform (in x) asymptotic behavior of the Bessel functions $I_\nu(x)$ and $K_\nu(x)$ at large ν [4], we obtain

$$\bar{Q}_l \simeq \frac{9}{16\,384}\frac{\eta^2}{\nu^2}(6-7\eta^2) + O(\nu^{-4}). \tag{27}$$

The sum in (26) converges. It can be estimated with the aid of the asymptotic expression (27):

$$\sum_{l=1}^{\infty}\bar{Q}_l \simeq \frac{9}{16\,384}\eta^2(6-7\eta^2)\sum_{l=1}^{\infty}\frac{1}{(l+1/2)^2} = \frac{9}{2^{14}}\eta^2(6-7\eta^2)\left(\frac{\pi^2}{2}-4\right). \tag{28}$$

Thus, the basic contribution to equation (26) is due to the second term. Therefore, with fairly good accuracy (a few percent), one can set $E_{\text{ball}} \simeq 3\eta^2/(64a)$. It was shown in the preceding section that, with the same accuracy, we have $E_{\text{shell}} = 3/(64a)$; therefore, $E_{\text{ball}} \simeq \eta^2 E_{\text{shell}}$. Taking into account (28), we obtain a more precise formula for the Casimir energy of a solid ball, $E_{\text{ball}} \simeq 3\eta^2(1.066 - 0.077\eta^2)/(64a)$ (cf. [6]).

4. CONCLUSION

The calculation of the Casimir effect for nonflat boundaries (specifically, for a sphere) by a direct summation of eigenfrequencies has been used only in the pioneering paper by Boyer [5]. The fact that it is done by us is actually a development and maximum simplification of the Boyer method. We recast it into a form requiring virtually no numerical calculations; what is more important is that no cutoff functions are used here.

ACKNOWLEDGMENTS

This work was supported in part by the Russian Foundation for Basic Research (project no. 97-01-00745).

REFERENCES

1. K. A. Milton, L. L. DeRaad, Jr., and J. Schwinger, Ann. Phys. **115**, 338 (1978); R. Balian and B. Duplantier, Ann. Phys. **112**, 165 (1978); S. Leseduarte and A. Romeo, Ann. Phys. **250**, 448 (1996); M. Bordag, E. Elizalde, and K. Kirsten, J. Math. Phys. **37**, 895 (1996).
2. V. V. Nesterenko and I. G. Pirozhenko, J. Math. Phys. **38**, 6265 (1997).
3. J. A. Stratton, *Electromagnetic Theory* (McGraw-Hill, New York, 1941).
4. *Handbook of Mathematical Functions*, Ed. by M. Abramowitz and I. A. Stegun (National Bureau of Standards, Washington, D.C., 1964).
5. T. H. Boyer, Phys. Rev. **174**, 1764 (1968).
6. I. Brevik and H. Kolbenstvedt, Ann. Phys. **143**, 179 (1982).

Physics of Atomic Nuclei, Vol. 63, No. 4, 2000, pp. 672–676. Fom Yadernaya Fizika, Vol. 63, No. 4, 2000, pp. 738–741.

VIII INTERNATIONAL CONFERENCE ON SYMMETRY METHODS IN PHYSICS

Role of the Q^2 Analyticity of α_s for Timelike Processes*

O. P. Solovtsova

Joint Institute for Nuclear Research, Dubna, Moscow oblast, 141980 Russia

Abstract—It is shown that, to describe processes with timelike momentum transfers, it is important to have a self-consistent determination of the running coupling constant in the timelike region. The technique of analytic perturbation theory allows a consistent determination of this running coupling constant. The results are found to disagree significantly with those obtained in the standard perturbative approach. © *2000 MAIK "Nauka/Interperiodica".*

1. A fundamental issue in quantum chromodynamics (QCD) is the behavior of the strong-interaction running coupling constant $\alpha_s = g_s^2/4\pi$. The basic research tool is perturbation theory (PT) with its renormalization-group improvement [1]. In the QCD case in the limit of large momentum transfers Q, this approach provides a logarithmic decrease of the running coupling constant $\alpha_s \sim 1/\ln(Q^2/\Lambda^2)$, where Λ is the QCD scale parameter that determines where the theory becomes asymptotically free. The study of the behavior of α_s outside of the asymptotic region is more difficult. It is known that the direct use of PT improved by the renormalization group leads to infrared instability of α_s and unphysical singularities—for instance, a ghost pole at $Q^2 = \Lambda^2$. Unphysical singularities of the PT running coupling constant preclude a self-consistent determination of the effective coupling constant for timelike momentum transfers. Recently, a new method has been proposed [2] for constructing the QCD running coupling constant in such a way as to retain the correct analytic properties. This method is called analytic perturbation theory (APT). The main purpose of this paper is to analyze the region of timelike momentum transfers on the basis of the APT approach. The running coupling constant in QCD as a function of Q^2 is determined by a renormalization-group analysis in the region of spacelike momentum transfers. However, to parametrize many physical processes, one needs to know the coupling constant in the timelike region. Therefore, a theoretical description of timelike processes (e^+e^- annihilation into hadrons, τ-lepton and Z-boson widths with respect to their decays into hadrons, and so on) requires analytic continuation of the running coupling constant from the spacelike (Euclidean) region of momentum transfers ($q^2 = -Q^2 < 0$) to the timelike (physical) region ($q^2 > 0$). It is obvious that information on the running coupling constant obtained from timelike processes corresponds to knowledge of the coupling constant extracted from spacelike processes such as deep-inelastic scattering, if the transition from the Euclidean to the physical region is performed in a correct manner (see [3, 4]) without violation of the analytic properties of the hadronic correlation function $\Pi(q^2)$ and the Adler function $D(q^2)$. When the analytic properties are not respected, the question arises: to what extent does this breakdown of analyticity affect the quantities extracted from physical processes? It is impossible to answer this question within standard perturbation theory. On the other hand, the APT method retains the correct analytic properties of the D function and, in addition, gives simple analytic expressions that can be compared with corresponding PT expressions; therefore, it allows a quantitative analysis of the effect that the breakdown of Q^2 analyticity has on the running coupling constant.

2. As is known, many experimentally measured ratios R_σ, where, e.g., $\sigma = e^+e^-$, τ, Z, …, can be written in the form $R_\sigma = R_\sigma^{(0)}(1 + \Delta_\sigma)$. Here, Δ_σ is a QCD correction and $R_\sigma^{(0)}$ represents the parton level of description of a given process with electroweak corrections. The quantity Δ_σ can be expressed in terms of the imaginary part of the hadronic correlation function as $\mathcal{R}(s) = \mathrm{Im}\Pi(s)/\pi$. To parametrize $\mathcal{R}(s)$ in terms of QCD parameters, a special procedure of analytic continuation is required. With this end in view, one usually employs the dispersion relation

$$D(z) = -z\int_0^\infty ds\frac{\mathcal{R}(s)}{(s-z)^2}, \qquad (1)$$

where $z = q^2$, and the inverse relation

$$\mathcal{R}(s) = \frac{1}{2\pi i}\int_{s-i\epsilon}^{s+i\epsilon} dz\frac{d\Pi(z)}{dz} = -\frac{1}{2\pi i}\int_{s-i\epsilon}^{s+i\epsilon} dz\frac{D(z)}{z}. \qquad (2)$$

We define the effective coupling constants $\bar{a}$ and $\bar{a}_s$, respectively, in the spacelike (t-channel) and timelike (s-channel) regions, using the notation $a = \alpha/4\pi$ and dimensionless (in units of the scaling parameter Λ)

* This article was submitted by the author in English.

1063-7788/00/6304-0672$20.00 © 2000 MAIK "Nauka/Interperiodica"

momentum variables, by

$$D(z) \propto 1 + d_1 a(z) + d_2 a^2(z) + \ldots = 1 + d_1 \bar{a}(z), \quad (3)$$

$$\mathcal{R}(s) \propto 1 + r_1 a_s(s) + r_2 a_s^2(s) + \ldots = 1 + r_1 \bar{a}_s(s). \quad (4)$$

Equations (1) and (2) and the equality $d_1 = r_1$ result in a relation between these coupling constants:

$$\bar{a}_s(s) = -\frac{1}{2\pi i}\int\limits_{s-i\epsilon}^{s+i\epsilon} \frac{dz}{z}\bar{a}(z), \quad (5)$$

$$\bar{a}(z) = -z\int\limits_0^\infty \frac{ds}{(s-z)^2}\bar{a}_s(s). \quad (6)$$

Therefore, the QCD corrections Δ_σ for the class of physical processes considered with timelike momentum transfers are to be parametrized, according to equation (4), by the effective coupling constant $\bar{a}_s(s)$, which is analytically related to $\bar{a}(z)$ by equations (5) and (6). In the one-loop approximation, the effective coupling constants coincide with the running coupling constants; in higher loops, the connection depends on the physical process.

3. Consider the above procedure of analytic continuation within PT with

$$\bar{a}^{PT}(z) = \frac{1}{\beta_0}\frac{1}{\ln(Q^2/\Lambda^2)} = \frac{1}{\beta_0}\frac{1}{\ln(-z)}, \quad z \equiv -Q^2/\Lambda^2. \quad (7)$$

Then, we obtain the following the expression for the PT running coupling constant in the s channel:

$$\bar{a}_s^{PT}(s) = -\frac{1}{2\pi i\beta_0}\int\limits_{s-i\epsilon}^{s+i\epsilon}\frac{dz}{z}\frac{1}{\ln(-z)} = -\frac{1}{\pi\beta_0}\left(\frac{\pi}{2} + \arctan\frac{\ln s}{\pi}\right). \quad (8)$$

This expression is physically meaningless, because it is negative for any s and does not have the correct asymptotic behavior, going as $1/\ln s$ as $s \longrightarrow \infty$; the reason will be explained below.

There is another way of calculating $\bar{a}_s$ based on the Shankar method [5]. Using analyticity of the D function in the complex z plane with the cut along the positive real axis, we may pass from the integral along the cut (see the contour C_1 in Fig. 1) to an integral around a circle of radius $|z| = s$ in the complex z plane, beginning at $z = s + i\epsilon$ and ending at $z = s - i\epsilon$ (the contour C_2 in Fig. 1) and parametrized by $z = -s\exp(i\varphi)$, $-\pi < \varphi < \pi$, to arrive at the expression

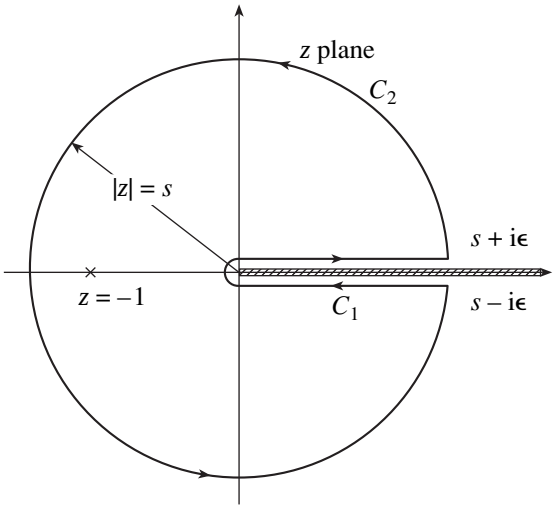

Fig. 1. Integration contours in the complex plane.

$$\frac{1}{2\pi i}\oint\limits_{C_2}\frac{dz}{z}\bar{a}^{PT}(z) = \frac{1}{2\pi\beta_0}\int\limits_{-\pi}^{\pi}\frac{d\varphi}{\ln s + i\varphi} = \frac{1}{\pi\beta_0}\arctan\frac{\pi}{\ln s}. \quad (9)$$

This is positive when s > 1 and possesses the correct ultraviolet asymptotic behavior. It is just this expression that is used as a one-loop PT result for all timelike momenta $s > 0$ (see, e.g., [6]): $\bar{\alpha}_s^{PT}(s) = \frac{4}{\beta_0}\arctan\frac{\pi}{\ln s}$.

Thus, a formal conversion of the PT one-loop running coupling constant in the spacelike region (7) into expressions for the coupling constant in the timelike region leads to the contradictory results (8) and (9). The reason can easily be understood if one applies the Cauchy theorem (see Fig. 1) to establish the connection between the integrals in equations (8) and (9),

$$\frac{1}{2\pi i}\oint\limits_{C_2} dz\psi(z) = -\frac{1}{2\pi i}\int\limits_{C_1} dz\psi(z) + \mathrm{res}[\psi(z), -1], \quad \psi(z) \equiv \frac{1}{z\ln(-z)}, \quad (10)$$

which is consistent with equations (8) and (9), because the residue of the function $\psi(z)$ at the point $z = -1$ is equal to unity. Therefore, the discrepancy between equations (8) and (9) is due to an unphysical ghost pole in (7) at $z = -1$, which violates the required analytic properties of the running coupling constant. The inclusion of multiloop corrections does not solve this problem, but it rather produces new unphysical singularities. Within standard PT approximations, which violate

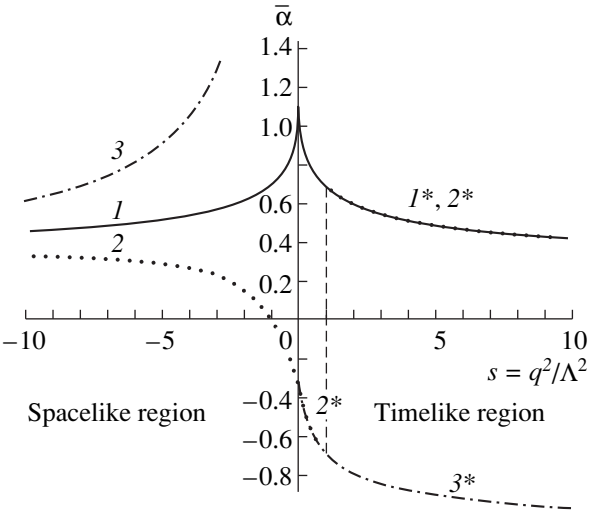

Fig. 2. The behavior of the running coupling constant calculated by various methods.

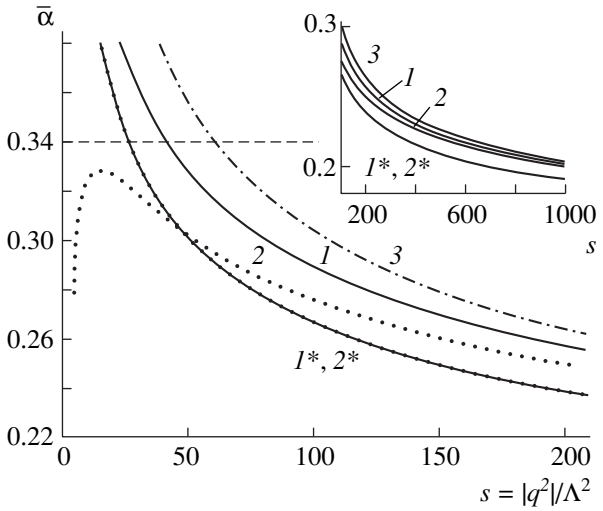

Fig. 3. Behavior of the running coupling constant. The notation is the same as in Fig. 2. The graph on the top right shows the behavior of the same curves for large values of s.

the necessary analytic properties of the running coupling constant, it is therefore impossible to pass into the timelike region in a self-consistent way.

4. The problem of how to make the correct transition between the space- and timelike regions can be solved within the APT method [2, 4], which ensures the correct analytic properties of the coupling constant without introducing extra parameters. The resulting one-loop expression for the analytic coupling constant in the Euclidean region is

$$\bar{a}^{\mathrm{APT}}(z) = \frac{1}{\beta_0}\left[\frac{1}{\ln(-z)} + \frac{1}{1+z}\right]. \qquad (11)$$

When one employs the analytic coupling constant (11), both methods for calculating $\bar{a}_s$ considered above produce the same result; i.e.,

$$\bar{a}_s^{\mathrm{APT}}(z) = -\frac{1}{2\pi\mathrm{i}}\int\limits_{C_1}\frac{dz}{z}\bar{a}^{\mathrm{APT}}(z) = \frac{1}{2\pi\mathrm{i}}\oint\limits_{C_2}\frac{dz}{z}\bar{a}^{\mathrm{APT}}(z)$$
$$= \frac{1}{\pi\beta_0}\left(\frac{\pi}{2} - \arctan\frac{\ln s}{\pi}\right). \qquad (12)$$

Consistency of the APT approach also follows from the fact that we can reconstruct the initial expression (11) when the timelike coupling (12) is substituted into equation (6). It is of interest to note that this consistency is due to the second term in equation (11), which compensates the pole, whose contribution to the contour integral is equal to zero when $s > 1$; i.e., we have the equality

$$\oint\limits_{C_2}\frac{dz}{z}\bar{a}^{\mathrm{APT}}(z) = \oint\limits_{C_2}\frac{dz}{z}\bar{a}^{\mathrm{PT}}(z), \quad s > 1, \qquad (13)$$

where the function $\bar{a}^{\mathrm{PT}}(z)$ is defined by equation (7). Therefore, the PT expression (7) gives the same result as the APT approach in the timelike region for $s > 1$ if the contour C_2 is used. However, there is no inverse correspondence for PT. Moreover, note that an equality analogous to equation (13) does not arise if the integrand contains the running coupling constant multiplied by a function of z. For the R_τ ratio, for instance, $\bar{a}$ is multiplied by a polynomial in z and, as is shown in [7], the contour integral along C_2 in PT turns out to be different from that in the APT approach.

5. The results obtained are illustrated in a series of figures. Firstly, we consider the region of small momentum transfers. Figure 2 shows the behavior of the running coupling constant computed by various methods in the region $-10 \le s = q^2/\Lambda^2 \le 10$. The solid curve represents the APT coupling constant calculated by formula (11) in the spacelike region (curve *1* in Fig. 2) and by formula (12) in the timelike region (curve *1**). Dots denote the coupling constant determined by equation (9) (curve *2**) and by making an inverse transition from the timelike to the spacelike region with the help of the dispersion relation (1). The dash-dotted curve *3* represents the PT coupling constant computed by formula (7) in the spacelike region, and curve *3**, the same by formula (8) in the timelike region.

Figure 3 shows the behavior of the running coupling constant in the region where the running coupling constant $\bar{\alpha}$ is about 0.3, which approximately corresponds to the mass scale of the τ lepton, $M_\tau = 1.78$ GeV. As is seen from Fig. 3, curves *1*, *2*, and *3*, which describe the spacelike region, noticeably differ from one another. With increasing s, they begin, as they should, to approach each other, which is demonstrated on the top right of Fig. 3. Values of the parameter Λ calculated

with the running coupling constants described by curves *1*, *2*, and *3* are different. For example, the value of APT function (curve *1*), equal to 0.34, is achieved at $s_0 = 41.5$, which corresponds to $\Lambda^{APT} = 276$ MeV. For the PT curve *3*, $s_0 = 60.5$ and $\Lambda^{PT} = 228$ MeV. Note that, for curve *2*, the value $\bar{\alpha} = 0.34$ cannot be achieved at any values of *s*. For timelike momentum transfers, recall that curves *1** and *2** as functions of the dimensionless variable *s* coincide when $s > 1$. However, they are characterized by different values of Λ, which results in different values of the running coupling constant in the timelike region, $\bar{\alpha}_s^{APT}(M_\tau) = 0.31$ and $\bar{\alpha}_s^{PT}(M_\tau) = 0.29$. With the accuracy attained at present for experimental data on the hadronic decay of the τ [8], this quantitative discrepancy becomes significant.

Finally, Fig. 4 shows the evolution of the running coupling constant in the region of momentum transfers of the order of the *Z*-boson mass $M_Z = 91.2$ GeV. The running coupling constant $\bar{\alpha}$ corresponding to the dimensionless variable *s* is drawn in Fig. 4. The curve denoted by $\bar{\alpha}$ represents all three curves *1*, *2*, and *3* drawn in Figs. 2 and 3 and describing the behavior of the running coupling constant in the spacelike region; they merge into one curve with high accuracy for these large values of *s*. The curve denoted by $\bar{\alpha}_s$ corresponds to the coupling constant in the timelike region and to curves *1** and *2** plotted in Figs. 2 and 3. In the region of sufficiently large values of *s*, the well-known approximate formula with the so-called π^2 term (see, e.g., [9]), $\bar{\alpha}_s = \bar{\alpha}[1 - (\pi^2/3)/\ln^2 s]$, works well (with an accuracy of about 0.1%) both for PT and for APT. This approximation gives a difference between $\bar{\alpha}_s$ and $\bar{\alpha}$ of about 2%. Substituting the value of the parameter Λ fixed at $q = M_\tau$, we obtain the corresponding values of the running coupling constant at $q = M_Z$: $\bar{\alpha}^{APT} = 0.120$, $\bar{\alpha}^{PT} = 0.117$ (spacelike region); $\bar{\alpha}_s^{APT} = 0.118$, $\bar{\alpha}_s^{PT} = 0.114$ (timelike region). Thus, even at such large values of *s*, the effect of analyticity on the running coupling constant amounts to ~2%; i.e., it is comparable with the contribution from the π^2 term and from higher PT loop corrections.

6. Let us briefly summarize our considerations. To determine the running coupling constant in the timelike region, we took advantage of APT because it provides a consistent procedure necessary for analytic continuation. It is to be noted that the APT method ensures not only correct analytic properties of the running coupling constant but also stability with respect to higher loop corrections, which is essential for the stability of our procedure of analytic continuation.

Quantitatively, our analysis shows that the effect of analytic continuation can be associated with π^2 terms only at very large momentum transfers of the order of the *Z*-boson mass, where the contribution of the π^2 terms is small. At intermediate and, especially, at low momentum transfers, it is important to take account of the correct analytic properties of α_s, which permits a consistent transition into the timelike region. The Q^2 dependence of $\bar{\alpha}_s$ is essentially different from the dependence of $\bar{\alpha}_s$ in PT. Our analysis shows that the popular PT expressions for $\bar{\alpha}_s$ as expansions in $1/\ln(Q^2/\Lambda^2)$, containing nonphysical singularities, do not allow a self-consistent interpretation of information obtained from various experiments that studied the evolution of α_s outside of the asymptotic region. From our numerical estimates, it follows that analyticity of the running coupling constant has a pronounced effect on the experimental value of the parameter Λ_{QCD} and on the Q^2 evolution of α_s. Note that these considerations are also important for the investigation of power-law corrections, which are now under intensive study (see, e.g., [10]). The analysis of power-law corrections in APT at the one-loop level naturally changes their importance relative to perturbative terms.

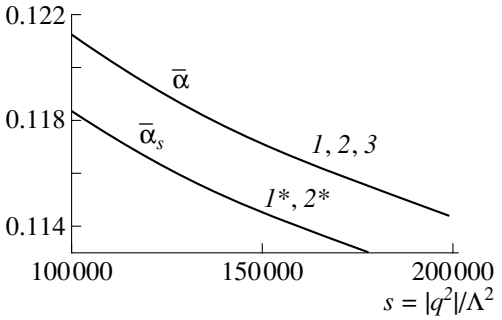

Fig. 4. Behavior of the running coupling constant in the vicinity of the *Z*-boson mass.

The APT method appears to be fruitful for studying the problem of analytic continuation of α_s to the timelike region. There is no doubt that extracting more detailed information from experimental data on timelike processes requires a more thorough theoretical analysis within APT, including the estimation of the contributions from higher order processes, mass corrections, and so on. These will be considered in our subsequent papers.

REFERENCES

1. N. N. Bogoliubov and D. V. Shirkov, *Introduction to the Theory of Quantized Fields*, 3rd ed. (Wiley, New York, 1980).
2. D. V. Shirkov and I. L. Solovtsov, JINR Rapid Commun., No. 2[76]-96, 5 (1996); Phys. Rev. Lett. **79**, 1209 (1997); hep-ph/9704333.

3. H. F. Jones and I. L. Solovtsov, Phys. Lett. B **349**, 519 (1995).
4. K. A. Milton and I. L. Solovtsov, Phys. Rev. D **54**, 5295 (1996); hep-ph/9611438.
5. R. Shankar, Phys. Rev. D **15**, 755 (1977).
6. A. A. Pivovarov, Nuovo Cimento A **105**, 813 (1992).
7. O. P. Solovtsova, JETP Lett. **64**, 714 (1996).
8. A. Pich, *Fourth Workshop on Tau Lepton Physics (TAU-96), Colorado, 1996*; hep-ph/9612308; hep-ph/97101305.
9. A. V. Radyushkin, JINR Rapid Commun., No. 4[78]-96, 9 (1996); Preprint No. E2-82-159, JINR (Dubna, 1982).
10. G. Grunberg, *32nd Rencontre de Moriond: QCD and High Energy Hadronic Interactions, Les Arcs, France, 1997*; hep-ph/9705290.

Physics of Atomic Nuclei, Vol. 63, No. 4, 2000, pp. 677–679. From Yadernaya Fizika, Vol. 63, No. 4, 2000, pp. 742–744.

VIII INTERNATIONAL CONFERENCE ON SYMMETRY METHODS IN PHYSICS

Symmetries and Invariant Solutions of Absolutely Unstable Media Equations*

A. V. Aksenov

Moscow State University, Vorob'evy gory, Moscow, 119899 Russia

Abstract—An algorithm for constructing fundamental solutions by using symmetries is proposed. The symmetries and the periodic invariant solutions of absolutely unstable media equations are found. © *2000 MAIK "Nauka/Interperiodica".*

1. BASIC EQUATIONS

We consider the system of equations

$$\begin{aligned}&\frac{\partial u}{\partial t}+u\frac{\partial u}{\partial x}-\lambda\frac{\partial \rho^{1/\lambda}}{\partial x}=0,\\&\frac{\partial \rho}{\partial t}+\frac{\partial(\rho u)}{\partial x}=0,\quad \lambda\in \mathrm{R}/\{0\},\end{aligned}\tag{1}$$

where ρ and u are density and pressure and λ is the parameter of the medium [1]. The system (1) is the long-wave approximation for the wide class of absolutely unstable media (for example, overturned shallow water, constrictions on a plasma pinch, and a flat gravitating gaseous layer).

We introduce the new dependent variables

$$r=\rho^{1/(2\lambda)},\quad z=u/(2\lambda).$$

In these variables, system (1) becomes

$$\begin{aligned}&\frac{\partial r}{\partial t}+2\lambda z\frac{\partial r}{\partial x}+r\frac{\partial z}{\partial x}=0,\\&\frac{\partial z}{\partial t}-r\frac{\partial r}{\partial x}+2\lambda z\frac{\partial z}{\partial x}=0.\end{aligned}\tag{2}$$

Using the godograph transformation, we obtain the system

$$\begin{aligned}&\frac{\partial x}{\partial r}=2\lambda z\frac{\partial t}{\partial r}+r\frac{\partial t}{\partial z},\\&\frac{\partial x}{\partial z}=-r\frac{\partial t}{\partial r}+2\lambda z\frac{\partial t}{\partial z}.\end{aligned}\tag{3}$$

We suppose that the Jacobian $D(r, z)/D(x, t)\neq 0$.

The compatibility condition for equations (3) is

$$\frac{\partial^2 t}{\partial r^2}+\frac{(2\lambda+1)}{r}\frac{\partial t}{\partial r}+\frac{\partial^2 t}{\partial z^2}=0.\tag{4}$$

Equation (4) is a complex analog of the Euler–Poisson–Darboux equation.

* This article was submitted by the author in English.

2. SYMMETRIES OF THE BASIC EQUATIONS

Proposition 2.1. System (2) admits Lie group symmetries with the following basis:

$$X_1=r\frac{\partial}{\partial r}+z\frac{\partial}{\partial z}+x\frac{\partial}{\partial x},$$

$$X_2=\frac{\partial}{\partial z}+2\lambda t\frac{\partial}{\partial x},$$

$$X_3=t\frac{\partial}{\partial t}+x\frac{\partial}{\partial x},$$

$$X_4=2rz\frac{\partial}{\partial r}+(z^2-r^2)\frac{\partial}{\partial z}+[x-2(2\lambda+1)zt]\frac{\partial}{\partial t}$$
$$-(2\lambda+1)(2\lambda z^2+r^2)t\frac{\partial}{\partial x}.$$

Proposition 2.2. Equation (4) admits Lie group symmetries with the following basis:

$$Y_1=\frac{\partial}{\partial z},\quad Y_2=t\frac{\partial}{\partial t},\quad Y_3=r\frac{\partial}{\partial r}+z\frac{\partial}{\partial z},$$

$$Y_4=2rz\frac{\partial}{\partial r}+(z^2-r^2)\frac{\partial}{\partial z}-(2\lambda+1)zt\frac{\partial}{\partial t},$$

provided that $4\lambda^2-1\neq 0$.

3. PERIODIC SOLUTIONS

Let us consider the equation

$$\frac{\partial^2 t}{\partial r^2}+\frac{(2\lambda+1)}{r}\frac{\partial t}{\partial r}+\frac{\partial^2 t}{\partial z^2}=\delta(r-1)\delta(z).\tag{5}$$

Equation (5) describes fundamental solutions to equation (4).

Proposition 3.1. Periodic (for space variable x) solutions to system (2) are fundamental solutions to equation (4).

1063-7788/00/6304-0677$20.00 © 2000 MAIK "Nauka/Interperiodica"

The proof follows from the identity

$$\oint_\Gamma dx = 2\lambda \oint_\Gamma d(zt) - \iint_\Sigma r\left[\frac{\partial^2 t}{\partial r^2} + \frac{(2\lambda+1)}{r}\frac{\partial t}{\partial r} + \frac{\partial^2 t}{\partial z^2}\right] dr dz.$$

Here, Γ is a closed path in the (r, z) plane where t = const and Σ is the inner domain.

Remark 3.1. The space period Λ is

$$\Lambda = \left|\oint_\Gamma dx\right|.$$

4. SYMMETRIES OF LINEAR PARTIAL DIFFERENTIAL EQUATIONS AND FUNDAMENTAL SOLUTIONS

Fundamental solutions to linear partial differential equations of mathematical physics are often invariant under the symmetry transformations admitted by the equation [2, 3]. Usually, fundamental solutions can be obtained by dimensional analysis [4] or, more generally, from the invariance under groups of scalings. Here, we formulate the algorithm for constructing fundamental solutions on the basis of our knowledge of the Lie group point symmetries.

Let us consider the pth order linear partial differential equation

$$Lu \equiv \sum_{|\alpha|=0}^{p} A_\alpha(x) D^\alpha u = 0, \quad x \in \mathrm{R}^m. \tag{6}$$

We use the standard notation: $\alpha = (\alpha_1, \ldots, \alpha_m)$ is a multi-index with integer-valued nonnegative components, $|\alpha| = \alpha_1 + \ldots + \alpha_m$,

$$D^\alpha \equiv \left(\frac{\partial}{\partial x^1}\right)^{\alpha_1} \ldots \left(\frac{\partial}{\partial x^m}\right)^{\alpha_m}.$$

Fundamental solutions of equation (6) satisfy the equation

$$Lu = \delta(x - x_0). \tag{7}$$

It was demonstrated in [5] that, in the cases $p \geq 2$ and $m \geq 2$, equation (6) admits symmetry operators only of the following special form:

$$X = \sum_{i=1}^{m} \xi^i(x)\frac{\partial}{\partial x^i} + \eta(x, u)\frac{\partial}{\partial u}, \quad \frac{\partial^2 \eta}{\partial u^2} = 0. \tag{8}$$

Let $\underset{p}{X}$ be the pth order prolongation of the operator (8).

Proposition 4.1. The necessary and sufficient condition for the infinitesimal operator of the form (8) to be the symmetry operator of equation (6) is the existence of the function $\lambda = \lambda(x)$ satisfying the identity

$$\underset{p}{X}(Lu) \equiv \lambda(x) Lu \tag{9}$$

for an arbitrary function $u = u(x)$.

Let us formulate the main result [6, 7].

Theorem 4.1. Lie algebra of symmetry operators of equation (7) is a subalgebra of the symmetry algebra of equation (6) distinguished by the relations

$$\xi^i(x_0) = 0, \quad i = 1, \ldots, m, \tag{10}$$

$$\lambda(x_0) + \sum_{i=1}^{m} \frac{\partial \xi^i(x_0)}{\partial x^i} = 0. \tag{11}$$

Let us formulate the algorithm for constructing fundamental solutions by using symmetries [7]:

(i) Find the general form of the symmetry operator of equation (6) and the corresponding function $\lambda(x)$ satisfying identity (9).

(ii) Find the general form of the equation (7) symmetry operator using restrictions (10) and (11).

(iii) Construct invariant fundamental solutions using the symmetries of equation (7).

(iv) Construct new fundamental solutions from the known ones using the symmetry group of equation (7).

5. THE INVARIANT PERIODIC SOLUTIONS

The general form of the equation (4) symmetry operator is

$$Y = (a^3 + 2a^4 z) r\frac{\partial}{\partial r} + [a^1 + a^3 z + a^4(z^2 - r^2)]\frac{\partial}{\partial z} + [a^2 - (2\lambda + 1)a^4 z] t\frac{\partial}{\partial t},$$

where a^i are some arbitrary constants. Then, the function $\lambda(r, z)$ is

$$\lambda(r, z) = a^2 - 2a^3 - (2\lambda + 5)a^4 z.$$

Proposition 5.1. Equation (5) admits only one symmetry operator

$$Y = 2rz\frac{\partial}{\partial r} + (z^2 - r^2 + 1)\frac{\partial}{\partial z} - (2\lambda + 1)zt\frac{\partial}{\partial t}. \tag{12}$$

Proposition 5.2. The symmetry operator (12) corresponds to the one-parameter group of transformations

$$r' = \frac{2r}{1 + r^2 + z^2 + (1 - r^2 - z^2)\cos(2\epsilon) - 2z\sin(2\epsilon)},$$

$$z' = \frac{2z\cos(2\epsilon) + (1 - r^2 - z^2)\sin(2\epsilon)}{1 + r^2 + z^2 + (1 - r^2 - z^2)\cos(2\epsilon) - 2z\sin(2\epsilon)},$$

$$t' = \left[\frac{1 + r^2 + z^2 + (1 - r^2 - z^2)\cos(2\epsilon) - 2z\sin(2\epsilon)}{2}\right]^\sigma t,$$

where ϵ is the group parameter and $\sigma = (2\lambda + 1)/2$.

The symmetry operator (12) has two functional independent invariants

$$\xi = \frac{r^2 + z^2 + 1}{2r}, \quad \omega = r^\sigma t.$$

Proposition 5.3. The invariant fundamental solution to equation (4) is

$$t = r^{-\sigma}\left[cP_{-\sigma}(\xi) - \frac{1}{2\pi}Q_{-\sigma}(\xi)\right], \qquad (13)$$

where $P_{-\sigma}(\xi)$ and $Q_{-\sigma}(\xi)$ are Legendre functions [8] and c is an arbitrary constant.

ACKNOWLEDGMENTS

This work was supported in part by the Russian Foundation for Basic Research (project no. 96-01-01742).

REFERENCES

1. S. K. Zhdanov and B. A. Trubnikov, *Quasi-gaseous Unstable Media* (Nauka, Moscow, 1991).
2. L. V. Ovsiannikov, *Group Analysis of Differential Equations* (Nauka, Moscow, 1978; Academic, New York, 1982).
3. N. H. Ibragimov, *Primer of the Group Analysis* (Znanie, Moscow, 1989), No. 8.
4. L. I. Sedov, *Similarity and Dimensional Methods* (Academic, New York, 1959).
5. G. W. Bluman, J. Math. Anal. Appl. **145** (1), 52 (1990).
6. A. V. Aksenov, Usp. Mat. Nauk **49** (4), 143 (1994).
7. A. V. Aksenov, Dokl. Akad. Nauk **342**, 151 (1995).
8. *Handbook of Mathematical Functions*, Ed. by M. Abramowitz and I. A. Stegun (Dover, New York, 1970).

Physics of Atomic Nuclei, Vol. 63, No. 4, 2000, pp. 680–683. From Yadernaya Fizika, Vol. 63, No. 4, 2000, pp. 745–748.

VIII INTERNATIONAL CONFERENCE ON SYMMETRY METHODS IN PHYSICS

The Exact Solution to the Cauchy Problem for Two Generalized "Linear" Vectorial Fokker–Planck Equations: Algebraic Approach*

A. A. Donkov[1)], A. D. Donkov[2)], and E. I. Grancharova

University of Sofia, Bulgaria

Abstract—The exact solutions to the Cauchy problem for two equations, which are slight generalizations of the so-called linear vectorial Fokker–Planck equation, are found using Feynman's disentangling techniques and algebraic (operational) methods. This approach may be considered as a generalization of the Suzuki method for solving the one-dimensional linear Fokker–Planck equation. *© 2000 MAIK "Nauka/Interperiodica".*

1. INTRODUCTION

The Fokker–Planck equations (FPE), the one-dimensional FPE

$$\frac{\partial W}{\partial t} = -\frac{\partial}{\partial x}[a(t,x)W] + \frac{\partial^2}{\partial x^2}[D(t,x)W(t,x)], \quad t \geq 0, \quad x \in \mathrm{R}, \tag{1}$$

and the "vectorial" FPE

$$\frac{\partial w}{\partial t} = -\nabla \cdot [\mathbf{a}(t,\mathbf{x}) \times \mathbf{w}] + \nabla\nabla : \{\hat{D}(t,\mathbf{x})\mathbf{w}(\mathbf{t},\mathbf{x})\}, \quad t \geq 0, \quad \mathbf{x} \in \mathrm{R}^n, \tag{2}$$

where $\mathbf{a}(t, \mathbf{x}) = (a_1(t, \mathbf{x}), a_2(t, \mathbf{x}), \ldots, a_n(t, \mathbf{x}))^T$ is the "drift vector", $\hat{D}(t, \mathbf{x})$ is a symmetric nonnegative definite rank-two "diffusion" tensor field, and $\nabla\nabla : \hat{D} = \partial^2 D_{ij}/\partial x_i \partial x_j$ (Einstein summation convention accepted), are widely used [1–19] as a tool in modeling various processes in many areas of theoretical and mathematical physics, chemistry and biology, pure and applied mathematics, and in engineering: nonequilibrium statistical mechanics (in particular, in the theory of Brownian motion and similar phenomena: random walks, fluctuations of liquid surfaces, local density fluctuations in fluids and solids, fluctuations of currents, etc.), metrology (Josephson voltage standards), laser physics, turbulence theory, cellular behavior, neurophysiology, population genetics, and the mathematical theory and applications of stochastic processes, to mention only a few of them.

Because of its importance, there have been many attempts to solve FPE exactly or approximately (for a review see [4, 6–11, 14]). Among the recent investigations of this problem, noteworthy for us is the Suzuki method [18].

In this paper, we find the exact solutions of the following Cauchy problems:

(a) The case with independent of t coefficients

$$\frac{\partial u}{\partial t} = a_1 u(t,\mathbf{x}) + \mathbf{a}_2 \cdot \nabla u + a_3 \mathbf{x} \cdot \nabla u + \hat{a}_4(t) : \nabla\nabla u, \quad u(0,\mathbf{x}) = \phi(\mathbf{x}), \tag{3}$$

where $\hat{a}_4$ is a symmetric nonnegative definite rank-two tensor.

(b) The case with t dependent coefficients

$$\frac{\partial u}{\partial t} = a_1(t)u(t,\mathbf{x}) + \mathbf{a}_2(t) \cdot \nabla u + a_3(t)\mathbf{x} \cdot \nabla u + \hat{a}_4(t) : \nabla\nabla u, \quad u(0,\mathbf{x}) = \phi(\mathbf{x}), \tag{4}$$

where

$$\hat{a}_4(t) = a_4(t)\hat{a}, \quad a_4(t) \geq 0, \quad \hat{a}^T = \hat{a} \geq 0,$$

and therefore $\hat{a}_4(t)$ is a symmetric nonnegative definite rank-two tensor function of the scalar parameter t.

It is easy to see that equations (3) and (4) are connected with the "linear" vectorial FPE (2) with a linear in $\mathbf{x}$ "drift vector" $\mathbf{a}(t, \mathbf{x}) = \mathbf{b}_1 + b_2\mathbf{x}$ and an independent of $\mathbf{x}$ diffusion tensor $\hat{D}$. (Here, $\mathbf{b}_1$, b_2, and $\hat{D}$ are constant in the case (a) and they are functions of t in the case (b).) Equations (3) and (4) are slight generalizations of the "linear" vectorial FPE (2) with independent of t and t-dependent coefficients, respectively.

We consider the Cauchy problems (3) and (4) separately because we have used different formulas to find the solutions, but obviously problem (3) with coefficients independent of t is a special case of problem (4).

* This article was submitted by the authors in English.

[1)] University of Wisconsin, Madison, WI USA

[2)] Bogolyubov Laboratory of Theoretical Physics, Joint Institute for Nuclear Research, Dubna, Moscow oblast, 141980 Russia.

1063-7788/00/6304-0680$20.00 © 2000 MAIK "Nauka/Interperiodica"

In the paper [20] the "isotropic" problems

$$\frac{\partial u}{\partial t} = a_1 u(t, \mathbf{x}) + \mathbf{a}_2 \cdot \nabla u + a_3 \mathbf{x} \cdot \nabla u + a_4 \Delta u, \quad u(0, \mathbf{x}) = \phi(\mathbf{x}) \tag{5}$$

and

$$\frac{\partial u}{\partial t} = a_1(t) u(t, \mathbf{x}) + \mathbf{a}_2(t) \cdot \nabla u + a_3(t) \mathbf{x} \cdot \nabla u + a_4(t) \Delta u, \quad u(0, \mathbf{x}) = \phi(\mathbf{x}) \tag{6}$$

have been exactly solved with similar techniques [here, a_4 and $a_4(t)$ are an arbitrary nonnegative constant and a function of t, respectively]. Our method may be regarded as a combination of Feynman's disentangling techniques [21], with the operational methods developed in functional analysis and, in particular, in the theory of pseudodifferential equations with partial derivatives [22–26]. As we have emphasized in [20], this approach is an extension and generalization of the Suzuki method [18] for solving the one-dimensional linear FPE (1).

2. EXACT SOLUTION TO THE CAUCHY PROBLEM (3)

In the spirit of the operational methods we can write the solution to the Cauchy problem (3) using the pseudodifferential operators [23–26] in the form

$$u(t, \mathbf{x}) = e^{t(a_1 + \mathbf{a}_2 \cdot \nabla + a_3 \mathbf{x} \cdot \nabla + \hat{a}_4 : \nabla\nabla)} \phi(\mathbf{x}) = e^{t a_1} e^{t\hat{A} + t\hat{B}} \phi(\mathbf{x}), \tag{7}$$

where

$$\hat{A} = \mathbf{a}_2 \cdot \nabla + a_3 \mathbf{x} \cdot \nabla, \quad \hat{B} = \hat{a}_4 : \nabla\nabla. \tag{8}$$

Therefore, to obtain the solution $u(t, \mathbf{x})$, we must find out how the pseudodifferential operator $e^{t\hat{A} + t\hat{B}}$ acts on $\phi(\mathbf{x})$. To do this, we will employ Feynman's disentangling techniques [21].

If we put

$$e^{t\hat{A} + t\hat{B}} = e^{t\hat{A}} \hat{F}(t), \tag{9}$$

we will find for $\hat{F}(t)$ the following initial value problem $d\hat{F}/dt = e^{-t\hat{A}} \hat{B} e^{t\hat{A}} \hat{F}(t)$, $\hat{F}(0) = 1$, the solution of which is

$$\hat{F}(t) = T - \exp \int_0^t e^{-s\hat{A}} \hat{B} e^{s\hat{A}} ds \equiv \exp_+ \int_0^t e^{-s\hat{A}} \hat{B} e^{s\hat{A}} ds, \tag{10}$$

where the symbols $T - \exp \equiv \exp_+$ designate the Volterra-ordered exponential.

Using the formula

$$e^{-s\hat{A}} B e^{s\hat{A}} = \hat{B} - s[\hat{A}, \hat{B}] + \frac{s^2}{2!}[\hat{A}, [\hat{A}, \hat{B}]] - \ldots$$

and the commutation relation $[\hat{A}, \hat{B}] = -2a_3 \hat{B}$, we obtain for $\hat{F}(t)$ an expression with the usual, not ordered, operator valued exponent function

$$\hat{F}(t) = \exp\left[\int_0^t e^{2a_3 s} ds \hat{B}\right] = \exp\left(\frac{e^{2a_3 t} - 1}{2a_3} \hat{a}_4 : \nabla\nabla\right) \equiv e^{\hat{\tau}(t) : \nabla\nabla}, \tag{11}$$

where

$$\hat{\tau}(t) = (e^{2a_3 t} - 1)\hat{a}_4 / (2a_3) \tag{12}$$

is a nonnegative definite symmetric rank-two tensor function of t.

Hence, from equations (7), (9), and (11), we have $u(t, \mathbf{x}) = e^{t a_1} e^{t(\mathbf{a}_2 \cdot \nabla + a_3 \mathbf{x} \cdot \nabla)} e^{\hat{\tau}(t) : \nabla\nabla} \phi(\mathbf{x})$. Taking into account the known formulas

$$e^{t(\mathbf{a}_2 \cdot \nabla + a_3 \mathbf{x} \cdot \nabla)} f(\mathbf{x}) = f\left(\mathbf{x} e^{a_3 t} + \frac{\mathbf{a}_2}{a_3}(e^{a_3 t} - 1)\right) \equiv f(\mathbf{z}) \tag{13}$$

and

$$e^{\hat{\tau}(t) : \nabla\nabla} f(\mathbf{x}) = \sqrt{\det \frac{\hat{\tau}^{-1}(t)}{4\pi}} \int_{R^n} \exp\left[-(\mathbf{x} - \mathbf{y}) \frac{\hat{\tau}^{-1}(t)}{4} (\mathbf{x} - \mathbf{y})\right] f(\mathbf{y}) dy, \tag{14}$$

we obtain the following expression for the exact solution to the Cauchy problem (3);

$$u(t, \mathbf{x}) = \frac{e^{t a_1}}{\sqrt{\det(4\pi \hat{\tau}(t))}} \times \int_{R^n} \left\{ \exp\left[-(\mathbf{z} - \mathbf{y}) \frac{\hat{\tau}^{-1}(t)}{4} (\mathbf{z} - \mathbf{y})\right] \right\} \phi(\mathbf{y}) dy, \tag{15}$$

where $dy = dy_1 \ldots dy_n$, $\hat{\tau}(t)$ is from (12) and $\mathbf{z}$ is defined in (13).

One may check that the function $u(t, \mathbf{x})$ from (15) is the solution to problem (3); according to the Cauchy theorem, it is the only classical solution of this problem.

3. EXACT SOLUTION TO THE CAUCHY PROBLEM (4)

We will proceed here by analogy with Section 2.

In view of the t dependence of the coefficients of equation (4), we formally have for the solution to prob-

lem (4) an ordered exponential

$$u(t, \mathbf{x})\left\{\exp_+\int_0^t [a_1(s) + \mathbf{a}_2 \cdot \nabla + a_3(s)\mathbf{x} \cdot \nabla + a_4(s)\hat{a} : \nabla\nabla]ds\right\}\phi(\mathbf{x}). \quad (16)$$

The linearity of the integral and the explicit form of the operators in (16) permit us to write $u(t, \mathbf{x})$ in terms of the usual, not ordered, operator-valued exponent

$$u(t, \mathbf{x}) = e^{\alpha_1(t)} e^{\alpha_2(t) \cdot \nabla + \alpha_3(t)\mathbf{x} \cdot \nabla + \alpha_4(t)\hat{a} : \nabla\nabla}\phi(\mathbf{x}), \quad (17)$$

where, for convenience, we have denoted

$$\alpha_1(t) = \int_0^t a_1(s)ds, \quad \alpha_2(t) = \int_0^t \mathbf{a}_2(s)ds,$$
$$\alpha_3(t) = \int_0^t \mathbf{a}_3(s)ds, \quad \alpha_4(t) = \int_0^t \mathbf{a}_4(s)ds. \quad (18)$$

If we introduce the operators

$$\hat{A}(t) = \alpha_2(t) \cdot \nabla + \alpha_3(t)\mathbf{x} \cdot \nabla,$$
$$\hat{B}(t) = \alpha_4(t)\hat{a} : \nabla\nabla, \quad (19)$$

we have (from now on ' means d/dt)

$$\hat{A}'(t) = \mathbf{a}_2(t) \cdot \nabla + a_3(t)\mathbf{x} \cdot \nabla, \quad \hat{B}'(t) = a_4(t)\hat{a} : \nabla\nabla,$$
$$[\hat{A}(t), \hat{B}'(s)] = -2\alpha_3(t)\hat{B}'(s), \quad (20)$$

and we can write (17) in the form

$$u(t, \mathbf{x}) = e^{\alpha_1(t)} e^{\hat{A}(t) + \hat{B}(t)}\phi(\mathbf{x}), \quad (21)$$

which is analogous to (7). In order to find the action of the pseudodifferential operator $e^{\hat{A}(t) + \hat{B}(t)}$ on the function $\phi(\mathbf{x})$, we put

$$e^{\hat{A}(t) + \hat{B}(t)} = e^{\hat{A}(t)}\hat{F}(t) \quad (22)$$

and, as in Section 2, we obtain

$$\hat{F}(t) = e^{\hat{\tau}(t) : \nabla\nabla}, \quad (23)$$

where

$$\hat{\tau}(t) = \left(\int_0^t e^{2\alpha_3(s)} a_4(s)ds\right)\hat{a} = \int_0^t a_4(s)\exp\left[2\int_0^s a_3(v)dv\right]ds\hat{a}. \quad (24)$$

From (24) and from the properties of $a_4(t)$ and $\hat{a}$, it is obvious that $\hat{\tau}(t)$ is a symmetric nonnegative definite rank-two tensor function of t.

Recalling (19) and (21)–(23), we can then write the solution to the problem (4) in the form

$$u(t, \mathbf{x}) = e^{\alpha_1(t)} e^{[\alpha_2(t) + \alpha_3(t)\mathbf{x}] \cdot \nabla} e^{\hat{\tau}(t) : \nabla\nabla}\phi(\mathbf{x}), \quad (25)$$

where the α's are from (18) and $\hat{\tau}(t)$ is from (24).

Now taking into account formula (14) and the analog to formula (13) [20],

$$e^{\left(\int_0^t \mathbf{a}_2(s)ds\right) \cdot \nabla + \left(\int_0^t a_3(s)ds\right)\mathbf{x} \cdot \nabla} f(\mathbf{x}) = f\left(\mathbf{x}e^{\int_0^t a_3(s)ds} + \int_0^t \mathbf{a}_2(s)e^{\int_0^s a_3(v)dv}ds\right) \equiv f(\mathbf{z}), \quad (26)$$

we obtain the following expression for the exact solution of the Cauchy problem (4):

$$u(t, \mathbf{x}) = \frac{e^{\int_0^t a_1(s)ds}}{\sqrt{\det(4\pi\hat{\tau}(t))}} \times \int_{R^n}\left\{\exp\left[-(\mathbf{z} - \mathbf{y})\frac{\hat{\tau}^{-1}(t)}{4}(\mathbf{z} - \mathbf{y})\right]\right\}\phi(\mathbf{y})dy, \quad (27)$$

where $dy = dy_1 \ldots dy_n$, $\hat{\tau}(t)$ is from (24) and $\mathbf{z}$ is defined in (26).

Substituting expression (27) into equations (4), we immediately see that the function $u(t, \mathbf{x})$ is the solution to the problem (4); and, according to the Cauchy theorem, it is the only the classical solution to this problem.

4. CONCLUDING REMARKS

The exact solutions to the Cauchy problems (3) and (4) are obtained using the algebraic method we have described.

When $\hat{a}_4$ [or $\hat{a}_4(t)$] is a scalar, $\hat{a}_4 = a_4\hat{1}$ [or $\hat{a}_4(t) = a_4(t)\hat{1}$] (in these cases, $\hat{a}_4 : \nabla\nabla = a_4\Delta$), the "anisotropic" problems (3) and (4) reduce to the "isotropic" ones with the exact solution found in [20]. It is easy to check that the solutions (15) and (27) reduce to the solutions obtained in [20] {there is an error in [20]: the sign before $\mathbf{a}_2$ in equations (17) and (34) should be (+)}.

For different choices of the coefficients a_j, equations (3) and (4) may be also regarded as a set of different diffusion equations. Therefore, from formulas (15) and (27) we obtain the exact solutions to the Cauchy problems for this set of diffusion equations.

ACKNOWLEDGMENTS

One of the authors (A. D. D.) would like to express his gratitude to the Directors of JINR and the Bogoliubov Laboratory of Theoretical Physics for their invitation to visit Dubna and to Profs. A.N. Sissakian and G.S. Pogosyan for granting the possibility to present this paper.

REFERENCES

1. A. D. Fokker, Ann. Phys. (Paris) **43**, 812 (1914).
2. M. V. Smoluchowski, Ann. Phys. (Paris) **48**, 1103 (1915).
3. M. Planck, Sitzungsber K. Preuss. Akad. Wiss., Phys. Math. Kl. 324 (1917).
4. G. E. Uhlenbeck and L.S. Ornstein, Phys. Rev. **36**, 823 (1930).
5. A. N. Kolmogorov, Math. Ann. **108**, 149 (1933).
6. H. Kramers, Physica **7**, 284 (1970).
7. S. Chandrasekhar, Rev. Mod. Phys. **15**, 1 (1943).
8. M. C. Wang and G. E. Uhlenbeck, Rev. Mod. Phys. **17**, 323 (1945).
9. M. Lax, Rev. Mod. Phys. **32**, 25 (1960); **38**, 359 (1966).
10. I. I. Gihman and A. V. Skorohod, *Stochastic Differential Equations* (Springer-Verlag, Berlin, 1972).
11. P. Hanggi and H. Thomas, Z. Phys. B **22**, 295 (1975); Phys. Rep. **88**, 209 (1982).
12. L. Ricciardi, *Diffusion Processes and Related Topics in Biology* (Springer-Verlag, Berlin, 1977).
13. N. G. van Kampen, *Stochastic Processes in Physics and Chemistry* (Amsterdam, 1983).
14. H. Risken, *The Fokker–Planck Equation,* 2nd ed. (Springer-Verlag, Berlin, 1989).
15. R. L. Kautz, Rep. Prog. Phys. **59**, 935 (1996).
16. Y. Abe *et al.*, Phys. Rep. **275**, 49 (1996).
17. R. Friedrich and J. Peinke, Phys. Rev. Lett. **78**, 863 (1997).
18. M. Suzuki, Physica A **117**, 103 (1983); J. Math. Phys. **26**, 601 (1985).
19. A. N. Drozdov, Phys. Rev. E **55**, 1496, 2496 (1997).
20. A. A. Donkov, A. D. Donkov, and E. I. Grancharova, Int. J. Mod. Phys. A **12**, 165 (1997).
21. R. Feynman, Phys. Rev. **84**, 108 (1951).
22. V. P. Maslov, *Operational Methods* (Mir, Moscow, 1976).
23. *Pseudodifferential Operators* (Mir, Moscow, 1967).
24. L. Hörmander, *Linear Partial Differential Operators* (Springer-Verlag, Berlin, 1963).
25. Ju. A. Dubinskiĭ, Sov. Mat. Dokl. **23**, 583 (1981); **38**, 206 (1989).
26. M. E. Taylor, *Pseudodifferential Operators* (Princeton Univ. Press, Princeton, 1981).

Physics of Atomic Nuclei, Vol. 63, No. 4, 2000, pp. 684–687. From Yadernaya Fizika, Vol. 63, No. 4, 2000, pp. 749–752.

VIII INTERNATIONAL CONFERENCE ON SYMMETRY METHODS IN PHYSICS

Linear Groups of Symmetries of State Equations in Relativistic Continuum Mechanics*

A. N. Golubiatnikov

Moscow State University, Vorob'evy gory, Moscow, 119899 Russia

Abstract—On the basis of classification of continuous subgroups of the SL_3 group and their invariants as functions of components of the rank-two tensor g_{ij}, a description of possible relativistic anisotropic continua is given. Stability of relativistic media (or hyperbolicity of motion equations) with high symmetry (≥4 group parameters) is investigated. © *2000 MAIK "Nauka/Interperiodica".*

1. The approach connected with affine symmetry in Newtonian continuum mechanics was proposed by Coleman [1] and Wang [2]. It is used for describing such anisotropic media as liquid crystals and plasma. The complete classifications of the continuous subgroup of groups SL_3 and GL_3, more exactly, their Lie algebras, and their invariants as functions of g_{ij}, was given in [3, 4]. The results for group $SL_3 \ni a$, $\det a = 1$ are presented in the table.

In the given work, an application of this theory to relativistic mechanics is considered. Let $\xi^i(x^\alpha)$, $i = 1, 2, 3$, be Lagrangian coordinates of a point in the medium; x^α, $\alpha = 1, 2, 3, 4$, be observer variables; and $\eta_{\alpha\beta}(x^\gamma)$ be components of the metric tensor of the spacetime with signature +++– and

$$g^{ij} = \xi^i_\alpha \xi^j_\beta \eta^{\alpha\beta}, \quad \xi^i_\alpha = \frac{\partial \xi^i}{\partial x^\alpha}, \tag{1}$$

so that $(g^{ij})^{-1} = (g_{ij})$ is a three-dimensional metric tensor (+++) of the manifold of world lines.

As is known, the energy density of a homogeneous simple medium has the form $\varepsilon(g_{ij}, s)$, s being the specific entropy. Thus, the results of Newtonian symmetry for the function of accompanying components of the space metric g_{ij} are transferred in the relativistic mechanics.

In the table, the following notation is used: n is the dimension of group Lie G_n, N^0 is its number; e^i_j is a matrix that has unity on the intersection of the i line and j column, the remaining elements being zeros; x is here the parameter of series of subgroups; and $g = \det(g_{ij})$. The groups act as transformation groups on the set of Lagrangian variables ξ^k, so that matrix e^i_j (with components $(e^i_j)^k_l = \delta^{ik}\delta_{jl}$) responds to the infinitesimal operator $X^j_i = \xi^j \partial/\partial\xi^i$.

2. Questions of the stability of media with G_4 symmetry and higher in the framework of Newtonian mechanics are considered in [5]. It is shown that in these cases only the media admitting G_5 symmetry can be stable [see the invariants of G_4, 5 and 6 ($x = –1$), and G_5, 2 and 3, in the table].

We shall examine the relativistic equations of isentropic (s = const) motion of an ideal continuum

$$\nabla_\alpha \frac{\partial \varepsilon}{\partial \xi^i_\alpha} = 0. \tag{2}$$

It should be noted that the motion equations in form (2) always have the divergent form of certain conservation laws. To trade form $\nabla_\alpha T^\alpha_\beta = 0$, they are reduced by contraction with ξ^i_β.

The motion of surface $f(x^\alpha) = 0$ of weak discontinuity is described by the condition of solubility of the following linear equations relative to w^j:

$$Q_{ij} w^j \equiv \frac{\partial^2 \varepsilon}{\partial \xi^i_\alpha \partial \xi^j_\beta} f_\alpha f_\beta w^j = 0, \quad f_\alpha = \frac{\partial f}{\partial x_\alpha}. \tag{3}$$

The functions $\eta_{\alpha\beta}(x^\gamma)$ are assumed to be smooth.

Let $n^i \sim \xi^i_\alpha \nabla^\alpha f$ be components of a unit normal vector and D be the value of the discontinuity speed with respect to the medium. Then,

$$\begin{aligned} Q_{ij} &\sim n^k n_l \left(\frac{\partial p^l_i}{\partial g^{jk}} + \frac{\partial p^l_j}{\partial g^{ik}} \right) + (g_{ij}\varepsilon - p_{ij}) \frac{D^2}{c^2} \\ &\equiv Q_{1,ij} + Q_{2,ij} \frac{D^2}{c^2}, \quad p_{ij} = -2\rho \frac{\partial u}{\partial g^{ij}}, \end{aligned} \tag{4}$$

where $u = \varepsilon/\rho$ is the specific inner energy, ρ is the mass density, p_{ij} is the stress tensor, and c is the velocity of light in vacuum.

For the stability of a given medium state, the tensors $Q_{1,ij}$ and $Q_{2,ij}$ must define at each vector n^i three linearly

* This article was submitted by the author in English.

1063-7788/00/6304-0684$20.00 © 2000 MAIK "Nauka/Interperiodica"

Symmetry groups and their invariants

No.	Lie algebra	Invariants
1.1	$x(e_1^1 + e_2^2 - 2e_3^3) + e_2^1 - e_1^2$, $x \geq 0$	g, $g_{33}(g_{11} + g_{22})^2$, $g^{33}(g^{11} + g^{22})^2$, $g_{33}g^{33}$, $g_{33}\exp\left(2x \arctan\frac{2g_{12}}{g_{11} - g_{22}}\right)$
1.2	$x(e_1^1 + e_2^2 - 2e_3^3) + e_2^1$, $x = 0, 1$	g, $g_{33}g_{11}^2$, $g_{11}g_{13}^2$, $g_{13}g^{23}$, $g_{11}\exp\left(-2x\frac{g_{12}}{g_{11}}\right)$
1.3	$e_1^1 + xe_2^2 - (1 + x)e_3^3$, $-1/2 < x \leq 1$	g, $g_{11}g_{22}g_{33}$, $g_{22}g_{13}^2$, $g_{11}g_{23}^2$, $g_{33}g_{11}^{1+x}$
1.4	$e_1^1 + e_3^2$	g, g_{11}, g^{33}, $g_{22} - 2g_{13}$, $g_{11}g^{23} + g_{12}g^{33}$
2.1	$e_1^1 + e_2^2 - 2e_3^3$, $e_2^1 - e_1^2$	g, $g_{33}(g_{11} + g_{22})^2$, $g^{33}(g^{11} + g^{22})^2$, $g_{33}g^{33}$
2.2	$e_1^1 - e_2^2$, $e_1^1 - e_3^3$	g, $g_{11}g_{22}g_{33}$, $g_{22}g_{13}^2$, $g_{11}g_{23}^2$
2.3	$e_2^1 + e_3^2$, e_3^1	g, g_{11}, g^{33}, $g_{11}g^{23} + g_{12}g^{33}$
2.4	$e_1^1 + e_2^2 - 2e_3^3$, e_2^1	g, $g_{33}g_{11}^2$, $g_{11}g_{13}^2$, $g_{13}g^{23}$
2.5	e_2^1, e_3^1	g, g_{11}, g^{22}, g^{23}
2.6	e_3^1, e_3^2	g, g_{11}, g_{12}, g_{22}
2.7	$e_1^1 - e_3^3$, $e_2^1 + e_3^2$	g, $g^{33}g_{11}^{-1}$, $g_{22} - 2g_{13}$, $(g_{11}g^{23} + g_{12}g^{33})g_{11}^{-3/2}$
2.8	$xe_1^1 + (1 + x)e_2^2 - (1 + 2x)e_3^3$, e_2^1	g, $g_{11}^{-1}g_{13}^2g_{33}^{-1}$, $g^{23}g_{11}^{-1/2}$, $g_{33}^x g_{11}^{1+2x}$
2.9	$e_1^1 + e_2^2 - 2e_3^3 - e_2^1$, e_3^1	g, $g^{23}g_{11}^{-1}$, $g^{33}g_{11}^{-2}$, $g_{11}\exp\left(\frac{2g_{12}}{g_{11}}\right)$
2.10	$2e_1^1 - e_2^2 - e_3^3 - e_3^2$, e_3^1	g, $g_{11}g_{22}^2$, $g_{11}^{-1}g_{12}^4$, $g^{33}\exp\left(-\frac{2g^{23}}{g^{33}}\right)$
3.1	$e_2^1 + e_1^2$, $e_3^1 + e_1^3$, $e_3^2 - e_2^3$	g, $g_{11} - g_{22} - g_{33}$, $g^{11} - g^{22} - g^{33}$
3.2	$e_1^1 - e_2^2$, e_2^1, e_1^2	g, g_{33}, g^{33}
3.3	$e_2^1 - e_1^2$, $e_3^1 - e_1^3$, $e_3^2 - e_2^3$	g, $g_{11} + g_{22} + g_{33}$, $g^{11} + g^{22} + g^{33}$
3.4	$e_1^1 - e_3^3$, $e_2^1 + e_3^2$, e_3^1	g, $g_{11}^{-1}g^{33}$, $(g_{11}g^{23} + g_{12}g^{33})g_{11}^{-3/2}$
3.5	$e_1^1 - e_2^2$, $e_2^2 - e_3^3$, e_2^1	g, $g_{11}^{-1}g_{13}^2g_{33}^{-1}$, $g^{23}g_{11}^{-1/2}$
3.6	$(1 + x)e_1^1 - xe_2^2 - e_3^3$, e_2^1, e_3^1 $\lvert x\rvert \leq 1$	g, $g^{23}g_{11}^{-1/2}$, $g_{11}^{-x}(g^{22})^{1+x}$
3.7	$x(2e_1^1 - e_2^2 - e_3^3) - e_3^2$, e_2^1, e_3^1 $x = 0, 1$	g, $g^{33}g_{11}^{-1/2}$, $g^{33}\exp\left(-2x\frac{g^{23}}{g^{33}}\right)$
3.8	$x(2e_1^1 - e_2^2 - e_3^3) - e_3^2 + e_2^3$, e_2^1, e_3^1 $x \geq 0$	g, $(g^{22} + g^{33})g_{11}^{-1/2}$, $g_{11}\exp\left(2x \arctan\frac{2g^{23}}{g^{22} - g^{33}}\right)$

Table. (Contd.)

No.	Lie algebra	Invariants
3.9	$xe_1^1 + e_2^2 - (1+x)e_3^3,\quad e_3^1,\quad e_3^2$ $\lvert x\rvert \le 1$	$g,\quad g_{11}^{-1}g_{12}^2g_{22}^{-1},\quad g_{11}g_{22}^{-x}$
3.10	$e_1^1 + e_2^2 - 2e_3^3 - e_2^1,\quad e_3^1,\quad e_3^2$	$g,\quad g_{11}^{-2}g^{33},\quad g_{11}\exp\left(\frac{2g_{12}}{g_{11}}\right)$
3.11	$x(2e_1^1 + e_2^2 - 2e_3^3) + e_2^1 - e_1^2,\quad e_3^1,\quad e_3^2$ $x \ge 0$	$g,\quad g^{33}(g_{11}+g_{22})^{-2},\quad g_{33}\exp\left(-2x\arctan\frac{2g_{12}}{g_{11}-g_{22}}\right)$
4.1	$e_1^1 - e_2^2,\quad e_2^2 - e_3^3,\quad e_2^1,\quad e_3^1$	$g,\quad g^{23}g_{11}^{-1/2}$
4.2	$2e_1^1 - e_2^2 - e_3^3,\quad e_2^1,\quad e_3^1,\quad e_3^2 - e_2^3$	$g,\quad (g^{22}+g^{33})g_{11}^{-1/2}$
4.3	$e_1^1 - e_2^2,\quad e_2^2 - e_3^3,\quad e_3^1,\quad e_3^2$	$g,\quad g_{11}^{-1}g_{12}^2g_{22}^{-1}$
4.4	$e_1^1 + e_2^2 - 2e_3^3,\quad e_2^1 - e_1^2,\quad e_3^1,\quad e_3^2$	$g,\quad g^{33}(g_{11}+g_{22})^{-2}$
4.5	$e_1^1 - e_2^2,\quad e_2^1,\quad e_3^1,\quad e_3^2$	$g,\quad g^{33}$
4.6	$(1+x)e_1^1 - xe_2^2 - e_3^3,\quad e_2^1,\quad e_3^1,\quad e_3^2$ $\lvert x\rvert \le 1$	$g,\quad g_{11}^{-1}(g^{33})^{1+x}$
4.7	$e_1^1 - e_2^2,\quad e_2^2 - e_3^3,\quad e_2^1,\quad e_1^2$	$g,\quad g_{33}g^{33}$
5.1	$e_1^1 - e_2^2,\quad e_2^2 - e_3^3,\quad e_2^1,\quad e_3^1,\quad e_3^2$	g
5.2	$e_1^1 - e_2^2,\quad e_2^1,\quad e_1^2,\quad e_3^1,\quad e_3^2$	$g,\quad g^{33}$
5.3	$e_2^2 - e_3^3,\quad e_2^1,\quad e_3^1,\quad e_3^2,\quad e_2^3$	$g,\quad g_{33}$
6.1	$e_1^1 - e_2^2,\quad e_2^2 - e_3^3,\quad e_2^1,\quad e_1^2,\quad e_3^1,\quad e_3^2$	g
6.2	$e_1^1 - e_2^2,\quad e_2^2 - e_3^3,\quad e_2^1,\quad e_3^1,\quad e_3^2,\quad e_2^3$	g
8.1	$e_1^1 - e_2^2,\quad e_2^2 - e_3^3,\quad e_2^1,\quad e_1^2,\quad e_3^1,\quad e_1^3,\quad e_3^2,\quad e_2^3$	g

independent vectors w^i and appropriate real speeds D. In the Newtonian approximation, the tensor $Q_{1,ij}$ depending on the vector n^i is the same. The tensor $Q_{2,ij}$ is independent of n^i ($Q_{2,ij} \approx g_{ij}\rho c^2$). Thus, the results of Newtonian mechanics in medium instability that are connected with the change of signature of the tensor $Q_{1,ij}$ at variations n^i [5] remain valid in the relativistic theory.

Let us give at the positive definiteness of tensor $Q_{2,ij}$ sufficient conditions of the strong hyperbolicity of equations (2) for the media with G_5 symmetry. Let $V = \sqrt{g} \sim 1/\rho$ be the relative volume, $I = \sqrt{g^{33}}$ be the length of the covector (in the proper basis), and $J = \sqrt{g_{33}}$ be the length of the vector. These vectors define the medium anisotropy.

In case 1, we have an isotropic fluid with $p_{ij} = -pg_{ij}$, where p is the pressure and $\partial p/\partial\varepsilon > 0$. In case 2,

$$\frac{u}{V} - u_V > 0,\quad u_I > 0,\quad u_{II} > 0,$$
$$u_{VV} > 0,\quad u_{II}u_{VV} > V^2\left(\frac{u_I}{V}\right)_V^2, \tag{5}$$

and in case 3,

$$uV - u_V - \frac{Ju_J}{V} > 0,\quad u_J > 0,\quad u_{JJ} > 0,$$
$$u_{VV} > 0,\quad u_{JJ}u_{VV} > u_{JV}^2, \tag{6}$$

where indices V, I, J indicate the partial derivatives.

In Newtonian mechanics, case 2 corresponds to layered liquid crystals or fluids with disk-shaped mole-

cules. In this case, it is the gradient field ($I = |\nabla\xi^3|$) dragged by the continuum. In case 3, we have fluids with prolate molecules and ideal magnetic hydrodynamics in the general case with "anisotropic pressure," where $H = J/V$ is the value of the magnetic field. If the model of the relativistic magnetic hydrodynamics is well known, then stable structures of case 3 can also have applications in problems of relativistic mechanics. Here, for example, the model with

$$u = f(s)VI^2 + u_1(V, s), \quad f > 0,$$
$$(u_1/V)_V < 0, \quad u_{1,VV} > 0$$

is possible.

ACKNOWLEDGMENTS

This work was supported in part by the Russian Foundation for Basic Research (project no. 97-01-00196).

REFERENCES

1. B. D. Coleman, Arch. Ration. Mech. Anal. **20**, 41 (1965).
2. C.-C. Wang, Arch. Ration. Mech. Anal. **20**, 1 (1965).
3. A. N. Golubiatnikov, Dokl. Akad. Nauk SSSR **240**, 298 (1978).
4. A. N. Golubiatnikov, *Modern Group Analysis* (MPhTI, Moscow, 1993), p. 25.
5. A. N. Golubiatnikov and A.G. Kalugin, Vestn. Mosk. Univ., Ser. 1: Mat. Mekh., No. 2, 59 (1996).

Physics of Atomic Nuclei, Vol. 63, No. 4, 2000, pp. 688–691. From Yadernaya Fizika, Vol. 63, No. 4, 2000, pp. 753–756.

VIII INTERNATIONAL CONFERENCE ON SYMMETRY METHODS IN PHYSICS

"Minus *c*" Symmetry in Classical Electrodynamics and Quantum Theory*

G. A. Kotel'nikov

Russian Research Centre Kurchatov Institute, pl. Kurchatova 1, Moscow, 123182 Russia

Abstract—A symmetry associated with the inversion of the speed of light is considered. © *2000 MAIK "Nauka/Interperiodica".*

1. INTRODUCTION

We shall mean by "minus *c*" symmetry that connected with discrete transformation as the inversion of the speed of light. Discrete transformations play an important role in theoretical physics. The space inversion $P(\mathbf{x} \longrightarrow -\mathbf{x})$, the time reversal $T(t \longrightarrow -t)$, and the charge conjugation C are examples of these symmetries [1, 2]. Recently, the existence of an additional discrete symmetry of such a type [3, 4] was established. It is the inversion of the speed of light $x^0 \longrightarrow x^0$, $\mathbf{x} \longrightarrow \mathbf{x}$, $c \longrightarrow -c$, where $x^0 = ct$. Let us designate this symmetry by the symbol Q. The equation of light cone $(x^0)^2 - \mathbf{x}^2 = 0$ can demonstrate the example of the Q symmetry. "Minus *c*" symmetry is also inherent in the D'Alembert equation, the Maxwell equation, the equation of motion of a charged particle in an electromagnetic field, and Schrödinger and Klein–Gordon–Fock equations [3]. The "$c \longrightarrow -c$" symmetry is connected closely with the charge conjugation C, which may be interpreted as the composition of the QPT transformations [4]. The purpose of the present work is the further study of the Q-symmetry.

2. G_8 GROUP OF DISCRETE TRANSFORMATIONS OF SPACE, TIME, AND THE SPEED OF LIGHT

Let us introduce the 5-dimensional space of events $V^5(x^0, \mathbf{x}, c)$ and two hyperplanes with $c = +3 \times 10^{10}$ cm/s and $c = -3 \times 10^{10}$ cm/s in it and construct four matrices of dimension 5×5:

$$\alpha^T = \begin{pmatrix} -1 & 0 & 0 \\ 0 & I & 0 \\ 0 & 0 & 1 \end{pmatrix}, \quad \alpha^P = \begin{pmatrix} 1 & 0 & 0 \\ 0 & -I & 0 \\ 0 & 0 & 1 \end{pmatrix},$$
$$\alpha^Q = \begin{pmatrix} 1 & 0 & 0 \\ 0 & I & 0 \\ 0 & 0 & -1 \end{pmatrix}. \tag{1}$$

Here, I is the 3×3 unit matrix and $[\alpha^T, \alpha^P] = [\alpha^T, \alpha^Q] = [\alpha^P, \alpha^Q] = 0$. Matrices and their products form the cyclic Abelian group and induce the 8-dimensional group G_8 of discrete transformations of time, space, and speed of light in the 5-space of events $V^5(x^0, \mathbf{x}, c)$:

$$x^{a'} = (\alpha^{T^k} \alpha^{P^l} \alpha^{Q^m})^{ab} x^b; \quad a, b = 0, 1, 2, 3, 5. \tag{2}$$

The matrices α^P, α^T, and α^Q are in conformity with operators P, T, and Q acting on field functions of the equations studied at replacement of variables (2).

We consider the place of the group G_8 and its subgroups in symmetry theory of classical and quantum equations.

3. DISCRETE SYMMETRY OF MAXWELL EQUATIONS

We take the one-charge Maxwell equations and consider them in the 5-dimensional space $V^5(x^0, \mathbf{x}, c)$ on hyperplanes with $+c$ and $-c$. Each hyperplane can be interpreted as the 4-Minkowski subspace, as long as the sign of speed of light does not affect the view of the metric tensor $g_{ab} = \mathrm{diag}(+, -, -, -)$. On the $+c$ hyperplane, we have

$$\nabla \times \mathbf{H} - \partial_0 \mathbf{E} = 4\pi \mathbf{J}; \quad \nabla \cdot \mathbf{H} = 0,$$
$$\nabla \times \mathbf{E} + \partial_0 \mathbf{H} = 0; \quad \nabla \cdot \mathbf{E} = 4\pi\rho. \tag{3}$$

Here, $x^0 = ct$, $x^{1,2,3} = x, y, z$; $\mathbf{E}$ and $\mathbf{H}$ are the electric and the magnetic field; ρ is the density of electric charge e; $\mathbf{J} = \rho\mathbf{v}/c$ is the density of current; $\mathbf{v}$ is the speed of charge; $\mathbf{E} = -\partial_0 \mathbf{A} - \nabla\phi$ and $\mathbf{H} = \nabla \times \mathbf{A}$; and $A = (\phi, \mathbf{A})$ is the 4-dimensional potential.

The following statement holds true: the group of transformations (2) is the group of discrete symmetry of the Maxwell equations.

The proof is convenient to do with the help of the 16-dimensional function

$$\Phi(x^0, \mathbf{x}, c) = \mathrm{column}(0, \mathbf{E}, 0, \mathbf{H}, \rho, \mathbf{j}, \phi, \mathbf{A})$$

* This article was submitted by the author in English.

1063-7788/00/6304-0688$20.00 © 2000 MAIK "Nauka/Interperiodica"

written on the $+c$ hyperplane. The Maxwell equations are transformed to themselves if the function Φ is transformed by the rules

$$\begin{aligned}
&T_1\Phi(x^0, \mathbf{x}, c)\\
&= \text{column}(0, +\mathbf{E}, 0, -\mathbf{H}, +\rho, -\mathbf{J}, +\phi, -\mathbf{A})_{(-x^0, \mathbf{x}, c)},\\
&T_2\Phi(x^0, \mathbf{x}, c)\\
&= \text{column}(0, -\mathbf{E}, 0, +\mathbf{H}, -\rho, +\mathbf{J}, -\phi, +\mathbf{A})_{(-x^0, \mathbf{x}, c)},\\
&P_1\Phi(x^0, \mathbf{x}, c)\\
&= \text{column}(0, -\mathbf{E}, 0, +\mathbf{H}, +\rho, -\mathbf{J}, +\phi, -\mathbf{A})_{(x^0, -\mathbf{x}, c)},\\
&P_2\Phi(x^0, \mathbf{x}, c)\\
&= \text{column}(0, +\mathbf{E}, 0, -\mathbf{H}, -\rho, +\mathbf{J}, -\phi, +\mathbf{A})_{(x^0, -\mathbf{x}, c)},
\end{aligned} \tag{4}$$

$$\begin{aligned}
&Q_1\Phi(x^0, \mathbf{x}, c)\\
&= \text{column}(0, -\mathbf{E}, 0, -\mathbf{H}, -\rho, -\mathbf{J}, -\phi, -\mathbf{A})_{(x^0, \mathbf{x}, -c)},\\
&Q_2\Phi(x^0, \mathbf{x}, c)\\
&= \text{column}(0, +\mathbf{E}, 0, +\mathbf{H}, +\rho, +\mathbf{J}, +\phi, +\mathbf{A})_{(x^0, \mathbf{x}, -c)}.
\end{aligned} \tag{5}$$

The given ratios generalize the ones from [2, 5, 6]. In addition to the Maxwell equations, they keep invariance of the D'Alembert equation for the 4-potential and the equation of motion of a charged particle in an electromagnetic field. By this they form a discrete symmetry in classical electrodynamics.

Below, we shall study the symmetry connected with the speed of light.

4. THE FREE MAXWELL EQUATIONS

The inversion of the speed of light is a particular case of discrete transformations of group G_8 and thus forms the symmetry of the Maxwell equations. Let us consider the properties of charge conjugation induced by the $c \longrightarrow -c$ inversion in the case of the free Maxwell equations.

4.1. The Charge Conjugation in the Classical Sense

We now consider the combination Q_1Q_2, which we denote by symbol C_e and which induces the transformations

$$\begin{aligned}
&C_e\Phi(x^0, \mathbf{x}, c)\\
&= \text{column}(0, -\mathbf{E}, 0, -\mathbf{H}, -\mathbf{j}, -\rho, -\phi, -\mathbf{A})_{(x^0, \mathbf{x}, c)}.
\end{aligned} \tag{6}$$

Operator C_e changes the sign of the electric charge and may be interpreted as the operator of charge-conjugation type.

In the case of free fields, the charge-conjugate function is $\Phi_{C_e} = \text{column}(0, -\mathbf{E}, 0, -\mathbf{H}, 0, 0, 0, -\phi, -\mathbf{A})$. By means of replacement $k^0 = \omega/c = \mathscr{E}/\hbar c = p^0/\hbar$, $\mathbf{k} = k^0\mathbf{n} = \mathbf{p}/\hbar$ (ω is the frequency of the electromagnetic field, $\hbar$ is the Planck constant, $\mathbf{n}$ is the guiding wave vector, $\mathscr{E}$ is the energy of field, and $\mathbf{p}$ is the momentum of the field) the result of charge conjugation (6) can be written as

$$\begin{aligned}
&C_e\Psi_{p\,\mathbf{n}\,\mathbf{l}}(x^0, \mathbf{x}, c)\\
&= \text{column}(0, -\mathbf{l}, 0, -\mathbf{m})e^{-\frac{i}{\hbar}(p^0x^0 - \mathbf{p}\cdot\mathbf{x})} = \Psi_{p\,\mathbf{n}\,-\mathbf{l}},
\end{aligned} \tag{7}$$

where $\Psi \in \Phi$. The charge conjugation C_e changes the signs of polarization vectors $\mathbf{l}$ and $\mathbf{m}$ and preserves the signs of the energy $C_e\mathscr{E} = \mathscr{E}$, momentum $C_e\mathbf{p} = \mathbf{p}$ and guiding wave vector of field $C_e\mathbf{n} = \mathbf{n}$. It agrees with the behavior of the density of the field energy and the field momentum calculated directly from Maxwell equations $W = (E^2 + H^2)/8\pi$, $\mathbf{S} = c(\mathbf{E} \times \mathbf{H})/4\pi$. By this, the charge conjugation $C_e = Q_1Q_2$, being the transformation of symmetry of the Maxwell equations, does not result in negative energies. It differs from the charge conjugation C in quantum theory. By the given attribute, it is possible to identify the C_e conjugation as the charge conjugation in the classical sense.

4.2. The Charge Conjugation in the Quantum Sense

Let us write the Maxwell equations in the form of the Dirac equation with the help of the 8-dimensional function $\Psi = \text{column}(0, E_1, E_2, E_3, 0, H_1, H_2, H_3)$ [6]:

$$\begin{aligned}
&\gamma^\alpha p_a\Psi(x^0, \mathbf{x}, c)\\
&= (i\hbar\gamma^0\partial_0 + i\hbar\boldsymbol{\gamma}\cdot\nabla)\Psi(x^0, \mathbf{x}, c) = 0,
\end{aligned} \tag{8}$$

where $x^a = (ct, x, y, z)$; $g_{ab} = \text{diag}(+, -, -, -)$; $p_a = i\hbar\partial/\partial x^a$; $a, b, = 0, k$; $k = 1, 2, 3$; the summation is carried out over dummy indices; $\gamma^a = (\gamma^0, \boldsymbol{\gamma})$; and $\boldsymbol{\gamma} \equiv \gamma^k = (\gamma^1, \gamma^2, \gamma^3)$ are the 8-matrices [4, 6]. Implying the conversion of Maxwell equations into the Dirac equation, we use the operator of charge conjugation C from the quantum theory and define the action of the operator C by analogy with [1] as

$$C\Psi(x^0, \mathbf{x}, c) = U_C\overline{\Psi}^T(x^0, \mathbf{x}, c) = U_C\gamma^0\Psi^*(x^0, \mathbf{x}, c). \tag{9}$$

Here, U_C is the charge-conjugation matrix, $\overline{\Psi} = \Psi^+\gamma^0$ is the Dirac conjugate function, * denotes complex conjugation, and T is transposition. The equation for the conjugate function is

$$\begin{aligned}
\gamma^a p_a\Psi = 0 \longrightarrow &(i\hbar U_C\gamma^{0T}U_C^{-1}\partial_0 + i\hbar U_C\boldsymbol{\gamma}^T U_C^{-1}\cdot\nabla)\\
&\times U_C(\Psi^+\gamma^0)^T = 0.
\end{aligned} \tag{10}$$

It coincides with the original equation (8) if

$$\begin{aligned}
&U_C\gamma^{0T}U_C^{-1} = \gamma^0; \quad U_C\gamma^{kT}U_C^{-1} = -\gamma^k;\\
&k = 1, 2, 3.
\end{aligned} \tag{11}$$

We have from here $U_C = \lambda\gamma^0$, where $\lambda = (\pm 1, \pm i)$ is a proportionality factor. Further, we write the function describing the initial photon state by analogy with [2] as

$$\Psi_{p\,\mathbf{n}\,\mathbf{l}}(x^0, \mathbf{x}, c) = \frac{1}{\sqrt{2}}\mathrm{column}(0, l_1, l_2, l_3, 0, m_1, m_2, m_3)e^{-\frac{i}{\hbar}(p^0x^0 - \mathbf{p}\cdot\mathbf{x})}, \quad (12)$$

where $\Psi^+\Psi = 1$, $p = (\mathscr{E}/c, \mathscr{E}\mathbf{n}/c)$ is the 4-momentum, $\mathscr{E} = \hbar\omega$ and $\mathbf{p} = \mathscr{E}\mathbf{n}/c$ are the energy and momentum of a photon, $\mathbf{n}$ is the guiding vector of the photon, and $\mathbf{l}$ is the vector of electric polarization. Applying the operator C to function (12), we find the charge-conjugate function in the form

$$C\Psi_{p\,\mathbf{n}\,\mathbf{l}}(x^0, \mathbf{x}, c) = \frac{i}{\sqrt{2}}\mathrm{column}(0, -\mathbf{l}, 0, -\mathbf{m})e^{\frac{i}{\hbar}(p^0x^0 - \mathbf{p}\cdot\mathbf{x})} = i\Psi_{-p\,\mathbf{n}\,-\mathbf{l}}, \quad (13)$$

where $\lambda = -i$. Similarly to the solution of the Dirac equation for a particle with a nonzero rest mass, it is possible for the photon charge-conjugate function to be considered as the function describing a particle with negative energy $\mathscr{E} = -\hbar\omega$ and opposite momentum $\mathbf{p} = -(\hbar\omega/c)\mathbf{n}$.

We introduce the notation $\Psi_C = i\Psi_{-p\,\mathbf{n}\,-\mathbf{l}}$ and, in the spirit of the Dirac interpretation of the solution with negative energy, shall consider the solution Ψ_C as that which describes directly unobservable vacuum photons. It follows from expressions of the quantum 8-currents $j^a = \overline{\Psi}\gamma^a\Psi$ and $j^a_C = \overline{\Psi}_C\gamma^a\Psi_C$ that the relations $j^0 = j^0_C = 1$ and $j^k = j^k_C = (n^1, n^2, n^3)$ are compatible with the fact that the photon has no charge. Due to this circumstance, we may interpret the charge-conjugate state as the antiphoton identical with the photon in accordance with [2].

Further, we shall find how the operator of charge conjugation C may be related to the operator of conjugation Q induced by the inversion of the speed of light $c \longrightarrow -c$. Let us define the conjugation Q as follows:

$$Q\Psi(x^0, \mathbf{x}, c) = U_Q\overline{\Psi}^T(x^0, \mathbf{x}, -c) = U_Q\gamma^0\Psi^*(x^0, \mathbf{x}, -c), \quad \hbar \longrightarrow -\hbar. \quad (14)$$

The inversion of the speed of light and Planck constant does not change equation (8), due to the absence of photon rest mass. Consequently, the conjugation Q formally transforms equation (8) into itself by means of the same matrix $U_Q = U_C = \lambda\gamma^0$ and the following interrelation is true:

$$C\Psi_{p\,\mathbf{n}\,\mathbf{l}}(x^0, \mathbf{x}, c) = Q\Psi_{p\,\mathbf{n}\,\mathbf{l}}(x^0, \mathbf{x}, c). \quad (15)$$

The most important conclusion may be drawn from here. The charge-conjugate function describing the vacuum photon state with negative energy on the $+c$ hyperplane coincides with the function describing the free photon state with positive energy on the $-c$ hyperplane:

$$\Psi_C(x^0, \mathbf{x}, c) = \Psi_Q(x^0, \mathbf{x}, -c) \longrightarrow \Psi_{-p\,-\mathscr{E}\,\mathbf{n}\,-\mathbf{l}}(x^0, \mathbf{x}, c) = \Psi_{-p\,+\mathscr{E}\,\mathbf{n}\,-\mathbf{l}}(x^0, \mathbf{x}, -c). \quad (16)$$

One can see that the vacuum photon from the $+c$ hyperplane is equivalent to the free photon from the $-c$ hyperplane. It is possible to admit that this is the same object with a different interpretation.

In the case of the vacuum interpretation, we may believe that the photon is located on a $+c$ hyperplane, with the positive Planck constant $\hbar > 0$. Its energy is negative $\mathscr{E} = -\hbar\omega < 0$, the frequency is negative $\omega < 0$, and the 4-momentum components have opposite signs $p^a = (-p^0, -\mathbf{p})$. The photon is in a condition of vacuum movement, with a positive speed of light and negative energy.

In the case of the "minus c" interpretation, we may believe that the photon is located on the $-c$ hyperplane, with the negative Planck constant $\hbar < 0$. Its energy is positive $\mathscr{E} = (-\hbar)(-\omega) > 0$, the frequency is negative $\omega < 0$, and the 4-momentum components have opposite signs $p^a = (-p^0, -\mathbf{p})$. The photon is in a condition of free movement with the negative speed of light and the positive energy.

Both interpretations reflect the invariance of Maxwell equations with respect to the inversion of the speed of light $c \longrightarrow -c$. The similar property is true not only for photon, but also for electron states from the Dirac equation. We note only that the operation of the Q conjugation in our case differs from the previous Q conjugation ([4], hep-ph/9703047), where the Planck constant kept the invariant significance. The choice of the Q conjugation in the form (9) seems more correct for those two reasons.

In the case of the Planck constant invariance, the fine-structure constant $\alpha = e^2/\hbar c$ is not invariant as far as $Q(e^2/\hbar c) = -e^2/\hbar c$, as this is undesirable.

In classical electrodynamics with a noninvariant speed of light, the new invariants hold true: $\hbar c$ [7] or $\hbar/c$ [8].

Below, we select the first version according to which the particle rest mass m is transformed as $Q(m) = m' = mc^2/(-c)^2 = m$—that is, it preserves the invariant significance on the hyperplane $-c$.

5. THE DIRAC EQUATION

We consider the case of the Dirac equation briefly and note that analogously to results (15) and (16) for photon states, those for electron states are

$$C\psi_{p\,\sigma\,\mathscr{E}}(x^0, \mathbf{x}, c) = Q\psi_{p\,\sigma\,\mathscr{E}}(x^0, \mathbf{x}, c) \longrightarrow \psi_{-p\,-\sigma\,-\mathscr{E}}(x^0, \mathbf{x}, c) = \psi_{-p\,-\sigma\,+\mathscr{E}}(x^0, \mathbf{x}, -c). \quad (17)$$

The difference consists in that the $\Psi_{p\,\mathbf{n}\,\mathbf{l}}$ field is 8-component field and describes the neutral bosonic particles (photons) when γ matrices γ^0 and γ^5 are commutative $[\gamma^0, \gamma^5] = 0$ [4], and the $\psi_{p\sigma\mathscr{E}}$ field is a 4-component field and describes the charge fermionic particles (electrons, positrons) when γ matrices γ^0 and γ^5 are anticommutative $\{\gamma^0, \gamma^5\} = 0$ [1, 2].

6. CONCLUSION

It is shown that the charge conjugation C_e in the classical sense and the charge conjugation C in the quantum sense may be interpreted as the consequence of symmetry of Maxwell and Dirac equations, with respect to the discrete transformations $x^0 \longrightarrow x^0$, $\mathbf{x} \longrightarrow \mathbf{x}$, $c \longrightarrow -c$.

We also note that the inversion of the speed of light is compatible with Lorentz transformations, because this inversion does not change the form of Lorentz transformations, as follows from

$$\begin{aligned} x^{0'} &= \frac{x^0 - \beta x^1}{\sqrt{1-\beta^2}}, \quad x^{1'} = \frac{x^1 - \beta x^0}{\sqrt{1-\beta^2}}, \quad x^{2'} = x^2, \\ x^{3'} &= x^3, \quad c' = +c; \\ x^{0'} &= \frac{x^0 - \beta x^1}{\sqrt{1-\beta^2}}, \quad x^{1'} = \frac{x^1 - \beta x^0}{\sqrt{1-\beta^2}}, \quad x^{2'} = x^2, \\ x^{3'} &= x^3, \quad c' = -c, \end{aligned} \tag{18}$$

where $\beta' = -\beta$. Consequently, the inversion of the speed of light does not violate the requirement of Lorentz and the relativistic invariance in physics. The reason for this lies in the fact that equations of classical and quantum electrodynamics satisfy the original principle of relativity: they are independent of the concrete value of the speed of light.

REFERENCES

1. S. S. Schweber, H. A. Bete, and F. de Hoffmann, *Mesons and Fields* (Peterson Row, Evanston, 1995; Russ. Transl., Inostrannaya Literatura, Moscow, 1957), Vol. 1.
2. V. B. Berestetskiĭ, E. M. Lifshitz, and L. P. Pitaevskiĭ, *Relativistic Quantum Theory* (Russ. original, Parts 1 and 2, Nauka, Moscow, 1968, 1971; Pergamon Press, Oxford, 1971).
3. G. A. Kotel'nikov, in *Proceedings of the Fifth Workshop on Symmetry Methods in Physics, Obninsk, July 1991* (Obninsk, 1992), p. 252; Izv. Vyssh. Uchebn. Zaved., Fiz. **12**, 69 (1992).
4. G. A. Kotel'nikov, http://xxx.lanl.gov/abs/quant-ph/9703047 (9707003).
5. J. Rosen, Am. J. Phys. **41**, 586 (1973).
6. V. I. Fushchich and A. G. Nikitin, *Symmetries of Maxwell's Equations* (Naukova Dumka, Kiev, 1983; Reidel, Dordrecht, 1987).
7. G. A. Kotel'nikov, Vestn. Mosk. Univ., Ser. 3: Fiz. Astron. **4**, 371 (1970); Izv. Vyssh. Uchebn. Zaved., Fiz. **9**, 93 (1979); **10**, 46 (1981); Teor. Mat. Fiz. **42**, 139 (1980).
8. J. P. Hsu, Found. Phys. **6**, 317 (1976).

Physics of Atomic Nuclei, Vol. 63, No. 4, 2000, pp. 692–694. From Yadernaya Fizika, Vol. 63, No. 4, 2000, pp. 757–759.

VIII INTERNATIONAL CONFERENCE ON SYMMETRY METHODS IN PHYSICS

Caldirola–Kanai Oscillator in the Classical Formulation of Quantum Mechanics*

S. S. Safonov

Moscow Institute for Physics and Technology, Institutskiĭ per. 9, Dolgoprudnyĭ, Moscow oblast, 141700 Russia

Abstract—The quadrature distribution for a quantum damped oscillator is introduced in the frame of formulation of quantum mechanics based on a tomography scheme. The probability distribution for coherent and Fock states of the damped oscillator is expressed explicitly in terms of Gaussian and Hermite polynomials, respectively. © *2000 MAIK "Nauka/Interperiodica".*

In classical mechanics, the description of motion with friction described by the equation of motion has no ambiguities present in quantum description. Quantum friction in the classical formulation of quantum mechanics was considered in [1]. The aim of this work is to discuss the problem of friction for a quantum Caldirola–Kanai oscillator [2, 3].

Moyal [4] obtained the evolution equation for quantum states in the form of the classical stochastic equation for a function which turned out to be the Wigner quasidistribution function [5], which cannot be considered as a probability since it takes negative values. Mancini *et al.* [6] obtained the evolution equation for the quantum state in the form of the classical stochastic equation for a function which turned out to be a probability distribution for a position measured in an ensemble of squeezed and rotated reference frames in the classical phase space of the system. The idea of this classical-like formulation of quantum dynamics uses the notion of optical tomography suggested by Vogel and Risken [7]. Man'ko [8] obtained the equation for energy levels in the frame of the classical-like formulation of quantum mechanics and rederived the energy spectrum of the quantum oscillator (see also [9]).

The distribution $w(X, \mu, \nu, t)$ for the generic linear combination of quadratures, which is a measurable observable,

$$\hat{X} = \mu\hat{q} + \nu\hat{p}, \tag{1}$$

where $\hat{q}$ and $\hat{p}$ are the position and momentum, respectively, depending on two extra real parameters μ, and ν, is related to the state of the quantum system expressed in terms of its Wigner function $W(q, p, t)$ as follows [6, 8]:

$$w(X, \mu, \nu, t) = \int \exp[-ik(X - \mu q - \nu q)] \times W(q, p, t)\frac{dk\,dq\,dp}{(2\pi)^2}. \tag{2}$$

The distribution is normalized,

$$\int w(X, \mu, \nu, t)dX = 1. \tag{3}$$

As was shown [2, 3], the quantum friction appears in a system with the Hamiltonian (we assume $\hbar = m = 1$)

$$\hat{H}(t) = \frac{\hat{p}^2}{2}\exp(-2\gamma t) + \omega^2\exp(2\gamma t)\frac{\hat{q}^2}{2}, \tag{4}$$

where the friction coefficient γ and the frequency of the quantum oscillator ω are taken to be constant. For this system, the wave functions of the coherent $|\alpha\rangle$ and Fock $|n\rangle$ states can be written as [10] (we assume $\omega = 1$)

$$\Psi_\alpha(q, t) = \frac{1}{\sqrt[4]{\pi}\sqrt{\varepsilon}}\exp\left(\frac{i\dot{\varepsilon}e^{2\gamma t}}{2\varepsilon}q^2 + \frac{\sqrt{2}\alpha}{\varepsilon}q - \frac{\dot{\varepsilon}^*}{2\varepsilon}\alpha^2 - \frac{|\alpha|^2}{2}\right), \tag{5}$$

$$\Psi_n(q, t) = \frac{1}{\sqrt[4]{\pi}\sqrt{\varepsilon}}\left(\frac{\varepsilon^*}{2\varepsilon}\right)^{n/2}\frac{1}{\sqrt{n!}}\exp\left(\frac{i\dot{\varepsilon}e^{2\gamma t}}{2\varepsilon}q^2\right)H_n\left(\frac{q}{\sqrt{\varepsilon\varepsilon^*}}\right). \tag{6}$$

In these formulas, the time-dependent function $\varepsilon(t)$ satisfies the equation

$$\ddot{\varepsilon}(t) + 2\gamma\dot{\varepsilon}(t) + \varepsilon(t) = 0 \tag{7}$$

and the initial conditions

$$\varepsilon(0) = \frac{1}{\sqrt{\Omega}}, \quad \dot{\varepsilon}(0) = \frac{i\Omega - \gamma}{\sqrt{\Omega}}, \tag{8}$$

where $\Omega^2 = 1 - \gamma^2$. The solution $\varepsilon(t)$ has the form

$$\varepsilon(t) = \frac{1}{\sqrt{\Omega}}e^{-\gamma t}[\cos(\Omega t) + i\sin(\Omega t)]. \tag{9}$$

The physical meaning of the Fock state of the Caldirola–Kanai oscillator (6) was discussed in [8]. It was shown that this state is a loss-energy state, and the wave function of this state has the property of periodicity in time with a purely imaginary period. Using the known

* This article was submitted by the author in English.

expression for the Wigner function in terms of the wave function of coherent state (5) (see [6, 8]) and calculating the integral (2), we obtain the probability distribution for the coherent state in the form

$$w_\alpha = \frac{1}{\sqrt{\pi\varepsilon\varepsilon^*(a^2+b^2)}}\exp(-|\alpha|^2)$$

$$\times \exp\left(-\frac{X^2}{\varepsilon\varepsilon^*(\alpha^2+b^2)}\right) \otimes \exp\left[-\alpha^2\frac{\varepsilon^{*2}(a-ib)^2}{2\varepsilon\varepsilon^*(\alpha^2+b^2)}\right. \quad (10)$$

$$\left. + \alpha\frac{\sqrt{2}\varepsilon^* X(\alpha-ib)}{\varepsilon\varepsilon^*(\alpha^2+b^2)}\right] \otimes \exp\left[-\alpha^{*2}\frac{\varepsilon^2(a+ib)^2}{2\varepsilon\varepsilon^*(\alpha^2+b^2)}\right.$$

$$\left. + \alpha^*\frac{\sqrt{2}\varepsilon X(\alpha+ib)}{\varepsilon\varepsilon^*(\alpha^2+b^2)}\right].$$

Using the wave function (6), we analogously find the probability distribution for the Fock state,

$$w_n(X,\mu,\nu,t) = w_0(X,\mu,\nu,t)\frac{1}{2^n n!}H_n^2\left(\frac{X}{\sqrt{\varepsilon\varepsilon^*(\alpha^2+b^2)}}\right), \quad (11)$$

where the probability distribution of the oscillator groundlike state is

$$w_0(X,\mu,\nu,t) = \frac{1}{\sqrt{\pi\varepsilon\varepsilon^*(\alpha^2+b^2)}}\exp\left(-\frac{X^2}{\varepsilon\varepsilon^*(\alpha^2+b^2)}\right), \quad (12)$$

where

$$a = \frac{\exp(2\gamma t)\nu(\varepsilon^*\dot{\varepsilon}+\varepsilon\dot{\varepsilon}^*)}{2\varepsilon\varepsilon^*}+\mu, \quad b = \frac{\nu}{\varepsilon\varepsilon^*}. \quad (13)$$

Here, $\varepsilon(t)$ is given by equation (9). In the figure, we show the probability distribution for the first excited state (loss-energy state) $w_1(X, \varphi, t)$ as a function of the rotation angle φ (abscissa) and homodyne output variable X (ordinate) [7]

$$\hat{X}(\varphi) = \hat{q}\cos\varphi - \hat{p}\sin\varphi. \quad (14)$$

In the figure, we assume $t = 5$ and $\gamma = 0.05$.

It was shown in [6] that, for the system with Hamiltonian

$$\hat{H}(t) = \frac{\hat{p}^2}{2} + \hat{V}(q,t), \quad (15)$$

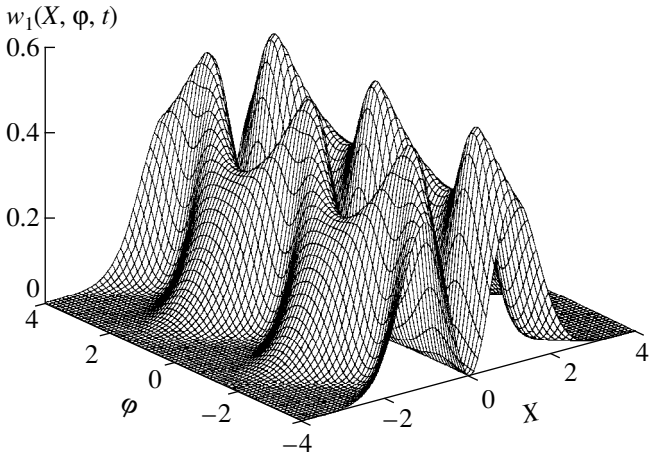

Marginal distribution of the excited (loss-energy) state $\gamma = 0.05$ and $t = 5$.

the quantum evolution equation alternative to the time-dependent Schrödinger equation has the form

$$\dot{w} - \mu\frac{\partial}{\partial\nu}w - i\left[V\left(-\frac{1}{\partial/\partial X}\frac{\partial}{\partial\mu} - i\frac{\nu}{2}\frac{\partial}{\partial X}, t\right)\right. \quad (16)$$
$$\left. - V\left(-\frac{1}{\partial/\partial X}\frac{\partial}{\partial\mu} + i\frac{\nu}{2}\frac{\partial}{\partial X}, t\right)\right]w = 0.$$

For the damped oscillator, this equation takes the form [1]

$$\dot{w} - \mu\frac{\partial}{\partial\nu}w - i\left[\tilde{V}\left(-\frac{1}{\partial/\partial X}\frac{\partial}{\partial\mu} - i\frac{\nu}{2}\frac{\partial}{\partial X}, t'\right)\right. \quad (17)$$
$$\left. - \tilde{V}\left(-\frac{1}{\partial/\partial X}\frac{\partial}{\partial\mu} + i\frac{\nu}{2}\frac{\partial}{\partial X}, t'\right)\right]w = 0,$$

where

$$\tilde{V}(q,t') = \exp[2\gamma t(t')]V[q,t(t')] = \exp[4\gamma t(t')]\frac{q^2}{2}, \quad (18)$$

$$t'(t) = \frac{1-\exp(-2\gamma t)}{2\gamma}, \quad t(t') = -\frac{\ln(1-2\gamma t')}{2\gamma}. \quad (19)$$

We have

$$\frac{\partial t(t')}{\partial t'} = \exp(2\gamma t). \quad (20)$$

In (16) and (17), overdots label partial derivatives with respect to t'. Using the relation (18), one can rewrite (17) as

$$\frac{\partial}{\partial t'}w - \mu\frac{\partial}{\partial\nu}w + \exp(4\gamma t)\nu\frac{\partial}{\partial\mu}w = 0. \quad (21)$$

One can check that the probability distributions w_α (10) and w_n (11) satisfy this equation.

Let us consider the invariants of the damped quantum oscillator $\hat{a}^\dagger\hat{a}(t)$ and $(\hat{a}^\dagger\hat{a})^*(t)$ in the classical for-

mulation of quantum mechanics. Here, the asterisk means the complex conjugate operator. The operator $\hat{a}^{\dagger}\hat{a}\,(t)$ acts on the variable q, and the operator $(\hat{a}^{\dagger}\hat{a}\,)^{*}(t)$ acts on the variable q' of the density matrix $\rho_n(q, q', t)$; these describe the Fock state $|n\rangle$ of the system. These invariants act on the distribution w_n of the Fock state (11) as

$$\hat{a}^{\dagger}\hat{a}(t)w_n(X, \mu, \nu, t) = nw_n(X, \mu, \nu, t), \qquad (22)$$

$$(\hat{a}^{\dagger}\hat{a})^{*}(t)w_n(X, \mu, \nu, t) = nw_n(X, \mu, \nu, t). \qquad (23)$$

Invariants $\hat{a}^{\dagger}\hat{a}\,(t)$ and $(\hat{a}^{\dagger}\hat{a}\,)^{*}(t)$ have the form

$$\hat{a}^{\dagger}\hat{a}(t) = \frac{1}{2}\left\{\left(\frac{\partial}{\partial X}\right)^{-2}\left[\varepsilon\varepsilon^{*}\left(\frac{\partial}{\partial \nu}\right)^{2} + \dot{\varepsilon}\dot{\varepsilon}^{*}e^{4\gamma t}\left(\frac{\partial}{\partial \mu}\right)^{2}\right.\right.$$

$$\left. - e^{2\gamma t}(\varepsilon^{*}\dot{\varepsilon} + \varepsilon\dot{\varepsilon}^{*})\frac{\partial^{2}}{\partial\mu\partial\nu}\right] - \left(\frac{\partial}{\partial X}\right)^{2}[\varepsilon\varepsilon^{*}\mu^{2} + \dot{\varepsilon}\dot{\varepsilon}^{*}e^{4\gamma t}\nu^{2}$$

$$+ e^{2\gamma t}(\varepsilon^{*}\dot{\varepsilon} + \varepsilon\dot{\varepsilon}^{*})\mu\nu] + i\left[\frac{\varepsilon\varepsilon^{*}}{2}\left(\mu\frac{\partial}{\partial \nu} + \frac{\partial}{\partial \nu}\mu\right)\right. \qquad (24)$$

$$+ \frac{\dot{\varepsilon}^{*}\varepsilon e^{2\gamma t}}{2}\nu\frac{\partial}{\partial \nu} + \frac{\varepsilon^{*}\dot{\varepsilon}e^{2\gamma t}}{2}\frac{\partial}{\partial \nu}\nu\Big] - i\left[\frac{\dot{\varepsilon}\dot{\varepsilon}^{*}}{2}\left(\nu\frac{\partial}{\partial \mu} + \frac{\partial}{\partial \mu}\nu\right)\right.$$

$$\left.\left. + \frac{\varepsilon^{*}\dot{\varepsilon}e^{2\gamma t}}{2}\mu\frac{\partial}{\partial \mu} + \frac{\dot{\varepsilon}^{*}\varepsilon e^{2\gamma t}}{2}\frac{\partial}{\partial \mu}\mu\right]\right\}$$

and

$$(\hat{a}^{\dagger}\hat{a})^{*}(t) = \frac{1}{2}\left\{\left(\frac{\partial}{\partial X}\right)^{-2}\left[\varepsilon\varepsilon^{*}\left(\frac{\partial}{\partial \nu}\right)^{2} + \dot{\varepsilon}\dot{\varepsilon}^{*}e^{4\gamma t}\left(\frac{\partial}{\partial \mu}\right)^{2}\right.\right.$$

$$\left. + e^{2\gamma t}(\varepsilon^{*}\dot{\varepsilon} + \varepsilon\dot{\varepsilon}^{*})\frac{\partial^{2}}{\partial\mu\partial\nu}\right] - \left(\frac{\partial}{\partial X}\right)^{2}[\varepsilon\varepsilon^{*}\mu^{2} + \dot{\varepsilon}\dot{\varepsilon}^{*}e^{4\gamma t}\nu^{2}$$

$$- e^{2\gamma t}(\varepsilon^{*}\dot{\varepsilon} + \varepsilon\dot{\varepsilon}^{*})\mu\nu] - i\left[\frac{\varepsilon\varepsilon^{*}}{2}\left(\mu\frac{\partial}{\partial \nu} + \frac{\partial}{\partial \nu}\mu\right)\right. \qquad (25)$$

$$- \frac{\varepsilon^{*}\dot{\varepsilon}e^{2\gamma t}}{2}\nu\frac{\partial}{\partial \nu} - \frac{\dot{\varepsilon}^{*}\varepsilon e^{2\gamma t}}{2}\frac{\partial}{\partial \nu}\nu\Big] + i\left[\frac{\dot{\varepsilon}\dot{\varepsilon}^{*}}{2}\left(\nu\frac{\partial}{\partial \mu} + \frac{\partial}{\partial \mu}\nu\right)\right.$$

$$\left.\left. - \frac{\dot{\varepsilon}^{*}\varepsilon e^{2\gamma t}}{2}\mu\frac{\partial}{\partial \mu} - \frac{\varepsilon^{*}\dot{\varepsilon}e^{2\gamma t}}{2}\frac{\partial}{\partial \mu}\mu\right]\right\}.$$

To obtain this form of the operators under discussion, we used the correspondence of the action of the operators on the Wigner function $W(q, p, t)$ and the probability distribution $w(X, \mu, \nu, t)$ [8].

The main result of this work is the introduction of the positive normalized distribution function (probability distribution) for describing the quantum states of the damped quantum oscillator. This distribution contains complete information about the state of the system. For the probability distribution of the damped oscillator, the quantum evolution equation is found, which is an alternative to the Schrödinger equation.

REFERENCES

1. V. I. Man'ko and S. S. Safonov, Teor. Mat. Fiz. **112**, 467 (1997).
2. P. Caldirola, Nuovo Cimento **18**, 393 (1941).
3. E. Kanai, Prog. Theor. Phys. **3**, 440 (1948).
4. J. E. Moyal, Proc. Cambridge Philos. Soc. **45**, 99 (1949).
5. E. Wigner, Phys. Rev. **40**, 749 (1932).
6. S. Mancini, V. I. Man'ko, and P. Tombesi, Phys. Lett. A **213**, 1 (1996); Found. Phys. (in press).
7. K. Vogel and H. Risken, Phys. Rev. A **40**, 2847 (1989).
8. V. I. Man'ko, J. Russ. Laser Res. **17**, 579 (1996).
9. V. I. Man'ko, J. Russ. Laser Res. **17**, 439 (1996).
10. V. V. Dodonov and V. I. Man'ko, Phys. Rev. A **20**, 550 (1979).

Physics of Atomic Nuclei, Vol. 63, No. 4, 2000, pp. 695–699. From Yadernaya Fizika, Vol. 63, No. 4, 2000, pp. 760–764.

VIII INTERNATIONAL CONFERENCE ON SYMMETRY METHODS IN PHYSICS

IBM: Discrete Symmetry Viewpoint*

A. M. Shirokov[1], N. A. Smirnova[1], Yu. F. Smirnov[1, 2], O. Castaños[2], and A. Frank[2]

Abstract—It is shown that the set of transformations of the *s* and *d* boson operators that maintain the IBM-like form of the Hamiltonian comprises a discrete point symmetry group D_2'. The transformations manifest themselves as a parameter symmetry of the IBM-1 Hamiltonian. The transformations considered are also necessary for constructing the most general IBM-2 Hamiltonian. The properties of the potential energy surfaces arising in connection with these transformations are discussed. © *2000 MAIK "Nauka/Interperiodica".*

1. INTRODUCTION

An ambiguity in the definition of the boson creation and annihilation operators within the Interacting Boson Model (IBM) was mentioned a long time ago [1, 2]. The gauge transformations

$$b^+_{lm} \longrightarrow \exp(i\phi_l) b^+_{lm}, \quad \tilde{b}_{lm} \longrightarrow \exp(-i\phi_l)\tilde{b}_{lm} \qquad (1)$$

do not change the spectrum of eigenvalues of the IBM-like Hamiltonian

$$H = H_0 + \sum_l \varepsilon_l [b^+_l \times \tilde{b}_l]^{(0)}_0 + \sum_{\lambda l_1 l_2 l_3 l_4} a(l_1 l_2 l_3 l_4)[[b^+_{l_1} \times b^+_{l_2}]^{(\lambda)} \times [\tilde{b}_{l_3} \times \tilde{b}_{l_4}]^{(\lambda)}]^{(0)}_0. \qquad (2)$$

Here and below, l and m are the angular momentum of the boson and its projection, respectively, $\tilde{b}_{lm} = (-1)^{l-m} b_{l,-m}$; $[t^{(\lambda_1)} \times u^{(\lambda_2)}]^{(\lambda)}_\mu = \sum_{\mu_1\mu_2} (\lambda_1\mu_1\lambda_2\mu_2|\lambda\mu) \times t^{(\lambda_1)}_{\mu_1} u^{(\lambda_2)}_{\mu_2}$, and $\lambda_1\mu_1\lambda_2\mu_2|\lambda\mu$ is an $O(3)$ Clebsch–Gordan coefficient. The parameters $a(l_1l_2l_3l_4)$ are assumed to be real. The Hamiltonian (2) is Hermitian and invariant with respect to the $O(3)$ group. It commutes with the boson number operator N. In general, the phases ϕ_l in transformations (1) are arbitrary. However, if we constrain ourselves to time-reversal invariant Hamiltonians, we should choose only discrete values: 0; π [3]; and, in some cases, $\pi/2$ [1, 2].

The following discrete transformations of the boson operators have been used before in the literature:

(1) **V** transformation [1, 2],

$$\mathbf{V}: b^+_{lm} \longrightarrow i b^+_{lm}, \quad \tilde{b}_{lm} \longrightarrow -i\tilde{b}_{lm}; \qquad (3)$$

(2) **S** transformation [3, 4],

$$\mathbf{S}: b^+_{lm} \longrightarrow -b^+_{lm}, \quad \tilde{b}_{lm} \longrightarrow -\tilde{b}_{lm}; \qquad (4)$$

(3) **F** transformation (particle–hole conjugation) [5],

$$\mathbf{F}: b^+_{lm} \longrightarrow \tilde{b}_{lm}, \quad \tilde{b}_{lm} \longrightarrow -b^+_{lm}. \qquad (5)$$

It is interesting to study the possible appearance of a discrete group associated with the transformations (3)–(5) and to consider some consequences of such discrete symmetry in the IBM. Note that all the transformations (3)–(5) are canonical ones; i.e., they preserve the boson commutation relations

$$[b^+_{lm}, b^+_{l'm'}] = [\tilde{b}_{lm}, \tilde{b}_{l'm'}] = 0,$$
$$[\tilde{b}_{lm}, b^+_{l'm'}] = (-1)^{l-m}\delta_{ll'}\delta_{m,-m'}. \qquad (6)$$

Thus, we look for a discrete subgroup of the continuous group $Sp(2, R)$ of linear canonical transformations [6]. It is easy to verify that the transformations **V**, $\mathbf{V}^{-1}$, **S**, and **F**, together with their products **FV**, $\mathbf{FV}^{-1}$, and **SF** and with a unit element **E**, form a double-point symmetry group D_2' acting in the two-dimensional space of the operators b^+_{lm} and $\tilde{b}_{lm}$. In fact, the transformations **V**, $\mathbf{V}^{-1}$, **F**, and $\mathbf{FV}^{-1}$ can be identified with the rotations C_{2z}, C^3_{2z}, C_{2y}, and C_{2x}, respectively, while $\mathbf{S} = \mathbf{V}^2$ is equivalent to the element Q of D_2' (here we use the notation of reference [7]).

Generally, the transformations (3) and (4) can be performed independently for each value of l. The transformation **F** does not conserve the total number of bosons N. Note that the transformation **F** was initially introduced for fermion systems and is incorrect for a boson system with bosons of one type. Therefore, to obtain a modified Hamiltonian of the IBM-like form (8), we should apply the particle–hole transformation **F** to *s* and *d* bosons simultaneously.

* This article was submitted by the authors in English.

[1] Institute of Nuclear Physics, Moscow State University, Vorob'evy gory, Moscow, 119899 Russia.
[2] Instituto de Ciencias Nucleares, UNAM, México, México.

1063-7788/00/6304-0695$20.00 © 2000 MAIK "Nauka/Interperiodica"

The group D_2' contains all discrete boson transformations used in the literature on IBM. For example, the transformation

$$Q = [d^+ \times s + s^+ \times \tilde{d}]^{(2)}_\mu - \frac{\sqrt{7}}{2}[d^+ \times \tilde{d}]^{(2)}_\mu \longrightarrow [d^+ \times s + s^+ \times \tilde{d}]^{(2)}_\mu + \frac{\sqrt{7}}{2}[d^+ \times \tilde{d}]^{(2)}_\mu, \quad (7)$$

introduced in [8] is equivalent to the product of the **F**-transformation for *s* and *d* bosons and the **S**-transformation for s bosons.

We now turn to the consequences of the D_2' symmetry in the boson Hamiltonians.

2. PARAMETER SYMMETRY OF IBM-1

The IBM-1 involves the bosons of two types, *s* and *d*, with angular momenta $l = 0$ and $l = 2$, respectively. The most general IBM-1 Hamiltonian has the form [2]

$$\begin{aligned} H = {} & \tilde{H}_0 + \varepsilon(d^+ \cdot \tilde{d}) \\ & + \sum_{\lambda = 0, 2, 4} \frac{1}{2}\sqrt{2\lambda + 1}\, c_\lambda [[d^+ \times d^+]^{(\lambda)} \times [\tilde{d} \times \tilde{d}]^{(\lambda)}]^{(0)}_0 \\ & + \frac{1}{2}\tilde{v}_0 [[d^+ \times d^+]^{(0)} \times [s \times s]^{(0)} \\ & + [s^+ \times s^+]^{(0)} \times [\tilde{d} \times \tilde{d}]^{(0)}]^{(0)}_0 \\ & + \frac{1}{\sqrt{2}}\tilde{v}_2 [[d^+ \times d^+]^{(2)} \times [\tilde{d} \times s]^{(2)} \\ & + [d^+ \times s^+]^{(2)} \times [\tilde{d} \times \tilde{d}]^{(2)}]^{(0)}_0. \end{aligned} \quad (8)$$

The Hamiltonian (8) can be equivalently expressed in terms of the first (C_1) and second order (C_2) Casimir invariants of the algebras entering the following reduction chains of the $U(6)$ algebra [2]:

$$U(6) \begin{cases} \nearrow & U(5) \supset SO(5) \supset SO(3) \supset SO(2) \\ \rightarrow & SU(3) \supset SO(3) \supset SO(2) \\ \searrow & SO(6) \supset SO(5) \supset SO(3) \supset SO(2), \end{cases} \quad (9)$$

i.e.,

$$\begin{aligned} H(\{k_i\}) = {} & H_0 + k_1 C_1(U(5)) \\ & + k_2 C_2(U(5)) + k_3 C_2(SO(5)) \\ & + k_4 C_2(SO(3)) + k_5 C_2(SO(6)) + k_6 C_2(SU(3)). \end{aligned} \quad (10)$$

Generally, one can find the eigenvalues diagonalizing the Hamiltonian *H* using an appropriate basis. However, if the Hamiltonian contains Casimir operators belonging to only one of the reduction chains (9), then the spectrum of the system can be found analytically. These cases, referred to as dynamical symmetries (DS) of the IBM, determine three typical nuclear spectra: vibrational (the $U(5)$ DS limit), rotational (the $SU(3)$ DS limit), and γ-unstable (the $SO(6)$ DS limit). The transitional nuclear Hamiltonian that does not pertain to any DS is conventionally believed to generate a spectrum different from those corresponding to any of the DS limits.

The transformation **S** applied to *s* bosons is equivalent to the substitution $\tilde{v}_2 \longrightarrow \tilde{v}_2' = -\tilde{v}_2$ in the equation (8). However, for the same Hamiltonian but expressed through Casimir operators [see (10)], it results in a more complicated transformation. Let us define the Casimir operators as in [3, 4]. The transformed Hamiltonian $H(\{k_i'\}) = SH(\{k_i\})S^{-1}$ with parameters

$$\begin{aligned} & H_0' = H_0, \quad k_1' = k_1 + 2k_6, \quad k_2' = k_2 + 2k_6, \\ & k_3' = k_3 - 6k_6, \quad k_4' = k_4 + 2k_6, \\ & k_5' = k_5 + 2k_6, \quad k_6' = -k_6 \end{aligned} \quad (11)$$

has the same spectrum of eigenvalues as the initial Hamiltonian (10). Therefore, the fit of the IBM-1 Hamiltonian parameters to the experimental data appears to be ambiguous.

If $k_6 = 0$ in the Hamiltonian (10), then the transformation **V** becomes compatible with time-reversal invariance. Applying the transformation **V** to only one type of boson (e.g., to *s* bosons), we obtain a new Hamiltonian $H(\{k_i'\}) = VH(\{k_i\})V^{-1}$ with parameters

$$\begin{aligned} & H_0' = H_0 + 20k_5 N, \quad k_1' = k_1 + 8k_5(N + 2), \\ & k_2' = k_2 - 8k_5, \quad k_3' = k_3 + 4k_5, \\ & k_4' = k_4, \quad k_5' = -k_5, \quad k_6' = k_6 = 0, \end{aligned} \quad (12)$$

which is also isospectral to *H*. It is important to note that applying the transformations **S** and **V** (to only one type of boson) and the transformation **F** to both types of bosons (in the case of DS limits $SO(6)$ or $SU(3)$), we obtain the Hamiltonian *H'*, which does not seem to correspond to any DS limit but is isospectral to the initial Hamiltonian *H*. The reason for this paradox is that **S**, **V**, and **F** transform the DS algebra *G* to the alternative algebra *G'*, which is isomorphic but not identical to *G*.

3. D_2' TRANSFORMATIONS AS A SOURCE OF NEW DYNAMICAL SYMMETRY ALGEBRAS

The transformation **V** for *s* bosons transforms the $SO(6)$ algebra with generators

$$[d^+ \times \tilde{d}]^{(\lambda)}_\mu \ (\lambda = 1, 3), \ D_\mu = [d^+ \times s + s^+ \times \tilde{d}]^{(2)}_\mu \quad (13)$$

into a new $SO'(6)$ algebra with generators [5]

$$[d^+ \times \tilde{d}]^{(\lambda)}_\mu \quad (\lambda = 1, 3),$$
$$D'_\mu = -i[d^+ \times s - s^+ \times \tilde{d}]^{(2)}_\mu. \tag{14}$$

The Casimir operator of $SO'(6)$ can be expressed in terms of $C_2(SO(6))$ and the rest of the Casimir operators as [4, 9]

$$C_2(SO'(6)) = 20N + 8(N+2)C_1(U(5)) - 8C_2(U(5)) + 4C_2(SO(5)) - C_2(SO(6)). \tag{15}$$

The substitution of $C_2(S0(6))$ by $C_2(SO'(6))$ in the Hamiltonian (10) with $k_6 = 0$ is seen from (15) to be equivalent to the parameter symmetry transformation (12).

Similarly, the transformation **S** transforms the $SU(3)$ algebra with generators

$$[d^+ \times \tilde{d}]^{(1)}_\mu,$$
$$Q_\mu = [d^+ \times s + s^+ \times \tilde{d}]^{(2)}_\mu - \frac{\sqrt{7}}{2}[d^+ \times \tilde{d}]^{(2)}_\mu \tag{16}$$

into the alternative $SU'(3)$ subalgebra of $U(6)$ with generators

$$[d^+ \times \tilde{d}]^{(1)}_\mu,$$
$$Q'_\mu = -[d^+ \times s + s^+ \times \tilde{d}]^{(2)}_\mu - \frac{\sqrt{7}}{2}[d^+ \times \tilde{d}]^{(2)}_\mu. \tag{17}$$

$C_2(SU'(3))$ can be expressed in terms of $C_2(SU(3))$ and the rest of the Casimir operators as [4, 9]

$$C_2(SU'(3)) = 2C_1(U(5)) + 2C_2(U(5)) - 6C_2(SO(5)) + 2C_2(SO(3)) + 2C_2(SO(6)) - C_2(SU(3)). \tag{18}$$

Due to (18), the substitution of $C_2(SU(3))$ into equation (10) by $C_2(SU'(3))$ is equivalent to the transformation (11) in the parameter space.

New algebras can be obtained by the application of the transformation **F** (see [5] for details) and the other elements of the D'_2 group. In the case of IBM-1, the corresponding algebras are not independent of the ones considered. However, this is not the case for IBM-2.

4. COMPLETE SET OF CASIMIR OPERATORS FOR THE GENERAL IBM-2 HAMILTONIAN

IBM-2 distinguishes proton and neutron degrees of freedom; i.e., it deals with proton and neutron boson operators s_ρ, d_ρ, where $\rho = \pi, \nu$. The general IBM-2 Hamiltonian H includes proton H_π and neutron H_ν Hamiltonians and the interaction between protons and neutrons $H_{\pi+\nu}$, i.e., [2]

$$H = H_\pi + H_\nu + H_{\pi+\nu}, \tag{19}$$

where H_ρ is given by (8) for each kind of boson, while

$$\begin{aligned} H_{\pi+\nu} &= w_0(d^+_\pi \cdot \tilde{d}_\pi) \cdot (d^+_\nu \cdot \tilde{d}_\nu) \\ &+ \sum_{\lambda=1}^{4} w_\lambda([d^+_\pi \times \tilde{d}_\pi]^{(\lambda)} \cdot [d^+_\nu \times \tilde{d}_\nu]^{(\lambda)}) \\ &+ w_8([s^+_\pi \times \tilde{d}_\pi + d^+_\pi \times s_\pi]^{(2)} \cdot [s^+_\nu \times \tilde{d}_\nu + d^+_\nu \times s_\nu]^{(2)}) \\ &+ w_9([s^+_\pi \times \tilde{d}_\pi - d^+_\pi \times s_\pi]^{(2)} \cdot [s^+_\nu \times \tilde{d}_\nu - d^+_\nu \times s_\nu]^{(2)}) \\ &+ w_{10}([d^+_\pi \times \tilde{d}_\pi]^{(2)} \cdot [s^+_\nu \times \tilde{d}_\nu + d^+_\nu \times s_\nu]^{(2)}) \\ &+ w_{11}([s^+_\pi \times \tilde{d}_\pi + d^+_\pi \times s_\pi]^{(2)} \cdot [d^+_\nu \times \tilde{d}_\nu]^{(2)}). \end{aligned} \tag{20}$$

We thus have 21 parameters which, in the framework of the IBM-2, describe the excitation spectrum of nuclei [2]. The general IBM-2 Hamiltonian can be equivalently expressed in terms of the first and second order Casimir invariants for the algebras entering the reduction chains of $U_\pi(6) \otimes U_\nu(6)$ algebra [2], i.e., each proton and neutron subsystem algebras $U_\rho(5)$, $SO_\rho(6)$, $SO_\rho(5)$, $SU_\rho(3)$, and $SO_\rho(3)$ and combined proton and neutron algebras $U_{\pi+\nu}(6)$, $U_{\pi+\nu}(5)$, $SO_{\pi+\nu}(6)$, $SO_{\pi+\nu}(5)$, $SU_{\pi+\nu}(3)$, and $SO_{\pi+\nu}(3)$ with generators

$$\mathcal{G}_{\pi+\nu} = \mathcal{G}_\pi + \mathcal{G}_\nu. \tag{21}$$

However, this results in only 18 independent Casimir operators instead of the needed 21. To the best of our knowledge, the general IBM-2 Hamiltonian has not been presented before in terms of Casimir operators.

Here, we propose to express the necessary three additional independent terms through the Casimir operators of the alternative algebras obtained by transformations (3)–(5).

(1) The new $SO'_{\pi+\nu}(6)$ algebra with generators

$$\mathcal{G}'_{\pi+\nu} = \mathcal{G}'_\pi + \mathcal{G}'_\nu, \tag{22}$$

where $\mathcal{G}'_\pi$ and $\mathcal{G}'_\nu$ are defined according to (14).

(2) The new $SU'_{\pi+\nu}(3)$ algebra with generators

$$\mathcal{G}'_{\pi+\nu} = \mathcal{G}_\pi + \mathcal{G}'_\nu, \tag{23}$$

where $\mathcal{G}_\pi$ and $\mathcal{G}'_\nu$ are defined according to (16) and (17), respectively. This algebra is not independent of the $SU^*(3)$ algebra introduced in [8].

(3) The new $SU''_{\pi+\nu}(3)$ algebra with generators

$$\mathcal{G}''_{\pi+\nu} = \mathcal{G}'_\pi + \mathcal{G}'_\nu, \tag{24}$$

where $\mathcal{G}'_\pi$ and $\mathcal{G}'_\nu$ are defined according to (17).

It can be verified that the general IBM-2 Hamiltonian (19) can be expressed in terms of the Casimir oper-

ators of the algebras given above, i.e.,

$$\begin{aligned} H(\{k_i\}) &= H_0 + k_1^{\pi} C_1(U_{\pi}(5)) \\ &+ k_2^{\pi} C_2(U_{\pi}(5)) + k_3^{\pi} C_2(SO_{\pi}(5)) \\ &+ k_4^{\pi} C_2(SO_{\pi}(3)) + k_5^{\pi} C_2(SO_{\pi}(6)) \\ &+ k_6^{\pi} C_2(SU_{\pi}(3)) + k_1^{\nu} C_1(U_{\nu}(5)) \\ &+ k_2^{\nu} C_2(U_{\nu}(5)) + k_3^{\nu} C_2(SO_{\nu}(5)) \\ &+ k_4^{\nu} C_2(SO_{\nu}(3)) + k_5^{\nu} C_2(SO_{\nu}(6)) \\ &+ k_6^{\nu} C_2(SU_{\nu}(3)) + kC_2(U_{\pi+\nu}(6)) \\ &+ k_2 C_2(U_{\pi+\nu}(5)) + k_3 C_2(SO_{\pi+\nu}(5)) \\ &+ k_4 C_2(SO_{\pi+\nu}(3)) + k_5 C_2(SO_{\pi+\nu}(6)) \\ &+ k_5' C_2(SO'_{\pi+\nu}(6)) + k_6 C_2(SU_{\pi+\nu}(3)) \\ &+ k_6' C_2(SU'_{\pi+\nu}(3)) + k_6'' C_2(SU''_{\pi+\nu}(3)). \end{aligned} \tag{25}$$

5. DISCRETE SYMMETRY OF THE IBM AND POTENTIAL-ENERGY SURFACES

Nuclear shapes are conventionally associated within the IBM-1 with the so-called potential-energy surfaces (PES) [10]

$$E(\beta, \gamma) = \frac{\langle N, \beta, \gamma | H | N, \beta, \gamma \rangle}{\langle N, \beta, \gamma | N, \beta, \gamma \rangle}, \tag{26}$$

where

$$|N, \beta, \gamma\rangle = \left(s^{+} + \sum_{\mu} \alpha_{\mu} d_{\mu}^{+} \right)^{N} |0\rangle \tag{27}$$

is a coherent state. The quadrupole parameters α_μ can be expressed in terms of Euler angles and the β and γ parameters of Bohr and Mottelson in the usual manner. The shape of the PES (26) depends on the parameters of the IBM Hamiltonian H. The PES behavior under transformation of the IBM-1 Hamiltonian parameters has been thoroughly investigated in [11] in the framework of the catastrophe theory. It has been shown that the points in the parameter space corresponding to the $U(5)$, $SO(6)$, $SO'(6)$, $SU(3)$, and $SU'(3)$ DS limits are of great importance for the determination of the PES. In this section, we discuss the relevance of the D_2' transformations in the PES.

The explicit expression for the PES corresponding to the IBM-1 Hamiltonian can be obtained using the results of [10], i.e.,

$$\begin{aligned} E(\beta, \gamma, k_i) &= 10N(k_5 + k_6) \\ &+ \frac{N\beta^2}{1+\beta^2}(k_1 + 5k_2 + 4k_3 + 6k_4) \\ &+ \frac{N(N-1)\beta^4}{(1+\beta^2)^2}(k_2 + k_6) + \frac{8N(N-1)\beta^2}{(1+\beta^2)^2}(k_5 + k_6) \\ &+ 4\sqrt{2}\frac{N(N-1)\beta^3 \cos 3\gamma}{(1+\beta^2)^2} k_6. \end{aligned} \tag{28}$$

It is seen from (28) that the transformation **S** applied to s bosons results in the transformation

$$E(\beta, \gamma) \longrightarrow E(-\beta, \gamma), \tag{29}$$

which corresponds, e.g., to the transformation from a prolate equilibrium shape to an oblate one and vice versa.

The transformation **V** (in the case $k_6 = 0$) applied to s bosons results only in a sign change of the term proportional to β^2. The difference between $SO(6)$ and $SO'(6)$ DS limits can be visually demonstrated in the particular case where $k_1 = k_2 = k_3 = k_4 = k_6 = 0$ and $H = k_5 C_2(SO(6))$. In this case, the PES is given by

$$E(\beta, \gamma) = \left(10Nk_5 + \frac{8N(N-1)\beta^2}{(1+\beta^2)^2} \right) k_5. \tag{30}$$

According to (15) the transformation **V** leads to a new Hamiltonian,

$$H' = k_5 C_2(SO'(6)). \tag{31}$$

In this case, we have a constant PES [11]:

$$E(\beta, \gamma) = 10Nk_5. \tag{32}$$

ACKNOWLEDGMENTS

We are thankful to R. Bijker, J. Cseh, D. Bonatsos, G. F. Filippov, F. Iachello, T. Otsuka, J. Patera, D.L. Pursey, V.N. Tolstoy, and P. Van Isacker for valuable discussions.

The paper is supported in part by the Russian Foundation for Basic Research, Competitive Center of Fundamental Science at St. Petersburg State University, the European Community, through project CI1*-CT94-0072; and DGAPA, UNAM, through project IN 101997.

REFERENCES

1. P. Van Isacker *et al.*, Phys. Rev. C **31**, 671 (1985).
2. F. Iachello and A. Arima, *The Interacting Boson Model* (Cambridge Univ. Press, Cambridge 1987).
3. N. A. Smirnova and A. M. Shirokov, Izv. Ross. Akad. Nauk, Ser. Fiz. **61**, 69 (1997) [Bull. Russ. Acad. Sci., Phys. Ser. **61**, 54 (1997)]; A. M. Shirokov, N. A. Smirnova, and Yu. F. Smirnov, Phys. Lett. B **434**, 237 (1998).

4. A. M. Shirokov and N. A. Smirnova, *Proceedings of the XXI International Coll. on Group Theoretical Methods in Physics* (World Sci., Singapore 1997), Vol. 2, p. 781.
5. A. Frank and P. van Isacker, *Algebraic Methods in Molecular and Nuclear Structure Physics* (Wiley, New York, 1994).
6. M. Moshinsky and Yu. F. Smirnov, *The Harmonic Oscillator in Modern Physics* (Harwood, 1996).
7. L. D. Landau and E. M. Lifshitz, *Quantum Mechanics: Non-Relativistic Theory* (Pergamon, Oxford, 1977; Russ. original, 4th ed., Nauka, Moscow, 1989).
8. A. E. L. Dieperink and R. Bijker, Phys. Lett. B **116**, 77 (1982).
9. D. Kusnezov, Phys. Rev. Lett. **79**, 537 (1997).
10. J. M. Ginocchio and M. W. Kirson, Nucl. Phys. A **350**, 31 (1980).
11. E. López-Moreno and O. Castaños, Phys. Rev. C **54**, 2374 (1996).

Physics of Atomic Nuclei, Vol. 63, No. 4, 2000, pp. 700–703. From Yadernaya Fizika, Vol. 63, No. 4, 2000, pp. 765–768.

VIII INTERNATIONAL CONFERENCE ON SYMMETRY METHODS IN PHYSICS

Dirac Equation in Curved Spacetime with the Metric in the Kerr–Schield Form*

V. P. Tsvetkov

Tver State University, ul. Zhelyabova 33, Tver, 170000 Russia

Abstract—The solution of the Dirac equation in the wave package form in a slightly curved spacetime (compared with the size of the wave package) was studied. For the metric in the Kerr–Schield form, a system of common differential equations describing spin conditions of massive neutral Dirac particles (neutrinos) was obtained. The effect of depolarization of the massive neutrinos in a gravitational field are discussed. This effect allows a considerable similarity between the theoretical and observed solar neutrino flows to be established if $m_{\nu_e} \geq 10^{-4}$ eV. *© 2000 MAIK "Nauka/Interperiodica".*

The study of spin phenomena in curved spacetime is one of the most important problems of modern astrophysics. A study of massive-neutrino spin behavior in gravitational fields with various geometries presents particular interest. As will be shown in the present work, the spin phenomena in curved spacetime are most simply described by the Dirac equation [1] for the class of the metrics presented in the Kerr–Schield form [2]: $g^{\mu\nu} = \eta^{\mu\nu} + \xi^\mu\xi^\nu$, where ξ^μ is an isotropic vector in relation to the Minkowski metric $\eta^{\mu\nu}$.

The Dirac equation in curved spacetime with the metric in the Kerr–Schield form can be presented in the form of the Schrödinger equation [3]:

$$i\frac{\partial\Psi}{\partial t} = \hat{\mathbf{H}}\Psi,$$

$$\begin{aligned}\hat{\mathbf{H}} = -i(1+\xi^2)^{-1}\Big[&-\Big(1+\frac{1}{2}\xi^2\Big)\gamma^5(\boldsymbol{\sigma}\cdot\nabla)\\ &+\Big(\xi+\frac{1}{2}\gamma^5(\boldsymbol{\sigma}\cdot\boldsymbol{\xi})\Big)(\boldsymbol{\xi}\cdot\nabla)+\frac{i}{2}\xi(\boldsymbol{\sigma}\cdot[\boldsymbol{\xi}\times\nabla])\\ &+\frac{1}{4}\frac{\partial}{\partial t}(\xi^2-\gamma^5(\boldsymbol{\sigma}\cdot\boldsymbol{\xi})\xi)+\frac{1}{4}(\nabla\cdot(\xi\boldsymbol{\xi}-\gamma^5(\boldsymbol{\sigma}\cdot\boldsymbol{\xi})\boldsymbol{\xi}))\\ &+im\beta\Big(1+\frac{1}{2}\xi^2+\frac{1}{2}\gamma^5\xi(\boldsymbol{\sigma}\cdot\boldsymbol{\xi})\Big)\Big],\end{aligned} \tag{1}$$

$$\xi_a = \eta_{ab}\xi^b, \quad \xi^0 = \xi, \quad \xi^\mu = (\xi, \boldsymbol{\xi}),$$

where γ^5, β, and σ^l are Dirac and Pauli matrices and m is the mass of the particle.

We present Ψ in the form of a combination of the conditions with left and right helicities:

$$\begin{aligned}\Psi &= \Psi_L + \Psi_R, \quad \Psi_L = \frac{1}{2}(1+\gamma^5)\Psi,\\ \Psi_R &= \frac{1}{2}(1-\gamma^5)\Psi.\end{aligned} \tag{2}$$

Then

$$\begin{aligned}i\frac{\partial\Psi_{L,R}}{\partial t} = -i(1+\xi^2)^{-1}\Big\{\Big[&\mp\Big(1+\frac{1}{2}\xi^2\Big)(\boldsymbol{\sigma}\cdot\nabla)\\ &+\Big(\xi\pm\frac{1}{2}(\boldsymbol{\sigma}\cdot\boldsymbol{\xi})\Big)(\boldsymbol{\xi}\cdot\nabla)+\frac{i}{2}\xi(\boldsymbol{\sigma}\cdot[\boldsymbol{\xi}\times\nabla])\\ &+\frac{1}{4}\frac{\partial}{\partial t}(\xi^2\mp(\boldsymbol{\sigma}\cdot\boldsymbol{\xi})\xi)+\frac{1}{4}(\nabla\cdot(\xi\boldsymbol{\xi}\mp(\boldsymbol{\sigma}\cdot\boldsymbol{\xi})\boldsymbol{\xi}))\Big]\Psi_{L,R}\\ &+im\beta\Big(1+\frac{1}{2}\xi^2\mp\xi(\boldsymbol{\sigma}\cdot\boldsymbol{\xi})\Big)\Psi_{R,L}\Big\}.\end{aligned} \tag{3}$$

The wave function Ψ will be normalized according to the following condition:

$$\int\overline{\Psi}e^0_{(a)}\gamma^a\Psi\sqrt{-g}d^3x = 1. \tag{4}$$

As follows from (2), the probability of a neutrino being in the conditions of right and left helicities equals

$$\begin{aligned}W_R &= \int\overline{\Psi}_R e^0_{(a)}\gamma^a\Psi_R\sqrt{-g}d^3x,\\ W_L &= \int\overline{\Psi}_L e^0_{(a)}\gamma^a\Psi_L\sqrt{-g}d^3x,\\ W_L + W_R &= 1.\end{aligned} \tag{5}$$

We look for the solution of equation (3) in the form of a wave package localized in a spatial area with a diameter l. We designate the length on which ξ is essentially changed as L_g. It is obvious that $L_g \sim 1/\max|\nabla\xi|$.

* This article was submitted by the author in English.

1063-7788/00/6304-0700$20.00 © 2000 MAIK "Nauka/Interperiodica"

Virtually, L_g is of the order of the sizes R of the gravitational field source. For black holes, L_g is of the order of the gravitational radius R_g of the collapsing astrophysical object, while R_g of stars with mass of the order of the Sun's mass is 1.5 km.

We seek the solution of (3) in the form of a wave packet with a width $L_p \gg L_g$:

$$\Psi_{L,R} = \frac{1}{\pi^{1/4} d^{-3/2}} \int d^3 q \exp\left(-\frac{(\mathbf{q}-\mathbf{p}_0)^2}{2d^2} + i\int_0^t E(\mathbf{q},\tau)d\tau - i(\mathbf{q}\cdot\mathbf{r}) \right) u(\mathbf{q},t)_{L,R}, \quad (6)$$

$$u_L = \begin{pmatrix} F \\ -F \end{pmatrix}, \quad u_R = \begin{pmatrix} H \\ H \end{pmatrix}.$$

Substituting (6) into (3), we obtain

$$\frac{d}{dt}F(H) = -i(1+\xi^2)^{-1}\left\{ \left(E(1+\xi^2) - \xi(\boldsymbol{\xi}\cdot\mathbf{q}) \pm (\boldsymbol{\sigma}\cdot\mathbf{Q}_{\mp}) \right) F(H) + m\left(1 + \frac{1}{2}\xi^2 \mp \frac{1}{2}\xi(\boldsymbol{\sigma}\cdot\boldsymbol{\xi}) \right) H(F) \right\}, \quad (7)$$

$$\mathbf{Q}_{\mp} = \mathbf{q} - \frac{1}{2}[\boldsymbol{\xi}\cdot[\boldsymbol{\xi}\times\mathbf{q}]] \mp \frac{i}{2}\xi[\boldsymbol{\xi}\times\mathbf{q}].$$

In (7), $\boldsymbol{\xi}$ is taken in the maximum of the wave package amplitude (6). Here, we have an accuracy of the order of L_p/L_g. The maximum of the wave package amplitude (6) is defined by the following condition:

$$\mathbf{r} = \int_0^t (\nabla_{\mathbf{q}} E(\mathbf{q},\tau))d\tau + \mathbf{r}_0, \quad (8)$$

which corresponds to the movement of the package's gravity center along the classical trajectory. The system of differential equations (7) describes the behavior of the massive-neutrino spin in curved spacetime with the Kerr–Schield metric. Contrary to the classical theory of spin in a gravitational field, the quantum system of equations (7) obviously includes the mass of the particle m. Moreover, in (7), there are terms which are stipulated by a nonhermiticity of the Hamiltonian $\hat{\mathbf{H}}$ for particles with spin $\frac{1}{2}$ in curved spacetime. This circumstance defines the character of the neutrino spin behavior in the gravitational field.

Let us present (7) in a more suitable form

$$\frac{d}{dt}F = -i\hat{\mathbf{H}}_1^{(+)}F - i\hat{\mathbf{H}}_2 H + i\hat{\mathbf{V}}_c H,$$
$$\frac{d}{dt}H = -i\hat{\mathbf{H}}_1^{(-)}H - i\hat{\mathbf{H}}_2 F - i\hat{\mathbf{V}}_c F, \quad (9)$$

where

$$\hat{\mathbf{H}}_1^{(\pm)} = (1+\xi^2)^{-1}(E(1+\xi^2) - \xi(\boldsymbol{\xi}\cdot\mathbf{q}) \pm (\boldsymbol{\sigma}\cdot\mathbf{Q}_{\mp})),$$
$$\hat{\mathbf{H}}_2 = \frac{m\left(1+\frac{1}{2}\xi^2\right)}{1+\xi^2},$$
$$\hat{\mathbf{V}}_c = \frac{m\xi}{2(1+\xi^2)}(\boldsymbol{\sigma}\cdot\boldsymbol{\xi}).$$

The term $\hat{\mathbf{V}}_c$ in (9) leads to the change of the spin conditions, i.e., $\frac{d}{dt}F \neq 0$ and $\frac{d}{dt}H \neq 0$. That is why we solve (9) for a stationary case $\hat{\mathbf{V}}_c = 0$. Then, we have

$$\hat{\mathbf{H}}_1^{(+)}F_0 + \hat{\mathbf{H}}_2 H_0 = 0, \quad \hat{\mathbf{H}}_1^{(-)}H_0 + \hat{\mathbf{H}}_2 F_0 = 0, \quad (10)$$

where F_0 and H_0 is a solution of the system of linear algebraic equations (10). The value of $E(\mathbf{q}, \boldsymbol{\xi})$ can be found from the conditions of compatibility of the system equations (10).

Due to the presence of the term $\frac{i}{2}\xi[\boldsymbol{\xi}\times\mathbf{q}]$ in $\hat{\mathbf{H}}_1^{(+)}$ and $\hat{\mathbf{H}}_1^{(-)}$, the values $E(\mathbf{q}, \boldsymbol{\xi})$ are complex and $\mathrm{Im}E(\mathbf{q}, \boldsymbol{\xi}) \sim m\xi^2 \sin\Theta$ (Θ is the angle between the vectors $\mathbf{q}$ and $\boldsymbol{\xi}$). In (10), we need to substitute only $\mathrm{Re}E(\mathbf{q}, \boldsymbol{\xi})$. We do not need the explicit form of F_0 and H_0. These solutions are normalized according to the conditions

$$F_0^{+}\left(1 + \frac{1}{2}\xi(\boldsymbol{\sigma}\cdot\boldsymbol{\xi})\right)F_0 = 1,$$
$$H_0^{+}\left(1 - \frac{1}{2}\xi(\boldsymbol{\sigma}\cdot\boldsymbol{\xi})\right)H_0 = 1. \quad (11)$$

We divide F_0 and H_0 into two linearly independent terms:

$$F_0 = f_0 - \frac{m\left(1+\frac{1}{2}\xi^2\right)}{\hat{\mathbf{H}}_1^{(+)}}h_0,$$
$$H_0 = h_0 - \frac{m\left(1+\frac{1}{2}\xi^2\right)}{\hat{\mathbf{H}}_1^{(-)}}f_0. \quad (12)$$

Then, the solution of the initial system (9) is to be searched for in the form

$$F = C_L(t) f_0 - C_R(t)\frac{m\left(1+\frac{1}{2}\xi^2\right)}{\hat{\mathbf{H}}_1^{(+)}}h_0,$$
$$H = C_R(t)h_0 - C_L(t)\frac{m\left(1+\frac{1}{2}\xi^2\right)}{\hat{\mathbf{H}}_1^{(-)}}f_0. \quad (13)$$

Substituting (13) into (9) and neglecting the terms of order (m/E), we obtain a system of differential equations for C_R and C_L:

$$\frac{d}{dt}C_L(t) = \frac{i}{2}\frac{m\xi}{(1+\xi^2)}(f_0^+(\boldsymbol{\sigma}\cdot\boldsymbol{\xi})h_0)C_R(t),$$
$$\frac{d}{dt}C_R(t) = -\frac{i}{2}\frac{m\xi}{(1+\xi^2)}(h_0^+(\boldsymbol{\sigma}\cdot\boldsymbol{\xi})f_0)C_L(t). \quad (14)$$

We indicate $\frac{m}{2}\xi(f_0^+(\boldsymbol{\sigma}\cdot\boldsymbol{\xi})h_0) = \omega$. Here, the notation "+" means Hermitian conjugation. The case of $C_R(0) = 0$ presents particular interest. After integrating (14), we get

$$C_L = A\cosh\int_0^t|\omega|d\tau, \quad C_R = -iA\frac{\omega^+}{\omega}\sinh\int_0^t|\omega|d\tau. \quad (15)$$

This kind of C_L and C_R behavior is radically different from the case of the effect of an electromagnetic field on the spin conditions of a neutral particle, with a spin of $\frac{1}{2}$ and anomalous magnetic moment. There, we deal with spin precession into the electromagnetic field, which, unlike (15), is described in trigonometric functions.

For defining W_L and W_R, we need to find $\exp(-2\mathrm{Im}\int_0^t E(\mathbf{q}, \boldsymbol{\xi})d\tau)$ explicitly; the result is presented together with C_L and C_R. Equation (17) gives several values of $\mathrm{Im}E(\mathbf{q}, \boldsymbol{\xi})$. The concrete values of $\mathrm{Im}E(\mathbf{q}, \boldsymbol{\xi})$ are estimated by the functions $C_L(t)$ and $C_R(t)$, which determine the particle's spin conditions. That is why we express $E(\mathbf{q}, \boldsymbol{\xi})$ by F and H, using the system

$$\mathrm{Im}E = \frac{\xi}{2(1+\xi^2)} \times \frac{H^+(\boldsymbol{\sigma}\cdot[\boldsymbol{\xi}\times\mathbf{q}])H + F^+(\boldsymbol{\sigma}\cdot[\boldsymbol{\xi}\times\mathbf{q}])F}{(F^+F)+(H^+H)}. \quad (16)$$

In the general case, the calculations in (16) are complicated and bulky. However, for $\xi^2 \ll 1$ and $\frac{m}{E} \ll 1$, calculation of (16) is considerably simplified:

$$\mathrm{Im}E(\mathbf{q}, \boldsymbol{\xi}) = \frac{1}{2}\frac{d}{dt}\ln(C_L^+C_L + C_R^+C_R),$$
$$|\omega| = \frac{1}{2}m\xi^2\sin\Theta. \quad (17)$$

As a result, for a weak gravitational field $\xi^2 \ll 1$ with the help of (5), (15), and (17), we find the dependence of W_L and W_R on time in the Kerr–Schield metric

$$W_L = \left[1+\tanh^2\left(\int_0^t|\omega|d\tau\right)\right]^{-1},$$
$$W_R = \left[1+\coth^2\left(\int_0^t|\omega|d\tau\right)\right]^{-1}. \quad (18)$$

From (18), an effect of massive-neutrino depolarization in the gravitational field follows. The gravitational field of a rotating gravitating body can be described by the following Kerr axial-symmetrical stationary metric under $r \gg a$:

$$\xi = \sqrt{\frac{R_g}{r}}, \quad \boldsymbol{\xi} = \frac{\xi}{r}\left(\mathbf{r} + \frac{[\mathbf{a}\times\mathbf{r}]}{r}\right). \quad (19)$$

Here, $a = J/M$, J is gravitating body's angular momentum and M is its mass. For the Sun, $a_\odot = 0.28$ km and $R_{g\odot} = 2.96$ km.

Assume that a particle is moving along the radius $\mathbf{r}$. Then, $|\omega| = \frac{1}{2}mR_g a r^{-2}\sin\alpha$ (α is the angle between the vectors $\mathbf{r}$ and $\mathbf{a}$). In this case, the effect of changing massive-neutrino helicity can be explained by the fact that the gravitating body has its own angular momentum, or rotation. Since (19) describes the external gravitational field, we shall calculate it with $t = 0$, $r = R$ (R is the gravitating body's radius). Making the necessary calculation, we have the evaluation at $r \gg R$:

$$\int_0^\infty|\omega|d\tau = \Omega = \frac{1}{2}mR_g a R^{-1}\sin\alpha. \quad (20)$$

The exact formula for Ω will evidently differ from (20) by a factor of the first order. It will also consider the particular geometry in the gravitational field of the rotating gravitating body. Let us assume that $\Omega = \ln 10$. Then, $W_L = 0.51$, $W_R = 0.49$, and $m = m_0 = \frac{1}{2}\ln 10(R/aR_g)\sin\alpha$. Hence, if $m \geq m_0$, the flows of right and left neutrinos emitted by a star will be virtually equal. The values of W_L and W_R change most consider-

ably if $0.1m_0 \le m \le 0.7m_0$. Here, $0.92 \ge W_L \ge 0.55$ and $0.45 \ge W_R \ge 0.08$.

For a solar neutrino, $m_0 = 3.14 \times 10^{-4}$ eV by $\alpha = \pi/2$. If the neutrino is emitted by a neutron star having the same moment and mass as those of the Sun and a radius of R = 10 km, then, if $\alpha = \pi/2$, m_0 will be greater than $m_0 = 3.14 \times 10^{-8}$ eV. The deficit of the left solar neutrinos on the Earth, D_{ν_L}, evidently amounts to W_R. The effect described in this work allows us to establish considerable similarity between the theoretical and observed solar-neutrino flows if $m_{\nu_e} \ge 10^{-4}$ eV. The effect of the massive-neutrino depolarization will also considerably influence cooling of rotating neutron stars, especially at the moment of their formation when supernova stars explode.

REFERENCES

1. V. Fock and D. Ivanenko, Z. Phys. **54**, 798 (1929).
2. R. P. Kerr, Phys. Rev. Lett. **11**, 237 (1963).
3. V. P. Tsvetkov and V. N. Ryshikov, *V International Workshop on High Energy Spin Physics, Protvino, 1994*, p. 191.